frontiers | Research Topics

Transcriptional and epigenetic landscapes of abiotic stress response in plants

Edited by
Aamir W. Khan, Yezhang Ding and Mehanathan Muthamilarasan

Published in
Frontiers in Plant Science

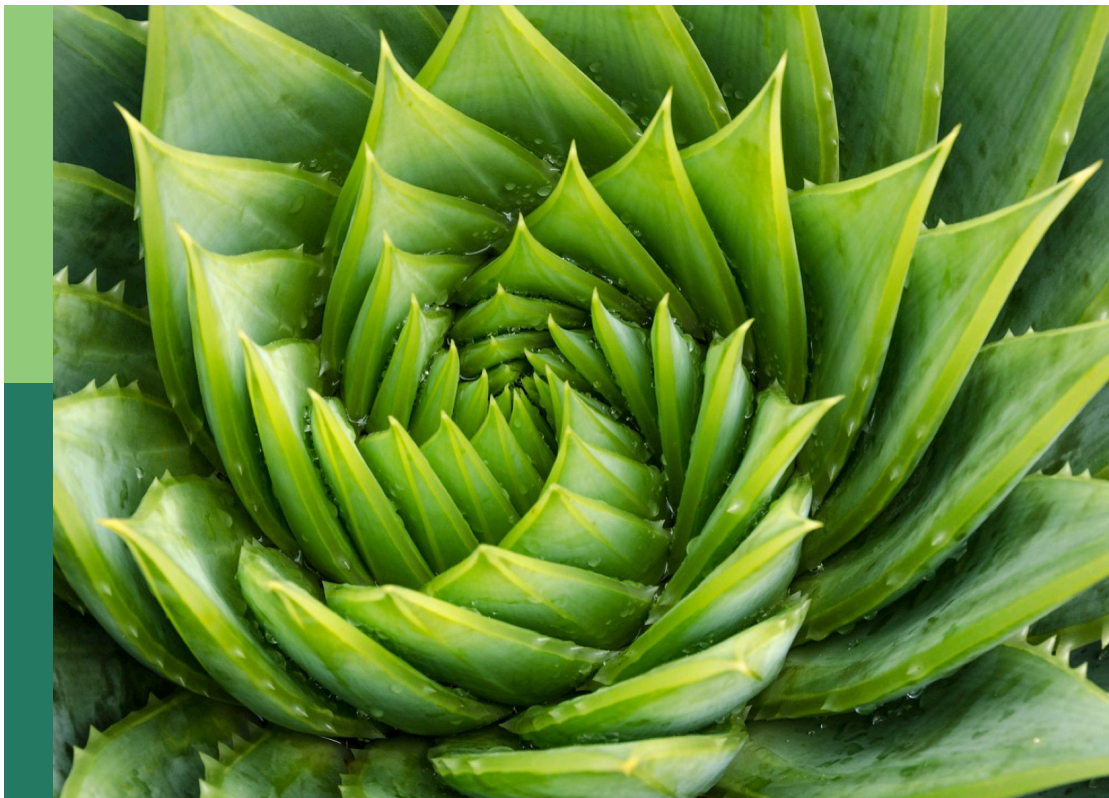

ISSN 1664-8714
ISBN 978-2-8325-5956-7
DOI 10.3389/978-2-8325-5956-7

About Frontiers

Frontiers is more than just an open access publisher of scholarly articles: it is a pioneering approach to the world of academia, radically improving the way scholarly research is managed. The grand vision of Frontiers is a world where all people have an equal opportunity to seek, share and generate knowledge. Frontiers provides immediate and permanent online open access to all its publications, but this alone is not enough to realize our grand goals.

Frontiers journal series

The Frontiers journal series is a multi-tier and interdisciplinary set of open-access, online journals, promising a paradigm shift from the current review, selection and dissemination processes in academic publishing. All Frontiers journals are driven by researchers for researchers; therefore, they constitute a service to the scholarly community. At the same time, the *Frontiers journal series* operates on a revolutionary invention, the tiered publishing system, initially addressing specific communities of scholars, and gradually climbing up to broader public understanding, thus serving the interests of the lay society, too.

Dedication to quality

Each Frontiers article is a landmark of the highest quality, thanks to genuinely collaborative interactions between authors and review editors, who include some of the world's best academicians. Research must be certified by peers before entering a stream of knowledge that may eventually reach the public - and shape society; therefore, Frontiers only applies the most rigorous and unbiased reviews. Frontiers revolutionizes research publishing by freely delivering the most outstanding research, evaluated with no bias from both the academic and social point of view. By applying the most advanced information technologies, Frontiers is catapulting scholarly publishing into a new generation.

What are Frontiers Research Topics?

Frontiers Research Topics are very popular trademarks of the *Frontiers journals series*: they are collections of at least ten articles, all centered on a particular subject. With their unique mix of varied contributions from Original Research to Review Articles, Frontiers Research Topics unify the most influential researchers, the latest key findings and historical advances in a hot research area.

Find out more on how to host your own Frontiers Research Topic or contribute to one as an author by contacting the Frontiers editorial office: frontiersin.org/about/contact

Transcriptional and epigenetic landscapes of abiotic stress response in plants

Topic editors

Aamir W. Khan — University of Missouri, United States

Yezhang Ding — Division of Environmental Genomics and Systems Biology, Berkeley Lab (DOE), United States

Mehanathan Muthamilarasan — University of Hyderabad, India

Citation

Khan, A. W., Ding, Y., Muthamilarasan, M., eds. (2025). *Transcriptional and epigenetic landscapes of abiotic stress response in plants*. Lausanne: Frontiers Media SA.

doi: 10.3389/978-2-8325-5956-7

Table of contents

frontiers | Frontiers in Plant Science

TYPE Editorial
PUBLISHED 20 January 2025
DOI 10.3389/fpls.2025.1541642

OPEN ACCESS

EDITED AND REVIEWED BY
Huihui Li,
Chinese Academy of Agricultural Sciences, China

*CORRESPONDENCE
Aamir W. Khan
maky74@missouri.edu
Yezhang Ding
yezhangding@lbl.gov
Mehanathan Muthamilarasan
muthu@uohyd.ac.in

RECEIVED 08 December 2024
ACCEPTED 07 January 2025
PUBLISHED 20 January 2025

CITATION
Khan AW, Ding Y and Muthamilarasan M (2025) Editorial: Transcriptional and epigenetic landscapes of abiotic stress response in plants.
Front. Plant Sci. 16:1541642.
doi: 10.3389/fpls.2025.1541642

Editorial: Transcriptional and epigenetic landscapes of abiotic stress response in plants

Aamir W. Khan[1]*, Yezhang Ding[2]* and Mehanathan Muthamilarasan[3]*

[1]Division of Plant Science and Technology, University of Missouri, Columbia, MO, United States, [2]Division of Environmental Genomics and Systems Biology, Lawrence Berkeley National Laboratory, Berkeley, CA, United States, [3]Department of Plant Sciences, University of Hyderabad, Hyderabad, India

KEYWORDS

transcriptome, epigenetics, abiotic, genomics, DNA methylation

Editorial on the Research Topic
Transcriptional and epigenetic landscapes of abiotic stress response in plants

In nature, plants constantly face various biotic and abiotic stresses that impact their growth, development, and productivity. Among these, abiotic stresses often have a more severe impact than biotic stresses. For instance, drought has been reported to cause greater yield losses than the combined impact of all plant pathogens (Gupta et al., 2020). Abiotic stresses are the immediate outcome of climate change, and the magnitude of these stresses has gradually increased every year with the rise in global temperatures. Thus, it has become imperative to study the impact of these stresses on plants and how plants respond to them at different levels to show resilient traits. This includes analysing the plants at morpho-physiological, biochemical, and molecular levels. Researchers often compare stressed plants to control (non-stressed) plants or evaluate contrasting genotypes, such as tolerant and sensitive lines, to elucidate the mechanisms underlying stress responses. While these studies have provided some insights, a comprehensive understanding of the intricate mechanisms governing plant responses to abiotic stress remains largely unknown. Recent advances in next-generation tools and technologies have enabled researchers to dissect the molecular basis of plant stress responses at genomic, transcriptomic, proteomic, metabolomic, epigenetic and epigenomic levels. Among these, knowledge of the transcriptional/epigenomic landscape of the trait-associated variations is limited. Given the importance of transcriptional changes and histone modifications in abiotic stress responses, this Research Topic was edited to collage the knowledge available on transcriptional and epigenetic landscapes of abiotic stress response in plants. The Research Topic features eight original research articles and one review, covering various aspects of transcriptome and epigenetic reprogramming in plants during abiotic stresses. Four of the research articles employ transcriptomics integrated with other omics approaches to explore transcriptome reprogramming, candidate gene identification, and the role of long non-coding RNA during different stresses. Two articles focus on the functional characterization of specific candidate genes involved in stress response, while another provides a genome-wide analysis of a stress-responsive gene family. Additionally, one study investigates genome-wide histone modifications, specifically H3K4me3 and H3K27me3, in response to abiotic stresses.

Wen et al. examined the transcriptional reprogramming in foxtail millet (*Setaria italica*) during foliar application of sodium selenite. The authors showed that selenium (Se) is sequentially transported and accumulated in the leaves, stems, and spikes. Transcriptome analysis revealed significant upregulation of Se metabolism and transporter genes, including those encoding sulfate, phosphate, and nitrate transporters, ABC transporters, antioxidants, phytohormone signaling components, and transcription factors. The study highlighted that these genes interact in complex networks, both synergistically and antagonistically, to regulate selenate transport mechanisms. Further, co-expression network analysis identified the key transcription factors and transporters significantly correlated with Se accumulation and transport. Expression profiling of candidate genes showed the upregulation of genes encoding sulfate transporters (SiSULTR1.2b and SiSULTR3.1a), a phosphate transporter (PHT1.3), a nitrate transporter (NRT1.1B), glutathione S-transferases (GSTs), and an ABC transporter (ABCC13), with an increase in SeO_4^{2-} accumulation. This study provided comprehensive insights into Se accumulation and transport mechanisms in foxtail millet. While selenium is considered an essential trace element, cadmium (Cd) is recognized as one of the most toxic elements. In a multi-omics study, Wu et al. investigated the physiological, transcriptomic, and metabolomic responses of *Abelmoschus manihot* to Cd stress. Exposure to Cd resulted in significant growth inhibition and oxidative stress in *A. manihot*. Transcriptomic analysis identified differentially expressed genes involved in metal transport, antioxidative defense, and stress signaling pathways. Metabolomic profiling revealed alterations in amino acid metabolism, organic acids, and secondary metabolites, indicating metabolic changes to mitigate Cd toxicity. Integrative analysis highlighted the activation of lipid metabolism and phenylpropanoid biosynthesis pathways, suggesting their roles in Cd detoxification and tolerance. Thus, Wu et al. provided insights into the molecular mechanisms of Cd response in *A. manihot*, which has implications for devising potential strategies for phytoremediation.

The early transcriptional and alternative splicing (AS) responses of tomato (*Solanum lycopersicum*) roots to salt stress were reported by Gan et al. Using DNBSEQ™ technology, Gan et al. identified 3590 differentially expressed genes (DEGs) and 3709 differentially alternatively spliced (DAS) genes during the initial hours of salt exposure. The DEGs were enriched in pathways related to protein metabolism, stress responses, and transcription regulation, indicating a rapid reprogramming of gene expression under salt stress. AS events, particularly exon skipping, were significantly enhanced under salt stress, affecting genes involved in signaling and metabolic processes. The study also reported that genes associated with splicing and spliceosome assembly were differentially expressed, suggesting their role in regulating AS events under stress conditions. These findings expand our knowledge of the molecular mechanisms underlying salt stress response in tomato roots, emphasizing the importance of AS in stress adaptation.

The use of transcriptome sequencing data to study the role of long non-coding RNAs (lncRNAs) was demonstrated by Babaei et al. The authors analyzed the publicly available RNA-seq data of four wheat cultivars (two sensitive and two tolerant cultivars) subjected to heat stress during the pollen development stage. The study identified 11,054 lncRNA-producing loci, with 5,482 lncRNAs showing differential expression in response to elevated temperatures. These heat-responsive lncRNAs potentially regulate protein-coding genes through *cis* and *trans* interactions, as well as within lncRNA-miRNA-mRNA networks. Gene ontology analysis revealed that the target genes of these lncRNAs are involved in processes such as hormonal responses, protein modification and folding, stress responses, and various biosynthetic and metabolic pathways. Specific lncRNA/protein-coding gene pairs and lncRNA-miRNA-mRNA regulatory modules were conserved across multiple cultivars, implicating them in heat stress responses. The study sheds light on lncRNA-mediated regulatory mechanisms during pollen development under heat stress. A similar study on heat stress was conducted by Niu et al., wherein the authors investigated the regulatory role of the SET domain protein SUVH2 in controlling the activity of the heat-activated retrotransposon ONSEN in *A. thaliana*. Under heat stress, ONSEN transcription levels were increased in the *suvh2* mutant; however, no transpositional activity was observed. Notably, the *suvh2* mutant produced small interfering RNAs (siRNAs) from the ONSEN locus during heat stress, indicating that siRNAs suppress transposition. These findings suggest that SUVH2 plays a critical role in the epigenetic regulation of ONSEN through mechanisms involving siRNA-mediated pathways. This study provides evidence of the complex regulatory networks governing retrotransposon activity in plants, particularly under abiotic stress conditions.

C2H2 zinc finger proteins (C2H2-ZFPs) are transcription factors that have critical roles in plant development and stress tolerance. Given this, Du et al. systematically analyzed the C2H2-ZFP gene family in sweet potato (*Ipomoea batatas*), identifying 178 *IbZFP* genes across 15 chromosomes. These proteins were phylogenetically categorized into six clades, and the expansion of this gene family was attributed to 24 tandem and 46 segmental duplications. *In silico* expression profiling of *IbZFP* genes in publicly available RNA-seq data on storage root development highlighted 44 *IbZFP* genes showing differential expression across cultivars. In another dataset on salt stress, 92 *IbZFP* genes showed differential expression to salt stress in salt-tolerant and salt-sensitive varieties. Six *IbZFP* genes were further investigated for tissue-specific and stress-responsive expression under drought, salt, abscisic acid, and gibberellic acid treatments. Further, heterologous expression of *IbZFP105* in *A. thaliana* conferred tolerance to salt stress and increased ABA sensitivity, indicating a positive role of C2H2-ZFPs in stress response. Similarly,Chen et al. examined the impact of overexpressing a ribosome-inactivating protein, OsRIP1, in rice (*Oryza sativa*). OsRIP1 is known to target ribosomal RNA, thereby inhibiting protein synthesis. The authors analyzed the previously developed overexpression lines at phenotypic, transcriptomic, and proteomic levels, in response to methyl jasmonate (MeJA) treatments. Overall, the study suggests that OsRIP1 may antagonize MeJA-induced shoot growth inhibition by modulating cytokinin-mediated leaf senescence and positively regulating cell cycle processes. Interactions between OsRIP1 and proteins, such as the 40S ribosomal protein S5 and

α-tubulin, facilitate this modulation. Thus, Chen et al. have provided insights into the complex regulatory roles of OsRIP1 in determining tolerance to exogenous MeJA application in rice.

From an epigenetic perspective, Faivre et al. examined the impact of cold stress on H3K4me3 (associated with gene activation) and H3K27me3 (associated with gene repression) in *A. thaliana*. Under stress conditions, both H3K4me3 and H3K27me3 exhibited rapid and gene-specific redistribution. Interestingly, changes in H3K4me3 and H3K27me3 levels occurred independently on different gene sets, confuting the notion that gene activation under cold stress involves a simple switch from H3K27me3-mediated repression to H3K4me3-mediated activation. Also, the study highlighted a weak correlation between these histone modifications and the changes in the expression of corresponding genes. Altogether, the study provided a genome-wide perspective on cold-triggered histone methylation dynamics, with a lead for further studies on the roles of these marks on corresponding genes.

Finally, a review by Liu et al. summarized the multifaceted roles of auxin response factors (ARFs) in plant development and stress tolerance, emphasizing their functions as transcriptional regulators in auxin signaling. The review provided structural insights into ARF-DNA interactions and explored non-canonical auxin signaling pathways independent of TIR1/AFB-mediated Aux/IAA degradation. This review highlights the versatility of ARFs in regulating organogenesis and abiotic and biotic stress responses.

In conclusion, the Research Topic provided valuable insights into the transcriptional and epigenetic mechanisms underlying abiotic stress responses. Overall, the studies discussed above have provided information on key genes and their potential roles in shared or common pathways and processes regulating stress responses; however, our understanding of the unique and novel mechanisms specific to certain genotypes, species, genera, and families is still limited. Moreover, studies on the effects of multiple or combined stresses on plants are scarce. While it is imperative to encourage more studies on the transcriptional and epigenetic responses of plants to different environmental cues, particularly under multiple or combined stresses, the Research Topic has paved the way for advancing such studies to gain a more comprehensive understanding of plant stress responses.

Author contributions

AK: Writing – original draft, Writing – review & editing. YD: Writing – review & editing. MM: Writing – review & editing.

Acknowledgments

We thank all the authors and reviewers who have participated in this Research Topic.

Conflict of interest

The authors declare that the research was conducted in the absence of any commercial or financial relationships that could be construed as a potential conflict of interest.

Publisher's note

Reference

Gupta, A., Rico-Medina, A., and Caño-Delgado, A. I. (2020). The physiology of plant responses to drought. *Science* 368, 266–269. doi: 10.1126/science.aaz7614

frontiers | Frontiers in Plant Science

TYPE Original Research
PUBLISHED 13 December 2023
DOI 10.3389/fpls.2023.1301848

OPEN ACCESS

EDITED BY
Aamir W. Khan,
University of Missouri, United States

REVIEWED BY
Mingzhe Sun,
Heilongjiang Bayi Agricultural University, China
Xin Liu,
Beijing Academy of Agriculture and Forestry Sciences, China

*CORRESPONDENCE
Fuyun Hou
houfuyun@shandong.cn
Liming Zhang
Zhanglm11@sina.com

RECEIVED 25 September 2023
ACCEPTED 27 November 2023
PUBLISHED 13 December 2023

CITATION
Du T, Zhou Y, Qin Z, Li A, Wang Q, Li Z, Hou F and Zhang L (2023) Genome-wide identification of the C2H2 zinc finger gene family and expression analysis under salt stress in sweetpotato.
Front. Plant Sci. 14:1301848.
doi: 10.3389/fpls.2023.1301848

Genome-wide identification of the C2H2 zinc finger gene family and expression analysis under salt stress in sweetpotato

Taifeng Du[1], Yuanyuan Zhou[2], Zhen Qin[2], Aixian Li[2], Qingmei Wang[2], Zongyun Li[1], Fuyun Hou[2]* and Liming Zhang[1,2]*

[1]Key Laboratory of Phylogeny and Comparative Genomics of the Jiangsu Province, School of Life Sciences, Jiangsu Normal University, Xuzhou, China, [2]Crop Research Institute, Shandong Academy of Agricultural Sciences/Scientific Observing and Experimental Station of Tuber and Root Crops in Huang-Huai-Hai Region, Ministry of Agriculture and Rural Affairs, Jinan, China

Introduction: The higher plant transcription factor C2H2 zinc finger protein (C2H2-ZFP) is essential for plant growth, development, and stress response. There are limited studies on *C2H2-ZFP* genes in sweetpotato, despite a substantial number of *C2H2-ZFP* genes having been systematically found in plants.

Methods: In this work, 178 *C2H2-ZFP* genes were found in sweetpotato, distributed randomly on 15 chromosomes, and given new names according to where they were located. These members of the zinc finger gene family are separated into six branches, as shown by the phylogenetic tree. 24 tandem repeats of *IbZFP* genes and 46 fragment repeats were identified, and a homology study revealed that *IbZFP* genes linked more regions with wild relative species of sweetpotato as well as rhizome plants like potato and cassava. And we analyzed the expression patterns of *IbZFP* genes during the early development of sweetpotato storage roots (SRs) and salt stress using transcriptome data, and identified 44 *IbZFP* genes that exhibited differences in expression levels during the early expansion of sweetpotato SRs in different varieties, and 92 *IbZFP* genes that exhibited differences in expression levels under salt stress in salt tolerant and salt sensitive sweetpotato varieties. Additionally, we cloned six *IbZFP* genes in sweetpotato and analyzed their expression patterns in different tissues, their expression patterns under abiotic stress and hormone treatment, and subcellular localization.

Results and discussion: The results showed that the *IbZFP* genes had tissue specificity in sweetpotato and were induced to varying degrees by drought and salt stress. ABA and GA_3 treatments also affected the expression of the *IbZFP* genes. We selected *IbZFP105*, which showed significant differences in expression levels under salt stress and ABA treatment, to be heterologously expressed in *Arabidopsis thaliana*. We found that *IbZFP105* OE lines exhibited higher tolerance to salt stress and ABA stress. This indicates that *IbZFP105* can enhance the salt

tolerance of plants. These results systematically identified the evolution and expression patterns of members of the *C2H2-ZFP* gene family in sweetpotato, providing a theoretical basis for studying the role of *IbZFP* genes in the development of sweetpotato SRs and in resistance to stress.

KEYWORDS

salt stress, C2H2-Zinc finger protein, expression profiles, synteny analysis, sweetpotato

1 Introduction

Sweetpotato (*Ipomoea batatas* (L.) Lam.) is an important food crop with ultra-high yield characteristics, and sweetpotato is rich in protein, dietary fiber, polyphenols, vitamins, mineral elements, and other nutrients needed by the human body. It is one of the globally recognized nutrients (Neela and Fanta, 2019). The sweetpotato planting area can reach 7.4 million hectares, with an annual production of about 88.9 million tonnes of storage roots (SRs). As the main edible tissue of sweetpotato, the production and development of SR are their most important agronomic traits (Du et al., 2023). However, adverse abiotic factors like salt and drought severely restrict the sweetpotato plant's growth, development, and output (Zhang et al., 2023). Transcription factors play an important regulatory role in the transmission of plant stress signals, regulating the expression of multiple stress related genes and improving plant stress resistance. The regulatory effects of many transcription factors have been reported, for example, the MYB transcription factor (Dubos et al., 2010; Li et al., 2016), the WRKY transcription factor (Chen et al., 2009; Raineri et al., 2015), the NAC transcription factor (Yuan et al., 2019; Diao et al., 2020), the bHLH transcription factor (Guo et al., 2021; Qian et al., 2021), the bZIP transcription factor (Joo et al., 2021; Han et al., 2023), and zinc finger transcription factor (Kiełbowicz-Matuk, 2012; Yin et al., 2017), *etc.* Zinc finger proteins (ZFPs) the largest transcription factor family in plants, are present in many different species. In controlling plant growth and development and responding to varied environmental challenges, they serve a critical regulatory role (Han et al., 2021).

ZFPs can be categorized into many subfamilies, such as C2H2, C3H, C3HC4, etc., depending on the quantity and arrangement of cysteine and histidine residues in their secondary structure. C2H2 zinc finger proteins (C2H2-ZFPs) are one of them that have undergone more in-depth study (Jiao et al., 2020). The *EPF1* gene of Petunia is the earliest zinc finger protein found in plants with a C2H2 zinc finger structure (Takatsuji et al., 1992). Numerous C2H2-ZFPs have so far been found in plants, including *Arabidopsis thaliana* 176 (Englbrecht et al., 2004), *Sorghum bicolor* 145 (Cui et al., 2022), *Vitis vinifera* 98 (Arrey-Salas et al., 2021), and *Panax ginseng* 115 (Jiang et al., 2022). The length of the long spacer between the two zinc fingers in plant-specific C2H2-ZFP (Q-type C2H2-ZFP) is different from that of other eukaryotes (Ciftci-Yilmaz and Mittler, 2008). A highly conservative QALGGH sequence is typically found in Q-type C2H2-ZFPs, allowing ZFPs to detect target genes and control their expression levels (Wang et al., 2019). There are several distinct classification types and standards used for C2H2-ZFPs. Usually, the number of zinc finger domains, the spacing between them, the series or dispersion of zinc finger domains, and the QALGGH sequence are used to categorize C2H2-ZFPs (Liu et al., 2022b).

C2H2-ZFP genes can regulate plants to cope with various abiotic stresses such as high salinity, drought, cold, etc. and plays a very important role in plant adaptation to the environment (Han et al., 2020). C2H2-ZFPs can typically interact with plant hormones to affect the phenotype of plants under stress. (Kiełbowicz-Matuk, 2012; Liu et al., 2022b). For example, overexpression of *OsZFP179* enhances the salt tolerance of rice, transgenic seedlings show hypersensitivity to exogenous ABA (Sun et al., 2010), *OsZFP36* is a key participant in rice abscisic acid induced antioxidant defense and oxidative stress tolerance (Zhang et al., 2014), and *PtrZPT2-1* encodes C2H2-ZFP from *Poncirus trifoliata*, which can enhance the tolerance of plants to various abiotic stresses (Liu et al., 2017).

In addition, C2H2-ZFP can also participate in the growth and development of many plant organs and structures. For instance, during seed germination and plant development, *Arabidopsis thaliana AtZFP3* interferes with the transmission of abscisic acid and light signals (Joseph et al., 2014), *Arabidopsis thaliana AtZFP1* acts upstream of the key trichome initiation factors GL3 and TRY, and overexpression of *AtZFP1* significantly increases the number of trichomes on the stem, leaf, lateral branch, and main stem (Zhang et al., 2020). *AtZFP5* is associated with ethylene signaling and regulates root hair development induced by phosphate and potassium deficiency in *Arabidopsis thaliana* (Huang et al., 2020).

In this study, we identified 178 C2H2 zinc-finger proteins (IbZFPs) from the genome of sweetpotato and analyzed their phylogenetic relationship, chromosome location, collinearity with other species, gene structure, conservative motif promoter cis-regulatory element, and subcellular location. In addition, we also analyzed the expression profile of *IbZFP* genes in sweetpotato SR development and salt stress. Some *IbZFP* genes were detected by real-time quantitative polymerase chain reaction (qRT-PCR). And overexpression of *IbZFP105* in *Arabidopsis thaliana* was revealed to enhance its tolerance to salt and ABA stress. These results should provide a very important theoretical basis for studying the function of *IbZFP* genes in the future.

2 Materials and methods

2.1 Identification of C2H2-ZFPs in sweetpotato

The hexaploid sweetpotato Taizhong6 genome sequence was extracted from the Ipomoea Genome Hub database (https://sweetpotao.com/download_genome.html, accessed on 7 March 2023). In order to screen the possible *C2H2-ZFP* coding genes in the genome, two methods were used. The HMM profile of the C2H2-ZFP domain (PF00096, PF13894, PF13912, PF18414, and PF16622) was downloaded from the Pfam database (http://www.ebi.ac.uk/interpro/, accessed on 8 March 2023) (Paysan-Lafosse et al., 2023) and was used to identify the *C2H2-ZFP* genes in the *Ipomoea batatas* genome using HMMER 3.0 software with an E value < $1e^{-5}$. Using all AtZFPs in the *Arabidopsis thaliana* genome database (https://www.Arabidopsisthaliana.org/index.jsp, accessed on 7 March 2023) as queries, the BLAST algorithm identifies the predicted IbZFPs (BLASTP, E value < $1e^{-5}$). All the protein sequences obtained by the two methods were subjected to domain analyses using NCBI Batch CD-Search programs (E value < $1e^{-2}$, https://www.ncbi.nlm.nih.gov/Structure/bwrpsb/bwrpsb.cgi, accessed on 10 March 2023) and SMART (https://smart.embl.de/, accessed on 11 March 2023) software (Letunic et al., 2021). Those protein sequences lacking the C2H2-ZFP domain were discarded.

2.2 Sequence characterization analysis and chromosomal location

The ExPASy program was used to evaluate the physical and chemical properties of IbZFPs, such as the length of amino acid residues, molecular weight (kDa), isoelectric point (pI), instability index, and aliphatic index of each IbZFP (https://www.expasy.org/, accessed on 14 March 2023) (Artimo et al., 2012). The phosphorylation sites of IbZFPs were detected using NetPhos-3.1 (https://services.healthtech.dtu.dk/services/NetPhos-3.1/, accessed on 15 March 2023) (Blom et al., 1999). The WoLF PSORT website predicted IbZFPs' subcellular localizations (https://wolfpsort.hgc.jp/aboutWoLF_PSORT.html.en, accessed on 21 March 2023) (Horton et al., 2007). Retrieve the location information of the *IbZFP* genes from the annotated GFF3 file of the Sweetpotato genome and rename it to IbZFP1-IbZFP178 based on their position on the chromosome.

2.3 Phylogenetic analysis of IbZFPs

Using the amino acid sequences of 178 IbZFPs in sweetpotato and 176 AtZFPs proteins in *Arabidopsis thaliana*, a phylogenetic tree was constructed using the maximum likelihood (ML) method by MEGA11 with the following parameters: 1000 bootstrap method, Jones-Taylor-Thornton (JTT) model, pairwise deletion (Tamura et al., 2021). The constructed phylogenetic tree was then classified, annotated, and modified by the Chiplot online tool (https://www.chiplot.online/, accessed on 11 May 2023) (Xie et al., 2023).

2.4 Collinearity relationship analysis of *IbZFP* genes

Using "One Step MCScanX Super Fast" of TBtools software v1.131 to analyze downloaded genome sequence files and genome structure annotation information files to obtain collinearity information between *IbZFP* genes (Chen et al., 2020). Then, use the "Advanced Circos" function of TBtools software to visualize the collinear relationship between members of the *IbZFP* gene family.

In addition, in order to conduct homology analysis between the *IbZFP* genes and genes from other plant species, the genome sequences and annotation files of *Ipomoea triloba* and *Ipomoea trifida* were downloaded from the diploid sweetpotato genome website (http://sweetpotato.uga.edu/), and the genome sequences and annotation files of *Arabidopsis thaliana*, *Oryza sativa*, *Solanum tuberosum*, *Manihot esculenta*, *Zea mays*, and *Hordeum vulgare* were downloaded from the Ensemble Plants website (http://plants.ensembl.org/index.html, accessed on 23 May 2023). The collinearity analysis and visualization of these eight plants with the *IbZFP* genes were completed using TBtools software.

2.5 Gene structures and conserved motifs analysis of *IbZFP* genes

Tbtools software (v1.131) was used to analyze the GFF annotation files of sweetpotato genome information and visualize the exon-intron structure. The conserved motifs of IbZFP were analyzed using the default parameters of the online website MEME 5.5.2 (https://meme-suite.org/meme/tools/meme, accessed May 21, 2023).

2.6 Cis-acting elements in promoter regions analysis of *IbZFP* genes

Use the PlantCARE online website (http://bioinformatics.psb.ugent.be/webtools/plantcare/html/, accessed on 15 June 2023) to analyze the 2000 bp sequence upstream of the start codon of the *IbZFP* gene (Lescot et al., 2002). After screening and simplification, TBtools software was used for visualization.

2.7 Expression patterns analysis of *IbZFP* genes

Transcriptome data on SR expansion of two different varieties of sweetpotato from a previous study with NCBI project ID PRJNA756699, including J25_D1, J25_D2, J25_D3, J29_D1,

J29_D2, and J29_D3 (Du et al., 2023). In addition, transcriptome data of salt tolerant and salt sensitive sweetpotato varieties under salt stress were obtained from previous studies under NCBI project number PRJNA552932 (Qin et al., 2020), including NL54_0 h, NL54_0.5 h, NL54_6 h, NL54_12 h, J26_0 h, J26_0.5 h, J26_6 h, and J26_12 h. The Chiplot online tool is used to generate heatmaps.

2.8 Analysis of *IbZFP* genes expression in different tissues, under stress, and hormone effects

The seedlings of sweetpotato variety 'Jishu26' were collected from the Crop Research Institute, Shandong Academy of Agricultural Sciences, China. Seedlings grow in Hoagland solution under a light cycle of 26°C, 16 h of illumination, and 8 h of darkness. When seedlings have 5 to 6 functional leaves and 8 to 10 centimeters of adventitious roots, they are subjected to four different treatments. Hoagland's solution containing 150 mmol/L NaCl, 20% PEG 6000, 100 mmol/L ABA and 50 mg/L GA3 was used respectively, treated fibrous roots were collected after 0, 3, 6, 12, 24 and 48 h (Hou et al., 2021a). Fibrous roots treated with liquid nitrogen freezing were used to extract total RNA from the sample using RNA isolator Total RNA Extraction Reagent (Vzayme, Nanjing). cDNA was obtained through reverse transcription using a reverse transcription kit (Takara, Beijing), and used as a template. The CFX Connect real-time system (Bio-RAD) and ChamQ Universal SYBR qPCR Master Mix (Vazyme, Nanjing) were used for qRT-PCR. The reaction procedure is 95°C for 30 seconds, followed by 40 cycles of 95 °C for 10 seconds and 60°C for 15 seconds. Using the *Ibactin* gene as an internal reference, Supplementary Table S5 lists the primer sequences of the examined genes. The experiment was repeated 3 times, and the data was calculated using the $2^{-\triangle\triangle CT}$ method (He et al., 2023).

2.9 Subcellular localization of IbZFPs

The coding sequences of several *IbZFP* genes were inserted into the pCAMBIA1300-GFP vector using homologous recombination method, and the constructed recombinant plasmid was transformed into *Agrobacterium tumefaciens* EHA105. It was then transiently expressed in tobacco leaf (*Nicotiana benthamiana*) cells through injection. Take the transformed GFP leaves as the control. Determine nuclear localization using DAPI staining, observe and take photos using a Laser confocal microscope (Olympus) 2-3 days after injection (Hou et al., 2021b).

2.10 Overexpressing *IbZFP105* in *Arabidopsis thaliana*

The coding sequence of IbZFP105 was inserted into the pCAMBIA1300 vector through homologous recombination, and transformed into *Arabidopsis thaliana* through *Agrobacterium tumefaciens* (EHA105) mediated transformation. Possible transgenic strains were obtained through HYG screening, and identified at the DNA and RNA levels using PCR and RT-PCR. The obtained transgenic lines were screened through planting to obtain T3 generation homozygous lines for subsequent experiments.

3 Results

3.1 Identifcation and phylogenetic analysis of *IbZFP* gene family

In this study, we identified 178 IbZFPs in the sweetpotato genome database and consistently named IbZFP1-IbZFP178 according to their chromosomal locations (Supplementary Table S1). The molecular characteristics of all proteins were analyzed, including the number of amino acid (aa) residues, molecular weight (MW), isoelectric point (pI), subcellular localization and phosphorylation sites, *etc.* (Supplementary Table S1). IbZFPs vary in length from 68 (IbZFP122) to 1888 (IbZFP8) amino acid residues, correspondingly, with molecular weights ranging from 7.5 to 211.1 kDa. Theoretical pI ranged from 4.05 (IbZFP98) to 11.54 (IbZFP178), and the isoelectric point of 55 IbZFPs was less than 7, indicating that most of the IbZFPs were basic proteins. There are 11 IbZFPs with an instability index less than 40, most of which are unstable proteins. The aliphatic index and grand average of hydropathicity showed that all proteins except IbZFP111 were hydrophilic proteins. Subcellular localization prediction showed that except for IbZFP17, which was localized in the cytoplasm, and IbZFP114 was localized in the chloroplast, all other IbZFPs were localized in the nucleus. The analysis of IbZFP phosphorylation sites showed that IbZFPs have multiple possible phosphorylation sites, with the least 2 (IbZFP73) and the most 209 (IbZFP8).

In order to explore the phylogenetic relationship of IbZFPs in sweetpotato, the unrooted phylogenetic tree of all 178 IbZFPs and 176 *Arabidopsis thaliana* AtZFPs was constructed by the ML method. Phylogenetic analysis showed that the *IbZFP* gene family could be divided into 6 subfamilies (I-VI) (Figure 1), and each clade contained 8, 39, 34, 10, 45, and 42 IbZFPs. Among them, Clade I includes *AtELF6* and *AtEMF2*, which can regulate the flowering of *Arabidopsis thaliana* (Yoshida et al., 2001; Noh et al., 2004). Clade III includes multiple reported functional *Arabidopsis thaliana ZAT* genes, among which *AtZAT10* and *AtZAT12* can enhance salt tolerance in *Arabidopsis thaliana* (Xie et al., 2012), *AtZAT1* can regulate the maturation of the outermost layer cells in the root cap of *Arabidopsis thaliana*, thereby inhibiting its growth (Song et al., 2020), and *AtZAT11* is a dual-function transcriptional regulator that positively regulates primary root growth but negatively regulates Ni^{2+} tolerance (Liu et al., 2014). Clade IV of *VRN2* genes can mediate epigenetic regulation of vernalization in *Arabidopsis thaliana* (Gendall et al., 2001). Clade V includes multiple *Arabidopsis thaliana WIP* members, with *AtWIP1* involved in seed coat development (Sagasser et al., 2002), the *AtWIP2* mutation severely inhibits pollen tube movement, leading to fertility decline in

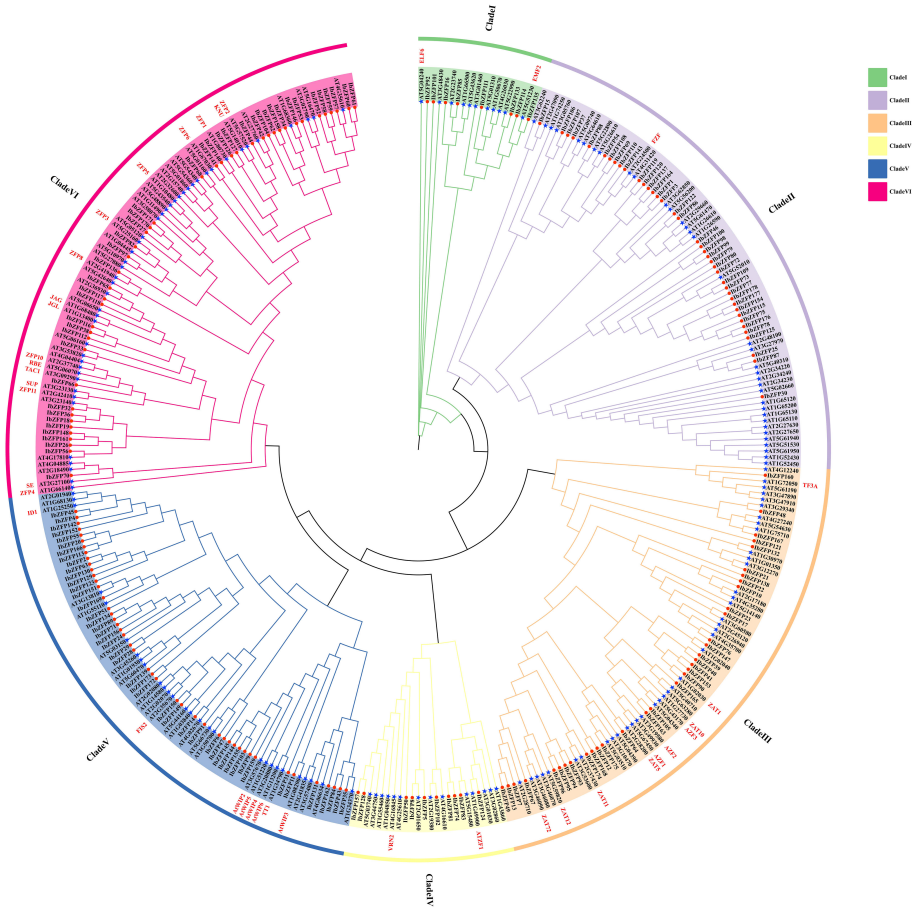

FIGURE 1
Phylogenetic classification of C2H2 zinc finger proteins (ZFPs) in *Arabidopsis thaliana* and *Ipomoea batatas*. The phylogenetic tree was established using the ML method of 1000 bootstraps. Used different colors to mark different subclasses of the *IbZFP* gene family (branch I-VI) with an arc outside the circular tree. The red circles and blue stars represented ZFPs from *Arabidopsis thaliana* and *Ipomoea batatas*, respectively. *Arabidopsis thaliana* genes that have reported their functions were marked in red font on the outer side of the branch.

Arabidopsis thaliana (Crawford et al., 2007), *AtWIP4* and *AtWIP5* are overexpressed in the pituitary gland and are necessary for the fate of distal stem cells in the root meristem tissue (Crawford et al., 2015). Clade VI includes several *AtZFP* genes with reported functions; for example, *AtZFP1* enhances salt tolerance in *Arabidopsis thaliana* (Han et al., 2014), *AtZFP3* participates in salt and osmotic stress responses (Liu et al., 2020b), and *AtZFP6* plays a key role in regulating trichome (Liu et al., 2020a).

3.2 Chromosome distribution and synteny analysis of *IbZFP* genes

Chromosomal location of *IbZFP* genes showed that 178 members of this gene family were distributed on all 15 chromosomes of *Ipomoea batatas* (Figure 2), among which Chr7 had the most with 23 *IbZFP* genes, while Chr9 and Chr13 had the least of 12 *IbZFP* genes.

Tandem repeat or local replication is the most common mechanism of gene family expansion (Cannon et al., 2004). We identified 15 tandem duplication events containing 24 *IbZFP* genes on Chr2, 4, 6, 7, 8, 9, and 11 (Figure 2). Moreover, some *IbZFP* genes participate in more than one tandem repeat event, such as *IbZFP58*, *59*, *60*, *78*, *79*, *etc*. In addition, all genes in tandem repeat events come from the same subfamily, which indicates that the subfamily classification of the evolutionary tree is accurate.Apart from that, collinearity analysis of the *IbZFP* gene family showed that a total of 71 *IbZFP* genes were involved in 46 segment repeat events (Figure 3), such as *IbZFP4* on Chr1 and *IbZFP45* on Chr5, *IbZFP13* on Chr2 and *IbZFP67* on Chr7, *IbZFP43* on Chr5, and *IbZFP84* on Chr7. These segmental duplication events are distributed across all 15 chromosomes, with Chr7 containing up to 15 *IbZFP* genes, followed by Chr5 containing 11, and Chr3, Chr9, and Chr12 containing at least 3 *IbZFP* genes, respectively. These results indicate that the evolution of the *IbZFP* gene family is related to gene duplication events, and tandem and segmental repeats play an important role in the amplification of the *IbZFP* genes.

In order to further infer the origin and evolutionary mechanism of the *IbZFP* genes in sweetpotato, we analyzed and compared the homology of *ZFP* genes between sweetpotato and several different species, including wild varieties *Ipomoea trifida* and *Ipomoea triloba* that are closely related to sweetpotato, two commonly used model

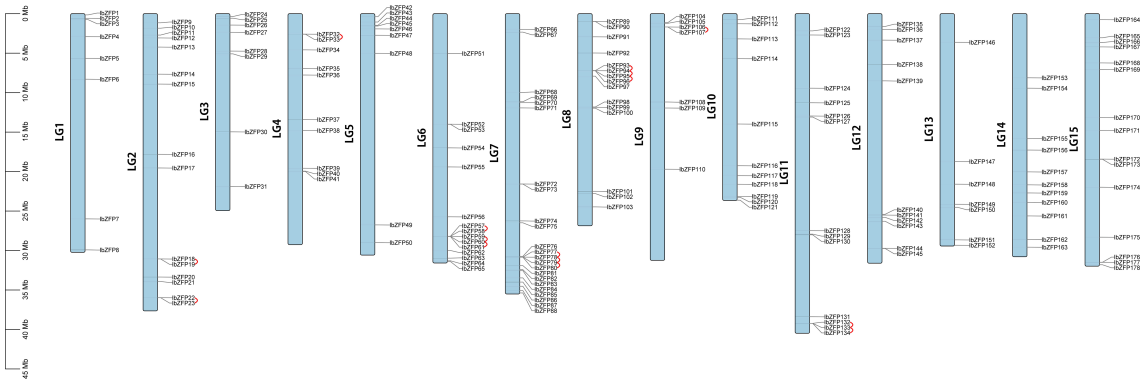

FIGURE 2
The gene locations of *IbZFP* genes in *Ipomoea batatas*. The scale bar on the left represents the length of the chromosome.

plants *Arabidopsis thaliana* and *Oryza sativa*, two edible rhizome plants *Solanum tuberosum* and *Manihot esculenta*, and two main grain plants *Zea mays* and *Hordeum vulgare* (Figure 4; Supplementary Table S2). Results display that 124 and 122 *IbZFP* genes showed syntenic connections with *Ipomoea trifida* and *Ipomoea triloba*, followed by *Manihot esculenta* (102), *Solanum tuberosum* (98), and *Arabidopsis thaliana* (67). The ones with less collinearity are *Oryza sativa* (18), *Hordeum vulgare* (17), and *Zea*

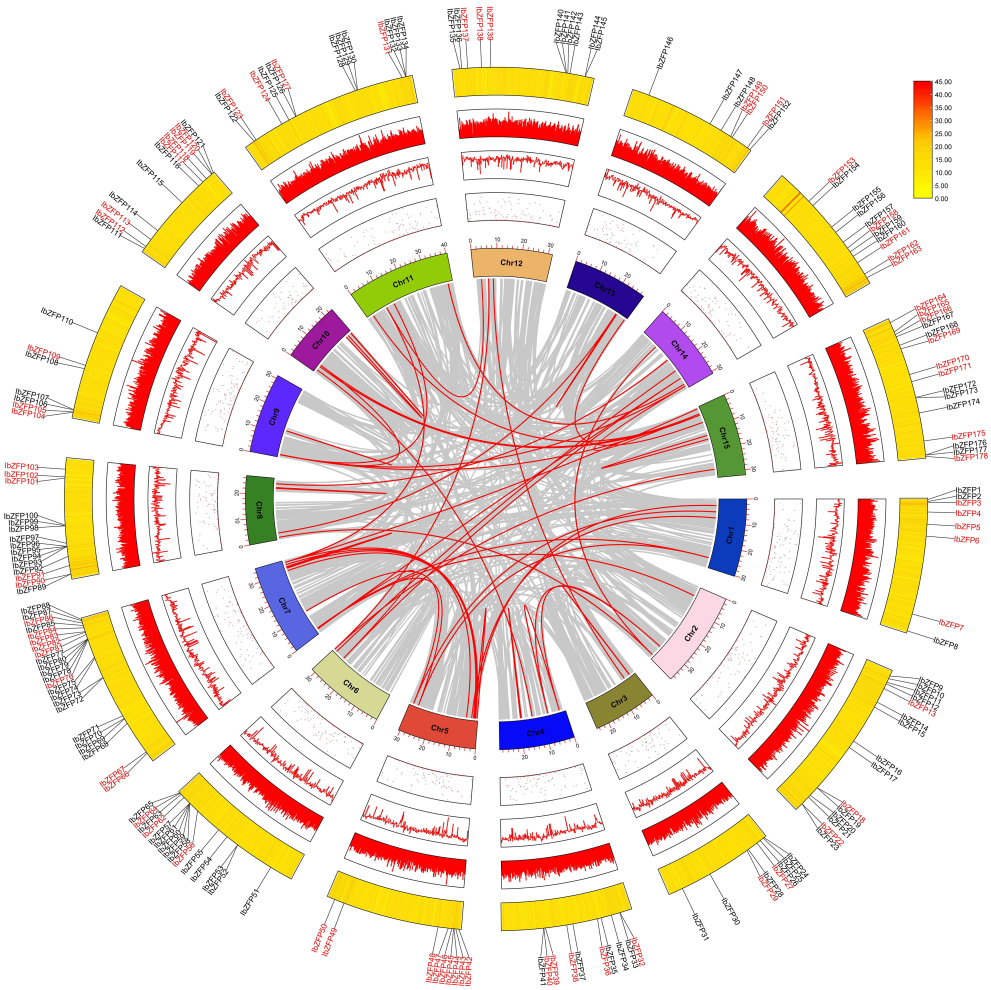

FIGURE 3
Schematic diagram of the homology relationship of the *IbZFP* genes. Grey represents all collinear fragments in the *Ipomoea batatas* genome, while red represents duplicate *IbZFP* gene pairs. The innermost circle shows the number of chromosomes, while the outer circle points, lines and heat maps show the distribution of unknown bases, the distribution of GC-content and the density of chromosomes, respectively.

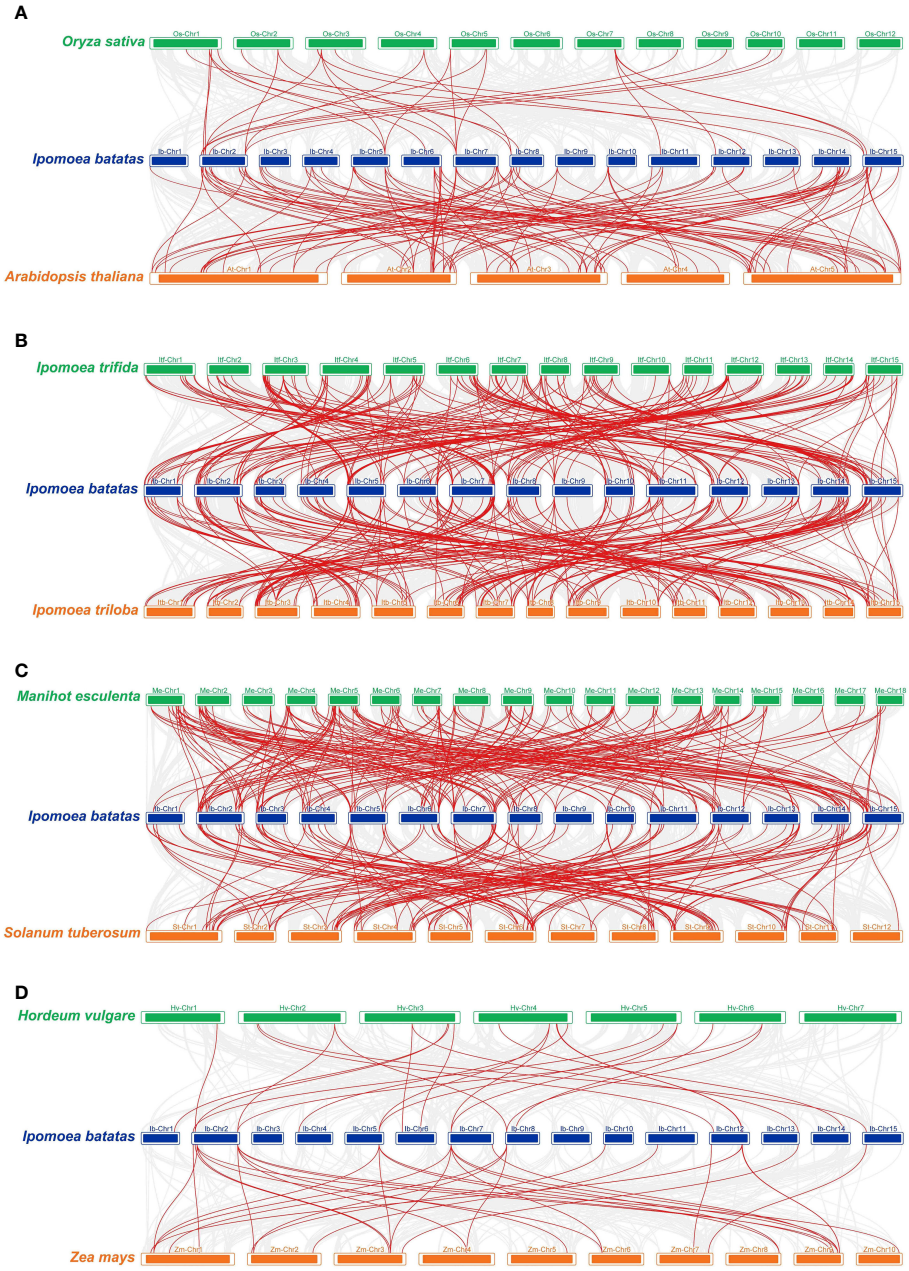

FIGURE 4
Synteny analyses of *IbZFP* genes between sweetpotato and eight representative plant species. **(A)** *Arabidopsis thaliana* and *Oryza sativa*, **(B)** *Ipomoea trifida* and *Ipomoea triloba*, **(C)** *Solanum tuberosum* and *Manihot esculenta*, **(D)** *Zea mays* and *Hordeum vulgare*. Blue represents the chromosomes of sweetpotato, while green and orange represent the chromosomes of the other two species compared. The red line connecting two different chromosomes highlights the *IbZFP* gene pairs in sweetpotato and other plant genomes.

mays (16). It is worth noting that *IbZFP* genes have the strongest collinearity with *Ipomoea trifida* and *Ipomoea triloba*. It may be that *Ipomoea trifida* and *Ipomoea triloba* are closely related wild species of sweetpotato, and *IbZFP* has much higher collinearity with edible rhizome plants such as *Manihot esculenta* and *Solanum tuberosum* than the model plant *Arabidopsis thaliana*, Poaceae plants *Oryza sativa*, *Hordeum vulgare*, and *Zea mays*, which may indicate that the *IbZFP* gene family is relatively conservative in the evolution of tuber or root tuber crops and may play a role in the expansion process of tubers or root tubers.

3.3 Gene structure and cis-acting elements analysis of *IbZFP* genes

In order to understand the structural diversity of these IbZFPs, we generated a phylogenetic tree using all IbZFPs (Figure 5A) and compared their exon/intron composition and conservative domain of IbZFPs (Figure 5C). The results showed that 65 of the 178 IbZFPs did not contain intron, accounting for 36.5% of the total number of IbZFPs. On the contrary, there are 11 IbZFPs with more than 10 intron, of which there are 28 intron in IbZFP8. The number of

FIGURE 5
Gene structure, motif composition and promoter cis-elements analysis of *IbZFP* genes. **(A)** The phylogenetic tree of IbZFPs was constructed using the ML method. **(B)** The distribution of ten largely conserved motifs found in IbZFPs is shown in the graph below **(C)** The exon/intron structures of IbZFPs, were predicted by TBtools. **(D)** Predicting cis-elements in the *IbZFP* genes promoter through the PlantCARE website.

intron in the remaining 102 IbZFPs ranges from 1 to 10. The exon/intron structure of the sequence reflects the structural diversity and complexity of IbZFPs. In addition, in the study of the conserved domains of the IbZFPs sequence, 10 conserved motifs were obtained (Figure 5B), among which motifs 1, 2, and 3 conform to the sequence characteristics of the C2H2 zinc finger (Supplementary Figure S1). Except for IbZFP9, 144, 145, and 155, which only have motif 2, motif 1 exists in all IbZFPs. We found the plant specific Q-type C2H2-ZFPs symbol "QALGGH" in motif 1, indicating that motif 1 should be a conserved and important motif in the *IbZFP* gene family of sweetpotato (Cui et al., 2022).

To further understand the potential regulatory mechanisms of the *IbZFP* genes in response to stress and various hormones. The 2000 bp promoter region upstream of the *IbZFP* genes was analyzed using PlantCARE online website, and nine cis-regulatory elements related to stress or hormone were identified (Figure 5D; Supplementary Table S3). Among them, 137 promoters of the *IbZFP* genes (77%) had elements corresponding to stress, such as low-temperature responsive elements, drought responsive elements, wound responsive elements, and defense and stress responsive elements. 174 promoters of the *IbZFP* genes (97.7%) had hormone responsive elements (auxin, gibberellin, abscisic acid,

MeJA, and salicylic acid responsive elements). More cis-elements were found in the promoters of *IbZFP80* (21), *IbZFP10* (19), and *IbZFP157* (19), while no cis-elements related to stress and hormone response were found in the promoter of *IbZFP2*. The analysis of the promoter of *IbZFP* genes showed that these cis-elements may have a potential role in affecting the development and responding to abiotic stress of sweetpotato.

3.4 Expression patterns analysis of *IbZFP* genes during SR development and salt stress

In order to study the expression patterns of *IbZFP* genes during SR expansion of sweetpotato, we used the transcriptome data of two different sweetpotato varieties at the early stage of SR expansion to analyze their expression levels (Du et al., 2023).

We identified 44 *IbZFP* genes from the SR transcriptome data 32 days, 46 days, and 67 days after planting (DAP) of two sweetpotato varieties ('Jishu25' and 'Jishu29'), and displayed the expression levels of these genes with a heatmap according to FPKM (Fragments Per Kilobase of exon model per Million mapped fragments) values (Figure 6A). The research results showed that some *IbZFP* genes, such as *IbZFP37*, *49*, *74*, *135*,*151*, and *169*, gradually increase in expression during SR development in two different varieties, while some genes (*IbZFP15* and *IbZFP160*) gradually decrease in expression levels during SR development in different varieties. In addition, we noticed that *IbZFP8* and *IbZFP128* exhibited significantly higher transcriptional accumulation than other *IbZFP* genes during SR development in

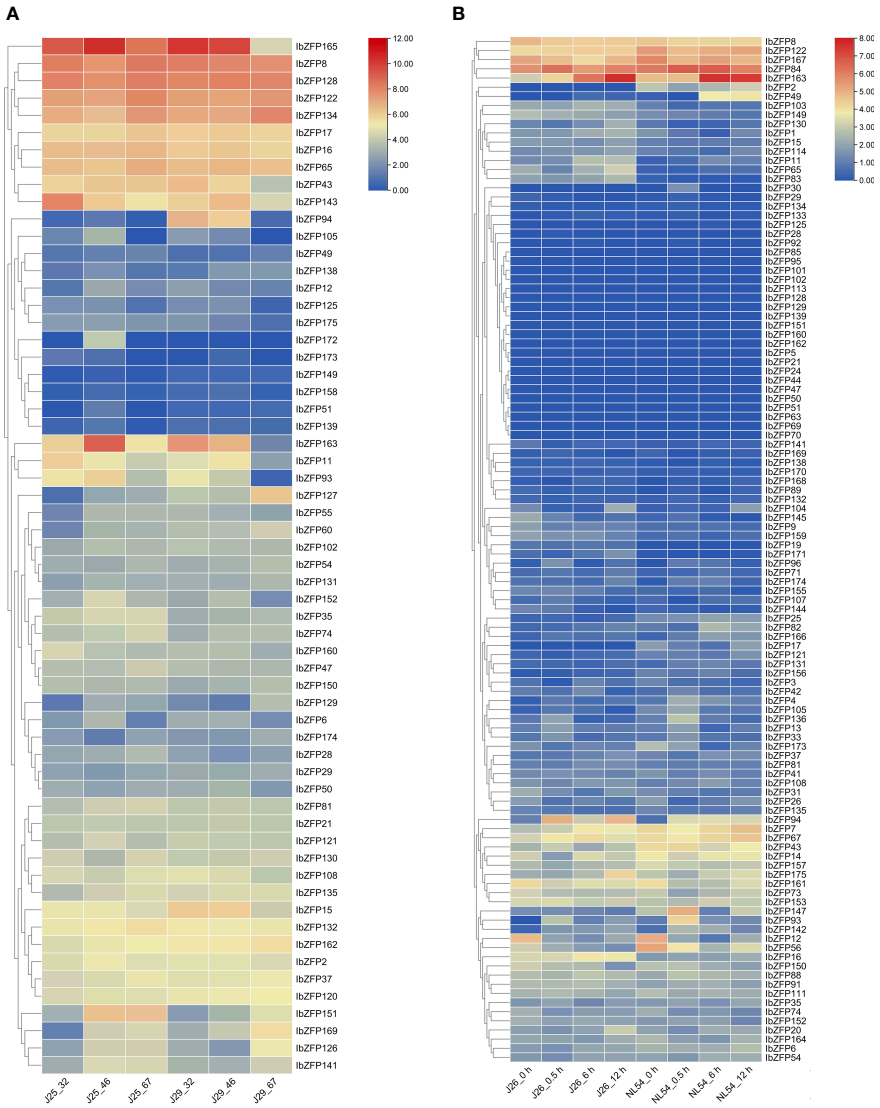

FIGURE 6
(A) Expression profiles of *IbZFP* genes during the development of sweetpotato storage roots. The horizontal axis represents the samples of sweetpotato varieties 'Jishu25' and 'Jishu29' at 32, 46, and 67 DAP, respectively **(B)** Expression profiles of *IbZFP* genes in sweetpotato under salt stress. The abscissa represents the samples of sweetpotato varieties 'Jishu26' and 'NL54' under salt treatment at 0, 0.5, 6, and 12 hours. All ratios undergo a $\log_2$ transformation, with red blocks indicating high relative expression levels and blue blocks indicating low relative expression levels.

different varieties (Supplementary Table S4). These results indicate that the *IbZFP* genes exhibit different expression patterns during SR development in sweetpotato, and some *IbZFP* genes may play an important regulatory role in the early expansion process of sweetpotato SR.

Similarly, in order to study the possible function of *IbZFP* genes in sweetpotato responses to stress, the transcriptome data of salt tolerant and salt sensitive sweetpotato varieties ('Jishu26' and 'NL54') under salt stress were used to analyze the expression pattern (Qin et al., 2020) of *IbZFP* genes under salt stress.

We identified 113 *IbZFP* genes in the sample transcriptome data of salt tolerant and salt sensitive varieties 0 h, 0.5 h, 6 h and 12 h after salt treatment, and mapped the expression calorimetry according to the FPKM value (Figure 6B). The research results showed that among two different salt stress resistant sweetpotato varieties, 21 *IbZFP* genes (18.6%) were not detected for expression in any treatment (FPKM value equals 0) (Supplementary Table S4), 8 *IbZFP* genes (such as *IbZFP9*, *41*, *63*, and *142*) were significantly upregulated after salt stress, and 14 *IbZFP* genes (such as *IbZFP12*, *56*, and *161*) were significantly downregulated after salt stress. It is worth noting that we found that 23 *IbZFP* genes (such as *IbZFP11*, *16*, and *65*) were expressed at higher levels in the salt tolerant variety 'Jishu26' compared to the salt sensitive variety 'NL54', while 19 *IbZFP* genes (*IbZFP2*, *14*, *43*, etc.) were expressed at higher levels in salt sensitive varieties. It is speculated that these genes may be related to the regulation of salt tolerance in sweetpotato.

3.5 Expression analysis of *IbZFP* genes in different tissues, hormones, and stress conditions and subcellular localization

Based on the results of the previous analysis, we screened 6 *IbZFP* genes (*IbZFP8*, *43*, *105*, *151*, *165*, and *167*) and examined their expression patterns in various tissues under abiotic stress (PEG6000-induced drought stress and NaCl-induced salt stress) and hormone-induced stress (ABA and GA_3) using qRT-PCR (Figure 7). This allowed us to better understand the role of the *IbZFP* gene in the development of the sweetpotato SR and stress tolerance.

The research results show that the *IbZFP* genes exhibits different expression patterns in different tissues of sweetpotato, with *IbZFP8*, *43*, *165*, and *167* having the highest expression levels in leaves, while *IbZFP105* and *IbZFP151* have the highest expression levels in FR and SR. This result suggests that the *IbZFP* genes may play a role in the development of sweetpotato. And under NaCl induced salt stress, except for the downregulation of *IbZFP151* expression with NaCl treatment time, the expression levels of *IbZFP43*, *105*, and *165* showed significant upregulation with stress time. Under drought stress, the expression of *IbZFP* genes showed a trend of upregulation and then downregulation, except for *IbZFP43*. Under ABA induction, the *IbZFP* genes showed a similar trend of first increasing and then decreasing. Different from ABA induction, the expression of the *IbZFP* genes showed a completely different trend under GA_3 induction. The expression of *IbZFP43* and *151* decreased significantly under GA_3 induction, while the expression of *IbZFP165* decreased first and then increased with GA_3 treatment time.

We previously predicted the subcellular localization information of all IbZFPs through the website (Supplementary Table S1), and it is important to determine whether transcription factors are located in the cell nucleus and study their regulatory function. Therefore, we recombined 6 IbZFPs (IbZFP8, 43, 105, 151, 165, and 167) onto GFP vectors to verify their subcellular localization results (Figure 8). The results showed that all six IbZFPs were located in the nucleus.

3.6 Overexpression of *IbZFP105* in *Arabidopsis thaliana*

To verify the function of the *IbZFP* genes in stress resistance, we cloned the *IbZFP105* gene in 'Jishu26' and constructed an overexpression vector pCAMBIA1300-*IbZFP105*, which was transferred into *Arabidopsis thaliana* (Col-0) through the *Agrobacterium* mediated inflorescence soaking method. Verify the positive lines by PCR amplification of the target gene and RT-PCR detection of gene expression levels (Supplementary Figure S1). We selected L2 and L7 with the highest relative expression levels from the 8 positive lines obtained for subsequent functional validation. To verify whether *IbZFP105* responds to salt stress, we planted wild-type (WT) and transgenic *Arabidopsis thaliana* in a 1/2 MS medium containing 100 mmol/L NaCl (Figures 9A, B) and 0.25 μmol/L of ABA (Figures 9C, D), measure its germination rate and root length after 15 DAP. The results showed that at 15 DAP, the OE lines of *IbZFP105* showed significantly better germination rate and growth status than the WT under salt stress and ABA treatment. This indicates that the heterologous expression of *IbZFP105* enhances salt tolerance and ABA tolerance in *Arabidopsis thaliana*, suggesting that *IbZFP105* enhances plant salt tolerance by responding to the ABA pathway.

4 Discussion

C2H2-ZFPs are one of the most important transcription factor families in higher plants, playing a crucial role in plant development and stress resistance (Han et al., 2021; Liu et al., 2022a; Liu et al., 2022b). Previous reports have shown that they can play important roles in *Arabidopsis thaliana*, wheat, grapevine, sorghum, and cotton (Englbrecht et al., 2004; Salih et al., 2019; Arrey-Salas et al., 2021; Cui et al., 2022; Wu et al., 2022). However, there are few reports on the C2H2-ZFPs in sweetpotato. In this study, we conducted a genome-wide study on the C2H2-ZFP family using genomic data from hexaploid sweetpotato Taizhong6. A total of 178 IbZFPs were screened and identified, encoding proteins with at least one C2H2-ZFP conserved motif.

By constructing phylogenetic evolution trees of *Arabidopsis thaliana* and sweetpotato ZFPs, we divided IbZFPs into six clades and found multiple reported functional *Arabidopsis thaliana* ZAT proteins, such as ZAT1, 5, and 10 (Xie et al., 2012; Liu et al., 2014; Yin et al., 2017), in clade III, which mostly regulate stress resistance

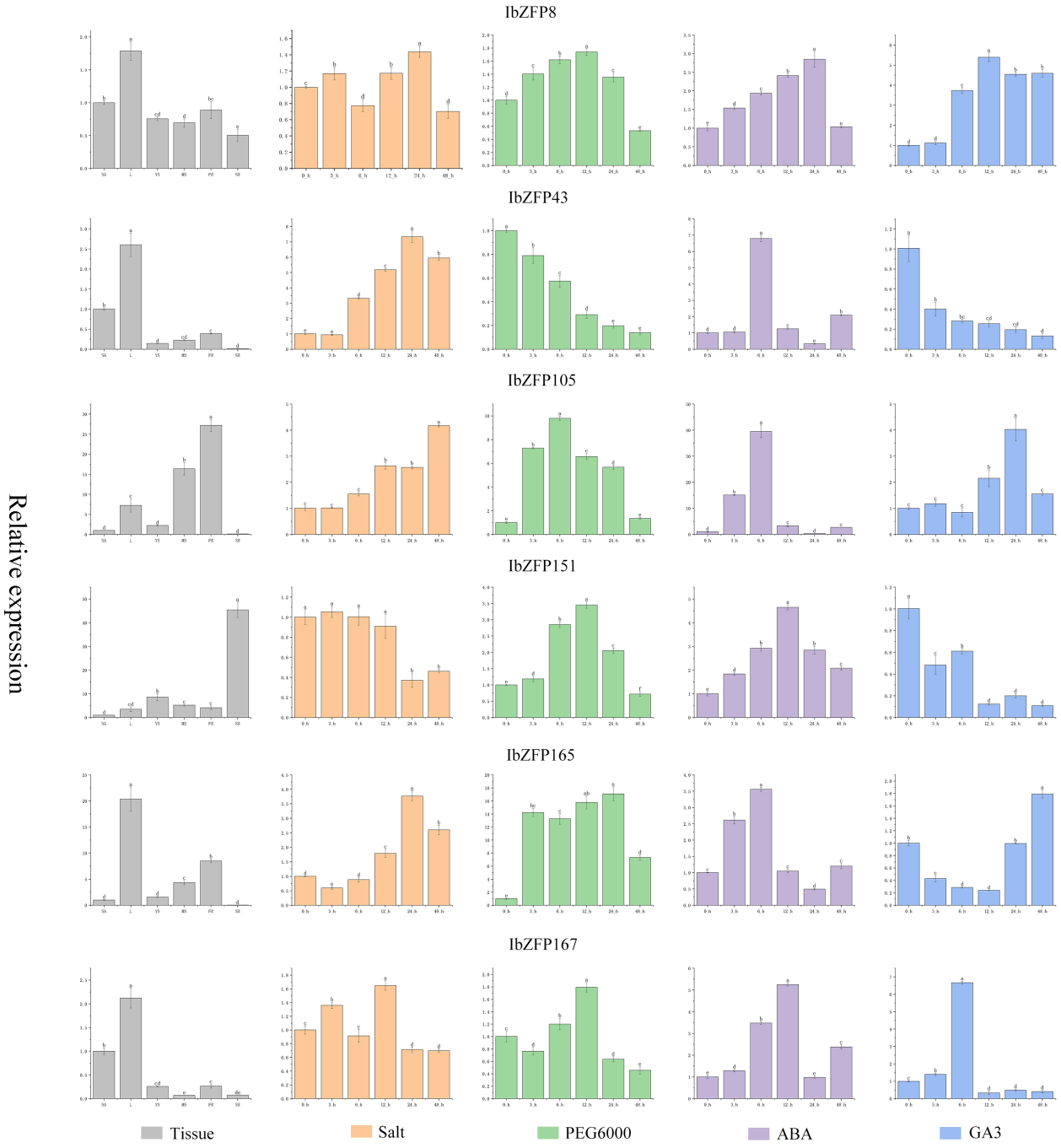

FIGURE 7
Expression profile of *IbZFP* genes in different tissues, under stress and hormone effects. The gray part in the figure represents the expression profile of *IbZFP* genes in different tissues of sweetpotato (where SA represents stem apex, L represents leaves, YS and MS represent young and mature stem, FR and SR represent fibrous root and storage root, respectively). And the orange part of the figure shows the expression profile of *IbZFP* genes under NaCl induced salt stress, the green part represents the expression profile under PEG6000 induced drought stress, the purple part represents the expression profile under ABA hormone induction, and the blue part represents the expression profile under GA_3 induction.

in *Arabidopsis thaliana*. We found that IbZFP43, 105, and 165 are closely related to these *Arabidopsis thaliana* ZAT proteins, indicating that these genes may also be involved in the response to stress in sweetpotato.

Then we analyzed the chromosomal localization and gene duplication events of IbZFPs. Gene duplication events, including tandem and segmental duplication, play an important role in the evolution and expansion of gene families (Vision et al., 2000). We investigated the mechanism of member amplification of *IbZFP* genes in sweetpotato and identified 15 tandem repeat events composed of 24 *IbZFP* genes, with some genes participating in multiple tandem repeats. We also identified 46 fragment replicates involving 71 *IbZFP* genes, indicating that segmental gene replicates play important roles in the evolution and diversification of the

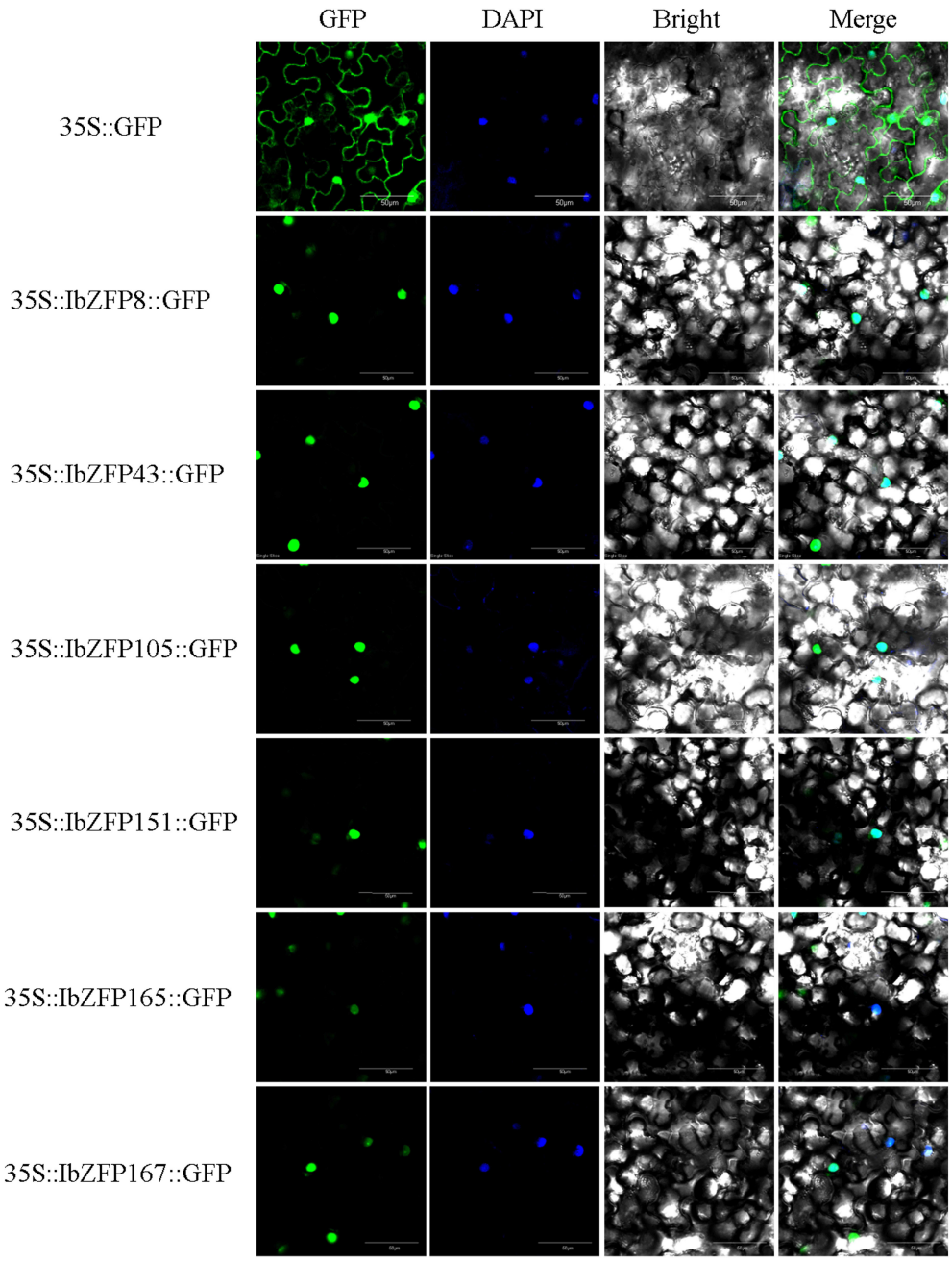

FIGURE 8
Subcellular localization of IbZFPs. Inject tobacco (*Nictiana benthamiana*) leaves after transforming *Agrobacterium tumefaciens* using recombinant plasmid (IbZFP-GFP) and empty control (GFP). The figure shows confocal images of GFP fluorescence, nuclear localization (DAPI), bright field, and composite field.

C2H2 zinc finger gene family in the sweetpotato genome. This result is similar to the analysis of the C2H2 zinc finger gene family in other species, such as poplar and sorghum (Liu et al., 2015; Cui et al., 2022).

By analyzing the collinearity of sweetpotato and other species in the C2H2 zinc finger gene family, we have discovered an interesting phenomenon where the *IbZFP* genes have 124 putative orthologous homologues in *Ipomoea trifida*, which is much higher than other plants, possibly due to the closer phylogenetic relationships between sweetpotato and *Ipomoea trifida*. In addition, the *IbZFP* genes have 102 and 98 putative orthologous compounds in cassava and potato, much higher than the model plant *Arabidopsis thaliana*. We believe that this means that the C2H2 zinc finger gene family is relatively conserved in the evolution of tuber or root crops and may play an important regulatory role in the expansion process of tubers or roots.

In addition, the gene structure and conserved motifs of IbZFPs were analyzed, with motifs 1, 2, and 3 being the characteristics of C2H2 zinc fingers. Among them, motif 1 has a conserved QLAGGH sequence, which is the symbol of plant specific Q type C2H2-ZFP. Q

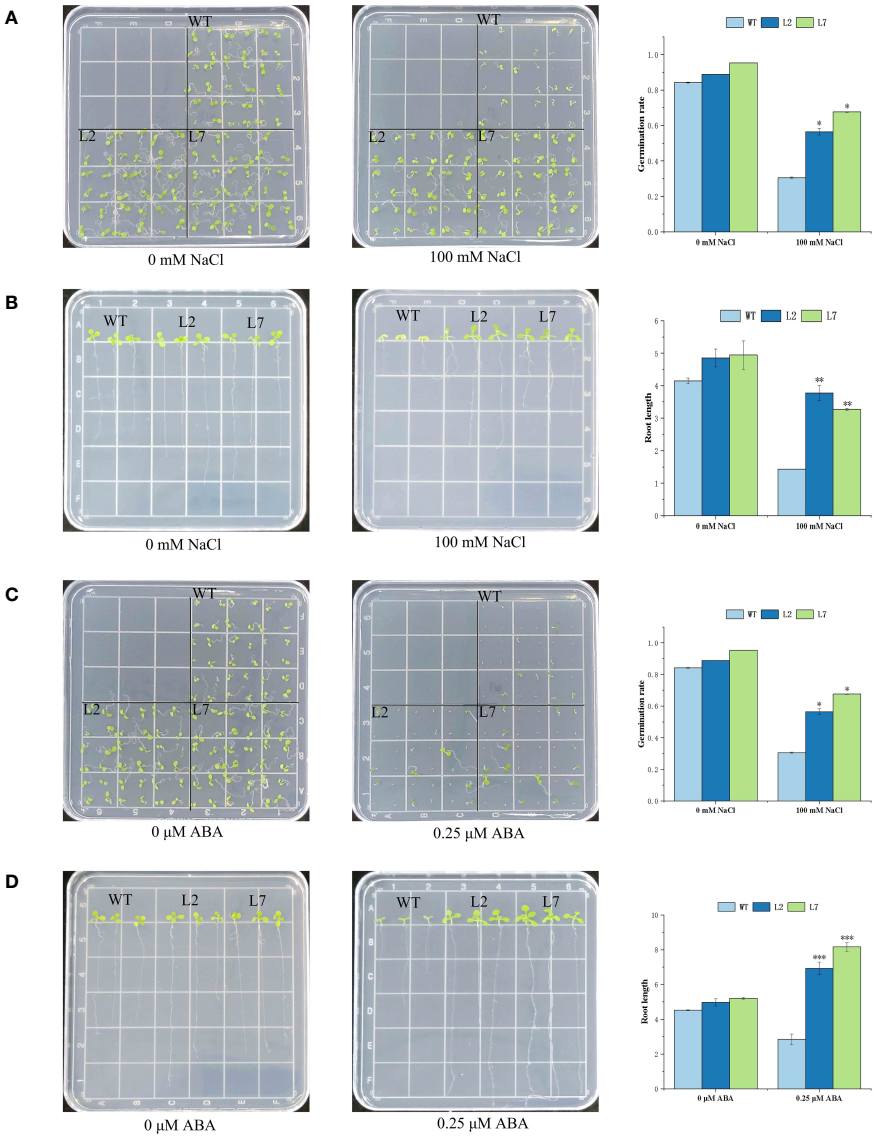

FIGURE 9
Functional Analysis of Overexpressed *IbZFP105* Gene in *Arabidopsis thaliana*. **(A, B)** Salt tolerance identification of germination and growth status of OE-L2, OE-L7, and WT in 1/2 MS medium containing 100 mmol/L NaCl. **(C, D)** OE-L2, OE-L7, and WT were subjected to ABA stress identification in 1/2 MS medium containing 0.25 μmol/L of ABA. The data consists of three independent biological replicates (* represents p<0.05, * * represents P<0.01, and * * * represents P<0.001).

type C2H2-ZFP is unique to plants and participates in the growth, development, organogenesis, and response to stress and defense in various plants (Cui et al., 2022), 174 IbZFPs (97.8%) have motif 1, indicating that motif 1 plays a crucial regulatory role in IbZFPs. In addition to C2H2 type motifs, IbZFPs also contain many other motifs, indicating that IbZFPs play a wide range of roles in sweetpotato.

We analyzed the expression profile of the *IbZFP* genes in the early development and salt stress transcriptome of sweetpotato SRs, identified several *IbZFP* genes that may be related to early development and salt stress tolerance of sweetpotato SRs. Subsequently, we cloned these genes in sweetpotato and analyzed their tissue specificity, expression patterns under drought and salt stress, and expression patterns under plant hormone ABA and GA_3 treatment, then their subcellular localization was verified in tobacco leaf cells. We found that the *IbZFP* genes exhibits different expression patterns in different parts of sweetpotato. Some genes are highly expressed in the leaves, while others are highly expressed in FR or SR. Multiple species such as cotton and wheat have also reported this phenomenon, indicating that the C2H2-ZFP may play a crucial role in the formation and development of various plant tissues.

Moreover, through RT-PCR analysis of the expression patterns of several *IbZFP* genes under abiotic stress and hormone treatment, we found that several *IbZFP* genes exhibited different expression patterns induced by different stresses and hormones. We selected the *IbZFP105* gene with the most significant difference in expression levels under salt stress and ABA treatment, constructed its

overexpression vector, and transformed it into *Arabidopsis thaliana*, through experiments on the germination rate and growth status of *Arabidopsis thaliana* seeds under salt and ABA stress, we found that the OE lines exhibited stronger salt tolerance and ABA stress resistance. Therefore, we speculate that IbZFP105 can improve plant salt tolerance by responding to ABA signals.

Data availability statement

The original contributions presented in the study are included in the article/Supplementary Material, further inquiries can be directed to the corresponding authors.

Author contributions

TD: Conceptualization, Data curation, Validation, Visualization, Writing – original draft. YZ: Validation, Writing – review & editing. ZQ: Project administration, Software, Writing – review & editing. AL: Formal Analysis, Funding acquisition, Writing – review & editing. QW: Formal Analysis, Funding acquisition, Writing – review & editing. ZL: Investigation, Writing – review & editing. FH: Conceptualization, Resources, Supervision, Writing – original draft, Writing – review & editing. LZ: Methodology, Resources, Writing – review & editing.

Funding

The author(s) declare financial support was received for the research, authorship, and/or publication of this article. This study was supported by the Key R&D Program of Shandong Province, China (2022TZXD0028), China Agriculture Research System of Sweet potato (CARS-10-GW08), Postgraduate Research & Practice Innovation Program of Jiangsu Province (KYCX21_2602), the Agricultural Seed Project of Shandong Province (2020LZGC004),3the Natural Science Foundation of Shandong Province (ZR2021MC092).

Acknowledgments

Thank you to the reviewers for their feedback and assistance on this manuscript.

Conflict of interest

The authors declare that the research was conducted in the absence of any commercial or financial relationships that could be construed as a potential conflict of interest.

Publisher's note

Supplementary material

The Supplementary Material for this article can be found online at: https://www.frontiersin.org/articles/10.3389/fpls.2023.1301848/full#supplementary-material

References

Arrey-Salas, O., Caris-Maldonado, J. C., Hernández-Rojas, B., and Gonzalez, E. (2021). Comprehensive genome-wide exploration of c2h2 zinc finger family in grapevine (Vitis vinifera L.): Insights into the roles in the pollen development regulation. *Genes* 12, 302. doi: 10.3390/genes12020302

Artimo, P., Jonnalagedda, M., Arnold, K., Baratin, D., Csardi, G., De Castro, E., et al. (2012). ExPASy: SIB bioinformatics resource portal. *Nucleic Acids Res.* 40, W597–W603. doi: 10.1093/nar/gks400

Blom, N., Gammeltoft, S., and Brunak, S. (1999). Sequence and structure-based prediction of eukaryotic protein phosphorylation sites. *J. Mol. Biol.* 294, 1351–1362. doi: 10.1006/jmbi.1999.3310

Cannon, S. B., Mitra, A., Baumgarten, A., Young, N. D., and May, G. (2004). The roles of segmental and tandem gene duplication in the evolution of large gene families in Arabidopsis thaliana. *BMC Plant Biol.* 4, 1–21. doi: 10.1186/1471-2229-4-10

Chen, C., Chen, H., Zhang, Y., Thomas, H. R., Frank, M. H., He, Y., et al. (2020). TBtools: an integrative toolkit developed for interactive analyses of big biological data. *Mol. Plant* 13, 1194–1202. doi: 10.1016/j.molp.2020.06.009

Chen, Y.-F., Li, L.-Q., Xu, Q., Kong, Y.-H., Wang, H., and Wu, W.-H. (2009). The WRKY6 transcription factor modulates PHOSPHATE1 expression in response to low Pi stress in Arabidopsis. *Plant Cell* 21, 3554–3566. doi: 10.1105/tpc.108.064980

Ciftci-Yilmaz, S., and Mittler, R. (2008). The zinc finger network of plants. *Cell. Mol. Life Sci.* 65, 1150–1160. doi: 10.1007/s00018-007-7473-4

Crawford, B. C., Ditta, G., and Yanofsky, M. F. (2007). The NTT gene is required for transmitting-tract development in carpels of Arabidopsis thaliana. *Curr. Biol.* 17, 1101–1108. doi: 10.1016/j.cub.2007.05.079

Crawford, B. C., Sewell, J., Golembeski, G., Roshan, C., Long, J. A., and Yanofsky, M. F. (2015). Genetic control of distal stem cell fate within root and embryonic meristems. *Science* 347, 655–659. doi: 10.1126/science.aaa0196

Cui, H., Chen, J., Liu, M., Zhang, H., Zhang, S., Liu, D., et al. (2022). Genome-wide analysis of C2H2 zinc finger gene family and its response to cold and drought stress in sorghum [Sorghum bicolor (L.) moench]. *Int. J. Mol. Sci.* 23, 5571. doi: 10.3390/ijms23105571

Diao, P., Chen, C., Zhang, Y., Meng, Q., Lv, W., and Ma, N. (2020). The role of NAC transcription factor in plant cold response. *Plant Signaling Behav.* 15, 1785668. doi: 10.1080/15592324.2020.1785668

Du, T., Qin, Z., Zhou, Y., Zhang, L., Wang, Q., Li, Z., et al. (2023). Comparative transcriptome analysis reveals the effect of lignin on storage roots formation in two sweetpotato (Ipomoea batatas (L.) lam.) cultivars. *Genes* 14, 1263. doi: 10.3390/genes14061263

Dubos, C., Stracke, R., Grotewold, E., Weisshaar, B., Martin, C., and Lepiniec, L. (2010). MYB transcription factors in Arabidopsis. *Trends Plant Sci.* 15, 573–581. doi: 10.1016/j.tplants.2010.06.005

Englbrecht, C. C., Schoof, H., and Böhm, S. (2004). Conservation, diversification and expansion of C2H2 zinc finger proteins in the Arabidopsis thaliana genome. *BMC Genomics* 5, 1–17. doi: 10.1186/1471-2164-5-39

Gendall, A. R., Levy, Y. Y., Wilson, A., and Dean, C. (2001). The VERNALIZATION 2 gene mediates the epigenetic regulation of vernalization in Arabidopsis. *Cell* 107, 525–535. doi: 10.1016/S0092-8674(01)00573-6

Guo, J., Sun, B., He, H., Zhang, Y., Tian, H., and Wang, B. (2021). Current understanding of bHLH transcription factors in plant abiotic stress tolerance. *Int. J. Mol. Sci.* 22, 4921. doi: 10.3390/ijms22094921

Han, G., Li, Y., Qiao, Z., Wang, C., Zhao, Y., Guo, J., et al. (2021). Advances in the regulation of epidermal cell development by C2H2 zinc finger proteins in plants. *Front. Plant Sci.* 12, 754512. doi: 10.3389/fpls.2021.754512

Han, G., Lu, C., Guo, J., Qiao, Z., Sui, N., Qiu, N., et al. (2020). C2H2 zinc finger proteins: master regulators of abiotic stress responses in plants. *Front. Plant Sci.* 11, 115. doi: 10.3389/fpls.2020.00115

Han, G., Wang, M., Yuan, F., Sui, N., Song, J., and Wang, B. (2014). The CCCH zinc finger protein gene AtZFP1 improves salt resistance in Arabidopsis thaliana. *Plant Mol. Biol.* 86, 237–253. doi: 10.1007/s11103-014-0226-5

Han, H., Wang, C., Yang, X., Wang, L., Ye, J., Xu, F., et al. (2023). Role of bZIP transcription factors in the regulation of plant secondary metabolism. *Planta* 258, 13. doi: 10.1007/s00425-023-04174-4

He, P., Zhang, J., Lv, Z., Cui, P., Xu, X., George, M. S., et al. (2023). Genome-wide identification and expression analysis of the polygalacturonase gene family in sweetpotato. *BMC Plant Biol.* 23, 1–13. doi: 10.1186/s12870-023-04272-1

Horton, P., Park, K.-J., Obayashi, T., Fujita, N., Harada, H., Adams-Collier, C., et al. (2007). WoLF PSORT: protein localization predictor. *Nucleic Acids Res.* 35, W585–W587. doi: 10.1093/nar/gkm259

Hou, F., Du, T., Qin, Z., Xu, T., Li, A., Dong, S., et al. (2021a). Genome-wide in silico identification and expression analysis of beta-galactosidase family members in sweetpotato [Ipomoea batatas (L.) Lam]. *BMC Genomics* 22, 1–13. doi: 10.1186/s12864-021-07436-1

Hou, W., Ren, L., Zhang, Y., Sun, H., Shi, T., Gu, Y., et al. (2021b). Characterization of BBX family genes and their expression profiles under various stresses in the sweet potato wild ancestor Ipomoea trifida. *Sci. Hortic.* 288, 110374. doi: 10.1016/j.scienta.2021.110374

Huang, L., Jiang, Q., Wu, J., An, L., Zhou, Z., Wong, C., et al. (2020). Zinc finger protein 5 (ZFP5) associates with ethylene signaling to regulate the phosphate and potassium deficiency-induced root hair development in Arabidopsis. *Plant Mol. Biol.* 102, 143–158. doi: 10.1007/s11103-019-00937-4

Jiang, Y., Liu, L., Pan, Z., Zhao, M., Zhu, L., Han, Y., et al. (2022). Genome-wide analysis of the C2H2 zinc finger protein gene family and its response to salt stress in ginseng, Panax ginseng Meyer. *Sci. Rep.* 12, 10165. doi: 10.1038/s41598-022-14357-w

Jiao, Z., Wang, L., Du, H., Wang, Y., Wang, W., Liu, J., et al. (2020). Genome-wide study of C2H2 zinc finger gene family in Medicago truncatula. *BMC Plant Biol.* 20, 1–17. doi: 10.1186/s12870-020-02619-6

Joo, H., Baek, W., Lim, C. W., and Lee, S. C. (2021). Post-translational modifications of bZIP transcription factors in abscisic acid signaling and drought responses. *Curr. Genomics* 22, 4–15. doi: 10.2174/18755488MTEx6OTQj0

Joseph, M. P., Papdi, C., Kozma-Bognár, L., Nagy, I., López-Carbonell, M., Rigó, G., et al. (2014). The Arabidopsis ZINC FINGER PROTEIN3 interferes with abscisic acid and light signaling in seed germination and plant development. *Plant Physiol.* 165, 1203–1220. doi: 10.1104/pp.113.234294

Kiełbowicz-Matuk, A. (2012). Involvement of plant C2H2-type zinc finger transcription factors in stress responses. *Plant Sci.* 185, 78–85. doi: 10.1016/j.plantsci.2011.11.015

Lescot, M., Déhais, P., Thijs, G., Marchal, K., Moreau, Y., Van De Peer, Y., et al. (2002). PlantCARE, a database of plant cis-acting regulatory elements and a portal to tools for in silico analysis of promoter sequences. *Nucleic Acids Res.* 30, 325–327. doi: 10.1093/nar/30.1.325

Letunic, I., Khedkar, S., and Bork, P. (2021). SMART: recent updates, new developments and status in 2020. *Nucleic Acids Res.* 49, D458–D460. doi: 10.1093/nar/gkaa937

Li, X., Xue, C., Li, J., Qiao, X., Li, L., Yu, L. A., et al. (2016). Genome-wide identification, evolution and functional divergence of MYB transcription factors in Chinese white pear (Pyrus bretschneideri). *Plant Cell Physiol.* 57, 824–847. doi: 10.1093/pcp/pcw029

Liu, X.-M., An, J., Han, H. J., Kim, S. H., Lim, C. O., Yun, D.-J., et al. (2014). ZAT11, a zinc finger transcription factor, is a negative regulator of nickel ion tolerance in Arabidopsis. *Plant Cell Rep.* 33, 2015–2021. doi: 10.1007/s00299-014-1675-7

Liu, Z., Coulter, J. A., Li, Y., Zhang, X., Meng, J., Zhang, J., et al. (2020b). Genome-wide identification and analysis of the Q-type C2H2 gene family in potato (Solanum tuberosum L.). *Int. J. Biol. Macromol.* 153, 327–340. doi: 10.1016/j.ijbiomac.2020.03.022

Liu, Y., Khan, A. R., Azhar, W., Wong, C. E., Li, Y., Huang, Y., et al. (2022a). Cys2/His2-type zinc finger proteins regulate plant growth and development. *Crit. Rev. Plant Sci.* 41, 351–363. doi: 10.1080/07352689.2022.2130370

Liu, Y., Khan, A. R., and Gan, Y. (2022b). C2H2 zinc finger proteins response to abiotic stress in plants. *Int. J. Mol. Sci.* 23, 2730. doi: 10.3390/ijms23052730

Liu, Y.-T., Shi, Q.-H., Cao, H.-J., Ma, Q.-B., Nian, H., and Zhang, X.-X. (2020a). Heterologous expression of a Glycine soja C2H2 zinc finger gene improves aluminum tolerance in Arabidopsis. *Int. J. Mol. Sci.* 21, 2754. doi: 10.3390/ijms21082754

Liu, Q., Wang, Z., Xu, X., Zhang, H., and Li, C. (2015). Genome-wide analysis of C2H2 zinc-finger family transcription factors and their responses to abiotic stresses in poplar (Populus trichocarpa). *PloS One* 10, e0134753. doi: 10.1371/journal.pone.0134753

Liu, D., Yang, L., Luo, M., Wu, Q., Liu, S., and Liu, Y. (2017). Molecular cloning and characterization of PtrZPT2-1, a ZPT2 family gene encoding a Cys2/His2-type zinc finger protein from trifoliate orange (Poncirus trifoliata (L.) Raf.) that enhances plant tolerance to multiple abiotic stresses. *Plant Sci.* 263, 66–78. doi: 10.1016/j.plantsci.2017.07.012

Neela, S., and Fanta, S. W. (2019). Review on nutritional composition of orange-fleshed sweet potato and its role in management of vitamin A deficiency. *Food Sci. Nutr.* 7, 1920–1945. doi: 10.1002/fsn3.1063

Noh, B., Lee, S.-H., Kim, H.-J., Yi, G., Shin, E.-A., Lee, M., et al. (2004). Divergent roles of a pair of homologous jumonji/zinc-finger–class transcription factor proteins in the regulation of Arabidopsis flowering time. *Plant Cell* 16, 2601–2613. doi: 10.1105/tpc.104.025353

Paysan-Lafosse, T., Blum, M., Chuguransky, S., Grego, T., Pinto, B. L., Salazar, G. A., et al. (2023). InterPro in 2022. *Nucleic Acids Res.* 51, D418–D427. doi: 10.1093/nar/gkac993

Qian, Y., Zhang, T., Yu, Y., Gou, L., Yang, J., Xu, J., et al. (2021). Regulatory mechanisms of bHLH transcription factors in plant adaptive responses to various abiotic stresses. *Front. Plant Sci.* 12, 677611. doi: 10.3389/fpls.2021.677611

Qin, Z., Hou, F., Li, A., Dong, S., Wang, Q., and Zhang, L. (2020). Transcriptome-wide identification of WRKY transcription factor and their expression profiles under salt stress in sweetpotato (Ipomoea batatas L.). *Plant Biotechnol. Rep.* 14, 599–611. doi: 10.1007/s11816-020-00635-4

Raineri, J., Wang, S., Peleg, Z., Blumwald, E., and Chan, R. L. (2015). The rice transcription factor OsWRKY47 is a positive regulator of the response to water deficit stress. *Plant Mol. Biol.* 88, 401–413. doi: 10.1007/s11103-015-0329-7

Sagasser, M., Lu, G.-H., Hahlbrock, K., and Weisshaar, B. (2002). Arabidopsis thaliana TRANSPARENT TESTA 1 is involved in seed coat development and defines the WIP subfamily of plant zinc finger proteins. *Genes Dev.* 16, 138–149. doi: 10.1101/gad.212702

Salih, H., Odongo, M. R., Gong, W., He, S., and Du, X. (2019). Genome-wide analysis of cotton C2H2-zinc finger transcription factor family and their expression analysis during fiber development. *BMC Plant Biol.* 19, 1–17. doi: 10.1186/s12870-019-2003-8

Song, S.-K., Jang, H.-U., Kim, Y. H., Lee, B. H., and Lee, M. M. (2020). Overexpression of three related root-cap outermost-cell-specific C2H2-type zinc-finger protein genes suppresses the growth of Arabidopsis in an EAR-motif-dependent manner. *BMB. Rep.* 53, 160. doi: 10.5483/BMBRep.2020.53.3.286

Sun, S.-J., Guo, S.-Q., Yang, X., Bao, Y.-M., Tang, H.-J., Sun, H., et al. (2010). Functional analysis of a novel Cys2/His2-type zinc finger protein involved in salt tolerance in rice. *J. Exp. Bot.* 61, 2807–2818. doi: 10.1093/jxb/erq120

Takatsuji, H., Mori, M., Benfey, P., Ren, L., and Chua, N. (1992). Characterization of a zinc finger DNA-binding protein expressed specifically in Petunia petals and seedlings. *EMBO J.* 11, 241–249. doi: 10.1002/j.1460-2075.1992.tb05047.x

Tamura, K., Stecher, G., and Kumar, S. (2021). MEGA11: molecular evolutionary genetics analysis version 11. *Mol. Biol. Evol.* 38, 3022–3027. doi: 10.1093/molbev/msab120

Vision, T. J., Brown, D. G., and Tanksley, S. D. (2000). The origins of genomic duplications in Arabidopsis. *Science* 290, 2114–2117. doi: 10.1126/science.290.5499.2114

Wang, K., Ding, Y., Cai, C., Chen, Z., and Zhu, C. (2019). The role of C2H2 zinc finger proteins in plant responses to abiotic stresses. *Physiol. Plant.* 165, 690–700. doi: 10.1111/ppl.12728

Wu, Z., Shen, S., Wang, Y., Tao, W., Zhao, Z., Hu, X., et al. (2022). Genome-wide identification and expression analysis of the Zinc Finger Protein gene subfamilies under drought stress in Triticum aestivum. *Plants* 11, 2511. doi: 10.3390/plants11192511

Xie, J., Chen, Y., Cai, G., Cai, R., Hu, Z., and Wang, H. (2023). Tree Visualization By One Table (tvBOT): a web application for visualizing, modifying and annotating phylogenetic trees. *Nucleic Acids Res.* 51(W1), W587–W592. doi: 10.1093/nar/gkad359

Xie, Y., Mao, Y., Lai, D., Zhang, W., and Shen, W. (2012). H2 enhances Arabidopsis salt tolerance by manipulating ZAT10/12-mediated antioxidant defence and controlling sodium exclusion. *PloS One* 7, e49800. doi: 10.1371/journal.pone.0049800

Yin, M., Wang, Y., Zhang, L., Li, J., Quan, W., Yang, L., et al. (2017). The Arabidopsis Cys2/His2 zinc finger transcription factor ZAT18 is a positive regulator of plant tolerance to drought stress. *J. Exp. Bot.* 68, 2991–3005. doi: 10.1093/jxb/erx157

Yoshida, N., Yanai, Y., Chen, L., Kato, Y., Hiratsuka, J., Miwa, T., et al. (2001). EMBRYONIC FLOWER2, a novel polycomb group protein homolog, mediates shoot development and flowering in Arabidopsis. *Plant Cell* 13, 2471–2481. doi: 10.1105/tpc.010227

Yuan, X., Wang, H., Cai, J., Li, D., and Song, F. (2019). NAC transcription factors in plant immunity. *Phytopathol. Res.* 1, 1–13. doi: 10.1186/s42483-018-0008-0

Zhang, C., Dong, T., Yu, J., Hong, H., Liu, S., Guo, F., et al. (2023). Genome-wide survey and expression analysis of Dof transcription factor family in sweetpotato shed light on their promising functions in stress tolerance. *Front. Plant Sci.* 14, 1140727. doi: 10.3389/fpls.2023.1140727

Zhang, H., Liu, Y., Wen, F., Yao, D., Wang, L., Guo, J., et al. (2014). A novel rice C2H2-type zinc finger protein, ZFP36, is a key player involved in abscisic acid-induced antioxidant defence and oxidative stress tolerance in rice. *J. Exp. Bot.* 65, 5795–5809. doi: 10.1093/jxb/eru313

Zhang, A., Liu, Y., Yu, C., Huang, L., Wu, M., Wu, J., et al. (2020). Zinc finger protein 1 (ZFP1) is involved in trichome initiation in Arabidopsis thaliana. *Agriculture* 10, 645. doi: 10.3390/agriculture10120645

frontiers | Frontiers in Plant Science

TYPE Original Research
PUBLISHED 06 February 2024
DOI 10.3389/fpls.2024.1344928

OPEN ACCESS

EDITED BY
Mehanathan Muthamilarasan,
University of Hyderabad, India

REVIEWED BY
Xuechen Tian,
Kean University-Wenzhou, China
Masood Jan,
Henan University, China

*CORRESPONDENCE
Mohan B. Singh
mohan@unimelb.edu.au

RECEIVED 27 November 2023
ACCEPTED 17 January 2024
PUBLISHED 06 February 2024

CITATION
Babaei S, Bhalla PL and Singh MB (2024) Identifying long non-coding RNAs involved in heat stress response during wheat pollen development. *Front. Plant Sci.* 15:1344928. doi: 10.3389/fpls.2024.1344928

Identifying long non-coding RNAs involved in heat stress response during wheat pollen development

Saeid Babaei, Prem L. Bhalla and Mohan B. Singh*

Plant Molecular Biology and Biotechnology Laboratory, School of Agriculture, Food and Ecosystem Sciences, The University of Melbourne, Melbourne, VIC, Australia

Introduction: Wheat is a staple food crop for over one-third of the global population. However, the stability of wheat productivity is threatened by heat waves associated with climate change. Heat stress at the reproductive stage can result in pollen sterility and failure of grain development.

Methods: This study used transcriptome data analysis to explore the specific expression of long non-coding RNAs (lncRNAs) in response to heat stress during pollen development in four wheat cultivars.

Results and discussion: We identified 11,054 lncRNA-producing loci, of which 5,482 lncRNAs showed differential expression in response to heat stress. Heat-responsive lncRNAs could target protein-coding genes in *cis* and *trans* and in lncRNA-miRNA-mRNA regulatory networks. Gene ontology analysis predicted that target protein-coding genes of lncRNAs regulate various biological processes such as hormonal responses, protein modification and folding, response to stress, and biosynthetic and metabolic processes. We also noted some paired lncRNA/protein-coding gene modules and some lncRNA-miRNA-mRNA regulatory modules shared in two or more wheat cultivars. These modules were related to regulating plant responses to heat stress, such as heat-shock proteins and transcription factors, and protein domains, such as MADS-box, Myc-type, and Alpha crystallin/Hsp20 domain.

Conclusion: Our results provide the basic knowledge and molecular resources for future functional studies investigating wheat reproductive development under heat stress.

KEYWORDS

wheat, lncRNA, heat stress, pollen development, transcriptome, pollen sterility

1 Introduction

Wheat is one of the most important staple crops in the world and plays a crucial role in global food security. Wheat is cultivated on more land area than any other crop globally. It is a primary source of dietary energy and protein for a significant portion of the global population, particularly in regions where it is a staple food. Given its central role in global food and nutrition security, maintaining stable wheat production is crucial to ensuring a steady food supply for a growing human population. However, environmental challenges such as high temperatures and heat waves associated with climate change impair proper plant growth and development, decreasing crop yield and quality (Lippmann et al., 2019; El-Sappah et al., 2022). With an estimated 6% decrease in global productivity for each degree Celsius temperature increase, wheat (*Triticum aestivum*), a key cereal crop and staple food growing worldwide, is not an exception to this disruptive phenomenon (Shewry, 2009; Asseng et al., 2015; Lal et al., 2021). Heat stress is a significant challenge for wheat production, especially during the reproductive stage, which is most vulnerable to environmental challenges. The reproductive phase of wheat starts with the emergence of flag leaf and finishes with grain maturity, and any stress during this stage can profoundly affect yield and quality (Farooq et al., 2011; Nawaz et al., 2015). The production of viable pollen is an essential component of the reproductive development of a plant as it determines crop fertility and productivity (Singh and Bhalla, 2007). According to transcriptomic investigations (Haerizadeh et al., 2009; Babaei et al., 2021; Golicz et al., 2021), distinct expressions for various protein- and nonprotein-coding genes drive developmental processes that result in mature pollen. However, environmental stresses can interrupt these developmental processes, reducing fertility and yield; (Browne et al., 2021; Lohani et al., 2021; Singh et al., 2021). At the molecular level, stress can disrupt various physiological and biochemical processes in developing pollen, leading to altered gene expression, protein synthesis, reactive oxygen species (ROS) metabolism, lipid metabolism, carbohydrate metabolism, and hormone signaling.

Genetic variability in the heat stress response of pollen development has been reported among wheat cultivars (Dong et al., 2017; Browne et al., 2021), and three days of heat stress (35°C) disrupted pollen development in two heat-sensitive cultivars, Cranbrook and Wyalkathem but not in two tolerant cultivars, Halberd and Young (Browne et al., 2021). At the molecular level, differential expression of protein-coding genes has been observed during pollen development following heat stress in the above two sensitive and two tolerant wheat cultivars (Browne et al., 2021). High temperature strongly up-regulated HEAT SHOCK TRANSCRIPTION FACTOR A9 (HSFA9), BCL-2-ASSOCIATED ATHANOGENE 6 (BAG6) and FK Binding Protein 65 (FKBP65) genes in anthers of all cultivars. Many genes were up-regulated differentially in heat-sensitive and tolerant cultivars. Additionally, by comparing the genes up-regulated in heat-tolerant and sensitive cultivars, Browne et al. (2021) have identified several genes, including MYELOBLASTOSIS VIRAL ONCOGENE HOMOLOG 30 (MYB30), BAX INHIBITOR-1 (BI-1), and MULTIPROTEIN BRIDGING FACTOR 1 (MBF1), that may contribute to heat tolerance in developing anthers.

Much is known about the protein-coding genes involved in the pollen heat stress response in wheat, but little is known about the contribution of lncRNAs underlying the vulnerability of pollen development to high-temperature exposure. LncRNAs are transcripts over 200 nucleotides that do not code for proteins but have diverse and significant regulatory functions within the cells based on the sequence composition and structure (Golicz et al., 2018a; Wierzbicki et al., 2021).

LncRNAs have been reported as regulatory molecules in various cellular processes such as chromatin organization, transcription, splicing, mRNA stability, translation, and protein modification (Herman et al., 2022). Based on their molecular function, lncRNAs can be categorized into signal, decoy, guide, and scaffold molecules (Wang et al., 2011). LncRNAs show lower inter-species sequence conservation, lower expression, and higher tissue-specificity expression compared to protein-coding RNAs (Golicz et al., 2018a). LncRNAs are classified as sense, antisense, intronic, or intergenic based on their genomic location and transcriptional direction (Babaei et al., 2022). In addition, lncRNAs can be identified as "*cis*-acting" when they control gene expression at or close to their transcriptional site or "*trans*-acting" when they move from their transcriptional sites to act in other locations in the nucleus or cytoplasm (Gil and Ulitsky, 2020).

In plants, lncRNAs have also been shown to function in different biological processes during growth and development (Zhao et al., 2022). For example, lncRNA ALTERNATIVE SPLICING COMPETITOR (ASCO), which is involved in root development in *Arabidopsis*, play a role as a decoy lncRNA to hijack nuclear speckle RNA-binding proteins (NSR) regulating the splicing of several mRNA targets (Bardou et al., 2014). In rice, lncRNA TWISTED LEAF regulates the expression of R2R3 MYB transcription factor to play its regulatory role in maintaining the leaf blades flattened (Liu et al., 2018). For instance, a DROUGHT-INDUCED lncRNA (DRIR) has been reported as the positive regulator of drought and salt stress in *Arabidopsis* involved in the regulation of many stress-responsive genes (Qin et al., 2017). LncRNA SVALKA has also been shown to tightly regulate the expression of CBF1 in *Arabidopsis* and promote the plant's ability to overcome severe cold stresses (Kindgren et al., 2018).

LncRNAs, as regulatory molecules, play crucial roles during pollen development and progression;(Xiao-Yan et al., 2004; Ding et al., 2012; Babaei et al., 2022). For example, sufficient expression of lncRNA LONG-DAY–SPECIFIC MALE-FERTILITY–ASSOCIATED RNA or in short, LDMAR is essential for pollen development and fertility in rice; even a single nucleotide mutation alters the secondary structure and expression of LDMAR, which leads to photoperiod-sensitive male sterility (Ding et al., 2012). Previously, the differential and specifical expression of several lncRNAs during pollen developmental stages has been reported in plants such as *Brassica rapa* (Huang et al., 2018; Lohani et al., 2023), *Camellia oleifera* (Kong et al., 2022), and *Oryza sativa* (Wang et al., 2021). During pollen development, lncRNAs can also be differently expressed in response to environmental challenges, which points to the regulatory role of lncRNAs as stress-responsive

molecules. For instance, 131 heat-stress response lncRNAs were discovered during *Arabidopsis* pollen development (Rutley et al., 2021), and a total of 3,053 drought-stress responsive lncRNAs were found in tomato anthers (Lamin-Samu et al., 2022). However, the knowledge of the expression profile of stress-responsive lncRNAs during pollen development in wheat is still lacking. To this end, we performed *in-silico* analysis to identify and characterize 5,482 heat-responsive lncRNAs during wheat pollen development. We predicted the potential function of lncRNAs as *cis* and *trans*-regulatory RNAs in various biological processes. We also explored lncRNA interactions with miRNAs and predicted lncRNA-miRNA-mRNA regulatory networks in response to heat stress during pollen development in wheat.

2 Materials and methods

2.1 Data

The RNA sequencing data with accession numbers PRJNA638225 and PRJNA433429 from a previously published study (Browne et al., 2021) were retrieved from the Sequence Read Archive (SRA) database at the National Center for Biotechnology Information (https://www.ncbi.nlm.nih.gov/sra/). The RNA-seq data represents the transcriptome of four wheat cultivars at two stages of pollen development: meiosis and tetrad (Supplementary Table S1). Wheat cultivars were Cranbrook and Wyalkatchem for stress-sensitive and Halberd and Young for stress-tolerant samples. All cultivars were grown under normal conditions (day/night: 22°C/15°C) as control samples and heat stress conditions (day/night: 35°C (for 12 hours)/15°C).

The wheat genomic reference sequence (*Triticum aestivum*, IWGSC, release-55) and its corresponding annotation were downloaded from the Plant Ensemble database (https://plants.ensembl.org/).

2.2 LncRNA identification and differential expression analysis

Reads were mapped to the wheat reference genome using alignment software HISAT2-v2.2.1 (Kim et al., 2015). Aligned reads were assembled into full-length transcripts and subsequently merged using StringTie-v2.2.1 (Pertea et al., 2015). Gffcompare-v0.11.2 (Pertea and Pertea, 2020) was used to annotate assembled transcript, and then transcripts that were tagged as class-code "i", "o", "u" and "x" were selected. The genomic sequence of selected transcripts was obtained using BEDTools-v2.30.0 (Quinlan and Hall, 2010) for subsequent analysis. Transcripts with sequence lengths shorter than 200 nucleotides were removed. The remaining transcripts were screened for protein-coding potential using CPC2-v1.0.1 (labelled as non-coding) (Kang et al., 2017), CNCI-v2.0 (indexed as non-coding) (Sun et al., 2013), and CPAT-v3.0.4 (coding probability < 0.365) (Wang et al., 2013). For CPAT, the cut-off coding probability was calculated using the provided CPAT R-code and ROCR-v1.0-11 (Sing et al., 2005). Transcripts selected as non-coding using CPC, CNCI, and CPAT were scanned against the Pfam database for homolog identification using HMMER-v3.3.2 (Eddy, 2011) to remove the remaining protein-coding RNAs.

Kallisto-v0.46.2 (Bray et al., 2016) was used to quantify the abundance of all protein-coding and non-protein-coding transcripts. We summarized the transcript abundance to the gene level and analyzed the differential expression using NOISeq-v2.42.0 (Tarazona et al., 2015). Trimmed Mean of M-values (TMM) was used as the normalization method, and Count Per Million smaller than one (CPM < 1) was used to filter out low-count genes. Given the typically lower expression levels of lncRNAs compared to messenger RNAs (mRNAs) (Grammatikakis and Lal, 2022; Li et al., 2023), a threshold of significance was established for lncRNA differential expression, requiring a minimum |log2 fold change| > 0.5. Additionally, lncRNAs with a false discovery rate exceeding 0.05 were excluded. These criteria align with methodologies employed in previous studies for the selection of differentially expressed lncRNAs (Li et al., 2020; Ping et al., 2021; Lohani et al., 2023).

Pandas-v1.5.2 (The Pandas Development Team, 2022) handled and manipulated large tabular and text files. Plots were made using R-v4.2.2 (R Core Team, 2021) with libraries gplots-v3.1.3 (Warnes et al., 2022), ggplot2-v3.4.0 (Wickham, 2016), and VennDiagram-v1.7.3 (Chen and Boutros, 2011).

2.3 Identification of *cis* and *trans* targets of lncRNAs

The co-expression network between differentially expressed lncRNAs and protein-coding genes was constructed for functional lncRNA prediction. We used BEDTools to locate 10 genes at either side of lncRNA's loci as their *cis* target; all other genes were considered to be the *trans* target. For the co-expression network, first, the CPM values were obtained using edgeR-v3.40.1 (Robinson et al., 2010). Then SciPy-v1.9.3 (Virtanen et al., 2020) was used to calculate the Pearson correlation coefficients (r) and corresponding *P* values (*P*). In *cis*, paired lncRNAs and protein-coding genes with $P < 0.05$ ($|r| > 0.81$) were selected. For *trans*-acting lncRNAs, MNE-Python-v1.3 (Gramfort et al., 2013) was used for multiple comparison correction using the Benjamini-Hochberg (BH) method, and paired lncRNAs and protein-coding genes with $P < 0.05$ were selected as co-expressed. As another filtering step for *trans*-acting lncRNAs, LncTar (Li et al., 2015) was used to measure the normalized binding free energy (ndG) between co-expressed lncRNA and its paired protein-coding gene. A cutoff of ndG = -0.15 was used to filter the LncTar results (Li et al., 2015; Zhao et al., 2021; Zhang et al., 2022).

2.4 Prediction of lncRNA-miRNA-mRNA regulatory network

The analysis of the interaction between lncRNAs and miRNAs and then miRNAs and mRNAs were also used to predict the function of differentially expressed lncRNAs. For this mean,

known sequence of wheat miRNAs were retrieved from the miRBase database (Kozomara and Griffiths-Jones, 2010) and TargetFinder-v1.7 (https://github.com/carringtonlab/TargetFinder) (Fahlgren and Carrington, 2010) with its default parameters was used to identify RNA-RNA interactions.

2.5 Functional prediction of lncRNAs

For functional prediction, Gene Ontology (GO) enrichment analysis was carried out using topGO-v2.50.0 (Alexa, 2022) for all the identified *cis* and *trans* targets of lncRNAs as well as the genes that were placed in the lncRNA-miRNA-mRNA network. Significant GO identifiers (ClassicFisher < 0.05) were summarized to their parent GO terms using rrvgo-v1.10 (Sayols, 2020).

2.6 Conservation analysis of lncRNAs

For conservation analysis, the sequence information of lncRNAs identified in other plant species was retrieved from PLncDB v2.0 (https://www.tobaccodb.org/plncdb/) (Jin et al., 2021). Then BLASTN (-word_size 11) was used to align lncRNAs detected in this study against lncRNAs identified in other plant species. For a lncRNA to be conserved, the 'E value' had to be less than 1e-5, and the aligned lncRNAs had to contain a minimum of 60% identical nucleotides covering at least 30% of the length of shorter lncRNA in the alignment. The phylogenetic tree was constructed using MEGA 11 (Tamura et al., 2021).

3 Results

3.1 Genome-wide identification and characteristics of heat-stress associated lncRNAs in wheat pollen

For the genome-wide discovery of heat stress-associated lncRNAs in wheat, we used publicly available RNA-seq libraries in the SRA database. The data represent the transcriptome of control and heat-stressed anthers at meiosis and the tetrad stages of pollen development in stress-tolerant (Halberd and Young) and stress-sensitive (Cranbrook and Wyalkatchem) wheat cultivars. The overall alignment rate of sequencing data to the wheat reference genome was more than 99% for all samples (Supplementary Table S1).

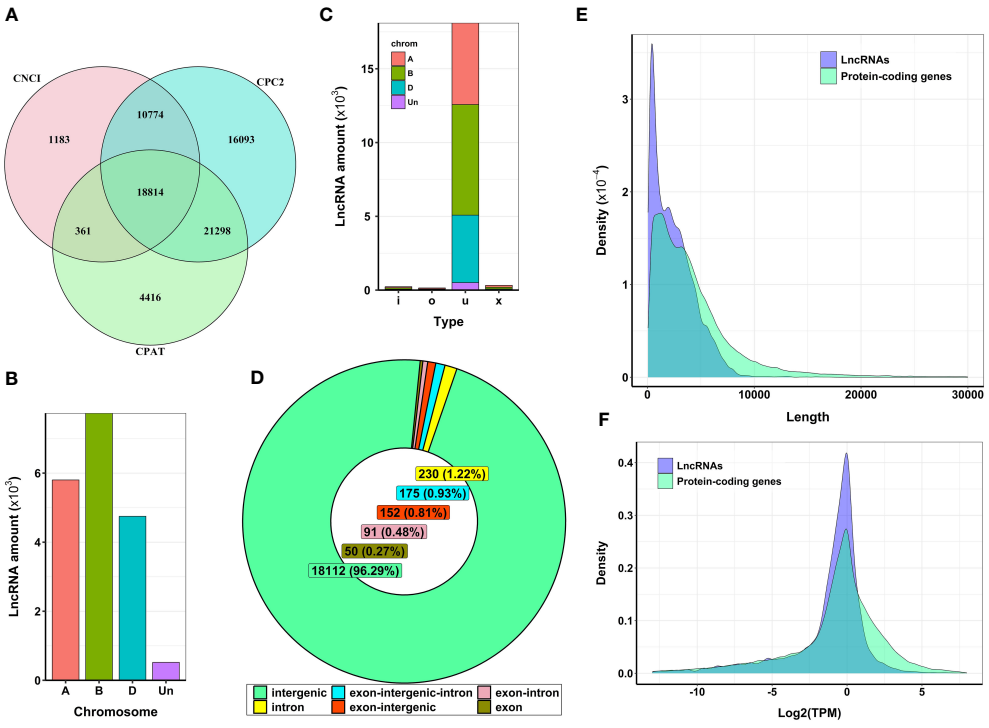

FIGURE 1
Features of expressed lncRNAs in wheat anthers. **(A)** Venn diagram representing the number of detected lncRNAs with no protein-coding potential. From 18,814 selected lncRNAs, four lncRNAs were filtered out using alignment against the Protein Families database (Pfam). **(B)** The distribution of lncRNAs generated from different sub-genomes. Most identified lncRNAs were generated from sub-genome **(B, C)** Type of lncRNAs identified in wheat. Most lncRNAs expressed from different wheat sub-genomes are classified as 'u', which means their genomic region is unknown or intergenic compared with known genomic regions. **(D)** The genomic location of lncRNA transcripts. The entire sequence of more than 96% of identified lncRNAs was derived from intergenic regions, and the remaining lncRNAs had some level of overlap with known protein-coding regions. **(E)** The length distribution of lncRNAs. The average length of lncRNAs was about 2,400 nucleotides. LncRNAs were shorter in length compared with protein-coding genes. **(F)** The expression level of lncRNAs and protein-coding genes. The mean $\log_2$ (TPM) values for lncRNAs were lower than those of protein-coding genes.

Transcript assembly analysis and abundance quantification identified a total of 181,096 genomic loci, among which 42,536 loci were tagged as class-code "i", "o", "u", and "x" and used for further lncRNA identification. Combining CPC2, CPAT, and CNCI methods (Figure 1A), our analysis detected 18,814 transcripts as potential lncRNAs. Further filtering against the Pfam database revealed four transcripts had protein-coding potential. Ultimately, we identified 18,810 transcripts (corresponding to 11,054 loci) as bona fide lncRNAs that lacked detectable protein-coding ability (Supplementary Table S2).

Hexaploid wheat (2n=6x=42), which evolved from three ancestral genomes (A, B, and D), comprises 21 pairs of chromosomes. Our analysis of lncRNA transcription in this species revealed an uneven distribution of these transcripts across the A, B, and D genomes, as shown in Figure 1B. Most identified lncRNAs in our samples were in intergenic regions (96.29%), although a small fraction also overlapped with genic regions (Figures 1C, D). In terms of length, most lncRNAs ranged from 200 to 5,000 nucleotides, with an average length of approximately 2,400 nucleotides. Notably, this was shorter than the average length of protein-coding transcripts, about 4,200 nucleotides (Figure 1E). Finally, we observed that the average expression levels of lncRNAs were lower than those of protein-coding genes (Figure 1F).

3.2 Identification of 5,482 heat-responsive lncRNAs

Further data analysis revealed that 5,482 lncRNAs were differentially expressed in response to heat stress in four wheat

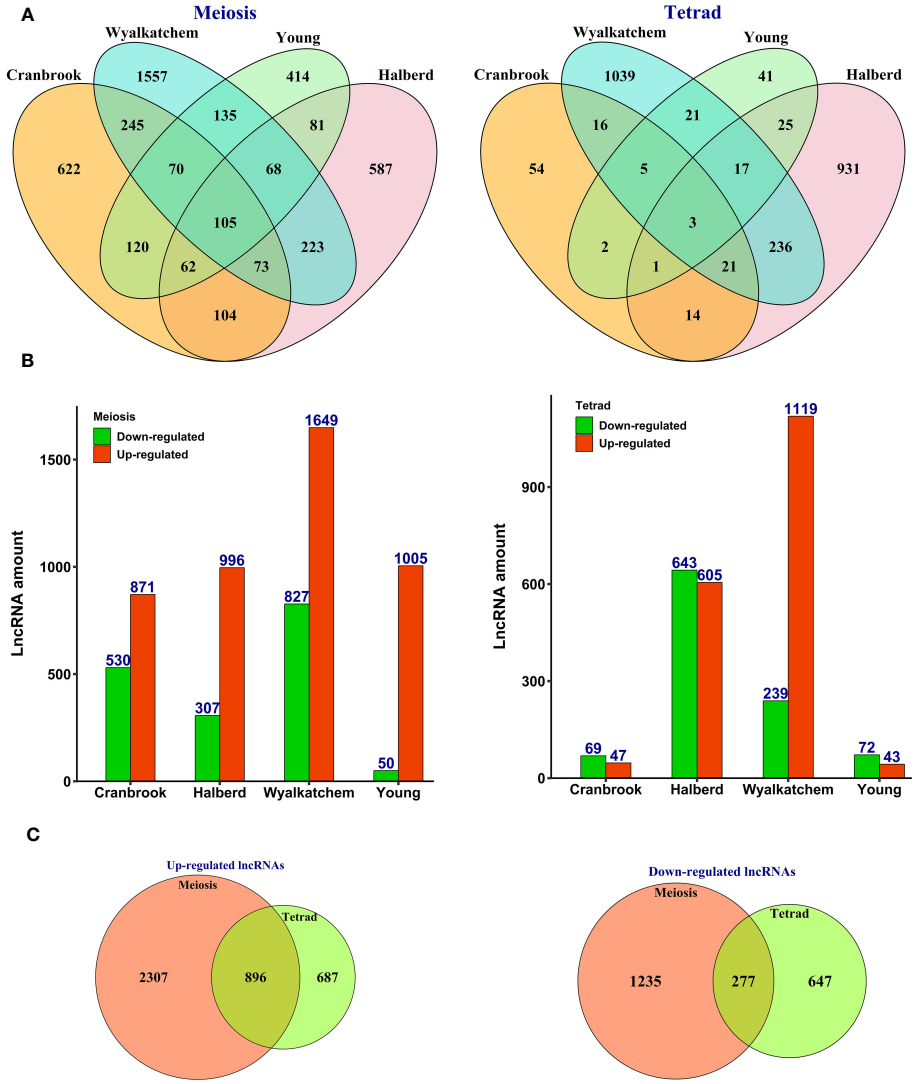

FIGURE 2
Expression pattern of heat-responsive lncRNAs during pollen development in heat-sensitive (Cranbrook and Wyalkatchem) or heat-tolerant (Halberd and Young) wheat cultivars. **(A)** The number of common and specific lncRNAs differentially expressed during meiosis or tetrad stages of pollen development. More lncRNAs showed cultivar-specific expression patterns, especially during the meiosis stage. **(B)** The number of lncRNAs with upregulation or downregulation trends in response to heat stress. LncRNAs had higher changes in their expression level with an upregulation trend in meiosis. **(C)** The number of stage-specific expressed lncRNAs. LncRNAs exhibited stage-specific expression patterns, with more lncRNAs showing differential expression in response to heat stress during meiosis than tetrad.

cultivars at meiosis and tetrad stages (Supplementary Table S3). We found that more lncRNAs showed differential expression patterns in meiosis than tetrad, with an up-regulation trend observed in all cultivars (Figure 2A). In tetrad, most of the differentially expressed lncRNAs were found in the Wyalkatchem and Halberd cultivars (Figure 2A), and Wyalkatchem also had the most significant number of differentially expressed lncRNAs in both meiosis and tetrad (Figures 2A, B).

Although the majority of lncRNAs displayed cultivar-specific expression patterns, we did identify a subset of lncRNAs that were commonly expressed between heat-sensitive cultivars (245), heat-tolerant cultivars (81), and all four cultivars (105) during meiosis (Figure 2A). Additionally, our analysis showed that while most of the identified lncRNAs were specific to either meiosis or tetrad stages, 1,173 lncRNAs exhibited common patterns of upregulation or downregulation between these two developmental stages (Figure 2C).

It's interesting to note that across all cultivars, we discovered a considerable variation in the expression of lncRNAs during pollen formation under heat stress. To further illustrate this, we present the expression pattern of the top 1,000 lncRNAs with the highest variability during pollen development in Figure 3. The heat-shock marker genes found to be upregulated in our analysis were also extracted through the differential expression analysis, and their details are provided in Supplementary Table S4. Among those, the most highly upregulated gene encodes chaperone protein and small heat shock protein HSP20/Alpha crystallin. Other notably upregulated genes encode members of the Heat shock factor (HSF) family.

3.3 Exploring the role of heat-responsive lncRNAs as *cis*- or *trans*-acting regulatory molecules

We focused on their regulation of nearby or distal protein-coding genes to gain insight into the potential functions of differentially expressed lncRNAs. We selected ten protein-coding genes located upstream and downstream of the lncRNAs as *cis* targets and all other protein-coding genes as *trans* targets. Pearson correlation coefficients were then calculated to identify co-expression patterns between lncRNAs and their target genes. The results predicted 5,306 significant correlated expressions between 2,922 lncRNAs and 4,638 neighboring protein-coding

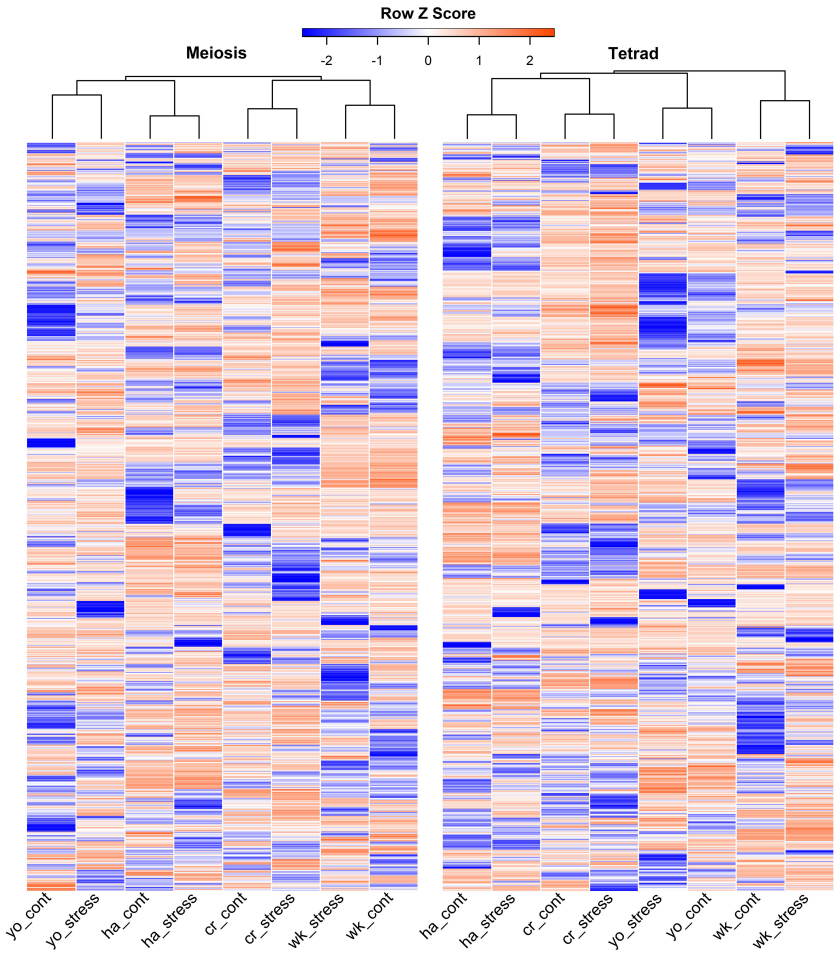

FIGURE 3
Top 1,000 highly variable expressed lncRNAs during pollen development in response to heat stress in heat-sensitive (cr, Cranbrook and wk, Wyalkatchem) or heat-tolerant (ha, Halberd and yo, Young) wheat cultivars. There was a high level of variability in the expression of lncRNAs, both between stress and control conditions and across different cultivars, during both meiosis and tetrad stages of pollen development.

10.3389/fpls.2024.1344928

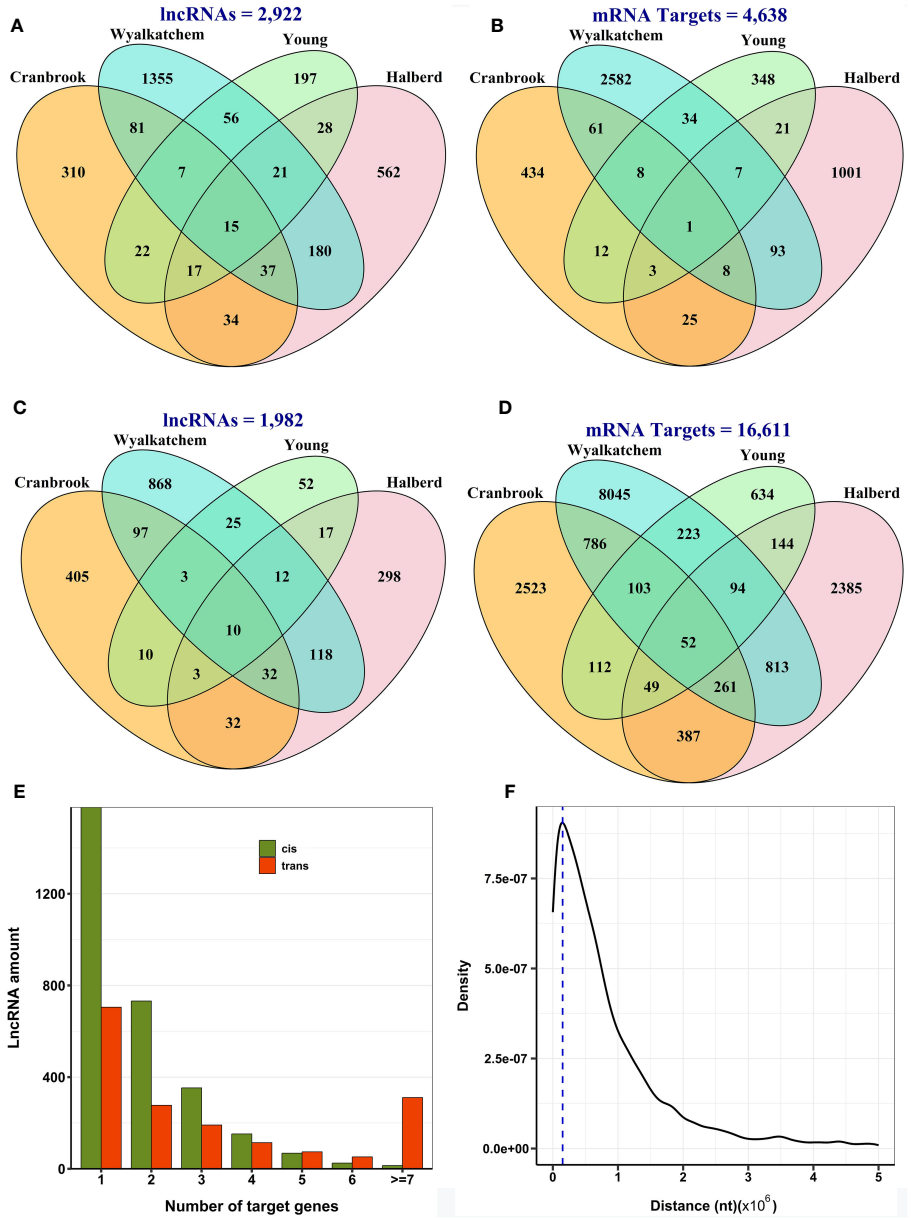

FIGURE 4
Predicted co-expression of lncRNAs and protein-coding genes in wheat. **(A)** The number of lncRNAs with *cis*-regulatory function. **(B)** The number of target protein-coding genes of lncRNAs in *cis*. **(C)** The number of lncRNAs with *trans*-regulatory function. **(D)** The number of target protein-coding genes of lncRNAs in *trans*. Most lncRNAs and their target genes showed cultivar-specific expression patterns in both *cis* and *trans*-regulatory mechanisms. **(E)** The number of target genes of lncRNAs in *cis* and *trans*, indicating that lncRNAs tend to target usually one to three genes. **(F)** The distance between lncRNAs and their target genes in *cis*, with the dashed line representing the peak density within a distance of 150 kb, indicating that lncRNAs generally regulate their target genes in close proximity.

genes in *cis* (Supplementary Table S5; Figures 4A, B) and 41,250 meaningful correlated expressions between 1,982 lncRNAs and 16,611 protein-coding genes in *trans* in all cultivars (Supplementary Table S6; Figures 4C, D). Again, we observed that most lncRNAs and their *cis* or *trans* targets showed a cultivar-specific association. Most lncRNAs exhibited a narrow range of target genes, with most regulating only one to three protein-coding genes. (Figure 4E). The peak density of distance between lncRNAs and their target protein-coding genes in *cis* was observed to be approximately 150 kb from the lncRNA. This suggests that lncRNAs often modulate the expression of genes in their immediate genomic vicinity (Figure 4F).

To investigate the potential regulatory role of lncRNAs in response to heat stress during pollen development in wheat, we conducted GO enrichment analysis on the target protein-coding genes of lncRNAs. Our findings demonstrated the involvement of lncRNAs in a range of biological processes, both as *cis* and *trans*-regulatory elements. For example, we observed that lncRNA target genes exhibiting an upregulation trend in response to heat stress were enriched in 505 GO terms under the biological category of *cis*

10.3389/fpls.2024.1344928

regulation. These GO terms were further consolidated into 121 parent terms, including RNA processing, response to temperature stimulus, regulation of jasmonic acid biosynthesis, response to abiotic stimulus, response to heat, and protein folding (Supplementary Table S7; Figure 5A). Enrichment analysis of lncRNA target genes exhibiting a downregulation trend in response to heat stress revealed 674 GO terms under various biological categories. Further consolidation of these GO terms yielded 155 parent terms, encompassing processes such as regulation of cell size, pigment biosynthesis, and chromatin organization (Supplementary Table S7).

Similarly, we investigated the *trans*-regulatory mechanism of lncRNAs. We found that the upregulated target genes of lncRNAs were enriched in 941 GO terms. In comparison, the downregulated ones were enriched in 1,019 GO terms, which were subsequently consolidated into 202 and 207 parent terms, respectively (Supplementary Table S8). Noteworthy GO terms for the upregulated target genes in *trans* included response to hydrogen peroxide, response to heat, protein ubiquitination, protein folding, and cuticle development (Figure 5B). Significant GO terms for the downregulated genes in *trans* were sister chromatid segregation, response to brassinosteroids, lipid modification, and ncRNA catabolic process (Supplementary Table S8).

3.4 LncRNAs regulate biological processes via lncRNA-miRNA-mRNA regulatory networks

To explore the potential post-transcriptional functions of lncRNAs, we predicted lncRNA-miRNA-mRNA regulatory networks. We identified lncRNA-miRNA modules by predicting interactions between differentially expressed lncRNAs identified in this study and known wheat miRNAs. Subsequently, we identified lncRNA-miRNA-mRNA regulatory networks by analyzing the interactions between selected miRNAs and differentially expressed mRNAs. To identify lncRNAs likely acting as miRNA sponges, we selected those lncRNAs and mRNAs in our lncRNA-miRNA-mRNA networks that showed similar expression trends, such as upregulated lncRNA and upregulated mRNA or downregulated lncRNA and downregulated mRNA. We defined lncRNAs as miRNA precursors if they had perfect complementary sequences with known wheat miRNAs and exhibited opposite expression trends with their target mRNAs, i.e., upregulated lncRNA-downregulated mRNA or downregulated lncRNA-upregulated mRNA. We identified 139 lncRNAs that potentially act as miRNA sponges, regulating the expression of 1,216 protein-coding genes through interactions with 50 miRNAs (Supplementary Table S9).

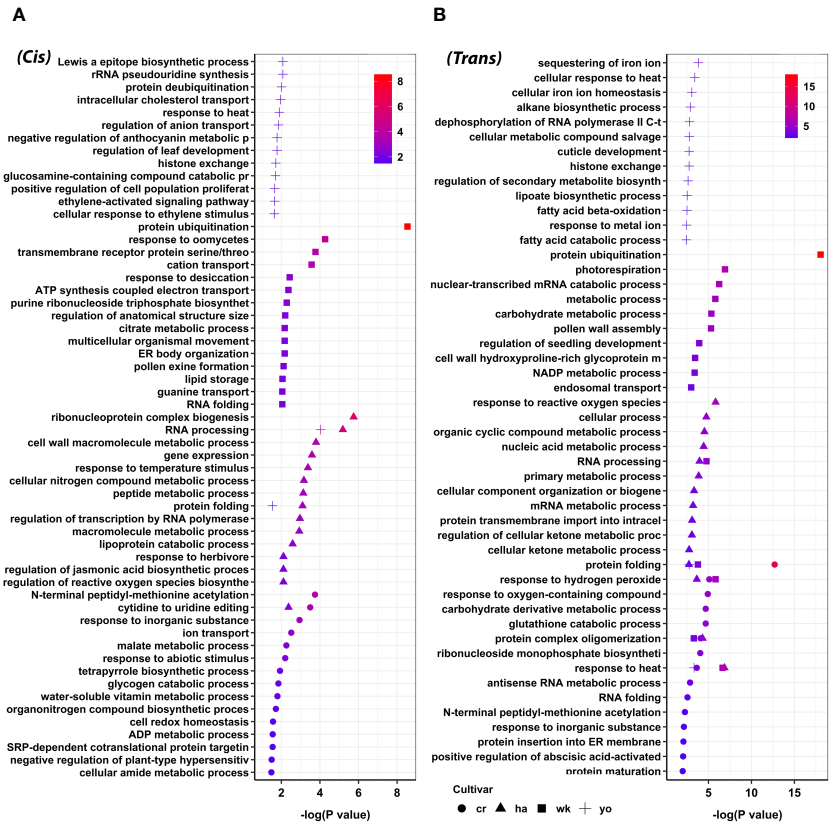

FIGURE 5
Functional annotation of upregulated target protein-coding genes of lncRNA during pollen development in wheat, categorized based on their *cis* **(A)** and *trans* **(B)** regulatory mechanisms. GO terms such as response to heat, response to hydrogen peroxide, protein complex oligomerization, protein folding, and RNA processing were enriched among different wheat cultivars. Cranbrook (cr) and Wyalkatchem (wk) are heat-sensitive, and Halberd (ha) and Young (yo) are heat-tolerant wheat cultivars.

10.3389/fpls.2024.1344928

Additionally, we identified 25 lncRNAs that could function as miRNA precursors, producing 11 miRNAs that potentially regulate the expression of 438 protein-coding genes (Supplementary Table S9). While some lncRNA-miRNA-mRNA modules were shared between two or more cultivars, most were specific to each cultivar (Figures 6A, B). Our analysis of miRNA target genes functionally annotated with GO terms revealed that lncRNAs can regulate several biological processes in response to heat stress through post-transcriptional mechanisms during wheat pollen development. Several GO terms were enriched, such as histone H3-K14 acetylation, cellular aromatic compound metabolic process, organic cyclic compound metabolic process, and cellular response to auxin stimulus (Supplementary Table S10). Figure 6C displays each wheat cultivar's top 15 enriched GO terms for miRNA target protein-coding genes. While some enriched GO terms were shared across multiple cultivars, others were cultivar specific.

3.5 Conservation of lncRNAs varies among plant species based on evolutionary distance

To investigate the evolutionary patterns of lncRNAs, we conducted alignment and conservation analyses between lncRNAs identified in this study and those from 13 plant species available in public databases (Figure 7A). Our research revealed that, among the 11,054 lncRNA loci in wheat, 3,263 loci (29.52%) contained conserved sequences with other plant species (Supplementary Table S11). Most sequence similarity in lncRNAs was observed between *Triticum aestivum* and *Hordeum vulgare*, followed by *Setaria viridis*, *Brachypodium distachyon*, *Zea mays*, *Oryza sativa*, and *Nicotiana tabacum* (Figure 7A). We identified 654 lncRNA loci in wheat that exhibited sequence homology with two or more other plant species. Among these, 20 loci showed homology with more than nine

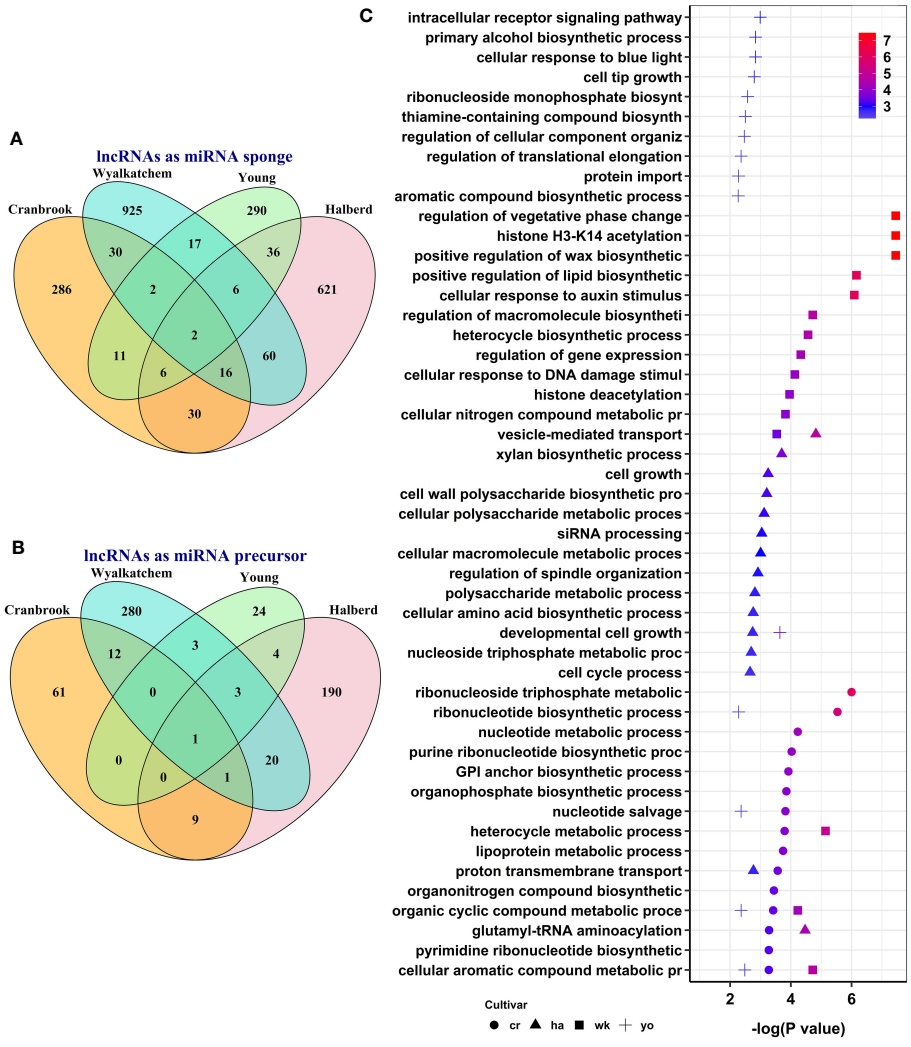

FIGURE 6
The number and potential function of predicted heat-responsive lncRNA-miRNA-mRNA regulatory networks during pollen development in four wheat cultivars. The number of cultivar-specific and common lncRNA-miRNA-mRNA modules when lncRNAs act as miRNA sponges **(A)** or as miRNA precursors **(B)**. **(C)** illustrates the enriched biological processes for the target genes of lncRNAs in the predicted lncRNA-miRNA-mRNA modules.

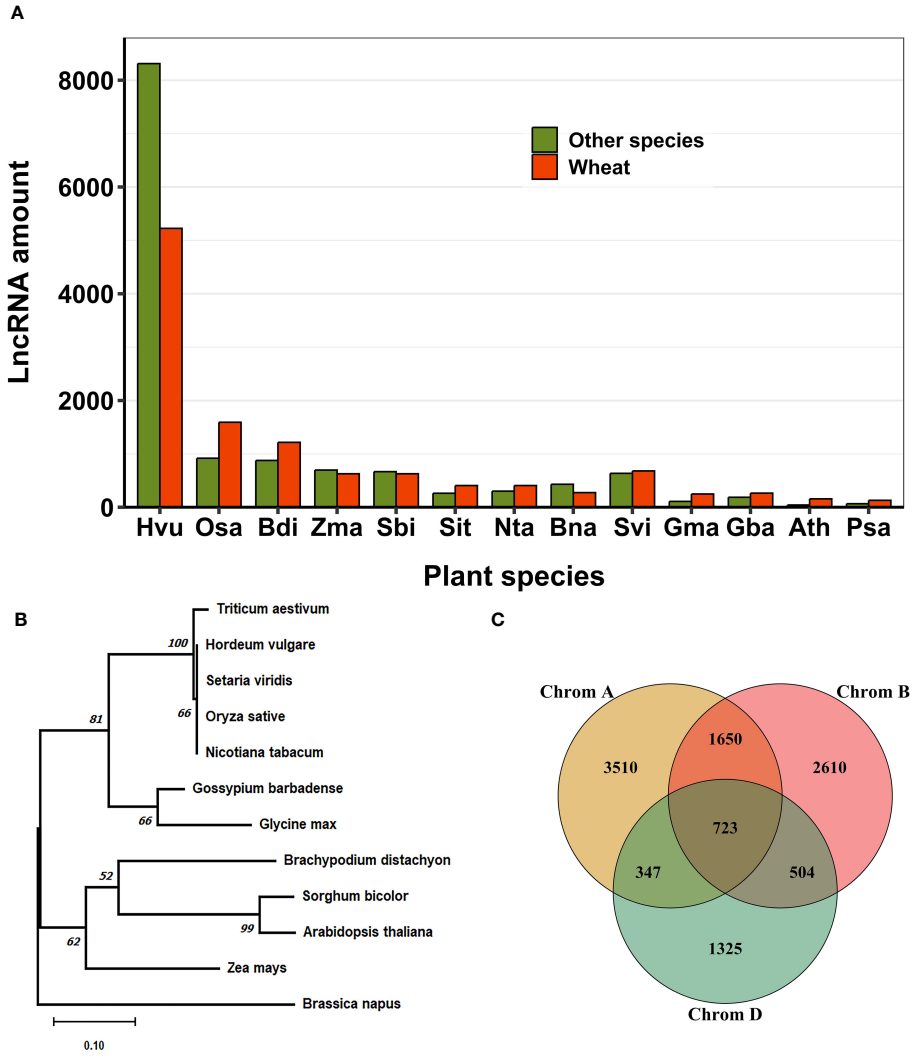

FIGURE 7
Conservation of lncRNAs in wheat. **(A)** Conservation of lncRNAs was determined by BLAST analysis with 13 other plant species. Most conserved lncRNAs in wheat showed sequence homology with closely related species, *Hordeum vulgare*. **(B)** The Neighbor joining phylogenetic tree with 1000 bootstrap replicates. It represents the evolutionary conservation of a specific lncRNA, MSTRG.56557.1, which is conserved across several plant species. **(C)** The conservation of lncRNAs between A, B, and D wheat genomes. Most lncRNAs exhibit sub-genome-specific expression patterns. Conserved lncRNAs are more common between genome A and B. Initials for plant species in **(A)** *Hordeum vulgare, Oryza sativa, Brachypodium distachyon, Zea mays, Sorghum bicolor, Setaria italica, Nicotiana tabacum, Brassica napus, Setaria viridis, Glycine max, Gossypium barbadense, Arabidopsis thaliana, Pisum sativum.*.

different species. We constructed a phylogenetic tree to investigate the evolutionary conservation of a highly conserved lncRNA, MSTRG.56557.1, identified in wheat and present in 11 other plant species. The phylogenetic tree revealed a close relationship between the identified lncRNA in wheat and those in *Hordeum vulgare*, *Setaria viridis*, *Oryza sativa*, and *Nicotiana tabacum*. (Figure 7B). We also investigated the conservation of lncRNAs in wheat's A, B, and D sub-genomes based on sequence homology (Supplementary Table S12). Our study revealed that the majority of lncRNAs exhibit sub-genome-specific expression patterns. However, 3,224 lncRNAs (29.17%) were conserved across all three sub-genomes, with the most frequently expressed lncRNAs shared between the A and B genomes. Additionally, we identified 723 (6.54%) lncRNAs that were conserved in all three genomes (A, B, and D) (Figure 7C).

4 Discussion

Environmental stresses such as high temperatures limit normal plant growth and development. In response to such stresses, plants activate a series of defense mechanisms that involve changes in the expression of several genes such as HSFA1s, DEHYDRATION-RESPONSIVE ELEMENT BINDING 2A (DREB2A), and JUNGBRUNNEN1 (JUB1) (Zhu, 2016; Ohama et al., 2017). Accumulating evidence reveals that lncRNAs function during normal plant growth and development and play essential roles in response to harsh environmental conditions (Wu et al., 2020b; Urquiaga et al., 2021). Previous studies reported abiotic stress-responsive lncRNAs in several plant species, such as cold-responsive lncRNAs in grapevine (Wang et al., 2019), drought

and heat-responsive lncRNAs in *Brassica juncea* (Bhatia et al., 2020), salt stress-responsive lncRNAs in maize (Liu et al., 2022) and rice (Tiwari et al., 2023), and drought-responsive lncRNAs in tomato (Lamin-Samu et al., 2022). In this study, we used transcriptomic data from four wheat cultivars to investigate the dynamic expression of lncRNAs during meiosis and tetrad stages of pollen development in response to heat stress. We identified the expression of lncRNAs from 11,054 loci, of which 5,482 loci showed differential expression patterns. The meiosis stage shows more response to heat stress as the more significant number of expressed lncRNAs and a higher level of changes in differential expression were observed in this stage of pollen development. Our results suggest that stress-responsive lncRNAs are part of the dynamic response of gene expression regulation during pollen development in wheat in response to heat stress (Table 1). Meiosis was also noted as the most sensitive stage to heat stress in previous studies (Bokshi et al., 2021). Meiosis processes are more vulnerable to high temperatures, which significantly affect how developing pollen functions as it matures. This sensitivity limits the quantity and quality of mature pollen (Bokshi et al., 2021). In wheat, high temperatures cause changes in pollen development, such as the breakdown of cells during meiosis, leading to two main outcomes. Firstly, the pollen grains might not develop properly, remaining immature. Alternatively, if the initial cell division is successful, there may be difficulties in progressing to the usual three-cell pollen grains (Saini et al., 1984; Bokszczanin et al., 2013). Additionally, heat stress during meiosis results in a decrease in pollen dispersal and noticeable irregularities in pollen shape, groups of pollen grains sticking together, and the formation of pollen grains with multiple nuclei (Jäger et al., 2008; Bokszczanin et al., 2013).

LncRNAs can function in *cis* to regulate the expression of their target genes in their proximity or in *trans* to regulate distal target gene expression (Rinn and Chang, 2020). However, in lncRNA identification pipelines, functional characterization of a lncRNA is still one of the most challenging tasks. The reason is that there are only a few lncRNAs validated functionally, and the inter-species sequence conservation among lncRNAs is lacking (Golicz et al., 2018b). As lncRNAs usually co-express with their target protein-coding genes, the primary method for lncRNA annotation is to identify the co-expression network between lncRNAs and protein-coding genes, and then, the potential function of lncRNAs is predicted based on the functional analysis of lncRNA's targets (Xu et al., 2018; Gasparis et al., 2021). With this regard, lncRNAs have been identified as *cis*- or *trans*-acting regulatory molecules in various processes in response to environmental stimuli (Urquiaga et al., 2021). For example, the target genes of *trans*-acting lncRNAs induced under salt stress in duckweed were related to amino acid metabolism, hormone metabolism, cytochrome P450, and CHO

TABLE 1 Selected upregulated lncRNAs in response to heat stress as heat tolerance or heat susceptible biomarkers in wheat.

Cultivar	Dev. Stage	LncRNA locus ID	Log2FC	LncRNA conservation (identity %)
Halberd/Young	Meiosis	MSTRG.93120	4.58/2.70	Bdi (75)
		MSTRG.66077	3.17/2.66	–
		MSTRG.4847	3.08/4.52	–
		MSTRG.51292	4.15/2.67	Huv (82)
		MSTRG.16221	3.69/2.72	–
	Tetrad	MSTRG.94397	3.80/3.62	Huv (86)
		MSTRG.53383	2.48/3.64	Huv (82)
		MSTRG.43348	2.52/3.55	–
		MSTRG.80946	1.86/3.37	–
		MSTRG.33763	1.88/3.06	–
Cranbrook/Wyalkatchem	Meiosis	MSTRG.6392	2.41/6.85	Huv (98), Svi (97), Osa (97), Nta (97)
		MSTRG.83325	3.09/5.51	–
		MSTRG.52667	4.56/2.83	–
		MSTRG.14617	3.02/3.44	Huv (78)
		MSTRG.10157	3.10/3.14	–
		MSTRG.3277	2.20/4.06	–
	Tetrad	MSTRG.8752	5.97/4.90	–
		MSTRG.105350	5.08/1.55	Huv (83), Zma (75), Svi (74), Sbi (73)
		MSTRG.18574	2.99/2.29	–
		MSTRG.47840	0.92/0.90	–

Symbol "-" : homolog of lncRNA was not found in other plant species.

metabolism (Fu et al., 2020). In response to drought stress during pollen development in tomatoes, *cis*-acting lncRNAs were found to be involved in abscisic acid (ABA) and jasmonic acid (JA) metabolism, sucrose, and starch metabolism, and tapetum development (Lamin-Samu et al., 2022). In this study, we also investigated the *cis* and *trans* function of lncRNAs in the regulation of gene expression in pollen in response to heat stress. We noted that lncRNAs could modulate gene expression and play roles in various biological processes such as RNA processing, protein folding, protein ubiquitination, regulation of jasmonic acid biosynthesis, and cuticle development (Table 2 and Figure 5). Similar results were also observed in previous studies. For

TABLE 2 Selected lncRNAs and their potential target protein-coding genes with specific expression in heat-tolerant or heat-sensitive cultivars.

Cultivars	LncRNA/ Target gene	Target gene Ortholog	Target gene GO term and/or description	LncRNA conservation (identity %)
Cis **Ha, Yo***	MSTRG.102721/ TraesCS7D02G520300	ERD7	Senescence/spartin-associated, response to abscisic acid and abiotic stress	Hvu (92)
	MSTRG.103361/ TraesCSU02G047300	Oshsp16.9B	Alpha crystallin/Hsp20 domain, 16.9 kDa heat shock protein 2	Hvu (90)
	MSTRG.26499/ TraesCS2D02G150600	CPN10	protein folding, response to heat, GroES chaperonin superfamily	Hvu (81)
	MSTRG.86324/ TraesCS6D02G273500	OsMADS57	Transcription factor, MADS-box	–
	MSTRG.90361/ TraesCS7A02G308900	RGLG4	jasmonic acid mediated signaling pathway, response to wounding, protein K63-linked ubiquitination	–
Wk, Cr	MSTRG.98330/ TraesCS7D02G057000	AT4G24340	Nucleoside phosphorylase domain, response to water deprivation, secondary metabolite biosynthetic process	–
	MSTRG.95589/ TraesCS7B02G259000	MBF1C	Cro/C1-type helix-turn-helix domain, response to abscisic acid, response to heat	Hvu (100), Svi (100), Osa (99), Nta (99), Zma (98)
	MSTRG.718/ TraesCS1A02G072200	WIN1	Pyridoxal phosphate-dependent transferase, arginine metabolic process, primary root development	Hvu (81)
	MSTRG.70350/ TraesCS5D02G083300	RPM1	Winged helix-like DNA-binding domain superfamily, defense response	–
	MSTRG.17875/ TraesCS2A02G405800	BPS1	shoot system development, root development	–
Trans **Ha, Yo**	MSTRG.105323/ TraesCS1B02G137100	OsSET30	Histone H3-K9 methyltransferase	Hvu (84), Zma (80), Svi (78), Sbi (76)
	MSTRG.105323/ TraesCS3A02G069900	CHR11	SANT/Myb domain, chromatin remodeling, positive regulation of cellular response to heat	
	MSTRG.105323/ TraesCS4A02G358000	REM16	B3 domain transcription factor	
	MSTRG.105323/ TraesCS5A02G272400	POM1	Glycoside hydrolase, regulation of salicylic acid metabolic process, response to heat	
	MSTRG.45186/ TraesCS6A02G276200	RSL1	Myc-type, basic helix-loop-helix (bHLH) domain, regulation of transcription by RNA polymerase II, root hair initiation	–
Wk, Cr	MSTRG.104324/ TraesCS2D02G091100	AT5G12010	Serine/threonine-protein kinase, response to abscisic acid and jasmonic acid, response to temperature stimulus	Hvu (84), Zma (78)
	MSTRG.104324/ TraesCS7B02G146900	XYLT	Glycosyltransferase 61, post-translational protein targeting to membrane, translocation	
	MSTRG.91627/ TraesCS4A02G355200	OsFd3	2Fe-2S ferredoxin-type iron-sulfur binding domain, electron transfer activity	–
	MSTRG.81272/ TraesCS2A02G088600	PDC2	Thiamine pyrophosphate enzyme, catalytic activity, cellular response to hypoxia	Bdi (99), Hvu (97), Nta (96), Gma (93), Svi (91)
	MSTRG.29264/ TraesCS6D02G197200	AT1G05785	Protein transport protein Got1, endoplasmic reticulum to Golgi vesicle-mediated transport	Osa (99), Nta (94)

*Wk and Cr, Wyalkatchem and Cranbrook (heat-sensitive cultivars); Yo and Ha, Young and Halberd (heat-tolerant cultivars).
Symbol "-" : homolog of lncRNA was not found in other plant species.

example, up-regulation of genes related to RNA processing and conversion of primary RNAs into mature RNAs were also observed in maize and *Brassica rapa* in response to heat stress (Byeon et al., 2019; He et al., 2019), representing the important function of transcriptional regulation during stress conditions. Protein folding is also vital in living organisms, including plants, as protein function is closely linked to their three-dimensional structures (Miernyk, 1999; Basharov, 2003). Environmental stresses such as heat stress can disrupt the bonds that maintain protein structure, leading to denaturation and loss of function (Freeman et al., 1999; Bischof and He, 2006; Huang and Xu, 2008). Previous studies reported the upregulation of genes related to protein folding in different plant species such as *Brachypodium distachyon* (Chen and Li, 2017), Orchard-grass (Luo et al., 2023) and maize (Wu et al., 2020a). During heat stress, the expression of genes that are related to protein folding and assembly, such as HSPs, can enhance heat tolerance in plants (Miernyk, 1999; Jacob et al., 2017; Ding et al., 2020).

LncRNAs can also regulate the expression of target protein-coding genes through lncRNA-small RNA-mRNA interactions. In this regulatory mechanism, lncRNAs can be the substrate for small RNA production, or they can act as competent endogenous RNAs (ceRNAs) and sequester miRNAs from their target mRNAs. Several studies reported the regulatory mechanism of plant lncRNAs through interacting with small RNAs during normal growth and development, or in response to environmental stresses (Yu et al., 2019; Zhang et al., 2019). In rice, for example, lncRNA PMS1T regulates male fertility by acting as a substrate for 21-nucleotide-phased small interfering RNAs (phasiRNAs) (Fan et al., 2016). LncRNA INDUCED BY PHOSPHATE STARVATION1 (IPS1) in *Arabidopsis* inhibits phosphate-starvation–induced miRNA, miR-399, from binding its target mRNA to regulate phosphate homeostasis in the plant (Franco-Zorrilla et al., 2007). The regulatory function of lncRNA-miRNA-mRNA interactions has also been reported in wheat. For instance, in response to drought stress, 10 lncRNA-miRNA-mRNA regulatory modules involving novel miRNAs such as miR417 and miRNA340 have been identified in drought-tolerant and drought-sensitive wheat varieties (Li et al., 2022). Similarly, four lncRNAs TalnRNA5, TahlnRNA27, TapmlnRNA19, and TapmlnRNA8, with upregulated expression in response to heat stress or powdery mildew infection, have been identified as precursors for miRNAs miR2004, miR2066, and miR2010. (Xin et al., 2011). By employing BLAST sequence comparison, TapmlnRNA8 was identified to exhibit sequence

TABLE 3 Selected heat-responsive lncRNA-miRNA-mRNA modules regulating pollen development under heat stress in two or more wheat cultivars.

lncRNA/miRNA/ Protein-coding gene	Target gene GO term and/or description	Cultivars				LncRNA conservation (identity %)
		Wk	Cr	Yo	Ha*	
lncRNA as miRNA inhibitor						
MSTRG.99184/miR1130b-3p/ TraesCS6B02G212900	Ribosome-inactivating protein superfamily, defense response	–	–	✓	✓	–
MSTRG.86324/ miR444b/TraesCS6D02G273500	Transcription factor, MADS-box, RNA polymerase II transcription	✓	–	✓	✓	–
MSTRG.96918/ miR10516/TraesCS3A02G085200	Leucine-rich repeat domain superfamily, defense response, ADP binding	✓	✓	–	✓	Hvu (88)
MSTRG.22283/miR1127b-3p/TraesCS2B02G527100	Transcription factor IBH1-like, bHLH domain, response to brassinosteroid	✓	✓	–	✓	Hvu (91)
MSTRG.22283/miR1127b-3p/TraesCS3B02G284800	Myc-type, basic helix-loop-helix (bHLH) domain, DNA-binding transcription factor activity	–	–	✓	✓	
MSTRG.75810/miR1120b-3p/TraesCS5B02G204100	SprT-like domain-containing protein Spartan, cellular response to DNA damage stimulus	–	–	✓	✓	–
MSTRG.68371/ miR10519/TraesCS2A02G547200	ATP synthase, F1 complex, alpha subunit, proton-transporting ATP synthase complex	✓	✓	✓	✓	Huv (79), Sbi (78)
lncRNA as miRNA precursor						
MSTRG.90453/ miR1121/TraesCS6D02G273500	Transcription factor, MADS-box, RNA polymerase II transcription	✓	–	–	✓	–
MSTRG.99184/miR1130b-3p/TraesCS2D02G254200	nucleic acid binding; Group II intron splicing, DEAD/DEAH box helicase domain	–	–	✓	✓	–
MSTRG.91287/ miR1128/TraesCS7D02G420400	E3 ubiquitin-protein ligase MBR1/2-like, ubiquitin protein ligase activity	✓	–	–	✓	–

*Wk and Cr, Wyalkatchem and Cranbrook (heat-sensitive cultivars); Yo and Ha, Young and Halberd (heat-tolerant cultivars).
Symbol "-" in column "Cultivars": lncRNA/miRNA/ Protein-coding gene module was not identified in the corresponding Cultivar.
Symbol "-" in the last column: homolog of lncRNA was not found in other plant species.
Symbol "✓" in column "Cultivars": lncRNA/miRNA/Protein-coding gene module was identified in the corresponding Cultivar.

similarity with three upregulated lncRNAs in this study, namely MSTRG.20144, MSTRG.31273, MSTRG.51285, and TapmlnRNA19 demonstrated sequence similarity with the upregulated lncRNAs MSTRG.24647 and MSTRG.38376. We also investigated the potential regulatory function of lncRNAs as either miRNA inhibitors or miRNA precursors during wheat pollen development in response to heat stress. We identified 139 lncRNAs inhibiting 50 miRNAs from 1,216 target protein-coding genes and 25 lncRNAs as the precursor for 11 miRNAs targeting 438 downstream protein-coding genes. Among the predicted miRNAs, there were some known stress-related miRNAs, such as miR1122, miR156, miR159, miR160, miR167, miR399, miR408, and miR444. In several plant species, these miRNAs regulate how plants respond to environmental challenges, including salt, drought, and nutrient deprivation (Islam et al., 2022a; Islam et al., 2022b; Singh et al., 2022). For instance, miR160 controls hormonal signaling pathways in response to salt stress in wheat (Lu et al., 2011) and rice (Barrera-Figueroa et al., 2012). We also discovered interactions between lncRNAs and other miRNAs, such as miR1117, miR1125, miR1130, and miR1135, previously identified in wheat heat shock-treated samples (Kumar et al., 2015). We observed that some of the lncRNA-miRNA-mRNA modules were present across several wheat cultivars, indicating the significance of these molecules during the development of heat-stressed pollen. Some of the such lncRNA-miRNA-mRNA modules were summarized in Table 3. Functional annotation on the miRNA's target protein-coding genes revealed that lncRNAs could regulate various biological processes related to plant stress response, several biosynthetic and metabolic processes, protein modification, and hormonal responses. Our results suggest that heat-responsive lncRNAs could regulate pollen development in wheat through the ceRNA mechanism or by producing miRNAs in post-transcriptional regulation processes.

In conclusion, our study reveals widespread and differential expression of lncRNAs in wheat pollen in response to heat stress. We identified 5,482 heat-responsive lncRNAs in meiosis and tetrad stages of pollen development in four different wheat cultivars. Our analysis suggested that lncRNAs could regulate the expression of their target protein-coding genes through *cis* or *trans*-regulatory mechanisms or through functioning as miRNA sequesters or miRNA precursors. Functional enrichment analysis on the target protein-coding genes of lncRNAs predicted the involvement of lncRNAs in many biological processes, including stress-responsive processes during pollen development in wheat. LncRNAs could regulate biological processes such as response to stress, protein modification, protein folding, hormonal response, and various metabolic and biosynthetic processes. We also noted some heat-responsive lncRNAs correlated with protein-coding genes in two or more different wheat cultivars that could be used for functional experiments in later studies. The present study reveals another layer of complex gene regulatory mechanisms in wheat pollen in response to stress conditions. It provides molecular resources and information for future experiments in this field of research.

Data availability statement

The original contributions presented in the study are included in the article/Supplementary Material. Further inquiries can be directed to the corresponding author.

Author contributions

SB: Methodology, Visualization, Writing – original draft. PB: Conceptualization, Funding acquisition, Project administration, Supervision, Writing – review & editing. MS: Conceptualization, Supervision, Writing – review & editing.

Funding

The author(s) declare that no financial support was received for the research, authorship, and/or publication of this article.

Acknowledgments

We acknowledge the University of Melbourne for supporting SB through a Melbourne Postgraduate Research Scholarship.

Conflict of interest

The authors declare that the research was conducted in the absence of any commercial or financial relationships that could be construed as a potential conflict of interest.

The author(s) declared that they were an editorial board member of Frontiers, at the time of submission. This had no impact on the peer review process and the final decision.

Publisher's note

Supplementary material

The Supplementary Material for this article can be found online at: https://www.frontiersin.org/articles/10.3389/fpls.2024.1344928/full#supplementary-material

References

Alexa, A. R. (2022). topGO: Enrichment Analysis for Gene Ontology. *R package version 2.50.0*. Available at: https://bioconductor.org/packages/topGO.

Asseng, S., Ewert, F., Martre, P., Rötter, R. P., Lobell, D. B., Cammarano, D., et al. (2015). Rising temperatures reduce global wheat production. *Nat. Climate Change* 5 (2), 143–147. doi: 10.1038/nclimate2470

Babaei, S., Singh, M. B., and Bhalla, P. L. (2021). Circular RNAs repertoire and expression profile during Brassica rapa pollen development. *Int. J. Mol. Sci.* 22 (19), 10297. doi: 10.3390/ijms221910297

Babaei, S., Singh, M. B., and Bhalla, P. L. (2022). Role of long non-coding RNAs in rice reproductive development. *Front. Plant Sci.* 13, 1040366. doi: 10.3389/fpls.2022.1040366

Bardou, F., Ariel, F., Simpson, C. G., Romero-Barrios, N., Laporte, P., Balzergue, S., et al. (2014). Long noncoding RNA modulates alternative splicing regulators in Arabidopsis. *Dev. Cell* 30 (2), 166–176. doi: 10.1016/j.devcel.2014.06.017

Barrera-Figueroa, B. E., Gao, L., Wu, Z., Zhou, X., Zhu, J., Jin, H., et al. (2012). High throughput sequencing reveals novel and abiotic stress-regulated microRNAs in the inflorescences of rice. *BMC Plant Biol.* 12 (1), 1–11. doi: 10.1186/1471-2229-12-132

Basharov, M. A. (2003). Protein folding. *J. Cell. Mol. Med.* 7 (3), 223–237. doi: 10.1111/j.1582-4934.2003.tb00223.x

Bhatia, G., Singh, A., Verma, D., Sharma, S., and Singh, K. (2020). Genome-wide investigation of regulatory roles of lncRNAs in response to heat and drought stress in Brassica juncea (Indian mustard). *Environ. Exp. Bot.* 171, 103922. doi: 10.1016/j.envexpbot.2019.103922

Bischof, J. C., and He, X. (2006). Thermal stability of proteins. *Ann. New York Acad. Sci.* 1066 (1), 12–33. doi: 10.1196/annals.1363.003

Bokshi, A. I., Tan, D. K. Y., Thistlethwaite, R. J., Trethowan, R., and Kunz, K. (2021). Impact of elevated CO2 and heat stress on wheat pollen viability and grain production. *Funct. Plant Biol.* 48 (5), 503–514. doi: 10.1071/FP20187

Bokszczanin, K. L.Solanaceae Pollen Thermotolerance Initial Training Network, C, , Fragkostefanakis, S. (2013). Perspectives on deciphering mechanisms underlying plant heat stress response and thermotolerance. *Front. Plant Sci.* 4, 315. doi: 10.3389/fpls.2013.00315

Bray, N. L., Pimentel, H., Melsted, P., and Pachter, L. (2016). Near-optimal probabilistic RNA-seq quantification. *Nat. Biotechnol.* 34 (5), 525–527. doi: 10.1038/nbt.3519

Browne, R. G., Li, S. F., Iacuone, S., Dolferus, R., and Parish, R. W. (2021). Differential responses of anthers of stress tolerant and sensitive wheat cultivars to high temperature stress. *Planta* 254 (1), 4. doi: 10.1007/s00425-021-03656-7

Byeon, B., Bilichak, A., and Kovalchuk, I. (2019). Transgenerational response to heat stress in the form of differential expression of noncoding RNA fragments in Brassica rapa plants. *Plant Genome* 12 (1), 180022. doi: 10.3835/plantgenome2018.04.0022

Chen, H., and Boutros, P. C. (2011). VennDiagram: a package for the generation of highly-customizable Venn and Euler diagrams in R. *BMC Bioinf.* 12 (1), 35. doi: 10.1186/1471-2105-12-35

Chen, S., and Li, H. (2017). Heat stress regulates the expression of genes at transcriptional and post-transcriptional levels, revealed by RNA-seq in Brachypodium distachyon. *Front. Plant Sci.* 7, 2067. doi: 10.3389/fpls.2016.02067

Ding, J., Lu, Q., Ouyang, Y., Mao, H., Zhang, P., Yao, J., et al. (2012). A long noncoding RNA regulates photoperiod-sensitive male sterility, an essential component of hybrid rice. *Proc. Natl. Acad. Sci.* 109 (7), 2654–2659. doi: 10.1073/pnas.1121374109

Ding, H., Mo, S., Qian, Y., Yuan, G., Wu, X., and Ge, C. (2020). Integrated proteome and transcriptome analyses revealed key factors involved in tomato (Solanum lycopersicum) under high temperature stress. *Food Energy Secur.* 9 (4), e239. doi: 10.1002/fes3.239

Dong, B., Zheng, X., Liu, H., Able, J. A., Yang, H., Zhao, H., et al. (2017). Effects of drought stress on pollen sterility, grain yield, abscisic acid and protective enzymes in two winter wheat cultivars. *Front. Plant Sci.* 8, 1008. doi: 10.3389/fpls.2017.01008

Eddy, S. R. (2011). Accelerated profile HMM searches. *PloS Comput. Biol.* 7 (10), e1002195. doi: 10.1371/journal.pcbi.1002195

El-Sappah, A. H., Rather, S. A., Wani, S. H., Elrys, A. S., Bilal, M., Huang, Q., et al. (2022). Heat stress-mediated constraints in maize (Zea mays) production: challenges and solutions. *Front. Plant Sci.* 13. doi: 10.3389/fpls.2022.879366

Fahlgren, N., and Carrington, J. C. (2010). miRNA Target Prediction in Plants. *Methods Mol. Biol.* 592, 51–57. doi: 10.1007/978-1-60327-005-2_4

Fan, Y., Yang, J., Mathioni, S. M., Yu, J., Shen, J., Yang, X., et al. (2016). PMS1T, producing phased small-interfering RNAs, regulates photoperiod-sensitive male sterility in rice. *Proc. Natl. Acad. Sci.* 113 (52), 15144–15149. doi: 10.1073/pnas.1619159114

Farooq, M., Bramley, H., Palta, J. A., and Siddique, K. H. M. (2011). Heat stress in wheat during reproductive and grain-filling phases. *Crit. Rev. Plant Sci.* 30 (6), 491–507. doi: 10.1080/07352689.2011.615687

Franco-Zorrilla, J. M., Valli, A., Todesco, M., Mateos, I., Puga, M. I., Rubio-Somoza, I., et al. (2007). Target mimicry provides a new mechanism for regulation of microRNA activity. *Nat. Genet.* 39 (8), 1033–1037. doi: 10.1038/ng2079

Freeman, M. L., Borrelli, M. J., Meredith, M. J., and Lepock, J. R. (1999). On the path to the heat shock response: destabilization and formation of partially folded protein intermediates, a consequence of protein thiol modification. *Free Radical Biol. Med.* 26 (5-6), 737–745. doi: 10.1016/S0891-5849(98)00258-5

Fu, L., Ding, Z., Tan, D., Han, B., Sun, X., and Zhang, J. (2020). Genome-wide discovery and functional prediction of salt-responsive lncRNAs in duckweed. *BMC Genomics* 21, 1–14. doi: 10.1186/s12864-020-6633-x

Gasparis, S., Przyborowski, M., and Nadolska-Orczyk, A. (2021). Genome-wide identification of barley long noncoding RNAs and analysis of their regulatory interactions during shoot and grain development. *Int. J. Mol. Sci.* 22 (10), 5087. doi: 10.3390/ijms22105087

Gil, N., and Ulitsky, I. (2020). Regulation of gene expression by cis-acting long non-coding RNAs. *Nat. Rev. Genet.* 21 (2), 102–117. doi: 10.1038/s41576-019-0184-5

Golicz, A. A., Allu, A. D., Li, W., Lohani, N., Singh, M. B., and Bhalla, P. L. (2021). A dynamic intron retention program regulates the expression of several hundred genes during pollen meiosis. *Plant Reprod.* 34 (3), 225–242. doi: 10.1007/s00497-021-00411-6

Golicz, A. A., Bhalla, P. L., and Singh, M. B. (2018a). lncRNAs in plant and animal sexual reproduction. *Trends Plant Sci.* 23 (3), 195–205. doi: 10.1016/j.tplants.2017.12.009

Golicz, A. A., Singh, M. B., and Bhalla, P. L. (2018b). The long intergenic noncoding RNA (LincRNA) landscape of the soybean genome. *Plant Physiol.* 176 (3), 2133–2147. doi: 10.1104/pp.17.01657

Gramfort, A., Luessi, M., Larson, E., Engemann, D. A., Strohmeier, D., Brodbeck, C., et al. (2013). MEG and EEG data analysis with MNE-Python. *Front. Neurosci.* 267. doi: 10.3389/fnins.2013.00267

Grammatikakis, I., and Lal, A. (2022). Significance of lncRNA abundance to function. *Mamm. Genome* 33 (2), 271–280. doi: 10.1007/s00335-021-09901-4

Haerizadeh, F., Wong, C. E., Bhalla, P. L., Gresshoff, P. M., and Singh, M. B. (2009). Genomic expression profiling of mature soybean (Glycine max) pollen. *BMC Plant Biol.* 9, 1–12. doi: 10.1186/1471-2229-9-25

He, J., Jiang, Z., Gao, L., You, C., Ma, X., Wang, X., et al. (2019). Genome-wide transcript and small RNA profiling reveals transcriptomic responses to heat stress. *Plant Physiol.* 181 (2), 609–629. doi: 10.1104/pp.19.00403

Herman, A. B., Tsitsipatis, D., and Gorospe, M. (2022). Integrated lncRNA function upon genomic and epigenomic regulation. *Mol. Cell* 82 (12), 2252–2266. doi: 10.1016/j.molcel.2022.05.027

Huang, L., Dong, H., Zhou, D., Li, M., Liu, Y., Zhang, F., et al. (2018). Systematic identification of long non-coding RNA s during pollen development and fertilization in Brassica rapa. *Plant J.* 96 (1), 203–222. doi: 10.1111/tpj.14016

Huang, B., and Xu, C. (2008). Identification and characterization of proteins associated with plant tolerance to heat stress. *J. Integr. Plant Biol.* 50 (10), 1230–1237. doi: 10.1111/j.1744-7909.2008.00735.x

Islam, W., Idrees, A., Waheed, A., and Zeng, F. (2022a). Plant responses to drought stress: microRNAs in action. *Environ. Res.* 215, 114282. doi: 10.1016/j.envres.2022.114282

Islam, W., Tauqeer, A., Waheed, A., and Zeng, F. (2022b). MicroRNA mediated plant responses to nutrient stress. *Int. J. Mol. Sci.* 23 (5), 2562. doi: 10.3390/ijms23052562

Jacob, P., Hirt, H., and Bendahmane, A. (2017). The heat-shock protein/chaperone network and multiple stress resistance. *Plant Biotechnol. J.* 15 (4), 405–414. doi: 10.1111/pbi.12659

Jäger, K., Fábián, A., and Barnabás, B. (2008). Effect of water deficit and elevated temperature on pollen development of drought sensitive and tolerant winter wheat (Triticum aestivum L.) genotypes. *Acta Biologica Szegediensis* 52 (1), 67–71.

Jin, J., Lu, P., Xu, Y., Li, Z., Yu, S., Liu, J., et al. (2021). PLncDB V2. 0: a comprehensive encyclopedia of plant long noncoding RNAs. *Nucleic Acids Res.* 49 (D1), D1489–D1495. doi: 10.1093/nar/gkaa910

Kang, Y.-J., Yang, D.-C., Kong, L., Hou, M., Meng, Y.-Q., Wei, L., et al. (2017). CPC2: a fast and accurate coding potential calculator based on sequence intrinsic features. *Nucleic Acids Res.* 45 (W1), W12–W16. doi: 10.1093/nar/gkx428

Kim, D., Langmead, B., and Salzberg, S. L. (2015). HISAT: a fast spliced aligner with low memory requirements. *Nat. Methods* 12 (4), 357–360. doi: 10.1038/nmeth.3317

Kindgren, P., Ard, R., Ivanov, M., and Marquardt, S. (2018). Transcriptional read-through of the long non-coding RNA SVALKA governs plant cold acclimation. *Nat. Commun.* 9 (1), 4561. doi: 10.1038/s41467-018-07010-6

Kong, L., Zhuo, Y., Xu, J., Meng, X., Wang, Y., Zhao, W., et al. (2022). Identification of long non-coding RNAs and microRNAs involved in anther development in the tropical Camellia oleifera. *BMC Genomics* 23 (1), 596. doi: 10.1186/s12864-022-08836-7

Kozomara, A., and Griffiths-Jones, S. (2010). miRBase: integrating microRNA annotation and deep-sequencing data. *Nucleic Acids Res.* 39 (suppl_1), D152–D157. doi: 10.1093/nar/gkq1027

Kumar, R. R., Goswami, S., Sharma, S. K., Kala, Y. K., Rai, G. K., Mishra, D. C., et al. (2015). Harnessing next generation sequencing in climate change: RNA-Seq analysis of heat stress-responsive genes in wheat (Triticum aestivum L.). *Omics: J. Integr. Biol.* 19 (10), 632–647. doi: 10.1089/omi.2015.0097

Lal, M. K., Tiwari, R. K., Gahlaut, V., Mangal, V., Kumar, A., Singh, M. P., et al. (2021). Physiological and molecular insights on wheat responses to heat stress. *Plant Cell Rep.* 41 (3), 501–518. doi: 10.1007/s00299-021-02784-4

Lamin-Samu, A. T., Zhuo, S., Ali, M., and Lu, G. (2022). Long non-coding RNA transcriptome landscape of anthers at different developmental stages in response to drought stress in tomato. *Genomics* 114 (4), 110383. doi: 10.1016/j.ygeno.2022.110383

Li, C., Lai, X., Yu, X., Xiong, Z., Chen, J., Lang, X., et al. (2023). Plant long noncoding RNAs: Recent progress in understanding their roles in growth, development, and stress responses. *Biochem. Biophys. Res. Commun.* 671, 270–277.

Li, N., Liu, T., Guo, F., Yang, J., Shi, Y., Wang, S., et al. (2022). Identification of long non-coding RNA-microRNA-mRNA regulatory modules and their potential roles in drought stress response in wheat (Triticum aestivum L.). *Front. Plant Sci.* 13. doi: 10.3389/fpls.2022.1011064

Li, J., Ma, W., Zeng, P., Wang, J., Geng, B., Yang, J., et al. (2015). LncTar: a tool for predicting the RNA targets of long noncoding RNAs. *Briefings Bioinf.* 16 (5), 806–812. doi: 10.1093/bib/bbu048

Li, F., Shi, T., He, A., Huang, X., Gong, J., Yi, Y., et al. (2020). Bacillus amyloliquefaciens LZ04 improves the resistance of Arabidopsis thaliana to high calcium stress and the potential role of lncRNA-miRNA-mRNA regulatory network in the resistance. *Plant Physiol. Biochem.* 151, 166–180. doi: 10.1016/j.plaphy.2020.03.022

Lippmann, R., Babben, S., Menger, A., Delker, C., and Quint, M. (2019). Development of wild and cultivated plants under global warming conditions. *Curr. Biol.* 29 (24), R1326–R1338.

Liu, X., Li, D., Zhang, D., Yin, D., Zhao, Y., Ji, C., et al. (2018). A novel antisense long noncoding RNA, TWISTED LEAF, maintains leaf blade flattening by regulating its associated sense R2R3-MYB gene in rice. *New Phytol.* 218 (2), 774–788.

Liu, P., Zhang, Y., Zou, C., Yang, C., Pan, G., Ma, L., et al. (2022). Integrated analysis of long non-coding RNAs and mRNAs reveals the regulatory network of maize seedling root responding to salt stress. *BMC Genomics* 23 (1), 1–16.

Lohani, N., Golicz, A. A., Allu, A. D., Bhalla, P. L., and Singh, M. B. (2023). Genome-wide analysis reveals the crucial role of lncRNAs in regulating the expression of genes controlling pollen development. *Plant Cell Rep.* 42 (2), 337–354. doi: 10.1007/s00299-022-02960-0

Lohani, N., Singh, M. B., and Bhalla, P. L. (2021). RNA-seq highlights molecular events associated with impaired pollen-pistil interactions following short-term heat stress in Brassica napus. *Front. Plant Sci.* 11, 622748. doi: 10.3389/fpls.2020.622748

Lu, W., Li, J., Liu, F., Gu, J., Guo, C., Xu, L., et al. (2011). Expression pattern of wheat miRNAs under salinity stress and prediction of salt-inducible miRNAs targets. *Front. Agric. China* 5, 413–422. doi: 10.1007/s11703-011-1133-z

Luo, D., Ding, Q., Ma, X., Zhu, J., Zou, K., Hong, W., et al. (2023). Proteomic and physiological responses of contrasting two different heat-resistant orchardgrass genotypes to heat stress. *Int. J. Biol. Macromolecules* 245, 125463. doi: 10.1016/j.ijbiomac.2023.125463

Miernyk, J. A. (1999). Protein folding in the plant cell. *Plant Physiol.* 121 (3), 695–703. doi: 10.1104/pp.121.3.695

Nawaz, H., Hussain, N., Yasmeen, A., Rehmani, M. I. A., and Nasrullah, H. M. (2015). Pictorial review of critical stages at vegetative and reproductive growth in wheat for irrigation water regimes. *Appl. Sci. Bus. Econ.* 2, 1–7.

Ohama, N., Sato, H., Shinozaki, K., and Yamaguchi-Shinozaki, K. (2017). Transcriptional regulatory network of plant heat stress response. *Trends Plant Sci.* 22 (1), 53–65. doi: 10.1016/j.tplants.2016.08.015

Pertea, G., and Pertea, M. (2020). GFF utilities: gffRead and gffCompare [version 2; peer review: 3]. *F1000Research* 9, 304. doi: 10.12688/f1000research.23297.1

Pertea, M., Pertea, G. M., Antonescu, C. M., Chang, T.-C., Mendell, J. T., and Salzberg, S. L. (2015). StringTie enables improved reconstruction of a transcriptome from RNA-seq reads. *Nat. Biotechnol.* 33 (3), 290–295. doi: 10.1038/nbt.3122

Ping, J., Huang, S., Wu, J., Bao, P., Su, T., Gu, K., et al. (2021). Association between lincRNA expression and overall survival for patients with triple-negative breast cancer. *Breast Cancer Res. Treat* 186, 769–777. doi: 10.1007/s10549-020-06021-6

Qin, T., Zhao, H., Cui, P., Albesher, N., and Xiong, L. (2017). A nucleus-localized long non-coding RNA enhances drought and salt stress tolerance. *Plant Physiol.* 175 (3), 1321–1336. doi: 10.1104/pp.17.00574

Quinlan, A. R., and Hall, I. M. (2010). BEDTools: a flexible suite of utilities for comparing genomic features. *Bioinformatics* 26 (6), 841–842. doi: 10.1093/bioinformatics/btq033

R Core Team. (2021). *R: A language and environment for statistical computing*. R Foundation for Statistical Computing, Vienna, Austria. Available at: https://www.R-project.org/.

Rinn, J. L., and Chang, H. Y. (2020). Long noncoding RNAs: molecular modalities to organismal functions. *Annu. Rev. Biochem.* 89, 283–308. doi: 10.1146/annurev-biochem-062917-012708

Robinson, M. D., McCarthy, D. J., and Smyth, G. K. (2010). edgeR: a Bioconductor package for differential expression analysis of digital gene expression data. *bioinformatics* 26 (1), 139–140. doi: 10.1093/bioinformatics/btp616

Rutley, N., Poidevin, L., Doniger, T., Tillett, R. L., Rath, A., Forment, J., et al. (2021). Characterization of novel pollen-expressed transcripts reveals their potential roles in pollen heat stress response in Arabidopsis thaliana. *Plant Reprod.* 34, 61–78. doi: 10.1007/s00497-020-00400-1

Saini, H. S., Sedgley, M., and Aspinall, D. (1984). Development anatomy in wheat of male sterility induced by heat stress, water deficit or abscisic acid. *Funct. Plant Biol.* 11 (4), 243–253. doi: 10.1071/PP9840243

Sayols, S. (2020). rrvgo: a Bioconductor package to reduce and visualize Gene Ontology terms. *Aust. Dent. J.* doi: 10.17912/micropub.biology.000811

Shewry, P. R. (2009). Wheat. *J. Exp. Bot.* 60 (6), 1537–1553. doi: 10.1093/jxb/erp058

Sing, T., Sander, O., Beerenwinkel, N., and Lengauer, T. (2005). ROCR: visualizing classifier performance in R. *Bioinformatics* 21 (20), 3940–3941. doi: 10.1093/bioinformatics/bti623

Singh, M. B., and Bhalla, P. L. (2007). Control of male germ-cell development in flowering plants. *Bioessays* 29 (11), 1124–1132. doi: 10.1002/bies.20660

Singh, A., Jain, D., Pandey, J., Yadav, M., Bansal, K. C., and Singh, I. K. (2022). Deciphering the role of miRNA in reprogramming plant responses to drought stress. *Crit. Rev. Biotechnol.* 43 (4), 613–627. doi: 10.1080/07388551.2022.2047880

Singh, M. B., Lohani, N., and Bhalla, P. L. (2021). The role of endoplasmic reticulum stress response in pollen development and heat stress tolerance. *Front. Plant Sci.* 12, 661062. doi: 10.3389/fpls.2021.661062

Sun, L., Luo, H., Bu, D., Zhao, G., Yu, K., Zhang, C., et al. (2013). Utilizing sequence intrinsic composition to classify protein-coding and long non-coding transcripts. *Nucleic Acids Res.* 41 (17), e166–e166. doi: 10.1093/nar/gkt646

Tamura, K., Stecher, G., and Kumar, S. (2021). MEGA11: molecular evolutionary genetics analysis version 11. *Mol. Biol. Evol.* 38 (7), 3022–3027. doi: 10.1093/molbev/msab120

Tarazona, S., Furió-Tarí, P., Turrà, D., Pietro, A. D., Nueda, M. J., Ferrer, A., et al. (2015). Data quality aware analysis of differential expression in RNA-seq with NOISeq R/Bioc package. *Nucleic Acids Res.* 43 (21), e140–e140. doi: 10.1093/nar/gkv711

The Pandas Development Team. (2022). pandas-dev/pandas: pandas. *Zenodo*. doi: 10.5281/zenodo.7344967

Tiwari, S., Jain, M., Singla-Pareek, S. L., Bhalla, P. L., Singh, M. B., and Pareek, A. (2023). Pokkali: A naturally evolved salt-tolerant rice shows a distinguished set of lncRNAs possibly contributing to the tolerant phenotype. *Int. J. Mol. Sci.* 24 (14), 11677. doi: 10.3390/ijms241411677

Urquiaga, M., Thiebaut, F., Hemerly, A. S., and Ferreira, P. C. G. (2021). From trash to luxury: The potential role of plant lncRNA in DNA methylation during abiotic stress. *Front. Plant Sci.* 11, 603246. doi: 10.3389/fpls.2020.603246

Virtanen, P., Gommers, R., Oliphant, T. E., Haberland, M., Reddy, T., Cournapeau, D., et al. (2020). SciPy 1.0: fundamental algorithms for scientific computing in Python. *Nat. Methods* 17 (3), 261–272. doi: 10.1038/s41592-019-0686-2

Wang, P., Dai, L., Ai, J., Wang, Y., and Ren, F. (2019). Identification and functional prediction of cold-related long non-coding RNA (lncRNA) in grapevine. *Sci. Rep.* 9 (1), 6638. doi: 10.1038/s41598-019-43269-5

Wang, L., Park, H. J., Dasari, S., Wang, S., Kocher, J.-P., and Li, W. (2013). CPAT: Coding-Potential Assessment Tool using an alignment-free logistic regression model. *Nucleic Acids Res.* 41 (6), e74–e74. doi: 10.1093/nar/gkt006

Wang, X., Wang, H., Wang, J., Sun, R., Wu, J., Liu, S., et al. (2011). The genome of the mesopolyploid crop species Brassica rapa. *Nat. Genet.* 43 (10), 1035–1039.

Wang, Y., Zhang, H., Li, Q., Jin, J., Chen, H., Zou, Y., et al. (2021). Genome-wide identification of lncRNAs involved in fertility transition in the photo-thermosensitive genic male sterile rice line wuxiang S. *Front. Plant Sci.* 11, 580050. doi: 10.3389/fpls.2020.580050

Warnes, G. R., Bonebakker, L., Gentleman, R., Huber, W., Liaw, A., Lumley, T., et al. (2022). *gplots: Various R Programming Tools for Plotting Data. R package version 3.1.3*. Available at: https://CRAN.R-project.org/package=gplots.

Wickham, H. (2016). *ggplot2: elegant graphics for data analysis* (springer).

Wierzbicki, A., Blevins, T., and Swiezewski, S. (2021). Long noncoding RNAs in plants. *Annu. Rev. Plant Biol.* 72 (1), 245–271. doi: 10.1146/annurev-arplant-093020-035446

Wu, L., Liu, S., Qi, H., Cai, H., and Xu, M. (2020b). Research progress on plant long non-coding RNA. *Plants* 9 (4), 408. doi: 10.3390/plants9040408

Wu, D.-C., Zhu, J.-F., Shu, Z.-Z., Wang, W., Yan, C., Xu, S.-B., et al. (2020a). Physiological and transcriptional response to heat stress in heat-resistant and heat-sensitive maize (Zea mays L.) inbred lines at seedling stage. *Protoplasma* 257, 1615–1637. doi: 10.1007/s00709-020-01538-5

Xiao-Yan, D., Jing-Juan, Y., Qian, Z., Deng-Yun, Z., and Guang-Ming, A. J. J. (2004). Non-coding RNA for ZM401, a pollen-specific gene of Zea mays. *J. Integr. Plant. Biol.* 46 (4), 497. Available at: https://api.semanticscholar.org/CorpusID:53370990.

Xin, M., Wang, Y., Yao, Y., Song, N., Hu, Z., Qin, D., et al. (2011). Identification and characterization of wheat long non-protein coding RNAs responsive to powdery mildew infection and heat stress by using microarray analysis and SBS sequencing. *BMC Plant Biol.* 11, 1–13. doi: 10.1186/1471-2229-11-61

Xu, W., Yang, T., Wang, B., Han, B., Zhou, H., Wang, Y., et al. (2018). Differential expression networks and inheritance patterns of long non-coding RNA s in castor bean seeds. *Plant J.* 95 (2), 324–340. doi: 10.1111/tpj.13953

Yu, Y., Zhang, Y., Chen, X., and Chen, Y. (2019). Plant noncoding RNAs: hidden players in development and stress responses. *Annu. Rev. Cell Dev. Biol.* 35, 407. doi: 10.1146/annurev-cellbio-100818-125218

Zhang, X., Wang, W., Zhu, W., Dong, J., Cheng, Y., Yin, Z., et al. (2019). Mechanisms and functions of long non-coding RNAs at multiple regulatory levels. *Int. J. Mol. Sci.* 20 (22), 5573. doi: 10.3390/ijms20225573

Zhang, Z., Zhong, H., Nan, B., and Xiao, B. (2022). Global identification and integrated analysis of heat-responsive long non-coding RNAs in contrasting rice cultivars. *Theor. Appl. Genet.* 135 (3), 833–852. doi: 10.1007/s00122-021-04001-y

Zhao, X., Yang, J., Li, G., Sun, Z., Hu, S., Chen, Y., et al. (2021). Genome-wide identification and comparative analysis of the WRKY gene family in aquatic plants and their response to abiotic stresses in giant duckweed (Spirodela polyrhiza). *Genomics* 113 (4), 1761–1777. doi: 10.1016/j.ygeno.2021.03.035

Zhao, Z., Zang, S., Zou, W., Pan, Y.-B., Yao, W., You, C., et al. (2022). Long non-coding RNAs: new players in plants. *Int. J. Mol. Sci.* 23 (16), 9301. doi: 10.3390/ijms23169301

Zhu, J.-K. (2016). Abiotic stress signaling and responses in plants. *Cell* 167 (2), 313–324. doi: 10.1016/j.cell.2016.08.029

frontiers | Frontiers in Plant Science

TYPE Original Research
PUBLISHED 08 February 2024
DOI 10.3389/fpls.2024.1355626

OPEN ACCESS

EDITED BY
Yezhang Ding,
Berkeley Lab (DOE), United States

REVIEWED BY
Ming-Bo Wang,
Commonwealth Scientific and Industrial Research Organisation (CSIRO), Australia
Yi Zhai,
Berkeley Lab (DOE), United States

*CORRESPONDENCE
Hidetaka Ito
hito@sci.hokudai.ac.jp

RECEIVED 14 December 2023
ACCEPTED 22 January 2024
PUBLISHED 08 February 2024

CITATION
Niu X, Ge Z and Ito H (2024) Regulatory mechanism of heat-active retrotransposons by the SET domain protein SUVH2.
Front. Plant Sci. 15:1355626.
doi: 10.3389/fpls.2024.1355626

Regulatory mechanism of heat-active retrotransposons by the SET domain protein SUVH2

Xiaoying Niu[1], Zhiyu Ge[1] and Hidetaka Ito[2*]

[1]Graduate School of Life Science, Hokkaido University, Sapporo, Hokkaido, Japan, [2]Faculty of Science, Hokkaido University, Sapporo, Hokkaido, Japan

New transposon insertions are deleterious to genome stability. The RNA-directed DNA methylation (RdDM) pathway evolved to regulate transposon activity via DNA methylation. However, current studies have not yet clearly described the transposition regulation. *ONSEN* is a heat-activated retrotransposon that is activated at 37°C. The plant-specific SUPPRESSOR OF VARIEGATION 3–9 HOMOLOG (SUVH) family proteins function downstream of the RdDM pathway. The SUVH protein families are linked to TE silencing by two pathways, one through DNA methylation and the other through chromatin remodeling. In this study, we analyzed the regulation of *ONSEN* activity by SUVH2. We observed that *ONSEN* transcripts were increased; however, there was no transpositional activity in Arabidopsis *suvh2* mutant. The *suvh2* mutant produced siRNAs from the *ONSEN* locus under heat stress, suggesting that siRNAs are involved in suppressing transposition. These results provide new insights into the regulatory mechanisms of retrotransposons that involve siRNA in the RdDM pathway.

KEYWORDS

epigenetics, transposon, environmental stress, *Arabidopsis thaliana*, *ONSEN*

1 Introduction

Plants and animals must cope with various environmental stressors. Environmental stress can activate transposable elements (TEs), and new insertions are inherited by the next generation of germ cells (Grandbastien et al., 1997; Oliver and Greene, 2009) contributing to genome evolution in plants (Oliver and Greene, 2009; Bennetzen and Wang, 2014). TEs are categorized into two main classes based on their mode of transposition: class I and II transposons (Bourque et al., 2018). Class I transposons are known as retrotransposons, and their transposition activity requires an RNA intermediate. Long terminal repeat (LTR) and non-LTR retrotransposons (long interspersed nuclear elements [LINEs] and short interspersed nuclear elements [SINEs]) are the two main classes of retrotransposons (Wicker et al., 2007). The transposition activity of the LTR retrotransposon begins at the promoter within the 5' LTR, where the TE is first transcribed into RNA by RNA polymerase

II. In the cytoplasm, the RNA is reverse-transcribed into cDNA and reintroduced into the nucleus, and, finally, the cDNA is reincorporated into the host DNA (Havecker et al., 2004). In contrast, most class II elements accomplish transposition activity by excising themselves and thus jumping to a new gene location (Wells and Feschotte, 2020). TEs regulate gene activity by transpositional insertions into or close to genes, manifesting either through the direct disruption of gene transcription or by indirectly affecting gene expression through epigenetic modifications (Niu et al., 2022a; Berthelier et al., 2023).

TEs are regulated through epigenetic modifications, such as two representative epigenetic processes: DNA methylation and histone modification (Lippman et al., 2004; Slotkin and Martienssen, 2007; Mhiri et al., 2022). In plants, *de novo* DNA methylation is induced by RNA-directed DNA methylation (RdDM), mediated by small interfering RNAs (siRNAs) and scaffolding RNAs (Gallego-Bartolome, 2020). RdDM is classified into canonical and non-canonical pathways (Matzke and Mosher, 2014). In the canonical RdDM pathway, Pol IV (RNA polymerase IV) and Pol V (RNA polymerase Pol V) are essential for the RdDM process and serve the production of 24 nt siRNA and long non-coding RNA (lncRNAs) (Onodera et al., 2005; Wierzbicki et al., 2008). Previous reports have shown that there are ten different suppressors of variegation 3–9 homolog (SUVH) family proteins in *Arabidopsis thaliana* (Naumann et al., 2005), of which SUVH2 and SUVH9 are closely associated with DNA methylation activities in RdDM (Johnson et al., 2008). SUVH2 and SUVH9 bind to methylated DNA and promote the recruitment of Pol V to the target locus to produce long non-coding RNAs by interacting with the DDR (DRD1-DMS3-RDM1; defective in RNA-directed DNA methylation 1 [drd1], defective in meristem silencing 3 [DMS3], and RNA-directed DNA methylation 1 [RDM1]) and MORC (microrchidia) complex (Kanno et al., 2004; Johnson et al., 2008; Ream et al., 2009; Law et al., 2010; Zhong et al., 2012; Brabbs et al., 2013; Liu et al., 2014).

ONSEN is an LTR retrotransposon defined in *A. thaliana* and is usually activated by heat stress (Ito et al., 2011). Previous studies have shown that some RdDM pathway mutants subjected to heat stress show transcriptional activation of *ONSEN* (Hayashi et al., 2020; Niu et al., 2022b). siRNAs are involved in transcriptional repression processes, especially in TEs (Moses et al., 2010). In the *nrpd1* mutant (siRNA biogenesis deficient mutant), *ONSEN* transcripts and extrachromosomal DNA levels increased, and transgenerational transposition was observed in the next generation (Ito et al., 2011). However, our understanding of *ONSEN* transposition repression has yet to be profound. This study focused on the contributions of SUVH2 and SUVH9 to the regulatory mechanism of *ONSEN*.

2 Materials and methods

2.1 Plant material

Arabidopsis thaliana accession Columbia (Col-0) was used as a wild-type control. The *suvh2* (*SALK_079574*) and *suvh9* (*SALK_048033*) mutants were obtained from the ABRC stock center, and the *nrpd1* (*C366150*) mutant was obtained from Ohio State University. *Suvh2* mutants were crossed with *suvh9* or *nrpd1* mutants to generate *suvh2/9* and *suvh2/nrpd1* double mutants, respectively. All mutants were of the Col-0 background.

2.2 Growth conditions

Seeds sterilized in a 1:1 solution of sodium hypochlorite and 0.04% Triton X-100 were planted in 0.5× Murashige and Skoog (MS) medium. Seeds were sowed at 4°C (dark conditions) for 2 days and then cultured in 0.5x MS medium or potting (soil: vermiculite = 1:7) at 21°C under continuous light.

2.3 Heat-stress treatment

Seven-day-old seedlings grown in 0.5× MS medium at 21°C under continuous light were subjected to heat stress at 37°C. For Southern blot experiments, we allowed them to recover to 21°C for two days before transferring them to the soil because the 7-day-old plants we analyzed would be weakened if transplanted directly into the soil immediately after heat treatment. Then, the seedlings were transferred to the soil at 21°C under continuous light. Progeny seeds were directly planted in the soil at 21°C under continuous light.

2.4 Southern blotting

DNA was extracted from 3-week-old plants using a Nucleon PhytoPure DNA Extraction Kit (Cytiva, Tokyo, Japan). The 2.4 μg of extracted DNA was processed with the restriction enzyme *EcoR*V overnight at 37°C, and the enzyme-treated DNA was purified by ethanol precipitation. DNA was electrophoresed on a 1% agarose gel for 24 h at 20 V. The DNA was transferred onto a Biodyne B Nylon Membrane (Thermo Fisher Scientific, Waltham, Massachusetts, USA) overnight. PCR product for the probe was generated by TaKaRa Ex Taq (TaKaRa, Kusatsu, Japan). The 577 bp of the predicted ORF of *ONSEN* was used as a probe. The PCR primers are shown in Supplementary Table 1. Hybridization signals were detected in a high SDS hybridization buffer using the Megaprime DNA Labeling System (Cytiva, Tokyo, Japan) with radioisotope-labeled probes.

2.5 Quantitative analysis

For qRT-PCR, total RNA was extracted using the TRI reagent (Sigma-Aldrich, St. Louis, Missouri, USA). After treatment with RQ1 Rnase-Free Dnase (Promega, Madison, Wisconsin, USA), RNA was reverse-transcribed using the ReverTra Ace qPCR RT Kit (TOYOBO, Osaka, Japan) to synthesize cDNA. The total DNA was extracted using the Nucleon PhytoPure DNA Extraction Kit (Cytiva, Tokyo, Japan) for qPCR. The Ct method was used to determine expression, and the expression of the 18S rRNA gene was used as an internal

control (Schmittgen and Livak, 2008). qPCR amplification was performed with the appropriate primers (Supplementary Table 1).

2.6 DNA methylation analysis

The DNA used for bisulfite sequencing was obtained from 7-day-old seedlings. Total DNA was bisulfite-converted and desulfated using a MethylCode Bisulfite Conversion Kit (Invitrogen, Waltham, Massachusetts, USA). The target fragments were amplified by PCR (40 cycles, 98°C for 10 s, 55°C for 30 s, 72°C for 1.5 min), and the PCR products were cloned. PCR amplification was performed with the appropriate primers (Supplementary Table 1). Twenty-four clones were sequenced, and the results were analyzed using the MEGA-X software and the Cymate website to detect DNA methylation levels.

2.7 Formaldehyde-assisted isolation of regulatory elements

Seven-day-old seedlings (0.3 g) were cross-linked in a 1% formaldehyde solution (Thermo Fisher Scientific, Waltham, Massachusetts, USA) under vacuum for 10 min (2 min + 8 min). The cross-linking was quenched by adding glycine at a final concentration of 0.125 M for 5 min under vacuum. The samples were ground to powder with liquid nitrogen, and separation buffer 1 (0.4 M sucrose, 10 mM Tris-HCl, pH 8, 10 mM MgCl2, 5 mM β-mercaptoethanol, and protease inhibitor [Roche, Basel, Switzerland]) was added, followed by filtration using Miracloth (Millipore, Burlington, Massachusetts, USA) to remove cell debris. After centrifugation at 2000 g for 20 min at 4°C, precipitated nuclei were dispersed in isolation buffer 2 (0.25 M sucrose, 10 mM Tris-HCl, pH 8, 10 mM MgCl2, 1% Triton X-100, 5 mM β-mercaptoethanol, and protease inhibitor [Roche, Basel, Switzerland]). After centrifugation at 13,000 rpm for 20 min at 4°C, the precipitated nuclei were re-dispersed in Isolation Buffer 2. Add Isolation Buffer 3 (0.25 M sucrose, 10 mM Tris-HCl, pH 8, 10 mM MgCl2, 1% Triton X-100, 5 mM β-mercaptoethanol, and protease inhibitor [Roche, Basel, Switzerland]) to keep the solution stratified and centrifuge for 60 min at 4°C at 13000 rpm. The precipitates were resuspended using 0.3 mL of SDS nuclear lysis buffer (50 mM Tris-HCl pH 8, 10 mM EDTA, 1% SDS, and protease inhibitor cocktail). The chromatin was sheared using Covaris M220 (Covaris, Woburn, Massachusetts, USA). Suspensions were centrifuged at 13,000 rpm for 10 min at 4°C to obtain a supernatant. DNA was purified using the phenol-chloroform method. The abundance of DNA fragments relative to the input DNA was determined using qPCR. qPCR amplification was performed with the appropriate primers (Supplementary Table 1). For input DNA treatment, 2 μL of supernatant was mixed with 198 μL of extraction buffer (10 mM Tris-HCl pH 8, 0.3 M NaCl, 5 mM EDTA, 0.5% SDS) and incubated overnight at 65°C to reverse formaldehyde cross-linking. The de-crosslinked DNA was purified using the phenol-chloroform method after treatment with Rnase and proteinase K. Input DNA was used as an internal control to identify the non-crosslinked portion of the condensed genomic region (NDR).

2.8 Cytology

The leaves of 7-day-old plants were fixed overnight with ethanol: acetic acid (3:1). Leaves were treated with the enzymes (boehmotoxin [Yakult Pharmaceutical Industries, Yakult Pharmaceutical Industries], pectinase [Kyowa Chemical Products, Tokyo, Japan], and cytochromes [Sigma-Aldrich, St. Louis, Missouri, USA] [1% (v/v) in citrate buffer]) at 37°C for 2 h. The leaves were placed on a slide on a heating plate at 45°C for 30 s, and the leaves were simultaneously torn with a needle to disperse the tissue in 45% acetic acid. After the acetic acid had evaporated, a fixative was added, and the slides were dried. Staining was performed by adding 4′,6-diamidino-2-phenylindole (DAPI) (Vector Laboratories, Newark, California, USA).

2.9 Northern blotting

Total RNA was extracted using the TRI reagent (Sigma-Aldrich, St. Louis, Missouri, USA). Low-molecular-weight RNA was purified by ethanol precipitation and dissolved in 100% formamide. RNA samples (1400ng) were denatured at 65°C for 5 min, and electrophoresis was performed on a 15% PAGE gel in 0.5× TBE buffer, run at 50 V for 20 min to make the dyes move at the same rate, and run at 200 V and 500 mA for 3 h. The RNA was transferred onto a Hybond-N+ hybridization membrane (Sigma-Aldrich, St. Louis, Missouri, USA) overnight and hybridized with a DIG-labeled RNA probe at 40°C overnight. We used synthetic oligonucleotides containing the T7 RNA polymerase promoter and the MRGA shortscript kit for generating probe (Thermo Fisher Scientific, Waltham, Massachusetts, USA). The PCR primers for the probe are shown in Supplementary Table 1. DIG-labeled RNA probes were synthesized using the DIG RNA Labeling Mix (Roche, Basel, Switzerland). Hybridized signals were detected using anti-dig (Roche, Basel, Switzerland) and CDP Star (Roche, Basel, Switzerland) using a LAS3000.

3 Results

3.1 Deletion of SUVH2 results in massive activation of *ONSEN* transcription

We investigated transcript levels and copy numbers (extrachromosomal cDNA levels) of *ONSEN* in WT, *suvh2*, *suvh9*, and *nrpd1*. We observed that after 24 h of heat stress, the transcript level and copy number of *ONSEN* in *suvh2* were significantly increased compared to those in the WT and exhibited approximately the same level as in *nrpd1* (Figures 1A, B), suggesting that deletion of *suvh2* released the transcriptional

10.3389/fpls.2024.1355626

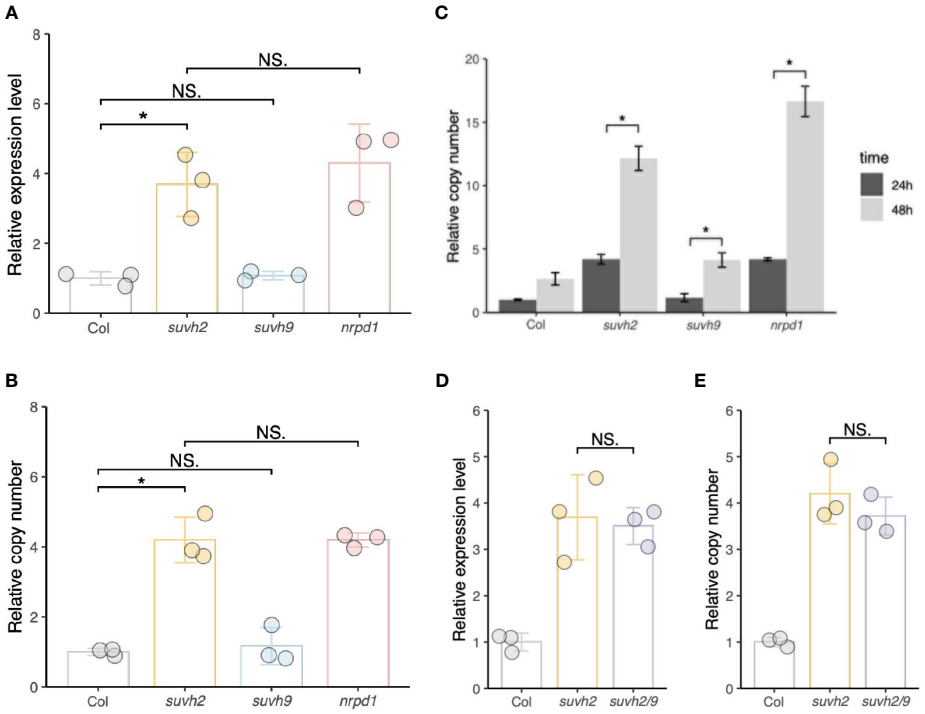

FIGURE 1
SUVH2 is essential for the transcriptional repression of *ONSEN* but not SUVH9. **(A)** and **(B)** Relative expression levels **(A)** and relative copy number **(B)** of *ONSEN* in wild-type, *suvh2*, *suvh9*, and *nrpd1* mutants at 24 h heat stress. **(C)** Relative copy number of *ONSEN* in wild type, *suvh2*, *suvh9*, and *nrpd1* at 24 h and 48 h heat stress. **(D)** and **(E)** Relative expression levels **(D)** and relative copy numbers **(E)** of *ONSEN* in wild-type, *suvh2*, and *suvh2/9* mutants at 24 h heat stress. Asterisks indicate significant differences between the two groups (Student's t-test, P ≤0.05). NS indicates no significant differences between the two groups (Student's t-test, P >0.05).

silencing of *ONSEN*. Consistent with previous findings, 48 h of heat treatment resulted in a further increase in *ONSEN* copy compared with 24 h of heat treatment (Figure 1C). In *suvh9*, *ONSEN* exhibited the same transcript levels and copy number as in the WT (Figures 1A, B). To determine the synergistic effect of SUVH2 and SUVH9 on the RdDM pathway, we investigated the transcript and copy number levels of *ONSEN* in the *suvh2/9* double mutant. However, *ONSEN* did not exhibit higher transcript levels or copy numbers in *suvh2/9* than in *suvh2* (Figures 1D, E), suggesting that SUVH9 was not involved in the transcriptional repression of *ONSEN* by RdDM.

3.2 The transposition of *ONSEN* is infrequent in *suvh2* mutants

To investigate whether the disruption of SUVH2 and SUVH9 affects *ONSEN* transposition, we investigated the transgenerational transposition of *ONSEN* in *suvh2* and *suvh9* mutants. Previous studies have shown that transposition frequency correlates with the duration of heat stress; *suvh2* and *suvh9* were subjected to heat stress for 24 and 48 h, respectively. Southern blot analysis showed that *ONSEN* transposition was observed in the *suvh2* mutant after 48 h of heat stress. In contrast, no transgenerational transposition occurred after 48 h of heat stress in the *suvh9* mutant (Figure 2A). This suggested that SUVH2 regulates *ONSEN* transposition. However, the frequency of *ONSEN* transposition in *suvh2* was much lower than *nrpd1* (Figure 2A). Because SUVH2 and SUVH9 are partially non-redundant in RdDM (Kuhlmann and Mette, 2012), we investigated *ONSEN* transposition in *suvh2/9*. The results showed that no new *ONSEN* insertion was observed in *suvh2/9* after 24 h of heat treatment; however, a new insertion was observed after 48 h of heat stress (Figure 2B). The frequency of *ONSEN* transposition was low in *suvh2/9* cells (Figure 2B), suggesting that SUVH2 and SUVH9 do not synergistically suppress *ONSEN* transposition. No *ONSEN* transposition was observed under heat stress in *suvh9* (Figure 2A), suggesting that SUVH9 was not directly involved in suppressing *ONSEN* transposition. Although *ONSEN* cDNA accumulated in *suvh2* after heat stress, it could not be inserted into new genomic loci. Next, we investigated the activity of *ONSEN* in *suvh2/nrpd1* double mutants. In the *suvh2/nrpd1* double mutant after 24 h of heat treatment, *ONSEN* exhibited a higher transposition frequency than *suvh2* (Figure 2C). However, the transposition frequency is similar to that in *nrpd1* (Figure 2C). Also, we analyzed the transposition and cDNA levels of *ONSEN* in *suvh2/nrpd1* under 48h HS. The results showed that *ONSEN* in *suvh2/nrpd1* after 48h heat treatment showed higher transposition frequency and cDNA levels. The copy number of *ONSEN* was significantly higher in *suvh2/nrpd1* than in *suvh2* or *nrpd1* (Figure 2D). This suggests that SUVH2 and NRPD1 synergistically affect the regulation of *ONSEN* transcription, but not transposition.

10.3389/fpls.2024.1355626

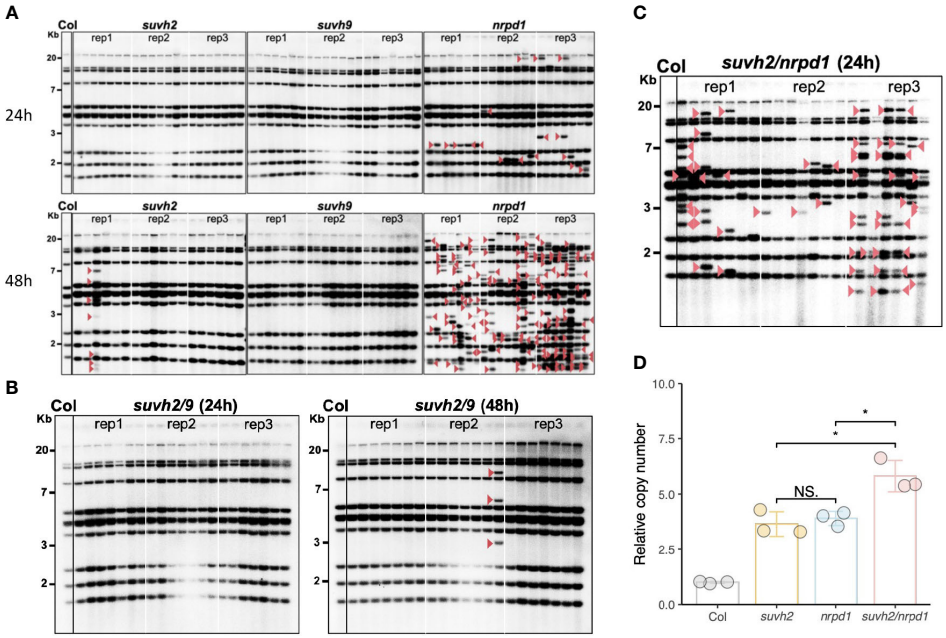

FIGURE 2
In *suvh2* mutants, the frequency of *ONSEN* transposition is low. **(A)** Southern blot results show transgenerational transposition of *ONSEN* in *suvh2*, *suvh9*, and *nrpd1* under heat stress of 24 h (top) or 48 h (bottom). **(B)** New insertions of *ONSEN* in *suvh2/9* under heat stress conditions at 24 h (left) or 48 h (right). The leftmost lane of each graph is the WT under non-stress conditions. For each mutant, three plants were subjected to heat stress (24 h or 48 h), and seven progenies were considered for *ONSEN* transposition analysis. Red arrow head indicates *ONSEN* insertions. **(C)** The next generation of *suvh2/nrpd1* mutants after 24 h heat stress was analyzed by Southern blot to examine the transgenerational transposition of *ONSEN*. The leftmost lane of each graph is the wild type under non-stress conditions. Three homozygous mutant plants were heat stressed, and seven progenies were considered for *ONSEN* transposition analysis for each individual. Red triangles indicate insertions of *ONSEN*. **(D)** Relative copy number of *ONSEN* in wild-type, *suvh2*, *nrpd1*, and *suvh2/nrpd1* under 24 h of heat stress. Asterisks indicate significant differences between the two groups (Student's t-test, P ≤0.05). NS indicates no significant differences between the two groups (Student's t-test, P >0.05).

3.3 DNA hypomethylation was independent of the transposition of *ONSEN* in *suvh2*

SUVH2 and SUVH9 are essential for DNA methylation (Liu et al., 2014). To determine what suppresses *ONSEN* transposition in *suvh2*, we investigated DNA methylation levels of the *ONSEN* in the SUVH mutant. We observed that the level of CHH methylation in *ONSEN* was significantly reduced in *suvh2* compared to WT (Figure 3; Table 1), suggesting that SUVH2 is essential for establishing CHH DNA methylation in *ONSEN*. This result was similar to that obtained for the single-copy SINE *AtSN1* (Johnson et al., 2008). The loss of SUVH2 and SUVH9 resulted in lower CHH methylation levels (Figure 3; Table 1), suggesting that SUVH2 and SUVH9 have synergistic effects in regulating methylation. However, the level of CHH methylation in *ONSEN* was significantly higher in *suvh9* mutants than in the WT (Figure 3; Table 1). The *ONSEN* promoter is present in the LTR region, and DNA methylation is present only in the CHH contexts. The CHH hypermethylation of *ONSEN* in *suvh9* may be responsible for the inability of *ONSEN* to be transcribed at a high level. Heat stress did not change the DNA methylation levels of the *ONSEN* region in *suvh2* (Supplementary Figure 1), which is consistent with our previous findings (Niu et al., 2022b). In addition, the DNA methylation pattern of *ONSEN* in *suvh2* was nearly identical to that of *nrpd1* (Figure 3), indicating that DNA hypomethylation released transcriptional silencing of *ONSEN* but did not affect transposition.

3.4 Chromatin condensation was independent of the activation of *ONSEN*

Chromatin repression causes transgene silencing in a non-DNA methylation-dependent manner. (Mittelsten Scheid et al., 2002). FAIRE-qPCR was used to examine the status of chromatin condensation in the LTR, or gene body region, of *ONSEN*. The levels of open chromatin in the LTR and gene body of *ONSEN* in *suvh2* and *suvh2/9* were much lower than those in *nrpd1* (Figures 4A, B). Since the promoter of *ONSEN* exists within LTRs, we concluded that the open chromatin of *ONSEN* does not directly correlate with the transcriptional repression of *ONSEN*. The open chromatin of the *ONSEN* gene body region appeared to be lower in *suvh2/nrpd1* double mutants than in *nrpd1* (Figure 4B). As heat stress activates *ONSEN*, producing extrachromosomal cDNAs, FAIRE of the *ONSEN* region after heat treatment is challenging. DAPI staining was used to investigate the condensation of heterochromatin in the nuclei of the mutants. We categorized heterochromatin as condensed or dispersed (Figure 4C). Heat stress loosened the heterochromatin; dispersed nuclei showed

10.3389/fpls.2024.1355626

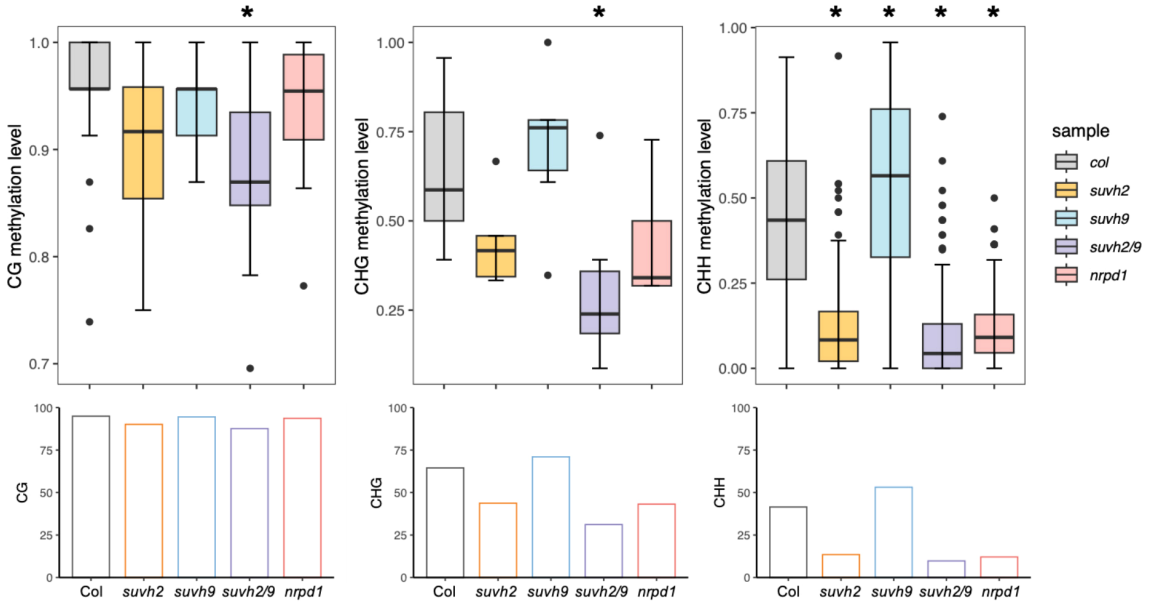

FIGURE 3
SUVH2 is essential for the establishment of DNA methylation on *ONSEN*. Box plots (top) showing CG (left), CHG (middle), and CHH (right, H = A, T, C) methylation levels of *ONSEN* (*At1g11265*) in wild-type, *suvh2*, *suvh9*, *suvh2/9*, and *nrpd1* mutants under non-stress conditions. Bar graphs (bottom) show the average levels of CG (left), CHG (middle), and CHH (right, H = A, T, C) methylation of *ONSEN* in each mutant. Asterisks indicate significant differences compared to Col (Student's t-test, P > 0.05).

TABLE 1 Results of significant difference analysis of methylation data and asterisks indicate significant differences in Figure 3 (Student's t-test, P < 0.05).

	group1	group2	p	p.adj	p.signif
CG	col	*suvh2*	0.0928273	0.62	ns
	col	*suvh9*	0.22078234	0.88	ns
	col	*suvh2/9*	0.00222573	0.022	**
	col	*nrpd1*	0.09985313	0.62	ns
	suvh2	*suvh9*	0.39217267	0.9	ns
	suvh2	*suvh2/9*	0.0886009	0.62	ns
	suvh2	*nrpd1*	0.39921964	0.9	ns
	suvh9	*suvh2/9*	0.00259797	0.023	**
	suvh9	*nrpd1*	0.30059472	0.9	ns
	suvh2/9	*nrpd1*	0.06608209	0.53	ns
	group1	group2	p	p.adj	p.signif
CG	col	*suvh2*	0.0928273	0.62	ns
	col	*suvh9*	0.22078234	0.88	ns
	col	*suvh2/9*	0.00222573	0.022	**
	col	*nrpd1*	0.09985313	0.62	ns
	suvh2	*suvh9*	0.39217267	0.9	ns
	suvh2	*suvh2/9*	0.0886009	0.62	ns
	suvh2	*nrpd1*	0.39921964	0.9	ns

(Continued)

TABLE 1 Continued

	group1	group2	p	p.adj	p.signif
	suvh9	*suvh2/9*	0.00259797	0.023	**
	suvh9	*nrpd1*	0.30059472	0.9	ns
	suvh2/9	*nrpd1*	0.06608209	0.53	ns
	group1	group2	p	p.adj	p.signif
CHH	col	*suvh2*	1.29E-20	7.70E-20	****
	col	*suvh9*	0.00037618	0.0011	***
	col	*suvh2/9*	4.64E-24	3.20E-23	****
	col	*nrpd1*	3.37E-19	1.70E-18	****
	suvh2	*suvh9*	9.21E-29	8.30E-28	****
	suvh2	*suvh2/9*	0.02640555	0.053	*
	suvh2	*nrpd1*	0.46133787	0.46	ns
	suvh9	*suvh2/9*	1.37E-31	1.40E-30	****
	suvh9	*nrpd1*	6.29E-28	5.00E-27	****
	suvh2/9	*nrpd1*	6.29E-05	0.00025	****

Student's t-test, ns means P>0.05, * means P ≤0.05, ** means P ≤0.01, *** means P <0.001, **** means P≤0.0001.

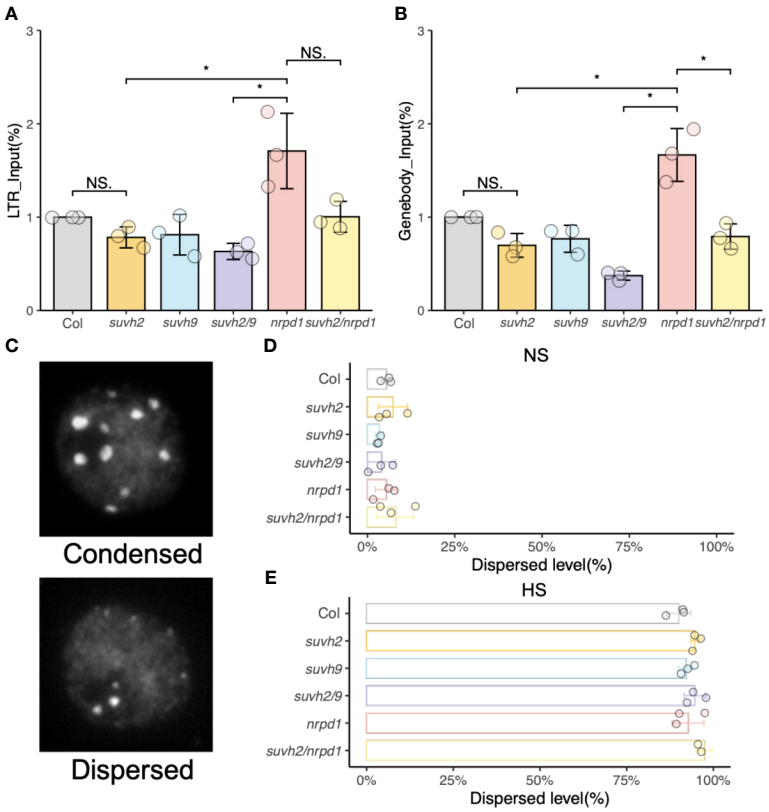

FIGURE 4
Analysis of open chromatin. **(A)** and **(B)** FAIRE-qPCR results show the level of open chromatin in a small region of LTR **(A)** and genebody **(B)** on *ONSEN*. **(C)** Representative images of nuclei under DAPI staining. **(D)** and **(E)** Percentage of chromatin in two (condensed or dispersed) states in wild-type, *suvh2*, *suvh9*, *suvh2/9*, *nrpd1*, and *suvh2/nrpd1* under non-stress (NS) **(C)** and 48 h heat stress (HS) **(D)** (n = 150). Asterisks indicate a significant difference between the two groups (Student's t-test, P <0.05). NS indicates no significant difference between the two groups (Student's t-test, P ≥0.05).

10.3389/fpls.2024.1355626

similar proportions across mutants with or without heat stress treatment (Figures 4D, E). These results imply that the chromatin state may not affect *ONSEN* transcription or transposition.

3.5 The siRNA regulates *ONSEN* transcription and transposition in *suvh2*

Pol IV is a significant factor in siRNA synthesis, and siRNAs are involved in *ONSEN*'s transcriptional repression regulation. Therefore, we explored the siRNA accumulation of *ONSEN* in each mutant. First, we investigated the accumulation of siRNAs in the LTR of *ONSEN* in WT plants under non-stress and heat-stress conditions. The results showed that siRNA was not produced immediately after heat stress and gradually accumulated in recovery at 21 degrees (Figure 5A). siRNA was produced in the WT plants under non-stressed conditions, and the amount of siRNA gradually increased over time (Figure 5A).

Because large amounts of siRNA were not produced immediately after heat stress, we investigated the accumulation levels of siRNA after heat stress and after 7 days of recovery. Accumulation of siRNA was observed in WT, *suvh2*, *suvh9*, and *suvh2/9* plants recovered at 21 degrees for 7 days after both 24-h and 48-h heat treatments (Figure 5B). As expected, we did not detect siRNA production in plants deficient in NRPD1 (Figure 5B). This suggests that the deletion of SUVH2 and/or SUVH9 did not completely disrupt siRNA production, inhibiting *ONSEN* transposition. In contrast, accumulation of siRNAs was observed in *suvh9* without heat stress, whereas siRNAs did not appear in *suvh2* and *suvh2/9* (Figure 5B). Because heat stress did not increase *ONSEN* transcription in *suvh9* (Figure 1A), we suggest that siRNA produced under non-stress conditions may make it difficult for *ONSEN* to be transcribed when subjected to heat stress. Since the deletion of SUVH2 reduced the production of *ONSEN* siRNA under non-stress conditions (Figure 5B), thereby diminishing siRNA involvement in heat stress, which could lead to the disruption of the siRNA-dependent transcriptional repression of *ONSEN*, However, *suvh2* mutant plants under heat stress showed similar amount of siRNAs to WT plants, and we propose that it is precisely the siRNAs produced after heat stress that result in the inhibition of *ONSEN* transposition in *suvh2* mutants (Figure 6).

4 Discussion

RdDM is essential for plant resistance to biotic and abiotic stresses (Erdmann and Picard, 2020). Downstream of the RdDM pathway, SUVH2 and SUVH9 are significant for the association of Pol V with chromatin (Johnson et al., 2014). In this study, we investigated the inhibition of *ONSEN* activity by SUVH2 and SUVH9. Our results show that SUVH2 represses a large amount of *ONSEN* transcription. In contrast, SUVH9 did not transcriptionally repress *ONSEN* (Figure 2A). *AtSN1*, a SINE retrotransposon found in *A. thaliana*, is a model target for studying RdDM and its transcriptional silencing. Liu et al. proposed that SUVH2 and SUVH9 have redundant functions in transcriptional silencing and observed that *AtSN1* expression was increased in the *suvh2/9* double mutant and not in the *suvh2* or *suvh9* single mutant (Liu et al., 2014). This result differed from the expression of *ONSEN*, and we hypothesized that SUVH2 and SUVH9 are partially non-redundant when involved in the transcriptional repression of *ONSEN*. Another possibility is that SUVH9 is not involved in the transcriptional repression of *ONSEN*.

We observed the new *ONSEN* insertions in the progeny of the 48-h heat-stressed *suvh2* (Figure 1A). In contrast, *ONSEN* transposition was suppressed in the plants after 24 h of heat stress (Figure 1A). The copy number of *ONSEN* was not reduced in *suvh2* compared to that in *nrpd1*, in which a high frequency of *ONSEN* transposition occurred (Figures 1A, 2C). This may be due to the post-transcriptional regulation of *ONSEN* in *suvh2*.

SUVH2 and SUVH9 lack the SET post-structural domain, and although they do not have histone methyltransferase activity, they can participate in RdDM by binding methylated DNA through their SET and RING-associated (SAR) domains (Johnson et al., 2008). The level of DNA methylation in the LTR region of *ONSEN* was lost in SUVH2-deficient plants, especially CHH methylation (Figure 3).

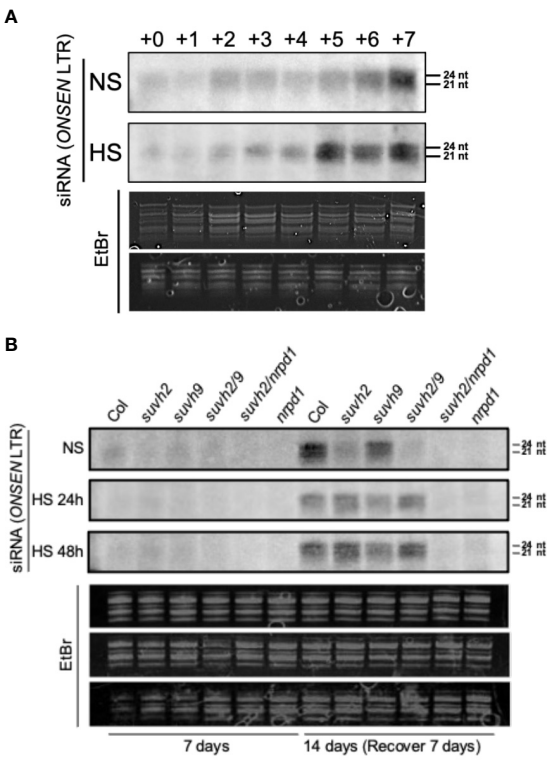

FIGURE 5
Northern blot analysis to investigate siRNA accumulation from the *ONSEN* LTR. **(A)** Levels of siRNA accumulation in WT under non-stress (NS) or heat stress (HS) conditions. The numbers above represent the accumulation levels of siRNAs in one-week-old seedlings placed under non-stress (NS) or heat stress (HS) conditions (37°C) for 24 h (+0) and recovery at normal conditions (21°C) for one day (+1), two days (+2)...seven days (+7) after heat stress treatment. **(B)** Accumulation levels of siRNAs in wild-type, *suvh2*, *suvh9*, *suvh2/9*, *nrpd1*, and *suvh2/nrpd1* in 7-week-old seedlings treated with non-stress (NS) or heat stress (HS) (24 h or 48 h) and recovered at normal conditions (21°C) for seven days (+7) after treatment.

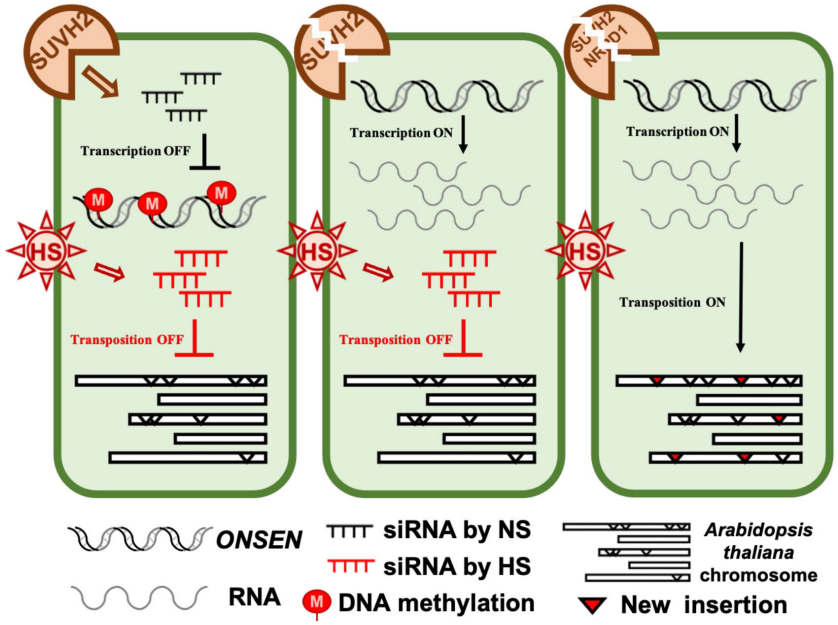

FIGURE 6
The model of SUVH2 involves *ONSEN* regulation. In the wild-type, intact RdDM can produce siRNAs to suppress *ONSEN* transcription. In the *suvh2* mutant, the RdDM pathway is disrupted, releasing *ONSEN* transcription by heat stress. Under heat stress, plants bypass the SUVH2-dependent pathway to produce new siRNAs, and these siRNAs produced by heat stress prevent *ONSEN* from transposing into other sites on the chromosome. In the *suvh2/nrpd1* double mutant, siRNA could not be synthesized under heat stress conditions releasing of transpositional silencing of *ONSEN*.

A related report on SDC showed that a lack of either *suvh2* or *suvh9* results in the loss of CHH methylation (Johnson et al., 2008). This contrasts with our finding that there was a slight increase instead of a decrease in DNA methylation in the *ONSEN* region of *suvh9* (Figure 3). The high DNA methylation level of *ONSEN* in *suvh9* is responsible for its low transcriptional activity. *ONSEN* showed a similar pattern of DNA methylation in *suvh2* and *nrpd1* (Figure 3). In conclusion, we suggest that the transcriptional activity of *ONSEN* depends on the level of DNA methylation.

Heterochromatin is enriched with transposable elements (Marsano and Dimitri, 2022). Although chromatin accessibility is associated with establishing DNA methylation (Zhong et al., 2021), it has been suggested that chromatin remodeling factors may occur independently of the DNA methylation process. For example, Morpheus Molecue 1 (MOM1) is required to silence repetitive heterochromatin sequences and is involved in epigenetic modification in a DNA methylation-independent manner (Amedeo et al., 2000). Similarly, AtMORC1 and AtMORC6 are involved in the RdDM pathway by controlling the decondensation of heterochromatin around filaments and not through DNA methylation (Moissiard et al., 2012). Jing et al. identified SUVH9 as a linker between MORC-mediated chromatin remodeling (Jing et al., 2016). We speculated that SUVH9 might be involved in silencing *ONSEN* via a non-DNA methylation pathway. Deletion of SUVH2 and/or SUVH9 did not result in open chromatin in the *ONSEN* LTR or gene body (Figures 4A, B). SUVH9 plays a minimal role in *ONSEN* silencing. In addition, the results of DAPI staining suggested that heat stress leads to the decondensation of heterochromatin. However, heat-induced decondensation of heterochromatin was not *nprd1* mutant-specific (Figures 4D, E). These results suggest that heterochromatin decondensation does not directly affect the transgenerational transposition of *ONSEN*. Open chromatin may be essential for transposition activity. However, it has been challenging to determine open chromatin in the promoter region of *ONSEN* under HS because of the presence of cDNA made from *ONSEN*. Whether open chromatin is required for *ONSEN* insertion is also considered, and information on the insertion site is needed. Previous studies have shown that *ONSEN* in *nrpd1* mutants exhibits random insertions (Ito et al., 2016). Investigating the open chromatin of heat-stressed random insertion sites is a challenge.

siRNAs are closely associated with gene silencing (Hamilton et al., 2002). *Pol IV* transcribes TE- and repeat-related genes as primary transcripts that are loaded by RDR2 (RNA-dependent RNA polymerase 2), DCL3 (Dicer-like 3), and AGO4 (ARGONAUTE 4) proteins to produce siRNAs (Ferrafiat et al., 2019). Transgenerational transposition of *ONSEN* often occurs in *nrpd1* mutants (Ito et al., 2011; Ito et al., 2016). Northern blot analysis showed that, although *ONSEN* siRNAs were not observed in *suvh2* and *suvh2/9* under non-stress conditions, new siRNAs were synthesized after heat stress (Figure 5B). In contrast, deletion of SUVH9 did not disrupt siRNA synthesis under non-stress or heat-stress conditions. This indicated that the absence of SUVH2 affected the siRNA synthesis activity of *ONSEN*.

In conclusion, our results showed that SUVH2 is involved in the transcriptional silencing of *ONSEN* in a siRNA pathway-dependent manner. We provide evidence that SUVH2 and SUVH9 are functionally non-redundant when involved in regulating retrotransposon activity. In addition, plants can adapt their protective mechanisms to cope with the possibility of genetic disruption resulting from adversity.

Data availability statement

The original contributions presented in the study are included in the article/Supplementary Material. Further inquiries can be directed to the corresponding author.

Author contributions

XN: Writing – original draft. ZG: Writing – original draft. HI: Writing – original draft, Writing – review & editing.

Funding

The author(s) declare financial support was received for the research, authorship, and/or publication of this article. This work was supported by JSPS Grant-in-Aid for Scientific Research C (21K06008), JSPS Fund for the Promotion of Joint International Research A (Fostering Joint International Research A) (21KK0263), and Hokkaido University Ambitious Doctoral Fellowship.

Acknowledgments

We would like to thank Dr. Yoko Ikeda for her assistance in FAIRE analysis, Mr. Yusuke Nakada for his technical advice in Northern blotting, and Dr. Leandro Quadrana for his comments on transposition analysis.

Conflict of interest

The authors declare that the research was conducted in the absence of any commercial or financial relationships that could be construed as a potential conflict of interest.

Publisher's note

Supplementary material

The Supplementary Material for this article can be found online at: https://www.frontiersin.org/articles/10.3389/fpls.2024.1355626/full#supplementary-material

References

Amedeo, P., Habu, Y., Afsar, K., Mittelsten Scheid, O., and Paszkowski, J. (2000). Disruption of the plant gene MOM releases transcriptional silencing of methylated genes. *Nature* 405 (6783), 203–206. doi: 10.1038/35012108

Bennetzen, J. L., and Wang, H. (2014). The contributions of transposable elements to the structure, function, and evolution of plant genomes. *Annu. Rev. Plant Biol.* 65, 505–530. doi: 10.1146/annurev-arplant-050213-035811

Berthelier, J., Furci, L., Asai, S., Sadykova, M., Shimazaki, T., Shirasu, K., et al. (2023). Long-read direct RNA sequencing reveals epigenetic regulation of chimeric gene-transposon transcripts in *Arabidopsis thaliana*. *Nat. Commun.* 14 (1), 3248. doi: 10.1038/s41467-023-38954-z

Bourque, G., Burns, K. H., Gehring, M., Gorbunova, V., Seluanov, A., Hammell, M., et al. (2018). Ten things you should know about transposable elements. *Genome Biol.* 19 (1), 199. doi: 10.1186/s13059-018-1577-z

Brabbs, T. R., He, Z., Hogg, K., Kamenski, A., Li, Y., Paszkiewicz, K. H., et al. (2013). The stochastic silencing phenotype of Arabidopsis morc6 mutants reveals a role in efficient RNA-directed DNA methylation. *Plant J.* 75 (5), 836–846. doi: 10.1111/tpj.12246

Erdmann, R. M., and Picard, C. L. (2020). RNA-directed DNA methylation. *PloS Genet.* 16 (10), e1009034. doi: 10.1371/journal.pgen.1009034

Ferrafiat, L., Pflieger, D., Singh, J., Thieme, M., Bohrer, M., Himber, C., et al. (2019). The NRPD1 N-terminus contains a Pol IV-specific motif that is critical for genome surveillance in Arabidopsis. *Nucleic Acids Res.* 47 (17), 9037–9052. doi: 10.1093/nar/gkz618

Gallego-Bartolome, J. (2020). DNA methylation in plants: mechanisms and tools for targeted manipulation. *New Phytol.* 227 (1), 38–44. doi: 10.1111/nph.16529

Grandbastien, M. A., Lucas, H., Morel, J. B., Mhiri, C., Vernhettes, S., and Casacuberta, J. M. (1997). The expression of the tobacco Tnt1 retrotransposon is linked to plant defense responses. *Genetica* 100 (1-3), 241–252. doi: 10.1007/978-94-011-4898-6_24

Hamilton, A., Voinnet, O., Chappell, L., and Baulcombe, D. (2002). Two classes of short interfering RNA in RNA silencing. *EMBO J.* 21 (17), 4671–4679. doi: 10.1093/emboj/cdf464

Havecker, E. R., Gao, X., and Voytas, D. F. (2004). The diversity of LTR retrotransposons. *Genome Biol.* 5 (6), 225. doi: 10.1186/gb-2004-5-6-225

Hayashi, Y., Takehira, K., Nozawa, K., Suzuki, T., Masuta, Y., Kato, A., et al. (2020). ONSEN shows different transposition activities in RdDM pathway mutants. *Genes Genet. Syst.* 95 (4), 183–190. doi: 10.1266/ggs.20-00019

Ito, H., Gaubert, H., Bucher, E., Mirouze, M., Vaillant, I., and Paszkowski, J. (2011). An siRNA pathway prevents transgenerational retrotransposition in plants subjected to stress. *Nature* 472 (7341), 115–U151. doi: 10.1038/Nature09861

Ito, H., Kim, J. M., Matsunaga, W., Saze, H., Matsui, A., Endo, T. A., et al. (2016). A stress-activated transposon in arabidopsis induces transgenerational abscisic acid insensitivity. *Sci. Rep.* 6. doi: 10.1038/Srep23181

Jing, Y., Sun, H., Yuan, W., Wang, Y., Li, Q., Liu, Y., et al. (2016). SUVH2 and SUVH9 couple two essential steps for transcriptional gene silencing in arabidopsis. *Mol. Plant* 9 (8), 1156–1167. doi: 10.1016/j.molp.2016.05.006

Johnson, L. M., Du, J., Hale, C. J., Bischof, S., Feng, S., Chodavarapu, R. K., et al. (2014). SRA- and SET-domain-containing proteins link RNA polymerase V occupancy to DNA methylation. *Nature* 507 (7490), 124–128. doi: 10.1038/nature12931

Johnson, L. M., Law, J. A., Khattar, A., Henderson, I. R., and Jacobsen, S. E. (2008). SRA-domain proteins required for DRM2-mediated *de novo* DNA methylation. *PloS Genet.* 4 (11), e1000280. doi: 10.1371/journal.pgen.1000280

Kanno, T., Mette, M. F., Kreil, D. P., Aufsatz, W., Matzke, M., and Matzke, A. J. (2004). Involvement of putative SNF2 chromatin remodeling protein DRD1 in RNA-directed DNA methylation. *Curr. Biol.* 14 (9), 801–805. doi: 10.1016/j.cub.2004.04.037

Kuhlmann, M., and Mette, M. F. (2012). Developmentally non-redundant SET domain proteins SUVH2 and SUVH9 are required for transcriptional gene silencing in *Arabidopsis thaliana*. *Plant Mol. Biol.* 79 (6), 623–633. doi: 10.1007/s11103-012-9934-x

Law, J. A., Ausin, I., Johnson, L. M., Vashisht, A. A., Zhu, J. K., Wohlschlegel, J. A., et al. (2010). A protein complex required for polymerase V transcripts and RNA-directed DNA methylation in Arabidopsis. *Curr. Biol.* 20 (10), 951–956. doi: 10.1016/j.cub.2010.03.062

Lippman, Z., Gendrel, A. V., Black, M., Vaughn, M. W., Dedhia, N., McCombie, W. R., et al. (2004). Role of transposable elements in heterochromatin and epigenetic control. *Nature* 430 (6998), 471–476. doi: 10.1038/nature02651

Liu, Z. W., Shao, C. R., Zhang, C. J., Zhou, J. X., Zhang, S. W., Li, L., et al. (2014). The SET domain proteins SUVH2 and SUVH9 are required for Pol V occupancy at RNA-directed DNA methylation loci. *PloS Genet.* 10 (1), e1003948. doi: 10.1371/journal.pgen.1003948

Marsano, R. M., and Dimitri, P. (2022). Constitutive heterochromatin in eukaryotic genomes: A mine of transposable elements. *Cells* 11 (5), 761. doi: 10.3390/cells11050761

Matzke, M. A., and Mosher, R. A. (2014). RNA-directed DNA methylation: an epigenetic pathway of increasing complexity. *Nat. Rev. Genet.* 15 (6), 394–408. doi: 10.1038/nrg3683

Mhiri, C., Borges, F., and Grandbastien, M. A. (2022). Specificities and dynamics of transposable elements in land plants. *Biol. (Basel)* 11 (4), 488. doi: 10.3390/biology11040488

Mittelsten Scheid, O., Probst, A. V., Afsar, K., and Paszkowski, J. (2002). Two regulatory levels of transcriptional gene silencing in Arabidopsis. *Proc. Natl. Acad. Sci. U.S.A.* 99 (21), 13659–13662. doi: 10.1073/pnas.202380499

Moissiard, G., Cokus, S. J., Cary, J., Feng, S., Billi, A. C., Stroud, H., et al. (2012). MORC family ATPases required for heterochromatin condensation and gene silencing. *Science* 336 (6087), 1448–1451. doi: 10.1126/science.1221472

Moses, J., Goodchild, A., and Rivory, L. P. (2010). Intended transcriptional silencing with siRNA results in gene repression through sequence-specific off-targeting. *RNA* 16 (2), 430–441. doi: 10.1261/rna.1808510

Naumann, K., Fischer, A., Hofmann, I., Krauss, V., Phalke, S., Irmler, K., et al. (2005). Pivotal role of AtSUVH2 in heterochromatic histone methylation and gene silencing in Arabidopsis. *EMBO J.* 24 (7), 1418–1429. doi: 10.1038/sj.emboj.7600604

Niu, C., Jiang, L., Cao, F., Liu, C., Guo, J., Zhang, Z., et al. (2022a). Methylation of a MITE insertion in the MdRFNR1-1 promoter is positively associated with its allelic expression in apple in response to drought stress. *Plant Cell* 34 (10), 3983–4006. doi: 10.1093/plcell/koac220

Niu, X., Chen, L., Kato, A., and Ito, H. (2022b). Regulatory mechanism of a heat-activated retrotransposon by DDR complex in *Arabidopsis thaliana*. *Front. Plant Sci.* 13. doi: 10.3389/fpls.2022.1048957

Oliver, K. R., and Greene, W. K. (2009). Transposable elements: powerful facilitators of evolution. *Bioessays* 31 (7), 703–714. doi: 10.1002/bies.200800219

Onodera, Y., Haag, J. R., Ream, T., Costa Nunes, P., Pontes, O., and Pikaard, C. S. (2005). Plant nuclear RNA polymerase IV mediates siRNA and DNA methylation-dependent heterochromatin formation. *Cell* 120 (5), 613–622. doi: 10.1016/j.cell.2005.02.007

Ream, T. S., Haag, J. R., Wierzbicki, A. T., Nicora, C. D., Norbeck, A. D., Zhu, J. K., et al. (2009). Subunit compositions of the RNA-silencing enzymes Pol IV and Pol V reveal their origins as specialized forms of. *Mol. Cell* 33 (2), 192–203. doi: 10.1016/j.molcel.2008.12.015

Schmittgen, T., and Livak, K. (2008). Analyzing real-time PCR data by the comparative CT method. *Nat. Protoc.* 3, 1101–1108. doi: 10.1038/nprot.2008.73

Slotkin, R. K., and Martienssen, R. (2007). Transposable elements and the epigenetic regulation of the genome. *Nat. Rev. Genet.* 8 (4), 272–285. doi: 10.1038/nrg2072

Wells, J. N., and Feschotte, C. (2020). A field guide to eukaryotic transposable elements. *Annu. Rev. Genet.* 23 (54), 539–561. doi: 10.1146/annurev-genet-040620-022145

Wicker, T., Sabot, F., Hua-Van, A., Bennetzen, J. L., Capy, P., Chalhoub, B., et al. (2007). A unified classification system for eukaryotic transposable elements. *Nat. Rev. Genet.* 8 (12), 973–982. doi: 10.1038/nrg2165

Wierzbicki, A. T., Haag, J. R., and Pikaard, C. S. (2008). Noncoding transcription by RNA polymerase Pol IVb/Pol V mediates transcriptional silencing of overlapping and adjacent genes. *Cell* 135 (4), 635–648. doi: 10.1016/j.cell.2008.09.035

Zhong, X., Hale, C. J., Law, J. A., Johnson, L. M., Feng, S., Tu, A., et al. (2012). DDR complex facilitates global association of RNA polymerase V to promoters and evolutionarily young transposons. *Nat. Struct. Mol. Biol.* 19 (9), 870–875. doi: 10.1038/nsmb.2354

Zhong, Z., Feng, S., Duttke, S. H., Potok, M. E., Zhang, Y., Gallego-Bartolome, J., et al. (2021). DNA methylation-linked chromatin accessibility affects genomic architecture in Arabidopsis. *Proc. Natl. Acad. Sci. U.S.A.* 118 (5). doi: 10.1073/pnas.2023347118

frontiers | Frontiers in Plant Science

TYPE Original Research
PUBLISHED 11 March 2024
DOI 10.3389/fpls.2024.1355518

OPEN ACCESS

EDITED BY
Mehanathan Muthamilarasan,
University of Hyderabad, India

REVIEWED BY
Reiaz Ul Rehman,
University of Kashmir, India
Xiaoli Fan,
Chinese Academy of Sciences (CAS), China

*CORRESPONDENCE
Xiangyang Yuan
Yuanxiangyang200@163.com
Meiqiang Yin
yinmq999@163.com

†These authors share first authorship

RECEIVED 14 December 2023
ACCEPTED 14 February 2024
PUBLISHED 11 March 2024

CITATION
Wen Y, Cheng L, Zhao Z, An M, Zhou S, Zhao J, Dong S, Yuan X and Yin M (2024) Transcriptome and co-expression network revealed molecular mechanism underlying selenium response of foxtail millet (*Setaria italica*). *Front. Plant Sci.* 15:1355518. doi: 10.3389/fpls.2024.1355518

Transcriptome and co-expression network revealed molecular mechanism underlying selenium response of foxtail millet (*Setaria italica*)

Yinyuan Wen[1†], Liuna Cheng[1,2†], Zeya Zhao[1,2], Mengyao An[1], Shixue Zhou[1], Juan Zhao[1], Shuqi Dong[1], Xiangyang Yuan[1*] and Meiqiang Yin[1,2*]

[1]College of Agronomy, Shanxi Agricultural University, Jinzhong, China, [2]Ministerial and Provincial Co-Innovation Centre for Endemic Crops Production with High-quality and Effciency in Loess Plateau, Jinzhong, China

Introduction: Selenium-enriched foxtail millet (*Setaria italica*) represents a functional cereal with significant health benefits for humans. This study endeavors to examine the impact of foliar application of sodium selenite (Na_2SeO_4) on foxtail millet, specifically focusing on selenium (Se) accumulation and transportation within various plant tissues.

Methods: To unravel the molecular mechanisms governing selenium accumulation and transportation in foxtail millet, we conducted a comprehensive analysis of selenium content and transcriptome responses in foxtail millet spikelets across different days (3, 5, 7, and 12) under Na_2SeO_4 treatment (200 μmol/L).

Results: Foxtail millet subjected to selenium fertilizer exhibited significantly elevated selenium levels in each tissue compared to the untreated control. Selenate was observed to be transported and accumulated sequentially in the leaf, stem, and spikes. Transcriptome analysis unveiled a substantial upregulation in the transcription levels of genes associated with selenium metabolism and transport, including sulfate, phosphate, and nitrate transporters, ABC transporters, antioxidants, phytohormone signaling, and transcription factors. These genes demonstrated intricate interactions, both synergistic and antagonistic, forming a complex network that regulated selenate transport mechanisms. Gene co-expression network analysis highlighted three transcription factors in the tan module and three transporters in the turquoise module that significantly correlated with selenium accumulation and transportation. Expression of sulfate transporters (SiSULTR1.2b and SiSULTR3.1a), phosphate transporter (PHT1.3), nitrate transporter 1 (NRT1.1B), glutathione S-transferase genes (GSTs), and ABC transporter (ABCC13) increased with SeO_4^{2-} accumulation. Transcription factors MYB, WRKY, and bHLH were also identified as players in selenium accumulation.

Conclusion: This study provides preliminary insights into the mechanisms of selenium accumulation and transportation in foxtail millet. The findings hold theoretical significance for the cultivation of selenium-enriched foxtail millet.

KEYWORDS

foxtail millet, Selenium biofortification, RNA-sequencing, WGCNA, sulfate transporters, phytohormones

1 Introduction

Selenium (Se), an essential trace element in the human body (Kieliszek, 2019), is crucial for forming the active site of glutathione peroxidase as selenocysteine. Its nutritional and health benefits include antioxidant, anti-tumor, anti-aging, radiation protection, antiviral effects, visual protection, and immune enhancement (Bjørklund et al., 2022), earning it the moniker "king of anticancer among trace elements" among trace elements in the human body. Se deficiency may result in various diseases such as Kaschin–Beck disease, chronic degenerative diseases, and skeletal muscle myopathy, potentially contributing to cancer and immune dysfunction (Zhang et al., 2022). A belt of Se deficiency exists in the Northern and Southern Hemispheres, involving over 40 countries and approximately one billion people, particularly in China, Africa, India, and Eastern Europe (Gao et al., 2011). As the human body cannot synthesize Se, dietary supplementation is the safest way to meet Se requirements (Rider et al., 2010). Utilizing biofortification techniques to enhance the nutritional value of staple crops is a cost-effective and feasible approach to mitigate micronutrient deficiencies (Ingle et al., 2023). Foxtail millet, rich in carbohydrates, proteins, fatty acids, vitamins, and minerals, is considered one of the most important nutritional cereals (Xiang et al., 2019), and its biofortification significantly contributes to nutritional security (Kaur et al., 2019). Biofortification with Se, effectively increasing the Se content of edible crops, has gained attention. Compared to soil application, foliar Se biofortification is more efficient and environmentally friendly, easily absorbed through leaves, and accumulates in the plant (Gao et al., 2023).

As a result of the chemical analogy of selanate/selenite with sulphate and phosphate, their behavior in metabolism and transport in plants is closely related (Raina et al., 2021). selenite may be transported through phosphate transporters and selenate through sulfate transporters (Mushtaq et al., 2022). Plants primarily absorb selenate (SeO_4^{2-}) or selenite (SeO_3^{2-}) through specific or non-specific Se transportation proteins, but not insoluble elemental Se (Se^0) or metal selenides (White and Broadley, 2009). Selenium is subsequently transformed into organic forms such as selenocysteine, selenomethionine, and other methylated derivatives (Holben and Smith, 1999). SeO_4^{2-} uptake in higher plants mainly occurs via sulfate transport, which is incorporated into the plant through the sulfur assimilation pathway (El Mehdawi et al., 2018). The complex mechanism of SeO_3^{2-} accumulation and transportation in plants remains unclear. Phosphate transporters (OsPHT1.2 and OsPHT1.8) and the aquaporin NIP2;1 in rice participate in SeO_3^{2-} accumulation and transportation (Li et al., 2008; Zhao et al., 2010; Zhang et al., 2014). The nitrate transporter (NRT1.1B) promotes the transport of selenomethionine (SeMet) in rice (Zhang et al., 2019). ABC transporters may also be involved in Se absorption and transport in plants. ABCC11, ABCC13, and ABCC10 are implicated in the accumulation and transportation of nanoselenium in cowpeas, regulating Se absorption and transformation (Li et al., 2023). Studies indicate that Se may regulate the expression levels of GSTs, affecting transcription factor activity or participating in signal transduction pathways (Zheng et al., 2023).

Compared with Arabidopsis and rice, research on the mechanism of Se transportation in foxtail millet is limited. This study aimed to investigate the effects of foliar spraying of sodium selenite (Na_2SeO_4) on foxtail millet (Setaria italica) concerning selenium (Se) accumulation and transportation within different plant tissues. Specific focus was given to the dynamics of Se content, RNA expression patterns, identification of differentially expressed genes (DEGs), functional annotations related to Se transport, and the role of various transporters, hormones, antioxidants, and transcription factors in Se accumulation. A detailed RNA-Seq analysis of the head stage of foxtail millet using selenium and water sprays was conducted, alongside the measurement of Se content in each foxtail millet tissue. These data offer a comprehensive system-level view of dynamic gene expression networks and their potential roles in Se accumulation and transportation. Using pairwise comparisons and weighted gene co-expression network analysis (WGCNA), candidate hub gene modules were identified. Through WGCNA, co-expressed gene modules were constructed, and a correlation analysis with selenium content data identified key modules related to selenium accumulation and transportation. Hub genes within these modules associated with Se accumulation and transportation were subsequently identified.

Abbreviations: WGCNA, Weighted Gene Co-expression Network Analysis; PCA, principal component analysis; DEG, differentially expressed genes; FPKM, fragments per kilobase of transcript per million mapped reads; GO, Gene Ontology; KEGG, Kyoto Encyclopedia of Genes and Genomes.

2 Materials and methods

2.1 Plant materials and treatments

Jingu 21 foxtail millet served as the test material. Field experiments were conducted from May to October 2022 at the Shanxi Agricultural University experimental station (Shenfeng Village, Taigu County, Jinzhong City, Shanxi Province, China). The experiment was performed using a completely randomized design with three replicates. Square plots, 25 m^2 in size, were used with 35-cm row spacing and 8 cm plant spacing. Nitrogen (150 $kg{\cdot}hm^{-2}$ of N), phosphorus (90 $kg{\cdot}hm^{-2}$ of P_2O_5), and Potassium (120 $kg{\cdot}hm^{-2}$ K_2O) fertilizers were applied before sowing. Local production recommendations were used in management of crops in the field. During the heading stage, we applied a foliar spray of 200 μmol/L Na_2SeO_4 for selenium treatment, while the control group received an equivalent volume of water (75 mL/m^2). Whole healthy roots, stems, functional leaves, stalks of spikelets, and spikes, along with seeds at the filling stage (S1-S5) (He et al., 2022), were collected on the 3rd, 5th, 7th, and 12th days of treatment. Each treatment comprised three biological replicates. For transcriptome analysis, spikes were collected, swiftly frozen in liquid nitrogen, and preserved at -80°C for subsequent physiological evaluations, RNA extraction, and gene expression analysis.

2.2 Foxtail millet selenium content measurement

We measured approximately 0.3 g of the sample (accurate to 0.0001 g) and placed it in a digestion tube. Subsequently, we introduced 6 mL of nitric acid and 2 mL of hydrogen peroxide into the tube, which was then sealed using a microwave digestion instrument. The digestion process involved heating to 120°C for 10 min, followed by heating to 150°C for another 10 min, and finally heating to 180°C for 30 min. After cooling, we added 5 mL of hydrochloric acid solution (6 mol/L). The tube was then opened and placed in a fume hood, and acid evaporation occurred at 170°C until 2 mL of liquid remained. Following digestion and cooling to ambient temperature, the samples were diluted with ultrapure water to a final volume of 10 mL and subjected to shaking. The Se content in various tissues was determined using inductively coupled plasma mass spectrometry (ICP-MS).

2.3 RNA sample collection and illumina sequencing

Total RNA samples from the spikes of JG21 under water and selenium treatments were extracted using RNAprep Pure reagent (QIAGEN, Germany) following the manufacturer's protocol. Illumina NovaSeq 6000 Sequencer at Beijing Novogene Biotechnologies Company, Beijing, China, was used for RNA-Seq. After filtering, clean sequence read segments were compared to the *Setaria_italica*_v2.0 reference genome using HISAT v.2.0.5. HTSeq was used to estimate the number of base fragments per kilobase of transcripts per million mapping reads (FPKM). Principal component analysis (PCA) was performed using log2 (FPKM+1) transformation and normalized gene expression values with the fast. Prcomp function from the models in R version 3.5.1.

2.4 DEG identification and functional analyses

DEG identification and functional analysis were conducted using DESeq v.1.20.0. In each pairwise comparison, DEGs were identified with a Benjamini and Hochberg false discovery rate (FDR) < 0.05, FPKM > 1, and |log2 fold change (FC)| > 0.5. Further analyses of DEGs, including Gene Ontology (GO) enrichment analysis, Clusters of Orthologous Groups of Proteins (COG) analysis, Kyoto Encyclopedia of Genes and Genomes (KEGG) analysis, and NCBI nonredundant protein sequence (Nr) annotation, were performed.

2.5 WGCNA

Gene co-expression modules were constructed using the R package WGCNA v3.5.0. To identify Se accumulation in the Se- and CK-related modules under treatment, we correlated the eigengene module with Se content and drew their correlation heat maps. Genes with an average FPKM > 1 out of 24 samples were analyzed. The soft threshold power β was set at five, and mergeCutHeight = 0.4 was used to merge similar modules. If the p-value of the module-trait association is 0.05, then the module is defined as significant (Wang et al., 2022). The OmicShare tool2 (https://www.omicshare.com/) was used to map the network visualization of genes within the module. Genes with high co-expression connectivity within the screening module were visualized using Cytoscape v.3.7.2 (Seattle, WA, USA).

2.6 qRT-PCR analysis

For the synthesis of first-strand cDNA, 0.5 μg of purified RNA underwent reverse transcription using the Takara PrimeScript RT Reagent Kit (TaKaRa, Beijing, China), including gDNA Erase, following the manufacturer's instructions. Subsequently, qRT-PCR was performed on a CFX96 Real-Time System (Bio-Rad, Hercules, CA, USA) using Super Real Premix Plus (SYBR Green) (TaKaRa, Beijing, China). Specific primers for the 10 selected genes were designed using the Primer Premier 5.0 design tool (Supplementary Table 1). The relative expression level of the gene was determined using the $2^{-\Delta\Delta Ct}$ method, with Actin (*SETIT_004277 mg*) as the internal reference gene. Bar charts were generated using Origin 2022, and significance analysis ($P < 0.05$) was performed using SPSS 26.

3 Results

3.1 Selenium content in each tissue of foxtail millet

The Se content in every tissue of foxtail millet exhibited an increase post-Se spraying (Figure 1). Interestingly, the Se content in leaves gradually decreased over time, while that in spikes exhibited a gradual increase. As the treatment duration extended, Se content decreased in leaves and stems, concomitant with an increase in spikes. This pattern suggests that foliar spraying of Na_2SeO_4 during the heading stage facilitated the sequential transport and accumulation of selenate in leaves, stems, and spikes.

3.2 Quality assessment of RNA-seq data

To explore the dynamic effects of Na_2SeO_4 on the expression of selenate transport-related genes during foxtail millet spike development, we conducted RNA-seq analysis on the spikes of JG21 plants treated with water and Na_2SeO_4 during the heading stage. Each sample, including CK3, Se3, CK5, Se5, CK7, Se7, CK12, and Se12, with three biological replicates, underwent quality assessment. A total of 154.03 G clean data was obtained from 24 samples, with individual samples ranging from 5.76 to 6.95 G. The Q30 value exceeded 91.26%, and the GC content distribution was 52.16-54.78% (Supplementary Table 2). After filtering low-quality reads, 84.38%-95.16% mapped to the *Setaria_italica*_v2.0 reference genome (Supplementary Table 2). PCA revealed significant differences between the eight treatments, with all replicates closely clustered. PC1 and PC2 contributed 42.48% and 17.29% to the total difference, respectively (Figure 2A). The results indicated varied gene expressions over time following foxtail millet water spraying and Na_2SeO_4 treatment, suggesting specific responses possibly linked to selenium transport in foxtail millet spikes. With high quality sampling, sequencing, and gene quantification, we identified differential genes associated with selenium transportation in foxtail millet spikes.

3.3 DEGs analysis and functional annotations

Evaluation of FPKM values depicted the expression of all genes (Figure 2B). Transcript abundance comparisons across samples led to the identification of differentially expressed genes (DEGs) in each sample (Figures 2C, D), revealing increased sensitivity of gene expression in foxtail millet spikes to Na_2SeO_4 treatment. Notably, comparing Na_2SeO_4 treatment with water treatment unveiled 3,262 unique DEGs across four comparisons (Figure 2D). Comparing 9,428 unique DEGs under Na_2SeO_4 treatment on adjacent days (days 3, 5, 7, and 12) revealed 98 common DEGs in the three comparisons (Figure 2D). These results strongly suggest that Na_2SeO_4 exerts regulatory control over the expression of a substantial number of genes.

For deeper insights into the potential mechanisms underlying selenium transport in foxtail millet spikes, functional classification of DEGs from all seven comparisons was conducted using GO enrichment analysis. Key terms included “thylakoid,” “thylakoid membrane,” “stroma,” and “photosynthetic membrane” under cellular components; “binding,” “transporter activity,” and “transferase activity” under molecular function, and “cellular processes,” “metabolic processes,” and “response to stimulus” under biological processes (Supplementary Table 3). Additionally, KEGG pathway analysis among the seven comparisons highlighted critical processes such as “selenocompound metabolism (map00450),” “plant hormone signal transduction (map04075),” “glutathion metabolism (map00480),” and “ABC transporters (map02010)” (Supplementary Figure 1). These findings illuminate the crucial biochemical pathways and genes regulating selenium accumulation after Se spraying on foxtail millet leaves, offering insights for the development of functional Se-enriched millet varieties. Further investigations are warranted to explore the DEGs involved in these pathways.

3.4 DEGs involved in selenium metabolism and transportation

To unravel the molecular intricacies governing selenium (Se) metabolism and transportation in millets, we pinpointed DEGs

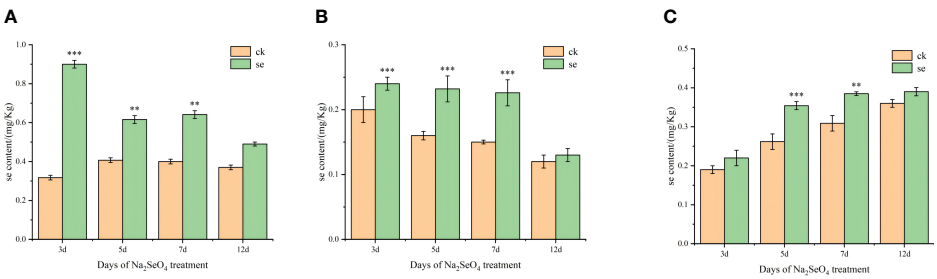

FIGURE 1
Effects of spraying sodium selenate on selenium content in leaves **(A)**, stems **(B)**, and spikes **(C)** of foxtail millet at the heading stage. *, ** and *** mean significant correlation at 0.05, 0.01 and 0.001 levels, respectively.

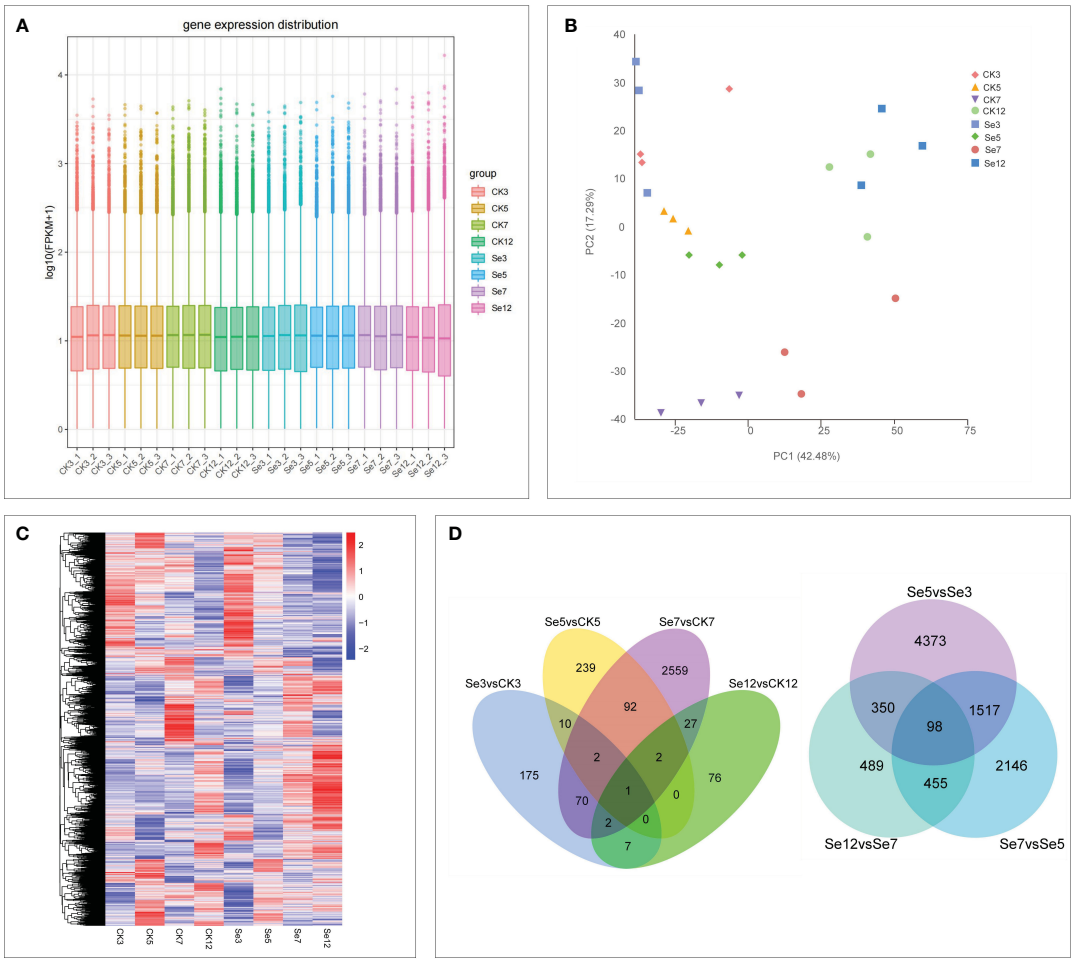

FIGURE 2
Global transcriptome sequencing and differentially expressed genes (DEGs) in CK and Se of foxtail millet. Principal component analysis (PCA) of RNA-sequencing (RNA-Seq) data **(A)**. Gene expression of all samples. The boxplots with different colors indicate different samples analyzed at regular intervals **(B)**. Cluster analysis of DEGs based on gene expression of all samples **(C)**. Venn diagrams showing the number of DEGs among seven comparisons **(D)**. CK3 (water treatment day 3), CK5 (water treatment day 5), CK7 (water treatment day 7), CK12 (water treatment day 12), Se3 (Na_2SeO_4 treatment day 3), Se5 (Na_2SeO_4 treatment day 5), Se7 (Na_2SeO_4 treatment day 7), Se12 (Na_2SeO_4 treatment day 12). The same below.

associated with selenocompound metabolism and sulfate transporters. In nature, Se manifests in organic and inorganic forms, further categorized based on its oxidation state as elemental selenium (Se^0), selenide (Se^{2-}), selenite (Se^{4+}), and selenate (Se^{6+}) (White and Broadley, 2009). Selenate, upon entering the chloroplast, undergoes activation by ATP sulfurylase (ATPs) to generate 5'-adenosine phosphoselenate (APSe). Subsequently, 5'-adenosine phosphosulfate reductase (APR) catalyzes APSe to form selenite. Notably, both externally absorbed selenate and selenite traverse the same assimilation pathway (Schiavon et al., 2015) (Figure 3A). Concurrently, sulfate transporters contribute to SeO_4^{2-} accumulation (Zou et al., 2021), phosphate transporters facilitate SeO_3^{2-} accumulation (Zhang et al., 2014), amino acid transporters engage in selenide metabolism (Taylor et al., 2015), and nitrate transporter promotes selenomethionine (SeMet) transport (Zhang et al., 2019). Additionally, the responses of ABC transporters to Se metabolism and transportation were explored.

Following the treatment of foxtail millet spikes with CK and Se on different days, we identified nine unique DEGs linked to the selenocompound metabolic pathway in five comparisons (Figure 3B; Supplementary Table 4). Moreover, 10 unique DEGs associated with sulfate transporters emerged from seven comparisons (Figure 3C; Supplementary Table 5), along with 13 unique DEGs related to phosphate transporters, 59 unique DEGs related to amino acid transporters, and 55 unique DEGs related to ABC transporters in seven comparisons (Figures 3D–F; Supplementary Tables 5, 6). Notable genes, including *SiSULTR1.2a*, *SiSULTR1.2b*, *SiSULTR2.1*, *SiSULTR3.1a*, *SiSULTR3.5*, and *PHO1-3*, exhibited increased expression post-Se spraying. *SiSULTR3.4* demonstrated involvement in both sulfate and phosphate transporters. The ABC transporter family prominently featured three subfamilies: ABCB, ABCC, and ABCG, underscoring their pivotal role in the ABC transporter family's response to Se stress in foxtail millet.

3.5 DEGs associated with plant hormone signal transduction

To scrutinize Se's impact on phytohormone signal transduction in foxtail millet, we delved into gene expression profiles within

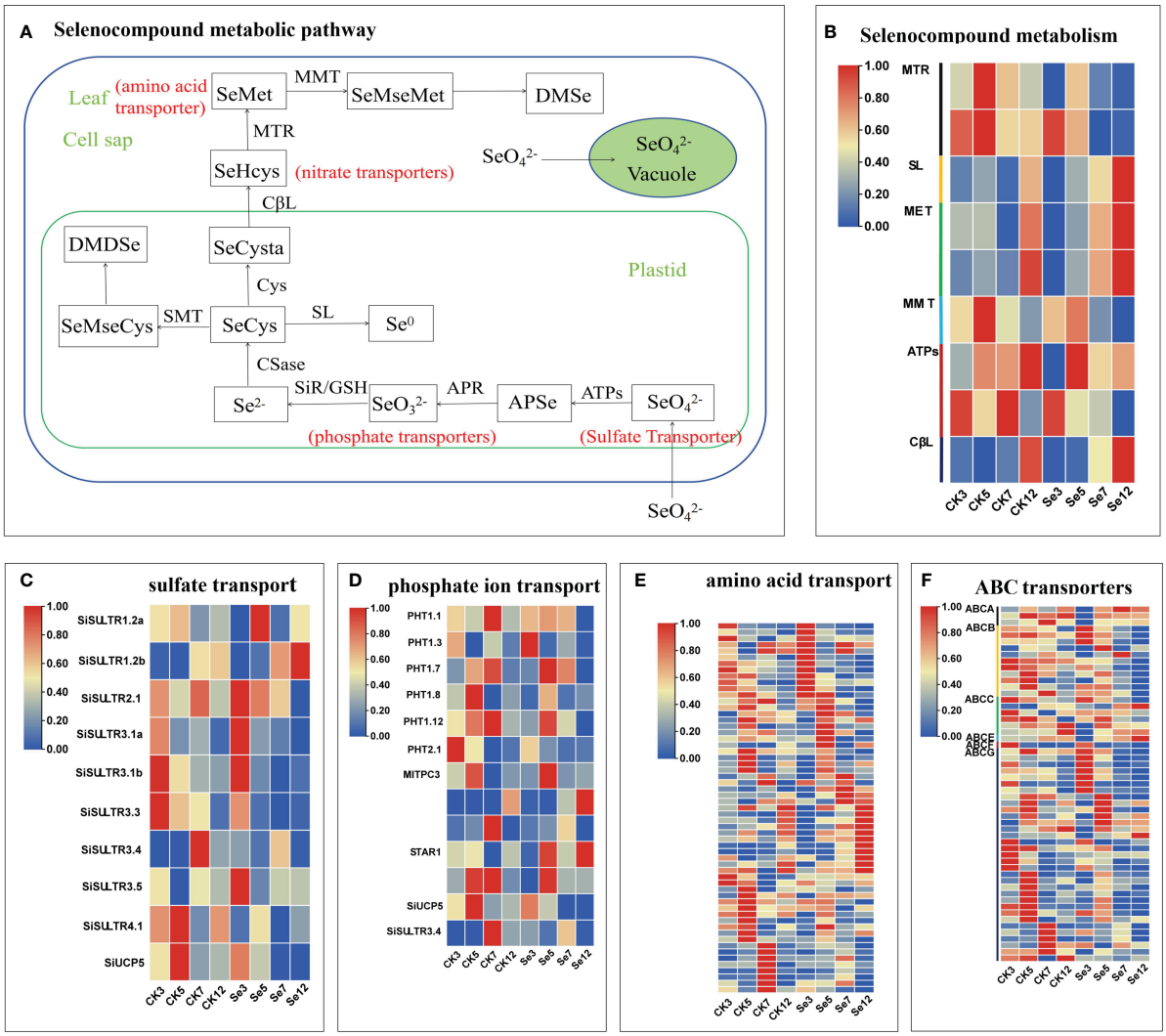

FIGURE 3
Selenocompound metabolism **(A)**. Expression profiles of differentially expressed genes (DEGs) involved in selenocompound metabolism **(B)**, sulfate transport **(C)**, phosphate transport **(D)**, amino acid transport **(E)**, and ABC transporter **(F)**. Different colors indicate different gene expression levels based on log2 FoldChange. The same below.

phytohormone signal transduction pathways. In the auxin pathway, Se upregulated the expression of key genes like auxin influx carrier *AUXIN1* (*AUX1*), *Auxin/indoleacetic acid* (*AUX/IAA*), and *Auxin response factor* (*ARF*) genes (Figure 4A; Supplementary Table 7). Cytokinin pathway analysis revealed Se-induced upregulation of most *Type A Arabidopsis response regulator* (*A-ARR*) genes (Figure 4B; Supplementary Table 8). Similarly, Se influenced the gibberellin pathway by upregulating one *DELLA protein* (*DELLA*) and three *phytochrome-interacting factor* (*TF*) genes (Figure 4C; Supplementary Table 9). The abscisic acid (ABA) pathway exhibited regulation by 27 unique DEGs (Figure 4D; Supplementary Table 10). Se, also modulated the ethylene pathway by downregulating certain components while upregulating others (Figure 4E; Supplementary Table 11). In the brassinosteroid pathway, Se exerted differential regulation on various genes (Figure 4F; Supplementary Table 12). Similarly, Se downregulated most *Jasmonate ZIM-domain* (*JAZ*) genes in the jasmonic acid pathway (Figure 4G; Supplementary Table 13). The salicylic acid pathway demonstrated a nuanced response with both upregulation and downregulation of specific genes (Figure 4H; Supplementary Table 14). Collectively, these results underscored Se's impact on phytohormone biosynthesis and signaling pathways.

3.6 DEGs associated with antioxidation

The application of Se treatment significantly upregulated genes associated with the antioxidant response, including superoxide dismutase (SOD), ascorbate peroxidase (APX), catalase (CAT), peroxidase (POD), monodehydroascorbate reductase (MDHAR), glutathione peroxidase (GSH-Px), and glutathione S-transferase (GST) (Supplementary Table 15; Figure 5). Noteworthy DEGs within the antioxidant system encompassed SOD, APX, CAT, and POD, with unique expressions and regulatory patterns. Similarly, GST-related genes exhibited diverse expression dynamics, with selenium. It was

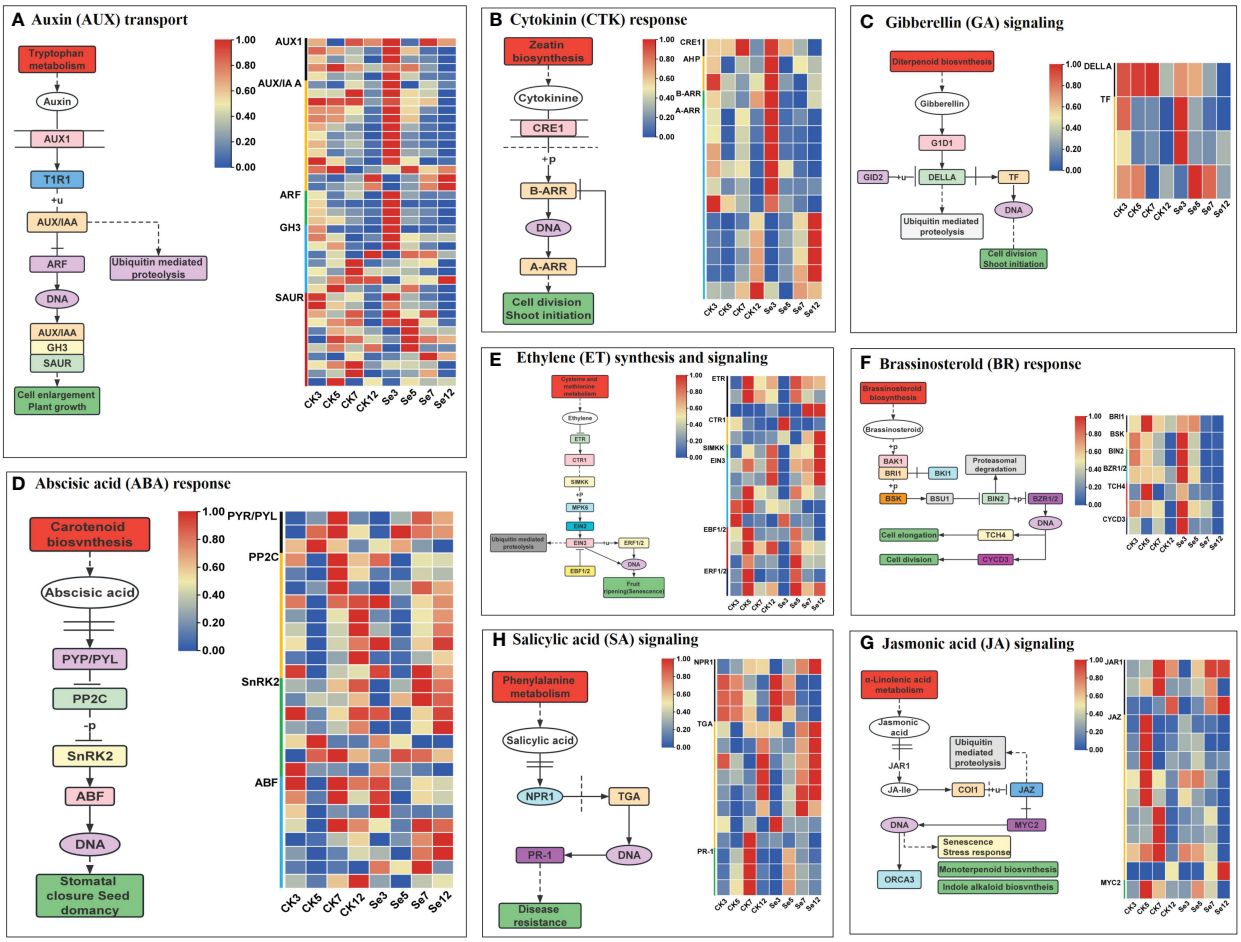

FIGURE 4
Eight plant hormone signal transduction pathways and expression profiles of differentially expressed genes (DEGs) involved in auxin (AUX; **A**), cytokinin (CTK; **B**), gibberellin (GA; **C**), abscisic acid (ABA; **D**), ethylene (ETH; **E**); brassinosteroid (BR; **F**), jasmonic acid (JA; **G**), and salicylic acid (SA; **H**) signal pathways of foxtail millet spikes after selenium and water spraying treatments.

identified one upregulated monodehydroascorbate reductase gene, three unique DEGs associated with the GSH-Px enzyme, and 22 unique DEGs associated with the GST enzyme, with 20 upregulated and two downregulated genes. Selenium spraying induced the early expression This response varied temporally, with certain genes showing altered expression on day 3 post-selenium treatment compared to their original expression on day 7 or 12.

3.7 WGCNA of foxtail millet after Se treatment

To unravel the specifically induced regulatory network response from leaves to spikes in foxtail millet following foliar Se application, we subjected expression datasets (FPKM >1) from 24 samples to WGCNA. This analysis identified nineteen co-expression modules (mergeCutHeight = 0.40) in foxtail millet spikes (Figure 6A). Subsequently, we explored the correlations between these modules using the eigengene module (Figure 6B). Two modules, namely "tan" (r= 0.62, p=0.000) and "turquoise" (r= 0.58, p=0.002), exhibited significant positive correlations with Se content, making them the focal point of our study.

Furthermore, GO and KEGG analyses were conducted on genes within the "tan" and "turquoise" modules to elucidate their biological functions. Both modules were enriched in GO terms related to "cellular processes," "metabolic processes," and "transport activities" (Figures 7A, B). The "tan" module demonstrated predominant enrichment in KEGG pathways such as "plant hormone signal transduction," "Glutathione metabolism," and "MAPK signaling pathway" (Figure 7C). In contrast, the "turquoise" module was enriched in pathways such as "plant hormone signal transduction," "sulfur metabolism," "selenocompound metabolism," "flavonoid biosynthesis," and "glutathione metabolism" (Figure 7D).

3.8 Identification of hub genes and interaction network in modules

Hub genes within the "tan" and "turquoise" modules, identified based on module membership >0.8 and GS>0.2, revealed three closely

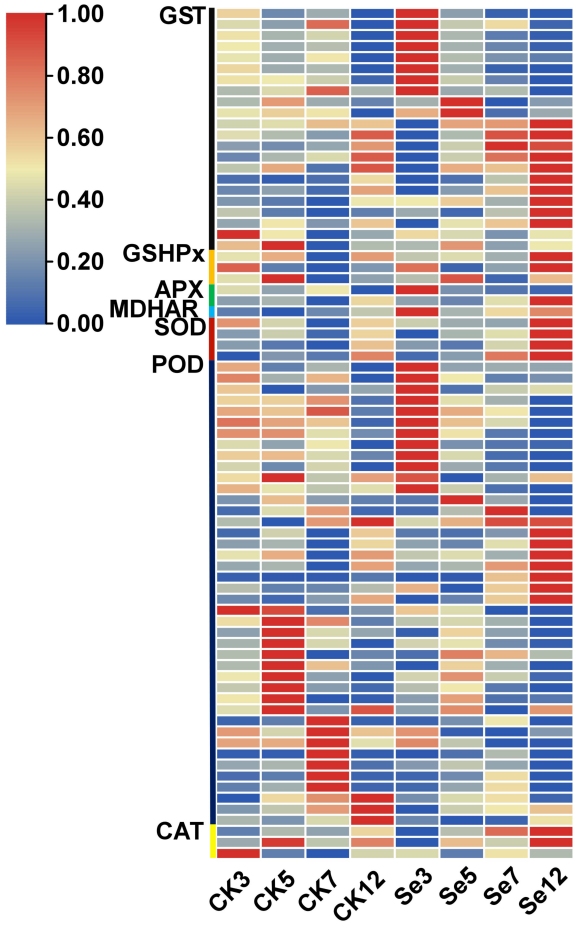

FIGURE 5
Expression profiles of differentially expressed genes (DEGs) involved in antioxidation.

related genes in each module (Figures 7E, F). Notably, the tan module featured three transcription factors— WRKY29 (SETIT_004791 mg), MYB3R-2 (SETIT_021484 mg), and bHLH130 (SETIT_030166 mg)—all implicated in Se regulation. The turquoise module highlighted hub genes such as *SiSULTR1.2* (SETIT_034596 mg), *SiNRT2.1* (SETIT_018372 mg), and *ABCC13* (SETIT_005820 mg), associated with sulfur transport (GO: 0008272), nitrate transport (GO: 0015706), and active transmembrane transport activity (GO: 0022804), respectively.

3.9 Analysis of sulfate transporter protein (SULTR) expression patterns

Given the mediation of SeO_4^{2-} uptake and transport by sulfate transporters, our focus turned to the sulfate transporter gene family (Figure 8A). Transcriptome analysis identified 10 genes encoding SULTRs (Figure 3C). The response patterns of *SiSULTR1.2a*, *SiSULTR1.2b*, *SiSULTR2.1*, *SiSULTR3.1a*, and *SiSULTR3.5* to selenium spraying varied temporally, with some genes responding on days 3, 7, or 12 post-treatment. Tissue-specific expression pattern analysis 12 days after selenium spraying (Figure 9A) and gene expression levels across five stages of grain filling (S1–S5) (Figure 9B) revealed *SiSULTR1.2b* as particularly notable, exhibiting high expression levels in foxtail millet spikes and maintaining consistent high expression throughout the grain -filling stages. This gene, accessed from the foxtail millet database (http://foxtail-millet.biocloud.net/home), displayed expression in grains, leaves, and roots during the grain-filling stage, with the highest expression observed in grains, suggesting a crucial role in Se transport from leaves to grains in foxtail millet (Figure 8B).

3.10 Gene expression validation through qRT-PCR

To validate the reliability and efficacy of the RNA-Seq data, we conducted qRT-PCR analysis on the relative expression levels of 10 selected genes, including six related to sulfur transport and four associated with plant hormone signal transduction. The qRT-PCR

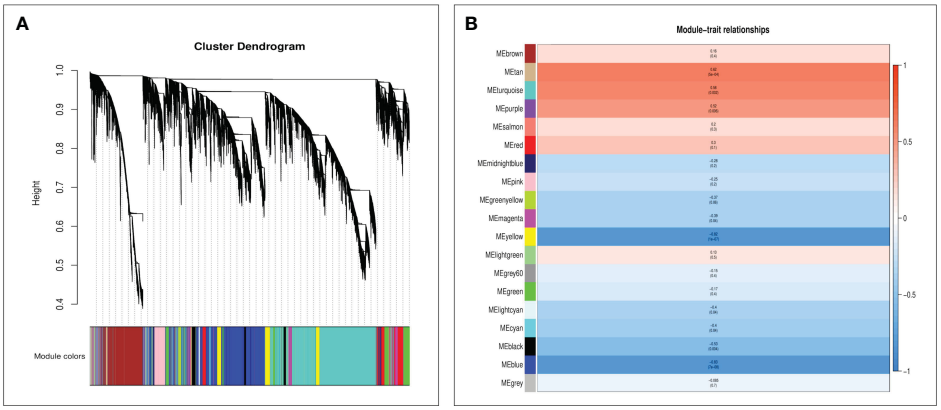

FIGURE 6
The WGCNA of foxtail millet panicle transcripts after selenium treatment used the average linkage hierarchical clustering method to construct the gene tree of CK and Se, and each row represents a gene. The module color under the clustering tree shows the result of the dynamic tree-cut module allocation **(A)**. Correlation between module characteristic genes and selenium content **(B)**. The color of each module was the same as that in **(A)**. The correlation coefficient (r) and p-value are shown in each cell.

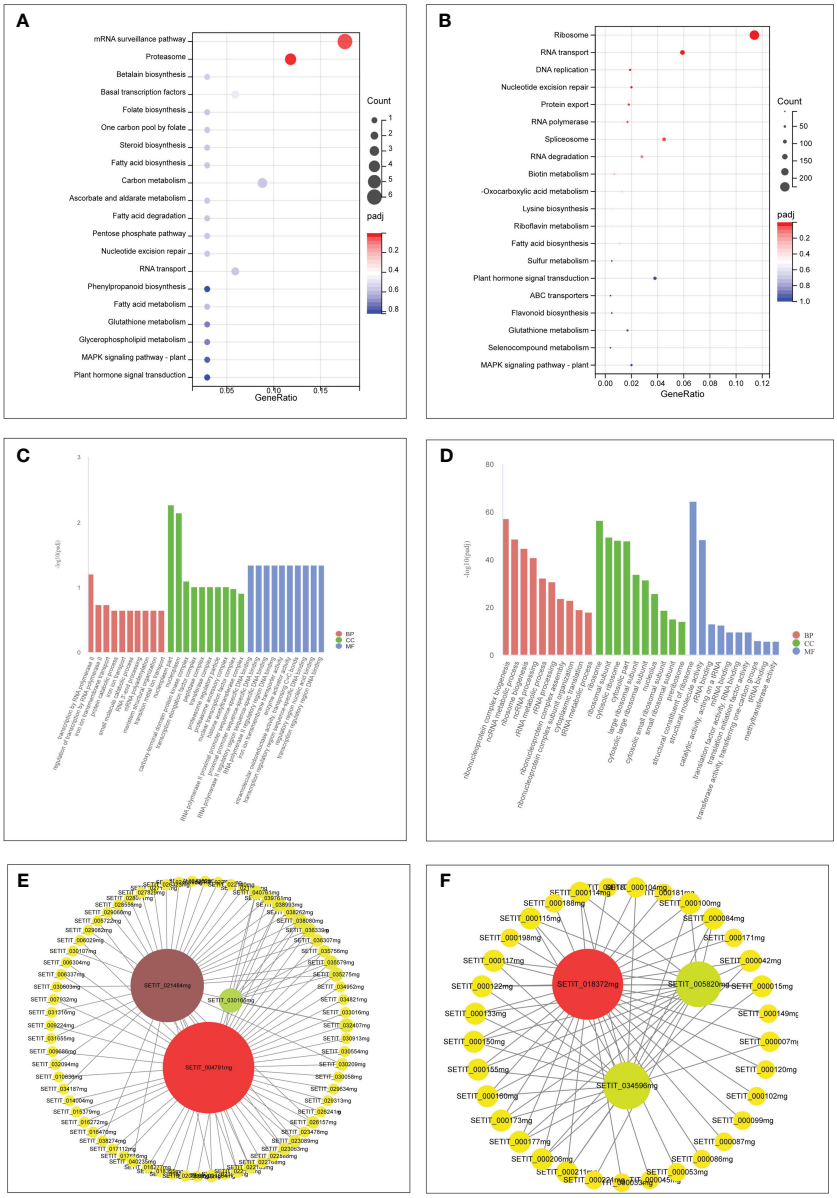

FIGURE 7
GO and KEGG analysis of unique genes in the tan module **(A, C)**. GO and KEGG analysis of unique genes in the turquoise module **(B, D)**. Hub genes network interaction in the tan module **(E)**. Hub genes network interaction in the turquoise module **(F)**.

expression trends of JG 21 spikes (Figure 10A) aligned with those observed in the RNA-Seq data (Figure 10B), affirming the consistency between the two analytical methods.

4 Discussion

In this study, transcriptome analysis was employed to investigate the temporal transcriptional changes in spikes treated with selenates, elucidating the primary mechanism underlying selenium transport in foxtail millet. Transcriptomic data were utilized to comprehensively explore the enrichment pathways associated with KEGG, and GO. The principal component analysis diagram directly depicted the degree of separation between samples from different groups. The biological repeats at 3d and 5d exhibited closer proximity, whereas those at 7d and 12d displayed slightly longer distances, yet still allowing for clear classification. The gene expression distribution chart indicated a similar expression trend among samples at the heading stage. Overall, the quality control and expression validation of the omics data confirmed the reliability of our findings, thereby providing valuable support for elucidating the mechanism of selenium enrichment in millet.

4.1 Effects of leaf spraying selenium on the selenium content of crops

Research on grain crops has revealed a positive correlation between selenium (Se) concentration in grains and foxtail millet's Se application.

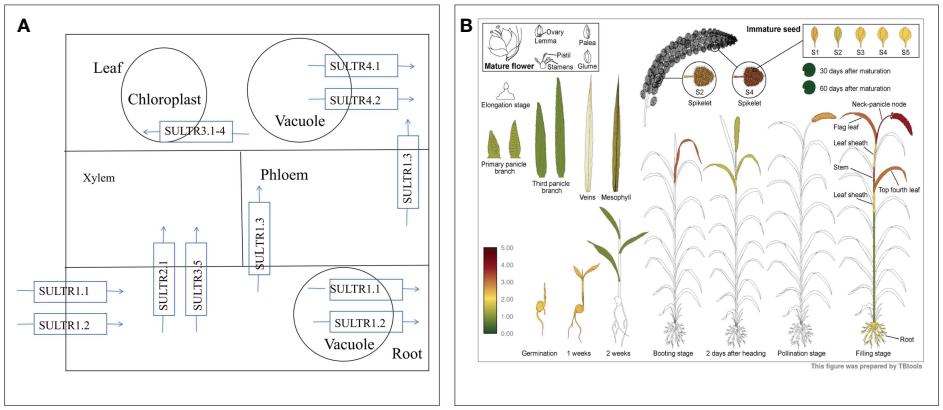

FIGURE 8
The absorption and transport mechanism of selenate by plants **(A)**. Expression of SiSULTR1.2b in different tissues of foxtail millet at different stages **(B)**.

The study recorded the highest Se concentration in grains (1.83 mg/kg) when spraying 61.5 g Se hm^{-2} (Li et al., 2022). Leaf spraying of sodium selenite increased Se content and yellow pigment in foxtail millet (Ning et al., 2016). On rice grains, selenite foliar application enhanced Se concentrations in glutelin and albumin proteins, such as SeCys2 and SeMet (Hu et al., 2018). Wheat grains exhibited increased Se concentration and highly bioavailable SeMet fraction with sodium selenate foliar fertilization (Ramkissoon et al., 2019). Potatoes treated with foliar selenate showed enhanced Se concentration, attributed to improved Se fluidity in the phloem (Poggi et al., 2000). In cash crops, Se spraying during the autumn tea-producing season increased Se and vitamin C contents in green tea (Huang et al., 2005). Grape leaves treated with amino acid-chelated selenium-enriched foliar fertilizer significantly increased Se content (Yin et al., 2020). Blueberries treated with foliar selenate and selenite (200 g/ha) during the young fruit stage showed enhanced Se accumulation in the fruit (Li et al., 2018). In our study, Se content significantly increased in all foxtail millet tissues after Se spraying. Over time, Se levels in leaves decreased, while in spikes, they gradually increased, indicating Se absorption and transport to the kernels in the leaves.

4.2 Transporters involved in Se accumulation and transportation in foxtail millet

In the botanical realm, selenium (Se) manifests in both organic and inorganic forms. Plant-hosted inorganic selenium encompasses

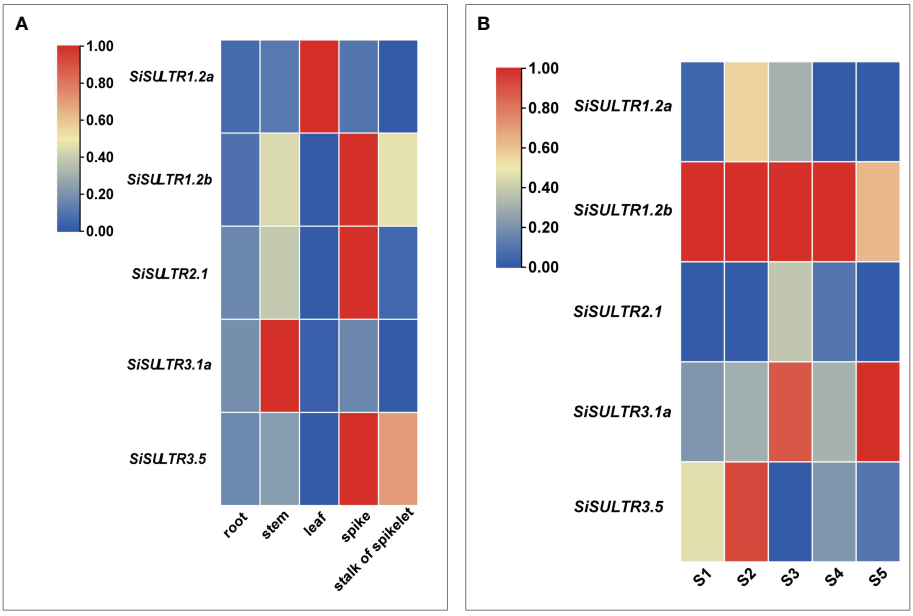

FIGURE 9
Analysis of the tissue expression pattern on the 12th day of selenium spraying **(A)**. Analysis of expression patterns in five stages of grain filling **(B)**.

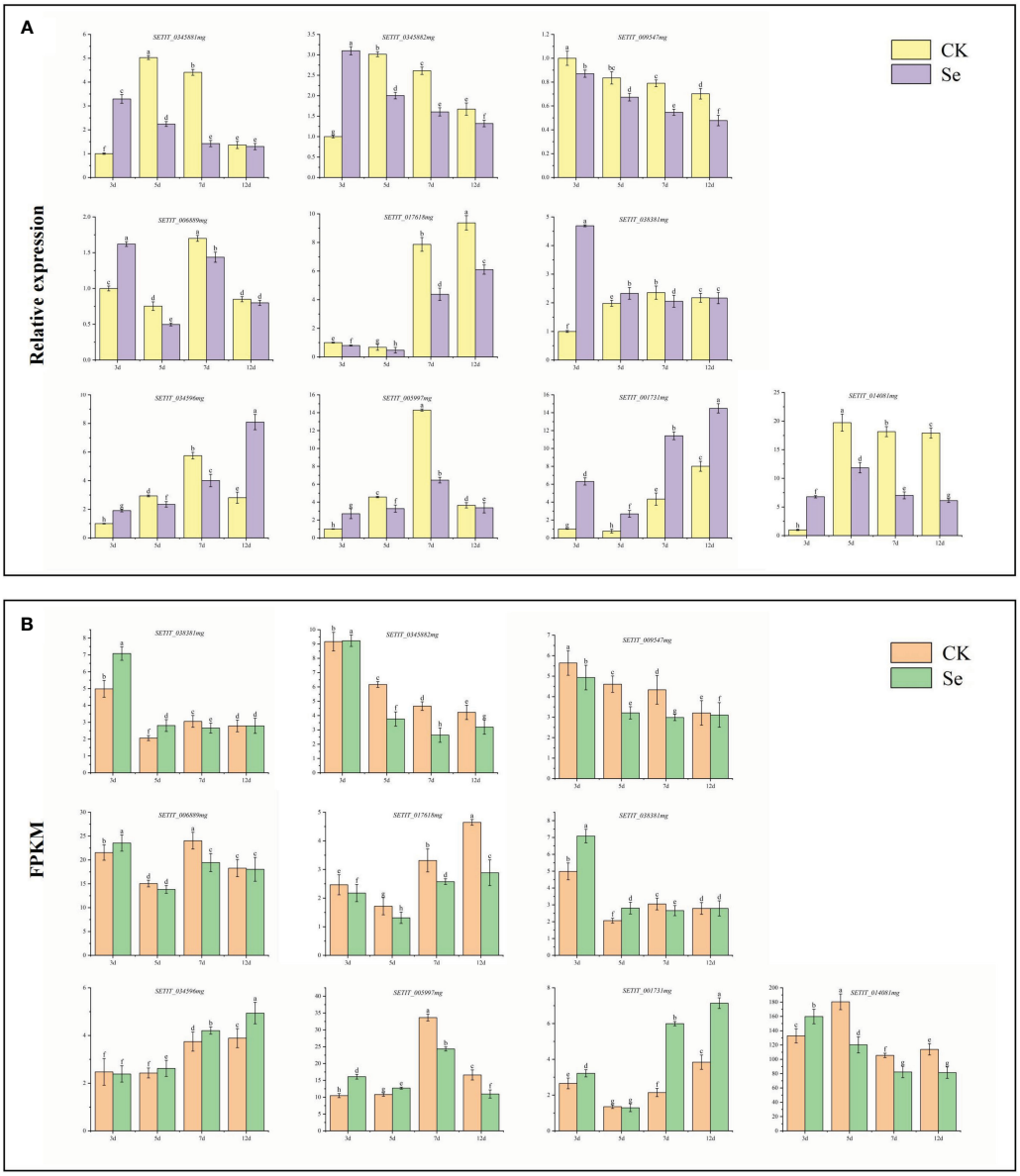

FIGURE 10
Candidate gene qRT-PCR verification **(A)**. Candidate gene RNA-Seq expression pattern **(B)**. Different lowercase letters above the bar indicate significant differences at the $p < 0.05$ level in the different treatment.

selenate (SeO_4^{2-}) and selenite (SeO_3^{2-}), while organic counterparts encompass selenocysteine (SeCys) and selenomethionine (SeMet) (White and Broadley, 2009). The intricate interplay of distinct absorption and transport mechanisms for varied Se forms, facilitated by specific transporters, results in the conversion of part of inorganic selenium into organic Se compounds, persisting within the plant structure. The remaining fraction undergoes metabolism, yielding volatile compounds—specifically dimethyl diselenide (DMDSe) and dimethyl selenide (DMSe) (Gui et al., 2022). SeO_4^{2-} and SeO_3^{2-} exhibit a robust affinity for plants. Sulfate transporters, such as SULTR1.2 in Arabidopsis, are instrumental in SeO_4^{2-} accumulation and transport (Shibagaki et al., 2002). In our investigation, nine SULTRs were identified, notably SiSULTR1.2b and SiSULTR3.1a, exhibiting upregulation during grain filling, suggesting their pivotal role in Se transport after foliar Se application (Figures 3C, 9B). Phosphate transporters, participate in SeO_3^{2-} accumulation, and hydrogen selenite (H_2SeO_3 and $HSeO^{3-}$) flows through silicon influx (NIP2;1) and phosphate (PT2) transporters (Zhang et al., 2014). Phosphate transporters (OsPHT1.2 and OsPHT1.8) engage in SeO_3^{2-} accumulation and transportation in rice (Zhang et al., 2014; Li et al., 2018). PHT1.3 in foxtail millet, play a role in accumulation, emphasizing their significance in Se transport (Figure 3D). The transport of Se in foxtail millet. The nitrate transporter protein NRT1.1B promotes the transport of SeMet in rice (Zhang et al., 2019). Three DEGs associated with nitrate transport were found in foxtail millet (Supplementary Table 5), and NRT2.1 (SETIT_ 018372mg), emerge as potential key players in Se transport in foxtail millet (Figure 7F).

ABC transporters, featuring a conserved ATPase domain and function by utilizing ATP to facilitate the transport of substrates across membranes. Consequently, they play a crucial role in various physiological processes, including the accumulation of plant secondary metabolites, as well as in biological and abiotic stress responses (Byrne et al., 2010). These transporters can be divided into eight subfamilies: ABCA, ABCG, and ABCI (Verrier et al., 2008). ABC transporters have been implicated in Se accumulation and transport in rice, and were detected after SeO_3^{2-} treatment, suggesting their potential involvement in Se accumulation and transport (Kong et al., 2021). ABCC11, ABCC13, and ABCC10 engage in nano-selenium accumulation and transport in cowpeas (Li et al., 2023). ABC transporter G family member 36 in alfalfa leaves is significantly upregulated after Se treatment, suggesting its involvement in the movement of Se into the leaf tissue (Wang et al., 2021). Zheng et al. observed the upregulation of 14 ABC genes in tea trees, suggesting that they may be involved in Se accumulation and transport in tea roots (Zheng et al., 2023). In perennial ryegrass, ABCA transporters regulate Se movement and accumulation. ATH genes in the ABCA subfamily were upregulated in response to selenite exposure (Byrne et al., 2010). ABCG14 participates in phytohormone transport (Gräfe and Schmitt, 2021). In this study, six ABC subfamilies were discerned, with ABCC13 posited to play a pivotal role in Se transport from leaves to spikes in foxtail millet (Figures 3F, 7E). This elucidation underscores the intricate orchestration of transporters in Se dynamics within foxtail millet, shedding light on the molecular mechanisms governing Se accumulation and transportation.

4.3 Plant hormone signaling pathway genes involved in Se accumulation and transportation in foxtail millet

Supplementation with Se enhances resistance to abiotic stress by modulating plant hormone homeostasis and regulating endogenous hormone levels. The generation of reactive oxygen species (ROS) in plants promotes the increase in levels of jasmonic acid and ethylene stress hormones (Overmyer et al., 2003). Se treatment triggers the expression of genes related to plant hormone signaling pathways, as demonstrated in pepper leaves treated with nano-selenium, resulting in elevated levels of jasmonic, abscisic, and salicylic acids (Li et al., 2020). The assimilation of Se is promoted by Jasmonic acid, gibberellin, and abscisic acid, subsequently increasing the transcriptional levels of genes encoding sulfate transporters (Zou et al., 2021). The influence of jasmonic acid compounds on selenium uptake appears to be dependent on the concentration of selenium treatment. Under high selenium conditions, jasmonic acid compounds can reduce selenium uptake and accumulation in rice plants as a protective response. Additionally, they can also lower the selenium accumulation levels in tea leaves treated with high concentrations of sodium selenate (135 $mg{\cdot}m^{-2}$). Conversely, jasmonic acid compounds exhibit a significant promoting effect on the selenium content of tea leaves treated with low concentrations of sodium selenate (Dai et al., 2021). The impact of salicylic acid on selenium uptake varies depending on the crop. It has been shown to reduce selenium content in the roots and leaves of rice plants, while enhancing the uptake of organic selenium and sodium selenite in lettuce (Kowalska et al., 2020; Mostofa et al., 2020). In our investigation, genes associated with auxin, cytokinin, gibberellin, and brassinosteroid response elements were upregulated on day 3 of Se treatment (Figures 4A–C, F). Salicylic acid response element genes exhibited upregulation on day 12 of Se treatment (Figure 4H), while genes related to the jasmonic acid pathway showed downregulation post-Se treatment (Figure 4G). These results indicated that plant hormones also regulate the transport and accumulation of selenium.

4.4 Transcription factors involved in Se accumulation and transportation in foxtail millet

Transcription factors function as pivotal molecular switches, regulating growth and development in response to various conditions (Yuan, 2008). Specifically, bHLH transcription factors are involved in the uptake and distribution of iron in Arabidopsis (Riaz and Guerinot, 2021). Additionally, the transcription factors bZIP19 and bZIP23 act as central regulators in the zinc deficiency response, functioning as sensors for zinc by utilizing their Cys/His rich motif to bind Zn^{2+} ions (Lilay et al., 2021). Notably, previous investigations on tea plants have underscored the involvement of transcription factors, such as ERF, bHLH, and MYB, in the modulation of defense networks in response to SeO_3^{2-} treatment, jasmonic acid, and ethylene exposure (Cao et al., 2018). Furthermore, the transcriptional level analysis has successfully established the association between selenium and the anthocyanin pathway through the participation of R2R3-MYB and bHLH in selenium metabolism (Pu et al., 2021). Moreover, the regulatory function of WRKY75 in tea roots has been identified in the accumulation of SeO_3^{2-} (Zheng et al., 2023). In the analysis conducted using WGCNA, three hub genes were identified. Thus, in foxtail millet, the transportation of SeO_4^{2-} from the leaf to the spike may be controlled by the transcription factors MYB, WRKY, and bHLH.

4.5 Selenium accumulation in foxtail millet enhanced antioxidant activity

Glutathione peroxidase and glutathione reductase are important enzymes and play a vital role in scavenging H_2O_2 and lipid peroxides to water and lipid alcohols, respectively (Hasanuzzaman and Fujita, 2011; Feng et al., 2013). GSH-Px is believed to be a key enzyme, which can be widely and robustly activated by Se in various plants exposed to several environmental stresses (Feng et al., 2013). In the presence of selenium, H_2O_2 (hydrogen peroxide) is primarily and majorly quenched by GSH-Px and then APX, CAT, and GR (Glutathione Reductase) eliminate the remnants of H_2O_2. Therefore, genes and proteins related to glutathione metabolism play important roles in assimilation and

tolerance of Se in plants (Chauhan et al., 2020; Rao et al., 2021). Se induces positive responses in plant growth and development by elevating antioxidant defense systems, including CAT, GSH-Px, and SOD. It also fosters the accumulation of secondary metabolites, such as total phenols and flavonoids, fortifying membrane integrity and enhancing nutrient quality and crop productivity under diverse abiotic stresses (Hawrylak-Nowak et al., 2014). The genes encoding GST, GSS (glutathione synthetase), GSH-Px, and GR are notably increased in tea plants treated with selenite (Cao et al., 2018). Remarkably, the expression of glutathione metabolism related genes and proteins were highly induced even 3 days after treatments of selenate in this study. The genes encoding GST, GSH-Px, APX, MDHAR, and SOD exhibited significant upregulation post-Se treatment in this study (Figure 5), indicating their potential role in enhancing Se accumulation in foxtail millet.

4.6 Conclusion

As the duration of Se treatment on leaves increased, Se nutrients exhibited sequential transport and accumulation along the leaf-stem-ear axis. RNA-Seq analysis unveiled the transcriptional mechanisms of Se treatment, highlighting key genes involved in selenium transport following foliar application. Upregulation was observed in the transcription levels of sulfate transporters, phosphate transporters, nitrate transporters, antioxidant enzymes, transcription factors, and enzymes associated with plant hormone synthesis after Se treatment. The accumulation of Na_2SeO_4 in foxtail millet spikes correlated with the upregulation of transcription factors ABCC13, PHT1.3, SiNRT2.1, GSTs, MYB, WRKY, and bHLH. Notably, Na_2SeO_4, a key player in Se accumulation, significantly induced the expression of SiSULTR1.2b and SiSULTR3.1a. These findings form a foundational understanding of Se accumulation and transportation in foxtail millet.

Data availability statement

The data presented in the study are deposited in the NCBI SRA database, accession number PRJNA1051663.

Author contributions

YW: Writing – original draft. LC: Writing – original draft. ZZ: Data curation, Writing – review & editing. MA: Data curation, Writing – review & editing. SZ: Data curation, Writing – review & editing. JZ: Formal Analysis, Writing – review & editing. SD: Conceptualization, Writing – review & editing. XY: Conceptualization, Writing – review & editing. MY: Conceptualization, Writing – review & editing.

Funding

The author(s) declare financial support was received for the research, authorship, and/or publication of this article. This research was funded by the Natural Science Foundation of Shanxi Province (20210302123373); Ministerial and Provincial Co-Innovation Centre for Endemic Crops Production with High-quality and Efficiency in Loess Plateau (SBGJXTZX-31); National Key R&D Plan(2021YFD1901103-5); Earmarked fund for CARS-foxtail millet and sorghum (CARS-06-14.5-A28); National Natural Science Foundation of China (30221803).

Acknowledgments

This is a short text to acknowledge the contributions of specific colleagues, institutions, or agencies that aided the efforts of the authors.

Conflict of interest

The authors declare that the research was conducted in the absence of any commercial or financial relationships that could be construed as a potential conflict of interest.

Publisher's note

Supplementary material

The Supplementary Material for this article can be found online at: https://www.frontiersin.org/articles/10.3389/fpls.2024.1355518/full#supplementary-material

References

Bjørklund, G., Shanaida, M., Lysiuk, R., Antonyak, H., Klishch, I., Shanaida, V., et al. (2022). Selenium: an antioxidant with a critical role in anti-aging. *Molecules* 27, 6613. doi: 10.3390/molecules27196613

Byrne, S. L., Durandeau, K., Nagy, I., and Barth, S. (2010). Identification of ABC transporters from Lolium perenne L. that are regulated by toxic levels of selenium. *Planta* 231, 901–911. doi: 10.1007/s00425-009-1096-y

Cao, D., Liu, Y., Ma, L., Jin, X., Guo, G., Tan, R., et al. (2018). Transcriptome analysis of differentially expressed genes involved in selenium accumulation in tea plant (Camellia sinensis). *PloS One* 13, e0197506. doi: 10.1371/journal.pone.0197506

Chauhan, R., Awasthi, S., Indoliya, Y., Chauhan, A. S., Mishra, S., Agrawal, L., et al. (2020). Transcriptome and proteome analyses reveal selenium mediated amelioration

of arsenic toxicity in rice (Oryza sativa L.). *J. Hazard. Mater.* 390, 122122. doi: 10.1016/j.jhazmat.2020.122122

Dai, Z., Yuan, Y., Huang, H., Hossain, M. M., Xiong, S., Cao, M., et al. (2021). Methyl jasmonate mitigates high selenium damage of rice via altering antioxidant capacity, selenium transportation and gene expression. *Sci. Total Environ.* 756, 143848. doi: 10.1016/j.scitotenv.2020.143848

El Mehdawi, A. F., Jiang, Y., Guignardi, Z. S., Esmat, A., Pilon, M., Pilon-Smits, E. A. H., et al. (2018). Influence of sulfate supply on selenium uptake dynamics and expression of sulfate/selenate transporters in selenium hyperaccumulator and nonhyperaccumulator Brassicaceae. *New Phytol.* 217, 194–205. doi: 10.1111/nph.14838

Feng, R., Wei, C., and Tu, S. (2013). The roles of selenium in protecting plants against abiotic stresses. *Environ. Exp. Bot.* 87, 58–68. doi: 10.1016/j.envexpbot.2012.09.002

Gao, C., Xiao, M., Gong, Z., Song, L., Wang, H., Ludlow, R. A., et al. (2023). Selenium biofortification and increased nutritional quality in alfalfa (Medicago sativa L.) using foliar application of selenium-rich nutrient solution. *J. Soil Sci. Plant Nutr.* 23, 3600–3611. doi: 10.1007/s42729-023-01278-4

Gao, J., Liu, Y., Huang, Y., Lin, Z. Q., Banuelos, G. S., Lam, M. H., et al. (2011). Daily selenium intake in a moderate selenium deficiency area of suzhou, China. *Food Chem.* 126, 1088–1093. doi: 10.1016/j.foodchem.2010.11.137

Gräfe, K., and Schmitt, L. (2021). The ABC transporter G subfamily in Arabidopsis thaliana. *J. Exp. Bot.* 72, 92–106. doi: 10.1093/jxb/eraa260

Gui, J. Y., Rao, S., Huang, X., Liu, X., Cheng, S., and Xu, F. (2022). Interaction between selenium and essential micronutrient elements in plants: A systematic review. *Sci. Total Environ.* 853, 158673. doi: 10.1016/j.scitotenv.2022.158673

Hasanuzzaman, M., and Fujita, M. (2011). Selenium pretreatment upregulates the antioxidant defense and methylglyoxal detoxification system and confers enhanced tolerance to drought stress in rapeseed seedlings. *Biol. Trace Elem. Res.* 143, 1758–1776. doi: 10.1007/s12011-011-8998-9

Hawrylak-Nowak, B., Dresler, S., and Wójcik, M. (2014). Selenium affects physiological parameters and phytochelatins accumulation in cucumber (Cucumis sativus L.) plants grown under cadmium exposure. *Sci. Hortic.* 172, 10–18. doi: 10.1016/j.scienta.2014.03.040

He, L., Cheng, L., Wang, J., Liu, J., Cheng, J., Yang, Z., et al. (2022). Carotenoid cleavage dioxygenase 1 catalyzes lutein degradation to influence carotenoid accumulation and color development in foxtail millet grains. *J. Agric. Food Chem.* 70, 9283–9294. doi: 10.1021/acs.jafc.2c01951

Holben, D. H., and Smith, A. M. (1999). The diverse role of selenium within selenoproteins: a review. *J. Am. Diet Assoc.* 99, 836–843. doi: 10.1016/S0002-8223(99)00198-4

Hu, Z., Cheng, Y., Suzuki, N., Guo, X., Xiong, H., and Ogra, Y. (2018). Speciation of selenium in brown rice fertilized with selenite and effects of selenium fertilization on rice proteins. *Int. J. Mol. Sci.* 19, 3494. doi: 10.3390/ijms19113494

Huang, Y., Xu, J., and Hu, Q. (2005). Effect of selenium on preservation quality of green tea during autumn tea-processing season. *J. Agric. Food Chem.* 53, 7444–7447. doi: 10.1021/jf048314j

Ingle, K. P., Suprasanna, P., Narkhede, G. W., Ceasar, A., Abdi, G., Raina, A., et al. (2023). Biofortified foxtail millet: towards a more nourishing future. *Plant Growth Regul.* 99, 25–34. doi: 10.1007/s10725-022-00900-2

Kaur, P., Purewal, S. S., Sandhu, K. S., Kaur, M., and Salar, R. K. (2019). Millets: a cereal grain with potent antioxidants and health benefits. *Food Measure* 13, 793–806. doi: 10.1007/s11694-018-9992-0

Kieliszek, M. (2019). Selenium-fascinating microelement, properties and sources in food. *Molecules* 24, 1298. doi: 10.3390/molecules24071298

Kong, Q., Li, F., Qin, L., and Chen, E. (2021). Screening and analysis of Se responsive genes in leaves of foxtail millet. *Mol. Plant Breed.* 19, 2798–2810. doi: 10.13271/j.mpb.019.002798

Kowalska, I., Smoleń, S., Czernicka, M., Halka, M., Kęska, K., and Pitala, J. (2020). Effect of selenium form and salicylic acid on the accumulation of selenium speciation forms in hydroponically grown lettuce. *Agriculture* 10, 584. doi: 10.3390/agriculture10120584

Li, H. F., McGrath, S. P., and Zhao, F. J. (2008). Selenium uptake, translocation and speciation in wheat supplied with selenate or selenite. *New Phytol.* 178, 92–102. doi: 10.1111/j.1469-8137.2007.02343.x

Li, X., Sun, J., Li, W., Gong, Z., Jia, C., and Li, P. (2022). Effect of foliar application of the selenium-rich nutrient solution on the selenium accumulation in grains of Foxtail millet (Zhangzagu 10). *Environ. Sci. pollut. Res. Int.* 29, 5569–5576. doi: 10.1007/s11356-021-16013-8

Li, L., Xiong, Y., Wang, Y., Wu, S., Xiao, C., Wang, S., et al. (2023). Effect of nano selenium on nutritional quality of cowpea and response of ABCC transporter family. *Molecules* 28, 1398. doi: 10.3390/molecules28031398

Li, M., Zhao, Z., Zhou, J., Zhou, D., Chen, B., Huang, L., et al. (2018). Effects of foliar spray of selenite or selenate at different growth stages on selenium distribution and quality of blueberries. *J. Sci. Food.* 98, 4700–4706. doi: 10.1002/jsfa.9004

Li, D., Zhou, C., Zhang, J., An, Q., Wu, Y., Li, J. Q., et al. (2020). Nanoselenium foliar applications enhance the nutrient quality of pepper by activating the capsaicinoid synthetic pathway. *J. Agric. Food Chem.* 68, 9888–9895. doi: 10.1021/acs.jafc.0c03044

Lilay, G. H., Persson, D. P., Castro, P. H., Liao, F., Alexander, R. D., Aarts, M. G. M., et al. (2021). Arabidopsis bZIP19 and bZIP23 act as zinc sensors to control plant zinc status. *Nat. Plants* 7, 137–143. doi: 10.1038/s41477-021-00856-7

Mostofa, M. G., Rahman, M. M., Siddiqui, M. N., Fujita, M., and Tran, L. P. (2020). Salicylic acid antagonizes selenium phytotoxicity in rice: selenium homeostasis, oxidative stress metabolism and methylglyoxal detoxification. *J. Hazard Mater.* 394, 122572. doi: 10.1016/j.jhazmat.2020.122572

Mushtaq, N. U., Alghamdi, K. M., Saleem, S., Shajar, F., Tahir, I., Bahieldin, A., et al. (2022). Selenate and selenite transporters in proso millet: Genome extensive detection and expression studies under salt stress and selenium. *Front. Plant Sci.* 13. doi: 10.3389/fpls.2022.1060154

Ning, N., Yuan, X. Y., Dong, S. Q., Wen, Y. Y., Gao, Z. P., Guo, M. J., et al. (2016). Increasing selenium and yellow pigment concentrations in foxtail millet (Setaria italica L.) grain with foliar application of selenite. *Biol. Trace Elem. Res.* 170, 245–252. doi: 10.1007/s12011-015-0440-2

Overmyer, K., Brosche, M., and Kangasjarvi, J. (2003). Reactive oxygen species and hormonal control of cell death. *Trends Plant Sci.* 8, 335–342. doi: 10.1016/S1360-1385(03)00135-3

Poggi, V., Arcioni, A., Filippini, P., and Pifferi, P. G. (2000). Foliar application of selenite and selenate to potato (Solanum tuberosum): effect of a ligand agent on selenium content of tubers. *J. Agric. Food Chem.* 48, 4749–4751. doi: 10.1021/jf000368f

Pu, Z., Wei, G., Liu, Z., Chen, L., Guo, H., Li, Y., et al. (2021). Selenium and anthocyanins share the same transcription factors R2R3MYB and bHLH in wheat. *Food Chem.* 356, 129699. doi: 10.1016/j.foodchem.2021.129699

Raina, M., Sharma, A., Nazir, M., Kumari, P., Rustagi, A., Hami, A., et al. (2021). Exploring the new dimensions of selenium research to understand the underlying mechanism of its uptake, translocation, and accumulation. *Physiol. Plantarum* 171, 882–895. doi: 10.1111/ppl.13275

Ramkissoon, C., Degryse, F., da Silva, R. C., Baird, R., Young, S. D., Bailey, E. H., et al. (2019). Improving the efficacy of selenium fertilizers for wheat biofortification. *Sci. Rep.* 9, 19520. doi: 10.1038/s41598-019-55914-0

Rao, S., Yu, T., Cong, X., Lai, X., Xiang, J., Cao, J., et al. (2021). Transcriptome, proteome, and metabolome reveal the mechanism of tolerance to selenate toxicity in Cardamine violifolia. *J. Hazard. Mater.* 406, 124283. doi: 10.1016/j.jhazmat.2020.124283

Riaz, N., and Guerinot, M. L. (2021). All together now: regulation of the iron deficiency response. *J. Exp. Bot.* 72, 2045–2055. doi: 10.1093/jxb/erab003

Rider, S. A., Davies, S. J., Jha, A. N., Clough, R., and Sweetman, J. W. (2010). Bioavailability of co-supplemented organic and inorganic zinc and selenium sources in a white fishmeal-based rainbow trout (Oncorhynchus mykiss) diet. *J. Anim. Physiol. Anim. Nutr.* 94, 99–110. doi: 10.1111/jpn.2009.94.issue-1

Schiavon, M., Pilon, M., Malagoli, M., and Pilon-Smits, E. A. (2015). Exploring the importance of sulfate transporters and ATP sulphurylases for selenium hyperaccumulation-a comparison of Stanleya pinnata and Brassica juncea (Brassicaceae). *Front. Plant Sci.* 6. doi: 10.3389/fpls.2015.00002

Shibagaki, N., Rose, A., McDermott, J. P., Fujiwara, T., Hayashi, H., Yoneyama., T., et al. (2002). Selenate-resistant mutants of Arabidopsis thaliana identify Sultr1; 2, a sulfate transporter required for efficient transport of sulfate into roots. *Plant J.* 29, 475–486. doi: 10.1046/j.0960-7412.2001.01232.x

Taylor, M. R., Reinders, A., and Ward, J. M. (2015). Transport function of rice amino acid permeases (AAPs). *Plant Cell Physiol.* 56, 1355–1363. doi: 10.1093/pcp/pcv053

Verrier, P. J., Bird, D., Buria, B., Dassa, E., Forestier, C., Geisler, M., et al. (2008). Plant ABC proteins - a unified nomenclature and updated inventory. *Trends Plant Sci.* 13, 151–159. doi: 10.1016/j.tplants.2008.02.001

Wang, Y., Nie, L., Ma, J., Zhou, B., Han, X., Cheng, J., et al. (2022). Transcriptomic variations and network hubs controlling seed size and weight during maize seed development. *Front. Plant Sci.* 13. doi: 10.3389/fpls.2022.828923

Wang, Q., Zhang, Y., Hu, H., Hu, J., Xiang, M., and Yang, Q. (2021). Comparative proteomics analysis of the responses to selenium in selenium-enriched alfalfa (Medicago sativa L.) leaves. *Plant Physiol. Biochem.* 165, 265–273. doi: 10.1016/j.plaphy.2021.04.039

White, P. J., and Broadley, M. R. (2009). Biofortification of crops with seven mineral elements often lacking in human diets–iron, zinc, copper, calcium, magnesium, selenium and iodine. *New Phytol.* 182, 49–84. doi: 10.1111/j.1469-8137.2008.02738.x

Xiang, J., Zhang, M., Apea-Bah, F. B., and Beta, T. (2019). Hydroxycinnamic acid amide (HCAA) derivatives, flavonoid C-glycosides, phenolic acids and antioxidant properties of foxtail millet. *Food Chem.* 295, 214–223. doi: 10.1016/j.foodchem.2019.05.058

Yin, N., Mu, L., Liang, Y. L., Hao, W. L., Yin, H. F., Zhu, S. M., et al. (2020). Effects of foliar selenium fertilizer on fruit yield, quality and selenium content of three varieties of Vitis vinifera. *Ying Yong Sheng Tai Xue Bao* 31, 953–958. doi: 10.13287/j.1001-9332.202003.007

Yuan, K. (2008). Functional and genetic analysis of plant transcription factors involved in the plant growth under various environmental conditions. *Dissertations Theses—Gradworks.* 2, 597–600. doi: 10.1109/APMC.1992.672172

Zhang, L., Hu, B., Deng, K., Gao, X., Sun, G., Zhang, Z., et al. (2019). NRT1.1B improves selenium concentrations in rice grains by facilitating selenomethinone translocation. *Plant Biotechnol.* 17, 1058–1068. doi: 10.1111/pbi.13037

Zhang, L., Hu, B., Li, W., Che, R., Deng, K., Li, H., et al. (2014). OsPT2, a phosphate transporter, is involved in the active uptake of selenite in rice. *New Phytol.* 201, 1183–1191. doi: 10.1111/nph.12596

Zhang, S., Li, B., and Luo, K. (2022). Differences of selenium and other trace elements abundances between the Kaschin-Beck disease area and nearby non-Kaschin-Beck disease area, Shaanxi Province, China. *Food Chem.* 373, 131481. doi: 10.1016/j.foodchem.2021.1314813

Zhao, X. Q., Mitani, N., Yamaji, N., Shen, R. F., and Ma, J. F. (2010). Involvement of silicon influx transporter OsNIP2;1 in selenite uptake in rice. *Plant Physiol.* 153, 1871–1877. doi: 10.1104/pp.110.157867

Zheng, Q., Guo, L., Huang, J., Hao, X., Li, X., Li, N., et al. (2023). Comparative transcriptomics provides novel insights into the mechanisms of selenium accumulation and transportation in tea cultivars. *Front. Plant Sci.* 14. doi: 10.3389/fpls.2023.1268537

Zou, Y., Han, C. Y., Wang, F., Tan, Y. H., Yang, S., Huang, C., et al. (2021). Integrated metabolome and transcriptome analysis reveal complex molecular mechanisms underlying selenium response of aloe vera L. *J. Plant Biol.* 64, 135–143. doi: 10.1007/s12374-020-09285-z

frontiers | Frontiers in Plant Science

TYPE Original Research
PUBLISHED 15 April 2024
DOI 10.3389/fpls.2024.1390144

OPEN ACCESS

EDITED BY
Aamir W. Khan,
University of Missouri, United States

REVIEWED BY
Chang Liu,
University of Hohenheim, Germany
Zhenhui Zhong,
Sichuan University, China
Sarah J. Whitcomb,
Agricultural Research Service (USDA), United States

*CORRESPONDENCE
Léa Faivre
lea.faivre@fu-berlin.de

RECEIVED 22 February 2024
ACCEPTED 27 March 2024
PUBLISHED 15 April 2024

CITATION
Faivre L, Kinscher N-F, Kuhlmann AB, Xu X, Kaufmann K and Schubert D (2024) Cold stress induces rapid gene-specific changes in the levels of H3K4me3 and H3K27me3 in *Arabidopsis thaliana*. *Front. Plant Sci.* 15:1390144. doi: 10.3389/fpls.2024.1390144

Cold stress induces rapid gene-specific changes in the levels of H3K4me3 and H3K27me3 in *Arabidopsis thaliana*

Léa Faivre[1]*, Nathalie-Francesca Kinscher[1], Ana Belén Kuhlmann[1], Xiaocai Xu[2], Kerstin Kaufmann[2] and Daniel Schubert[1]

[1]Epigenetics of Plants, Freie Universität Berlin, Berlin, Germany, [2]Department for Plant Cell and Molecular Biology, Institute for Biology, Humboldt-Universität zu Berlin, Berlin, Germany

When exposed to low temperatures, plants undergo a drastic reprogramming of their transcriptome in order to adapt to their new environmental conditions, which primes them for potential freezing temperatures. While the involvement of transcription factors in this process, termed cold acclimation, has been deeply investigated, the potential contribution of chromatin regulation remains largely unclear. A large proportion of cold-inducible genes carries the repressive mark histone 3 lysine 27 trimethylation (H3K27me3), which has been hypothesized as maintaining them in a silenced state in the absence of stress, but which would need to be removed or counteracted upon stress perception. However, the fate of H3K27me3 during cold exposure has not been studied genome-wide. In this study, we offer an epigenome profiling of H3K27me3 and its antagonistic active mark H3K4me3 during short-term cold exposure. Both chromatin marks undergo rapid redistribution upon cold exposure, however, the gene sets undergoing H3K4me3 or H3K27me3 differential methylation are distinct, refuting the simplistic idea that gene activation relies on a switch from an H3K27me3 repressed chromatin to an active form enriched in H3K4me3. Coupling the ChIP-seq experiments with transcriptome profiling reveals that differential histone methylation only weakly correlates with changes in expression. Interestingly, only a subset of cold-regulated genes lose H3K27me3 during their induction, indicating that H3K27me3 is not an obstacle to transcriptional activation. In the H3K27me3 methyltransferase *curly leaf (clf)* mutant, many cold regulated genes display reduced H3K27me3 levels but their transcriptional activity is not altered prior or during a cold exposure, suggesting that H3K27me3 may serve a more intricate role in the cold response than simply repressing the cold-inducible genes in naïve conditions.

KEYWORDS

chromatin, histone methylation, cold stress, polycomb, trithorax, Arabidopsis

Abbreviations: COR, Cold Responsive; DE, Differentially Expressed; DM, Differentially Methylated; GO, Gene Ontology; H3K4me3, Histone 3 Lysine 4 trimethylation; H3K27me3, Histone 3 Lysine 27 trimethylation; TES, Transcription End Site; TSS, Transcription Start Site; PTM, Post-Translational Modification; PcG, Polycomb Group; TrxG, Trithorax Group; PRC2, Polycomb Repressive Complex 2; log2FC, log2 fold change; RPKM, Read Per Kilobase per Million mapped read.

1 Introduction

Low temperatures negatively affect both plant growth and productivity. Low temperature stress can be divided into chilling stress (0-15°C for temperate plants such as *Arabidopsis thaliana*) and freezing stress (subzero temperatures) and plants devised strategies to cope with both of these stress types (Zarka et al., 2003). While plants have a constitutive tolerance towards chilling stress, the freezing tolerance of most plants growing in a temperate climate is increased during an exposure to low but non-freezing temperatures, a process known as cold acclimation (Gilmour et al., 1988; Jan et al., 2009). Cold acclimation relies on the production of a variety of proteins whose function is to limit the damage caused by a putative future freezing event and is therefore associated with a significant transcriptional reprogrammation (Calixto et al., 2018; Shi et al., 2018). Upon perception of low temperature, the ICE1 transcription factor is activated, thereby inducing the expression of the C-repeat Binding Factors (CBFs) (Wang et al., 2017). In turn, the CBFs bind to the C-Repeat motifs of cold-responsive (*COR*) genes (Yamaguchi-Shinozaki and Shinozaki, 1994; Medina et al., 1999). This results in the transcriptional activation of thousands of *COR* genes within a few hours of exposure to low temperatures. While numerous transcription regulators have been identified as playing a role in cold acclimation, the putative contribution of the chromatin status to this transcriptional reprogramming remains underinvestigated.

Chromatin is an important contributor to the regulation of transcription, as it controls the accessibility of the underlying DNA to the transcriptional machinery. Within the nucleus, DNA is wrapped around octamers of histones, forming the nucleosome, which is the basic organizational unit of the chromatin (Kornberg, 1977; Luger et al., 1997). Histones tails protrude from the nucleosome and can be heavily post-translationally modified by acetylation, methylation and phosphorylation, among others (Luger and Richmond, 1998; Zhao and Garcia, 2015). Those histone post-translational marks (PTMs) can affect the transcriptional activity of the underlying gene directly, by modulating the strength of the interaction between DNA and histones, or indirectly, by recruiting other proteins called histone readers that recognize and bind to specific histone PTMs (Blakey and Litt, 2015). Depending on whether they are associated with transcribed or silenced genes, histone PTMs are classified as active or repressive marks, respectively. Some of the most characterized histone PTMs are the trimethylation on lysine 4 (H3K4me3) and 27 (H3K27me3) of histone 3, which respectively act as an active and a repressive mark (Roudier et al., 2011; Cheng et al., 2020). H3K27me3 is deposited by the Polycomb Repressive Complex 2 (PRC2) and contributes to the silencing of its targets (Müller et al., 2002; Zhang et al., 2007). PRC2, which was initially identified in *Drosophila*, consists of four subunits, including the Enhancer of zeste [E(z)] methyltransferase (Müller et al., 2002). Three homologs of E(z) have been identified in *Arabidopsis thaliana*: CURLY LEAF (CLF), SWINGER (SWN) and MEDEA (MEA) (Chanvivattana et al., 2004). The action of PRC2 is counteracted by methyltransferases from the Trithorax (TrxG) group, which deposit H3K4me3 (Ingham, 1983; Ringrose and Paro, 2004). H3K27me3 and H3K4me3 have long been described as being mutually exclusive, with genes undergoing a Polycomb (PcG)/TrxG switch during their transcriptional activation, where H3K27me3 is removed and replaced by H3K4me3 (Ringrose and Paro, 2004; Köhler and Hennig, 2010; Kuroda et al., 2020).

In plants, both H3K4me3 and H3K27me3 have been implicated in the control of development, but also of stress responses (Köhler and Hennig, 2010; Kleinmanns and Schubert, 2014; Engelhorn et al., 2017; Faivre and Schubert, 2023). Indeed, several PcG proteins are necessary for the repression of stress responses in plants growing in optimal conditions (Alexandre et al., 2009; Kim et al., 2010; Kleinmanns et al., 2017) while numerous TrxG members have been shown to be essential to the proper induction of stress responses (Ding et al., 2011; Song et al., 2021). In addition to the immediate control of stress responses, both H3K4me3 and H3K27me3 also regulate the memory of past stress episodes (Friedrich et al., 2018; Yamaguchi et al., 2021). However, the potential role of both methylation marks in the response to cold and in cold acclimation remains largely underinvestigated. Numerous *COR* genes carry H3K27me3 in the absence of cold (Vyse et al., 2020) and the repressive mark is lost on certain loci during cold exposure (Kwon et al., 2009). H3K27me3 has therefore been hypothesized to maintain the *COR* genes in a silenced state until the plant perceives low temperatures, at which point the repression is lifted through demethylation. However, previous work from our lab demonstrated that not all H3K27me3-carrying *COR* genes undergo demethylation during cold exposure (Vyse et al., 2020), raising questions on both the role of H3K27me3 and its removal in the control of cold responses. In order to shed more light on the putative contribution of H3K27me3 to cold acclimation, we performed a genome-wide profiling of its distribution during cold exposure. As stress-responsive genes are commonly thought to be undergoing a PcG/TrxG switch during their activation, the distribution of H3K4me3 was also examined. We uncovered a rapid redistribution of both methylation marks upon cold exposure, albeit on distinct sets of genes. By combining the epigenomic approach with a transcriptomic study, we identified a correlation between differential methylation and differential expression. However, differential methylation was not required for the transcriptional activation of *COR* genes, but might favor a higher amplitude of induction. Finally, we examined the impact of reduced H3K27me3 levels in the *clf* mutant on the cold acclimation response and could not detect any significant difference in physiological or transcriptional responses, suggesting that H3K27me3 might not participate directly in the cold response but rather in more long-term responses or to the deacclimation process. Alternatively, H3K27me3 levels may only be sufficiently reduced in *clf swn* double mutants for unmasking the role of H3K27me3 in cold acclimation.

2 Materials and methods

2.1 Plant material and growth conditions

Arabidopsis thaliana accession Columbia (Col-0) was used as a wild type. The *clf-28* line (SALK_139371) was obtained from the Nottingham Arabidopsis Stock Centre (NASC). The primers used for genotyping are listed in Supplementary Table S1. The seeds were surface-sterilized, stratified in the dark at 4°C for three days and grown on ½ MS media supplemented with Gamborg B5 vitamins

(Duchefa) containing 1.5% (w/v) plant agar (Duchefa) in short day conditions (8 h light, 16 h darkness) at 20°C for 21 days. Cold treatments were performed at 4°C in short day conditions (8 h light, 16 h darkness) for 3 hours or 3 days, with the treatment starting one hour after light onset.

2.2 Electrolyte leakage

Plants were grown as described previously for 21 days and placed at 4°C for three days. The freezing tolerance was then measured by electrolyte leakage assay using a protocol adapted from Hincha and Zuther (2014). Four technical replicates were performed for each biological replicate. For each sample, six temperature points were measured, using a pool of shoot tissue of five to eight seedlings. The LT50 was determined using the non-linear regression log(agonist) vs response from the GraphPad Prism version 7.0 (GraphPad Software).

2.3 Western blot

100 mg of 21 day-old seedlings were harvested 4 hours after the light onset and flash-frozen in liquid nitrogen. The histones were extracted following the protocol described in Bowler et al. (2004) with the following modifications: the samples were resuspended in 1 mL of buffer 1. After filtration through Miracloth, the samples were centrifuged 20 min at 4000 rpm at 4°C. The pellets were resuspended in 300 µL of buffer 2, centrifuged 10 min at 13000 rpm at 4°C and resuspended in 300 µL of buffer 3 and layered on 300 µL of clean buffer 3. After a 1 h centrifugation at 13000 rpm at 4°C, the pellets were resuspended in 100 µL of nuclei lysis buffer. The protein concentration was assessed using the Qubit protein assay (ThermoFisher Scientific) and all samples were adjusted to the same concentration using nuclear lysis buffer. The immunoblot analysis was performed as described in Hisanaga et al. (2023) using the following antibodies: α-H3K27me3 (C15410195 Diagenode), α-H3K4me3 (C15410003, Diagenode) and α-H3pan (C15200011 Diagenode). The imaging was performed using the Image Studio Lite software (Li-Cor, version 5.2). The intensity of the H3K27me3 and H3K4me3 signals were normalized to the intensity of the H3 signal.

2.4 ChIP-qPCR

1 g of 21 day-old seedlings was harvested 4 hours after the light onset. The cross-linking reaction, chromatin extraction and immunoprecipitation were performed as previously described in Vyse et al. (2020). The chromatin was incubated with 1 µg of α-H3K27me3 (C15410195 Diagenode), α-H3K4me3 (C15410003, Diagenode), α-H3pan (C15200011 Diagenode) or IgG (C15410206 Diagenode) antibodies. The qPCR was performed using the Takyon ROX SYBR MasterMix blue dTTP kit and the QuantStudio5 (Applied Biosystems). The primers used for the ChIP-qPCR analysis are listed in Supplementary Table S1.

2.5 ChIP-seq

After DNA recovery, the DNA was purified and concentrated using the ChIP DNA Clean and Concentrator lit (Zymo Research). The libraries were prepared using the ThruPLEX DNA-seq kit (Takara Bio) and indexes from the SMARTer DNA HT Dual Index kit (Takara Bio). DNA fragments were then selected based on size using AMPure beds (Beckman Coulter). The concentration of the samples was measured using the Qubit dsDNA High Sensitivity kit and the Qubit Fluorometer (ThermoFisher Scientific) and the library quality was assessed using the High Sensitivity DNA ScreenTape and the TapeStation (Agilent). The libraries were sequenced by Novogene (UK) using a HiSeq instrument (Illumina) in 150bp paired-end mode. Two biological replicates were performed, a summary of the reads number is given in Supplementary Table S2.

Bioinformatic analyses were performed using Curta, the High Performance Computing of the Freie Universitaet Berlin (Bennet, Melchers and Proppe, 2020). The reads were mapped to the TAIR10 reference genome of *Arabidopsis thaliana* using Bowtie2 (Langmead and Salzberg, 2012). PCR duplicates and reads with an aligment quality MAPQ < 10 were removed using samtools rmdup and samtools view respectively (Li et al., 2009). The peak calling was performed using MACS2, using the broad option and a p-value threshold of 0.01 (Gaspar, 2018). Bigwig tracks were generated by pooling the two replicates and normalizing as RPKM using DeepTools bamCoverage, using a bin size of 10bp (Ramírez et al., 2016) and visualized using the IGV genome browser (Robinson et al., 2011).

Read counts for each nuclear-encoded gene (from TSS to TES) were obtained using featureCounts (Liao et al., 2014) and fold changes were computed using DESeq2 (Love et al., 2014). A gene was considered differentially methylated if (i) at least 150bp of its coding sequence (from TSS to TES) was included within a peak of the histone mark in at least one of the tested condition and (ii) it showed an absolute log2 fold change (log2FC) of at least 0.5. The metagenes plots were produced using deepTools (Ramírez et al., 2016) on the merged RPKM bigwig files, scaling all genes to 2000 bp and examining a region starting 500 bp upstream from the TSS and ending 500 bp downstream form the TES.

2.6 RT-qPCR

100 mg of seedlings were harvested 4 hours after light onset and flash-frozen in liquid nitrogen. After grinding to a fine powder, total RNA was extracted using the innuPREP Plant RNA kit (Analytik Jena). Samples were treated with DNaseI (ThermoFisher Scientific) and cDNA was synthesized using the RevertAid Reverse Transcriptase kit (ThermoFisher Scientific). The qPCR was performed using the Takyon ROX SYBR MasterMix blue dTTP kit and the QuantStudio5 (Applied Biosystems). The primers used for the RT-qPCR analysis are listed in Supplementary Table S1. The Ct values were normalized by subtracting the mean of three housekeeping genes (*ACTIN2*, *PDF* and *TIP41*) from the Ct value of each gene of interest (ΔCt). Transcript abundance was expressed as $2^{-\Delta Ct}$.

2.7 RNA-seq

RNA samples were extracted and DNaseI-treated as previously described. The libraries were prepared using poly-A enrichment by Novogene (UK) and the sequencing was performed on the NovaSeq 600 platform (Illumina) in 150bp paired-end mode. Three biological replicates were analysed and a summary of the reads number is given in Supplementary Table S2.

Bioinformatic analyses were performed using Curta, the High Performance Computing of the Freie Universitaet Berlin (Bennet et al., 2020). The reads were mapped to the reference genome of Arabidopsis thaliana (TAIR10) using STAR (Dobin et al., 2013), using a minimum and maximum intron size of 60 and 6000 bases respectively. The counting was performed using featureCounts (Liao et al., 2014), using only reads with an alignment score superior to 10. The differential expression analysis was performed using the DESeq2 package (Love et al., 2014). A gene was considered to be differentially expressed (DEG) if it presented an absolute log2 fold change of at least 1 and a Benjamini-Hochberg adjusted p-value inferior to 0.05. As the differences in expression were correlated to the differences in histone methylation levels, only nuclear-encoded DEGs were retained in the analysis.

2.8 Statistics and data visualization

Unless stated otherwise, statistical analyses and plots were generated using R or GraphPad Prism (GraphPad Software). Normal distribution was tested using the Shapiro-Wilks' method. For normally distributed data, ANOVA tests and any *post-hoc* tests were performed using the agricolae package (de Mendiburu and Yaseen, 2020). Gene ontology enrichment analyses were performed in RStudio using the topGO package (Alexa and Rahnenfuhrer, 2021), the TAIR10 annotation and the gene-GO term relationships from the org.At.tair.db package, version 3.17.0 (Carlson, 2019). The enrichment analysis was done using the weight01 algorithm and statistical testing was performed using the Fisher exact test. Only terms with a p-value < 0.01 were retained as significantly enriched. Upset plots were generated using the UpSetR package, version 1.4.0 (Conway et al., 2017).

3 Results

3.1 H3K4me3 and H3K27me3 undergo differential methylation upon short cold exposure

To determine whether cold exposure triggers genome-wide changes in the levels of H3K27me3 and H3K4me3, a Western-Blot was conducted on plants exposed to 4°C for three hours or three days (Figures 1A, B). Those two time points have been selected as "early" and "late" time points of cold stress response, respectively. Indeed, transcriptomic responses to cold can already be detected after only three hours of cold exposure (Calixto et al., 2018), while after three days the plants already show a significant cold acclimation at the physiological level (Zuther et al., 2019). For both chromatin marks, no genome wide changes could be detected at the time points tested here. However, previous studies indicated that H3K27me3 is removed from certain loci upon cold exposure while H3K4me3 was shown to be accumulated at others, suggesting that both marks might undergo differential methylation in a loci-specific manner that does not lead to changes detectable at the genome wide scale (Kwon et al., 2009; Miura et al., 2020; Vyse et al., 2020). To assess this possibility, an epigenome profiling of the distribution of H3K4me3 and H3K27me3 was performed at the same time points described above. In total, 13829, 14152 and 14430 H3K4me3 peaks were detected in naïve, 3h and 3d samples respectively while 5753, 5665 and 5802 H3K27me3 peaks were detected in those same samples. These peaks largely overlapped for the individual marks, indicating that short cold exposure did not lead to a substantial redistribution of the chromatin methylation marks investigated here. In order to detect lower magnitudes of methylation levels changes, reads mapped between the transcription start site (TSS) and transcription end site (TES) of genes targeted by each methylation mark were counted and normalized for each condition (Figures 1C–F). The correlation plots indicated that H3K4me3 is accumulated after three hours of cold exposure while after three days, this tendency mostly disappeared (Figures 1C, E). On the other hand, H3K27me3 correlation plots displayed an accumulation of the mark at both time points (Figures 1D, F). The differentially methylated genes were identified as genes targeted by the respective mark (i.e. covered by a peak in a least one condition) and showing an absolute log2FC of the normalized counts of at least 0.5. The complete list of differentially methylated (DM) genes can be found in Supplementary Table 3. Consistent with the general trend observed on the correlation plots, more genes were found to significantly gain H3K4me3 or H3K27me3 than losing it. 3619 and 2309 DM genes were identified for H3K4me3 after three hours and three days of cold treatment, respectively, while H3K27me3 differential methylation was detected only on 735 and 922 genes, respectively. This substantial disparity in the number of DM genes between H3K4me3 and H3K27me3 can be largely explained by the fact that H3K4me3 targets a broader proportion of genes than H3K27me3 (17366 vs 8128): between 13 and 20% of H3K4me3 targets are differentially methylated while only 9 to 11% of H3K37me3 targets undergo changes during cold exposure.

While the proportion of DM genes is not strikingly different between H3K4me3 and H3K27me3, the magnitude of the changes differs significantly, with H3K4me3 DM genes presenting higher absolute fold change values than H3K27me3 DM genes (Figures 1C–F; Supplementary Figure 1). These observations were confirmed when examining the levels of both methylation marks at specific loci (Figure 2A): the changes of H3K4me3 were drastic, leading to peaks appearing (*CBF3*, *LTI30* and *COR15A*) or disappearing (*HSP90.1*). The changes were prominently located just downstream of the TSS, consistent with the known localization of H3K4me3, whose peaks usually center around the TSS of its target genes, and were more pronounced after three days than after three hours (Supplementary Figure 1A). On the other hand, while H3K27me3 loss led to the almost-complete loss of peaks at certain loci such as

10.3389/fpls.2024.1390144

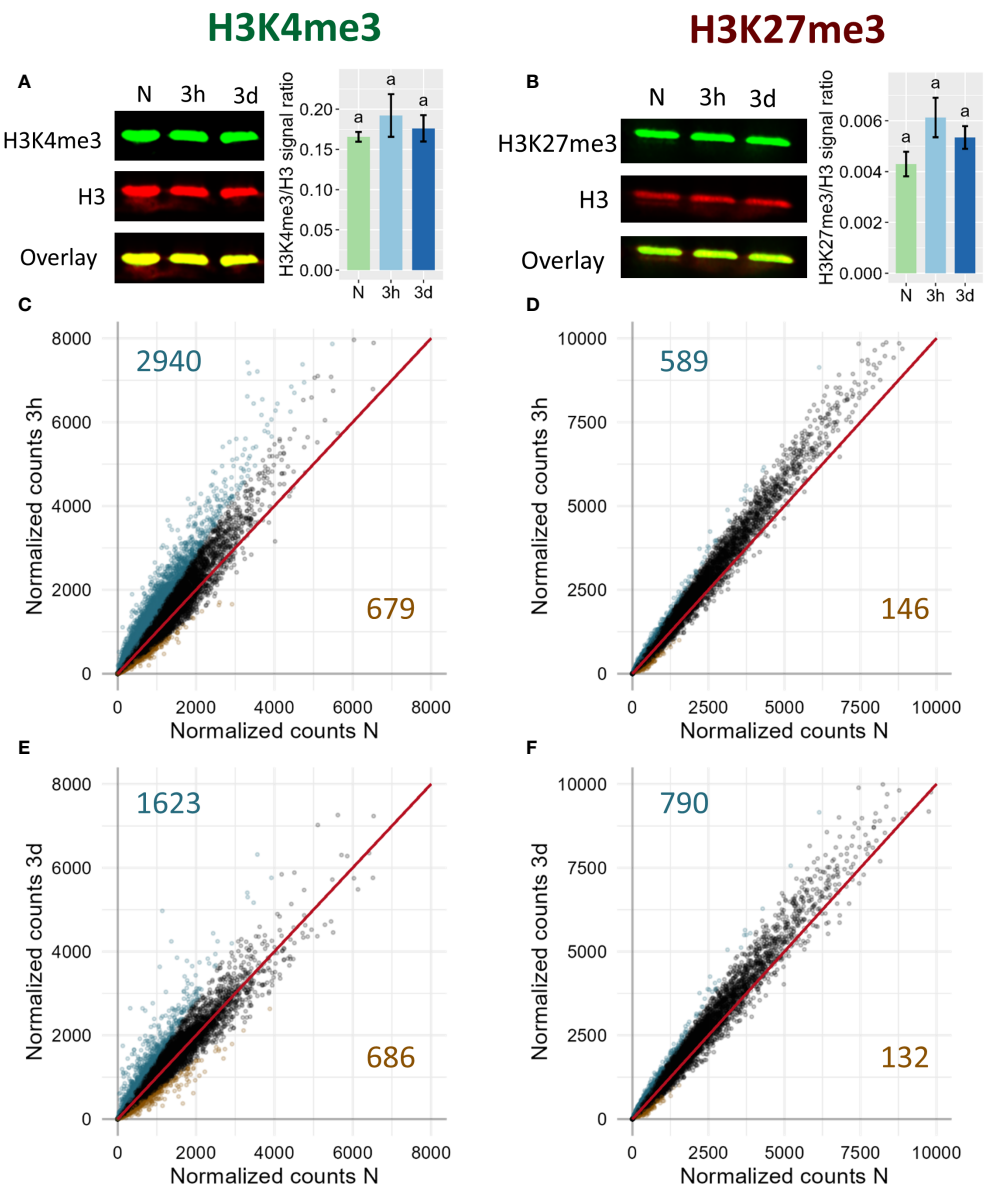

FIGURE 1
Genome-wide dynamics of H3K4me3 (left) and H3K27me3 (right) upon cold exposure. Plants were grown for 21 days at 20°C (N) and then exposed to 4°C for three hours (3h) or three days (3d). **(A, B)** Global levels of H3K4me3 and H3K27me3, respectively, as measured by Western Blot. The membrane images show the signal of the histone methylation mark in green, of total histone 3 in red and the overlay of both signals in yellow. The bar charts on the right of the membrane images display the modification/H3 signal ratio of four independent biological replicates. Significance was tested by one-way ANOVA followed by a Tukey *post-hoc* test ($\alpha = 0.05$). Identical letters indicate no significant difference. **(C–F)** Correlation plot of H3K4me3 **(C, E)** and H3K27me3 **(D, F)** levels on genes targeted by the respective mark after 3h **(C, D)** or 3d **(E, F)** of cold exposure. Each point represents a gene targeted by the respective mark. Reads were counted over the gene body and were normalized to library size using DESeq2 (See Materials and Methods). Genes showing a log2 fold change of the respective mark smaller than -0.5 are displayed in orange, while genes showing log2 fold change of at least 0.5 are displayed in turquoise. Total number of genes satisfying these criteria are indicated in orange in the lower right quadrant and turquoise in the upper left quadrant respectively.

LTI30, it was more limited on others such as *COR15A*, where the H3K27me3 peaks were still visible after three days of cold treatment. Genes gaining H3K27me3 showed moderately increased levels of the repressive mark on the sides of the original peak (*END1* and *AT5G43570*). The variations in H3K27me3 occurred on the whole gene body of the DM genes and were more pronounced in the case of loss than of gain (Supplementary Figure 1B). Overall, even short cold exposure times of three hours were sufficient to trigger significant alteration of the level of both methylation marks on thousands of loci.

3.2 H3K4me3 and H3K27me3 differential methylation occurs on stress responsive and developmental genes, respectively

Overlapping the sets of DM genes at each time point revealed that only a minor proportion of them undergo a change in both H3K4me3 and H3K27me3 levels, totaling 35 genes at the 3h time point and 58 at the 3d time point (Figures 2B, C). As those marks are commonly described as antagonists, genes differentially

10.3389/fpls.2024.1390144

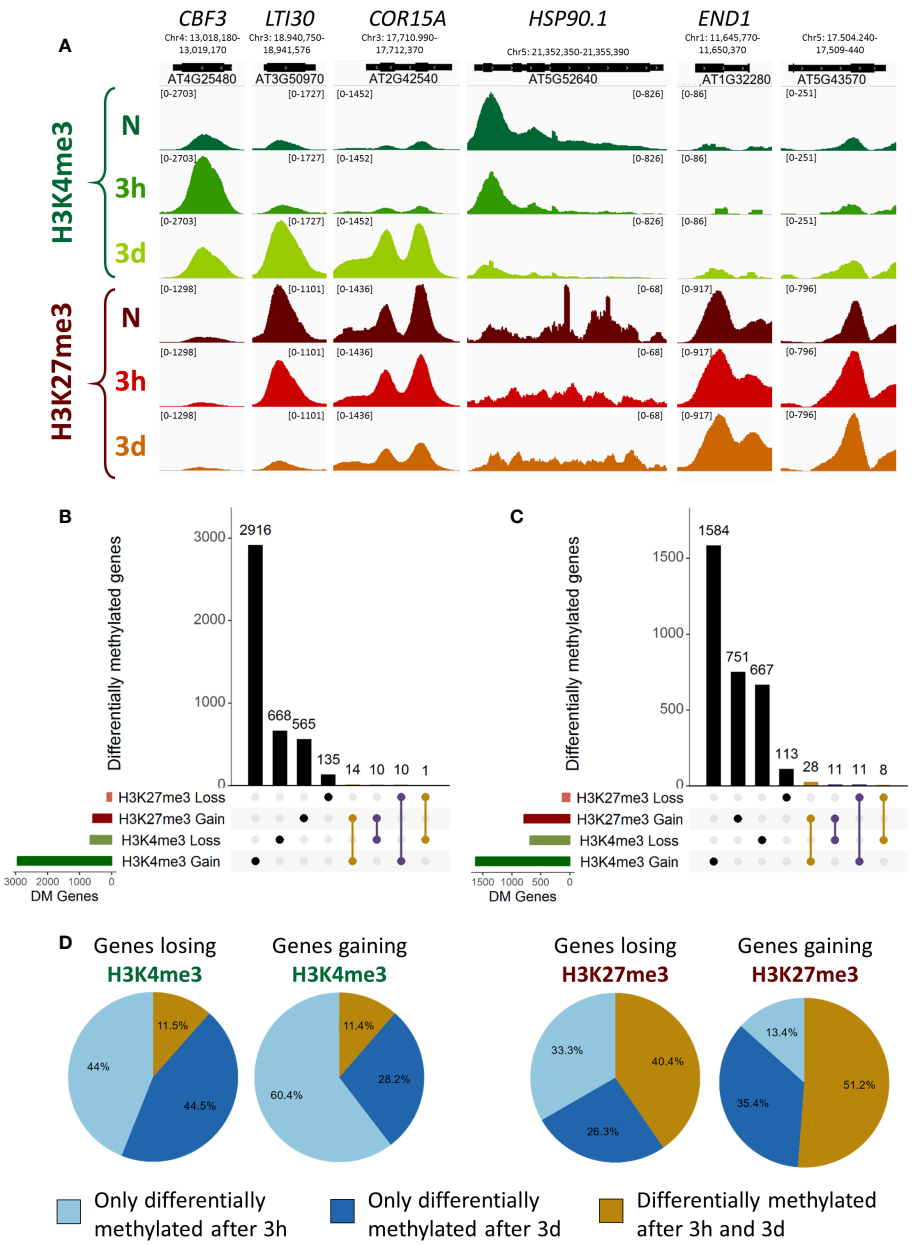

FIGURE 2
Characterization of differentially methylated genes. A differentially methylated gene is defined as a gene targeted by H3K4me3 or H3K27me3, respectively, and showing an absolute log2 fold change of the respective methylation level of at least 0.5. **(A)** Genome browser views of H3K4me3 and H3K27me3 ChIP-seq signals at selected differentially methylated genes, in naïve plants (N) or plants exposed to 4°C for 3h or 3d. The numbers in bracket at the top of each track indicate the scale of that track in reads per million per bin. **(B, C)** UpSet plots showing the overlaps of differentially methylated genes for both histone methylation marks after 3h or 3d in the cold respectively. Intersections of same direction of change are highlighted in yellow while intersections of opposite direction of change are highlighted in purple. **(D)** Pie charts indicating the percentage of differentially methylated genes being specifically regulated at a single time point or at both time points examined, for each histone mark and direction of differential methylation.

methylated for both marks would be expected to display opposite changes. However, there are only slightly fewer genes showing same direction changes than opposite (10 vs 25 at 3h, 22 vs 36 at 3d), suggesting that the loss of one mark does not entail a gain of the other and vice versa. As the DM gene sets of H3K4me3 and H3K27me3 displayed such a reduced overlap, we hypothesized that H3K4me3 and H3K27me3 differential methylation might serve distinct purposes. To explore this hypothesis, a gene ontology (GO) term analysis for biological function was performed on each DM gene set (Supplementary Figures 2, 3; Supplementary Table 5). Genes gaining H3K4me3 during a cold treatment were enriched for terms related to the cold response, cold acclimation and freezing tolerance as well as terms linked to the response to other abiotic and biotic stresses (water deprivation, hypoxia, fungus) (Supplementary Figures 2A, C). After three hours of cold exposure, genes losing H3K4me3 were enriched for terms

related to protein refolding and chromatid cohesion, while after three days the set showed an enrichment for development and photosynthesis related terms (Supplementary Figures 2B, D). Few terms were found to be enriched among the genes losing H3K27me3, which might be due to the smaller size of the sets (Supplementary Figures 3B, C). Some terms related to stress responses were identified (response to salicylic acid and to fungus) but surprisingly, no term associated to the cold response was found to be enriched. Genes gaining H3K27me3 upon cold exposure were mostly enriched for development related terms (Supplementary Figures 3A, C). H3K4me3 and H3K27me3 differential methylation therefore occur on different sets of genes, with H3K4me3 DM mostly targeting stress responsive genes and H3K27me3 DM developmental genes. This could suggest that differential histone methylation holds a distinct role in the cold response depending on the specific mark.

To determine whether the methylation changes triggered by cold exposure were stable over time or dynamic, their persistence was examined by computing the percentage of genes differentially methylated at both time points (Figure 2D). In the case of H3K4me3, only 11% of the DM genes were identified at both time points, indicating that the variations in the level of the active mark were rather transient. On the contrary, 40 to 50% of H3K27me3 DM genes displayed a change at both time points, revealing H3K27me3 changes to be more stable over time than those of H3K4me3. Taken together with the results of the GO analysis and the small overlap between the genes which are DM for H3K4me3 and H3K27me3, this suggests that H3K4me3 and H3K27me3 differential methylation might serve distinct purposes.

3.3 Differential methylation only partially correlates with differential expression

As H3K4me3 and H3K27me3 are commonly described as favoring and silencing transcription, respectively, we hypothesized that the changes in the levels of those two chromatin marks might associate with differences in the transcriptional activity of the underlying genes. A transcriptome analysis was therefore performed on the same seedlings used for the epigenome investigations, leading to the identification of the nuclear-encoded genes up- and down-regulated after three hours or three days of cold exposure (Supplementary Table 4). As expected, at all the tested time points, the absolute levels of H3K4me3 and H3K27me3 positively and negatively correlated with the absolute expression level of the genes, respectively (Supplementary Figure 5). Next, the potential correlations between differential methylation and differential expression were examined. After three hours of cold treatment, no correlation between the changes in H3K4me3 levels and the changes in expression could be detected (Figure 3A), while a weak negative correlation was observed for H3K27me3 (Figure 3B). However, after three days, the changes in expression were positively and negatively correlated with the variations in H3K4me3 and H3K27me3, respectively (Figures 3C, D), indicating that genes up-regulated by a cold treatment were more likely to gain H3K4me3 and/or lose H3K27me3. Still, the correlation coefficients were modest and the scatterplots revealed that they did not hold true for all differentially expressed (DE) genes, indicating that the correlations between differential expression and methylation are only partial. Furthermore, since those correlations were seen after three days of cold exposure but not (or to a lesser extend) after three hours, it is likely that the two phenomena (differential expression and differential methylation) occur at a different pace. Indeed, after three days at 4°C, the plants are accustomed to the cold and cold acclimation can already be detected at a physiological level, while after only three hours, the plant is only starting its acclimation process and not all responses are fully accomplished yet (Calixto et al., 2018; Zuther et al., 2019). To try and decipher whether chromatin or expression changes first, the correlations analyses were repeated across time points (Figure 3E). The early methylation changes did not strongly correlate with the late expression changes. However, early expression changes correlated positively and negatively with the variations in H3K4me3 and H3K27me3 levels at the late time point, respectively. Those results collectively suggest that the transcriptional activity of a gene is modulated ahead of its chromatin methylation status, but more precise time-course experiments would be required to fully confirm this observation.

Although significant correlations between methylation and expression changes could be detected, their magnitude was relatively modest. The lists of significantly DE and DM genes exhibited a moderate overlap (Supplementary Figure 6), indicating that differential methylation is not required for differential expression and that differential expression does not necessarily result in differential methylation. Whether differential methylation contributes, even partially, to the transcriptome reprogramming remains unelucidated. In order to examine whether it might facilitate the induction of cold responsive genes, the transcriptional activity of non DM and DM genes was compared for each chromatin mark (Figures 4 and 5). Out of the 17366 genes detected as carrying H3K4me3 at any time point of the stress regimen, 1714 were up-regulated upon cold treatment (Figure 4A). The majority (57%) of these genes did not undergo differential methylation, as observed on the UpSet plots (Supplementary Figure 6), while the levels of H3K4me3 increased on 37% of the genes and decreased for 6% of them, consistent with the correlation analyses (Figure 3). The genes undergoing differential methylation had slightly lower H3K4me3 levels than non-DM genes prior to cold exposure (Figure 4D). This was associated with a lower basal expression of genes losing H3K4me3, but no difference in expression in naïve conditions could be seen between non DM genes and genes gaining H3K4me3 upon cold exposure (Figure 4B). During a cold stress, the expression of genes gaining H3K4me3 increased significantly more than those of non DM and genes losing H3K4me3 and reached higher overall expression levels (Figures 4B, C). There was however no difference in the fold change of gene expression between non DM and genes losing H3K4me3. This suggests that H3K4me3 gain, while not strictly necessary for gene activation, might facilitate it, leading to a higher magnitude of induction.

8128 genes have been detected as carrying H3K27me3 in at least one time point during the stress regiment, of which 550 were induced by cold (Figure 5A). Only 3.6% of those genes lost

10.3389/fpls.2024.1390144

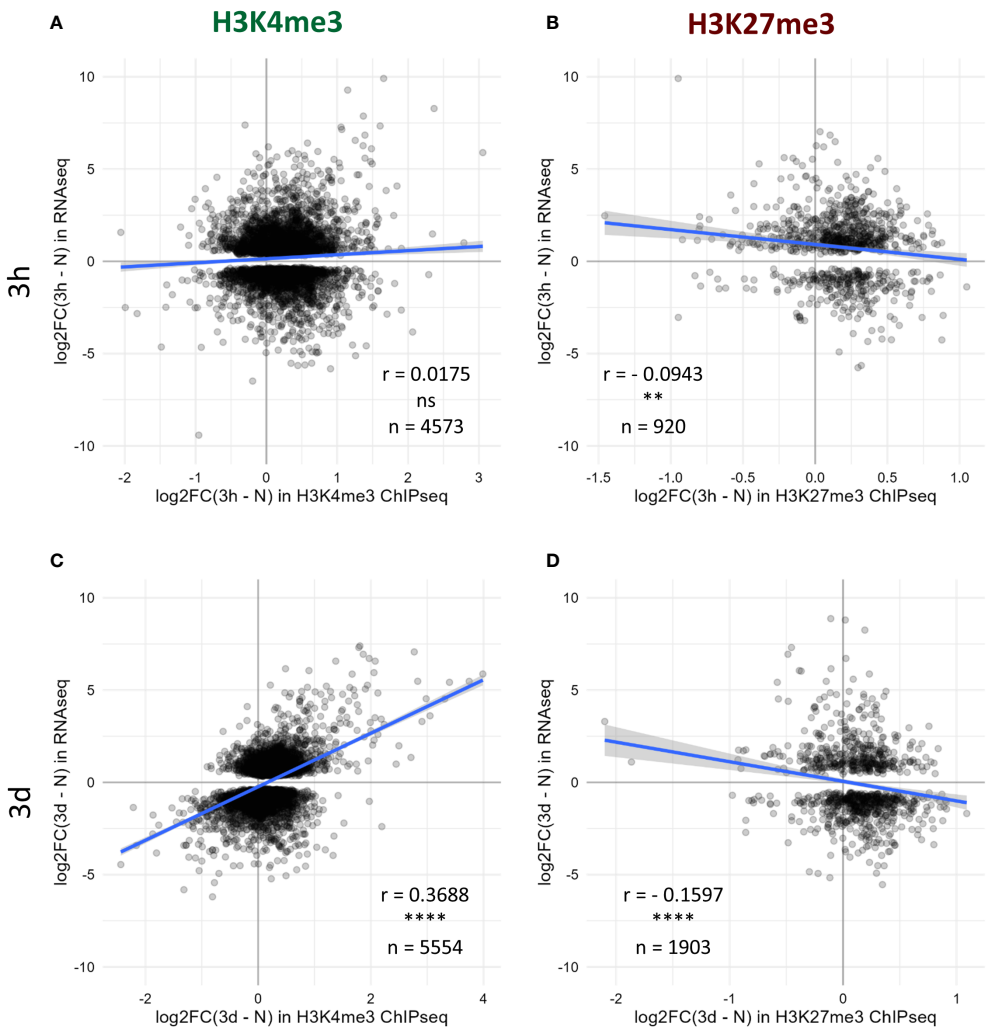

E

	H3K4me3	H3K27me3
Early (3h) expression changes vs Late (3d) methylation changes	r = 0.2242 ****	r = - 0.1337 ****
Late (3d) expression changes vs Early (3h) methylation changes	r = - 0.0705 ****	r = - 0.1053 **

FIGURE 3
Correlation between histone methylation and expression changes upon cold exposure. Plants were grown for 21 days at 20°C (N) and then exposed to 4°C for three hours (3h) or three days (3d). H3K4me3 and H3K27me3 levels were measured by ChIP-seq while the changes in expression were detected by an RNA-seq conducted on RNA isolated from the same seedlings. Correlation between changes in expression and changes in H3K4me3 **(A, C)** or H3K27me3 **(B, D)** levels after 3h **(A, B)** or 3d **(C, D)** of cold exposure. For each graph, the X axis denotes the log2 fold change in methylation signal over the whole gene body at the respective time point compared to non-cold treated plants while the Y axis shows the log2 fold change in expression for the same comparison. Only genes which are differentially expressed at the considered time point, i.e. present an absolute log2 fold change >= 1 and a p-adj < 0.05, and are targeted by the respective mark are shown on the scatterplot, their number is indicated as n. The correlation analyses were performed using the Spearman method, the correlation coefficient is indicated as r. ns indicates a non-significant correlation, ** denotes a p-value < 0.01 and **** a p-value < 0.0001. **(E)** Table summarizing the correlation between changes in expression and in methylation levels across time points, performed as described above.

H3K27me3 during cold exposure, confirming that H3K27me3 is not an obstacle to gene induction (Vyse et al., 2020). Surprisingly, a higher proportion (7.6%) showed an increase in H3K27me3 levels. Both genes gaining or losing H3K27me3 upon cold treatment had lower H3K27me3 levels in naïve conditions compared to non DM H3K27me3 targets (Figure 5D). However, this difference in the levels of the repressive mark was not associated with a difference in expression in naïve conditions (Figure 5B). The expression of non DM and DM genes remained similar upon cold exposure, but the genes losing H3K27me3 showed a higher fold change of expression

10.3389/fpls.2024.1390144

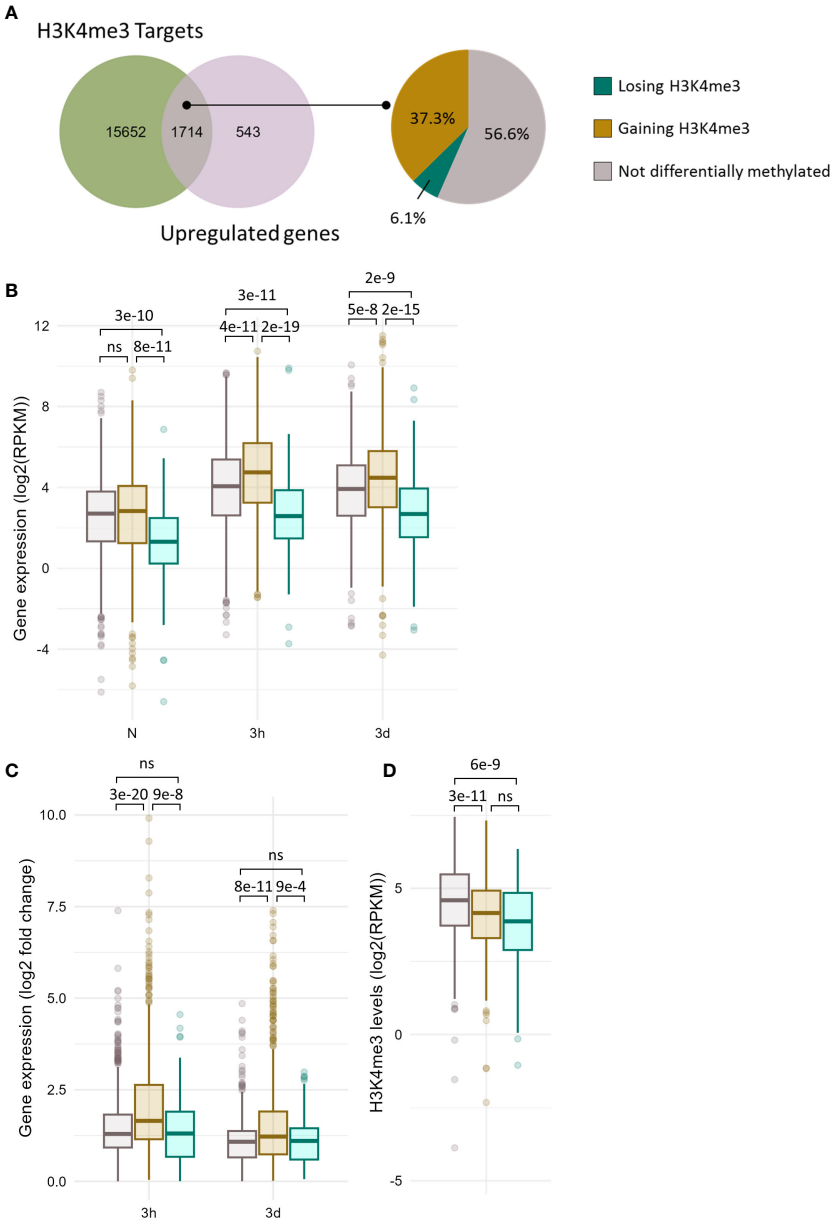

FIGURE 4
A subset of cold induced genes gains H3K4me3 upon cold exposure. **(A)** Venn diagram showing the overlap between the genes carrying H3K4me3 and the genes induced at any time point during cold exposure (left panel). Pie chart showing the percentage of genes gaining or losing H3K4me3 at any time point during cold exposure among the 1714 genes which are induced by cold and carry H3K4me3 (right panel). **(B)** Box plot showing the distribution of gene expression during cold exposure for the three gene categories listed in **(A)**. Gene expression is shown as log2 of the RPKM (Read Per Kilobase per Million mapped read). **(C)** Box plot showing the distribution of log2 fold change in gene expression after 3h and 3 days of cold exposure for the three gene categories listed in **(A)**. **(D)** Box plot showing the distribution of H3K4me3 levels as RPKM for the three gene categories listed in **(A)**. The p-values were computed using a two-sided Wilcoxon rank-sum test. ns indicates no significance.

after three days of cold treatment compared to genes which gained H3K27me3 (Figures 5B, C). This suggests that H3K27me3 loss might also contribute to the amplitude of induction. Still, it is worth noting that the differences observed here, while significant, had a relatively modest magnitude, both for H3K4me3 and H3K27me3. Investigating gene induction in mutants were H3K4me3 deposition or H3K27me3 removal is impaired would allow to determine whether differential methylation really contributes to the magnitude of transcriptional induction.

3.4 Reduced levels of H3K27me3 do not impact the cold stress response

While some H3K27me3 targets which are induced by cold showed a reduction in the level of this mark during a cold treatment (such as *LTI30* and *COR15A*), others did not show any differential methylation (*GOLS3*, *WRKY40*). To examine whether H3K27me3 might hold different roles on those two types of genes, their transcriptional activity during a cold treatment was monitored

10.3389/fpls.2024.1390144

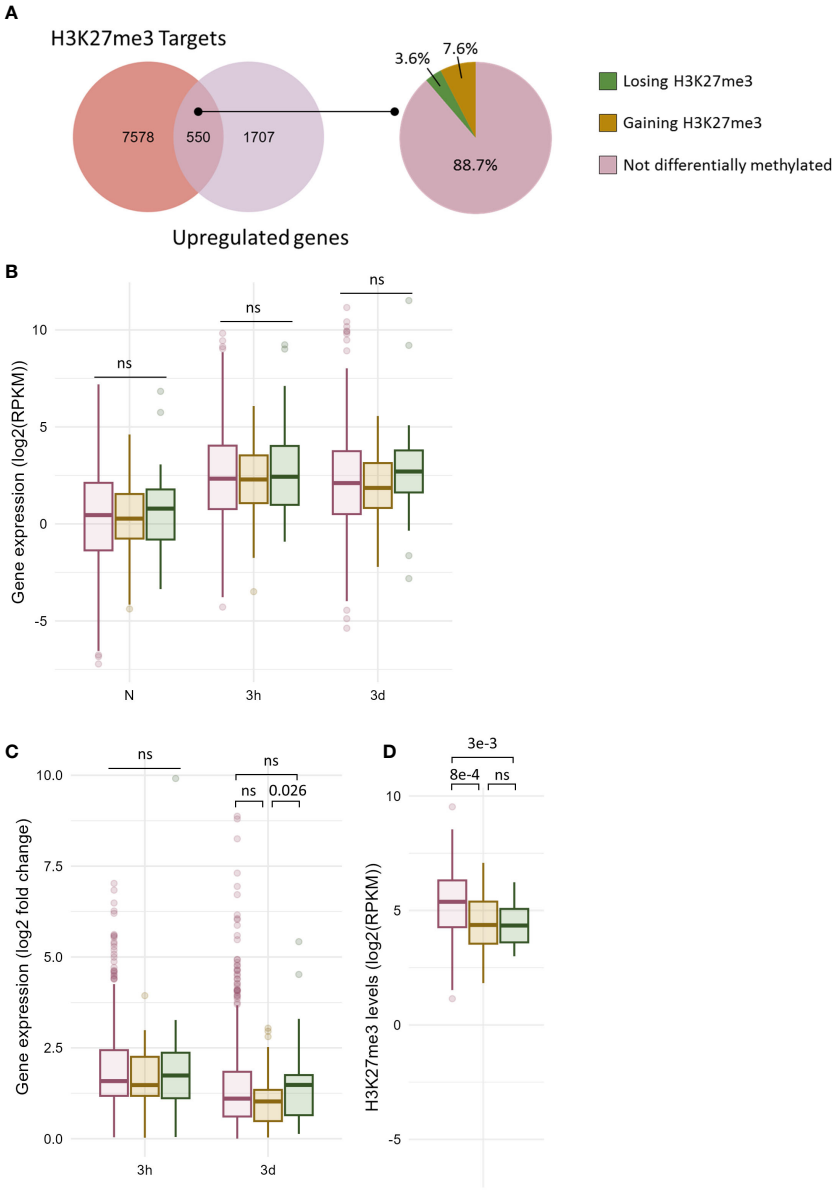

FIGURE 5
Only a fraction of cold induced genes carrying H3K27me3 undergo differential methylation. **(A)** Venn diagram showing the overlap between the genes carrying H3K27me3 and the genes induced at any time point during cold exposure (left panel). Pie chart showing the percentage of genes gaining or losing H3K27me3 at any time point during cold exposure among the 550 genes which are induced by cold and carry H3K27me3 (right panel). **(B)** Box plot showing the distribution of gene expression during cold exposure for the three gene categories listed in **(A)**. Gene expression is shown as log2 of the RPKM (Read Per Kilobase per Million mapped read). **(C)** Box plot showing the distribution of log2 fold change in gene expression after 3h and 3 days of cold exposure for the three gene categories listed in **(A)**. **(D)** Box plot showing the distribution of H3K27me3 levels as RPKM for the three gene categories listed in **(A)**. The p-values were computed using a two-sided Wilcoxon rank-sum test. ns indicates no significance.

in the H3K27 methyltransferase mutant *curly leaf* (*clf*) (Figure 6). In *clf*, H3K27me3 levels were reduced by around 50% on those cold-responsive genes, suggesting that, while they are targeted by CLF, a second methyltransferase (likely SWN) is also able to deposit H3K27me3 at those loci (Figure 6A). Interestingly, the levels of H3K27me3 in the *clf* mutant in naïve conditions are similar to that observed after three days of cold exposure in wild-type plants (data not shown). Despite the reduced H3K27me3 levels, the expression of those genes was not altered in *clf*, neither in naïve conditions nor after a cold treatment (Figure 6C). Reduced levels of H3K27me3 did not impact the basal level of expression nor the speed or magnitude of induction. On the other hand, *FLC*, whose H3K27me3 were significantly reduced in *clf*, displayed a higher expression in this mutant in all the examined conditions. This increased expression was associated with elevated H3K4me3 levels in *clf* while the levels of this mark remained constant on the other genes (Figure 6B). Both the basal and the acquired freezing tolerance of the *clf* mutant were measured during an electrolyte leakage assay (Figure 6D). No significant difference to wild-type could be observed, confirming that reduced H3K27me3 levels do not impact cold tolerance. Altogether, these data reject the simplistic model whereby a reduction of H3K27me3 would directly lead to increased

10.3389/fpls.2024.1390144

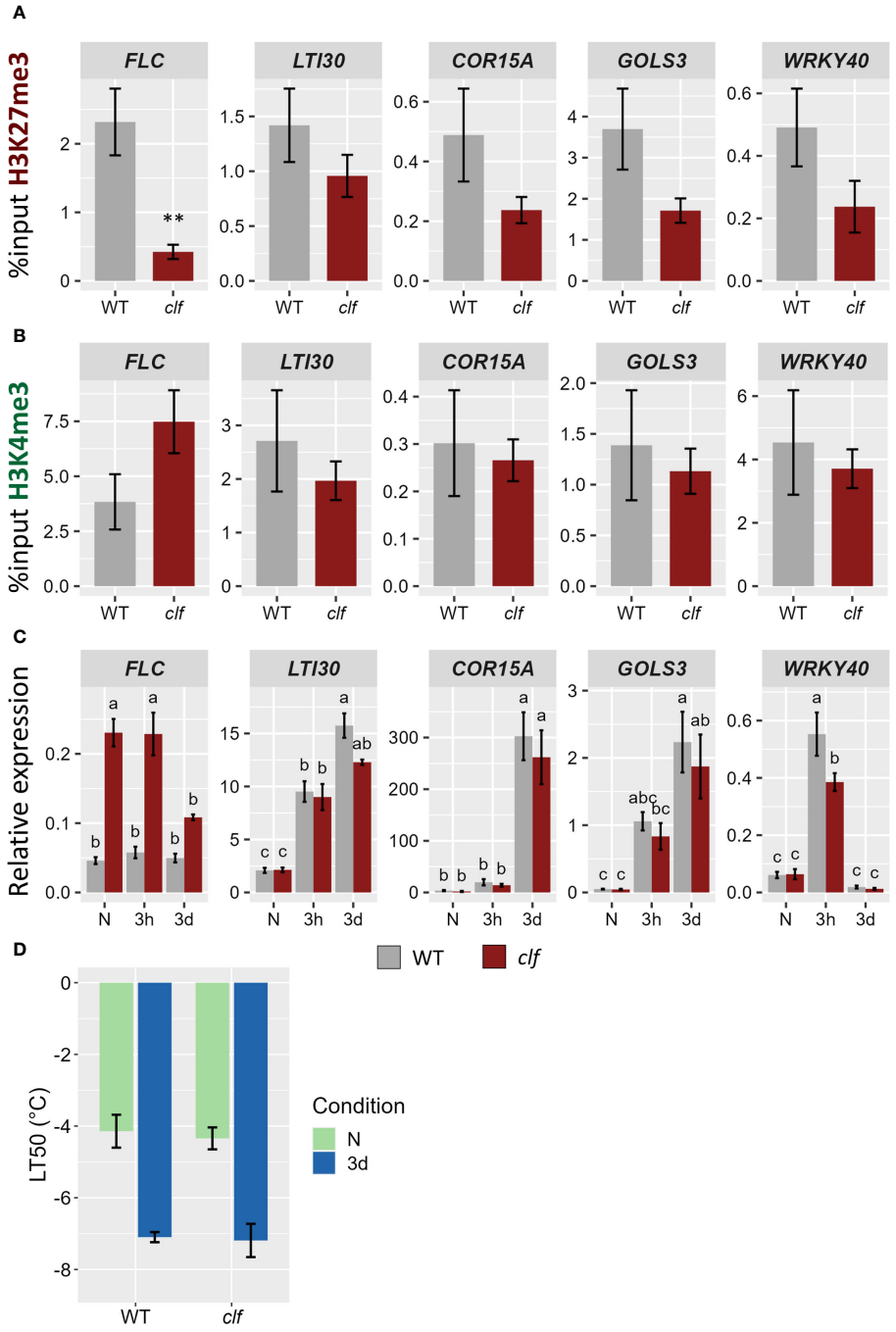

FIGURE 6
Reduced levels of H3K27me3 do not impact the transcriptional activity of cold-induced genes. **(A, B)** H3K27me3 **(A)** and H3K4me3 **(B)** levels on five H3K27me3-targeted genes in 21 day-old WT and *clf* mutant plants grown at 20°C. After cross-linking, chromatin was extracted and precipitated using H3K27me3 and H3K4me3 antibodies, respectively. The purified DNA was amplified by quantitative PCR. Results are presented as %input. Error bars indicate the sem of four biological replicates. Significance was tested using t-test, ** indicates a p-value < 0.01. **(C)** Relative expression level of five H3K27me3-targeted genes in 21 day-old WT and *clf* mutant plants grown at 20°C (N) and exposed to 4°C for three hours (3h) or three days (3d). Transcript levels were measured by RT-qPCR and normalized to three internal controls (*TIP41*, *ACTIN2* and *PDF*). Error bars indicate the sem of three biological replicates. Significance was tested by two-way ANOVA followed by a Tukey *post-hoc* test ($\alpha = 0.05$). Identical letters indicate no significant difference. All primer sequences used for this experiment can be found in Supplementary Table 1. **(D)** Freezing tolerance of clf mutant before or after cold acclimation, measured by electrolyte leakage assay. Plants were grown for 21 days at 20°C (N) and then exposed to 4°C for three days (3d). Error bars represent the sem of three biological replicates. Statistical significance was assessed by 2-way ANOVA followed by a Dunnett *post hoc* test, no significant difference was found.

H3K4me3 levels and to the transcriptional activation of previously silenced genes.

4 Discussion

4.1 Chilling stress alters the levels of both H3K4me3 and H3K27me3 at specific loci

Low temperatures are known to alter the distribution and levels of both H3K4me3 and H3K27me3 in the genome of *Arabidopsis thaliana* (Xi et al., 2020). However, studies have so far either focused on long cold treatments, with the aim of investigating vernalization, or examined only a handful of loci (Kwon et al., 2009; Vyse et al., 2020; Xi et al., 2020). The potential contribution of histone methylation to the response to cold stress therefore remains unelucidated. Here, we attempt to shed some light on this question by performing a genome-wide investigation of H3K4me3 and H3K27me3 dynamics after short (three hours or three days) 4°C treatments. While H3K27me3 was shown to be accumulated in Arabidopsis growing in moderate heat (Kim et al., 2023), Western Blots did not reveal drastic changes in the levels of either mark upon cold exposure (Figures 1A, B), similarly to what was observed during chilling stress in grapevine leaves (Zhu et al., 2023). In order to gain a more detailed view on potential changes, ChIP-seq were performed. The distributions of both H3K4me3 and H3K27me3 were not dramatically altered upon cold treatment: the number of peaks and of genes carrying the marks were sensibly the same in all conditions. This is in stark contrast to the consequences of cold treatment in *Oryza sativa*, where only 38% of genes enriched in H3K27me3 were common to the naïve and cold-stress conditions (Dasgupta et al., 2022). However, it led to many local changes in the levels of both H3K4me3 and H3K27me3, with around 5 300 and 1 100 genes showing an absolute log2 fold change of at least 0.5, respectively (Figures 1C–F). Differentially methylated genes were already detected after only three hours of cold treatment, indicating that this process happens on a time scale similar to that of differential expression (Calixto et al., 2018). For both marks, differential methylation was skewed towards a gain of the modification, while after 40 days of cold treatment, Xi et al. (2020) observed a trend of gain for H3K27me3 and of loss for H3K4me3, hinting that varying lengths of cold treatment might impact the distribution of histone marks differently. Significantly more genes underwent H3K4me3 differential methylation than H3K27me3, but once reported to the total number of genes targeted by each mark, the difference was not substantial anymore. However, H3K4me3 changes were, on average, of a larger magnitude than those observed for H3K27me3 (Figures 1C–F; Supplementary Figure 1).

4.2 The induction of cold stress responsive genes does not rely on a PcG-TrxG switch

Both H3K4me3 and H3K27me3 differential methylation partially correlated with differential expression, especially after a longer (three days) cold exposure (Figure 3). While this was not observed for all DE genes, genes induced by cold were more likely to display a gain of H3K4me3 and/or a loss of H3K27me3. However, very little overlap between H3K4me3 and H3K27me3 DM genes was observed, refuting the simplistic model of stress-responsive genes transitioning from a silenced H3K27me3 chromatin to an active form enriched in H3K4me3 during their transcriptional activation. This was further confirmed by examining the levels of H3K4me3 on cold-inducible genes in the *clf* mutant (Figure 6): while their H3K27me3 status was reduced, no significant difference in H3K4me3 could be observed, indicating that H3K27me3 is not automatically replaced by H3K4me3. Such a PcG/TrxG switch has been demonstrated for transcriptional activation during development (Engelhorn et al., 2017), but in this context, the expression of the gene is altered indefinitely. By contrast, stress responses only require a transient adjustement of the transcriptional activity. It is therefore possible that the chromatin status of cold responsive genes is not as dramatically altered, to allow for reversion to the initial state once the stress subsides. Instead of a H3K27me3-to-H3K4me3 switch, H3K4me3 and H3K27me3 differential methylations appear to be mostly independent from one another, suggesting that they might hold very distinct functions. Indeed, the GO analyses uncovered that distinct categories of terms were enriched for H3K4me3 and H3K27me3 DM genes (Supplementary Figures 2, 3). Furthermore, the correlation between differential methylation and differential expression was stronger for H3K4me3 than H3K27me3. This is consistent with a previous study from Engelhorn et al. (2017) on the floral transition, which reported H3K4me3 to be a stronger predictor of transcriptional changes than H3K27me3. The levels of the active mark were also altered prior to the ones of its silencing counterpart during seasonal oscillations (Nishio et al., 2020). In the present study, while both marks already displayed variations after only three hours of cold exposure, only about 11% of H3K4me3 changes were detected both after three hours and three days of cold treatment, suggesting that they are mostly transient (Figure 2D). On the contrary, the majority of H3K27me3 changes were shared by both time points, indicating a higher stability of H3K27me3 modifications. This is consistent with previous analyses of H3K4me3 and H3K27me3 dynamics in HeLa cells, which reported H3K4me3 as having a faster turn-over and re-establishment speed than H3K27me3 (Zheng et al., 2014; Alabert et al., 2015; Reverón-Gómez et al., 2018). Mathematical modelling demonstrated that chromatin marks with slower dynamics are more robust against rapidly fluctuating environmental conditions, as the signal has to persist longer for a new equilibrium for the level of the mark to be reached (Berry et al., 2017). The different dynamics of H3K4me3 and H3K27me3 could therefore confer them different responsiveness to environmental variations, with H3K4me3 contributing to the immediate stress response to lower temperature (as suggested by the enrichment of abiotic and biotic stress-response related GO terms) and H3K27me3 mediating more long term responses such as developmental adaptations (Supplementary Figures 2, 3).

While the current study examined H3K4me3 and H3K27me3 individually, revealing them to be antagonistic and mutually exclusive at a large fraction of examined loci, several studies

report that they can be present on the same locus, forming a specific chromatin state called H3K4me3-H3K27me3 bivalency (Bernstein et al., 2006; Voigt et al., 2013; Faivre and Schubert, 2023). Chromatin bivalency was initially identified in embryonic stem cells but its existence has also been reported in plants, where it has been suggested to control both developmental and stress responses (Jiang et al., 2008; Berr et al., 2010; Zeng et al., 2019). While the ChIP-seq performed here are not sufficient to prove the existence of bivalency (Faivre and Schubert, 2023), overlapping the individual tracks obtained for each mark revealed that numerous cold stress-responsive genes carry both H3K4me3 and H3K27me3 either before or during cold exposure (Figure 2A, *LTI30* and *COR15A*). This observation raises the possibility that they are bivalent and that H3K4me3-H3K27me3 might contribute to the cold stress response in *Arabidopsis thaliana*, similarly to what has been suggested in *Solanum tuberosum* (Zeng et al., 2019). However, it is also possible that the apparent co-occurrence of H3K4me3 and H3K27me3 on those genes is simply due to the existence of distinct cell populations where the genes are decorated with either H3K4me3 or H3K27me3, and more precise investigations, using e.g. sequential ChIP, are required to draw definite conclusions.

4.3 Role of differential methylation in gene regulation

It has been reported that cold-inducible H3K27me3 targets lose the repressive mark upon induction (Kwon et al., 2009), but in a previous work, we demonstrated that loss of H3K27me3 is not required for induction (Vyse et al., 2020). This new genome wide analysis confirms our prior report and refutes the idea that H3K27me3 is an absolute obstacle for transcriptional activation of cold-responsive genes. To further dissect the potential role of cold-induced H3K27me3 loss on those genes, we used the *clf* mutant, in which many cold-responsive genes present a reduced H3K27me3 status. The reduced H3K27me3 levels in the *clf* mutant did not lead to a change in the basal expression of the genes investigated here (Figure 6C), suggesting that additional factors are required for their transcriptional activation, likely transcription factors such as the CBFs. Similar observations were made by Liu et al. (2014), where the absence of a functional CLF and therefore the reduction of H3K27me3 at drought inducible genes did not trigger their induction in naïve conditions. However, the authors observed a higher magnitude of induction upon stress exposure, which was not detected in the present study. It is therefore likely that H3K27me3 holds a different function in the response to drought and in the response to cold. Instead, the silencing mark might control the induction speed of the genes: reduced H3K27me3 status has been reported as allowing a faster transcriptional activation in the case of camalexin biosynthesis genes during pathogen infection (Zhao et al., 2021). This does not seem to hold true for cold-inducible genes: the expression levels in WT and *clf* were comparable both after three hours and three days of cold exposure, suggesting that lower H3K27me3 status does not lead to a faster induction. However, more detailed time-course transcriptomic experiments would be required in order to reach a definite conclusion. Interestingly, the levels of H3K27me3 on cold inducible genes in the *clf* mutants are similar to those observed after three days of cold exposure. The lack of higher or faster induction of those genes upon cold stress in *clf* is therefore consistent with observations from Kwon et al. (2009), where a persisting cold-induced lower H3K27me3 status did not lead to an altered expression of the genes upon cold re-exposure. Furthermore, H3K27me3 does not appear to directly contribute to the regulation of the cold stress response (at least for the tested conditions), as *clf* mutants also did not show an altered basal or acquired freezing tolerance compared to wild-type (Figure 6D). Instead, H3K27me3 might contribute to the regulation of deacclimation or memory processes, only affecting transcriptional activity after the cold episode subsides. In addition, many development-related terms were identified in the gene sets gaining H3K27me3, suggesting that they might be down-regulated upon cold exposure. However, when performing a GO term analysis on the lists of genes differentially expressed after three hours and three days of cold exposure, no such enrichment for development-related genes could be detected (Supplementary Figures 4B, D). This suggests that the changes in the methylation level of these genes might serve another purpose than an immediate adjustment of their transcriptional activity. Alternatively, the role of CLF in the cold stress response may be masked by its paralogue SWN, as both proteins have overlapping functions, at least for developmental processes (Chanvivattana et al., 2004).

Similarly, while many cold-inducible genes underwent a gain of H3K4me3 upon cold exposure, this could not be generalized to all up-regulated genes. This was also observed for other abiotic stresses (Sani et al., 2013; Yamaguchi et al., 2021). The correlation analyses between differential methylation and expression suggest that both phenomena have different dynamics, with expression changes occurring prior to methylation status alterations. This would indicate that H3K4me3 gain is not necessary for the initiation of the transcriptional activation but it might positively feed back into it, as genes gaining H3K4me3 displayed a higher magnitude of induction than non DM genes (Figure 4C). While H3K4me3 has long been described as being necessary for transcription initiation, this idea has recently been refuted (Shilatifard, 2012; Lauberth et al., 2013; Wang et al., 2023). Instead, H3K4me3 was demonstrated to prevent RNA polymerase II pausing, thereby accelerating elongation. This suggests that higher H3K4me3 levels would lead to higher accumulation of transcripts, as observed in this study for genes gaining H3K4me3 upon cold exposure (Figure 4B).

Despite the observed correlations between differential methylation and differential expression, it is important to note that numerous cold-regulated genes did not undergo differential methylation and vice-versa (Supplementary Figure 6), indicating that differential methylation is neither required for differential expression nor it is a direct consequence. However, differential methylation might allow for a larger magnitude of induction of cold-responsive genes, as both H3K4me3-gaining and H3K27me3-losing genes displayed slightly higher fold-change of gene expression than non-differentially methylated genes (Figures 4 and 5). Alternatively, the limited overlap between differential methylation and expression might be explained by the fact that all the epigenomic and transcriptomic experiments of the current

study have been performed on whole seedlings. This prevents us from testing whether different tissues or cell types respond differently to lower temperatures. In tomatoes for example, nitrogen treatment triggered H3K4me3 and H3K27me3 differential methylation on distinct sets of genes in shoots and roots (Julian et al., 2023). Performing similar investigations in a tissue-specific approach might allow us to decipher more precisely the relationship between histone methylation and transcriptional activity.

Uncovering the exact potential role of differential histone methylation in the response to cold will require the identification of the mechanisms controlling it. For both H3K4me3 and H3K27me3, differential methylation was not associated with altered nucleosome density (data not shown), suggesting that differential methylation is due to active mechanisms rather than H3 depletion or accumulation. H3K4me3 is deposited by methyltransferases, which are known to act redundantly in *Arabidopsis thaliana* (Chen et al., 2017; Cheng et al., 2020). According to the transcriptomic data generated in this study and previously generated data, both *ATX1* and *ATX4* are induced by exposure to low temperatures (Supplementary Figure 7A; Vyse et al., 2020), suggesting them as first candidates. In particular, ATX1 has already been shown to deposit H3K4me3 on specific genes upon cold treatment (Miura et al., 2020). H3K27me3 loss upon heat has been demonstrated to be redundantly controlled by JMJ30, JMJ32, ELF6 and REF6 (Yamaguchi et al., 2021), the same methyltransferases might therefore regulate H3K27me3 levels during cold stress. In particular, both ELF6, JMJ13 and JMJ30 were found to be induced during cold exposure (Supplementary Figure 7B; Vyse et al., 2020). It would therefore be of high interest to examine the cold tolerance abilities and transcriptional response of such mutants to cold exposure, in order to determine whether alterations of H3K4me3 and/or H3K27me3 levels on cold-responsive genes directly contribute to their transcriptional regulation.

While H3K4me3 and H3K27me3 are among the most well-characterized histone marks, numerous other modifications contribute to the chromatin status of a specific locus. Histone acetylation, in particular H3K9ac and H3K14ac, has been shown to be accumulated at the promoters of *COR* genes during cold exposure, where it contributes to their transcriptional activation (Pavangadkar et al., 2010; Lim et al., 2020). Histone deacetylases such as HDA6 were identified as essential for the acquisition of freezing tolerance during cold acclimation (To et al., 2011). It would therefore be highly interesting to examine whether other chromatin marks could contribute to the cold stress response. There is significant interplay between diverse histone modifications, such as H3K27me3-H3K18ac or H3K4me3-H3K27me3 bivalency (Zhao et al., 2021; Faivre and Schubert, 2023), highlighting the need for more holistic approaches in epigenomic studies to decipher the influence not only of a single mark but of the chromatin status as a whole on transcriptional activity.

In conclusion, this study provides a genome wide perspective on cold-triggered histone methylation dynamics and demonstrates that H3K4me3 and H3K27me3 differential methylations are independent from one another. H3K4me3 correlates more strongly with differential expression and appears to regulate immediate stress responses, while H3K27me3 might contribute to longer term responses such as developmental adaptation. As reduced H3K27me3 levels did not impact the transcriptional activity of cold-responsive genes, further work is required to finally elucidate the role played by this repressive mark at those genes. It would especially interesting to examine whether it might contribute to deacclimation processes.

Data availability statement

The datasets presented in this study can be found in online repositories. The names of the repository/repositories and accession number(s) can be found below: https://www.ncbi.nlm.nih.gov/, GSE255445.

Author contributions

LF: Conceptualization, Data curation, Formal Analysis, Investigation, Methodology, Project administration, Supervision, Validation, Visualization, Writing – original draft, Writing – review & editing. NK: Formal Analysis, Investigation, Validation, Writing – review & editing. AK: Formal Analysis, Investigation, Validation, Writing – review & editing. XX: Investigation, Methodology, Writing – review & editing. KK: Conceptualization, Methodology, Resources, Supervision, Writing – review & editing. DS: Conceptualization, Funding acquisition, Project administration, Resources, Supervision, Writing – review & editing.

Funding

The author(s) declare that financial support was received for the research, authorship, and/or publication of this article. This work was supported by the Deutsche Forschungsgemeinschaft-funded Collaborative Research Center CRC973, project C7.

Acknowledgments

The authors would like to thank Jose M. Muino for his precious expertise in ChIP-seq analysis and the HPC Service of ZEDAT, Freie Universität Berlin, for computing time. This manuscript was previously published as a preprint (Faivre et al., 2024), available at: https://www.biorxiv.org/content/10.1101/2024.02.29.582735v1.

Conflict of interest

The authors declare that the research was conducted in the absence of any commercial or financial relationships that could be construed as a potential conflict of interest.

The author(s) declared that they were an editorial board member of Frontiers, at the time of submission. This had no impact on the peer review process and the final decision.

Publisher's note

All claims expressed in this article are solely those of the authors and do not necessarily represent those of their affiliated organizations, or those of the publisher, the editors and the reviewers. Any product that may be evaluated in this article, or claim that may be made by its manufacturer, is not guaranteed or endorsed by the publisher.

Supplementary material

The Supplementary Material for this article can be found online at: https://www.frontiersin.org/articles/10.3389/fpls.2024.1390144/full#supplementary-material

References

Alabert, C., Barth, T. K., Reverón-Gómez, N., Sidoli, S., Schmidt, A., Jensen, O. N., et al. (2015). Two distinct modes for propagation of histone PTMs across the cell cycle. *Genes Dev.* 29, 585–590. doi: 10.1101/gad.256354.114

Alexa, A., and Rahnenfuhrer, J. (2023). topGO: Enrichment Analysis for Gene Ontology. doi: 10.18129/B9.bioc.topGO, R package version 2.54.0, Available at: https://bioconductor.org/packages/topGO.

Alexandre, C., Möller-Steinbach, S., Schönrock, N., and Gruissem and Hennig, W. L. (2009). Arabidopsis MSI1 is required for negative regulation of the response to drought stress. *Mol. Plant* 2, 675–687. doi: 10.1093/mp/ssp012

Bennet, L., Melchers, B., and Proppe, B. (2020). *Curta: A general-purpose high-performance computer at ZEDAT* (Berlin, Germany: Freie Universität Berlin). doi: 10.17169/refubium-26754

Bernstein, B. E., Mikkelsen, T. S., Xie, X., Kamal, M., Huebert, D. J., Cuff, J., et al. (2006). A bivalent chromatin structure marks key developmental genes in embryonic stem cells. *Cell* 125, 315–326. doi: 10.1016/j.cell.2006.02.041

Berr, A., McCallum, E. J., Ménard, R., Meyer, D., Fuchs, J., Dong, A., et al. (2010). Arabidopsis SET DOMAIN GROUP2 is required for H3K4 trimethylation and is crucial for both sporophyte and gametophyte development. *Plant Cell* 22, 3232–3248. doi: 10.1105/tpc.110.079962

Berry, S., Dean, C., and Howard, M. (2017). Slow chromatin dynamics allow polycomb target genes to filter fluctuations in transcription factor activity. *Cell Syst.* 4, 445–457.e8. doi: 10.1016/j.cels.2017.02.013

Blakey, C. A., and Litt, M. D. (2015). Histone modifications-models and mechanisms. *Epigenetic Gene Expression Regul.*, 21–42. doi: 10.1016/B978-0-12-799958-6.00002-0

Bowler, C., Benvenuto, G., Laflamme, P., Molino, D., Probst, A. V., Tariq, M., et al. (2004). Chromatin techniques for plant cells. *Plant J.* 39, 776–789. doi: 10.1111/j.1365-313X.2004.02169.x

Calixto, C. P. G., Gui, W., James, A. B., Tzioutziou, N. A., Entizne, J. C., Panter, P. E., et al. (2018). Rapid and dynamic alternative splicing impacts the Arabidopsis cold response transcriptome. *Plant Cell* 30, 1424-1444. doi: 10.1105/tpc.18.00177

Carlson, M. (2019). org.At.tair.db: Genome wide annotation for Arabidopsis. doi:10.18129/B9.bioc.org.At.tair.db, R package version 3.17.0, Available at: https://bioconductor.org/packages/org.At.tair.db

Chanvivattana, Y., Bishopp, A., Schubert, D., Stock, C., Moon, Y.-H., Sung, Z. R., et al. (2004). Interaction of Polycomb-group proteins controlling flowering in Arabidopsis. *Development* 131, 5263–5276. doi: 10.1242/dev.01400

Chen, L. Q., Luo, J.-H., Cui, Z.-H., Xue, M., Wang, L., Zhang, X.-Y., et al. (2017). ATX3, ATX4, and ATX5 encode putative H3K4 methyltransferases and are critical for plant development. *Plant Physiol.* 174, 1795–1806. doi: 10.1104/pp.16.01944

Cheng, K., Xu, Y., Yang, C., Ouellette Niu, L. L., Zhou, X., et al. (2020). Histone tales : lysine methylation, a protagonist in Arabidopsis development. *J. Exp. Bot.* 71, 3, 793–807. doi: 10.1093/jxb/erz435

Conway, J. R., Lex, A., and Gehlenborg, N. (2017). UpSetR: An R package for the visualization of intersecting sets and their properties. *Bioinformatics* 33, 2938–2940. doi: 10.1093/bioinformatics/btx364

Dasgupta, P., Prasad, P., Bag, S. K., and Chaudhuri, S. (2022). Dynamicity of histone H3K27ac and H3K27me3 modifications regulate the cold-responsive gene expression in Oryza sativa Lssp. indica. *Genomics* 114, 110433. doi: 10.1016/j.ygeno.2022.110433

de Mendiburu, F., and Yaseen, M. (2020). agricolae: Statistical Procedures for Agricultural Research. R package version 1.4.0, Available at: https://myaseen208.github.io/agricolae/https://cran.r-project.org/package=agricolae

Ding, Y., Avramova, Z., and Fromm, M. (2011). The Arabidopsis trithorax-like factor ATX1 functions in dehydration stress responses via ABA-dependent and ABA-independent pathways. *Plant J.* 66, 735–744. doi: 10.1111/j.1365-313X.2011.04534.x

Dobin, A., Davis, C. A., Schlesinger, F., Drenkow, J., Zaleski, C., Jha, S., et al. (2013). STAR: Ultrafast universal RNA-seq aligner. *Bioinformatics* 29, 15–21. doi: 10.1093/bioinformatics/bts635

Engelhorn, J., Blanvillain, R., Kröner, C., Parrinello, H., Rohmer, M., Posé, D., et al. (2017). Dynamics of H3K4me3 Chromatin Marks Prevails over H3K27me3 for Gene Regulation during Flower Morphogenesis in Arabidopsis thaliana. *Epigenomes* 1, 8. doi: 10.3390/epigenomes1020008

Faivre, L., Kinscher, N.-F., Kuhlmann, A. B., Xu, X., Kaufmann, K., Schubert, D., et al. (2024). Cold stress induces a rapid redistribution of the antagonistic marks H3K4me3 and H3K27me3 in Arabidopsis thaliana. *BioRxiv*, 1–24. doi: 10.1101/2024.02.29.582735

Faivre, L., and Schubert, D. (2023). Facilitating transcriptional transitions: an overview of chromatin bivalency in plants. *J. Exp. Bot.* 74, 1770–1783. doi: 10.1093/jxb/erad029

Friedrich, T., Faivre, L., Bäurle, I., and Schubert, D. (2018). Chromatin-based mechanisms of temperature memory in plants 1–9. doi: 10.1111/pce.13373

Gaspar, J. M. (2018). Improved peak-calling with MACS2. *BioRxiv*, 1–16. doi: 10.1101/496521

Gilmour, S. J., Hajela, R. K., and Thomashow, M. F. (1988). Cold acclimation in arabidopsis thaliana. *Plant Physiol.* 87, 745–750. doi: 10.1104/pp.87.3.745

Hincha, D. K., and Zuther, E. (2014). *Plant cold acclimation: methods and protocols* (New York: Springer). doi: 10.1007/978-1-4939-2687-9

Hisanaga, T., Romani, F., Wu, S., Kowar, T., Wu, Y., Lintermann, R., et al. (2023). The Polycomb repressive complex 2 deposits H3K27me3 and represses transposable elements in a broad range of eukaryotes. *Curr. Biol.* 33 (20), 4367-4380. doi: 10.1016/j.cub.2023.08.073

Ingham, P. W. (1983). Differential expression of bithorax complex genes in the absence of the extra sex combs and trithorax genes. *Nature* 306, 591–593. doi: 10.1038/306591a0

Jan, N., Hussain, M., and Andrabi, K. I. (2009). Cold resistance in plants: A mystery unresolved. *Electronic J. Biotechnol.* 12, 14–15. doi: 10.4067/S0717-34582009000300014

Jiang, D., Wang, Y., Wang, Y., and He, Y. (2008). Repression of FLOWERING LOCUS C and FLOWERING LOCUS T by the arabidopsis polycomb repressive complex 2 components. *PloS One* 3, e3404. doi: 10.1371/journal.pone.0003404

Julian, R., Patrick, R. M., and Li, Y. (2023). Organ-specific characteristics govern the relationship between histone code dynamics and transcriptional reprogramming during nitrogen response in tomato. *Commun. Biol.* 6, 1225. doi: 10.1038/s42003-023-05601-8

Kim, J., Bordiya, Y., Xi, Y., Zhao, B., Kim, D.-H., Pyo, Y., et al. (2023). Warm temperature-triggered developmental reprogramming requires VIL1-mediated, genome-wide H3K27me3 accumulation in Arabidopsis. *Development* 150. doi: 10.1242/dev.201343

Kim, S. Y., Zhu, T., and Renee Sung, Z. (2010). Epigenetic regulation of gene programs by EMF1 and EMF2 in Arabidopsis. *Plant Physiol.* 152, 516–528. doi: 10.1104/pp.109.143495

Kleinmanns, J. A., Schatlowski, N., Heckmann, D., and Schubert, D. (2017). BLISTER regulates polycomb-target genes, represses stress-regulated genes and promotes stress responses in Arabidopsis thaliana. *Front. Plant Sci.* 8. doi: 10.3389/fpls.2017.01530

Kleinmanns, J. A., and Schubert, D. (2014). Polycomb and Trithorax group protein-mediated control of stress responses in plants. *Biol. Chem.* 395, 1291–1300. doi: 10.1515/hsz-2014-0197

Köhler, C., and Hennig, L. (2010). Regulation of cell identity by plant Polycomb and trithorax group proteins. *Curr. Opin. Genet. Dev.* 20, 541–547. doi: 10.1016/j.gde.2010.04.015

Kornberg, R. D. (1977). Structure of chromatin. *Annu. Rev. Biochem.* 46, 931–954. doi: 10.1146/annurev.bi.46.070177.004435

Kuroda, M. I., Kang, H., De, S., and Kassis, J. A. (2020). Dynamic competition of polycomb and trithorax in transcriptional programming. *Annu. Rev. Biochem.* 89, 235–253. doi: 10.1146/annurev-biochem-120219-103641

Kwon, C. S., Lee, D., Choi, G., and Chung, W.-I. (2009). Histone occupancy-dependent and -independent removal of H3K27 trimethylation at cold-responsive genes in Arabidopsis. *Plant J.* 60, 112–121. doi: 10.1111/j.1365-313X.2009.03938.x

Langmead, B., and Salzberg, S. L. (2012). Fast gapped-read alignment with Bowtie 2. *Nat. Methods* 9, 357–359. doi: 10.1038/nmeth.1923

Lauberth, S. M., Nakayama, T., Wu, X., Ferris, A. L., Tang, Z., Hughes, S. H., et al (2013). H3K4me3 interactions with TAF3 regulate preinitiation complex assembly and selective gene activation. *Cell* 152, 1021–1036. doi: 10.1016/j.cell.2013.01.052

Li, H., Handsaker, B., Wysoker, A., Fennell, T., Ruan, J., Homer, N., et al. (2009). The sequence alignment/map format and SAMtools. *Bioinformatics* 25, 2078–2079. doi: 10.1093/bioinformatics/btp352

Liao, Y., Smyth, G. K., and Shi, W. (2014). FeatureCounts: An efficient general purpose program for assigning sequence reads to genomic features. *Bioinformatics* 30, 923–930. doi: 10.1093/bioinformatics/btt656

Lim, C. J., Park, J., Shen, M., Park, H. J., Cheong, M. S., Park, K. S., et al. (2020). The Histone-modifying complex PWR/HOS15/HD2C epigenetically regulates cold tolerance1[OPEN]. *Plant Physiol.* 184, 1097–1111. doi: 10.1104/pp.20.00439

Liu, N., Fromm, M., and Avramova, Z. (2014). H3K27me3 and H3K4me3 chromatin environment at super-induced dehydration stress memory genes of arabidopsis thaliana. *Mol. Plant* 7, 502–513. doi: 10.1093/mp/ssu001

Love, M. I., Huber, W., and Anders, S. (2014). Moderated estimation of fold change and dispersion for RNA-seq data with DESeq2. *Genome Biol.* 15, 1–21. doi: 10.1186/s13059-014-0550-8

Luger, K., Mäder, A. W., Richmond, R. K., Sargent, D. F., and Richmond, T. J. (1997). Crystal structure of the nucleosome core particle at 2.8 Å resolution. *Nature* 389, 251–260. doi: 10.1038/38444

Luger, K., and Richmond, T. J. (1998). The histone tails of the nucleosome. *Curr. Opin. Genet. Dev.* 8, 140–146. doi: 10.1016/S0959-437X(98)80134-2

Medina, J., Bargues, M., Terol, J., Pérez-Alonso, M., and Salinas, J. (1999). The Arabidopsis CBF gene family is composed of three genes encoding AP2 domain-containing proteins whose expression is regulated by low temperature but not by abscisic acid or dehydration. *Plant Physiol.* 119, 463–469. doi: 10.1104/pp.119.2.463

Miura, K., Renhu, N., and Suzaki, T. (2020). The PHD finger of Arabidopsis SIZ1 recognizes trimethylated histone H3K4 mediating SIZ1 function and abiotic stress response. *Commun. Biol.* 3, 1–10. doi: 10.1038/s42003-019-0746-2

Müller, J., Hart, C. M., Francis, N. J., Vargas, M. L., Sengupta, A., Wild, B., et al. (2002). Histone methyltransferase activity of a Drosophila Polycomb group repressor complex. *Cell* 111, 197–208. doi: 10.1016/S0092-8674(02)00976-5

Nishio, H., Nagano, A. J., Ito, T., Suzuki, Y., and Kudoh, H. (2020). Seasonal plasticity and diel stability of H3K27me3 in natural fluctuating environments. *Nat. Plants* 6, 1091–1097. doi: 10.1038/s41477-020-00757-1

Pavangadkar, K., Thomashow, M. F., and Triezenberg, S. J. (2010). Histone dynamics and roles of histone acetyltransferases during cold-induced gene regulation in Arabidopsis. *Plant Mol. Biol.* 74, 183–200. doi: 10.1007/s11103-010-9665-9

Ramírez, F., Ryan, D. P., Grüning, B., Bhardwaj, V., Kilpert, F., Richter, A. S., et al. (2016). deepTools2: a next generation web server for deep-sequencing data analysis. *Nucleic Acids Res.* 44, W160–W165. doi: 10.1093/nar/gkw257

Reverón-Gómez, N., Gonzáles-Aguilera, C., Stewart-Morgan, K. R., Petryk, N., Flury, V., Graziano, S., et al. (2018). Accurate recycling of parental histones reproduces the histone modification landscape during DNA replication. *Mol. Cell* 72, 239–249.e5. doi: 10.1016/j.molcel.2018.08.010

Ringrose, L., and Paro, R. (2004). Epigenetic regulation of cellular memory by the polycomb and trithorax group proteins. *Annu. Rev. Genet.* 38, 413–443. doi: 10.1146/annurev.genet.38.072902.091907

Robinson, J. T., Thorvaldsdóttir, H., Winckler, W., Guttman, M., Lander, E. S., Getz, G., et al. (2011). Integrative genomics viewer. *Nat. Biotechnol.* 29, 24–26. doi: 10.1038/nbt.1754

Roudier, F., Ahmed, I., Bérard, C., Sarazin, A., Mary-Huard, T., Cortijo, S., et al. (2011). Integrative epigenomic mapping defines four main chromatin states in Arabidopsis. *EMBO J.* 30, 1928–1938. doi: 10.1038/emboj.2011.103

Sani, E., Herzyk, P., Perrella, G., Colot, V., and Amtmann, A. (2013). Hyperosmotic priming of Arabidopsis seedlings establishes a long-term somatic memory accompanied by specific changes of the epigenome. *Genome Biol.* 14, 1–24. doi: 10.1186/gb-2013-14-6-r59

Shi, Y., Ding, Y., and Yang, S. (2018). Molecular regulation of CBF signaling in cold acclimation. *Trends Plant Sci.* 23, 623–637. doi: 10.1016/j.tplants.2018.04.002

Shilatifard, A. (2012). The COMPASS family of histone H3K4 methylases: Mechanisms of regulation in development and disease pathogenesis. *Annu. Rev. Biochem.* 81, 65–95. doi: 10.1146/annurev-biochem-051710-134100

Song, Z. T., Zhang, X., Li, M., Yang, H., Fu, D., Lv, J., et al. (2021). Histone H3K4 methyltransferases SDG25 and ATX1 maintain heat-stress gene expression during recovery in Arabidopsis. *Plant J.* 105, 1326–1338. doi: 10.1111/tpj.15114

To, T. K., Nakaminami, K., Kim, J.-M., Morosawa, T., Ishida, J., Tanaka, M., et al. (2011). Arabidopsis HDA6 is required for freezing tolerance. *Biochem. Biophys. Res. Commun.* 406, 414–419. doi: 10.1016/j.bbrc.2011.02.058

Voigt, P., Tee, W. W., and Reinberg, D. (2013). A double take on bivalent promoters. *Genes Dev.* 27, 1318–1338. doi: 10.1101/gad.219626.113

Vyse, K., Faivre, L., Romich, M., Pagter, M., Schubert, D., Hincha, D. K., et al. (2020). Transcriptional and post-transcriptional regulation and transcriptional memory of chromatin regulators in response to low temperature. *Front. Plant Sci.* 11. doi: 10.3389/fpls.2020.00039

Wang, D. Z., Jin, Y.-N., Ding, X.-H., Wang, W.-J., Zhai, S.-S., Bai, L.-P., et al. (2017). Gene regulation and signal transduction in the ICE–CBF–COR signaling pathway during cold stress in plants. *Biochem. (Moscow)* 82, 1103–1117. doi: 10.1134/S0006297917100030

Wang, H., Fan, Z., Shliaha, P. V., Miele, M., Hendrickson, R. C., Jiang, X., et al. (2023). H3K4me3 regulates RNA polymerase II promoter-proximal pause-release. *Nature* 615, 339–348. doi: 10.1038/s41586-023-05780-8

Xi, Y., Park, S.-R., Kim, D.-H., Kim, E.-D., and Sung, S. (2020). Transcriptome and epigenome analyses of vernalization in Arabidopsis thaliana. *Plant J.* 103, 1490–1502. doi: 10.1111/tpj.14817

Yamaguchi, N., Matsubara, S., Yoshimizu, K., Seki, M., and Hamada Kamitani, K. M. (2021). H3K27me3 demethylases alter HSP22 and HSP17.6C expression in response to recurring heat in Arabidopsis. *Nat. Commun.* 12, 1–16. doi: 10.1038/s41467-021-23766-w

Yamaguchi-Shinozaki, K., and Shinozaki, K. (1994). A novel cis-acting element in an arabidopsis gene is involved in responsiveness to drought, low-temperature, or high-salt stress. *Plant Cell* 6, 251–264. doi: 10.2307/3869643

Zarka, D. G., Vogel, J. T., Cook, D., and Thomashow, M. F. (2003). Cold induction of arabidopsis CBF genes involves multiple ICE (Inducer of CBF expression) promoter elements and a cold-regulatory circuit that is desensitized by low temperature. *Plant Physiol.* 133, 910–918. doi: 10.1104/pp.103.027169

Zeng, Z., Zhang, W., Marand, A. P., Zhu, B., Buell, C. R., Jiang, J., et al. (2019). Cold stress induces enhanced chromatin accessibility and bivalent histone modifications H3K4me3 and H3K27me3 of active genes in potato. *Genome Biol.* 20, 1–17. doi: 10.1186/s13059-019-1731-2

Zhang, X., Clarenz, O., Cokus, S., Bernatavichute, Y. V., Pellegrini, M., Goodrich, J., et al. (2007). Whole-genome analysis of histone H3 lysine 27 trimethylation in Arabidopsis. *PloS Biol.* 5, 1026–1035. doi: 10.1371/journal.pbio.0050129

Zhao, K., Kong, D., Jin, B., Smolke, C. D., and Rhee, S. Y. (2021). A novel form of bivalent chromatin associates with rapid induction of camalexin biosynthesis genes in response to a pathogen signal in Arabidopsis. *Elife* 10, 1–15. doi: 10.7554/eLife.69508

Zhao, Y., and Garcia, B. A. (2015). Comprehensive catalog of currently documented histone modifications. *Cold Spring Harbor Perspect. Biol.* 7. doi: 10.1101/cshperspect.a025064

Zheng, Y., Tipton, J. D., Thomas, P. M., Kelleher, N. L., Sweet, S. M.M. , et al. (2014). Site-specific human histone H3 methylation stability: fast K4me3 turnover. *Proteomics* 23, 1–7. doi: 10.1002/pmic.201400060.Site-specific

Zhu, Z., Li, Q., Gichuki, D. K., Hou, Y., Liu, Y., Zhou, H., et al. (2023). Genome-wide profiling of histone H3 lysine 27 trimethylation and its modification in response to chilling stress in grapevine leaves. *Hortic. Plant J.* 9, 496–508. doi: 10.1016/j.hpj.2023.03.002

Zuther, E., Schaarschmidt, S., Fischer, A., Erban, A., Pagter, M., Mubeen, U., et al. (2019). Molecular signatures associated with increased freezing tolerance due to low temperature memory in Arabidopsis. *Plant Cell Environ.* 42, 854–873. doi: 10.1111/pce.13502

frontiers | Frontiers in Plant Science

TYPE Review
PUBLISHED 10 June 2024
DOI 10.3389/fpls.2024.1398818

OPEN ACCESS

EDITED BY
Aamir W. Khan,
University of Missouri, United States

REVIEWED BY
Mingku Zhu,
Jiangsu Normal University, China
Xiaoli Sun,
Heilongjiang Bayi Agricultural University, China

*CORRESPONDENCE
Fengkai Wu
wfk124@sicau.edu.cn

†These authors have contributed equally to this work

RECEIVED 10 March 2024
ACCEPTED 23 May 2024
PUBLISHED 10 June 2024

CITATION
Liu L, Yahaya BS, Li J and Wu F (2024) Enigmatic role of auxin response factors in plant growth and stress tolerance. *Front. Plant Sci.* 15:1398818. doi: 10.3389/fpls.2024.1398818

Enigmatic role of auxin response factors in plant growth and stress tolerance

Ling Liu[1†], Baba Salifu Yahaya[2,3†], Jing Li[2,3] and Fengkai Wu[2,3*]

[1]Faculty of Agriculture, Forestry and Food Engineering, Yibin University, Yibin, Sichuan, China, [2]Maize Research Institute, Sichuan Agricultural University, Wenjiang, Sichuan, China, [3]Key Laboratory of Biology and Genetic Improvement of Maize in Southwest Region, Ministry of Agriculture, Wenjiang, Sichuan, China

Abiotic and biotic stresses globally constrain plant growth and impede the optimization of crop productivity. The phytohormone auxin is involved in nearly every aspect of plant development. Auxin acts as a chemical messenger that influences gene expression through a short nuclear pathway, mediated by a family of specific DNA-binding transcription factors known as Auxin Response Factors (ARFs). ARFs thus act as effectors of auxin response and translate chemical signals into the regulation of auxin responsive genes. Since the initial discovery of the first ARF in Arabidopsis, advancements in genetics, biochemistry, genomics, and structural biology have facilitated the development of models elucidating ARF action and their contributions to generating specific auxin responses. Yet, significant gaps persist in our understanding of ARF transcription factors despite these endeavors. Unraveling the functional roles of ARFs in regulating stress response, alongside elucidating their genetic and molecular mechanisms, is still in its nascent phase. Here, we review recent research outcomes on ARFs, detailing their involvement in regulating leaf, flower, and root organogenesis and development, as well as stress responses and their corresponding regulatory mechanisms: including gene expression patterns, functional characterization, transcriptional, post-transcriptional and post-translational regulation across diverse stress conditions. Furthermore, we delineate unresolved questions and forthcoming challenges in ARF research.

KEYWORDS

ARF, Aux/IAA, growth and development, abiotic stresses, regulatory mechanisms

1 Introduction

Plants face numerous abiotic and biotic stresses due to their sessile nature, including water and nutrient deficiencies, high salinity, extreme temperatures, radiation, heavy metal toxicity, and biotic infections. An estimated 90% of global arable lands are exposed to one or more of the above abiotic stresses (Dos Reis et al., 2012), projected to cause up to 70% yield loss in major crops (Mantri et al., 2012). The biotic stress caused by viral, fungal, and

bacterial infections cause reduction in level of photosynthesis in all major crops and is the major cause of pre- and post-harvest losses. Biotic stresses are responsible for approximately, 28.2%, 37.4%, 31.2%, 40.3%, 26.3%, and 28.8% yield losses in wheat, rice, maize, potatoes, soybeans, and cotton, respectively (Wang et al., 2013). Adaptation to such stresses is crucial for optimizing performance of plants and stability of their successive generations. Developing stress-tolerant plants remains the ultimate goal of plant breeders due to their superior yields and stability (Kambona et al., 2023). Genetic manipulation of plants remains the most prominent approach to alleviating poverty, due to its potential to increasing crop yield and mitigating nutrient deficiencies, enabling the cultivation of salt affected lands, overcoming energy crisis and production of cost-efficient biopharmaceuticals using plants as cellular factories (Ahmad and Mukhtar, 2017). Additionally, genetic modification offers the possibility of identifying candidate genes, miRNAs and transcription factors (TFs) that participate in regulating specific plant processes to improve tolerance to abiotic stresses and enhance productivity. For example, overexpression of *McWRKY57* conferred tolerance to drought stress in *Arabidopsis* (Bai et al., 2023). miRNAq and nuclear factor YA8 enhanced salt tolerance by activating PEROSIDASE expression in response to reactive oxygen species (ROS) (Xing et al., 2021).

Plants have evolved intricate stress response mechanisms, including proper perception, signal transduction and respective physiological adjustments informed by the kind and duration of stress (Kranner et al., 2010). The perception of stress cues in plant is a complex network of input signals integrated in signal pathways that target regulators of plant growth and physiology (Scheres and van der Putten, 2017). Transcription regulation of stress-responsive genes is a pivotal biological process that confers stress tolerance in plants, and allows plants to strictly define and sustain their cellular identity and coordinates cellular activity during its life cycle (Casamassimi and Ciccodicola, 2019). Such regulations are mainly mediated by the temporal and spatial functioning of TFs that contain highly conserved DNA-binding domains (DBDs), with which they bind to specific DNA sequences in promoters of their target genes (Wang G. et al., 2015). On the other hand, TFs are either upregulated or downregulated by kinases or phosphatases and inturn binds to cis-regulatory elements in promoter of stress-inducible genes to enhance or suppress their transcription (Baillo et al., 2019). TFs also regulate stress induced responses in plants through mechanisms like posttranslational and epigenetic modifications such as variable nucleosome distribution, histone modification, DNA methylation, and synthesis of non-protein-coding RNAs (npcRNAs).

2 Molecular structure and classification of ARF proteins

Recent studies have traced the evolutionary origins of ARFs back to early charophyte algae, where a single proto-ARF gene existed (Mutte et al., 2018). Following an initial duplication event, proto-ARFs diversified into two classes (A/B and C) during the late-divergence charophytes. In the transition to land plants, a subsequent division of class A/B into distinct classes A and B established the three evolutionary classes recognized today: A, B, and C. Further duplications within these classes expanded and diversified the ARF family in higher land plants (Mutte et al., 2018). Since the identification of the first ARF (ARF1) in Arabidopsis, 22 more ARFs have been identified and characterized from the Arabidopsis genome (Moller et al., 2017). Homology cloning and genetic approaches have since been employed ino identifying numerous homologous ARF genes in various plant species after the release of genomic data and development of bioinformatics analyses. The 23 ARFs in Arabidopsis canbe divided into three subclasses: A, B, and C (Finet et al., 2013). Most ARFs possess similar topology, with three conserved protein domains, whose properties must be understood in details. Majority of ARFs generally contain a conserved N-terminus DNA-binding domain (DBD), a variable middle region (MR) that functions as either an activator or repressor domain and a conserved C-terminal dimerization domain (CTD), which is involved in protein-protein interactions (Dinesh et al., 2015). The functions and properties of each of these domains are enumerated below.

2.1 The DNA-binding domain of ARFs

Transcription factors are universal master regulators of gene expression that bind to unique DNA sequences in the promoter of their target genes to regulate their expression (Suter, 2020). A critical, yet unresolved in aspect of auxin biology is the mechanism by which the simple tryptophan-like indole-3-acetic acid triggers a wide range of cellular responses. During the last step of auxin signaling prior to gene regulation, the ARFs confer specificity to auxin response through selection of target genes. ARF TFs possess typical B3 DBD at their N-terminus, which allows them to bind to DNA motifs called Auxin Response Elements (AuxREs) (Boer et al., 2014; Weijers and Wagner, 2016). The first AuxRE was identified in pea (Ballas et al., 1993) and soybean (Ulmasov et al., 1995) in the promoters of auxin-responsive genes as TGTCTC (Liu et al., 1994). The identification of AuxRE is one of the most significant events that has enhanced the understanding of auxin-mediated regulation of gene expression and the creation of auxin-reporter systems (Hagen and Guilfoyle, 2002), and the identification of the first ARF protein (Ulmasov et al., 1997). The crystal structures of the DBD of ARF1 and ARF5/MONOPTEROS (MP) homodimers, as well as complex of ARF1 DBD with DNA has permitted visualization of protein-DNA interaction (Roosjen et al., 2018), and depicts how amino acids in the DBD interact with the DNA-binding motif TGTCTC (Freire-Rios et al., 2020). The higher affinity of ARFs to the TGTCGG element is because of deeper rotation of H136 into the major DNA groove, which forms additional hydrogen bonds with G5 and G6 in the TGTCGG structure (Boer et al., 2014; Freire-Rios et al., 2020). Mutations in these DNA-interacting amino acids interfered with the DNA binding properties of these ARFs and their biological functions. The TGTC serves as the invariable core element crucial for auxin response, while the final two nucleotides are variable (Boer et al., 2014). In recent years, adoption of advanced techniques has

contributed to the identification of other AuxREs and the revelation that variation in the last two nucleotides of an AuxRE were permitted and could play a role in the affinity of ARFs for DNA binding. Although TGTCTC DNA-binding motif was the first to be identified, protein-binding microarrays (PBMs) has revealed that TGTCGG motif possesses relatively higher ARF binding affinity than the TGTCTC motif (Boer et al., 2014). It has been revealed through a 'cistrome' analysis that ARF2 and ARF5/MP have higher affinity for TGTCGG than the classical TGTCTC (O'Malley et al., 2016).

Through crystal structures, *in vitro*, and heterologous studies, a model in which ARF dimers bind with high affinity to distinct repeats of canonical AuxRE motifs has been unraveled. Like all TFs, ARFs bind to DNA as dimers and can homodimerize through their DBD by binding to tandem repeat motifs of TGTCNN elements. Configurations of the tandem repeat and the number of bases between the individual motifs determine their nomenclature: Inverted repeats (IR) where two AuxREs are oriented towards each other in different strands of DNA, direct repeat (DR) where two AuxREs follow each other in the same DNA strand and everted repeat (ER) where two AuxREs orient back to back in different strands of DNA (Freire-Rios et al., 2020). Yeast synthetic auxin signaling system suggest that some ARFs may activate transcription on a single AuxRE, but dimerization between the ARFs is necessary for transcription to occur (Lanctot et al., 2020). Enrichment for single AuxREs upstream of auxin-responsive genes has also been detectable (Freire-Rios et al., 2020), in affirmation to the yeast synthetic auxin signaling system. The biochemical mechanism underlying the differences in DNA-binding specificity of ARFs to single AuxRE binding sites is yet to be proven. Genome-wide DNA binding by ARFs has revealed both overlapping and distinct motif preferences for class A and B ARFs (Galli et al., 2018; Stigliani et al., 2019). DNA affinity purification and sequencing (DAP-seq) experiments performed on maize and Arabidopsis revealed that both class A and class B ARFs can bind IR7/8 motifs, while class A ARFs are additionally capable of binding to several DR and ER motifs (O'Malley et al., 2016; Galli et al., 2018; Stigliani et al., 2019). Although C-ARFs have been proven not to be involved in auxin-dependent transcriptional responses, at least in Marchantia (Mutte et al., 2018), one algal ARF related to the class C ARFs bind to the TGTCNN motifs (Carrillo-Carrasco et al., 2023).

Another element that determines the specificity of the DBD binding is the spacing between both sites of the AuxRE. The binding affinity of two ARFs differ significantly based on spacing between the AuxRE repeats, which dictates the formulation of a caliper model that determine specificity of ARFs binding sites (Boer et al., 2014). The dimerization ability of ARFs through their DBD or C-terminal PB1 domain permits strong binding to double-stranded DNA (dsDNA) carrying a pair of AuxREs with a spacer of a specific length (Boer et al., 2014; Pierre-Jerome et al., 2016). It has been reported that spacing of 7 or 8 bp in ARF1 and 5 to 9 bp in ARF5/MP is required between AuxRE repeats to enhance the interaction between these ARFs and their targeted AuxRE (Boer et al., 2014). Fluorophore or enzyme reporter genes under the control of synthetic promoters including DR5 promoter, characterized by tandem direct repeat of TGTCTC spaced at 5-bp intervals, has often been used for visualizing the distribution pattern of auxin signal in many plant species (Goldental-Cohen et al., 2017), suggesting that this repeat constellation is biologically meaningful.

2.2 Regulation of ARF activity through the C-terminal PB1 domain

The C-terminal of ARFs is a classical type -I/II PB1domain of 80-100 amino acids, which was previously named domain III/IV for ARFs and Aux/IAAs (Guilfoyle and Hagen, 2007). Besides the DBD, the PB1 domain is also an ARF interacting domain. Structural analysis on the C-terminal domain of ARFs revealed the structural basis of such heterotypic interaction of ARF5/MP (Nanao et al., 2014), ARF7 (Korasick et al., 2014), *IAA17* (Han et al., 2014), and *PsIAA4* (Dinesh et al., 2015). PB1 domains are also present in fungi, animals, amoeba, and in several protein families in plants. Characteristic of the type -I/II PB1 domains, the ARF PB1 domain permits for head to tail oligomerization, such that the positive face of one PB1 domain interacts with the negative face of another PB1 domain (Korasick et al., 2014). ARFs and Aux/IAAPB1s interact due to similarity in their 3D structure, such that one negative and one positive face will permit ARF-PB1 interact with AUX/IAA-PB1 in a head-to-tail manner through electrostatic interactions and hydrogen bonds (Vernoux et al., 2011; Piya et al., 2014). The positive face is characterized by an invariant lysine residue that interacts with an array of conserved aspartic and glutamic acids (Korasick et al., 2014), such that alteration in the lysine residue of the positive face hinders interactions with the negative face and preventing oligomerization (Powers et al., 2019).

The PB1 domain of ARFs contributes to their functioning in numerous ways. The PB1 domain mediates the interaction between ARFs and the AUX/IAA proteins, which is required for appropriate canonical auxin signal transduction, which will be discussed briefly. Mutation on the positive face of ARF19 that ablates oligomerization resulted in increased transcription of both auxin-responsive genes and novel targets in the absence of auxin (Powers et al., 2019), suggesting that the ARF19 PB1 mutant is acting as a constitutive auxin signaling factor probably due to its lack of interaction with its transcriptional corepressor Aux/IAAs. Further *in vivo* oligomerization assay revealed that ARF19 PB1 mutant did not display nuclear dimerization (Powers et al., 2019), which could be inferred that the ARF PB1 domain rather than the DBD primarily promotes ARF homodimerization. Besides the Aux/IAA-ARF interaction, the PB1 domain of ARFs is involved in transcriptional regulations. For example, ARF19 with a mutant PB1 domain that inhibits dimerization did not activate transcription of single AuxRE, but activated paired AuxRE without any hindrance. In the case of the DBD, DBD dimerization is required for both single and paired AuxRE. This data outlines the possibility that the PB1 domain confers on ARFs the ability to activate transcription of AuxREs and could stabilize ARF dimerization under less ideal AuxRE numbers.

Interestingly, the PB1 domain seems to have diverse effects on different class A ARFs, as its deletion in *Marchantia polymorpha*

ARF1 generates a loss-of-function mutant (Kato et al., 2020), whereas in *A. thaliana* ARF5/MP, the mutant maintains its function and is hyperactive (Krogan et al., 2012). Although heterotypic interactions are stronger than ARF or Aux/IAA homotypic interactions, most PB1s of class A ARFs interact with Aux/IAAs. The disparity between the strength of heterotypic and homotypic interactions result from higher number of electrostatic bonds between ARF and Aux/IAA-PB1s (Parcy et al., 2016; Kim et al., 2020). However, a limited set of interactions between Aux/IAAs and Class B or C ARFs have been identified (Vernoux et al., 2011; Piya et al., 2014), which suggest that the repressor ARF proteins function independently of auxin regulation, and instead compete for DNA binding sites or heterodimerize with other ARF proteins to block transcription (Lavy et al., 2016).

2.3 The middle region

Between the N-terminal DBD and C-terminal of ARFs is the middle region (MR), which is highly variable among ARF TFs. Functional characterization of the middle region thus far has been quite elusive owing to its variability. Nonetheless, the middle region provides the framework for classifying the ARF family proteins. The amino acid composition of the middle region is critical in determining an ARF's function, with glutamine-rich ARFs acting as transcriptional activators (Wu et al., 2015), whiles those enriched in serines, prolines, and threonines functioning as transcription repressors (Tiwari et al., 2003; Guilfoyle and Hagen, 2007). The activator/repressor classification correlates with the division in subgroups A/B/C, such that those ARFs tested as activators belong to class A, while class B and C ARFs encompass those tested as repressors (Tiwari et al., 2003). The activation and repressive activity of ARFs was decoupled from auxin induction by expressing the MR alone in a synthetic transcription factor assay in carrot protoplasts (Tiwari et al., 2003).

In contrast to the ARF repressor domains, the ARF activation domain remains unknown. This occurrence is probably due in part to the intrinsic disorder in the middle region of class A ARFs. Most activation domains are not characterized by semblance in their sequence, but by sequence characteristics such as hydrophobicity and negative charge (Erijman et al., 2020). It is however worth mentioning that the intrinsic disorder predominantly found in the MR of class A ARFs does not only dictate transcription potential but extends to other cellular features. For example, the MR of ARF7 and ARF19 dictates their subcellular localization (Powers et al., 2019), which is significantly influenced by the C-terminal PB1 domain. ARF19 is differentially localized to the nucleus of young roots and cytoplasm of matured roots. This tissues specific localization of ARF19 is altered by mutation in the PB1 domain, such that more ARF19 is driven to the nucleus of matured roots compared to wild-type. This cooperative relationship between ARF MR and the PB1 is believed to drive the nucleocytoplasmic partitition of ARFs through protein condensation. The PB1 domain probably increases the local concentration of ARF19 and that the intrinsic disorder of the MR contributes to phase separation and protein condensation (Powers and Strader, 2020). Just like other transcription factors, the relationship between ARF localization and transcriptional activity provides further insight into the regulatory mechanism governing the auxin signaling cascade. It is instructive to unravel the mechanisms that drive ARF condensation and the level of participation of other ARFs in this regulatory process, which will significantly broaden our understanding of auxin signaling specificity. The MR also acts as an interaction domain for the recruitment of different types of cofactors such as chromatin remodelers that aid ARFs to carry out their functions. It however remains unknown whether class B ARFs can function as transcriptional activators at certain loci or in the presence of other unknown cofactors.

Transcription activators belonging to the class A ARFs may also induce transcription indirectly by recruiting the SWITCH/SUCROSE NONFERMENTING (SWI/SNF) chromatin-remodeling complex (Clapier and Cairns, 2009). For example, the MR of *ARF5*/*MP* increases chromatin accessibility at its binding sites by recruiting the SWI/SWF complex through interactions with BRAHMA and SPLAYED, respectively (Wu et al., 2015). This result reveals a mechanism in which *ARF5*/MP, and most likely other activator ARFs, alter nucleosome positioning to make more transcription factor-binding sites accessible (Wu et al., 2015; Weijers and Wagner, 2016). In contrast, *Arabidopsis* class B ARF harbor a conserved TPL-binding motif (RLFGV), and may additionally encode a canonical ethylene-responsive element binding factor (EAR motif), which act as repressor domains *in vivo* (Choi et al., 2018). For example, both the conserved RLFGV motif and the additional EAR motif are needed for ARF2 to function as a transcriptional corepressor, but only the RLFGV motif is required for TPL interactions in yeast two-hybrid experiments (Choi et al., 2018). These evidences suggest that class B ARFs act as auxin-insensitive negative regulators of auxin-responsive genes (Kato et al., 2020). Additionally, the MR of *AtARF2* also harbors the EAR motif (Causier et al., 2012) which bears semblance to that found on Aux/IAAs and which permits interaction with the N-terminal part of TPL/TPRs (Ke et al., 2015). Class C ARFs possess a BRD-like domain with a slightly different sequence (VLFG).

3 The canonical and non-canonical auxin response

3.1 The canonical nuclear auxin pathway

Auxin regulates multiple outputs in plants primarily by controlling the activity of thousands of genes through the nuclear auxin pathway. The canonical auxin transcriptional response system was originally characterized in flowering plants. The nuclear auxin signaling pathway consists of a small number of core components which are represented by a large gene family. Changes in cellular auxin concentrations trigger transcriptional responses of numerous genes, mediated by ARF transcription factors (Weijers and Wagner, 2016). Significant advancement in understanding the auxin signaling machinery has been achieved in recent years (Weijers and Friml, 2009). The core components of the

auxin signaling pathway comprises the F-box-containing Transport Inhibitor Response 1 (TIR1) and its homologous Auxin-signaling F Box Proteins (AFBs) proteins, the transcriptional co-repressors AUXIN/INDOLE-3-ACETIC ACID (Aux/IAA), and the ARF transcription factors (Wright and Nemhauser, 2015; Kong et al., 2016). Activation of gene expression as a result of IAA-mediated assembly of TIR1/AFB proteins with AUX/IAA transcriptional regulators has been accepted as the canonical auxin signalling pathway (Figure 1**).** During auxin limitation, Aux/IAA protein binds to the C-terminal domain of ARFs and its co-repressor TOPLESS (TPL) to repress transcription. TPL recruits chromatin remodeling enzymes such as Histone Deacetylase 19 (HDA19) (Figure 1A) and also interacts with Mediator multiprotein complex (Figure 1B) to prevent ARF transcriptional output. For one case, the HDA19 acts as a physical impediment to maintain chromatin closure at the promoters of ARF-regulated auxin responsive genes (Szemenyei et al., 2008; Qiao et al., 2018) (Figure 1A). For another, ARFs interacts with the Mediator complex via its MR region and Aux/IAA via their PB1domains. The recruited TPL by the domain I of Aux/IAA inturn interacts with the CDK8 of the Mediator complex. Under high auxin concentration, TIR1/AFB forms $SCF^{TIR1/AFBs}$ ubiquitin complex and triggers Aux/IAAs polyubiquitylation and degradation via the 26S proteasome, resulting in the dissociation of ARFs to TPL-HDA19 and Mediator complex. The eviction of TPL facilitates a permissive chromatin conformation and an increase in the accessibility of transcription factors on the promoters of auxin responsive genes (Wang and Estelle, 2014; Jing et al., 2015) (Figure 1A), and permits the ARFs-Mediator complex to recruit RNA polymerase II and leading to the initiation of gene expression (Figure 1B). Comparison of TIR1, AUX/IAA and ARF orthologues across land plants and charophycean algae indicate that the assembly of the canonical auxin transcriptional response pathway is a land plant innovation.

3.2 Non-canonical auxin–dependent signaling

The auxin-related developmental defects of *ett* mutants suggested that ETT/ARF3 could regulate auxin signaling independently of the canonical pathway. A fundamental

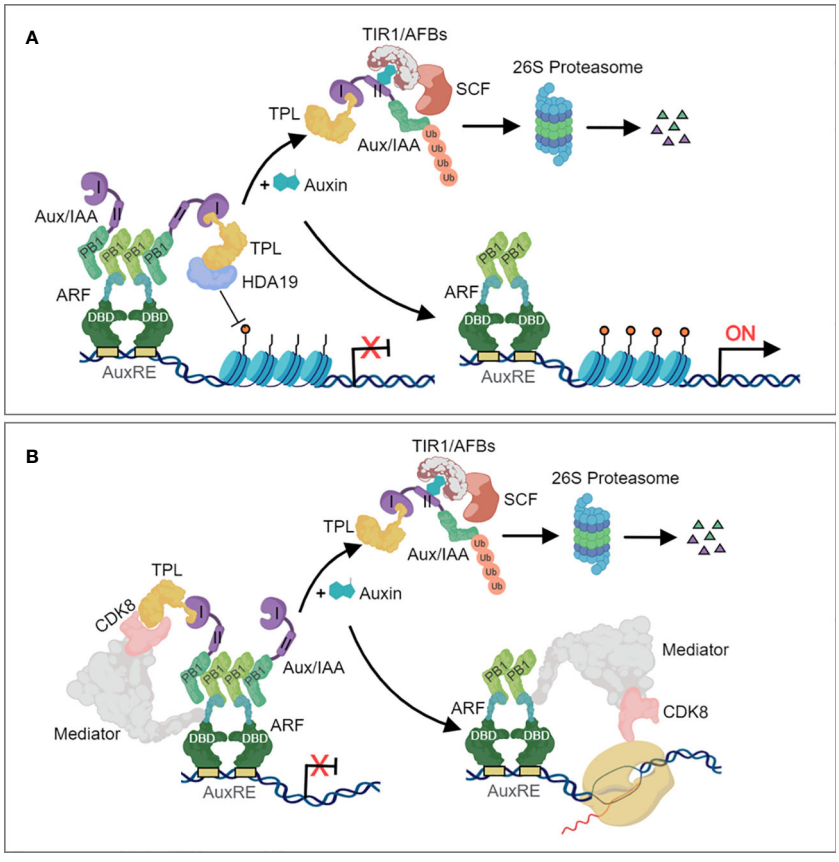

FIGURE 1
The canonical nuclear auxin signaling pathway. **(A)** Auxin signaling involving chromatin remodeling. **(B)** Auxin signaling involving the Mediator complex. In the absence of auxin, ARFs are bound by Aux/IAA repressor proteins, which recruit the TOPLESS (TPL) corepressor to constitute a repressor complex that repress transcription of auxin-responsive genes. ARFs, through their DBD domain, bind to the AuxRE of auxin-responsive genes and repress their transcriptional activity through interaction between the ARF Phox and Bem1 (PB1) domain and the Aux/IAA PB1 domain. TPL recruits histone deacetylases **(A)** and also interacts with Mediator **(B)** to prevent ARF transcriptional output. Auxin increases the affinity between the SKP1-CULLIN1-F-BOX (SCF) TIR1/AFB auxin receptor complex and Aux/IAAs, which stimulates Aux/IAA polyubiquitylation and degradation via the proteasome. Once free from TPL and Aux/IAA repression, ARFs then activates the expression of auxin-responsive genes.

difference between the ETT/ARF3-mediated and the canonical models of auxin signaling is that the former does not primarily require protein degradation to activate gene expression. It was suggested that ETT/ARF3 translates local auxin concentrations to developmental outputs in the gynoecium, although the molecular mechanisms governing this occurrence had not yet been discovered (Simonini et al., 2016). ETT/ARF3 has been reported to participate in auxin dependent protein-protein interactions with several transcription factors belonging to different families, and that these interactions are relevant for auxin responsiveness of specific tissues or cell types during development (Simonini et al., 2016). In the absence of auxin, ETT/ARF3 recruits TPL to its target loci via its ES domain. TPL, in turn, recruits HDA19 to promote deacetylation of histones and repress target gene expression (Figure 2A). In the presence of auxin, ETT/ARF3 can directly interact with the auxin molecule via the ES domain, suggesting that binding of auxin disrupts the interaction between ETT/ARF3 and its corepressor TPL (Kuhn et al., 2020) (Figure 2A), which permits the regulation of auxin-responsive genes.

Another non-canonical auxin-dependent signaling mechanism involves the Trans-Membrane Protein Kinases (TMPKs) pathway. The TMPK subfamily was first linked to auxin signal transduction when the phenotypes of double, triple, and quadruple *tmpk* mutants showed cell expansion and proliferation defects, miniaturized organs, infertility, and a reduced sensitivity to exogenously applied auxin (Dai et al., 2013). Kinase cascades are rapid and could be involved in rapid, non-canonical signalling. At high auxin concentration, TMPK phosphorylates AUX/IAA at its domain II, which interferes with the poly-ubiquitination and degradation of the AUX/IAA-TPL repressor complex by the $SCF^{TIR1/AFBs}$ ubiquitin complex, thus inhibiting the transcriptional regulation of auxin-responsive genes (Figure 2B).

4 ARF-mediated auxin pathway in growth and development

Plant growth and development are physiological processes coordinated by phytohormones. Physiological mechanisms regulating growth and development in plants are coordinated by hormonal signals, among which auxin has been implicated in virtually every aspect. Growth and development are intrinsic processes sustained by coordinated cell division, cell expansion, and cell differentiation. Auxin promotes cell division and meristem maintenance, and also plays an important role in the establishment of cellular patterning (Perrot-Rechenmann, 2010). Transcription factors are key regulators of cellular processes, both intrinsic, such as development and differentiation (Spitz and Furlong, 2012), as well as extrinsic, such as response to external signals (Lambert et al., 2018), through hormonal signaling pathways. At the molecular level, ARF TFs transduce auxin response signals by binding to the AuxRE in promoters of early auxin response genes (Wan et al., 2014). The ARFs are key components of the auxin signaling pathway known to regulate cellular processes of growth and development under normal cellular conditions (Guilfoyle and Hagen, 2007; Chandler, 2016). Several ARF genes have been reported to regulate various auxin-induced developmental processes in several plant species. ARFs are predominantly expressed during through all the periods of plant growth and development, and in different plant organs (Table 1), indicating its intricate role in plants.

4.1 Root morphogenesis and architecture

Plant root system plays crucial role in regulating and optimizing plant growth and development. They are important plant organs

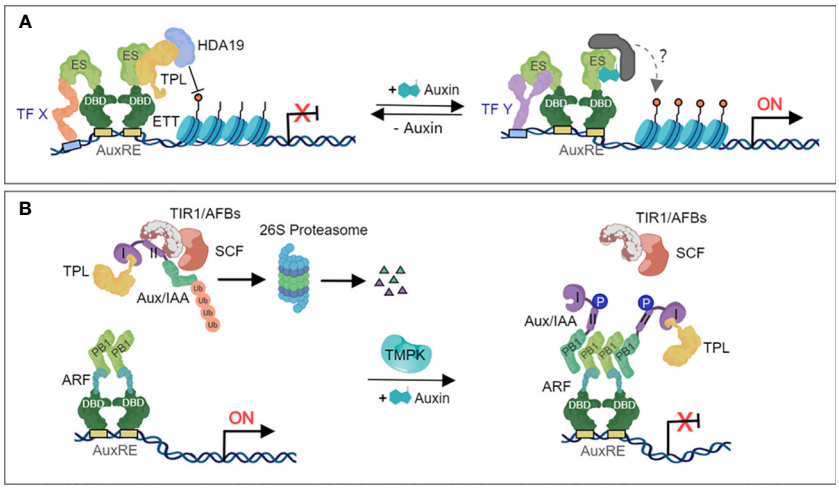

FIGURE 2
Mechanism of the non-canonical auxin-dependent signaling pathway. **(A)** The ETT-mediated non-canonical auxin signaling pathway. In the absence of auxin, the ETT-specific (ES) domain recruits the co-repressor TPL, which in turn, recruits HDA19 to deacetylate histones and repress target gene expression. Under elevated auxin levels, auxin binds to the ES domain of ETT and triggers the dissociation of the repressive complex, which releasing the repression of HDA19 and triggers histone acetylation and initiates gene expression. **(B)** The regulation of noncanonical Aux/IAAs. Certain ARFs heterodimerize with noncanonical Aux/IAAs, under no or low auxin concentrations leading to their polyubiquitylation and degradation. Auxin availability triggers phosphorylation of Aux/IAAs 4, leading to their stabilization and accumulation. These nondegradable Aux/IAAs will maintain the repression of their interactor ARFs, inhibiting the transcriptional regulation of auxin-responsive genes.

TABLE 1 Characterization of ARFs function in various plant species.

Species	Gene name	Function	References
Arabidopsis	AtARF1/2/3	Floral organ formation	(Nishimura et al., 2005)
	AtARF1/2	*F. oxysporum* infestation response	(Lyons et al., 2015)
	AtARF2	Seed germination and primary root growth	(Wang et al., 2011)
		Lateral root growth	(Marin et al., 2010)
		Leaf flattening	(Guan et al., 2017)
		Potassium stress response regulation	(Zhao et al., 2016)
	AtARF2/ARF7	Chlorophyll accumulation	(Luo et al., 2023)
	AtARF3	Rosette leaf formation	(Schuetz et al., 2019)
	AtARF3/4	Lateral root growth	(Marin et al., 2010)
		Leaf flattening	(Guan et al., 2017)
	AtARF5	Embryonic/primary root formation	(Dastidar et al., 2019; Zhang et al., 2023)
	AtARF6/8	Adventitious root formation	(Gutierrez et al., 2009; Kou et al., 2022)
		Leaf shape/leaf reproductive organs	(Tabata et al., 2010; Xiong et al., 2021)
	AtARF8	Turnip mosaic virus response	(Jay et al., 2011)
	AtARF7/19	Lateral root formation	(Okushima et al., 2005, Okushima et al., 2007)
		Adventitious root formation	(Lee et al., 2019)
	AtARF10/16	Root cap formation	(Wang et al., 2005)
Rice	OsARF1	Crown root growth	(Waller et al., 2002)
		Leaf inclination regulation	(Xing et al., 2022)
		Somatic and reproductive tissues	(Attia et al., 2009)
	OsARF1/5/6/17/19/24/25	Nitrogen use efficiency/ grain yield	(Zhang S. et al., 2021)
	OsARF3	Lemina development	(Si et al., 2022)
	OsARF4	Leaf inclination regulation	(Qiao et al., 2022)
	OsARF6/12/17/25	Flower opening and stigma size	(Zhao et al., 2022)
	OsARF11	Leaf angle regulation	(Sakamoto et al., 2013)
	OsARF12	Primary root growth	(Qi et al., 2012)
		Pi homeostasis	(Wang et al., 2014)
		Root elongation and Fe accumulation	(Qi et al., 2012)
	OsARF12/16	RDV immune response	(Qin et al., 2020)
	OsARF16	Adventitious crown root primordial formation	(Wang et al., 2007)
		Pi starvation response	(Shen et al., 2013)
		Fe-deficiency response	(Shen et al., 2013)
	OsARF17	Rice black-streaked dwarf virus response	(Zhang et al., 2020)
	OsARF19	Constitutive aerenchyma/Lateral root formation	(Yamauchi et al., 2019)
		Leaf angle regulation	(Zhang et al., 2015)
	OsARF21	Drought stress response	(Uga et al., 2013)
	OsARF23/24	Root elongation	(Li et al., 2014)
	OsARF25	Primary/crown root growth	(Mao et al., 2020)
Maize	ZmARF2/7/*25*	Maize inflorescence regulation	(Ma et al., 2023)
		Potassium uptake and homeostasis	(Sheng et al., 2020)
	ZmARF3	Leaf structure regulation	(Dotto et al., 2014)
	ZmARF4	Growth and development	(Li et al., 2022)
		Low Pi stress response	(Li et al., 2022)
	ZmARF5	Root growth and development	(Yang et al., 2022)
	ZmARf23		(Liang et al., 2023)

(Continued)

TABLE 1 Continued

(Continued)

TABLE 1 Continued

Species	Gene name	Function	References
		Embryonic callus and primary root development	
	ZmARF25/35	Seminal and lateral root regulation	(von Behrens et al., 2011)
	ZmARF34	Crown root formation	(Majer et al., 2012; Xu et al., 2015)
Wheat	TaARF15	Senescence regulation	(Li et al., 2023)
Tomato	SiARF2	Salt and drought stress response	(El Mamoun et al., 2023)
	SiARF4	Drought stress response	(Chen M. et al., 2021)
	SiARF5	Fruit set and development	(Liu S. et al., 2018)
	SiARF6	Photosynthesis/ sugar accumulation/ fruit development	(Yuan et al., 2019)
	SiARF8/10	Salt stress response	(Bouzroud et al., 2020)
	SiARF10	Chlorophyll and sugar accumulation	(Yuan et al., 2018)
Potato	StARF10	*P. infestans* infestation response	(Natarajan et al., 2018)
	StARF16	Necrotrophic pathogen infection response	(Kalsi et al., 2022)
Poplar	PdPapARF1	*Trichoderma asperellum* infestation response	(Wang et al., 2020)
Medicago	MdARF2/3/4	Lateral Root and Nitrogen Fixing Nodule Development	(Kirolinko et al., 2021)
Betula	BpARF1	Drought stress response	(Li H. et al., 2020)
Soybean	GmARF8	Nodulation and lateral root formation	(Wang Y. et al., 2015)

that absorb water and nutrients from soils and translocate them to the shoot (Stone et al., 2001; Sainju et al., 2005), as well as providing a means to monitor the soil for a range of environmental conditions (Overvoorde et al., 2010). Moreover, roots provide mechanical support to plants and distribute hormones that regulate numerous physiological and biochemical processes associated with growth and development of plants. Seed plants have evolved a complex root system consisting of at least three root types, i.e., the primary root, lateral roots, and adventitious roots. Since the discovery of auxins, they have been characterized to be closely related to root development. Root phenotypes associated with auxin signaling are dosage dependent, and include the length of epidermal-derived root hairs, primary root length, number and length of lateral roots and response to gravity (Ishida et al., 2008; Peret et al., 2009). ARFs have been reported to regulate various aspects of root morphogenesis and architecture in several plant species (Table 1).

4.1.1 Arabidopsis thaliana

Primary roots develop from an embryonically formed meristem (De Smet et al., 2010) and is the first organ to emerge from a germinating seed in the form of a radicle. Among the five genes encoding *Arabidopsis* clade A ARFs, ARF5/MP is essentially involved in primary root organogenesis (Aida et al., 2002). During embryogenesis, the hypophysis acts as the primary root founder cell in Arabidopsis (Petricka et al., 2012) and requires the auxin-dependent release of MP transcription factor from its inhibition by the Aux/IAA protein BODENLOS (BDL)/IAA12 (Herud et al., 2016). MP binds directly to the AuxRE in promoter of miR390 to regulates its expression in the *A. thaliana* primary root meristem (Dastidar et al., 2019), and also controls embryonic root initiation by regulating genes that mediate signaling from embryo to hypophysis. ARF5/MP, *TARGET OF MP 5* (*TMO5*) and *TMO7* encode basic helix–loop–helix (bHLH) TFs, that are expressed in the hypophysis-adjacent embryo cells, and are required and partially sufficient for MP-dependent root initiation (Schlereth et al., 2010). Both Wuschel-related Homeobox 9 (*WOX9*) and *ARF5*/MP are required for hypophysis specification and primary root formation, with mutations in either *WOX9* or *ARF5*/MP resulting in defective stem cell niche establishment of the primary root (Breuninger et al., 2008). The WOX9-ARF5/MP complex initiates primary root formation by activating RGF1 INSENSITIVEs (RGIs) in the primary root founder cell (Zhang et al., 2023). Root cap formation in *Arabidopsis* is regulated by miRNA160, which targets ARF10 and ARF16. The Pro(35S): MIR160 and *arf10-2 arf16-2* double mutants displayed the same root tip defect, with uncontrolled cell division and blocked cell differentiation in the root distal region and showed a tumor-like root apex and loss of gravity-sensing (Wang et al., 2005). Moreover, ARF2 acted as an ABA positive responsive regulator that functions in both seed germination and primary root growth by directly regulating the expression of a homeodomain gene HB33, with ABA treatment reducing cell division and altering auxin distribution more in *arf2* mutant than in WT (Wang et al., 2011).

Lateral roots (LR) are post-embryonic roots that arise from existing roots (Atkinson et al., 2014). LRs increase the volume of soil reached by roots, provide anchorage, and participate in water and nutrient uptake and transport (Dubrovsky and Laskowski, 2017). Auxin is a crucial hormone for lateral root formation, while ARFs act as key components of auxin biosynthesis, transport, signaling, and play important roles in lateral root initiation and lateral root primordium development (Jing and Strader, 2019). The *de novo* formation of lateral root organs requires tightly coordinated asymmetric cell division of a limited number of pericycle cells located at the xylem pole. This typically involves the formation of founder cells, followed by a number of cellular changes until the cells divide and give rise to two unequally sized daughter cells.

During LR initiation, a pair of xylem pole pericycle cells are primed by auxin signaling and specified as founder cells that undergo asymmetric cell division to develop as a stage I LR primordium. This process is activated by an AUX/IAA–ARF-dependent auxin signaling cascade (Luo L. et al., 2022). The module regulating founder cell formation involves the perception of auxin signaling by the auxin receptor TIR1, which acts in the basal meristem (Figure 3). Several Aux/IAA-ARF modules have been implicated in driving lateral root formation (Stoeckle et al., 2018). The IAA28-ARF5/6/7/19 module is specific for priming cell specification (De Smet et al., 2007; De Rybel et al., 2010), and positioning new lateral root primodia (LRP) and for specifying lateral root founder cell (LRFC) identity (Du and Scheres, 2018). Auxin-regulated GATA23 TF, considered as the first molecular marker for LRFCs, is regulated in XPP cells that leave the basal meristem by the IAA28-ARF5/6/7/19 auxin signaling cascade in the basal meristem (De Rybel et al., 2010), to regulate the process of lateral root founder cell identity (Figure 3). Prohibitin 3-Nitric oxide (PHB3–NO) signaling module regulates LR initiation through modulation of the canonical AUX/IAA-mediated auxin signaling cascade. PHB3 accumulates NO in pericycle cells and LRPs, and NO in turn triggers the degradation of AUX/IAA28 and IAA14 and the activation of ARFs, thereby inducing the expression of transcription factor genes *GATA23* and *Lateral organ boundaries domain 16* (*LBD16*) to promote LR initiation and LRP development (Luo L. et al., 2022). The SLR/IAA14–ARF7–ARF19 module regulates LR initiation by activating several auxin-responsive genes (Okushima et al., 2007). ARF7 and ARF19 directly regulate the auxin-mediated transcription of *LBD16/ASL18* and/or *LBD29/ASL16* in roots (Okushima et al., 2007), and contributes to asymmetric breakage of root cell wall (Figure 3). Auxin-dependent cell wall remodeling also has an important patterning function during LRP formation. ARF7/19 regulates the expression of Mustache (MUS) and Mustache-like (MUL) genes during LRP initiation. MUS and MUL encoding inactive LRR-RLKs, are expressed in early-stage LRPs via regulating cell wall biosynthesis and remodeling genes such as Xyloglucan Endotransglycosylase6 (XTR6), Expansin1 (EXP1), EXP17, and Polygalacturonase Abscission Zone A. Thaliana (PGAZAT) (Xun et al., 2020) (Figure 3). ARF7/19 also regulates *HAESA-LIKE 2* (HSL2) which is known to affect the expression of cell wall modifying and defense related genes (Niederhuth et al., 2013) (Figure 3). ARF7/19 module regulates the expression of LBD16/18/29, which inturn regulate the expression of downstream genes PUCHI (Goh et al., 2019), ERF2A (Berckmans et al., 2011), and CDKA1 (Feng et al., 2012), which have been implicated in lateral root initiation (Figure 3). ARF7/19 also regulates *Lateral Root Primordium1* (*LRP1*) (Figure 3), whose expression has been shown to be induced during lateral root initiation in *Arabidopsis* (Singh et al., 2020). Two callose-degrading enzymes plasmodesmal-localized β-1,3 glucanase1 (PdBG1) and PdBG2, are both transcriptionally regulated by auxin in an IAA14-ARF7/19-dependent manner, which control callose deposition in LRPs during lateral root morphogenesis (Figure 3). ARF7/19 and ARF5/MP regulate Plethora 5 (PLT5), which interacts with Wuschel-related Homeobox 5 (WOX5) to regulate lateral root morphogenesis.

Adventitious roots are those secondary roots that arrive from non-root tissues (Atkinson et al., 2014) whose initiation is controlled by precise balance of activator and repressor ARF transcripts, which is maintained by a complex regulatory network (Gutierrez et al., 2009). ARF6/8 are among the five genes encoding *Arabidopsis* clade A ARFs, and are required for adventitious root formation from hypocotyls (Gutierrez et al., 2009). *ARF6* and *ARF8* regulate adventitious root formation with the involvement of miRNA160 and miRNA167, such that, *ARF6* positively controls the development of adventitious roots (Kou et al., 2022). The WOX11-ARF6/8 complex activates RGIs and LBD16 to initiate the adventitious root primordium (Zhang et al., 2023). The auxin

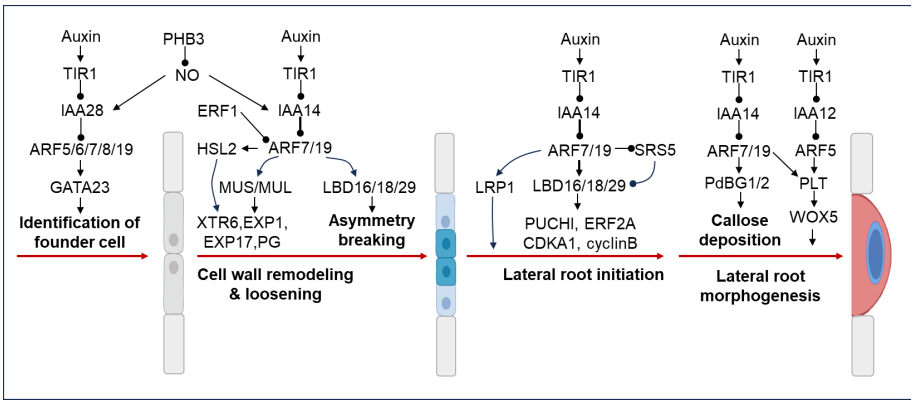

FIGURE 3
Lateral root regulation by ARFs. The IAA28-ARF5/6/7/8/19 module regulates positioning of new LRP and specification of LRFC identity by controlling the expression of GATA23 TF. PHB3 accumulates NO in pericycle cells and LRPs, which in turn triggers the degradation of AUX/IAA28/14 and the activation of ARFs and induction of *GATA23* to promote LR initiation and LRP development. ARF7 and ARF19 directly regulate the auxin-mediated transcription of *LBD16/ASL18* and/or *LBD29/ASL16* in roots and contribute to asymmetric breakage of root cell wall. Moreover, ARF7/19 regulates the expression of HSL2, MUS and MUL genes to modulate LRP initiation via regulating cell wall biosynthesis and remodeling genes such as XTR6, EXP1/17, and PGAZAT. ARF7/19 module regulates the expression of LRP1, LBD16/18/29, which inturn regulate the expression of downstream genes PUCHI, ERF2A, and CDKA1, which have been implicated in lateral root initiation. The IAA14-ARF7/19 module regulates callose deposition in LRPs during lateral root morphogenesis. ARF7/19 and ARF5/MP regulate PLETHORA 5 (PLT5), which interacts with Wuschel-related Homeobox 5 (WOX5) to regulate lateral root morphogenesis.

signaling module, *ARF7/ARF19-LBD16/LBD18* via AUXIN1 (AUX1)/LIKE-AUXIN3 (LAX3) auxin influx carriers, is involved in adventitious root formation in *Arabidopsis*: single mutants *aux1*, *lax3*, *arf7*, *arf19*, *lbd16* and *lbd18* recorded reduced numbers of adventitious roots than in the WT (Lee et al., 2019). At the same time, double and triple mutants exhibited further decrease in adventitious root numbers compared with the corresponding single or double mutants, respectively, and the *aux1 lax3 lbd16 lbd18* quadruple mutant lacked adventitious roots.

4.1.2 Rice

OsARF are large multigene family that plays essential roles in different tissues of the rice plant. OsARFs play crucial roles in modulating root developmental processes and optimal architecture of root system (RSA) essential for normal growth and development (Table 1). For example, *OsARF1* regulates auxin-dependent differential growth in the crown roots of rice coleoptiles, and that, *OsARF1* transcript abundance was stimulated by gravitropism in the lower fast-growing flank (Waller et al., 2002). Knockout of *OSARF12* resulted in decreased primary root length, with *osarf12* and *osarf12/25* mutants displaying shorter root elongation zone compared to WT: This was occasioned by decreased expression of auxin synthesis genes OsYUCCAs and auxin efflux carriers OsPINs and OsPGPs (Qi et al., 2012). *OsNAC2* functions as an upstream integrator of auxin and cytokinin signals by binding directly to the promoters of *OsARF25* and a cytokinin oxidase gene (*OsCKX4*) to regulate primary root length and the number of crown roots in rice (Mao et al., 2020). OsARF23/24 heterodimers binds to the promoter of an actin-binding protein (RMD) and promote its expression in the auxin signaling pathway to trigger changes in F-actin organization that controls root elongation in rice (Li et al., 2014). AUX/IAA-ARF-dependent auxin signaling controls aerenchyma and lateral root development: LR number and constitutive aerenchyma formation were reduced by the dominant-negative effect of a mutated AUX/IAA protein in the *iaa13* mutant. It was further revealed that ARF19 interacted with IAA13, and that LBD1-8 acted as a downstream target of ARF19; IAA13, ARF19, and LBD1-8 were highly expressed in the cortex and LR primordia, suggesting that these genes function in the initiation of constitutive aerenchyma and LR formation (Yamauchi et al., 2019). Rice stems develop adventitious root primordia at each node but mature slowly and eventually emerge only when the plant gets flooded (Lin and Sauter, 2018) to provide water, nutrients, and anchorage. In rice, *OsARF16* regulates the initiation of adventitious crown root primordia by activating the expression of *Crow Rootless1/Adventitious Rootless1* (*CRL1/ARL1*), which encodes an LBD protein (Liu et al., 2005; Wang et al., 2007).

4.1.3 Maize

Auxin synthesis, transport and signal transduction have been proven to be involved in regulating maize root growth and development (Nestler et al., 2016). The unique roles of ARF genes in maize growth and development are emerging from molecular genetic studies (Table 1). Auxin signal transduction is mainly controlled by ARF and Aux/IAA genes. Multiple *AUX/IAA*-ARF-mediated signaling plays an important role in regulating plant root formation (Goh et al., 2012). *ZmIAA5* interacts with *ZmARF5* to regulate maize root growth and development. Primary root length and the number of lateral roots at the seedling stage, and total number of roots and the dry root weight at the matured stage of maize overexpressing *ZmIAA5* increased compared to the WT, while those of mutant *zmiaa5* was significantly reduced (Yang et al., 2022). Auxin has also been implicated as the starting signal that induces crown root formation in maize. Auxin induces the degradation of AUX/IAA proteins so that *ZmARF34* activate the expression of downstream target *Rootless Concerning Crown and Seminal Roots* (*RTCS*), an LOB domain protein regulating shoot-borne root initiation in maize. The induced *RTCS* proteins bind to the promoter of *ZmARF34* and activate its transcription, which inturn promotes RTCs expression, representing an amplified mutual feedback loop that regulates *ZmARF34* and *RTCS* transcription during coleoptilar node development and crown root formation in maize (Majer et al., 2012; Xu et al., 2015). The *Rootless with Undetectable Meristems 1* (*RUM1*) gene encodes *ZmIAA10* which is required for the initiation of embryonic seminal and post-embryonic lateral root initiation in primary roots of maize (Wang et al., 2010). RUM1 could interact with, and form complexes with transcriptional activators *ZmARF25* and *ZmARF34* to regulate initiation of embryonic seminal and post-embryonic lateral root initiation in primary roots of maize (von Behrens et al., 2011). *ZmARF23* bound to the promoter of a known causal gene for embryonic callus induction, *ZmSAUR15*, and positively regulated its expression at the transcription level to promote embryonic callus formation and primary root development (Liang et al., 2023).

4.2 Leaf regulation mechanism

Photosynthesis is crucial for the existence of the vast majority of life on earth. Plants are primary producers that form the base of every ecosystem and fuel the next tropic level by utilizing photosynthesis to transform water, sunlight and carbon dioxide into oxygen and simple energy for utilization. The photosynthetic process is the principal energy source for all organisms on earth. Leaf anatomy, such as mesophyll thickness and chloroplast abundance and distribution, influences the photosynthetic capacity of plants (Oguchi et al., 2003). Moreover, the shape, size, and chlorophyll content of plant leave influence its photosynthetic capability and efficiency (Guan et al., 2017). Auxin has been proven to play central roles in leaf developmental processes such as leaf initiation, blade formation, compound leaf patterning and leaf inclination (Xiong and Jiao, 2019), with active participation of ARFs in numerous plant species (Schuetz et al., 2019), as outlined in Table 1.

The flattening of leaves to form broad blades with wider surface area is a pronounced adaptation by plants to maximize photosynthetic ability and efficiency. Adaxial-expressed ARF5/MP directly binds to the promoters of *WOX1* and *Pressed Flower* (PRS) and activate their expression in the leaf marginal domain to enable leaf flattening, while redundant abaxial-enriched ARF2/ARF3/ARF4 repressors suppress *WOX1* and *PRS* expression to maintain

the abaxial identity (Guan et al., 2017). While *arf3*, *arf5* and *arf7* single mutants formed normal leaves in *Arabidopsis*, *mp/arf3* or *mp/arf7* displayed a breakdown in leaf formation with novel leaf structure not present in any of the single mutants, suggesting that ARF3 and ARF7 regulates rosette leaf formation and that their functions overlap and act parallel with those of ARF5/MP (Schuetz et al., 2019). ARF6 and ARF8 activate the expression of *DWARF4* (*DWF4*), a pivotal enzyme in brassinosteroids (BR) synthesis. BRs, in turn, facilitate the demethylation of cell wall pectin, resulting in isotropic in-plane cell wall loosening, which ultimately gives rise to leaves with diverse shapes and overseeing the proximal-distal growth of leaf reproductive organs (Xiong et al., 2021). ARF2 and ARF7, with the help of IAA14, suppressed the expression of chlorophyll biosynthesis gene *Protochlorophyllide Oxidoreductase A* (*PORA*) and *Genomes Uncoupled 5* (*GUN5*) in matured leaves, resulting in reduced chloroplast number and structure in mesophyll cells and eventual reduction in photosynthetic efficiency (Luo et al., 2023).

Leaf inclination/angle is a component of crop architecture and fundamental property of plant canopy structure, which is required for light interception, canopy photosynthesis, and energy balance. Leaf inclination of rice results mainly from the asymmetric cell division and elongation of adaxial and abaxial cells at the lamina joint (Zhou et al., 2017), which is regulated by the biosynthesis or signaling of auxin. In rice, *OsARF4* participates in leaf inclination regulation via auxin and brassinosteroid (BR) signaling pathways: *osarf4* mutants displayed increase in cell differentiation on the adaxial side, resulting in increased leaf inclination; however, *OsARF4*-overexpressing lines manifested a decrease in leaf inclination, resulting in erect leaves (Qiao et al., 2022). In another experiment, *OsIAA6* interacts with *OsARF1* to suppress auxin signaling and regulates leaf inclination, with rice brassinazole resistant (*OsBZR1*), the key transcription factor in BR signaling, binding directly to the promoter of *OsIAA6* to stimulate its transcription (Xing et al., 2022), suggesting that *OsIAA6–OsARF1* module regulates rice leaf inclination through synergistic action of auxin and BR. The mutant *ds1* showed reduced BR sensitivity and leaf angle through a mechanism involving DS1's interaction with *OsARF11* to regulate *OsBRI1* expression (Liu X. et al., 2018). Loss-of-function mutant of *OsARF11*, *osarf11-1*, displayed phenotypes with reduced plant height and leaf angle of flag leaves compared to WT in rice (Sakamoto et al., 2013). *OsARF19* controls rice leaf angles by positively regulating *OsGH3-5* and *OsBRI1*. *OsARF19*-overexpression rice lines showed an enlarged lamina inclination compared to WT due to its increased adaxial cell division in an auxin and brassinosteroid-dependent manner, resulting from direct activation of the early auxin responsive gene *OsGH3-1* and *Brassinosteroid Insensitive 1* (*OsBRI1*) (Zhang et al., 2015). Auxin induces *OsARF6* and *OsARF17* to independently and synergistically bind directly to the *Increased Leaf Angle1* (ILA1) promoter and activate its expression to control secondary cell wall composition of the lamina joint to determine flag leaf angle (Zhang et al., 2015).

Mutation in maize *leafbladeless1* (*lbl1*), that disrupt ta-siRNA biogenesis, give rise to plants with thread-like leaves that have lost top/bottom polarity. Misregulation of tasiR-ARFs target, ETT/*ARF3*, has emerged as the basis for the *lbl1* leaf polarity defects, with plants expressing *arf3a* transcripts displaying insensitivity to tasiR-ARF-directed cleavage and recapitulating the phenotypes observed in *lbl1* (Dotto et al., 2014). Auxin plays important roles in regulating both age-dependent and dark-induced senescence through the actions of several auxin-related genes, such as *YUCCA6*, *Small Auxin Upregulated RNA36* (*SAUR36*), and *Indole-3-acetic Acid Inducible 29* (*IAA29*) (Kim et al., 2011; Hou et al., 2013; Jiang et al., 2014). *ZmbHLH112* can repress the expression of *Aux/IAA* related genes, and promote the binding of ARF to AUXRE in the promoter of their target genes to regulate the elongation of leaf angle cells (Zhang et al., 2022).

4.3 Mechanism of floral structure and sexual reproduction regulation

Flowers constitute the reproductive structures in plants and lead to formation of fruit and seed after fertilization. Unlike leaves and roots that appear as single organs, flowers have evolved into a stable plant reproductive composite structure, composed of multiple organs arranged in an orderly pattern (Endress, 2010). ARFs have been reported to modulate auxin-dependent regulation of floral organ organization mostly in Arabidopsis (Table 1). The *ett/arf3*mutant displayed phenotypes with abnormal floral meristem patterning and gynoecium development in *Arabidopsis* (Sessions et al., 1997), whiles *arf1* and *arf2* loss-of-function mutants illustrated abnormal abscission of floral organs (Ellis et al., 2005). Mutation analyses revealed that *ARF1* and *ARF2* regulated plant leaf senescence and floral organ exfoliation, and the ETT/ARF3 gene influenced defect in pistil and flower meristem formation in *Arabidopsis thaliana* (Nishimura et al., 2005; Quint and Gray, 2006). ARF3 has been functionally characterized to participate in regulatory pathway that modulate gynoecium morphogenesis, self-incompatibility, *de novo* organ-regeneration, and organ polarity (Tantikanjana and Nasrallah, 2012). *ARF6* and *ARF8* regulated JA biosynthesis and floral organ development via suppression of class I KNOX genes *KNAT2* and *KNAT6*, with a*rf6arf8* plants displaying defective phenotypes such as aberrant vascular patterning and lack of epidermal cell differentiation in petals, which were partially suppressed by mutations in *KNAT2* or *KNAT6* (Tabata et al., 2010).

Floral organ development significantly influences plant reproduction and seed quality, yet its underlying regulatory mechanisms are still largely unknown, especially in crop plants. Disruption of *OsARF19* regulates floral organ development and plant architecture in rice. *ARF6*, *ARF12*, *ARF17*, and *ARF25*, manifested overlapping functions in flower opening and stigma size: Single mutant, *arf12*, showed a reduced plant height and aborted apical spikelets, while mutation in *ARF12* together with mutation in either *ARF6*, *ARF17*, or *ARF25* led to the same defective phenotypes including the failed elongation of stamen filaments, increased stigma size, and morphological alteration of lodicule (Zhao et al., 2022). AUX/IAA-ZmARF complexes have been reported to predominantly affect maize reproductive growth (Ori, 2019). *ZmIAA29* can influence maize florescence by interacting with *ZmARF2*, *ZmARF7*, and *ZmARF25* (Ma et al., 2023). AUX/IAA proteins Barren Inflorescence 1 and Barren Inflorescence4 and

ARFs forms multiple BIF1/BIF4-ARFs transcriptional repression modules involved in the regulation of the boundary basic helix-loop-helix transcription factor *Barren Stalk1* (*BA1*), during the initial stages of reproductive organogenesis in maize and influence its inflorescence architecture (Galli et al., 2015).

5 The mechanism of ARFs involvement in abiotic and biotic stress responses

5.1 Abiotic stress

Most of the gains made towards functional characterization of ARF family proteins have focused largely on their role in plant growth and development. On the contrary, the role of auxin in regulating stress responses in plants has not received much attention. However, recent molecular approaches such as expression profiling have hinted that auxin might exert some regulatory role on plant responses to environmental stress conditions (Ha et al., 2013). It is suggested that auxin might either be acting alone or together with other key phytohormones in regulating plant response to abiotic stresses such as drought, cold, temperature extremities and salinity (Zahir et al., 2010; Lee et al., 2012). These abiotic stresses affect plant viability and development, which may result in changes in plant growth and crop yield, as well as, disturbance of physiological processes such as photosynthetic or mineral uptake rates (Kou et al., 2022). Genomic studies and expression analysis revealed that, numerous ARF family proteins were differentially expressed in various species in response to key abiotic stress such as drought, salinity or cold (Jain and Khurana, 2009), suggesting that these ARFs are active participants in abiotic stress response in plant species (Table 1).

5.1.1 Arabidopsis thaliana

Nutrient deficiencies are major abiotic stresses that impact the growth, development and productivity of plants. Macronutrients are the building blocks of crucial cellular components like proteins and nucleic acids. Macronutrient deficiencies have far reaching consequence for optimum crop growth and yield optimization. Some ARFs have been implicated to participate in regulating macronutrient deficiency responses in plants. The framework of molecular components composing a cascade of auxin synthesis, transport, and signaling that triggers root hair (RH) elongation in response to low N has been proposed (Jia et al., 2023). Low N upregulates Tryptophan Aminotransferase of Arabidopsis 1 (TAA1) and YUCCA8 activities, which increase auxin accumulation in the root apex. Auxin is then translocated from the root apex to the RH differentiation zone by the auxin transport machinery comprising Auxin Transporter Protein 1 (AUX1) and Pin-formed 2 (PIN2). At the RH differentiation zone, auxin activates the transcription of ARF6/8 to stimulate epidermal and auxin-inducible transcriptional module Root Hair Defective 6 (RHD6)-Lotus Japonica Root Hairless-like 3 (LRL3) to steer RH elongation in response to low N (Jia et al., 2023) (Figure 4).

IAA14-ARF7/19 module has been reported to modulate LR development and confer low P stress tolerance. ARF7 and ARF19, which are transcriptional activators of early auxin response genes, acts downstream of IAA14 and regulates LR formation in Arabidopsis by directly regulating the auxin-mediated transcription of LBD16/29 in roots (Okushima et al., 2007) as shown in Figure 4. Auxin-responsive LBD18 acts as a specific DNA-binding transcriptional activator that directly regulates expression of Expansin (EXP) *genes* (Figure 4), which encode cell wall-loosening factor that promotes lateral root emergence in *Arabidopsis thaliana* (Lee et al., 2013). PHOSPHATE STARVATION RESPONSE1 (PHR1)/MYB are recognized as key regulatory component of the response to Pi starvation by directly regulating various *P starvation-induced* (*PSI*) genes, which consequently affects P uptake and transport, and modulates RSA (Puga et al., 2017; Huang et al., 2018). ARF7 and ARF19, are the upstream regulators of the genes encoding PHR1/MYB family members (Figure 4).

CLSY1, a key component of the RNA-directed DNA-methylation machinery, mechanistically mediates the transcriptional repression of a negative regulator of root branching, *IAA27*, and promotes lateral root development under K deficiency (Shahzad et al., 2020) (Figure 4). IAA27 interacts with ARF2, which inturn modulates the expression of the K^+ transporter gene HAK5 (High Affinity K^+ transporter 5), with *arf2* mutant plants displaying a tolerant phenotype similar to the HAK5-overexpressing lines on low-K^+ medium (Zhao et al., 2016) (Figure 4), and suggests that ARF2 acts as a negative regulator of low K stress response in Arabidopsis.

The molecular link that integrates plant abscisic acid (ABA) responses to drought stress in plants has been demonstrated (Meng et al., 2015). Drought signal perception leads to activation of dehydration-responsive element-binding protein (DREB2A/B) TFs which directly promote transcription of IAA genes in response to drought stress (Figure 4). The molecular and genetic evidence presented indicate that ARF2, ANT and Cold-regulated15A (COR15A) form an ABA-mediated signaling pathway that modulates drought stress response, with ARF2 serving as a molecular link that integrates plant ABA responses to drought stress (Meng et al., 2015) (Figure 4).

5.1.2 Rice

Expression of seven ARF TFs, *OsARF1*, *OsARF5*, *OsARF6*, *OsARF17*, *OsARF19*, *OsARF24* and *OsARF25*, is upregulated in *dnr1* but downregulated in pAct : DNR1-Flag overexpression line relative to WT. Upregulation of these ARF TFs mediates auxin-dependent activation of NO_3^- transporter and N-metabolism genes, resulting in improved NUE and grain yield in rice (Zhang S. et al., 2021). The *osarf12* and *osarf12/25* mutants with P-intoxicated phenotypes recorded higher P concentrations, up-regulation of Pi transporter encoding genes (*OsIPS1*, *OsIPS2*, *OsSPX1*), *OsSQD2*, *OsMYB2P-1* and *OsTIR1*) and increased APase activity under Pi-sufficient/-deficient (+Pi/-Pi, 0.32/0 mM NaH_2PO_4) conditions compared to WT, suggesting that *OsARF12* is a negative regulator of Pi homeostasis in rice (Wang et al., 2014). Knockout of *OsARF16*

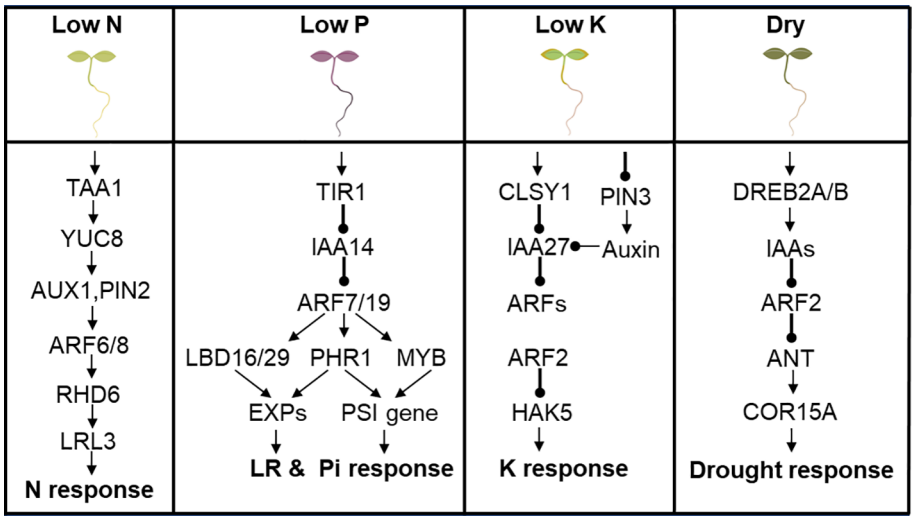

FIGURE 4
ARF is involved in abiotic stress response in Arabidopsis. **(A)** Low N upregulates TAA1 and YUCCA8 activity to regulate downstream genes ending with LRL3 to confer low N stress response. **(B)** IAA14-ARF7/19 modulates LBD16/29 and PHR1 to regulate cell wall loosening EXPs to promote lateral root development. IAA14-ARF7/19-PHR1 or IAA14-ARF7/19-MYB modulates expression of PSI genes to confer tolerance to low Pi stress. **(C)** *CLSY1* mediates the transcriptional repression of *IAA27*, an upstream regulator of ARF2, which inturn modulate the expression of the K^+ transporter gene HAK5 and confer tolerance to low K stress. **(D)** Drought signal perception activates DREB2A/B, which directly promote transcription of IAA genes in response to drought, through a mechanism mediated by ARF2, ANT and COR15A in an ABA-dependent manner.

led to loss of sensitivity of primary roots, lateral roots and root hairs to auxin and Pi response, with *osarf16* mutant displaying slightly reduced shoot biomass, inhibited root growth, and reduced induction of phosphate starvation-induced genes (Shen et al., 2013). Compared to WT, *osarf16* mutant displayed compromised cytokinin-induced inhibition of Pi uptake and higher Pi content under cytokinin treatment, which was occasioned by higher expression of *Phosphate Transporter1* (*PHT1*) genes, *PSI* genes and *purple PAPase* genes (Shen et al., 2014), suggesting that *OsARF16* participates in cytokinin mediated inhibition of phosphate transport and phosphate signaling in rice. Besides regulating adaptation mechanisms to macronutrient deficiencies, OsARFs have also been reported to modulate iron deficiency response adaptation in rice. *OSARF16* has been reported to regulate iron deficiency response in rice by regulating auxin redistribution: Expression of *OsARF16* is induced by Fe limitation in root and shoot, which inturn upregulates Fe-deficiency response genes; Consequently, in the auxin insensitive mutant, *osarf16*, most Fe-deficiency symptoms were partially restored, including dwarfing, decreased photosynthesis, reduced iron content and the regulation of RSA (Shen et al., 2015). An *OsARF12* knockout mutant, *osarf12*, displayed short primary root length, altered abundance of mitochondrial iron-regulated (*OsMIR*), iron (Fe)-regulated transporter 1 (*OsIRT1*) and short postembryonic root (*OsSPR1*) in roots of rice, and resulted in limited Fe content (Qi et al., 2012).

OsARF21 directly binds to the promoter of the early auxin responsive genes, *Deep rooting 1* (*DRO1*), and regulates its expression in the auxin signaling pathway to modulate cell elongation in the root tip, causing asymmetric root growth and downward bending of the root in response to gravity to maintain high yield performance under drought conditions (Uga et al., 2013). The rice auxin response factors, *OsARF11* and *OsARF15*, have both been reported to show differential expression under salt stress condition, suggesting that they might participate in response to salt stress response in rice (Jain and Khurana, 2009). Evaluation of changes in endogenous indole-3-acetic acid (IAA) and jasmonic acid (JA) levels and their responsive genes in rice under various abiotic stress condition revealed that *OsARF4/14/18/19* were induced by cold stress, whiles *OsARF11/13/16* were induced by heat stress (Du et al., 2013).

5.1.3 Maize

Functional characterization of ZmARFs in stress response in maize remains largely limited. Nonetheless, a few ZmARF TFs have been reported to participate in stress response and adaptation. Cytonuclear localized *ZmARF2* interacts with promoter of the maize high-affinity K transporter (*ZmHAK1*) to promote K^+ uptake and homeostasis (Sheng et al., 2020). Nucleotide diversity and favorable alleles of *ZmARF31* were found to be significantly associated with low P responses traits and root architecture in maize. Thirty, fourteen, and nine natural variations were identified in *ZmARF31* that were associated with P-deficiency-tolerance traits in maize (Wu et al., 2016). Overexpression of the maize ARF, *ZmARF4*, in Arabidopsis conferred low phosphate (Pi) stress tolerance; transgenic Arabidopsis overexpressing *ZmARF4* displayed better root development, increased Pi mobilization, up-regulation of low Pi stress inducible gene (*AtRNS1*) and down-regulation of anthocyanin biosynthesis genes (*AtDER* and *AtANS*), under low Pi stress compared to WT (Li et al., 2022).

5.2 Biotic stresses

Biotic stresses are those adverse conditions that normally affectplant growth due to their interaction with deleterious microorganisms such as fungi, bacteria, viruses, viroids, phytoplasmas and nematodes. These microorganisms mainly growth either on or inside plant tissues and inflict varied damages leading to symptoms like chlorosis, stunting, rotting, or local lesions formation. Compared to the role of ARF TFs in regulating responses to abiotic stresses, the role of theses TFs in biotic stress response regulation has not received much research attention. The role of auxin and its signaling pathway on plan- pathogen association has long been reported (Bari and Jones, 2009).

In *Arabidopsis*, the transcript of *ARF1* and *ARF2* were repressed by *F. oxysporum*, whiles *arf2*, *arf1* and *arf2/arf1* displayed phenotypes with increased resistance to *F. oxysporum* relative to WT, these outcomes suggest that *ARF1* and *ARF2* promote susceptibility to *F. oxysporum* infestation (Lyons et al., 2015). Misregulation of *ARF8* results in developmental abnormalities manifested by viral suppressors of RNA (VSR) transgenic plants and also for the phenotypes displayed during normal viral infection caused by the HcPro-encoding Turnip mosaic virus (TuMV) (Jay et al., 2011). Some OsARFs also play crucial roles in host antiviral immune defense. *OsARF12* and *OsARF16* interacted with *OsIAA10* to positively regulate rice antiviral defense against rice dwarf virus (RDV) through a mechanism involving binding of *OsARF12* to the AuxRE in promoter of *OsWRK13* to activate its transcription (Qin et al., 2020). Overexpression of *OsARF17* reduced accumulation of the black-streaked dwarf virus (BSDV) and rice black-streaked dwarf virus (RBSDV), whiles the accumulation of these virus and severity of their symptoms increased in *osarf17* knockout mutant rice lines (Zhang et al., 2020). In maize, expression of *ZmARF6* and *ZmARF18* genes increased significantly in response to *Colletotrichum graminicola* and *F. verticillioides* (Saidi and Hajibarat, 2020), suggesting that these ARFs could act as positive regulators to stresses induced by *Colletotrichum graminicola* and *F. verticillioides*.

6 Transcriptional and post transcriptional regulation of ARFs

ARFs have been proven to be regulated by other TFs to mediate biological process of growth and development, as well as, stress responses (Wang and Estelle, 2014). Yeast two-hybrid and *in vitro* pull down assays revealed heterodimerization between the III/IV domain of ARF5/MP and the *Arabidopsis* BREVIS RADIX (BRX) transcription co-regulator, which promotes the transactivation potential of ARF5/MP (Guilfoyle and Hagen, 2007) (Figure 5A), which control root meristem growth (Scacchi et al., 2010). LBD18 interacts with ARFs (Figure 5A) such as ARF7 and ARF19 via the Phox and BemI domains to promote the transcriptional activity of ARF7 on the AuxRE, inhibiting the negative feedback loop exerted by AUX/IAA repressor, to constitute a double positive feedback, that ensures continued lateral root growth in response to auxin in Arabidopsis (Pandey et al., 2018). A recent study showed that *Dull Nitrogen Response* TF (*DNR1*) regulates auxin homeostasis and induction of ARFs (Figure 5A) to promote ARF-mediated activation of *NPF/NRT1* and *NRT2* to regulate NO_3^- uptake in roots, resulting in enhanced NUE and grain yield (Xing et al., 2023). Other regulatory models have been proposed to inhibit transcription of ARFs during growth and stress responses. For example, induction of *Agamous* (AG) represses ARF3 expression indirectly through *Giant Killer* (GIK) (Figure 5A) which harbors an AT-hook DNA binding motif, and is crucial for floral meristem development (Zhang et al., 2018). The *Apetala2* (APT2), encoding a putative TF characterized by a novel DNA binding motif referred to as AP2 domain, directly represses ARF3 transcription (Figure 5A) during floral meristem determination (Liu et al., 2014). The rice P8 proteins have been reported to interact with the C-terminus domain of *OsARF17* to prevent its dimerization with other proteins, leading to suppression of its role in conferring resistance to RBSDV and RBSD (Zhang et al., 2020). Several post-transcriptional events contribute to the cell-specific expression patterns and functions of genes. Majority of the post-transcriptional regulations of gene expression are occasioned by activities of RNA binding proteins and processing factors that are closely related with RNAs, spanning from transcription initiation to eventual death of the RNA in the cytoplasm (Dassi, 2017). MicroRNA (miRNA)-mediated regulation of auxin signaling pathway during plant development and stress responses has been reported (Luo P. et al., 2022). Numerous miRNAs have been characterized to target ARFs, leading to regulation of the downstream auxin responsive genes related to both development and stress response in plants. Two conserved miRNAs, miRNA160 and miRNA167, constitutes a complex feedback loop that regulates processes in the auxin signaling pathway by modulating the expression of ARFs (Singh and Singh, 2021)(Figure 5B). The miRNA160 and miRNA167 actively regulate mRNA abundance of ARFs in Arabidopsis, miRNA160 targets and cleaves *ARF10/16/17*, while miRNA167 targets and cleaves *ARF6/8* (Mallory et al., 2005; Wu et al., 2006) (Figure 5B). The miRNA160/miRNA167 and their associated targets *ARF6/8/17* form a regulatory network that modulates adventitious root development. Whiles miRNA167 targets ARF6 and ARF8, which functions as positive regulators of adventitious root development, miRNA160 targets ARF17, which acts as a negative regulator of adventitious root development (Gutierrez et al., 2009). However, *ARF6/8/17* control their own expression at both transcriptional and posttranscriptional level by regulating the abundance of miRNA160 and miRNA167, which completes the miRNA160/miRNA167-*AtARF6/8/17* feedback loop that regulates adventitious root development (Gutierrez et al., 2009). OsmiRi167a targets *OsARF12*, *OsARF17* and *OsARF25* to control tiller angle in rice, with repression of *OsARF12*, *OsARF17* and *OsARF25* in transgenic plants overexpressing OsmiRi167a, which displayed phenotypes with larger tiller angle similar to *osarf12/osarf17* and *osarf12/osarf25* plants (Li Y. et al., 2020). The miRNA167a positively regulates grain length and weight by dictating *OsARF6* mRNA silencing to mediate *OsAUX3* expression in a novel *miRNA167a-OsARF6-OsAUX3* regulatory model (Qiao et al., 2021). The miRNA160 has also been reported to target ARF10 and ARF16,

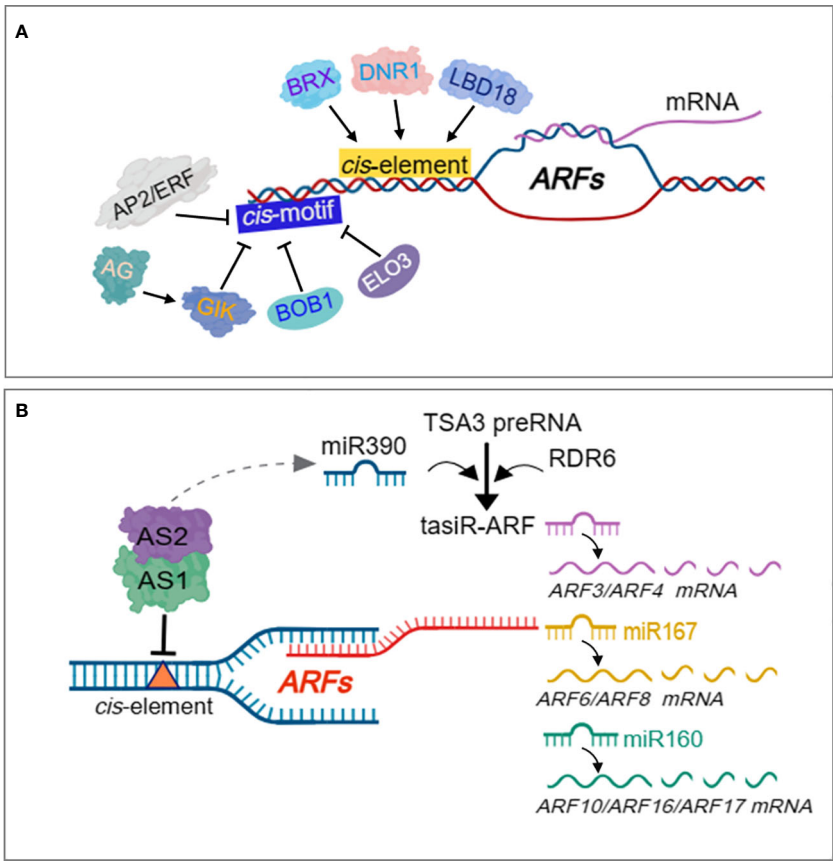

FIGURE 5
Regulation of ARFs by transcriptional and post-transcriptional events. BRX transcription co-regulator, DNR1 and LBD18, directly induce ARF expression to promote several aspects of plant growth and development. AP2/ERF, BOB1 and ELO3 directly repress expression of ARFs. AG indirectly represses ARF3 expression through GIK. AS1-AS2 complex indirectly activates miR390-and RDR6-dependent gene silencing to negatively regulate both ARF3 and ARF4 activities. The TAS3 genes encode tasiR-ARF species which target the mRNA of three ARF TFs, ARF2, ARF3/ETT and ARF4, for subsequent degradation. TAS3 harbors two miR390 target sites that are cleaved by miR138 to trigger the production of tasiR-ARF from the cleaved fragments. miRNA160 targets and cleaves *ARF10/16/17*, while miRNA167 targets and cleaves *ARF6/8* in a regulatory network that modulates adventitious root development.

which act as transcription repressors, and regulate the expression of their downstream responsive genes to mediate the regulation of developmental processes in plants (Huang et al., 2016; Liu et al., 2016).

The most well studied Trans-acting SIRNA (TAS)-derived short interfering RNAs (siRNAs) are tasiR-ARFs, which are widely conserved across plant species and target several ARF genes (Allen et al., 2005). The TAS3 genes encode tasiR-ARF species which target the mRNA of three ARF TFs, ARF2, ETT/ARF3 and ARF4, for subsequent degradation (Ozerova et al., 2013) (Figure 5B). miRNA can trigger the biogenesis of secondary siRNAs in phase (phasiRNAs) such as the TAS by targeting their transcripts for cleavage (Liu et al., 2020). The cleaved TAS transcripts is bound to and converted to double-stranded RNAs (dsRNAs) by RNA-binding protein SUPPRSSOR OF GENE SILENCING 3 (SGS3), through RNA-dependent RNA polymerase (RDR6), and undergoes further processing to generate phasiRNAs such as tasiR-ARF (Zhang et al., 2019) (Figure 5B). In another mechanism, TAS RNA precursor TAS3 transcript bears two targets sites of miR390, cleavage at these sites trigger the production of phasiRNAs such as tasiR-ARF from the cleaved fragments (Axtell et al., 2006) (Figure 5B). ARF2, ARF3 and ARF4 have been demonstrated to be targeted and regulated by TAS3 ta-siRNA (tasiRNA-ARF) (Hunter et al., 2006) (Figure 5B), which affects developmental timing and patterning in *Arabidopsis* (Fahlgren et al., 2006). Assymetric leaves 1 (AS1)-AS2 also indirectly activates miR390-and RDR6-dependent post-transcriptional gene silencing to negatively regulate both ARF3 and ARF4 activities (Iwasaki et al., 2013) (Figure 5B).

miR167 positively regulates nodulation and lateral root development in *Glycine max* by targeting and inhibiting its target genes *GmARF8a* and *GmARF8b* (Wang Y. et al., 2015). miR167 has also been reported to positively regulate plant development and root plasticity by targetingARF6 and Indole acetic acid alanine resistant3 (IAR3) (Kinoshita et al., 2012). Digital gene expression profile revealed that microRNA response element, miRNA167, targets *TcARF6* to constitute a tch-miRNA167-TcARF6 negative response module that downregulates the expression of *TcARF6* in roots of *Tamarix chinensis* in response to salt stress (Ye et al., 2020). The expression of miRNA160a/b was strongly upregulated whiles

their target ARF10 was downregulated in two cowpea genotypes under drought stress treatment (Barrera-Figueroa et al., 2011). Analysis of ta-siRNA synthesis mutants and mutated *ARF3*-overexpressing plants that escape tasiRNA-ARF targeting indicated that, self-pollination was hampered by short stamens in plants under drought and high salinity stress, suggesting that tasiRNA-ARF is involved in maintaining the normal morphogenesis of flowers in plants under drought and high salinity stress conditions (Matsui et al., 2014). Salt stress treatment (100 mM NaCl) induced expression of miR390, increased cleavage of TAS3, produced higher levels of tasiARFs, and subsequently enhanced cleavage of ARF3/4 (Wen et al., 2020). A miRNA160-ARF regulatory network modulates male sterility caused by long exposure to high temperature stress: overexpression of miRNA160 increased sensitivity of cotton to high temperature stress, with a reduction in ARF10/17 mRNA, leading to activation of the auxin response at the sporogenous cell proliferation stage (Ding et al., 2017; Chen et al., 2020). *NtmiRNA167a* transcriptionally regulates *NtARF6* and *NtARF8* to mediate drastic plant Pi-starvation response via modulation of various biological processes in a miRNA167a-ARF6-ARF8 negative response regulatory module, where *NtmiRNA167a* overexpression and *NtARF6* knockdown mutant displayed reduced plant growth, biomass and increased ROS accumulation under Pi-starvation condition compared to WT (Chen et al., 2018). Interaction between miRNA160 and miRNA165/166 modulates numerous downstream responsive biological processes, in which ARFs and HD-ZIP IIIs play opposite roles in regulating leaf development and drought stress response (Yang et al., 2019). The miRNA167-ARF8 regulatory module has been revealed to regulate cell type-specific response to available nitrogen status and plastic development of lateral roots in Arabidopsis (Gifford et al., 2008).

Analysis of differentially expressed miRNA target genes revealed that, miRNA160 was induced by bacterial and fungal pathogen infection, whiles its ARF target genes were downregulated in a miRNA160-ARF module, which regulated defense response in Arabidopsis against *Botrytis cinerea* (Xue and Yi, 2018), in banana against *Fusarium oxysporum* (Cheng et al., 2019) and in cassava against *Colletotrichum gloeosporioides* (Pinweha et al., 2015). AtmiRNA167a targets the transcription of ARF6 and ARF8 to regulate the closure of leaf stomata to prevent entry of *Pseudomonas syringae*, with P_{35S}:MIRNA167a overexpression and *arf6-2 arf8-3* plants displaying extreme resistant phenotypes compared to WT (Caruana et al., 2020). The miRNA390-tasiRNA-ARF regulatory module regulates lateral root development under salt stress, with significant inhibition in expression of ARF3.1, ARF3.2 and ARF4 in miRNA390-overexpressing line under salt stress but increased in the miRNA390-knockout line (He et al., 2018).

7 Regulation of ARFs by epigenetic modes

Epigenetic mechanisms play crucial roles during the life cycle of living organisms (Duan et al., 2018), which help cells to control gene activity without changing the DNA sequence. These mechanisms help determine whether specific genes are tuned on or off, and ensure that each cell produces only the proteins that are necessary for its function (Gayon, 2016). The three most prominent epigenetic mechanisms are histone modification, DNA methylation, and noncoding RNA (ncRNA) regulation (Fessele and Wright, 2018). ARF-dependent induction of downstream auxin-responsive genes is regulated by multiple epigenetic factors, including histone modifications and the chromatin remodeling factor PICKLE (PKL) (Weiste and Droge-Laser, 2014).

7.1 Histone modifications

Histone acetylation is a key histone modification mechanism that appears to be a dynamic reversible switch for inter-conversion between permissive and repressive transcriptional states of chromatin domains (Zhou and Hu, 2010). The co-repressor TOPLESS (TPL) recruits *HDA19* to the auxin signaling repressor, AUX/IAA, in an EAR motif-dependent manner, and that the function of GCN5/HAG1 histone acetylase is directly opposed to the function of *IAA12/BDL-TPL-HDA19* repressor complex in the ARF-dependent expression of auxin responsive genes (Long et al., 2006; Szemenyei et al., 2008). ARF18-HISTONEDEACETYLASE6 (HDA6) module regulates floral organ identity in *Rosa hybrid*: Silencing of *RhHAD6* increases H3K9/K14 acetylation levels at the site adjacent to the *RhARF18*-binding site in the promoter of its downstream target, *RhAG*, and reduces petal number (Chen J. et al., 2021), which indicates that *RhARF18* probably recruit *RhHDA6* to the *RhAG* promoter to repress *RhAG* transcription.

7.2 DNA methylation

DNA methylation is one of the prominent epigenetic modifications that occur extensively in living organisms (Wang et al., 2009). DNA methylation causes changes in chromatin state in plant cells undergoing dedifferentiation (Koukalova et al., 2005), and can also help to establish or maintain the undifferentiated cell state in plants (Berdasco et al., 2008). In plants, DNA demethylation depends on four bifunctional 5-methylcytosine glycosylases: Repressor of silencing 1 (ROS1), Demeter (DME), DME-like 2 (DML2), and DML3, which remove methylated bases and cleave the DNA backbone at abasic sites. The increased expression of *AUXIN RESPONSE FACTOR3 (ARF3)* in *met1* indeed was due to DNA demethylation, suggesting that DNA methylation regulates *de novo* shoot regeneration by modulating auxin signaling (Li et al., 2011). BOBBERY1 (BOB1), an Arabidopsis orthologue of eukaryotic NudC domain proteins, and ELONGATA3 (ELO3), the catalytic subunit of the hioghly conserved elongator complex in Arabidopsis, has been revealed through genetic analysis to repress expression of ARF3 and ARF4, along with AS1-AS2 (Takahashi et al., 2013). BIN2 has been reported to phosphorylate ARF7 and ARF19, and in contrast to reducing activity of ARF2, ARF7, and ARF19 phosphorylation enhanced their transactivation activity, which is attributed to reduced ARF7 and ARF19 interactions with the Aux/IAA repressors.

8 Post-translational regulation of ARFs

Post-translational regulation refers to those cellular events that regulate the abundance of active proteins. It predominantly occurs either by means of reversible events as evident through post-translational modifications (PTMs) or through irreversible events such as proteolysis. PTMs are covalent processing activities that modify the properties of active proteins via proteolytic cleavage and addition of modifying group such as acetyl, phosphoryl, glycosyl and methyl, to one or multiple amino acids (Ramazi et al., 2020).

8.1 Phosphorylation

Protein phosphorylation is the most prominent PTM that acts as a crucial cellular regulatory mechanism to either activate or deactivate enzymes and receptors by phosphorylation or dephosphorylation events, which are respectively catalyzed by kinases and phosphatases at serine, threonine, or tyrosine residues (Ardito et al., 2017). The mitogen-activated protein kinases (MAPK) cascades are conserved signaling mechanism comprising reversible phosphorylation through a cascade of ATP-dependent protein kinases, which regulates multiple aspects of plant growth and development. It has been proposed that auxin signal transduction is mediated by the conserved MAPK signaling cascade (Mizoguchi et al., 1994). Auxin-induced MPK14 phosphorylated and stabilized non-canonical IAA33 and enhanced its competitiveness over canonical repressor IAA5 for binding site on promoters of ARF10 and ARF16, which mitigated inhibition of ARF10 and ARF16 by IAA5 and promoted the identity of root distal stem cell (DSC) and negatively regulated auxin signaling (Lv et al., 2020). In the canonical NAP, drought-induced MPK3/MPK6 phosphorylates and stabilizes IAA15 by inhibiting TIR1-mediated ubiquitination of IAA15, which inturn represses the transcriptional activation of LBD genes by ARF7 and ARF19, leading to limited lateral root development under drought stress in Arabidopsis (Kim et al., 2022). In the non-canonical NAP, some TMK1 family members function as PM-resident receptors or part of a receptor complex, perceiving extracellular auxin and transducing these signals into various phosphorylation events (Tan et al., 2021). The cytosolic and nucleus-translocated C terminus of TMK1 specifically interacts with and phosphorylates non-canonical IAA32 and IAA34 repressors of auxin signaling, thereby regulating ARF transcription factors to dictate differential growth of the apical hook (Cao et al., 2019). Other phosphorylation events have been reported to regulate ARF protein functions. For example, ARF2 mostly represses the expression of the HAK5 potassium transporter gene, meanwhile ARF2 is phosphorylated under low potassium stress to abolish its ability to bind to the promoter of HAK5 and diminishes its repressive effects on HAK5 (Zhao et al., 2016). The BRASSINOSTEROID-INSENSITIVE 2 (BIN2) has been implicated to target and phosphorylate ARF7 and ARF19: Phosphorylation of ARF7 and ARF19 suppresses their interaction the AUX/IAA repressor, which eventually enhances the transcription activity of ARF7 and ARF19 to regulate their downstream target gene *LBD16* and *LBD29* to promote lateral root organogenesis (Cho et al., 2014).

8.2 Ubiquitination

Previous studies on the role of proteolytic regulation in auxin signaling have focused on degradation of their interacting partner, the Aux/IAA proteins, as described above. Although ARF proteins have been shown to be degraded through the 26S mediated ubiquitination, and the degradation process occurs independent of IAAs (Salmon et al., 2008), not much data has been generated regarding degradation of ARFs. Degradation analysis in ARFs show that 37°C treatment increased the protein levels of *HA-ARF5*/MP, *HA-ARF6*, and *HA-ARF10*. On the contrary, there was a pronounced reduction in protein levels of these *HA-ARF*s by ABA, 4°C and salt treatments, whiles MG132 inhibited the reduction of *HA-ARF6* level by ABA and 4°C treatments, suggesting that the *ARF* protein levels are regulated by multiple factors and that these treatments decrease *HA-ARF6* level through 26S proteasome-mediated protein degradation (Li K. et al., 2020). MG132 suppressed the ethylene-dependent decrease in ARF2 protein levels during apical hook development, which strongly suggests that the ethylene-mediated degradation of ARF2 protein is via 26S proteasome degradation pathway (Li et al., 2004). Functional characterization of F-box protein AUXIN RESPONSE FACTOR F-BOX1 (ARF1) SCF^{ARF1}) revealed that this E3 ubiquitin ligase directly interacts with ARF7 and ARF19 to promote their degradation, and regulate their accumulation, condensation, and nucleo-cytoplasmic partitioning, which triggers downstream auxin responses (Jing et al., 2022).

8.3 SUMO modification

Small ubiquitin-like modifier (SUMO) is emerging as an important posttranslational modification that regulates plant development and defense pathways (Orosa-Puente et al., 2018; Niu et al., 2019). SUMO is covalently attached to the lysine residues of target proteins, which could modulate protein activity, stability, localization, and protein-protein interactions of target proteins (Vierstra, 2009), converse to protein degradation as witnessed during ubiquitination. SUMOylation is a crucial PTM that has significantly affected various plant responses to stress and environmental changes (Benlloch and Lois, 2018). MdARF8 is directly SUMOylated by apple SUMO E3 ligase MdSIZ1, which enhances protein stability of MdARF8, and facilitates LR formation in apple (Zhang C. L. et al., 2021). The uneven distribution of water in the soil has a direct influence on plant growth and root architecture, which are regulated by the SUMOylation of ARF7 (Bao et al., 2014; Orosa-Puente et al., 2018). SUMOylated ARF7 enhances its binding capacity to IAA3 and negatively regulates ARF7 activity, thereby inhibiting the expression of LBD16 (Orosa-Puente et al., 2018). Conversely, nonSUMOylated ARF7 cannot recruit IAA3 on the

moisture side, which leads to an increased expression of LBD16 and promoted LR development (Orosa-Puente et al., 2018).

9 Conclusions and perspectives

Over the past decades, the auxin signaling pathway has emerged as a complex regulatory system that modulates plant growth, development, and stresses response. ARF transcription factors serve as effectors of auxin response that transduce and translate auxin signals into the regulation of auxin responsive genes. Both forward and reverse genetic approaches have deepened our understanding of the influence of ARFs on plant development and stress responses. The differential expression of various ARFs in response to various abiotic and biotic stresses suggests that ARFs might exhibit overlapping regulatory roles in response to these stresses. We have also reviewed the modulation of ARF expression by other molecular regulators and how these transcriptional regulations influence the role of ARFs in stress response in plants.

So far, studies on ARF TFs have primarily emphasized on gene cloning and functional characterization, with majority of them focusing transcriptional levels where ARFs bind to cis-acting elements in promoter of their target genes to regulate their expression. Comparably, research on post-translational modification of ARF TFs, including mRNA precursor splicing, editing, stability, nuclear transport, and siRNA-mediated modification—critical for stress response regulation in plants—remains very limited. We propose that future analyses of ARF TFs should emphasize the synergy between transcription regulatory factors, post-transcriptional and post-translational modifications, with a strong focus on the mechanisms of action governing the post-translational modifications of ARF TFs.

Moreover, studies on ARFs have predominantly concentrated on the function of individual ARF TFs or their interaction with other proteins. However, the mechanism governing ARFs function is highly complex due to the larger number of the ARF TF family members and the scattered nature of recent research. Consequently, the regulatory network of ARF TFs remains poorly understood. Further exploration and investigation are needed to understand the role of ARF TFs in perception and transduction of internal and external signals and the interaction among various ARF TFs on physiological and biochemical processes.

It is also important to note that, although plants often encounter multiple stresses, most ARF research has focused on the function of ARFs under single stress conditions. Future functional characterization of ARF TFs should include analyses in response to multiple stresses, followed by comparison of the differences and similarities between single and multiple stresses conditions. This approach is expected to identify key nodes in the complex regulatory network of ARFs. It is also worth highlighting that many datasets related to ARF TFs are scattered and requires integration into a specific online database, which will enable researchers to access relevant ARF TF information quickly.

Research findings have revealed the potential of ARFs in regulating multiple stress conditions, highlighting the functional complexity of ARFs and emphasizing the need to address all aspects of their functioning. Recent studies have shown the existence of crosstalk in some ARF TFs, and ARFs exert their function through various signaling pathways, which can be influenced by both crosstalk and mutual coordination mechanisms.

Conflicts of interest

The authors declare that the research was conducted in the absence of any commercial or financial relationships that could be construed as a potential conflict of interest.

Author contributions

LL: Funding acquisition, Writing – review & editing, Conceptualization, Data curation, Investigation, Writing – original draft. BY: Writing – original draft, Writing – review & editing, Data curation, Investigation. JL: Writing – review & editing, Formal analysis. FW: Conceptualization, Funding acquisition, Supervision, Writing – review & editing.

Funding

The author(s) declare financial support was received for the research, authorship, and/or publication of this article. This research was supported by the National Natural Science Foundation of China (32101785), the General Project of Natural Science Foundation of Sichuan Province (2022NSFSC0147 and 24NSFSC0766), and the Sailing Project Plan of Yibin University (2021QH09).

Conflict of interest

The authors declare that the research was conducted in the absence of any commercial or financial relationships that could be construed as a potential conflict of interest.

Publisher's note

References

Ahmad, N., and Mukhtar, Z. (2017). Genetic manipulations in crops: Challenges and opportunities. *Genomics* 109, 494–505. doi: 10.1016/j.ygeno.2017.07.007

Aida, M., Vernoux, T., Furutani, M., Traas, J., and Tasaka, M. (2002). Roles of PIN-FORMED1 and MONOPTEROS in pattern formation of the apical region of the Arabidopsis embryo. *Development* 129, 3965–3974. doi: 10.1242/dev.129.17.3965

Allen, E., Xie, Z., Gustafson, A. M., and Carrington, J. C. (2005). microRNA-directed phasing during trans-acting siRNA biogenesis in plants. *Cell* 121, 207–221. doi: 10.1016/j.cell.2005.04.004

Ardito, F., Giuliani, M., Perrone, D., Troiano, G., and Lo Muzio, L. (2017). The crucial role of protein phosphorylation in cell signaling and its use as targeted therapy (Review). *Int. J. Mol. Med.* 40, 271–280. doi: 10.3892/ijmm.2017.3036

Atkinson, J. A., Rasmussen, A., Traini, R., Voss, U., Sturrock, C., Mooney, S. J., et al. (2014). Branching out in roots: uncovering form, function, and regulation. *Plant Physiol.* 166, 538–550. doi: 10.1104/pp.114.245423

Attia, K. A., Abdelkhalik, A. F., Ammar, M. H., Wei, C., Yang, J., Lightfoot, D. A., et al. (2009). Antisense phenotypes reveal a functional expression of OsARF1, an auxin response factor, in transgenic rice. *Curr. Issues Mol. Biol.* 11 Suppl 1, i29–i34. doi: 10.21775/9781912530069

Axtell, M. J., Jan, C., Rajagopalan, R., and Bartel, D. P. (2006). A two-hit trigger for siRNA biogenesis in plants. *Cell* 127, 565–577. doi: 10.1016/j.cell.2006.09.032

Bai, Y., Zhang, T., Zheng, X., Li, B., Qi, X., Xu, Y., et al. (2023). Overexpression of a WRKY transcription factor McWRKY57-like from Mentha canadensis L. enhances drought tolerance in transgenic Arabidopsis. *BMC Plant Biol.* 23, 216. doi: 10.1186/s12870-023-04213-y

Baillo, E. H., Kimotho, R. N., Zhang, Z., and Xu, P. (2019). Transcription factors associated with abiotic and biotic stress tolerance and their potential for crops improvement. *Genes (Basel)* 10, 771. doi: 10.3390/genes10100771

Ballas, N., Wong, L. M., and Theologis, A. (1993). Identification of the auxin-responsive element, AuxRE, in the primary indoleacetic acid-inducible gene, PS-IAA4/5, of pea (Pisum sativum). *J. Mol. Biol.* 233, 580–596. doi: 10.1006/jmbi.1993.1537

Bao, Y., Aggarwal, P., Robbins, N. E. 2nd, Sturrock, C. J., Thompson, M. C., Tan, H. Q., et al. (2014). Plant roots use a patterning mechanism to position lateral root branches toward available water. Proc Natl Acad Sci U S A, 111(25), 9319-9324. https://doi.org/10.1073/pnas.1400966111

Bari, R., and Jones, J. D. (2009). Role of plant hormones in plant defence responses. *Plant Mol. Biol.* 69, 473–488. doi: 10.1007/s11103-008-9435-0

Barrera-Figueroa, B. E., Gao, L., Diop, N. N., Wu, Z., Ehlers, J. D., Roberts, P. A., et al. (2011). Identification and comparative analysis of drought-associated microRNAs in two cowpea genotypes. *BMC Plant Biol.* 11, 127. doi: 10.1186/1471-2229-11-127

Benlloch, R., and Lois, L. M. (2018). Sumoylation in plants: mechanistic insights and its role in drought stress. *J. Exp. Bot.* 69, 4539–4554. doi: 10.1093/jxb/ery233

Berckmans, B., Vassileva, V., Schmid, S. P., Maes, S., Parizot, B., Naramoto, S., et al. (2011). Auxin-dependent cell cycle reactivation through transcriptional regulation of Arabidopsis E2Fa by lateral organ boundary proteins. *Plant Cell* 23, 3671–3683. doi: 10.1105/tpc.111.088377

Berdasco, M., Alcázar, R., García-Ortiz, M. V., Ballestar, E., Fernández, A. F., Roldán-Arjona, T., et al. (2008). Promoter DNA hypermethylation and gene repression in undifferentiated arabidopsis cells. *PloS One* 3, e3306. doi: 10.1371/journal.pone.0003306

Boer, D. R., Freire-Rios, A., van den Berg, W. A., Saaki, T., Manfield, I. W., Kepinski, S., et al. (2014). Structural basis for DNA binding specificity by the auxin-dependent ARF transcription factors. *Cell* 156, 577–589. doi: 10.1016/j.cell.2013.12.027

Bouzroud, S., Gasparini, K., Hu, G., Barbosa, M. A. M., Rosa, B. L., Fahr, M., et al. (2020). Down regulation and loss of auxin response factor 4 function using CRISPR/cas9 alters plant growth, stomatal function and improves tomato tolerance to salinity and osmotic stress. *Genes (Basel)* 11, 272. doi: 10.3390/genes11030272

Breuninger, H., Rikirsch, E., Hermann, M., Ueda, M., and Laux, T. (2008). Differential expression of WOX genes mediates apical-basal axis formation in the Arabidopsis embryo. *Dev. Cell* 14, 867–876. doi: 10.1016/j.devcel.2008.03.008

Cao, M., Chen, R., Li, P., Yu, Y., Zheng, R., Ge, D., et al. (2019). TMK1-mediated auxin signalling regulates differential growth of the apical hook. *Nature* 568, 240–243. doi: 10.1038/s41586-019-1069-7

Carrillo-Carrasco, V. P., Hernandez-Garcia, J., Mutte, S. K., and Weijers, D. (2023). The birth of a giant: evolutionary insights into the origin of auxin responses in plants. *EMBO J.* 42, e113018. doi: 10.15252/embj.2022113018

Caruana, J. C., Dhar, N., and Raina, R. (2020). Overexpression of Arabidopsis microRNA167 induces salicylic acid-dependent defense against Pseudomonas syringae through the regulation of its targets ARF6 and ARF8. *Plant Direct* 4, e00270. doi: 10.1002/pld3.270

Casamassimi, A., and Ciccodicola, A. (2019). Transcriptional regulation: molecules, involved mechanisms, and misregulation. *Int. J. Mol. Sci.* 20, 1281. doi: 10.3390/ijms20061281

Causier, B., Ashworth, M., Guo, W., and Davies, B. (2012). The TOPLESS interactome: a framework for gene repression in Arabidopsis. *Plant Physiol.* 158, 423–438. doi: 10.1104/pp.111.186999

Chandler, J. W. (2016). Auxin response factors. *Plant Cell Environ.* 39, 1014–1028. doi: 10.1111/pce.12662

Chen, J., Li, Y., Li, Y., Li, Y., Wang, Y., Jiang, C., et al. (2021). AUXIN RESPONSE FACTOR 18-HISTONE DEACETYLASE 6 module regulates floral organ identity in rose (Rosa hybrida). *Plant Physiol.* 186, 1074–1087. doi: 10.1093/plphys/kiab130

Chen, J., Pan, A., He, S., Su, P., Yuan, X., Zhu, S., et al. (2020). Different MicroRNA Families Involved in Regulating High Temperature Stress Response during Cotton (Gossypium hirsutum L.) Anther Development. *Int. J. Mol. Sci.* 21, 1280. doi: 10.3390/ijms21041280

Chen, M., Zhu, X., Liu, X., Wu, C., Yu, C., Hu, G., et al. (2021). Knockout of auxin response factor slARF4 improves tomato resistance to water deficit. *Int. J. Mol. Sci.* 22, 3347. doi: 10.3390/ijms22073347

Chen, X., Liu, Z., Shi, G., Bai, Q., Guo, C., and Xiao, K. (2018). MIR167a transcriptionally regulates ARF6 and ARF8 and mediates drastically plant Pi-starvation response via modulation of various biological processes. *Plant Cell Tissue Organ Culture* 133, 177–191. doi: 10.1007/s11240-017-1371-8

Cheng, C., Liu, F., Sun, X., Tian, N., Mensah, R. A., Li, D., et al. (2019). Identification of Fusarium oxysporum f. sp. cubense tropical race 4 (Foc TR4) responsive miRNAs in banana root. *Sci. Rep.* 9, 13682. doi: 10.1038/s41598-019-50130-2

Cho, H., Ryu, H., Rho, S., Hill, K., Smith, S., Audenaert, D., et al. (2014). A secreted peptide acts on BIN2-mediated phosphorylation of ARFs to potentiate auxin response during lateral root development. *Nat. Cell Biol.* 16, 66–76. doi: 10.1038/ncb2893

Choi, H. S., Seo, M., and Cho, H. T. (2018). Two TPL-binding motifs of ARF2 are involved in repression of auxin responses. *Front. Plant Sci.* 9. doi: 10.3389/fpls.2018.00372

Clapier, C. R., and Cairns, B. R. (2009). The biology of chromatin remodeling complexes. *Annu. Rev. Biochem.* 78, 273–304. doi: 10.1146/annurev.biochem.77.062706.153223

Dai, N., Wang, W., Patterson, S. E., and Bleecker, A. B. (2013). The TMK subfamily of receptor-like kinases in Arabidopsis display an essential role in growth and a reduced sensitivity to auxin. *PloS One* 8, e60990. doi: 10.1371/journal.pone.0060990

Dassi, E. (2017). Handshakes and fights: the regulatory interplay of RNA-binding proteins. *Front. Mol. Biosci.* 4. doi: 10.3389/fmolb.2017.00067

Dastidar, M. G., Scarpa, A., Magele, I., Ruiz-Duarte, P., von Born, P., Bald, L., et al. (2019). ARF5/MONOPTEROS directly regulates miR390 expression in the Arabidopsis thaliana primary root meristem. *Plant Direct* 3, e00116. doi: 10.1002/pld3.116

De Rybel, B., Vassileva, V., Parizot, B., Demeulenaere, M., Grunewald, W., Audenaert, D., et al. (2010). A novel aux/IAA28 signaling cascade activates GATA23-dependent specification of lateral root founder cell identity. *Curr. Biol.* 20, 1697–1706. doi: 10.1016/j.cub.2010.09.007

De Smet, I., Lau, S., Mayer, U., and Jurgens, G. (2010). Embryogenesis - the humble beginnings of plant life. *Plant J.* 61, 959–970. doi: 10.1111/j.1365-313X.2010.04143.x

De Smet, I., Tetsumura, T., De Rybel, B., Frei dit Frey, N., Laplaze, L., Casimiro, I., et al. (2007). Auxin-dependent regulation of lateral root positioning in the basal meristem of Arabidopsis. *Development* 134, 681–690. doi: 10.1242/dev.02753

Dinesh, D. C., Kovermann, M., Gopalswamy, M., Hellmuth, A., Calderon Villalobos, L. I., Lilie, H., et al. (2015). Solution structure of the PsIAA4 oligomerization domain reveals interaction modes for transcription factors in early auxin response. *Proc. Natl. Acad. Sci. U.S.A.* 112, 6230–6235. doi: 10.1073/pnas.1424077112

Ding, Y., Ma, Y., Liu, N., Xu, J., Hu, Q., Li, Y., et al. (2017). microRNAs involved in auxin signalling modulate male sterility under high-temperature stress in cotton (Gossypium hirsutum). *Plant J.* 91, 977–994. doi: 10.1111/tpj.13620

Dos Reis, S. P., Lima, A. M., and De Souza, C. R. B. (2012). Recent molecular advances on downstream plant responses to abiotic stress. *Int. J. Mol. Sci.* 13, 8628–8647. doi: 10.3390/ijms13078628

Dotto, M. C., Petsch, K. A., Aukerman, M. J., Beatty, M., Hammell, M., and Timmermans, M. C. (2014). Genome-wide analysis of leafbladeless1-regulated and phased small RNAs underscores the importance of the TAS3 ta-siRNA pathway to maize development. *PloS Genet.* 10, e1004826. doi: 10.1371/journal.pgen.1004826

Du, H., Liu, H., and Xiong, L. (2013). Endogenous auxin and jasmonic acid levels are differentially modulated by abiotic stresses in rice. *Front. Plant Sci.* 4. doi: 10.3389/fpls.2013.00397

Du, Y., and Scheres, B. (2018). Lateral root formation and the multiple roles of auxin. *J. Exp. Bot.* 69, 155–167. doi: 10.1093/jxb/erx223

Duan, C. G., Zhu, J. K., and Cao, X. (2018). Retrospective and perspective of plant epigenetics in China. *J. Genet. Genomics* 45, 621–638. doi: 10.1016/j.jgg.2018.09.004

Dubrovsky, J. G., and Laskowski, M. (2017). Lateral root initiation. *Encyclopedia Appl. Plant Sci.* 1, 256–264. doi: 10.1016/B978-0-12-394807-6.00126-X

Ellis, C. M., Nagpal, P., Young, J. C., Hagen, G., Guilfoyle, T. J., and Reed, J. W. (2005). AUXIN RESPONSE FACTOR1 and AUXIN RESPONSE FACTOR2 regulate senescence and floral organ abscission in Arabidopsis thaliana. *Development* 132, 4563–4574. doi: 10.1242/dev.02012

El Mamoun, I., Bouzroud, S., Zouine, M., and Smouni, A. (2023). The knockdown of AUXIN RESPONSE FACTOR 2 confers enhanced tolerance to salt and drought

stresses in tomato (Solanum lycopersicum L.). *Plants (Basel)* 12, 2804. doi: 10.3390/plants12152804

Endress, P. K. (2010). The evolution of floral biology in basal angiosperms. *Philos. Trans. R Soc. Lond B Biol. Sci.* 365, 411–421. doi: 10.1098/rstb.2009.0228

Erijman, A., Kozlowski, L., Sohrabi-Jahromi, S., Fishburn, J., Warfield, L., Schreiber, J., et al. (2020). A high-throughput screen for transcription activation domains reveals their sequence features and permits prediction by deep learning. *Mol. Cell* 78, 890–902 e896. doi: 10.1016/j.molcel.2020.08.013

Fahlgren, N., Montgomery, T. A., Howell, M. D., Allen, E., Dvorak, S. K., Alexander, A. L., et al. (2006). Regulation of AUXIN RESPONSE FACTOR3 by TAS3 ta-siRNA affects developmental timing and patterning in Arabidopsis. *Curr. Biol.* 16, 939–944. doi: 10.1016/j.cub.2006.03.065

Feng, Z., Sun, X., Wang, G., Liu, H., and Zhu, J. (2012). LBD29 regulates the cell cycle progression in response to auxin during lateral root formation in Arabidopsis thaliana. *Ann. Bot.* 110, 1–10. doi: 10.1093/aob/mcs019

Fessele, K. L., and Wright, F. (2018). Primer in genetics and genomics, article 6: basics of epigenetic control. *Biol. Res. Nurs.* 20, 103–110. doi: 10.1177/1099800417742967

Finet, C., Berne-Dedieu, A., Scutt, C. P., and Marletaz, F. (2013). Evolution of the ARF gene family in land plants: old domains, new tricks. *Mol. Biol. Evol.* 30, 45–56. doi: 10.1093/molbev/mss220

Freire-Rios, A., Tanaka, K., Crespo, I., van der Wijk, E., Sizentsova, Y., Levitsky, V., et al. (2020). Architecture of DNA elements mediating ARF transcription factor binding and auxin-responsive gene expression in *Arabidopsis*. *Proc. Natl. Acad. Sci.* 117, 24557–24566. doi: 10.1073/pnas.2009554117

Galli, M., Khakhar, A., Lu, Z., Chen, Z., Sen, S., Joshi, T., et al. (2018). The DNA binding landscape of the maize AUXIN RESPONSE FACTOR family. *Nat. Commun.* 9, 4526. doi: 10.1038/s41467-018-06977-6

Galli, M., Liu, Q., Moss, B. L., Malcomber, S., Li, W., Gaines, C., et al. (2015). Auxin signaling modules regulate maize inflorescence architecture. *Proc. Natl. Acad. Sci. U.S.A.* 112, 13372–13377. doi: 10.1073/pnas.1516473112

Gayon, J. (2016). From Mendel to epigenetics: History of genetics. *C R Biol.* 339, 225–230. doi: 10.1016/j.crvi.2016.05.009

Gifford, M. L., Dean, A., Gutierrez, R. A., Coruzzi, G. M., and Birnbaum, K. D. (2008). Cell-specific nitrogen responses mediate developmental plasticity. *Proc. Natl. Acad. Sci. U.S.A.* 105, 803–808. doi: 10.1073/pnas.0709559105

Goh, T., Kasahara, H., Mimura, T., Kamiya, Y., and Fukaki, H. (2012). Multiple AUX/IAA-ARF modules regulate lateral root formation: the role of Arabidopsis SHY2/IAA3-mediated auxin signalling. *Philos. Trans. R Soc. Lond B Biol. Sci.* 367, 1461–1468. doi: 10.1098/rstb.2011.0232

Goh, T., Toyokura, K., Yamaguchi, N., Okamoto, Y., Uehara, T., Kaneko, S., et al. (2019). Lateral root initiation requires the sequential induction of transcription factors LBD16 and PUCHI in Arabidopsis thaliana. *New Phytol.* 224, 749–760. doi: 10.1111/nph.16065

Goldental-Cohen, S., Israeli, A., Ori, N., and Yasuor, H. (2017). Auxin response dynamics during wild-type and entire flower development in tomato. *Plant Cell Physiol.* 58, 1661–1672. doi: 10.1093/pcp/pcx102

Guan, C., Wu, B., Yu, T., Wang, Q., Krogan, N. T., Liu, X., et al. (2017). Spatial auxin signaling controls leaf flattening in Arabidopsis. *Curr. Biol.* 27, 2940–2950 e2944. doi: 10.1016/j.cub.2017.08.042

Guilfoyle, T. J., and Hagen, G. (2007). Auxin response factors. *Curr. Opin. Plant Biol.* 10, 453–460. doi: 10.1016/j.pbi.2007.08.014

Gutierrez, L., Bussell, J. D., Pacurar, D. I., Schwambach, J., Pacurar, M., and Bellini, C. (2009). Phenotypic plasticity of adventitious rooting in Arabidopsis is controlled by complex regulation of AUXIN RESPONSE FACTOR transcripts and microRNA abundance. *Plant Cell* 21, 3119–3132. doi: 10.1105/tpc.108.064758

Ha, C. V., Le, D. T., Nishiyama, R., Watanabe, Y., Sulieman, S., Tran, U. T., et al. (2013). The auxin response factor transcription factor family in soybean: genome-wide identification and expression analyses during development and water stress. *DNA Res.* 20, 511–524. doi: 10.1093/dnares/dst027

Hagen, G., and Guilfoyle, T. (2002). Auxin-responsive gene expression: genes, promoters and regulatory factors. *Plant Mol. Biol.* 49, 373–385. doi: 10.1023/A:1015207114117

Han, M., Park, Y., Kim, I., Kim, E.-H., Yu, T.-K., Rhee, S., et al. (2014). Structural basis for the auxin-induced transcriptional regulation by Aux/IAA17. *Proc. Natl. Acad. Sci.* 111, 18613–18618. doi: 10.1073/pnas.1419525112

He, F., Xu, C., Fu, X., Shen, Y., Guo, L., Leng, M., et al. (2018). The MicroRNA390/TRANS-ACTING SHORT INTERFERING RNA3 Module Mediates Lateral Root Growth under Salt Stress via the Auxin Pathway. *Plant Physiol.* 177, 775–791. doi: 10.1104/pp.17.01559

Herud, O., Weijers, D., Lau, S., and Jurgens, G. (2016). Auxin responsiveness of the MONOPTEROS-BODENLOS module in primary root initiation critically depends on the nuclear import kinetics of the Aux/IAA inhibitor BODENLOS. *Plant J.* 85, 269–277. doi: 10.1111/tpj.13108

Hou, K., Wu, W., and Gan, S. S. (2013). SAUR36, a small auxin up RNA gene, is involved in the promotion of leaf senescence in Arabidopsis. *Plant Physiol.* 161, 1002–1009. doi: 10.1104/pp.112.212787

Huang, J., Li, Z., and Zhao, D. (2016). Deregulation of the osmiR160 target gene osARF18 causes growth and developmental defects with an alteration of auxin signaling in rice. *Sci. Rep.* 6, 29938. doi: 10.1038/srep29938

Huang, K. L., Ma, G. J., Zhang, M. L., Xiong, H., Wu, H., Zhao, C. Z., et al. (2018). The ARF7 and ARF19 transcription factors positively regulate PHOSPHATE STARVATION RESPONSE1 in Arabidopsis roots. *Plant Physiol.* 178, 413–427. doi: 10.1104/pp.17.01713

Hunter, C., Willmann, M. R., Wu, G., Yoshikawa, M., de la Luz Gutierrez-Nava, M., and Poethig, S. R. (2006). Trans-acting siRNA-mediated repression of ETTIN and ARF4 regulates heteroblasty in Arabidopsis. *Development* 133, 2973–2981. doi: 10.1242/dev.02491

Ishida, T., Kurata, T., Okada, K., and Wada, T. (2008). A genetic regulatory network in the development of trichomes and root hairs. *Annu. Rev. Plant Biol.* 59, 365–386. doi: 10.1146/annurev.arplant.59.032607.092949

Iwasaki, M., Takahashi, H., Iwakawa, H., Nakagawa, A., Ishikawa, T., Tanaka, H., et al. (2013). Dual regulation of ETTIN (ARF3) gene expression by AS1-AS2, which maintains the DNA methylation level, is involved in stabilization of leaf adaxial-abaxial partitioning in Arabidopsis. *Development* 140, 1958–1969. doi: 10.1242/dev.085365

Jain, M., and Khurana, J. P. (2009). Transcript profiling reveals diverse roles of auxin-responsive genes during reproductive development and abiotic stress in rice. *FEBS J.* 276, 3148–3162. doi: 10.1111/j.1742-4658.2009.07033.x

Jay, F., Wang, Y., Yu, A., Taconnat, L., Pelletier, S., Colot, V., et al. (2011). Misregulation of AUXIN RESPONSE FACTOR 8 underlies the developmental abnormalities caused by three distinct viral silencing suppressors in Arabidopsis. *PloS Pathog.* 7, e1002035. doi: 10.1371/journal.ppat.1002035

Jia, Z., Giehl, R. F. H., Hartmann, A., Estevez, J. M., Bennett, M. J., and von Wiren, N. (2023). A spatially concerted epidermal auxin signaling framework steers the root hair foraging response under low nitrogen. *Curr. Biol.* 33, 3926–3941 e3925. doi: 10.1016/j.cub.2023.08.040

Jiang, Y., Liang, G., Yang, S., and Yu, D. (2014). Arabidopsis WRKY57 functions as a node of convergence for jasmonic acid- and auxin-mediated signaling in jasmonic acid-induced leaf senescence. *Plant Cell* 26, 230–245. doi: 10.1105/tpc.113.117838

Jing, H., Korasick, D. A., Emenecker, R. J., Morffy, N., Wilkinson, E. G., Powers, S. K., et al. (2022). Regulation of AUXIN RESPONSE FACTOR condensation and nucleo-cytoplasmic partitioning. *Nat. Commun.* 13, 4015. doi: 10.1038/s41467-022-31628-2

Jing, H., and Strader, L. C. (2019). Interplay of auxin and cytokinin in lateral root development. *Int. J. Mol. Sci.* 20, 486. doi: 10.3390/ijms20030486

Jing, H., Yang, X., Zhang, J., Liu, X., Zheng, H., Dong, G., et al. (2015). Peptidyl-prolyl isomerization targets rice Aux/IAAs for proteasomal degradation during auxin signalling. *Nat. Commun.* 6, 7395. doi: 10.1038/ncomms8395

Kalsi, H. S., Karkhanis, A. A., Natarajan, B., Bhide, A. J., and Banerjee, A. K. (2022). AUXIN RESPONSE FACTOR 16 (StARF16) regulates defense gene StNPR1 upon infection with necrotrophic pathogen in potato. *Plant Mol. Biol.* 109, 13–28. doi: 10.1007/s11103-022-01261-0

Kambona, C. M., Koua, P. A., Leon, J., and Ballvora, A. (2023). Stress memory and its regulation in plants experiencing recurrent drought conditions. *Theor. Appl. Genet.* 136, 26. doi: 10.1007/s00122-023-04313-1

Kato, H., Mutte, S. K., Suzuki, H., Crespo, I., Das, S., Radoeva, T., et al. (2020). Design principles of a minimal auxin response system. *Nat. Plants* 6, 473–482. doi: 10.1038/s41477-020-0662-y

Ke, J., Ma, H., Gu, X., Thelen, A., Brunzelle, J. S., Li, J., et al. (2015). Structural basis for recognition of diverse transcriptional repressors by the TOPLESS family of corepressors. *Sci. Adv.* 1, e1500107. doi: 10.1126/sciadv.1500107

Kim, S. H., Bahk, S., Nguyen, N. T., Pham, M. L. A., Kadam, U. S., Hong, J. C., et al. (2022). Phosphorylation of the auxin signaling transcriptional repressor IAA15 by MPKs is required for the suppression of root development under drought stress in Arabidopsis. *Nucleic Acids Res.* 50, 10544–10561. doi: 10.1093/nar/gkac798

Kim, J. I., Murphy, A. S., Baek, D., Lee, S. W., Yun, D. J., Bressan, R. A., et al. (2011). YUCCA6 over-expression demonstrates auxin function in delaying leaf senescence in Arabidopsis thaliana. *J. Exp. Bot.* 62, 3981–3992. doi: 10.1093/jxb/err094

Kim, Y., Park, C., Cha, S., Han, M., Ryu, K. S., and Suh, J. Y. (2020). Determinants of PB1 domain interactions in auxin response factor ARF5 and repressor IAA17. *J. Mol. Biol.* 432, 4010–4022. doi: 10.1016/j.jmb.2020.04.007

Kinoshita, N., Wang, H., Kasahara, H., Liu, J., Macpherson, C., Machida, Y., et al. (2012). IAA-Ala Resistant3, an evolutionarily conserved target of miR167, mediates Arabidopsis root architecture changes during high osmotic stress. *Plant Cell* 24, 3590–3602. doi: 10.1105/tpc.112.097006

Kirolinko, C., Hobecker, K., Wen, J., Mysore, K. S., Niebel, A., Blanco, F. A., et al. (2021). Auxin response factor 2 (ARF2), ARF3, and ARF4 mediate both lateral root and nitrogen fixing nodule development in medicago truncatula. *Front. Plant Sci.* 12. doi: 10.3389/fpls.2021.659061

Kong, X., Zhang, L., and Ding, Z. (2016). 26S proteasome: hunter and prey in auxin signaling. *Trends Plant Sci.* 21, 546–548. doi: 10.1016/j.tplants.2016.05.007

Korasick, D. A., Westfall, C. S., Lee, S. G., Nanao, M. H., Dumas, R., Hagen, G., et al. (2014). Molecular basis for AUXIN RESPONSE FACTOR protein interaction and the control of auxin response repression. *Proc. Natl. Acad. Sci.* 111, 5427–5432. doi: 10.1073/pnas.1400074111

Kou, X. Z. X., Wu, B., Wang, C. W. C., Yang, S., Zhou, J., and Xue, Z. (2022). Auxin response factors are ubiquitous in plant growth and development, and involved in crosstalk between plant hormoness: A review. *Appl. Sci.* 22, 1360. doi: 10.3390/app12031360

Koukalova, B., Fojtova, M., Lim, K. Y., Fulnecek, J., Leitch, A. R., and Kovarik, A. (2005). Dedifferentiation of tobacco cells is associated with ribosomal RNA gene hypomethylation, increased transcription, and chromatin alterations. *Plant Physiol.* 139, 275–286. doi: 10.1104/pp.105.061788

Kranner, I., Minibayeva, F. V., Beckett, R. P., and Seal, C. E. (2010). What is stress? Concepts, definitions and applications in seed science. *New Phytol.* 188, 655–673. doi: 10.1111/j.1469-8137.2010.03461.x

Krogan, N. T., Ckurshumova, W., Marcos, D., Caragea, A. E., and Berleth, T. (2012). Deletion of MP/ARF5 domains III and IV reveals a requirement for Aux/IAA regulation in Arabidopsis leaf vascular patterning. *New Phytol.* 194, 391–401. doi: 10.1111/j.1469-8137.2012.04064.x

Kuhn, A., Ramans Harborough, S., McLaughlin, H. M., Natarajan, B., Verstraeten, I., Friml, J., et al. (2020). Direct ETTIN-auxin interaction controls chromatin states in gynoecium development. *Elife* 9, e51787. doi: 10.7554/eLife.51787.sa2

Lambert, S. A., Jolma, A., Campitelli, L. F., Das, P. K., Yin, Y., Albu, M., et al. (2018). The human transcription factors. *Cell* 172, 650–665. doi: 10.1016/j.cell.2018.01.029

Lanctot, A., Taylor-Teeples, M., Oki, E. A., and Nemhauser, J. L. (2020). Specificity in auxin responses is not explained by the promoter preferences of activator ARFs. *Plant Physiol.* 182, 1533–1536. doi: 10.1104/pp.19.01474

Lavy, M., Prigge, M. J., Tao, S., Shain, S., Kuo, A., Kirchsteiger, K., et al. (2016). Constitutive auxin response in Physcomitrella reveals complex interactions between Aux/IAA and ARF proteins. *Elife* 5, e13325. doi: 10.7554/eLife.13325.025

Lee, H. W., Cho, C., Pandey, S. K., Park, Y., Kim, M. J., and Kim, J. (2019). LBD16 and LBD18 acting downstream of ARF7 and ARF19 are involved in adventitious root formation in Arabidopsis. *BMC Plant Biol.* 19, 46. doi: 10.1186/s12870-019-1659-4

Lee, M., Jung, J. H., Han, D. Y., Seo, P. J., Park, W. J., and Park, C. M. (2012). Activation of a flavin monooxygenase gene YUCCA7 enhances drought resistance in Arabidopsis. *Planta* 235, 923–938. doi: 10.1007/s00425-011-1552-3

Lee, H. W., Kim, M. J., Kim, N. Y., Lee, S. H., and Kim, J. (2013). LBD18 acts as a transcriptional activator that directly binds to the EXPANSIN14 promoter in promoting lateral root emergence of Arabidopsis. *Plant J.* 73, 212–224. doi: 10.1111/tpj.12013

Li, H., Johnson, P., Stepanova, A., Alonso, J. M., and Ecker, J. R. (2004). Convergence of signaling pathways in the control of differential cell growth in Arabidopsis. *Dev. Cell* 7, 193–204. doi: 10.1016/j.devcel.2004.07.002

Li, Y., Li, J., Chen, Z., Wei, Y., Qi, Y., and Wu, C. (2020). OsmiR167a-targeted auxin response factors modulate tiller angle via fine-tuning auxin distribution in rice. *Plant Biotechnol. J.* 18, 2015–2026. doi: 10.1111/pbi.13360

Li, G., Liang, W., Zhang, X., Ren, H., Hu, J., Bennett, M. J., et al. (2014). Rice actin-binding protein RMD is a key link in the auxin–actin regulatory loop that controls cell growth. *Proc. Natl. Acad. Sci.* 111, 10377–10382. doi: 10.1073/pnas.1401680111

Li, W., Liu, H., Cheng, Z. J., Su, Y. H., Han, H. N., Zhang, Y., et al. (2011). DNA methylation and histone modifications regulate *de novo* shoot regeneration in Arabidopsis by modulating WUSCHEL expression and auxin signaling. *PloS Genet.* 7, e1002243. doi: 10.1371/journal.pgen.1002243

Li, H., Liu, H., Hao, C., Li, T., Liu, Y., Wang, X., et al. (2023). The auxin response factor TaARF15-A1 negatively regulates senescence in common wheat (Triticum aestivum L.). *Plant Physiol.* 191, 1254–1271. doi: 10.1093/plphys/kiac497

Li, K., Wang, S., Wu, H., and Wang, H. (2020). Protein levels of several Arabidopsis auxin response factors are regulated by multiple factors and ABA promotes ARF6 protein ubiquitination. *Int. J. Mol. Sci.* 21, 9437. doi: 10.3390/ijms21249437

Li, J., Wu, F., He, Y., He, B., Gong, Y., Yahaya, B. S., et al. (2022). Maize transcription factor zmARF4 confers phosphorus tolerance by promoting root morphological development. *Int. J. Mol. Sci.* 23, 2361. doi: 10.3390/ijms23042361

Li, H., Zhang, X., Tong, B., Wang, Y., and Yang, C. (2020). Expression analysis of the BpARF genes in Betula platyphylla under drought stress. *Plant Physiol. Biochem.* 148, 273–281. doi: 10.1016/j.plaphy.2020.01.028

Liang, T., Hu, Y., Xi, N., Zhang, M., Zou, C., Ge, F., et al. (2023). GWAS across multiple environments and WGCNA suggest the involvement of ZmARF23 in embryonic callus induction from immature maize embryos. *Theor. Appl. Genet.* 136, 93. doi: 10.1007/s00122-023-04341-x

Lin, C., and Sauter, M. (2018). Control of adventitious root architecture in rice by darkness, light, and gravity. *Plant Physiol.* 176, 1352–1364. doi: 10.1104/pp.17.01540

Liu, X., Dinh, T. T., Li, D., Shi, B., Li, Y., Cao, X., et al. (2014). AUXIN RESPONSE FACTOR 3 integrates the functions of AGAMOUS and APETALA2 in floral meristem determinacy. *Plant J.* 80, 629–641. doi: 10.1111/tpj.12658

Liu, X., Dong, X., Liu, Z., Shi, Z., Jiang, Y., Qi, M., et al. (2016). Repression of ARF10 by microRNA160 plays an important role in the mediation of leaf water loss. *Plant Mol. Biol.* 92, 313–336. doi: 10.1007/s11103-016-0514-3

Liu, Y., Teng, C., Xia, R., and Meyers, B. C. (2020). PhasiRNAs in plants: their biogenesis, genic sources, and roles in stress responses, development, and reproduction. *Plant Cell* 32, 3059–3080. doi: 10.1105/tpc.20.00335

Liu, Z. B., Ulmasov, T., Shi, X., Hagen, G., and Guilfoyle, T. J. (1994). Soybean GH3 promoter contains multiple auxin-inducible elements. *Plant Cell* 6, 645–657. doi: 10.1105/tpc.6.5.645

Liu, H., Wang, S., Yu, X., Yu, J., He, X., Zhang, S., et al. (2005). ARL1, a LOB-domain protein required for adventitious root formation in rice. *Plant J.* 43, 47–56. doi: 10.1111/j.1365-313X.2005.02434.x

Liu, X., Yang, C. Y., Miao, R., Zhou, C. L., Cao, P. H., Lan, J., et al. (2018). DS1/OsEMF1 interacts with OsARF11 to control rice architecture by regulation of brassinosteroid signaling. *Rice (N Y)* 11, 46. doi: 10.1186/s12284-018-0239-9

Liu, S., Zhang, Y., Feng, Q., Qin, L., Pan, C., Lamin-Samu, A. T., et al. (2018). Tomato AUXIN RESPONSE FACTOR 5 regulates fruit set and development via the mediation of auxin and gibberellin signaling. *Sci. Rep.* 8, 2971. doi: 10.1038/s41598-018-21315-y

Long, J. A., Ohno, C., Smith, Z. R., and Meyerowitz, E. M. (2006). TOPLESS regulates apical embryonic fate in Arabidopsis. *Science* 312, 1520–1523. doi: 10.1126/science.1123841

Luo, P., Di, D., Wu, L., Yang, J., Lu, Y., and Shi, W. (2022). MicroRNAs are involved in regulating plant development and stress response through fine-tuning of TIR1/AFB-dependent auxin signaling. *Int. J. Mol. Sci.* 23, 510. doi: 10.3390/ijms23010510

Luo, W. G., Liang, Q. W., Su, Y., Huang, C., Mo, B. X., Yu, Y., et al. (2023). Auxin inhibits chlorophyll accumulation through ARF7-IAA14-mediated repression of chlorophyll biosynthesis genes in Arabidopsis. *Front. Plant Sci.* 14, 1172059. doi: 10.3389/fpls.2023.1172059

Luo, L., Xie, Y., and Xuan, W. (2022). Prohibitin 3 gives birth to a new lateral root primordium. *J. Exp. Bot.* 73, 3828–3830. doi: 10.1093/jxb/erac175

Lv, B., Yu, Q., Liu, J., Wen, X., Yan, Z., Hu, K., et al. (2020). Non-canonical AUX/IAA protein IAA33 competes with canonical AUX/IAA repressor IAA5 to negatively regulate auxin signaling. *EMBO J.* 39, e101515. doi: 10.15252/embj.2019101515

Lyons, R., Stiller, J., Powell, J., Rusu, A., Manners, J. M., and Kazan, K. (2015). Fusarium oxysporum triggers tissue-specific transcriptional reprogramming in Arabidopsis thaliana. *PloS One* 10, e0121902. doi: 10.1371/journal.pone.0121902

Ma, C., Dang, K., Xie, Q., Sahito, J. H., Yuan, B., Wan, J., et al. (2023). Over-expression of zmIAA29, an AUX/IAA transcription factor, improved maize flowering time. *Agronomy* 13, 2028. doi: 10.3390/agronomy13082028

Majer, C., Xu, C., Berendzen, K. W., and Hochholdinger, F. (2012). Molecular interactions of ROOTLESS CONCERNING CROWN AND SEMINAL ROOTS, a LOB domain protein regulating shoot-borne root initiation in maize (Zea mays L.). *Philos. Trans. R Soc. Lond B Biol. Sci.* 367, 1542–1551. doi: 10.1098/rstb.2011.0238

Mallory, A. C., Bartel, D. P., and Bartel, B. (2005). MicroRNA-directed regulation of Arabidopsis AUXIN RESPONSE FACTOR17 is essential for proper development and modulates expression of early auxin response genes. *Plant Cell* 17, 1360–1375. doi: 10.1105/tpc.105.031716

Mantri, N., Patade, V., Penna, S., Ford, R., and Pang, E. (2012). "Abiotic stress responses in plants: present and future," in *Abiotic stress responses in plants* (Springer, New York), 1–19. doi: 10.1007/978-1-4614-0634-1_1

Mao, C., He, J., Liu, L., Deng, Q., Yao, X., Liu, C., et al. (2020). OsNAC2 integrates auxin and cytokinin pathways to modulate rice root development. *Plant Biotechnol. J.* 18, 429–442. doi: 10.1111/pbi.13209

Marin, E., Jouannet, V., Herz, A., Lokerse, A. S., Weijers, D., Vaucheret, H., et al. (2010). miR390, Arabidopsis TAS3 tasiRNAs, and their AUXIN RESPONSE FACTOR targets define an autoregulatory network quantitatively regulating lateral root growth. *Plant Cell* 22, 1104–1117. doi: 10.1105/tpc.109.072553

Matsui, A., Mizunashi, K., Tanaka, M., Kaminuma, E., Nguyen, A. H., Nakajima, M., et al. (2014). tasiRNA-ARF pathway moderates floral architecture in *Arabidopsis* Plants subjected to drought stress. *BioMed. Res. Int.* 2014, 1–10. doi: 10.1155/2014/303451

Meng, L. S., Wang, Z. B., Yao, S. Q., and Liu, A. (2015). The ARF2-ANT-COR15A gene cascade regulates ABA-signaling-mediated resistance of large seeds to drought in Arabidopsis. *J. Cell Sci.* 128, 3922–3932. doi: 10.1242/jcs.171207

Mizoguchi, T., Gotoh, Y., Nishida, E., Yamaguchi-Shinozaki, K., Hayashida, N., Iwasaki, T., et al. (1994). Characterization of two cDNAs that encode MAP kinase homologues in Arabidopsis thaliana and analysis of the possible role of auxin in activating such kinase activities in cultured cells. *Plant J.* 5, 111–122. doi: 10.1046/j.1365-313X.1994.5010111.x

Moller, B. K., Ten Hove, C. A., Xiang, D., Williams, N., Lopez, L. G., Yoshida, S., et al. (2017). Auxin response cell-autonomously controls ground tissue initiation in the early Arabidopsis embryo. *Proc. Natl. Acad. Sci. U.S.A.* 114, E2533–E2539. doi: 10.1073/pnas.1616493114

Mutte, S. K., Kato, H., Rothfels, C., Melkonian, M., Wong, G. K., and Weijers, D. (2018). Origin and evolution of the nuclear auxin response system. *Elife* 7, e33399. doi: 10.7554/eLife.33399.035

Nanao, M. H., Vinos-Poyo, T., Brunoud, G., Thevenon, E., Mazzoleni, M., Mast, D., et al. (2014). Structural basis for oligomerization of auxin transcriptional regulators. *Nat. Commun.* 5, 3617. doi: 10.1038/ncomms4617

Natarajan, B., Kalsi, H. S., Godbole, P., Malankar, N., Thiagarayaselvam, A., Siddappa, S., et al. (2018). MiRNA160 is associated with local defense and systemic acquired resistance against Phytophthora infestans infection in potato. *J. Exp. Bot.* 69, 2023–2036. doi: 10.1093/jxb/ery025

Nestler, J., Keyes, S. D., and Wissuwa, M. (2016). Root hair formation in rice (Oryza sativa L.) differs between root types and is altered in artificial growth conditions. *J. Exp. Bot.* 67, 3699–3708. doi: 10.1093/jxb/erw115

Niederhuth, C. E., Patharkar, O. R., and Walker, J. C. (2013). Transcriptional profiling of the Arabidopsis abscission mutant hae hsl2 by RNA-Seq. *BMC Genomics* 14, 37. doi: 10.1186/1471-2164-14-37

Nishimura, T., Wada, T., Yamamoto, K. T., and Okada, K. (2005). The Arabidopsis STV1 protein, responsible for translation reinitiation, is required for auxin-mediated gynoecium patterning. *Plant Cell* 17, 2940–2953. doi: 10.1105/tpc.105.036533

Niu, D., Lin, X. L., Kong, X., Qu, G. P., Cai, B., Lee, J., et al. (2019). SIZ1-mediated SUMOylation of TPR1 suppresses plant immunity in Arabidopsis. *Mol. Plant* 12, 215–228. doi: 10.1016/j.molp.2018.12.002

Oguchi, R., Hikosaka, K., and Hirose, T. (2003). Does the photosynthetic light-acclimation need change in leaf anatomy? *Plant Cell Environ.* 26, 505–512. doi: 10.1046/j.1365-3040.2003.00981.x

Okushima, Y., Fukaki, H., Onoda, M., Theologis, A., and Tasaka, M. (2007). ARF7 and ARF19 regulate lateral root formation via direct activation of LBD/ASL genes in Arabidopsis. *Plant Cell* 19, 118–130. doi: 10.1105/tpc.106.047761

Okushima, Y., Overvoorde, P. J., Arima, K., Alonso, J. M., Chan, A., Chang, C., et al. (2005). Functional genomic analysis of the AUXIN RESPONSE FACTOR gene family members in Arabidopsis thaliana: unique and overlapping functions of ARF7 and ARF19. *Plant Cell* 17, 444–463. doi: 10.1105/tpc.104.028316

O'Malley, R. C., Huang, S. C., Song, L., Lewsey, M. G., Bartlett, A., Nery, J. R., et al. (2016). Cistrome and epicistrome features shape the regulatory DNA landscape. *Cell* 166, 1598. doi: 10.1016/j.cell.2016.08.063

Ori, N. (2019). Dissecting the biological functions of ARF and aux/IAA genes. *Plant Cell* 31, 1210–1211. doi: 10.1105/tpc.19.00330

Orosa-Puente, B., Leftley, N., von Wangenheim, D., Banda, J., Srivastava, A. K., Hill, K., et al. (2018). Root branching toward water involves posttranslational modification of transcription factor ARF7. *Science* 362, 1407–1410. doi: 10.1126/science.aau3956

Overvoorde, P., Fukaki, H., and Beeckman, T. (2010). Auxin control of root development. *Cold Spring Harb. Perspect. Biol.* 2, a001537. doi: 10.1101/cshperspect.a001537

Ozerova, L. V., Krasnikova, M. S., Troitsky, A. V., Solovyev, A. G., and Morozov, S. Y. (2013). TAS3 Genes for small ta-siARF RNAs in plants belonging to subtribe Senecioninae: occurrence of prematurely terminated RNA precursors. *Mol. Gen. Mikrobiol Virusol* 2), 33–36. doi: 10.3103/S0891416813020043

Pandey, S. K., Lee, H. W., Kim, M. J., Cho, C., Oh, E., and Kim, J. (2018). LBD18 uses a dual mode of a positive feedback loop to regulate ARF expression and transcriptional activity in Arabidopsis. *Plant J.* 95, 233–251. doi: 10.1111/tpj.13945

Parcy, F., Vernoux, T., and Dumas, R. (2016). A glimpse beyond structures in auxin-dependent transcription. *Trends Plant Sci.* 21, 574–583. doi: 10.1016/j.tplants.2016.02.002

Peret, B., De Rybel, B., Casimiro, I., Benkova, E., Swarup, R., Laplaze, L., et al. (2009). Arabidopsis lateral root development: an emerging story. *Trends Plant Sci.* 14, 399–408. doi: 10.1016/j.tplants.2009.05.002

Perrot-Rechenmann, C. (2010). Cellular responses to auxin: division versus expansion. *Cold Spring Harb. Perspect. Biol.* 2, a001446. doi: 10.1101/cshperspect.a001446

Petricka, J. J., Winter, C. M., and Benfey, P. N. (2012). Control of *Arabidopsis* root development. *Annu. Rev. Plant Biol.* 63, 563–590. doi: 10.1146/annurev-arplant-042811-105501

Pierre-Jerome, E., Moss, B. L., Lanctot, A., Hageman, A., and Nemhauser, J. L. (2016). Functional analysis of molecular interactions in synthetic auxin response circuits. *Proc. Natl. Acad. Sci. U.S.A.* 113, 11354–11359. doi: 10.1073/pnas.1604379113

Pinweha, N., Asvarak, T., Viboonjun, U., and Narangajavana, J. (2015). Involvement of miR160/miR393 and their targets in cassava responses to anthracnose disease. *J. Plant Physiol.* 174, 26–35. doi: 10.1016/j.jplph.2014.09.006

Piya, S., Shrestha, S. K., Binder, B., Stewart, C. N. Jr., and Hewezi, T. (2014). Protein-protein interaction and gene co-expression maps of ARFs and Aux/IAAs in Arabidopsis. *Front. Plant Sci.* 5. doi: 10.3389/fpls.2014.00744

Powers, S. K., Holehouse, A. S., Korasick, D. A., Schreiber, K. H., Clark, N. M., Jing, H., et al. (2019). Nucleo-cytoplasmic partitioning of ARF proteins controls auxin responses in Arabidopsis thaliana. *Mol. Cell* 76, 177–190 e175. doi: 10.1016/j.molcel.2019.06.044

Powers, S. K., and Strader, L. C. (2020). Regulation of auxin transcriptional responses. *Dev. Dyn* 249, 483–495. doi: 10.1002/dvdy.139

Puga, M. I., Rojas-Triana, M., de Lorenzo, L., Leyva, A., Rubio, V., and Paz-Ares, J. (2017). Novel signals in the regulation of Pi starvation responses in plants: facts and promises. *Curr. Opin. Plant Biol.* 39, 40–49. doi: 10.1016/j.pbi.2017.05.007

Qi, Y., Wang, S., Shen, C., Zhang, S., Chen, Y., Xu, Y., et al. (2012). OsARF12, a transcription activator on auxin response gene, regulates root elongation and affects iron accumulation in rice (Oryza sativa). *New Phytol.* 193, 109–120. doi: 10.1111/j.1469-8137.2011.03910.x

Qiao, J., Jiang, H., Lin, Y., Shang, L., Wang, M., Li, D., et al. (2021). A novel miR167a-OsARF6-OsAUX3 module regulates grain length and weight in rice. *Mol. Plant* 14, 1683–1698. doi: 10.1016/j.molp.2021.06.023

Qiao, J., Zhang, Y., Han, S., Chang, S., Gao, Z., Qi, Y., et al. (2022). OsARF4 regulates leaf inclination via auxin and brassinosteroid pathways in rice. *Front. Plant Sci.* 13. doi: 10.3389/fpls.2022.979033

Qiao, L., Zhang, W., Li, X., Zhang, L., Zhang, X., Li, X., et al. (2018). Characterization and expression patterns of auxin response factors in wheat. *Front. Plant Sci.* 9. doi: 10.3389/fpls.2018.01395

Qin, Q., Li, G., Jin, L., Huang, Y., Wang, Y., Wei, C., et al. (2020). Auxin response factors (ARFs) differentially regulate rice antiviral immune response against rice dwarf virus. *PloS Pathog.* 16, e1009118. doi: 10.1371/journal.ppat.1009118

Quint, M., and Gray, W. M. (2006). Auxin signaling. *Curr. Opin. Plant Biol.* 9, 448–453. doi: 10.1016/j.pbi.2006.07.006

Ramazi, S., Allahverdi, A., and Zahiri, J. (2020). Evaluation of post-translational modifications in histone proteins: A review on histone modification defects in developmental and neurological disorders. *J. Biosci.* 45, 135. doi: 10.1007/s12038-020-00099-2

Roosjen, M., Paque, S., and Weijers, D. (2018). Auxin Response Factors: output control in auxin biology. *J. Exp. Bot.* 69, 179–188. doi: 10.1093/jxb/erx237

Saidi, A., and Hajibarat, Z. (2020). Computational study of environmental stress-related transcription factor binding sites in the promoter regions of maize auxin response factor (ARF) gene family. *Not Sci. Biol.* 12, 646–657. doi: 10.15835/nsb12310823

Sainju, U. M., Singh, B. P., and Whitehead, W. F. (2005). Tillage, cover crops, and nitrogen effects on cotton and sorghum root biomass, carbon, and nitrogen. *Agron. J.* 97, 1279–1290. doi: 10.2134/agronj2004.0213

Sakamoto, T., Morinaka, Y., Inukai, Y., Kitano, H., and Fujioka, S. (2013). Auxin signal transcription factor regulates expression of the brassinosteroid receptor gene in rice. *Plant J.* 73, 676–688. doi: 10.1111/tpj.12071

Salmon, J., Ramos, J., and Callis, J. (2008). Degradation of the auxin response factor ARF1. *Plant J.* 54, 118–128. doi: 10.1111/j.1365-313X.2007.03396.x

Scacchi, E., Salinas, P., Gujas, B., Santuari, L., Krogan, N., Ragni, L., et al. (2010). Spatio-temporal sequence of cross-regulatory events in root meristem growth. *Proc. Natl. Acad. Sci. U.S.A.* 107, 22734–22739. doi: 10.1073/pnas.1014716108

Scheres, B., and van der Putten, W. H. (2017). The plant perceptron connects environment to development. *Nature* 543, 337–345. doi: 10.1038/nature22010

Schlereth, A., Moller, B., Liu, W., Kientz, M., Flipse, J., Rademacher, E. H., et al. (2010). MONOPTEROS controls embryonic root initiation by regulating a mobile transcription factor. *Nature* 464, 913–916. doi: 10.1038/nature08836

Schuetz, M., Fidanza, M., and Mattsson, J. (2019). Identification of auxin response factor-encoding genes expressed in distinct phases of leaf vein development and with overlapping functions in leaf formation. *Plants (Basel)* 8, 242. doi: 10.3390/plants8070242

Sessions, A., Nemhauser, J. L., McColl, A., Roe, J. L., Feldmann, K. A., and Zambryski, P. C. (1997). ETTIN patterns the Arabidopsis floral meristem and reproductive organs. *Development* 124, 4481–4491. doi: 10.1242/dev.124.22.4481

Shahzad, Z., Eaglesfield, R., Carr, C., and Amtmann, A. (2020). Cryptic variation in RNA-directed DNA-methylation controls lateral root development when auxin signalling is perturbed. *Nat. Commun.* 11, 218. doi: 10.1038/s41467-019-13927-3

Shen, C., Wang, S., Zhang, S., Xu, Y., Qian, Q., Qi, Y., et al. (2013). OsARF16, a transcription factor, is required for auxin and phosphate starvation response in rice (Oryza sativa L.). *Plant Cell Environ.* 36, 607–620. doi: 10.1111/pce.12001

Shen, C., Yue, R., Sun, T., Zhang, L., Yang, Y., and Wang, H. (2015). OsARF16, a transcription factor regulating auxin redistribution, is required for iron deficiency response in rice (Oryza sativa L.). *Plant Sci.* 231, 148–158. doi: 10.1016/j.plantsci.2014.12.003

Shen, C., Yue, R., Yang, Y., Zhang, L., Sun, T., Tie, S., et al. (2014). OsARF16 is involved in cytokinin-mediated inhibition of phosphate transport and phosphate signaling in rice (Oryza sativa L.). *PloS One* 9, e112906. doi: 10.1371/journal.pone.0112906

Sheng, H., Cong, D. L., and Ju, H. Y. (2020). [Functional characterization of zmHAK1 promoter and its regulatory transcription factors in maize]. *Mol. Biol. (Mosk)* 54, 374–388. doi: 10.1134/S0026893320030152

Si, F., Yang, C., Yan, B., Yan, W., Tang, S., Yan, Y., et al. (2022). Control of OsARF3a by OsKANADI1 contributes to lemma development in rice. *Plant J.* 110, 1717–1730. doi: 10.1111/tpj.15766

Simonini, S., Deb, J., Moubayidin, L., Stephenson, P., Valluru, M., Freire-Rios, A., et al. (2016). A noncanonical auxin-sensing mechanism is required for organ morphogenesis in Arabidopsis. *Genes Dev.* 30, 2286–2296. doi: 10.1101/gad.285361.116

Singh, S., and Singh, A. (2021). A prescient evolutionary model for genesis, duplication and differentiation of MIR160 homologs in Brassicaceae. *Mol. Genet. Genomics* 296, 985–1003. doi: 10.1007/s00438-021-01797-8

Singh, S., Yadav, S., Singh, A., Mahima, M., Singh, A., Gautam, V., et al. (2020). Auxin signaling modulates LATERAL ROOT PRIMORDIUM1 (LRP1) expression during lateral root development in Arabidopsis. *Plant J.* 101, 87–100. doi: 10.1111/tpj.14520

Spitz, F., and Furlong, E. E. (2012). Transcription factors: from enhancer binding to developmental control. *Nat. Rev. Genet.* 13, 613–626. doi: 10.1038/nrg3207

Stigliani, A., Martin-Arevalillo, R., Lucas, J., Bessy, A., Vinos-Poyo, T., Mironova, V., et al. (2019). Capturing auxin response factors syntax using DNA binding models. *Mol. Plant* 12, 822–832. doi: 10.1016/j.molp.2018.09.010

Stoeckle, D., Thellmann, M., and Vermeer, J. E. (2018). Breakout-lateral root emergence in Arabidopsis thaliana. *Curr. Opin. Plant Biol.* 41, 67–72. doi: 10.1016/j.pbi.2017.09.005

Stone, L. R., Goodrum, D. E., Jaafar, M. N., and Khan, A. H. (2001). Rooting front and water depletion depths in grain sorghum and sunflower. *Agron. J.* 93, 1105–1110. doi: 10.2134/agronj2001.9351105x

Suter, D. M. (2020). Transcription factors and DNA play hide and seek. *Trends Cell Biol.* 30, 491–500. doi: 10.1016/j.tcb.2020.03.003

Szemenyei, H., Hannon, M., and Long, J. A. (2008). TOPLESS mediates auxin-dependent transcriptional repression during Arabidopsis embryogenesis. *Science* 319, 1384–1386. doi: 10.1126/science.1151461

Tabata, R., Ikezaki, M., Fujibe, T., Aida, M., Tian, C. E., Ueno, Y., et al. (2010). Arabidopsis auxin response factor6 and 8 regulate jasmonic acid biosynthesis and floral organ development via repression of class 1 KNOX genes. *Plant Cell Physiol.* 51, 164–175. doi: 10.1093/pcp/pcp176

Takahashi, H., Iwakawa, H., Ishibashi, N., Kojima, S., Matsumura, Y., Prananingrum, P., et al. (2013). Meta-analyses of microarrays of Arabidopsis asymmetric leaves1 (as1), as2 and their modifying mutants reveal a critical role for the ETT pathway in stabilization of adaxial-abaxial patterning and cell division during leaf development. *Plant Cell Physiol.* 54, 418–431. doi: 10.1093/pcp/pct027

Tan, S., Luschnig, C., and Friml, J. (2021). Pho-view of auxin: reversible protein phosphorylation in auxin biosynthesis, transport and signaling. *Mol. Plant* 14, 151–165. doi: 10.1016/j.molp.2020.11.004

Tantikanjana, T., and Nasrallah, J. B. (2012). Non-cell-autonomous regulation of crucifer self-incompatibility by Auxin Response Factor ARF3. *Proc. Natl. Acad. Sci. U.S.A.* 109, 19468–19473. doi: 10.1073/pnas.1217343109

Tiwari, S. B., Hagen, G., and Guilfoyle, T. (2003). The roles of auxin response factor domains in auxin-responsive transcription. *Plant Cell* 15, 533–543. doi: 10.1105/tpc.008417

Uga, Y., Sugimoto, K., Ogawa, S., Rane, J., Ishitani, M., Hara, N., et al. (2013). Control of root system architecture by DEEPER ROOTING 1 increases rice yield under drought conditions. *Nat. Genet.* 45, 1097–1102. doi: 10.1038/ng.2725

Ulmasov, T., Hagen, G., and Guilfoyle, T. J. (1997). ARF1, a transcription factor that binds to auxin response elements. *Science* 276, 1865–1868. doi: 10.1126/science.276.5320.1865

Ulmasov, T., Liu, Z. B., Hagen, G., and Guilfoyle, T. J. (1995). Composite structure of auxin response elements. *Plant Cell* 7, 1611–1623. doi: 10.1105/tpc.7.10.1611

Vernoux, T., Brunoud, G., Farcot, E., Morin, V., Van den Daele, H., Legrand, J., et al. (2011). The auxin signalling network translates dynamic input into robust patterning at the shoot apex. *Mol. Syst. Biol.* 7, 508. doi: 10.1038/msb.2011.39

Vierstra, R. D. (2009). The ubiquitin-26S proteasome system at the nexus of plant biology. *Nat. Rev. Mol. Cell Biol.* 10, 385–397. doi: 10.1038/nrm2688

von Behrens, I., Komatsu, M., Zhang, Y., Berendzen, K. W., Niu, X., Sakai, H., et al. (2011). Rootless with undetectable meristem 1 encodes a monocot-specific AUX/IAA protein that controls embryonic seminal and post-embryonic lateral root initiation in maize. *Plant J.* 66, 341–353. doi: 10.1111/j.1365-313X.2011.04495.x

Waller, F., Furuya, M., and Nick, P. (2002). OsARF1, an auxin response factor from rice, is auxin-regulated and classifies as a primary auxin responsive gene. *Plant Mol. Biol. 50*, 415–425. doi: 10.1023/A:1019818110761

Wan, S., Li, W., Zhu, Y., Liu, Z., Huang, W., and Zhan, J. (2014). Genome-wide identification, characterization and expression analysis of the auxin response factor gene family in Vitis vinifera. *Plant Cell Rep.* 33, 1365–1375. doi: 10.1007/s00299-014-1622-7

Wang, K., Chen, Y., Chang, E. A., Knott, J. G., and Cibelli, J. B. (2009). Dynamic epigenetic regulation of the Oct4 and Nanog regulatory regions during neural differentiation in rhesus nuclear transfer embryonic stem cells. *Cloning Stem Cells* 11, 483–496. doi: 10.1089/clo.2009.0019

Wang, Y., Deng, D., Bian, Y., Lv, Y., and Xie, Q. (2010). Genome-wide analysis of primary auxin-responsive Aux/IAA gene family in maize (Zea mays. L.). *Mol. Biol. Rep.* 37, 3991–4001. doi: 10.1007/s11033-010-0058-6

Wang, R., and Estelle, M. (2014). Diversity and specificity: auxin perception and signaling through the TIR1/AFB pathway. *Curr. Opin. Plant Biol.* 21, 51–58. doi: 10.1016/j.pbi.2014.06.006

Wang, M., Zheng, Q., Shen, Q., and Guo, S. (2013). The critical role of potassium in plant stress response. *Int. J. Mol. Sci.* 14, 7370–7390. doi: 10.3390/ijms14047370

Wang, Y. F., Hou, X. Y., Deng, J. J., Yao, Z. H., Lyu, M. M., and Zhang, R. S. (2020). AUXIN RESPONSE FACTOR 1 acts as a positive regulator in the response of poplar to trichoderma asperellum inoculation in overexpressing plants. *Plants (Basel)* 9, 272. doi: 10.3390/plants9020272

Wang, L., Hua, D., He, J., Duan, Y., Chen, Z., Hong, X., et al. (2011). Auxin Response Factor2 (ARF2) and its regulated homeodomain gene HB33 mediate abscisic acid response in Arabidopsis. *PloS Genet.* 7, e1002172. doi: 10.1371/journal.pgen.1002172

Wang, Y., Li, K., Chen, L., Zou, Y., Liu, H., Tian, Y., et al. (2015). MicroRNA167-directed regulation of the auxin response factors gmARF8a and gmARF8b is required for soybean nodulation and lateral root development. *Plant Physiol.* 168, 984–999. doi: 10.1104/pp.15.00265

Wang, D., Pei, K., Fu, Y., Sun, Z., Li, S., Liu, H., et al. (2007). Genome-wide analysis of the auxin response factors (ARF) gene family in rice (Oryza sativa). *Gene* 394, 13–24. doi: 10.1016/j.gene.2007.01.006

Wang, G., Wang, F., Huang, Q., Li, Y., Liu, Y., and Wang, Y. (2015). Understanding transcription factor regulation by integrating gene expression and DNase I hypersensitive sites. *BioMed. Res. Int.* 2015, 757530. doi: 10.1155/2015/757530

Wang, J. W., Wang, L. J., Mao, Y. B., Cai, W. J., Xue, H. W., and Chen, X. Y. (2005). Control of root cap formation by MicroRNA-targeted auxin response factors in Arabidopsis. *Plant Cell* 17, 2204–2216. doi: 10.1105/tpc.105.033076

Wang, S., Zhang, S., Sun, C., Xu, Y., Chen, Y., Yu, C., et al. (2014). Auxin response factor (OsARF12), a novel regulator for phosphate homeostasis in rice (Oryza sativa). *New Phytol.* 201, 91–103. doi: 10.1111/nph.12499

Weijers, D., and Friml, J. (2009). SnapShot: Auxin signaling and transport. *Cell* 136, 1172 e1171. doi: 10.1016/j.cell.2009.03.009

Weijers, D., and Wagner, D. (2016). Transcriptional responses to the auxin hormone. *Annu. Rev. Plant Biol.* 67, 539–574. doi: 10.1146/annurev-arplant-043015-112122

Weiste, C., and Droge-Laser, W. (2014). The Arabidopsis transcription factor bZIP11 activates auxin-mediated transcription by recruiting the histone acetylation machinery. *Nat. Commun.* 5, 3883. doi: 10.1038/ncomms4883

Wen, F. L., Yue, Y., He, T. F., Gao, X. M., Zhou, Z. S., and Long, X. H. (2020). Identification of miR390-TAS3-ARF pathway in response to salt stress in Helianthus tuberosus L. *Gene* 738, 144460. doi: 10.1016/j.gene.2020.144460

Wright, R. C., and Nemhauser, J. L. (2015). New tangles in the auxin signaling web. *F1000Prime Rep.* 7, 19. doi: 10.12703/P7-19

Wu, F., Liu, Z., Xu, J., Gao, S., Lin, H., Liu, L., et al. (2016). Molecular evolution and association of natural variation in zmARF31 with low phosphorus tolerance in maize. *Front. Plant Sci.* 7. doi: 10.3389/fpls.2016.01076

Wu, M. F., Tian, Q., and Reed, J. W. (2006). Arabidopsis microRNA167 controls patterns of ARF6 and ARF8 expression, and regulates both female and male reproduction. *Development* 133, 4211–4218. doi: 10.1242/dev.02602

Wu, M. F., Yamaguchi, N., Xiao, J., Bargmann, B., Estelle, M., Sang, Y., et al. (2015). Auxin-regulated chromatin switch directs acquisition of flower primordium founder fate. *Elife* 4, e09269. doi: 10.7554/eLife.09269.027

Xing, J., Cao, X., Zhang, M., Wei, X., Zhang, J., and Wan, X. (2023). Plant nitrogen availability and crosstalk with phytohormones signallings and their biotechnology breeding application in crops. *Plant Biotechnol. J.* 21, 1320–1342. doi: 10.1111/pbi.13971

Xing, M., Wang, W., Fang, X., and H., X. (2022). Rice OsIAA6 interacts with OsARF1 and regulates leaf inclination. *Crop J.* 10, 1580–1588. doi: 10.1016/j.cj.2022.02.010

Xing, L., Zhu, M., Luan, M., Zhang, M., Jin, L., Liu, Y., et al. (2021). miR169q and NUCLEAR FACTOR YA8 enhance salt tolerance by activating PEROXIDASE1 expression in response to ROS. *Plant Physiol.* 188, 608–623. doi: 10.1093/plphys/kiab498

Xiong, Y., and Jiao, Y. (2019). The diverse roles of auxin in regulating leaf development. *Plants (Basel)* 8, 243. doi: 10.3390/plants8070243

Xiong, Y., Wu, B., Du, F., Guo, X., Tian, C., Hu, J., et al. (2021). A crosstalk between auxin and brassinosteroid regulates leaf shape by modulating growth anisotropy. *Mol. Plant* 14, 949–962. doi: 10.1016/j.molp.2021.03.011

Xu, C., Tai, H., Saleem, M., Ludwig, Y., Majer, C., Berendzen, K. W., et al. (2015). Cooperative action of the paralogous maize lateral organ boundaries (LOB) domain proteins RTCS and RTCL in shoot-borne root formation. *New Phytol.* 207, 1123–1133. doi: 10.1111/nph.13420

Xue, M., and Yi, H. (2018). Enhanced Arabidopsis disease resistance against Botrytis cinerea induced by sulfur dioxide. *Ecotoxicol Environ. Saf.* 147, 523–529. doi: 10.1016/j.ecoenv.2017.09.011

Xun, Q., Wu, Y., Li, H., Chang, J., Ou, Y., He, K., et al. (2020). Two receptor-like protein kinases, MUSTACHES and MUSTACHES-LIKE, regulate lateral root development in Arabidopsis thaliana. *New Phytol.* 227, 1157–1173. doi: 10.1111/nph.16599

Yamauchi, T., Tanaka, A., Inahashi, H., Nishizawa, N. K., Tsutsumi, N., Inukai, Y., et al. (2019). Fine control of aerenchyma and lateral root development through AUX/IAA- and ARF-dependent auxin signaling. *Proc. Natl. Acad. Sci. U.S.A.* 116, 20770–20775. doi: 10.1073/pnas.1907181116

Yang, F., Shi, Y., Zhao, M., Cheng, B., and Li, X. (2022). ZmIAA5 regulates maize root growth and development by interacting with ZmARF5 under the specific binding of ZmTCP15/16/17. *PeerJ* 10, e13710. doi: 10.7717/peerj.13710

Yang, T., Wang, Y., Teotia, S., Wang, Z., Shi, C., Sun, H., et al. (2019). The interaction between miR160 and miR165/166 in the control of leaf development and drought tolerance in Arabidopsis. *Sci. Rep.* 9, 2832. doi: 10.1038/s41598-019-39397-7

Ye, Y., Wang, J., Wang, W., and Xu, L. A. (2020). ARF family identification in Tamarix chinensis reveals the salt responsive expression of TcARF6 targeted by miR167. *PeerJ* 8, e8829. doi: 10.7717/peerj.8829

Yuan, Y., Mei, L., Wu, M., Wei, W., Shan, W., Gong, Z., et al. (2018). SlARF10, an auxin response factor, is involved in chlorophyll and sugar accumulation during tomato fruit development. *J. Exp. Bot.* 69, 5507–5518. doi: 10.1093/jxb/ery328

Yuan, Y., Xu, X., Gong, Z., Tang, Y., Wu, M., Yan, F., et al. (2019). Auxin response factor 6A regulates photosynthesis, sugar accumulation, and fruit development in tomato. *Hortic. Res.* 6, 85. doi: 10.1038/s41438-019-0167-x

Zahir, Z. A., Shah, M. K., Naveed, M., and Akhter, M. J. (2010). Substrate-dependent auxin production by Rhizobium phaseoli improves the growth and yield of Vigna radiata L. under salt stress conditions. *J. Microbiol. Biotechnol.* 20, 1288–1294. doi: 10.4014/jmb.1002.02010

Zhang, T., Ge, Y., Cai, G., Pan, X., and Xu, L. (2023). WOX-ARF modules initiate different types of roots. *Cell Rep.* 42, 112966. doi: 10.1016/j.celrep.2023.112966

Zhang, Y., Ji, X., Xian, J., Wang, Y., and Peng, Y. (2022). Morphological characterization and transcriptome analysis of leaf angle mutant bhlh112 in maize [Zea mays L.]. *Front. Plant Sci.* 13. doi: 10.3389/fpls.2022.995815

Zhang, H., Li, L., He, Y., Qin, Q., Chen, C., Wei, Z., et al. (2020). Distinct modes of manipulation of rice auxin response factor OsARF17 by different plant RNA viruses for infection. *Proc. Natl. Acad. Sci. U.S.A.* 117, 9112–9121. doi: 10.1073/pnas.1918254117

Zhang, Z., Teotia, S., Tang, J., and Tang, G. (2019). Perspectives on microRNAs and Phased Small Interfering RNAs in Maize (Zea mays L.): Functions and Big Impact on Agronomic Traits Enhancement. *Plants* 8, 170. doi: 10.3390/plants8060170

Zhang, S., Wang, S., Xu, Y., Yu, C., Shen, C., Qian, Q., et al. (2015). The auxin response factor, OsARF19, controls rice leaf angles through positively regulating OsGH3-5 and OsBRI1. *Plant Cell Environ.* 38, 638–654. doi: 10.1111/pce.12397

Zhang, C. L., Wang, G. L., Zhang, Y. L., Hu, X., Zhou, L. J., You, C. X., et al. (2021). Apple SUMO E3 ligase MdSIZ1 facilitates SUMOylation of MdARF8 to regulate lateral root formation. *New Phytol.* 229, 2206–2222. doi: 10.1111/nph.16978

Zhang, K., Wang, R., Zi, H., Li, Y., Cao, X., Li, D., et al. (2018). AUXIN RESPONSE FACTOR3 regulates floral meristem determinacy by repressing cytokinin biosynthesis and signaling. *Plant Cell* 30, 324–346. doi: 10.1105/tpc.17.00705

Zhang, S., Zhu, L., Shen, C., Ji, Z., Zhang, H., Zhang, T., et al. (2021). Natural allelic variation in a modulator of auxin homeostasis improves grain yield and nitrogen use efficiency in rice. *Plant Cell* 33, 566–580. doi: 10.1093/plcell/koaa037

Zhao, Z. X., Yin, X. X., Li, S., Peng, Y. T., Yan, X. L., Chen, C., et al. (2022). miR167d-ARFs module regulates flower opening and stigma size in rice. *Rice (N Y)* 15, 40. doi: 10.1186/s12284-022-00587-z

Zhao, S., Zhang, M.-L., Ma, T.-L., and Wang, Y. (2016). Phosphorylation of ARF2 relieves its repression of transcription of the K+ Transporter gene HAK5 in response to low potassium stress. *Plant Cell* 28, 3005–3019. doi: 10.1105/tpc.16.00684

Zhou, D.-X., and Hu, Y. (2010). Regulatory function of histone modifications in controlling rice gene expression and plant growth. *Rice* 3, 103–111. doi: 10.1007/s12284-010-9045-8

Zhou, L. J., Xiao, L. T., and Xue, H. W. (2017). Dynamic cytology and transcriptional regulation of rice lamina joint development. *Plant Physiol.* 174, 1728–1746. doi: 10.1104/pp.17.00413

frontiers | Frontiers in Plant Science

TYPE Original Research
PUBLISHED 10 June 2024
DOI 10.3389/fpls.2024.1389207

OPEN ACCESS

EDITED BY
Hamada AbdElgawad,
Beni-Suef University, Egypt

REVIEWED BY
Hajar Salehi,
Catholic University of the Sacred Heart, Italy
Zaid Ulhassan,
Zhejiang University, China
Shikha Verma,
Ben-Gurion University of the Negev, Israel
Saeed ur Rahman,
Shanghai Jiao Tong University, China

*CORRESPONDENCE
Yuanzhi Pan
scpyzls@163.com

†These authors have contributed equally to this work and share first authorship

RECEIVED 21 February 2024
ACCEPTED 21 May 2024
PUBLISHED 10 June 2024

CITATION
Wu M, Xu Q, Tang T, Li X and Pan Y (2024) Integrative physiological, transcriptomic, and metabolomic analysis of *Abelmoschus manihot* in response to Cd toxicity. *Front. Plant Sci.* 15:1389207. doi: 10.3389/fpls.2024.1389207

Integrative physiological, transcriptomic, and metabolomic analysis of *Abelmoschus manihot* in response to Cd toxicity

Mengxi Wu[1†], Qian Xu[1†], Tingting Tang[1], Xia Li[1] and Yuanzhi Pan[2*]

[1]College of Landscape Architecture, Sichuan Agricultural University, Chengdu, China, [2]College of Forestry, Sichuan Agricultural University, Chengdu, Sichuan, China

Rapid industrialization and urbanization have caused severe soil contamination with cadmium (Cd) necessitating effective remediation strategies. Phytoremediation is a widely adopted technology for remediating Cd-contaminated soil. Previous studies have shown that *Abelmoschus manihot* has a high Cd accumulation capacity and tolerance indicating its potential for Cd soil remediation. However, the mechanisms underlying its response to Cd stress remain unclear. In this study, physiological, transcriptomic, and metabolomic analyses were conducted to explore the response of *A. manihot* roots to Cd stress at different time points. The results revealed that Cd stress significantly increased malondialdehyde (MDA) levels in *A. manihot*, which simultaneously activated its antioxidant defense system, enhancing the activities of superoxide dismutase (SOD), peroxidase (POD), and catalase (CAT) by 19.73%–50%, 22.87%–38.89%, and 32.31%–45.40% at 12 h, 36 h, 72 h, and 7 days, respectively, compared with those in the control (CK). Moreover, transcriptomic and metabolomic analyses revealed 245, 5,708, 9,834, and 2,323 differentially expressed genes (DEGs), along with 66, 62, 156, and 90 differentially expressed metabolites (DEMs) at 12 h, 36 h, 72 h, and 7 days, respectively. Through weighted gene coexpression network analysis (WGCNA) of physiological indicators and transcript expression, eight hub genes involved in phenylpropanoid biosynthesis, signal transduction, and metal transport were identified. In addition, integrative analyses of metabolomic and transcriptomic data highlighted the activation of lipid metabolism and phenylpropanoid biosynthesis pathways under Cd stress suggesting that these pathways play crucial roles in the detoxification process and in enhancing Cd tolerance in *A. manihot*. This comprehensive study provides detailed insights into the response mechanisms of *A. manihot* to Cd toxicity.

KEYWORDS

transcriptomic, metabolomics, Cd stress, lipids, phenylpropanoid, *Abelmoschus manihot*

1 Introduction

Cadmium (Cd) is widely recognized as one of the most toxic heavy metals, and the rapid development of modern industry and agriculture has contributed to the increasing prevalence of Cd pollution (Balali-Mood et al., 2021; Rezapour et al., 2022). Importantly, Cd accumulation in soil can easily be transferred to plants and subsequently enter the human food chain posing significant threats to both the soil environment and human health even at low concentrations (Liang et al., 2018). Therefore, it is crucial to implement effective strategies for remediating Cd-contaminated soil. Over the past decade, a variety of strategies, including physical, chemical, and biological methods, have been utilized to decontaminate soil contaminated with Cd. Among these methods, phytoremediation has emerged as a cost-effective and environmentally friendly approach for removing Cd contaminants from soil (Mahar et al., 2016; Suman et al., 2018).

In plants, Cd toxicity either directly or indirectly disrupts various physiological processes, including photosynthesis, respiration, nutrient uptake, and hormonal balance, ultimately resulting in growth retardation, leaf chlorosis, and reduced biomass (Mwamba et al., 2020; Hamid et al., 2022; Nazir et al., 2022). Unlike normal plants, Cd hyperaccumulators are capable of maintaining normal physiological functions in high-Cd environments and accumulate significant amounts of Cd in their tissues (Corso et al., 2018; Haider et al., 2021). Therefore, hyperaccumulators are considered ideal materials for phytoremediation. Identifying new Cd hyperaccumulators and understanding the mechanisms underlying Cd detoxification and accumulation in these plants are crucial for improving the efficiency of phytoremediation (Suman et al., 2018; Kanwar et al., 2020; Yan et al., 2020). Under Cd stress, hyperaccumulators demonstrate an exceptional ability to accumulate Cd in their tissues attributed to the evolution of detoxification mechanisms that mitigate its toxic effects. For instance, in the Cd hyperaccumulator *Solanum nigrum*, Cd binding to sulfur ligands serves as a detoxification mechanism, which likely involves the sequestration of Cd complexes with glutathione or phytochelatins in plant vacuoles leading to greater Cd accumulation than in the nonaccumulator *Solanum melongena* (Pons et al., 2021). Moreover, the cell wall biosynthesis pathway has also been identified as another significant contributor to Cd detoxification in *S. nigrum* (Wang et al., 2022). Similarly, root cell wall modification serves as an important defense strategy for the Cd hyperaccumulator *Sedum alfredii* against Cd stress (Guo et al., 2021). The primary mechanism by which the Cd hyperaccumulator *Erigeron annuus* alleviates Cd toxicity is through the acceleration of antioxidation mechanisms facilitating the removal of reactive oxygen species (ROS) (Zhang et al., 2021). In addition, various metal transporter families, including the ATP-binding cassette transporter (ABC) family, heavy metal ATPase (HMA) family, zinc transporter (ZIP) family, and natural resistance-As-associated macrophage proteins (NRAMPs), have been identified to play crucial roles in the detoxification and accumulation mechanisms of hyperaccumulators (Liu et al., 2017; Zhang et al., 2020). For example, SpHMA3, which is isolated from the Cd/zinc (Zn) hyperaccumulator *Sedum plumbizincicola*, has been demonstrated to play an essential role in Cd detoxification by sequestering Cd into vacuoles in young leaves and stems (Liu et al., 2017). SaNramp1, a plasma membrane-localized transporter, is involved in Cd accumulation in *S. alfredii* (Zhang et al., 2020). However, the majority of proposed Cd detoxification and accumulation mechanisms have focused on specific plants or even specific genotypes. Therefore, expanding the scope of information on the genetics, proteins, and biochemistry of other hyperaccumulators in response to Cd stress is necessary.

Abelmoschus manihot (Supplementary Figure S1) has been identified as a potential Cd hyperaccumulator that has high ornamental and economic value (Wu et al., 2018). However, the mechanisms underlying the response of *A. manihot* to Cd toxicity remain unknown. Recently, high-throughput omics technologies, including transcriptomics, proteomics, and metabolomics, have been widely applied to study the responses of hyperaccumulators, such as *Phytolacca americana* (Zhao et al., 2011), *S. nigrum* (Wang et al., 2022), *S. alfredii* (Wu et al., 2020), and *Brassica napus* (Zhang et al., 2019), to heavy metal stress. These omics technologies have further expanded our understanding of the complex biological processes induced by Cd stress (Wang et al., 2022; Wei et al., 2023). Therefore, in the present study, we employed a combination of physiological, transcriptomic, and metabolomic analyses to investigate how *A. manihot* acclimates to Cd stress. The objectives of this study were (1) to investigate the physiological response of *A. manihot* to Cd exposure in its roots, (2) to reveal the dynamic adjustments in transcriptional and metabolic processes in *A. manihot* roots in response to Cd stress, and (3) to explore a potential regulatory network between genes and metabolites in *A. manihot* under Cd stress. The results will contribute to a better understanding of the Cd detoxification and accumulation mechanisms of *A. manihot* and further facilitate the decontamination of Cd-contaminated soils.

2 Materials and methods

2.1 Plant materials and treatments

The seeds of *A. manihot*, sourced from a noncontaminated area in Sichuan Province, China, were subjected to surface sterilization by soaking in 0.05% sodium hypochlorite (NaClO) for 30 min followed by rinsing with deionized water. The sterilized seeds were directly planted in baskets filled with sterilized ceramsite stones and placed within the planting basket of an automatic hydroponic culture device (Supplementary Figure S2). Germination occurred under controlled conditions maintaining a constant temperature of 25°C and a photoperiod of 14/10 h (day/night). After 2 weeks, the seedlings were precultured in a greenhouse using Hoagland nutrient solution, with a temperature setting of 28°C/24°C (day/night), a photoperiod of 14/10 h (day/night), and humidity maintained between 60% and 80%. The components of the nutrient solution were as follows: 4 mM $Ca(NO_3)_2{\cdot}4H_2O$, 4 mM $(NH_4)_2SO_4$, 4 mM K_2SO_4, 4 mM KNO_3, 1.3 mM KH_2PO_4, 1 mM $MgSO_4{\cdot}7H_2O$, 50 μM

Fe-EDTA, 10 μM H_3BO_3, 5 μM $MnSO_4·H_2O$, 5 μM $ZnSO_4·7H_2O$, 1 μM $CuSO_4·5H_2O$, and 0.5 μM $Na_2MoO_4·2H_2O$ (Mwamba et al., 2016). After 30 days of growth, the plants were transferred to Hoagland nutrient solution containing $CdCl_2$, while the control plants were not treated with $CdCl_2$ (CK). An additional preliminary experiment assessed the physiological parameters of *A. manihot* roots under a range of Cd concentrations, including 0, 50, 100, 200, and 400 μM (data not shown), which allowed the level of Cd exposure to be set at 100 μM in the present study. Plant samples were collected at four different time points: 12 h, 36 h, 72 h, and 7 days. At each time point, a total of 12 individuals were subdivided into three biological replicates. The harvested plants were washed with tap water, and the roots were treated with 20 mM ethylenediaminetetraacetic acid disodium salt (Na_2-EDTA) for 15 min to remove the Cd adsorbed on the root surface.

2.2 Determination of Cd concentrations in plant tissues

Dried samples of roots, stems, and leaves were ground, passed through a 0.15-mm mesh sieve, and digested using an acid mixture of nitric acid (HNO_3) and perchloric acid ($HClO_4$) (v:v, 4:1) (Wu et al., 2018). The Cd concentrations in the different plant tissues were analyzed by atomic absorption spectrometry (PinAAcle 900 H, Perkin Elmer, USA). Electrodeless discharge lamp at 228.8 nm (with a slit width of 0.7 nm) was used as the radiation source for the Cd.

2.3 Biochemical parameters

Fresh root tissues were utilized directly for the detection of biochemical parameters. The malondialdehyde (MDA) content was measured using the thiobarbituric acid (TBA) reaction method (Peever and Higgins, 1989). The activities of superoxide dismutase (SOD), peroxidase (POD), and catalase (CAT) were determined following the procedure described by Wu et al. (2018). SOD activity was determined by nitroblue tetrazolium (NBT) reduction, POD activity through guaiacol oxidation, and CAT activity by measuring the decrease in H_2O_2 concentration.

2.4 Transcriptomic analysis

2.4.1 RNA extraction and transcriptome sequencing

Fresh roots harvested from both Cd-treated and CK samples at different time points were immediately frozen in liquid nitrogen and stored at −80°C for future analysis. Total RNA was extracted using a Plant RNA Purification Kit (Omega, USA). Subsequently, the quantity and quality of total RNA were assessed using spectrophotometry (NanoDrop 2000, Thermo Scientific) and RNase-free agarose gel electrophoresis, respectively. Briefly, mRNAs were enriched from total RNA using oligo(dT)-rich magnetic beads and randomly fragmented using fragmentation buffer. Then, first-strand cDNAs were synthesized with random hexamer primers and reverse transcriptase using mRNA fragments as templates followed by second-strand cDNA synthesis using dNTPs, RNase H, and DNA polymerase I. The resulting cDNA fragments were purified using a QiaQuick PCR extraction kit (Qiagen, Duesseldorf, Germany), end-repaired, poly(A) tailed, and ligated to Illumina sequencing adapters. The ligation products were size selected via agarose gel electrophoresis, PCR amplified, and sequenced on the Illumina HiSeq™4000 platform by Gene Denovo Biotechnology Co., Ltd. (Guangzhou, China) (Grabherr et al., 2011).

Before assembly, the raw reads were filtered by removing low-quality reads containing more than 40% low-quality bases (Q value ≤ 10 bases), adaptor-contaminated reads, and reads with more than 10% unknown bases. The high-quality clean reads were subsequently *de novo* assembled using the Trinity package to construct unique consensus sequences as reference sequences (Grabherr et al., 2011). The assembled unigenes were aligned using the BLASTx program with an E-value ≤ 10^{-5} to various protein databases, including the Nonredundant Protein Sequence Database (Nr, ftp://ftp.ncbi.nih.gov/blast/db/), Swissprot (http://www.uniprot.org/), Kyoto Encyclopedia of Genes and Genomes (KEGG, http://www.genome.jp/kegg/), Gene Ontology (GO, http://geneontology.org/), and Eukaryotic Ortholog Groups (KOG, http://www.ncbi.nlm.nih.gov/KOG/).

The expression levels of unigenes were calculated using RPKM (Reads Per Kilobase of exon Model per Million mapped reads), based on the number of uniquely mapped reads, to eliminate the influence of unigene length and sequencing discrepancies on the expression calculation. The longest transcript was selected for genes with more than one alternative transcript to calculate the RPKM. The differentially expressed genes (DEGs) between the Cd treatment and CK groups at different time points were identified by the DESeq R package with a false discovery rate (FDR) ≤ 0.05 and a |log2(fold change)| ≥ 1. GO enrichment analysis was implemented to assess the functions of DEGs using the GOseq R package, and GO terms with a corrected p ≤ 0.05 were considered significantly enriched. All RNA-seq read data reported in this study have been deposited in the NCBI under project accession number PRJNA1078221.

2.4.2 Gene expression pattern analysis

Short Time-series Expression Miner (STEM) software was used to cluster all DEGs resulting from pairwise comparisons between the Cd treatment and CK groups at four time points (Ernst and Bar-Joseph, 2006). Only expression profiles with p ≤ 0.05 were considered significant temporal expression profiles. Subsequently, GO enrichment analysis was performed on the major expression profiles.

2.4.3 Gene coexpression network analysis

A coexpression network for genes was constructed using the weighted gene coexpression network analysis (WGCNA, v1.47) package in R (Langfelder and Horvath, 2008). After filtering out genes that were not expressed in more than half of the samples, a

total of 24,689 genes were selected and imported into WGCNA to construct coexpression modules using the automatic network construction function (blockwise modules). The modules were generated with default settings except for adjustments made to the power (set to 7), TOMType (set to unsigned), and minModuleSize (set to 50). To identify biologically significant modules, module eigengenes were used to calculate correlation coefficients with physiological traits. The networks were visualized using Cytoscape_3.9.1.

2.4.4 Quantitative real-time PCR

Twelve DEGs were randomly selected for qRT–PCR assays to validate the RNA sequencing (RNA–seq) results. Primers were designed using the Primer3 website and are listed in Supplementary Table 1. *Actin* was selected as the reference control gene. The PCR system (10 μl) consisted of 1 μl of template cDNA, 0.5 μl of each forward and reverse primer (4 μM), 5 μl of 2× SYBR® Green Supermix, and 3 μl of ddH_2O. The reaction program consisted of an initial denaturation step at 95°C for 3 min followed by 40 cycles of 95°C for 10 s and 60°C for 30 s. Melting curves were generated from 65°C to 95°C with increments of 1°C for 4 s. Three technical replicates were performed for each sample, and transcript levels were calculated using the $2^{-\Delta\Delta CT}$ method. Correlation analysis was conducted between the qPCR and RNA-seq results.

2.5 Metabolomic analysis

2.5.1 Metabolite extraction and liquid chromatography with mass spectrometry metabolome analysis

The samples from the Cd-treated and CK groups at different time points were retrieved from storage at −80°C, vacuum freeze dried, and ground into a powder. For each sample, approximately 100 mg of the ground material was extracted overnight at 4°C with 1.0 ml of 70% methanol containing 0.1 $mg{\cdot}L^{-1}$ lidocaine as the internal standard. After centrifugation at 10,000 × *g* for 10 min at 4°C, the supernatants were collected, filtered, and transferred to an injection bottle for liquid chromatography with tandem mass spectrometry (LC–MS/MS) analysis (UPLC, Shim-pack UFLC Shimadzu CBM20A system, MS/MS, Applied Biosystems 4500 QTRAP). Quality control (QC) samples were prepared by mixing 20 μl from each sample to monitor deviations in the analytical results and ensure system stability throughout the entire experiment. The UPLC conditions, as well as the mass spectrometry parameters, were set up as described previously (Chen et al., 2013).

2.5.2 Metabolomic data analysis

The qualitative analysis of metabolites was performed by referencing existing mass spectrometry databases, including MassBank (http://www.massbank.jp/), HMDB (http://www.hmdb.ca/), MoToDB (http://www.ab.wur.nl/moto/), KNAPSAcK (http://kanaya.naist.jp/KNApSAcK/), METLIN (http://metlin.scripps.edu/index.php), and the commercial database MWDB (MetWare Biological Science and Technology Co., Ltd., Wuhan, China) (Zhu et al., 2018). For the quantitative analysis of metabolites, the multiple reaction monitoring (MRM) mode of triple quadrupole mass spectrometry was used (Chen et al., 2013). After obtaining the metabolite spectra for each sample, the areas of the mass spectrum peaks were integrated, and the mass spectra of the same metabolites in different samples were corrected.

Principal component analysis (PCA) and orthogonal partial least squares discriminant analysis (OPLS-DA) were performed using the R package ropls. The model's stability was assessed through seven cycles of interactive verification. Additionally, Student's t-test was used. Significantly differentially expressed metabolites (DEMs) between the Cd treatment and CK groups were selected based on the variable weight value (VIP) from the OPLS-DA model and the p-value from Student's t-test. The metabolites with VIP > 0.1 and $p < 0.05$ were considered significantly different metabolites (Hu et al., 2020). These DEMs were then subjected to metabolic pathway analysis.

2.6 Integrated analysis of the metabolomic and transcriptomic data

The transcriptome and metabolome data were normalized and subjected to statistical analysis to elucidate the relationships between the genes and metabolites implicated in the Cd stress response. Pearson correlation analysis between DEGs and DEMs was performed using the COR function in R with normalized data. Subsequently, DEGs and DEMs with Pearson correlation coefficient (PCC) thresholds of ≥0.8 or ≤−0.8 were subjected to KEGG analysis.

2.7 Statistical analysis

Statistical analysis was performed using SPSS 20.0 (SPSS Inc., Chicago, IL, USA). Statistical significance was calculated using two- or one-way ANOVA followed by Tukey's multiple comparison test with differences deemed significant at $p < 0.05$. Graphs were generated using GraphPad Prism 9 software (GraphPad Software Inc., La Jolla, CA, USA).

3 Results

3.1 Cd concentrations in different tissues

The present study analyzed the Cd concentrations in the roots, stems, and leaves of *A. manihot* at four different time points following exposure to 100 μM Cd. The results revealed a significant increase in the Cd content in *A. manihot* with increasing duration of Cd exposure (Figure 1). The average Cd

10.3389/fpls.2024.1389207

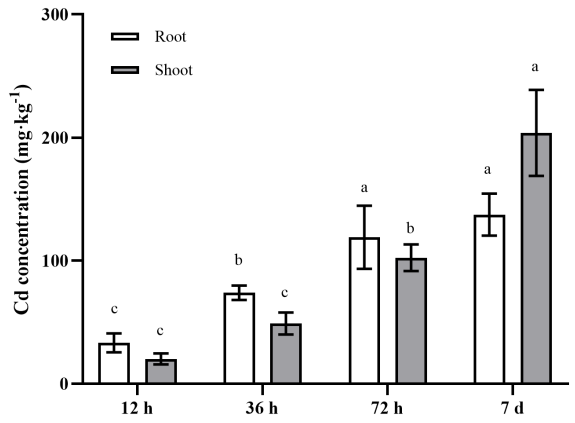

FIGURE 1
Cd concentrations in different tissues of *A. manihot* at 12 h, 36 h, 72 h, and 7 days. Each error bar represents the mean ± SD. Different small letters indicate significant differences at the $p < 0.05$ level among different time points in the same tissue.

concentrations in the roots were 33.21, 73.95, 119.00, and 137.38 $mg{\cdot}kg^{-1}$ at 12 h, 36 h, 72 h, and 7 days after Cd treatment, respectively. Initially, the Cd concentrations in the shoots remained lower than those in the roots at 12–36 h. However, the Cd concentration in the shoots significantly increased to 203.81 $mg{\cdot}kg^{-1}$ at 7 days indicating a 1.48-fold increase over that in the roots. These results verified the high Cd accumulation capability of *A. manihot*, as indicated by a previous study (Wu et al., 2018).

3.2 Effect of Cd stress on physiological characteristics

A. manihot demonstrated strong tolerance to Cd treatment showing no visible phytotoxicity symptoms. To evaluate the response of *A. manihot* roots to Cd stress, several biochemical indices associated with the oxidative stress response were monitored. MDA, one of the final products of cell membrane lipid peroxidation, is recognized as a well-known biomarker for oxidative lipid damage caused by increased ROS under abiotic stress (Wu et al., 2018; Yu et al., 2021). Compared with that in the control plants, the MDA content in the Cd-treated plants significantly increased by 64.0%–104.12% indicating that Cd induced cellular oxidative stress (Figure 2A). Plants respond to oxidative stress by enhancing their antioxidant defense systems (Wu et al., 2018; Zhang et al., 2021). In the roots of *A. manihot*, compared with those in the CK treatment, Cd stress significantly increased the activity of SOD, POD, and CAT by 19.73%–50%, 22.87%–38.89%, and 32.31%–45.40%, respectively, at 12 h, 36 h, 72 h, and 7 days. SOD activity significantly increased under Cd stress, peaking at 36 h, and then gradually decreased (Figure 2B). A similar pattern was observed for POD activity, which peaked at 72 h (Figure 2C). Additionally, the CAT activity in roots increased continuously with the duration of Cd exposure (Figure 2D).

3.3 Transcriptome analysis of *A. manihot* roots under Cd stress

After data filtering, approximately 40.61–66.83 million 150-bp high-quality clean reads were obtained from the RNA-seq data of 24 samples. The clean read Q20 and Q30 values for all test samples were greater than 97.51% and 92.74%, respectively (Supplementary Table S2) demonstrating the high quality of sequencing and the feasibility of subsequent analyses. *De novo* assembly of the clean reads using the Trinity program generated a reference transcriptome comprising 73,122 unigenes, with an average length of 873 bp, a maximum length of 13,204 bp, a minimum length of 201 bp, and an N50 of 1,268 bp. Using the BLASTX tool with a cutoff E-value of 10^{-5}, a total of 56,752 unigenes were functionally annotated (Supplementary Table S3). Based on extensive database searches, *Gossypium hirsutum* (22.47%), *Gossypium arboreum* (22.14%), and *Gossypium raimondii* (21.91%) exhibited high similarity to *A. manihot* (Supplementary Figure S3).

To further evaluate the validity of the RNA-seq data, 12 unigenes were randomly selected for qPCR analysis. The RT-qPCR results for these genes showed similar expression trends to the RNA-seq data (Supplementary Figure S4) indicating the accuracy of the RNA-seq data. Furthermore, a strong positive correlation was observed between the qPCR and RNA-seq data ($r = 0.7581$, $p < 0.001$) (Supplementary Figure S5). These results confirm the validity of RNA-seq and suggest that the RNA-seq data can be reliably used for further analyses.

3.4 Analysis of the DEGs in *A. manihot* at different time points under Cd stress

The DEGs of *A. manihot* were identified by comparing RNA-seq data from Cd-treated root samples with CK samples at the same time points. Comparative DEG analysis revealed a total of 245 DEGs (122 upregulated and 123 downregulated) at 12 h, 5,708 DEGs (629 upregulated and 5,079 downregulated) at 36 h, 9,834 DEGs (3,606 upregulated and 6,228 downregulated) at 72 h, and 2,323 DEGs (647 upregulated and 1,676 downregulated) at 7 days (Figure 3A).

Subsequently, the functions of the DEGs were classified according to GO classifications. The downregulated DEGs were predominantly associated with "structural molecule activity" in the molecular function category, "intracellular ribonucleoprotein complex" and "ribonucleoprotein complex" in the cellular component category, and "phenylpropanoid metabolic process," "lignin metabolic process," and "cell wall organization or biogenesis" in the biological process category (Figure 3B, Supplementary Table S4). These results suggest that Cd stress impacts the cell wall organization or biogenesis of *A. manihot*. In addition, the upregulated DEGs were significantly enriched in molecular function categories, such as "tetrapyrrole binding," "catalytic activity," and "oxidoreductase activity," while the

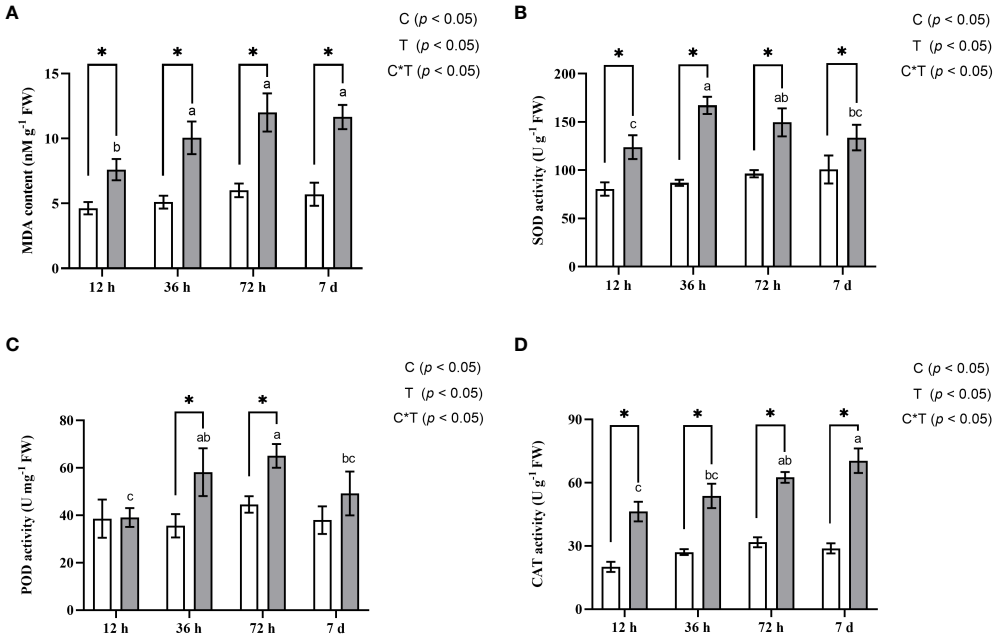

FIGURE 2
Effects of Cd stress on the content of MDA **(A)** and the activities of SOD **(B)**, POD **(C)**, and CAT **(D)** in the roots of *A. manihot* at four time points. The white columns represent the CK group, and the gray columns represent the Cd treatment group. Each error bar represents the mean ± SD. Different lowercase letters denote statistically significant differences among the various Cd stress durations (Duncan's test, $p < 0.05$). The symbol "*" indicates a significant difference (t-test, $p < 0.05$) between the Cd and CK treatments at the corresponding sampling time. Two-way ANOVA results for treatment (T) and treatment time (T) are shown in the insets.

cellular component category was dominated by "intracellular ribonucleoprotein complex," "ribonucleoprotein complex," and "ribosome." In addition, the biological process category was the most enriched in "defense response," "metabolic process," and "salicylic acid-mediated signaling pathway" (Figure 3B, Supplementary Table S4). These results indicate that *A. manihot* can enhance catalytic activity and tetrapyrrole binding and activate defense mechanisms and salicylic acid-mediated signaling pathways to achieve stable Cd detoxification or improve Cd tolerance (Yan et al., 2020).

3.5 Temporal trends in DEGs responding to Cd stress

To analyze the temporal expression patterns of Cd-responsive genes, STEM analysis was employed to cluster DEGs with similar expression patterns (Supplementary Figure S6). In the STEM analysis, profiles 1, 5, 7, 8, and 11 with $p < 0.05$ were considered significant profiles (Figure 4A). Subsequently, GO enrichment analysis of the DEGs within these significant profiles was performed to elucidate the functional significance of the transcriptional changes induced by Cd stress (Figure 4B). In profiles 1 and 7, genes associated with cell wall biosynthetic and metabolic pathways were particularly enriched, including "glucuronoxylan metabolic process," "xylan metabolic process," "lignin metabolic process," "phenylpropanoid metabolic process," and "polysaccharide catabolic process." Gene expression in profile 7 decreased after 36 h, whereas in profile 1, there was a decrease in gene expression from 12 to 72 h, which subsequently increased after 72 h. Profiles 5 and 8 also shared a similar expression pattern to profile 1, where genes were primarily associated with energy and substance metabolism. Profile 5, enriched in GO terms related to "glycerol-3-phosphate metabolic process," showed a decrease in gene expression levels from 12 to 36 h followed by an increase thereafter. Profile 8, enriched in GO terms, such as "ATP biosynthetic process," "purine nucleoside triphosphate biosynthetic process," and "purine ribonucleoside triphosphate biosynthetic process," demonstrated a decrease in gene expression from 36 to 72 h but an increase afterward. In contrast, profile 11 exhibited genes that were upregulated between 36 and 72 h and subsequently downregulated after 72 h. The enriched pathways represented in this profile included "lipid homeostasis," "acylglycerol homeostasis," "response to toxic substances," and "response to zinc ion" (Figure 4B).

3.6 Coexpression network analysis and identification of hub genes related to the response to Cd stress

WGCNA was used to investigate various physiological parameters and key genes involved in Cd detoxification and accumulation in *A. manihot*. This analysis identified 17 modules with an unsigned TOM through the dynamic tree cutting (Supplementary Figure S7). Notably, the purple module exhibited significant positive correlations with Cd accumulation in both roots ($r = 0.77$, $p < 0.05$) and shoots ($r = 0.74$, $p < 0.05$), as did MDA ($r =$

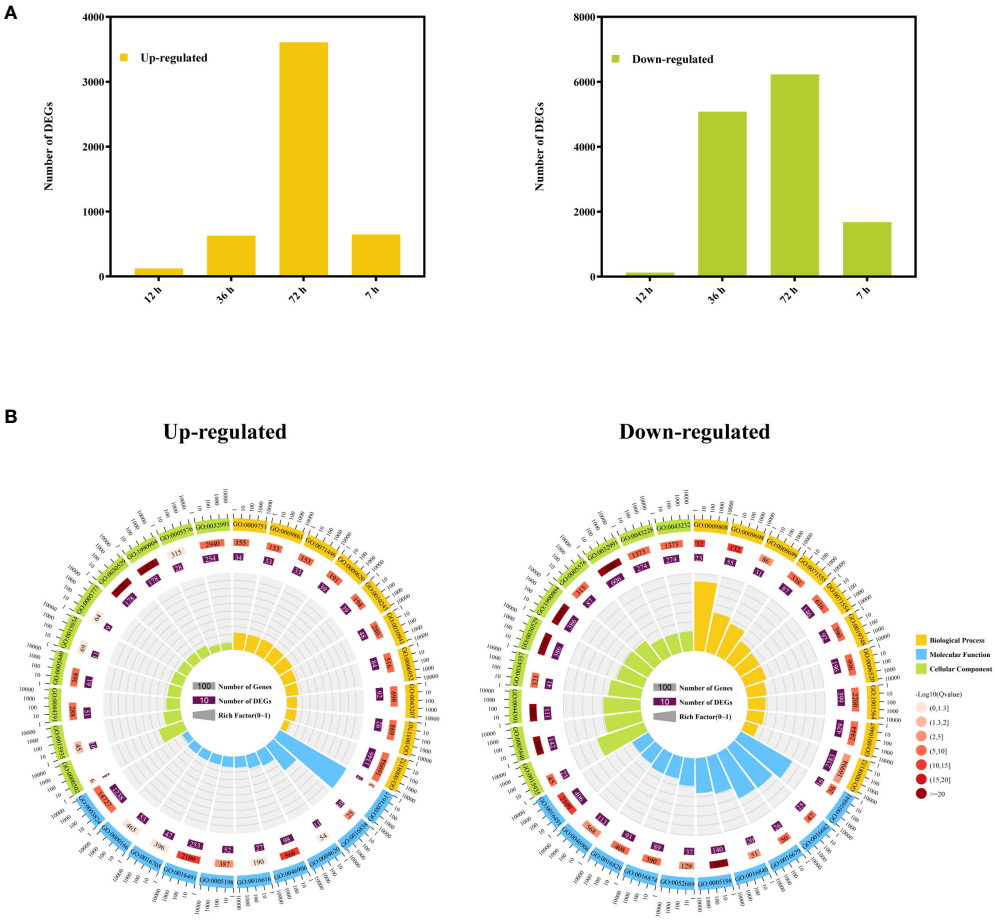

FIGURE 3
Cd-responsive differentially expressed genes at different time points. **(A)** The numbers of Cd-responsive DEGs in the roots of *A. manihot* at four time points. **(B)** GO enrichment circle diagram of upregulated and downregulated DEGs. The first 10 enrichment cycles of GO terms are depicted, and the number of genes is presented outside the circle on a logarithmic scale. Different colors represent different GO domains. The second circle displays the number of genes enriched in each GO term along with the Q value. The length of the bar corresponds to the number of genes, with a shorter bar and a redder color indicating a lower Q value. The third circle represents the number of DEGs enriched in each GO term. The fourth circle shows the enrichment factor value for each GO term, with each grid line representing 0.1 in the background.

0.67, $p < 0.05$), POD ($r = 0.50$, $p < 0.05$), and CAT ($r = 0.71$, $p < 0.05$) (Figure 5A). We speculated that genes in the purple module were associated with enhanced resistance and Cd accumulation in *A. manihot*. Therefore, the purple module was selected for further analysis.

There were 577 genes in the purple module. Based on the gene expression heatmaps and eigengene histograms, the genes within the purple module were upregulated at 72 h and 7 days following Cd treatment (Figure 5B). Among them, 321 and 85 genes in the purple module were differentially expressed at 72 h and 7 days, respectively (Figure 5C). Subsequently, KEGG pathway analysis was conducted on the overlapping DEGs (344 genes in total). The overlapping DEGs predominantly mapped to pathways, such as "phenylpropanoid biosynthesis," "glutathione metabolism," "vitamin B6 metabolism," and various lipid metabolism-related pathways, including "glycerolipid metabolism," "glycerophospholipid metabolism," "fatty acid elongation," and "linoleic acid metabolism" (Figure 5D).

In the purple module, the eight genes with the most connections in the network were considered hub genes (Figure 5E, Supplementary Table S5). Among these genes, four hub genes were involved in the phenylpropanoid biosynthesis pathway, including three *POD* homologs (*Unigene0046043*, *Unigene0046044*, and *Unigene0010159*) and a *coniferyl-aldehyde dehydrogenase* (*REF1*) homolog (*Unigene0006924*). Additionally, *Unigene0053629* is a homolog of the ethylene-responsive transcription factor ERF98, which belongs to the AP2/ERF transcription factor family. Other hub genes included an ABC transporter homolog (*Unigene0055296*), a cytochrome P450 CYP82D47 homolog (*Unigene0041804*), and a RING-H2 finger protein ATL3 homolog (*Unigene0035257*). Taken together, these core physiological processes and the hub genes that regulate them may be involved in the regulation of *A. manihot*'s response to Cd in terms of uptake, translocation, and detoxification.

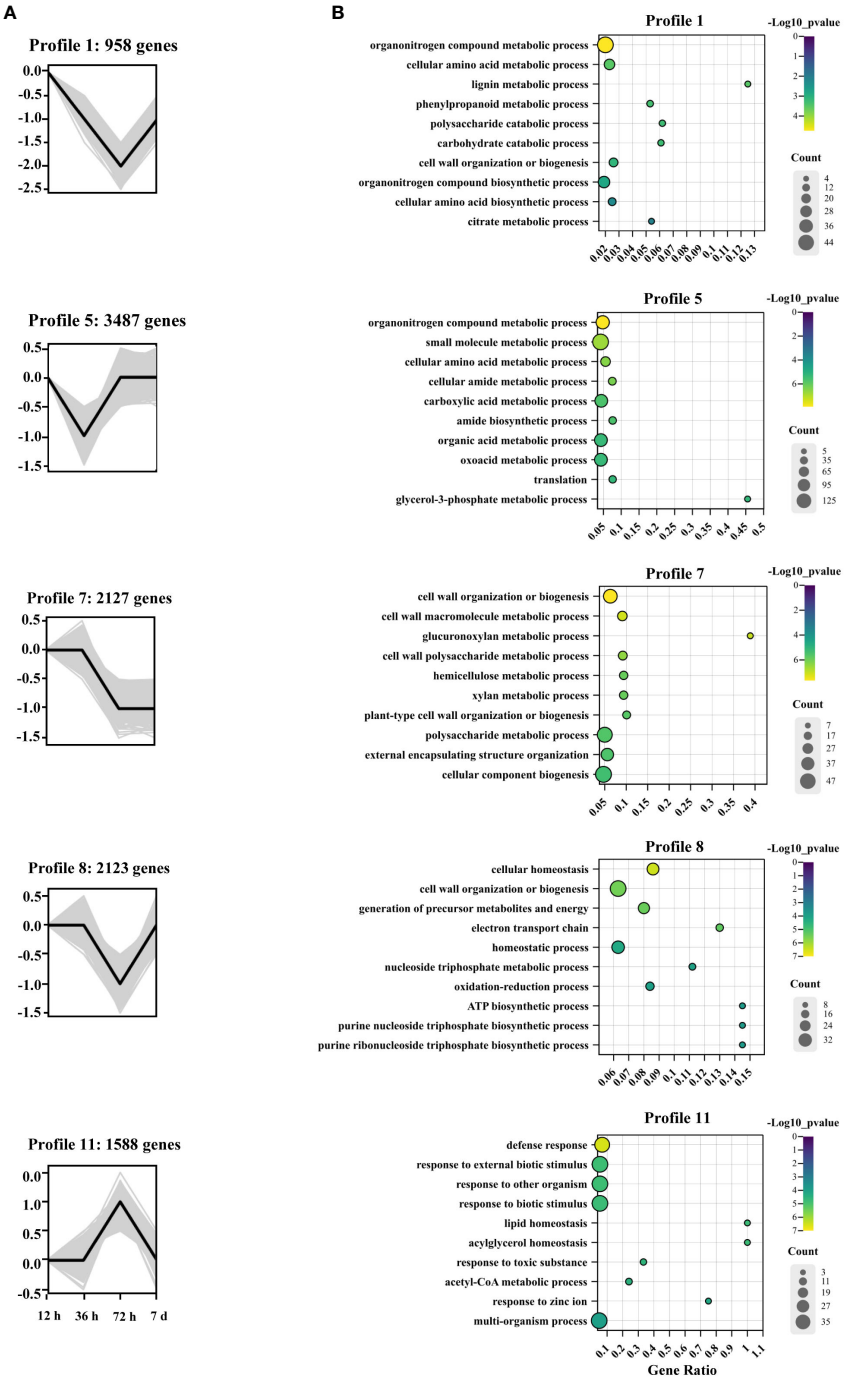

FIGURE 4
Patterns of gene expression and GO enrichment across four time points in the roots of *A. manihot*. **(A)** Expression profiles of five significant DEGs ($p < 0.05$). In each frame, the black lines represent the expression tendencies of genes. The number of genes belonging to each pattern is labeled above the frame. **(B)** GO enrichment analysis of significant gene expression profiles. The GO analysis diagram was generated using ChiPlot (https://www.chiplot.online/). The significance of the most represented GO-slims in each profile is indicated by the p-value. The top 10 significant pathways according to the biological process results are displayed.

3.7 Effects of Cd stress on root metabolism in *A. manihot*

To investigate the simultaneous changes in the metabolome and identify the metabolic adaptations of *A. manihot* to Cd stress, a broadly targeted metabolomic analysis of its roots was performed. Using an LC-MS/MS-based widely targeted metabolomics approach, we detected a total of 722 metabolites (Supplementary Table S6). Multivariate PCA and OPLS-DA were subsequently applied to identify differentially abundant metabolites across various time points. The PCA results showed that biological repeat samples within each group clustered together

10.3389/fpls.2024.1389207

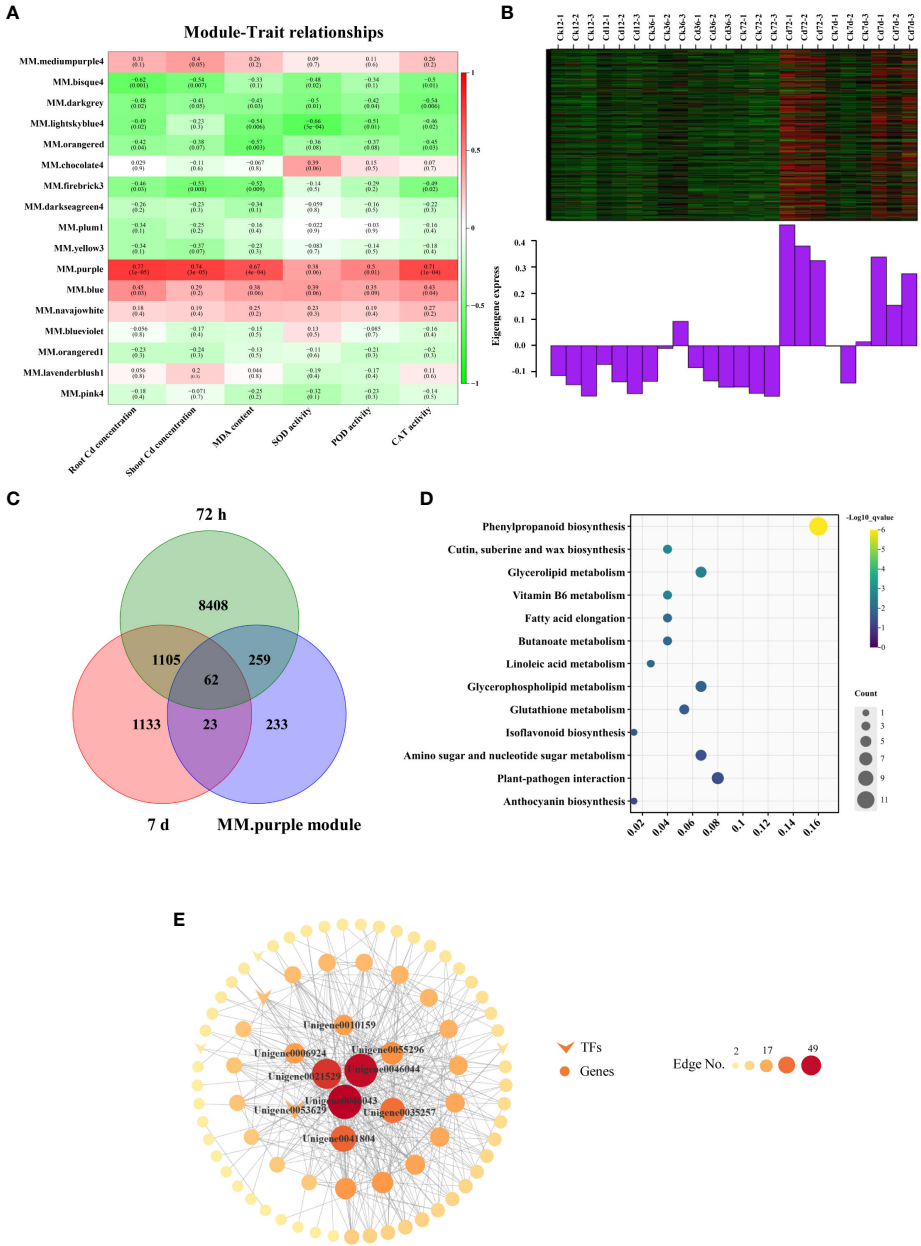

FIGURE 5
Module–trait relationships based on WGCNA. **(A)** Heatmap of the correlation coefficients between WGCNA modules and traits. Each row represents a specific module, and each column represents a trait. The numbers in each cell indicate the correlation coefficients and the corresponding p-values (in parentheses). **(B)** Gene coexpression heatmap for the purple module (upper panel) and the expression level of the corresponding eigengene in each sample (lower panel). **(C)** Common genes between DEGs (72 h and 7 days) and the purple module. **(D)** KEGG analyses of the overlapping DEGs. **(E)** The correlation network of the purple module. Genes with edge weights >0.17 were visualized by Cytoscape. The size and color of each node represent the number of connections.

demonstrating the stability and reliability of the sequencing results and confirming good reproducibility among samples in each group (Figure 6A). Notably, as the duration of Cd exposure increased, distinct differences emerged among the samples. According to predefined criteria, a total of 66 (20 upregulated, 46 downregulated), 62 (16 upregulated, 46 downregulated), 156 (89 upregulated, 67 downregulated), and 90 (55 upregulated, 35 downregulated) DEMs were identified at 12 h, 36 h, 72 h, and 7 days, respectively (Figure 6B). These findings highlight the differences in metabolic responses at various stages of Cd stress, suggesting the occurrence of adaptive metabolic adjustments in *A. manihot* as the stress progresses.

Among the identified DEMs, six metabolites consistently appeared across all time points, including D-pipecolinic acid, adenosine O-ribose, melatonin, N,N-didesvenlafaxine, LysoPE 18:3, and LysoPE 18:1 (Figure 6C). The upregulated DEMs were categorized into 12 major groups, predominantly including alkaloids, lipids, flavonoids, phenolic acids, organic acids, amino

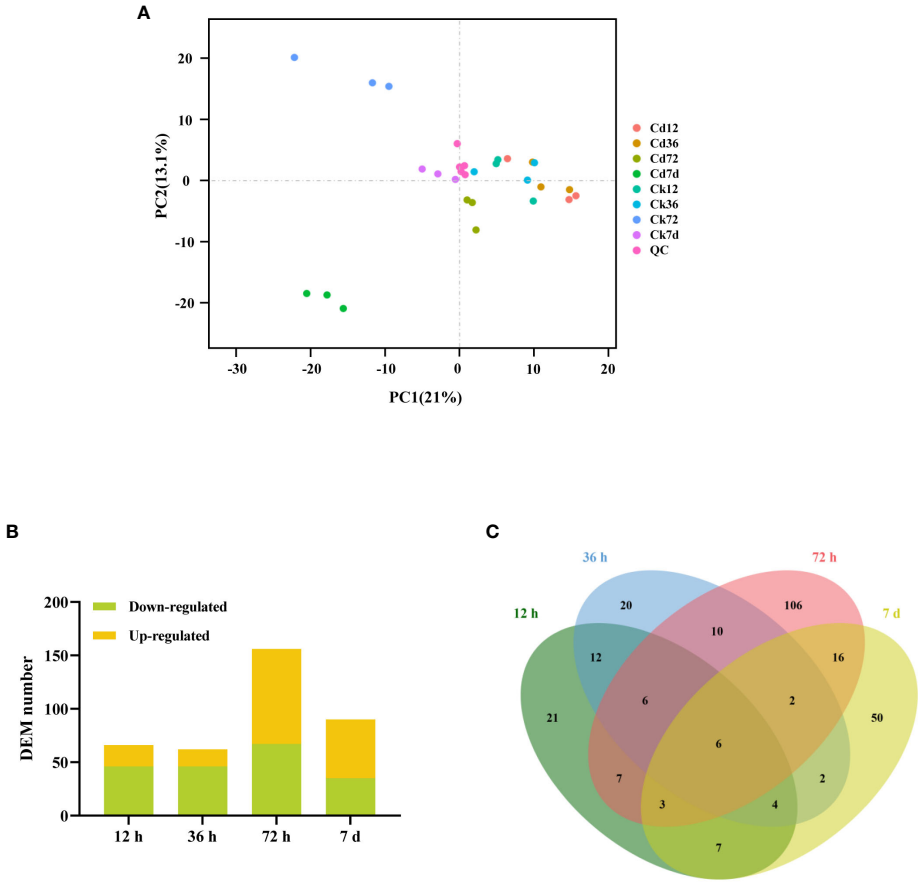

FIGURE 6
Metabolite accumulation in *A. manihot* roots at different time points under Cd stress. **(A)** PCA score plot based on metabolome data, with PC1 and PC2 plotted on the x- and y-axes, respectively. Quality control (QC) samples, prepared from a mixture of sample extracts, were used to ensure the reproducibility of measurements under the same treatment method. **(B)** Total numbers of up- and downregulated DEMs at different time points. **(C)** Venn diagram comparing the DEM numbers in pairwise groups.

acids, and nucleotide and its derivatives (Supplementary Table S7). Furthermore, the analysis revealed the participation of several phytohormones, including abscisic acid and gibberellin, in the plant's adaptive response to Cd stress (Supplementary Table S7, Supplementary Figure S8). Further analysis through KEGG pathway analysis of these upregulated DEMs highlighted their involvement in fatty acid-related pathways such as "linoleic acid metabolism," "α-linolenic acid metabolism," "fatty acid biosynthesis," and "fatty acid degradation" (Supplementary Figure S8).

3.8 Integrated analysis of metabolomic and transcriptomic data

To gain further insight into the potential regulatory mechanisms influenced by Cd stress, we conducted an integrated analysis of the metabolome and transcriptome data from the roots of *A. manihot*. KEGG enrichment analysis of correlated DEGs and DEMs revealed that phenylpropanoid biosynthesis was significantly enriched in both the metabolome and transcriptome datasets across the four time points (Figure 7, Supplementary Table S8). Furthermore, lipid metabolism-related pathways, which were enriched at all four time points, exhibited temporal differences. In summary, the analysis of metabolome and transcriptome data identified lipid metabolism, especially α-linolenic acid metabolism, and phenylpropanoid biosynthesis as key metabolic pathways involved in the response of *A. manihot* to Cd stress. Hence, a detailed analysis of the lipid metabolism and phenylpropanoid biosynthesis pathways was conducted (Figures 8, 9).

In the lipid metabolism pathway, significant variations in the levels of lysophospholipids, including lysophosphatidylcholines (LysoPCs), lysophosphatidylethanolamines (LysoPEs), and lysophosphatidylserines (LysoPSs), were observed. At 12 h, there were significant increases in the levels of lysoPC C16:0 (2) and C18:3 (2). Interestingly, most lysoPEs showed significant decreases relative to the controls, except for lysoPE 18:0 (2), which increased at 72 h. Furthermore, *phospholipase A* (*PLA*), a crucial gene involved in the metabolism of fatty acids and lysophospholipids, was significantly downregulated at 36 h and subsequently upregulated at 72 h. At common time points, significant upregulation of metabolites, such as 13-hydroperoxyoctadecatrienoic acid (13-HPOTrE), 9-hydroxy-10E,12Z,15Z-octadecatrienoic acid (9-HOTrE), and stearidonic acid in α-linolenic acid metabolism, was also observed under Cd stress.

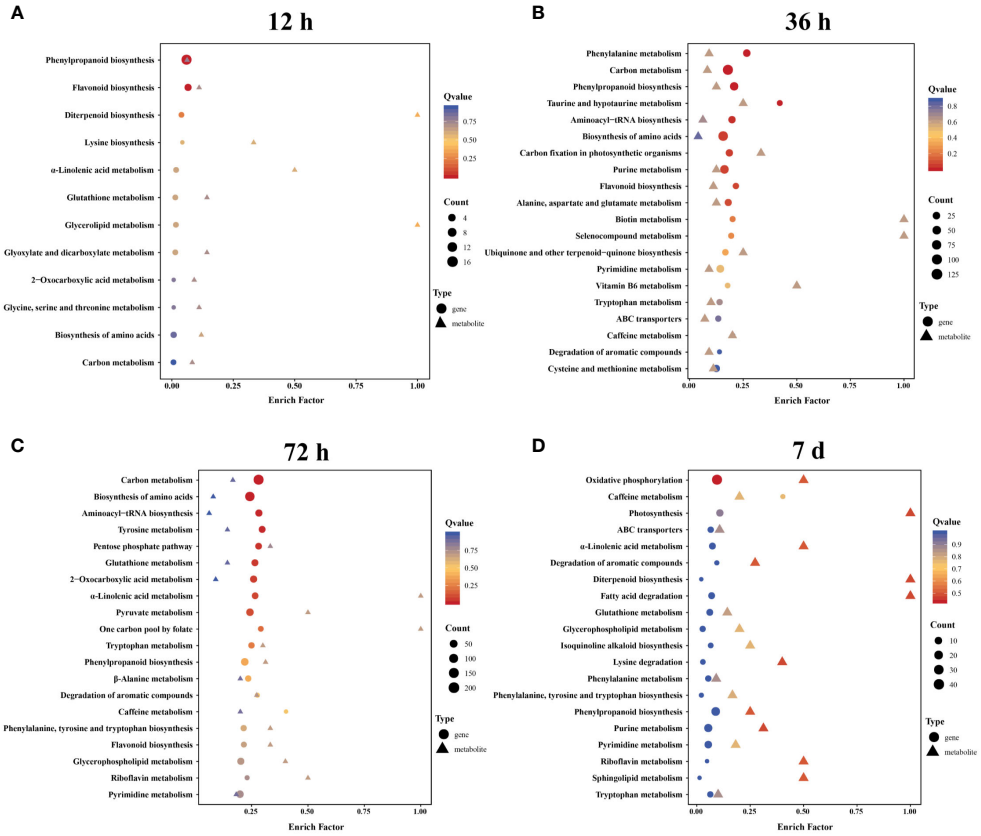

FIGURE 7
The KEGG enrichment pathways that integrate metabolomic and transcriptomic data at 12 h **(A)**, 36 h **(B)**, 72 h **(C)**, and 7 days **(D)**. The color gradient from red to yellow to blue represents the significance of enrichment, which changes from high to medium to low, as indicated by the Q value.

Consistent with these findings, the reaction products of upstream genes, including *fatty acid desaturase* (*FAD*) and *lipoxygenase* (*LOX*), were significantly upregulated at 72 h in response to Cd stress.

13-HPOTrE serves as the key intermediate in the biosynthesis pathway of jasmonic acid (JA) from the α-linolenic acid metabolic pathway (Feussner and Wasternack, 2002). The sustained upregulation of 13-HPOTrE suggested that the synthesis of JA from α-linolenic acid is strongly induced by Cd stress. Moreover, the expression levels of several JA pathway-related structural genes, including *allene oxide synthase* (*AOS*) and *12-oxophytodienoate reductase* (*OPR*), and β-oxidation-related genes, such as *acyl-CoA oxidase* (*ACX*), *enoyl-CoA hydratase/3-hydroxyacyl-CoA dehydrogenase* (*MFP2*), and *acetyl-CoA acyltransferase* (*ACAA1*), were upregulated at 72 h. These results provide further evidence that the synthesis of JA was strongly induced by Cd stress.

In the phenylpropanoid biosynthesis pathway, Cd stress triggered the upregulation of *phenylalanine ammonia lyase* (*PAL*), *cinnamate 4-hydroxylase* (*C4H*), *caffeic acid O-methyltransferase* (*COMT*), *ferulate 5-hydroxylase* (*F5H*), *4-coumarate-CoA ligase* (*4CL*), and *POD* expression at 72 h or 7 days. This resulted in marked increases in the production of p-coumaric acid, trans-cinnamic acid, ferulic acid, and sinapic acid. In addition, REF1 exhibited upregulated expression at 72 h and 7 days. Concurrently, there were significant decreases in the concentrations of three primary monolignols: sinapyl alcohol, *p*-coumaryl alcohol, and coniferyl alcohol. Given the critical role of POD in the final steps of phenylpropanoid biosynthesis, particularly in lignin polymerization through the oxidation of monolignols, the reductions in these precursors coupled with the upregulation of POD may lead to an increase in lignin content.

4 Discussion

Cd, a deleterious nonessential element, has negative effects on plant growth and development (Asgari Lajayer et al., 2017; Haider et al., 2021; Khalid et al., 2022). Despite their high Cd accumulation capacity, many hyperaccumulators exhibit slow growth and low biomass, which limits their effectiveness in remediation (Yan et al., 2020; Wang et al., 2022). Our previous study revealed that concentrations of Cd below 100 $mg{\cdot}kg^{-1}$ stimulate the growth of *A. manihot* in Cd-polluted soil while maintaining a high translocation factor (Wu et al., 2018). Similarly, in this study, *A. manihot* demonstrated the ability to accumulate high amounts of Cd in aboveground tissues without exhibiting obvious physiological toxicity when exposed to 100 μM Cd. Furthermore, Cd accumulation in the roots and shoots of *A. manihot* significantly increased as the duration of Cd stress increased (Figure 1). Given its ability to hyperaccumulate Cd, *A. manihot* has significant application prospects. Therefore, further investigations are

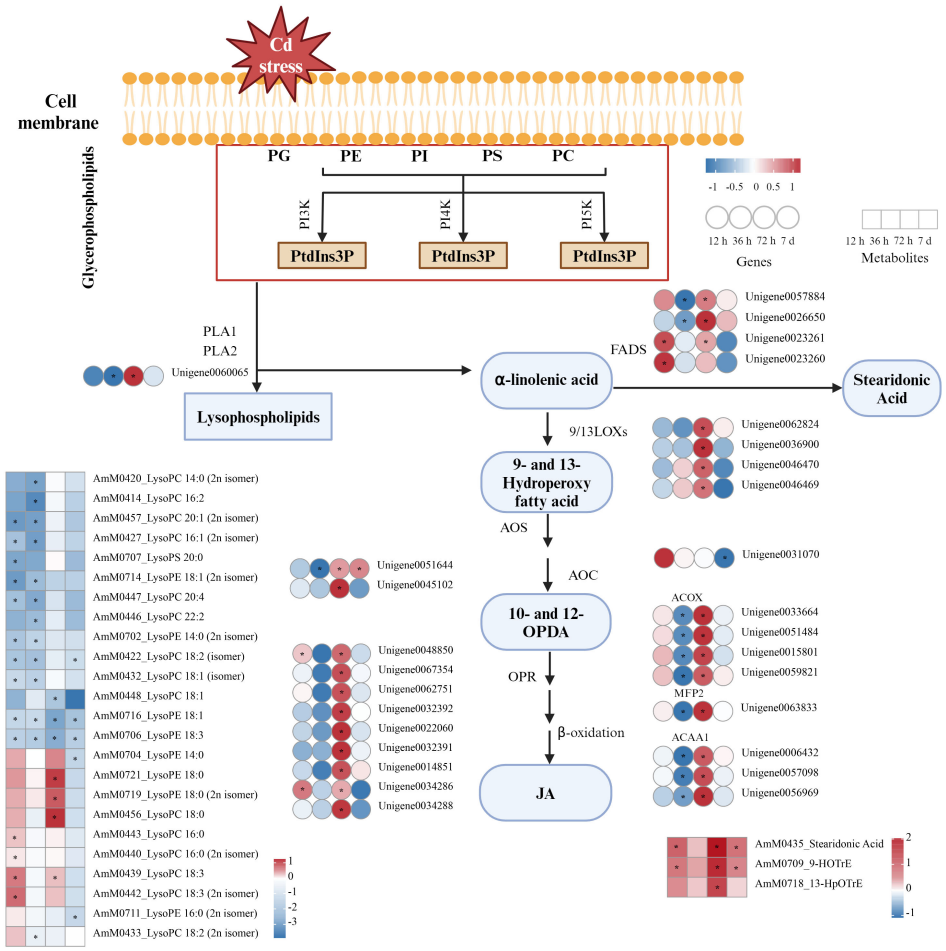

FIGURE 8
DEGs and DEMs associated with lipid metabolism pathways in *A. manihot* roots in response to Cd stress. The heatmap was constructed using Log_2FC values. An asterisk "*" denotes a significant difference between the Cd treatment group and the control group ($p < 0.05$). Different colors represent differential expression, with red indicating high expression and green indicating low expression. PC, phosphatidylcholine; PE, phosphatidylethanolamine; PG, phosphatidylglycerol; PI, phosphatidylinositol; PS, phosphatidylserine; PI3K, PI4K, PI5K, phosphatidylinositol 3-kinase, 4-kinase, and 5-kinase, respectively; PtdIns3P, PtdIns4P, and PtdIns5P, phosphatidylinositol 3-phosphate, 4-phosphate, and 5-phosphate, respectively; PLA, phospholipase A; LOX, lipoxygenase; AOS, allene oxide synthase; AOC, allene oxide cyclase; FAD, fatty acid desaturase; OPR, 12-oxophytodienoate reductase; ACX, acyl-CoA oxidase; MFP2, enoyl-CoA hydratase/3-hydroxyacyl-CoA dehydrogenase; ACCA1, acetyl-CoA acyltransferase; JA, jasmonic acid; 10-OPDA, 10-oxo-11,15-phytodienoic acid; 12-OPDA, 12-oxo-10,15-phytodienoic acid.

necessary to explore the mechanisms underlying the response to Cd stress in *A. manihot*.

4.1 Antioxidant enzymes alleviate the toxicity of Cd in *A. manihot*

Exposure to Cd disturbs the redox homeostasis of plants, leading to pronounced increases in ROS production and lipid peroxidation, consequently triggering oxidative stress (Asgari Lajayer et al., 2017; Haider et al., 2021). In response to Cd stress, physiological traits, which are pivotal for plant survival and adaptation under challenging conditions, play significant roles in orchestrating defense strategies (Pan et al., 2021; Xu et al., 2022). A noteworthy example of such physiological responses is the activation and regulation of antioxidant enzymes under Cd stress, which play essential roles in restoring cellular functions and maintaining homeostasis (Yu et al., 2021; Liu et al., 2023). Our findings indicate that Cd stress induced a significant increase in the content of the lipid peroxidation product MDA suggesting increased lipid oxidative damage in plant cells (Figure 2A). Moreover, exposure to Cd stress significantly elevated the activity of antioxidant enzymes (SOD, POD, and CAT) in *A. manihot* roots in this study (Figures 2B–D), consistent with findings in Cd hyperaccumulators such as *Youngia japonica* (Yu et al., 2021), *Pterocypsela laciniata* (Zhong et al., 2019), and *Arabis paniculate* (Liu et al., 2023). Among these enzymes, POD plays pivotal roles in regulating diverse plant physiological processes under Cd stress (Rui et al., 2016; Loix et al., 2017). In the roots of *A. manihot*, there was no significant difference in POD activity compared to that in the CK group at 12 h, but a significant increase was observed thereafter (Figure 2C). This finding aligns with previous research suggesting that POD becomes particularly important in the later stages of exposure to Cd toxicity (Yang et al., 2007; Rui et al., 2016).

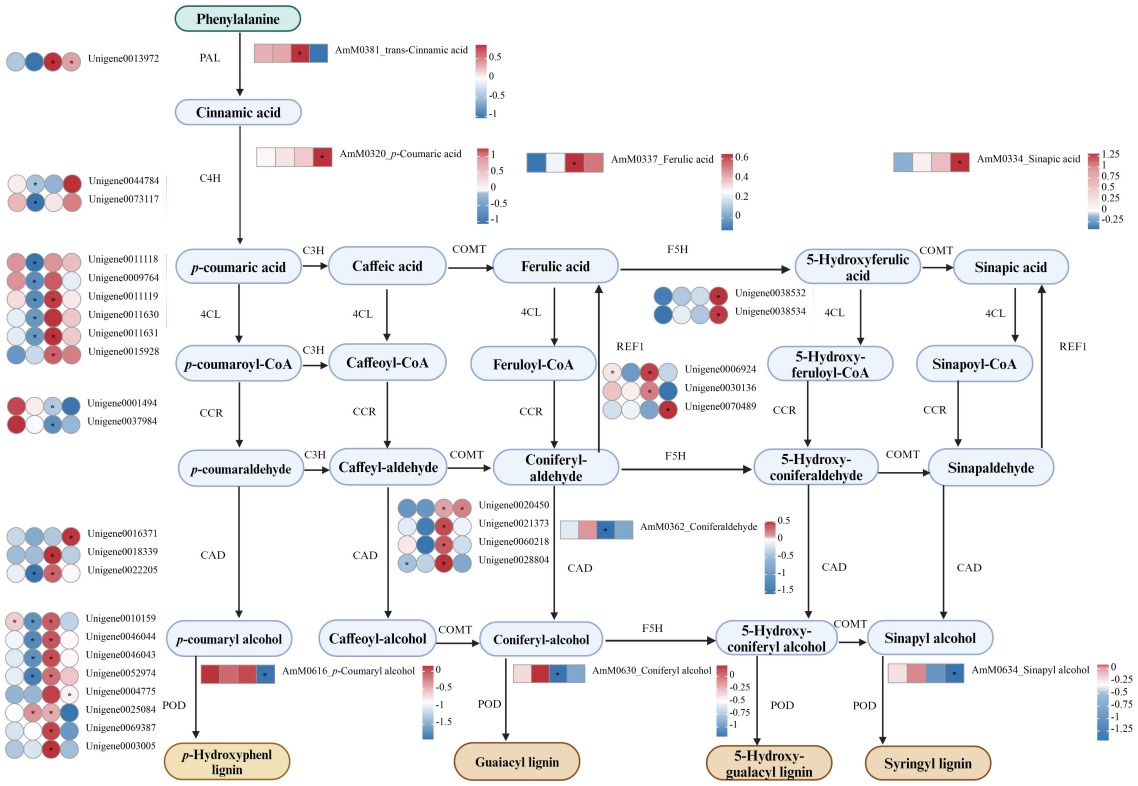

FIGURE 9
DEGs and DEMs involved in phenylpropanoid biosynthesis pathways in *A. manihot* roots in response to Cd stress. The heatmap was constructed using Log_2FC values. An asterisk "*" denotes a significant difference between the Cd treatment group and the control group ($p < 0.05$). Different colors represent differential expression, with red indicating high expression and green indicating low expression. PAL, phenylalanine ammonia lyase; C4H, cinnamate 4-hydroxylase; COMT caffeic acid O-methyltransferase; F5H ferulate 5-hydroxylase; 4CL, 4-coumarate-CoA ligase; C3H, *p*-coumarate 3-hydroxylase; POD, peroxidase; REF1, coniferyl-aldehyde dehydrogenase.

4.2 *A. manihot* copes with Cd stress by adjusting gene expression

In this study, transcriptome analysis revealed significant changes in the transcripts of *A. manihot* roots from 12 h to 7 days under Cd stress. At the initial stage of Cd stress, only a limited number of genes exhibited differential regulation. Notably, the transcript-level responses of *A. manihot* to Cd stress became more pronounced during the medium term (36–72 h) (Figure 3A). Moreover, more downregulated DEGs were identified in *A. manihot* roots than upregulated DEGs under Cd stress at different time points (Figures 3A and 6B). These downregulated DEGs were mainly enriched in metabolic pathways related to cell wall organization or biogenesis (Figure 3B, Supplementary Table S4). Interestingly, DEGs involved in secondary cell wall synthesis exhibited diverse temporal expression patterns in response to Cd stress. For example, DEGs related to hemicelluloses, such as xylan and glucuronoxylan, decreased after 36 h, while those linked to lignin metabolic processes declined continuously from 12 to 72 h before increasing thereafter (Figure 4). The cell wall is a dynamic structure whose composition rapidly changes in response to Cd stress (Loix et al., 2017). In general, elevated levels of polysaccharide components result in greater accumulation of metal ions within the cell wall, thereby impeding their entry into the protoplast (Guo et al., 2021; Wang et al., 2022). This serves as a significant defense mechanism against trace metal stress across many plant species. However, studies on hyperaccumulators have revealed that the fixation of metal ions by root cell walls is less stable than that in non-hyperaccumulator plants potentially leading to the transportation of metal ions to the shoots (Loix et al., 2017; Guo et al., 2020). For example, the Cd non-hyperaccumulating ecotype of *S. alfredii* exhibits abundant functional groups and xyloglucan in hemicellulose resulting in tighter Cd binding within the root cell wall. Conversely, the Cd-hyperaccumulating ecotype of *S. alfredii* shows lower levels of hemicellulose-bound Cd, which allows easier transport into the shoot (Guo et al., 2020). Therefore, during a period of Cd exposure, the dynamic inhibition of the secondary cell wall in *A. manihot* may facilitate the upward transport of Cd ions.

Similarly, we found that other metabolic processes were also dynamically regulated under Cd stress in *A. manihot*. For example, during the middle of Cd exposure, the STEM analysis revealed initial increases followed by decreases in the expression levels of DEGs related to lipid and acylglycerol homeostasis, while DEGs in pathways involved in ATP synthesis exhibited decreased expression followed by increased expression (Figure 4). Lipid homeostasis involves a balance between the accumulation of membrane lipids and the accumulation of storage lipids such as triacylglycerol.

Previous studies have demonstrated that lipid homeostasis is known to exert systemic effects capable of influencing plant survival, growth, and development during stress (Boutté and Jaillais, 2020). In *A. manihot*, the dynamic control of lipid homeostasis responds to disruptions in lipid metabolism induced by Cd stress. Taken together, these findings demonstrate that Cd stress dynamically affects the gene expression of *A. manihot* in a temporally specific manner.

We utilized physiological indicators as trait files to conduct further analysis of these DEGs. By performing WGCNA, we identified eight hub genes that likely play key roles in Cd stress responses (Figure 5, Supplementary Table S5). Interestingly, among these hub genes, four were homologous genes related to lignin biosynthesis, including three *POD* genes and one *REF1* homolog. In terms of the antioxidant system, POD assists plants in coping with the excess H_2O_2 induced by Cd exposure. In addition to its role in redox homeostasis, this enzyme family participates in various cellular processes, including cell wall loosening, cross-linking, and lignification (Rui et al., 2016; Loix et al., 2017). *POD* is involved in a complex redox network in *A. manihot* playing a regulatory role in response to Cd in terms of accumulation and detoxification. Furthermore, a crucial transcription factor has been identified. *ERF98*, an ethylene response factor, serves as a central regulatory hub in plant responses to abiotic stresses (Wu et al., 2022). Among the identified hub genes, we also identified a homolog of an ABC transporter, a homolog of cytochrome P450 CYP82D47, and a homolog of the RING-H2 finger protein ATL3. ABC transporters, a significant portion of the membrane protein family, play vital roles in the transport and detoxification of heavy metals. In *Arabidopsis*, *AtABCC3* acts as a transporter for PC–Cd complexes influencing Cd accumulation and tolerance (Brunetti et al., 2015). Similarly, *OsABCG36* is activated under heavy metal stress serving as one of the root hub genes responsible for exporting Cd or Cd conjugates, thereby increasing Cd tolerance in *Oryza sativa* (Fu et al., 2019).

4.3 Metabolite expression in *A. manihot* is affected by Cd stress

Metabolites represent the biochemical end products of gene activity reflecting the adaptability of organisms (Wu et al., 2023). In this study, we observed a trend of increasing changes in the number of DEMs with prolonged Cd stress peaking at 72 h before decreasing thereafter. (Figure 6B). The upregulated DEMs were predominantly composed of alkaloids, lipids, flavonoids, phenolic acids, organic acids, amino acids, nucleotides, and their derivatives (Supplementary Table S7). Interestingly, at the early stage of Cd stress, there was a significant increase in the level of abscisic acid potentially triggering intricate stress-adaptive signaling cascades (Shen et al., 2022). Additionally, melatonin was significantly upregulated at all time points (Figure 6C) consistent with previous findings (Ahammed et al., 2024). Remarkably, exogenous melatonin application has been demonstrated to enhance Cd tolerance in *Solanum lycopersicum* through increased antioxidant potential and phytochelatin biosynthesis (Hasan et al., 2015). Therefore, the sustained increase in melatonin levels may have contributed to the enhanced tolerance of *A. manihot* to Cd stress. Subsequently, KEGG analysis of the metabolome revealed that the response of *A. manihot* to Cd stress involves various metabolic pathways at different stages (Supplementary Figure S8). These upregulated DEMs were mainly enriched in fatty acid-related pathways indicating the importance of fatty acid metabolism in the response of *A. manihot* to Cd stress.

4.4 Involvement of lipid metabolism in the adaptive regulation of *A. manihot* under Cd stress

In this study, analysis of time-course metabolome and transcriptome data, along with their integrated results, revealed the crucial role of lipid metabolism-related pathways in the defense response of *A. manihot* to Cd stress (Figures 4, 5, 7, and S8). Similarly, a study on *Tamarix hispida* reported that lipid synthesis and metabolism play key roles in enhancing Cd tolerance (Xie et al., 2023). Lipids, which are fundamental components of plant cell biofilms, participate in a wide range of biological processes, including growth, development, and stress responses (Hou et al., 2016; Hu et al., 2023; Liang et al., 2023). Furthermore, accumulating evidence suggests a role for lipid molecules, such as lysophospholipids, fatty acids, and phosphatidic acid, in plant signaling processes (Liang et al., 2023).

In this study, the levels of various types of lysophospholipids exhibited diverse patterns of change (Figure 8). LysoPCs [C16:0 (2) and C18:3 (2)] significantly increased under Cd exposure at 12 h. LysoPCs are typically present in trace quantities in plant tissues, but their levels substantially increase under abiotic or biotic stress conditions (Okazaki and Saito, 2014). Previously, it was reported that the amounts of lysoPCs (C14:0, C15:0, C16, C17:1, and C18:3) significantly increased under cold stress (Sun et al., 2021). At an early stage, the increased generation of lysoPCs in *A. manihot* roots may mediate signaling cascades leading to alterations in gene expression during Cd stress responses (Cappa and Pilon-Smits, 2014). Interestingly, the majority of the detected LysoPEs, specifically LysoPE 18:3 and LysoPE 18:1, decreased consistently at all treatment time points. This result is consistent with findings on *T. hispida* under Cd stress (Xie et al., 2023). However, there have been few reports regarding the functions of lysophospholipids in response to Cd stress in higher plants.

In addition, we observed that with continuous Cd stimulation, the gene expression of *PLA* was initially downregulated at 36 h followed by upregulation at 72 h (Figure 8). PLA is critically important because it hydrolyzes the sn-1 and sn-2 positions of glycerophospholipids to produce lysophospholipids and free fatty acids (Hou et al., 2016). Previous studies have indicated a strong correlation between PLA and plant stress defense through its roles in the biosynthesis of JA and oxylipins, as well as the activation of downstream defense (Hou et al., 2016; Hu et al., 2023; Liang et al., 2023). Moreover, genes involved in α-linolenic acid metabolism, including FAD, *LOX*, *AOS*, *OPR*, and β-oxidation genes, exhibited significant upregulation at 72 h under Cd stress corresponding to significant increases in metabolites such as 13-HPOTrE, 9-HOTrE,

and stearidonic acid (Figure 8). These findings suggest that phospholipase is activated in the plasma membrane promoting α-linolenic acid metabolism in *A. manihot* roots. The upregulation of the *LOX* and *AOS* genes, along with the increased levels of the crucial intermediate metabolite 13-HPOTrE, implies activation of the downstream JA pathway. Previous studies have indicated that under heavy metal stress, JA regulates antioxidant activity to enhance plant tolerance to heavy metal stress (Hewedy et al., 2023).

Interestingly, stearidonic acid, a nontraditional fatty acid, significantly increased at multiple time points. This may be attributed to the upregulation of *FAD* genes, which increases the conversion of α-linolenic acid to γ-linolenic and stearidonic acids (Lee et al., 2019). In *B. napus*, the transcript levels of the *FAD* genes were greater in the Cd-tolerant cultivar than in the sensitive cultivar under 250 μM Cd stress (Xu et al., 2019). Moreover, *FAD* genes have been extensively identified in diverse plant species; these genes are activated under various abiotic stress conditions and thereby augment plant stress resistance (Zhang et al., 2005; Yu et al., 2009; Xu et al., 2019). For instance, in tomatoes, *LeFAD3* overexpression significantly enhanced resistance to both salt and cold stress (Zhang et al., 2005; Yu et al., 2009). Therefore, we speculate that lipid metabolism maintains the stable cell membrane state in *A. manihot* under Cd stress and participates in the signaling processes involved in the plant stress response, thereby enhancing the Cd tolerance of plants.

4.5 Phenylpropanoid biosynthesis as an important metabolic pathway in response to Cd stress in *A. manihot*

Recent studies have highlighted the important role of phenylpropanoid biosynthesis in mitigating the adverse effects of Cd stress (Chen et al., 2020; Wang et al., 2022; Yu et al., 2023). In our studies, significant increases in the levels of trans-cinnamic acid and ferulic acid were detected at 72 h followed by pronounced increases in *p*-coumaric acid and sinapic acid levels at 7 days (Figure 9). Similarly, the accumulation of phenolic acids was detected in the roots of *Kandelia obovata* under Cd stress (Chen et al., 2020). On the one hand, enhancing phenolic acid biosynthesis in response to Cd exposure plays a crucial role in scavenging ROS due to their potent antioxidant activity (Sharma et al., 2019; Chen et al., 2020). On the other hand, phenolic acids are capable of chelating Cd or rendering Cd biologically unavailable, thereby mitigating its toxicity (Chen et al., 2020). It should be noted that the composition and concentration of phenolic acids differ among plants exposed to diverse heavy metal stresses (Anjitha et al., 2021). Such variations may be determinants of the specific defense strategies plants employ to cope with these environmental stresses. Consistent with these findings, structural genes involved in the synthesis of these compounds, including *PAL*, *C4H*, *COMT*, *F5H*, and *4CL*, were significantly upregulated at 72 h or 7 days (Figure 9). PAL is the first enzyme in the general phenylpropanoid pathway, catalyzing the nonoxidative elimination of ammonia to yield trans-cinnamic acid, which is then transformed into p-coumaric acid through a process catalyzed by C4H (Dong and Lin, 2021). Both trans-cinnamic acid and *p*-coumaric acid serve as precursors for a wide range of organic compounds and can be influenced by the metabolic efficiency of the phenylpropanoid, lignin, and flavonoid pathways (Chen et al., 2020; Dong and Lin, 2021).

In addition, significant reductions in the levels of three primary monolignols, namely, sinapyl alcohol, *p*-coumaryl alcohol, and coniferyl alcohol, were observed in the later stages of Cd stress (Figure 9). This phenomenon could be associated with the activation of REF1, which enzymatically converts coniferaldehyde and sinapaldehyde into sinapic acid and ferulic acid, respectively, thereby depleting the substrates necessary for monolignol synthesis (Nair et al., 2004). Interestingly, *REF1* was identified as a hub gene in the present study (Figure 5C). Nevertheless, the precise mechanism by which *REF1* influences the phenylpropanoid biosynthesis pathway in response to Cd stress requires further investigation. Additionally, an increase in the *POD* transcript level might also influence the monolignol content. The expression of the *GhPER8* gene, a ligninolytic peroxidase in tobacco leaves, significantly reduced the levels of coniferyl alcohol and sinapic acid, which are substrates for G-lignin and S-lignin biosynthesis, respectively (Gao et al., 2019). In summary, phenylpropanoid biosynthesis, through the production of phenolic acids and the modulation of lignin, plays a vital role in detoxifying *A. manihot* against Cd.

5 Conclusion

In this study, we conducted a comprehensive investigation of the physiology, transcriptome, and metabolome to elucidate the response mechanisms of *A. manihot* under Cd stress. At the physiological level, we identified the activation of the antioxidant system, including SOD, POD, and CAT, as a key mechanism for Cd detoxification in *A. manihot*. Analysis of the transcriptome and metabolome revealed dynamic effects of Cd stress on gene expression and metabolites in *A. manihot*. Integration of the physiology and transcriptome datasets allowed us to identify eight hub genes involved in processes, such as metal ion transport, ethylene response factors, and lignin biosynthesis, which are likely to play key roles in Cd stress responses. Moreover, the integration of transcriptome and metabolome datasets highlighted the critical role of phenylpropanoid biosynthesis, as well as lipid synthesis and metabolic pathways, in enhancing the tolerance of *A. manihot* to Cd. Overall, our study offers valuable insights into the mechanisms underlying the response of *A. manihot* to Cd toxicity. Moreover, these findings provide essential information for further exploration into the functional characterization of genes associated with Cd tolerance paving the way for future research aimed at improving Cd stress resilience in *A. manihot* and potentially other related plant species.

Data availability statement

The data presented in the study are deposited in the NCBI repository, accession number PRJNA1078221.

Author contributions

MW: Conceptualization, Data curation, Formal analysis, Methodology, Validation, Writing – original draft. QX: Data curation, Formal analysis, Validation, Software, Writing – review & editing. TT: Data curation, Software, Writing – review & editing. XL: Data curation, Software, Writing – review & editing. YP: Conceptualization, Formal analysis, Funding acquisition, Investigation, Methodology, Project administration, Resources, Supervision, Writing – review & editing.

Funding

The author(s) declare financial support was received for the research, authorship, and/or publication of this article. This study was supported by the National Natural Science Foundation of China (Grant No. 31670622).

Conflict of interest

The authors declare that the research was conducted in the absence of any commercial or financial relationships that could be construed as a potential conflict of interest.

Publisher's note

Supplementary material

The Supplementary Material for this article can be found online at: https://www.frontiersin.org/articles/10.3389/fpls.2024.1389207/full#supplementary-material

References

Ahammed, G. J., Li, Z., Chen, J., Dong, Y., Qu, K., Guo, T., et al. (2024). Reactive oxygen species signaling in melatonin-mediated plant stress response. *Plant Physiol. Biochem.* 207, 108398. doi: 10.1016/j.plaphy.2024.108398

Anjitha, K. S., Sameena, P. P., and Puthur, J. T. (2021). Functional aspects of plant secondary metabolites in metal stress tolerance and their importance in pharmacology. *Plant Stress* 2, 100038. doi: 10.1016/j.stress.2021.100038

Asgari Lajayer, B., Ghorbanpour, M., and Nikabadi, S. (2017). Heavy metals in contaminated environment: Destiny of secondary metabolite biosynthesis, oxidative status and phytoextraction in medicinal plants. *Ecotoxicol. Environ. Saf.* 145, 377–390. doi: 10.1016/j.ecoenv.2017.07.035

Balali-Mood, M., Naseri, K., Tahergorabi, Z., Khazdair, M. R., and Sadeghi, M. (2021). Toxic mechanisms of five heavy metals: mercury, lead, chromium, cadmium, and arsenic. *Front. Pharmacol.* 12. doi: 10.3389/fphar.2021.643972

Boutté, Y., and Jaillais, Y. (2020). Metabolic cellular communications: feedback mechanisms between membrane lipid homeostasis and plant development. *Dev. Cell* 54, 171–182. doi: 10.1016/j.devcel.2020.05.005

Brunetti, P., Zanella, L., De Paolis, A., Di Litta, D., Cecchetti, V., Falasca, G., et al. (2015). Cadmium-inducible expression of the ABC-type transporter *AtABCC3* increases phytochelatin-mediated cadmium tolerance in *Arabidopsis*. *J. Exp. Bot.* 66, 3815–3829. doi: 10.1093/jxb/erv185

Cappa, J. J., and Pilon-Smits, E. A. (2014). Evolutionary aspects of elemental hyperaccumulation. *Planta* 239, 267–275. doi: 10.1007/s00425-013-1983-0

Chen, S., Lin, R., Lu, H., Wang, Q., Yang, J., Liu, J., et al. (2020). Effects of phenolic acids on free radical scavenging and heavy metal bioavailability in *kandelia obovata* under cadmium and zinc stress. *Chemosphere* 249, 126341. doi: 10.1016/j.chemosphere.2020.126341

Chen, W., Gong, L., Guo, Z., Wang, W., Zhang, H., Liu, X., et al. (2013). A novel integrated method for large-scale detection, identification, and quantification of widely targeted metabolites: application in the study of rice metabolomics. *Mol. Plant* 6, 1769–1780. doi: 10.1093/mp/sst080

Corso, M., Schvartzman, M. S., Guzzo, F., Souard, F., Malkowski, E., Hanikenne, M., et al. (2018). Contrasting cadmium resistance strategies in two metallicolous populations of *Arabidopsis halleri*. *New Phytol.* 218, 283–297. doi: 10.1111/nph.14948

Dong, N. Q., and Lin, H. X. (2021). Contribution of phenylpropanoid metabolism to plant development and plant-environment interactions. *J. Integr. Plant Biol.* 63, 180–209. doi: 10.1111/jipb.13054

Ernst, J., and Bar-Joseph, Z. (2006). STEM: a tool for the analysis of short time series gene expression data. *BMC Bioinf.* 7, 191. doi: 10.1186/1471-2105-7-191

Feussner, I., and Wasternack, C. (2002). The lipoxygenase pathway. *Annu. Rev. Plant Biol.* 53, 275–297. doi: 10.1146/annurev.arplant.53.100301.135248

Fu, S., Lu, Y., Zhang, X., Yang, G., Chao, D., Wang, Z., et al. (2019). The ABC transporter ABCG36 is required for cadmium tolerance in rice. *J. Exp. Bot.* 70, 5909–5918. doi: 10.1093/jxb/erz335

Gao, Z., Sun, W., Wang, J., Zhao, C., and Zuo, K. (2019). GhbHLH18 negatively regulates fiber strength and length by enhancing lignin biosynthesis in cotton fibers. *Plant Sci.* 286, 7–16. doi: 10.1016/j.plantsci.2019.05.020

Grabherr, M. G., Haas, B. J., Yassour, M., Levin, J. Z., Thompson, D. A., Amit, I., et al. (2011). Full-length transcriptome assembly from RNA-Seq data without a reference genome. *Nat. Biotechnol.* 29, 644–652. doi: 10.1038/nbt.1883

Guo, X., Liu, Y., Zhang, R., Luo, J., Song, Y., Li, J., et al. (2020). Hemicellulose modification promotes cadmium hyperaccumulation by decreasing its retention on roots in *Sedum alfredii*. *Plant Soil* 447, 241–255. doi: 10.1007/s11104-019-04339-9

Guo, X., Luo, J., Du, Y., Li, J., Liu, Y., Liang, Y., et al. (2021). Coordination between root cell wall thickening and pectin modification is involved in cadmium accumulation in *Sedum alfredii*. *Environ. pollut.* 268, 115665. doi: 10.1016/j.envpol.2020.115665

Haider, F. U., Liqun, C., Coulter, J. A., Cheema, S. A., Wu, J., Zhang, R., et al. (2021). Cadmium toxicity in plants: Impacts and remediation strategies. *Ecotoxicol. Environ. Saf.* 211, 111887. doi: 10.1016/j.ecoenv.2020.111887

Hamid, Y., Liu, L., Usman, M., Tang, L., Lin, Q., Saqib Rashid, M., et al. (2022). Organic/inorganic amendments for the remediation of a red paddy soil artificially contaminated with different cadmium levels: Leaching, speciation, and phytoavailability tests. *J. Environ. Manage.* 303, 114148. doi: 10.1016/j.jenvman.2021.114148

Hasan, M. K., Ahammed, G. J., Yin, L., Shi, K., Xia, X., Zhou, Y., et al. (2015). Melatonin mitigates cadmium phytotoxicity through modulation of phytochelatins biosynthesis, vacuolar sequestration, and antioxidant potential in *Solanum lycopersicum* L. *Front. Plant Sci.* 6. doi: 10.3389/fpls.2015.00601

Hewedy, O. A., Elsheery, N. I., Karkour, A. M., Elhamouly, N., Arafa, R. A., Mahmoud, G. A.-E., et al. (2023). Jasmonic acid regulates plant development and orchestrates stress response during tough times. *Environ. Exp. Bot.* 208, 105260. doi: 10.1016/j.envexpbot.2023.105260

Hou, Q., Ufer, G., and Bartels, D. (2016). Lipid signalling in plant responses to abiotic stress. *Plant Cell Environ.* 39, 1029–1048. doi: 10.1111/pce.12666

Hu, Z., Fu, Q., Zheng, J., Zhang, A., and Wang, H. (2020). Transcriptomic and metabolomic analyses reveal that melatonin promotes melon root development under

copper stress by inhibiting jasmonic acid biosynthesis. *Hortic. Res.* 7, 79. doi: 10.1038/s41438-020-0293-5

Hu, H., Jia, Y., Hao, Z., Ma, G., Xie, Y., Wang, C., et al. (2023). Lipidomics-based insights into the physiological mechanism of wheat in response to heat stress. *Plant Physiol. Biochem.* 205, 108190. doi: 10.1016/j.plaphy.2023.108190

Kanwar, V. S., Sharma, A., Srivastav, A. L., and Rani, L. (2020). Correction to: Phytoremediation of toxic metals present in soil and water environment: a critical review. *Environ. Sci. pollut. Res. Int.* 27, 44861–44862. doi: 10.1007/s11356-020-11461-0

Khalid, M., Ur-rahman, S., Tan, H. X., Su, L. T., Zhou, P., and Hui, N. (2022). Mutualistic fungus *Piriformospora indica* modulates cadmium phytoremediation properties of host plant *via* concerted action of enzymatic and non-enzymatic biochemicals. *Pedosphere* 32, 256–267. doi: 10.1016/S1002-0160(21)60014-0

Langfelder, P., and Horvath, S. (2008). WGCNA: an R package for weighted correlation network analysis. *BMC Bioinf.* 9, 559. doi: 10.1186/1471-2105-9-559

Lee, K. R., Kim, K. H., Kim, J. B., Hong, S. B., Jeon, I., Kim, H. U., et al. (2019). High accumulation of γ-linolenic acid and Stearidonic acid in transgenic Perilla (*Perilla frutescens* var. *frutescens*) seeds. *BMC Plant Biol.* 19, 120. doi: 10.1186/s12870-019-1713-2

Liang, Y., Huang, Y., Liu, C., Chen, K., and Li, M. (2023). Functions and interaction of plant lipid signalling under abiotic stresses. *Plant Biol.* 25, 361–378. doi: 10.1111/plb.13507

Liang, H., Wu, W. L., Zhang, Y. H., Zhou, S. J., Long, C. Y., Wen, J., et al. (2018). Levels, temporal trend and health risk assessment of five heavy metals in fresh vegetables marketed in Guangdong Province of China during 2014–2017. *Food Control* 92, 107–120. doi: 10.1016/j.foodcont.2018.04.051

Liu, H., Zhao, H., Wu, L., Liu, A., Zhao, F. J., and Xu, W. (2017). Heavy metal ATPase 3 (HMA3) confers cadmium hypertolerance on the cadmium/zinc hyperaccumulator *Sedum plumbizincicola*. *New Phytol.* 215, 687–698. doi: 10.1111/nph.14622

Liu, Z., Zhou, L., Gan, C., Hu, L., Pang, B., Zuo, D., et al. (2023). Transcriptomic analysis reveals key genes and pathways corresponding to Cd and Pb in the hyperaccumulator *Arabis paniculata*. *Ecotoxicol. Environ. Saf.* 254, 114757. doi: 10.1016/j.ecoenv.2023.114757

Loix, C., Huybrechts, M., Vangronsveld, J., Gielen, M., Keunen, E., and Cuypers, A. (2017). Reciprocal interactions between cadmium-induced cell wall responses and oxidative stress in plants. *Front. Plant Sci.* 8. doi: 10.3389/fpls.2017.01867

Mahar, A., Wang, P., Ali, A., Awasthi, M. K., Lahori, A. H., Wang, Q., et al. (2016). Challenges and opportunities in the phytoremediation of heavy metals contaminated soils: A review. *Ecotoxicol. Environ. Saf.* 126, 111–121. doi: 10.1016/j.ecoenv.2015.12.023

Mwamba, T. M., Ali, S., Ali, B., Lwalaba, J. L., Liu, H., Farooq, M. A., et al. (2016). Interactive effects of cadmium and copper on metal accumulation, oxidative stress, and mineral composition in *Brassica napus*. *Int. J. Environ. Sci. Technol.* 13, 2163–2174. doi: 10.1007/s13762-016-1040-1

Mwamba, T. M., Islam, F., Ali, B., Lwalaba, J. L. W., Gill, R. A., Zhang, F., et al. (2020). Comparative metabolomic responses of low- and high-cadmium accumulating genotypes reveal the cadmium adaptive mechanism in *Brassica napus*. *Chemosphere* 250, 126308. doi: 10.1016/j.chemosphere.2020.126308

Nair, R. B., Bastress, K. L., Ruegger, M. O., Denault, J. W., and Chapple, C. (2004). The *Arabidopsis thaliana REDUCED EPIDERMAL FLUORESCENCE1* gene encodes an aldehyde dehydrogenase involved in ferulic acid and sinapic acid biosynthesis. *Plant Cell* 16, 544–554. doi: 10.1105/tpc.017509

Nazir, M. M., Noman, M., Ahmed, T., Ali, S., Ulhassan, Z., Zeng, F., et al. (2022). Exogenous calcium oxide nanoparticles alleviate cadmium toxicity by reducing Cd uptake and enhancing antioxidative capacity in barley seedlings. *J. Hazard. Mater.* 438, 129498. doi: 10.1016/j.jhazmat.2022.129498

Okazaki, Y., and Saito, K. (2014). Roles of lipids as signaling molecules and mitigators during stress response in plants. *Plant J.* 79, 584–596. doi: 10.1111/tpj.12556

Pan, C., Lu, H., Yang, C., Wang, L., Chen, J., and Yan, C. (2021). Comparative transcriptome analysis reveals different functions of *Kandelia obovata* superoxide dismutases in regulation of cadmium translocation. *Sci. Total. Environ.* 771, 144922. doi: 10.1016/j.scitotenv.2020.144922

Peever, T. L., and Higgins, V. J. (1989). Electrolyte leakage, lipoxygenase, and lipid peroxidation induced in tomato leaf tissue by specific and nonspecific elicitors from *Cladosporium fulvum*. *Plant Physiol.* 90, 867–875. doi: 10.1104/pp.90.3.867

Pons, M. L., Collin, B., Doelsch, E., Chaurand, P., Fehlauer, T., Levard, C., et al. (2021). X-ray absorption spectroscopy evidence of sulfur-bound cadmium in the Cd-hyperaccumulator Solanum nigrum and the non-accumulator *Solanum melongena*. *Environ. pollut.* 279, 116897. doi: 10.1016/j.envpol.2021.116897

Rezapour, S., Siavash Moghaddam, S., Nouri, A., and Khosravi Aqdam, K. (2022). Urbanization influences the distribution, enrichment, and ecological health risk of heavy metals in croplands. *Sci. Rep.* 12, 3868. doi: 10.1038/s41598–022-07789-x

Rui, H., Chen, C., Zhang, X., Shen, Z., and Zhang, F. (2016). Cd-induced oxidative stress and lignification in the roots of two *Vicia sativa* L. varieties with different Cd tolerances. *J. Hazard. Mater.* 301, 304–313. doi: 10.1016/j.jhazmat.2015.08.052

Sharma, A., Shahzad, B., Rehman, A., Bhardwaj, R., Landi, M., and Zheng, B. (2019). Response of phenylpropanoid pathway and the role of polyphenols in plants under abiotic stress. *Molecules* 24 (13):2452. doi: 10.3390/molecules24132452

Shen, C., Yang, Y. M., Sun, Y. F., Zhang, M., Chen, X. J., and Huang, Y. Y. (2022). The regulatory role of abscisic acid on cadmium uptake, accumulation and translocation in plants. *Front. Plant Sci.* 13. doi: 10.3389/fpls.2022.953717

Suman, J., Uhlik, O., Viktorova, J., and Macek, T. (2018). Phytoextraction of heavy metals: A promising tool for clean-up of polluted environment? *Front. Plant Sci.* 9. doi: 10.3389/fpls.2018.01476

Sun, S., Fang, J., Lin, M., Hu, C., Qi, X., Chen, J., et al. (2021). Comparative metabolomic and transcriptomic studies reveal key metabolism pathways contributing to freezing tolerance under cold stress in Kiwifruit. *Front. Plant Sci.* 12. doi: 10.3389/fpls.2021.628969

Wang, J., Chen, X., Chu, S., You, Y., Chi, Y., Wang, R., et al. (2022). Comparative cytology combined with transcriptomic and metabolomic analyses of *Solanum nigrum* L. @ in response to Cd toxicity. *J. Hazard. Mater* 423, 127168. doi: 10.1016/j.jhazmat.2021.127168

Wei, Z., Zhongbing, C., Xiuqin, Y., Luying, S., Huan, M., and Sixi, Z. (2023). Integrated transcriptomics and metabolomics reveal key metabolic pathway responses in *Pistia stratiotes* under Cd stress. *J. Hazard. Mater.* 452, 131214. doi: 10.1016/j.jhazmat.2023.131214

Wu, Y., Li, X., Zhang, J., Zhao, H., Tan, S., Xu, W., et al. (2022). ERF subfamily transcription factors and their function in plant responses to abiotic stresses. *Front. Plant Sci.* 13. doi: 10.3389/fpls.2022.1042084

Wu, M., Luo, Q., Zhao, Y., Long, Y., Liu, S., and Pan, Y. (2018). Physiological and biochemical mechanisms preventing cd toxicity in the new hyperaccumulator *Abelmoschus manihot*. *J. Plant Growth Regul.* 37, 709–718. doi: 10.1007/s00344-017-9765-8

Wu, Y., Ma, L., Liu, Q., Vestergard, M., Topalovic, O., Wang, Q., et al. (2020). The plant-growth promoting bacteria promote cadmium uptake by inducing a hormonal crosstalk and lateral root formation in a hyperaccumulator plant *Sedum alfredii*. *J. Hazard. Mater.* 395, 122661. doi: 10.1016/j.jhazmat.2020.122661

Wu, M., Northen, T. R., and Ding, Y. (2023). Stressing the importance of plant specialized metabolites: omics-based approaches for discovering specialized metabolism in plant stress responses. *Front. Plant Sci.* 14. doi: 10.3389/fpls.2023.1272363

Xie, Q., Liu, B., Dong, W., Li, J., Wang, D., Liu, Z., et al. (2023). Comparative transcriptomic and metabolomic analyses provide insights into the responses to NaCl and Cd stress in *Tamarix hispida*. *Sci. Total. Environ.* 884, 163889. doi: 10.1016/j.scitotenv.2023.163889

Xu, C., Li, Z., and Wang, J. (2022). Temporal and tissue-specific transcriptome analyses reveal mechanistic insights into the *Solidago canadensis* response to cadmium contamination. *Chemosphere* 292, 133501. doi: 10.1016/j.chemosphere.2021.133501

Xu, L., Zeng, W., Li, J., Liu, H., Yan, G., Si, P., et al. (2019). Characteristics of membrane-bound fatty acid desaturase (FAD) genes in *Brassica napus* L. and their expressions under different cadmium and salinity stresses. *Environ. Exp. Bot.* 162, 144–156. doi: 10.1016/j.envexpbot.2019.02.016

Yan, A., Wang, Y., Tan, S. N., Mohd Yusof, M. L., Ghosh, S., and Chen, Z. (2020). Phytoremediation: A promising approach for revegetation of heavy metal-polluted land. *Front. Plant Sci.* 11. doi: 10.3389/fpls.2020.00359

Yang, Y. J., Cheng, L. M., and Liu, Z. H. (2007). Rapid effect of cadmium on lignin biosynthesis in soybean roots. *Plant Sci.* 172, 632–639. doi: 10.1016/j.plantsci.2006.11.018

Yu, B., Peng, Y., Xu, J., Qin, D., Gao, T., Zhu, H., et al. (2021). Phytoremediation potential of *Youngia japonica* (L.) DC: a newly discovered cadmium hyperaccumulator. *Environ. Sci. pollut. Res. Int.* 28, 6044–6057. doi: 10.1007/s11356-020-10853-6

Yu, C., Wang, H. S., Yang, S., Tang, X. F., Duan, M., and Meng, Q. W. (2009). Overexpression of endoplasmic reticulum omega-3 fatty acid desaturase gene improves chilling tolerance in tomato. *Plant Physiol. Biochem.* 47, 1102–1112. doi: 10.1016/j.plaphy.2009.07.008

Yu, M., Zhuo, R., Lu, Z., Li, S., Chen, J., Wang, Y., et al. (2023). Molecular insights into lignin biosynthesis on cadmium tolerance: Morphology, transcriptome and proteome profiling in *Salix matSudana*. *J. Hazard. Mater.* 441, 129909. doi: 10.1016/j.jhazmat.2022.129909

Zhang, M., Barg, R., Yin, M., Gueta-Dahan, Y., Leikin-Frenkel, A., Salts, Y., et al. (2005). Modulated fatty acid desaturation via overexpression of two distinct omega-3 desaturases differentially alters tolerance to various abiotic stresses in transgenic tobacco cells and plants. *Plant J.* 44, 361–371. doi: 10.1111/j.1365-313X.2005.02536.x

Zhang, H., Heal, K., Zhu, X., Tigabu, M., Xue, Y., and Zhou, C. (2021). Tolerance and detoxification mechanisms to cadmium stress by hyperaccumulator *Erigeron annuus* include molecule synthesis in root exudate. *Ecotoxicol. Environ. Saf.* 219, 112359. doi: 10.1016/j.ecoenv.2021.112359

Zhang, J., Zhang, M., Song, H., Zhao, J., Shabala, S., Tian, S., et al. (2020). A novel plasma membrane-based NRAMP transporter contributes to Cd and Zn hyperaccumulation in *Sedum alfredii* Hance. *Environ. Exp. Bot.* 176, 104121. doi: 10.1016/j.envexpbot.2020.104121

Zhang, Z. H., Zhou, T., Tang, T. J., Song, H. X., Guan, C. Y., Huang, J. Y., et al. (2019). A multiomics approach reveals the pivotal role of subcellular reallocation in determining rapeseed resistance to cadmium toxicity. *J. Exp. Bot.* 70, 5437–5455. doi: 10.1093/jxb/erz295

Zhao, L., Sun, Y. L., Cui, S. X., Chen, M., Yang, H. M., Liu, H. M., et al. (2011). Cd-induced changes in leaf proteome of the hyperaccumulator plant *Phytolacca americana*. *Chemosphere* 85, 56–66. doi: 10.1016/j.chemosphere.2011.06.029

Zhong, L., Lin, L., Liao, M., Wang, J., Tang, Y., Sun, G., et al. (2019). Phytoremediation potential of Pterocypsela laciniata as a cadmium hyperaccumulator. *Environ. Sci. pollut. Res. Int.* 26, 13311–13319. doi: 10.1007/s11356-019-04702-4

Zhu, G., Wang, S., Huang, Z., Zhang, S., Liao, Q., Zhang, C., et al. (2018). Rewiring of the fruit metabolome in tomato breeding. *Cell* 172, 249–261, e212. doi: 10.1016/j.cell.2017.12.019

frontiers | Frontiers in Plant Science

TYPE Original Research
PUBLISHED 20 June 2024
DOI 10.3389/fpls.2024.1394223

OPEN ACCESS

EDITED BY
Mehanathan Muthamilarasan,
University of Hyderabad, India

REVIEWED BY
Md Mostofa Uddin Helal,
Shanxi Agricultural University, China
Nunzio D'Agostino,
University of Naples Federico II, Italy

*CORRESPONDENCE
Li Tian
li.tian@zafu.edu.cn
Yanyan Yan
yanyan@zafu.edu.cn

†These authors have contributed equally to this work

RECEIVED 01 March 2024
ACCEPTED 30 May 2024
PUBLISHED 20 June 2024

CITATION
Gan J, Qiu Y, Tao Y, Zhang L, Okita TW, Yan Y and Tian L (2024) RNA-seq analysis reveals transcriptome reprogramming and alternative splicing during early response to salt stress in tomato root. *Front. Plant Sci.* 15:1394223. doi: 10.3389/fpls.2024.1394223

RNA-seq analysis reveals transcriptome reprogramming and alternative splicing during early response to salt stress in tomato root

Jianghuang Gan[1,2†], Yongqi Qiu[1,2†], Yilin Tao[1,2], Laining Zhang[1,2], Thomas W. Okita[3], Yanyan Yan[1,2*] and Li Tian[1,2*]

[1]Collaborative Innovation Center for Efficient and Green Production of Agriculture in Mountainous Areas of Zhejiang Province, College of Horticulture Science, Zhejiang A&F University, Hangzhou, Zhejiang, China, [2]Key Laboratory of Quality and Safety Control for Subtropical Fruit and Vegetable, Ministry of Agriculture and Rural Affairs, College of Horticulture Science, Zhejiang A&F University, Hangzhou, Zhejiang, China, [3]Institute of Biological Chemistry, Washington State University, Pullman, WA, United States

Salt stress is one of the dominant abiotic stress conditions that cause severe damage to plant growth and, in turn, limiting crop productivity. It is therefore crucial to understand the molecular mechanism underlying plant root responses to high salinity as such knowledge will aid in efforts to develop salt-tolerant crops. Alternative splicing (AS) of precursor RNA is one of the important RNA processing steps that regulate gene expression and proteome diversity, and, consequently, many physiological and biochemical processes in plants, including responses to abiotic stresses like salt stress. In the current study, we utilized high-throughput RNA-sequencing to analyze the changes in the transcriptome and characterize AS landscape during the early response of tomato root to salt stress. Under salt stress conditions, 10,588 genes were found to be differentially expressed, including those involved in hormone signaling transduction, amino acid metabolism, and cell cycle regulation. More than 700 transcription factors (TFs), including members of the MYB, bHLH, and WRKY families, potentially regulated tomato root response to salt stress. AS events were found to be greatly enhanced under salt stress, where exon skipping was the most prevalent event. There were 3709 genes identified as differentially alternatively spliced (DAS), the most prominent of which were serine/threonine protein kinase, pentatricopeptide repeat (PPR)-containing protein, E3 ubiquitin-protein ligase. More than 100 DEGs were implicated in splicing and spliceosome assembly, which may regulate salt-responsive AS events in tomato roots. This study uncovers the stimulation of AS during tomato root response to salt stress and provides a valuable resource of salt-responsive genes for future studies to improve tomato salt tolerance.

KEYWORDS

***Solanum lycopersicum*, tomato root, salt stress, alternative splicing, RNA sequencing, transcription factors**

Introduction

Soil salinization has become an increasingly serious global problem. It is estimated that more than 833 million hectares (8.7% of the Earth's surface) are salinized worldwide with an annual increase of 10% (FAO, 2021). Soil salinization is projected to extend to more than 50% of the arable land by 2050 (Jamil et al., 2011). There are various reasons for soil salinization, including low rainfall, weathering of indigenous rocks, and inappropriate irrigation and fertilization during the cultivation process (Shrivastava and Kumar, 2015). Saline soils are known to suppress plant growth and development, which in turn severely affects crop yields in agricultural production (Yuan et al., 2016; van Zelm et al., 2020). Tomato (*Solanum lycopersicum* L.) is one of the most grown and valuable vegetable crops in the world, ranking the first among vegetable crops with an annual production of 186 million tons globally (FAO, 2022). Although tomato is thought to be moderately tolerant to salt stress, tomato yield and quality are severely affected by high salinity (Bonarota et al., 2022). The development of salt-tolerant tomato crops is therefore an important goal of plant breeding.

Salt stress can damage plant growth and development in many ways. High salt concentration in the soil modifies the structure of soil porosity and, in turn, hydraulic conductivity. This results in low water potential and nutrient availability, causing osmotic stress and eventually leading to metabolic toxicity and physiological disorders that affect plant growth and development (Tester and Davenport, 2003; Hasanuzzaman and Fujita, 2022; 2023). The rapid accumulation of reactive oxygen species (ROS) frequently occurs during salt stress, which induces oxidative stress, causes damage to cellular macromolecules like proteins and DNA, and destabilizes membranes and organelles (Kesawat et al., 2023). Furthermore, salt stress also decreases stomatal conductance and inhibits photosynthesis (Lawlor and Cornic, 2002; Chaves et al., 2009; Sayyad-Amin et al., 2016; Kesawat et al., 2023). All these negative effects impair most plant growth phases, from seed germination, vegetative growth, flowering and fruiting and eventually overall yield.

Along with the development of multi-omics technology, extensive studies have applied transcriptomics, proteomics, metabolomics or the combined analysis with biochemical and physiological characteristics to investigate the molecular mechanism underlying plant salt tolerance. Based on current understanding, plants adapt various mechanisms, including activation of osmotic adjustment, regulation of ion transport and homeostasis, clearance of reactive oxygen species, regulation of plant hormone signaling, modulation of cytoskeletal dynamics and the cell wall composition, to negate the adverse effects and survive at salinity condition (Wang et al., 2011; Hasanuzzaman and Fujita, 2022; Balasubramaniam et al., 2023). More importantly, regulation of gene expression is the integral part that activates and coordinates all these regulatory pathways.

Gene expression is regulated at transcriptional level mainly exerted by transcription factors and post-transcriptional events involving RNA processing, maturation, transport and turn-over (Zhao et al., 2017; Zhang et al., 2019). Alternative splicing (AS) is the main step during RNA processing to regulate gene expression and proteome diversity. As AS can generate multiple transcripts from a single RNA precursor via exon skipping, intron retention, and selection of alternative donor site or acceptor site as well as other intricate forms of splicing (Keren et al., 2010), AS eventually cause differential expression of the corresponding gene and modulate gene function via altering a protein domain or affecting the stability of the spliced transcript and the corresponding protein. Previous studies have demonstrated that high salinity stress can promote the occurrence of alternative splicing of stress-responsive genes and affect the expression of the genes coding spliceosome components in *Arabidopsis* (Ding et al., 2014b; Feng et al., 2015; Gu et al., 2018), rice (Yu et al., 2021; Jian et al., 2022), wheat (Liu et al., 2018), Barley (Fu et al., 2019), Date Palm (Xu et al., 2021), grapevine (Jin et al., 2021), cotton (Zhu et al., 2018), *Opisthopappus* (Han et al., 2024), etc. However, the alternative splicing events in tomato root under salt stress remains to be resolved.

In this study, we investigated the transcriptomic response of tomato root to salt stress, focusing on the global dynamics of transcriptome reprogramming and AS changes during the initial 12 hours under salt exposure. We found a large number of early response differentially expressed (DE) genes induced by salt stress while simultaneously elevating AS events of both DE and non-DE genes. Our findings provide a comprehensive understanding of tomato root response to salt stress and highlights the vital role of AS in tomato's adaptation to salt stress.

Results

Overview of morphological performance of tomato seedlings and RNA-seq data of tomato roots in response to salt stress

To study the rapid response of tomato roots to salt stress, five-leaf-stage tomato seedlings were treated with 150 mM NaCl for 12 hours. At 1 hour post treatment (hpt), tomato leaves became dehydrated and wilted, exhibiting leaf curling and petiole softening. The dehydration of plants was more severe at 3 hpt but started to slightly recover at 6 hpt (Figure 1A). At 12 hpt, tomato plants apparently recovered from salt stress as plants showed upright growth without dehydration. The recovery beyond 6 hours suggests that tomato regulates changes in osmotic stress and restores ion homeostasis in a short amount of time after exposure to salt stress. In order to examine the underlying molecular mechanism of tomato's early responses to salt stress, tomato roots were sampled at 0, 1, 3, 6 and 12 hpt (S0, S1, S3, S6, S12) and subjected to next generation RNA-sequencing. Three biological repeats per time point were performed and a total of 15 cDNA libraries were generated for sequencing. Approximately 6.9 billion raw reads were obtained and eventually around 6.6 billion high-quality reads (Supplementary Tables S1, S2) were mapped against the tomato genome to determine transcriptomic changes during early salt stress. Principal component analysis (PCA) (Figure 1B; Supplementary Table S3) and correlation analysis on RNA levels (Figure 1C; Supplementary Table S4) revealed excellent

10.3389/fpls.2024.1394223

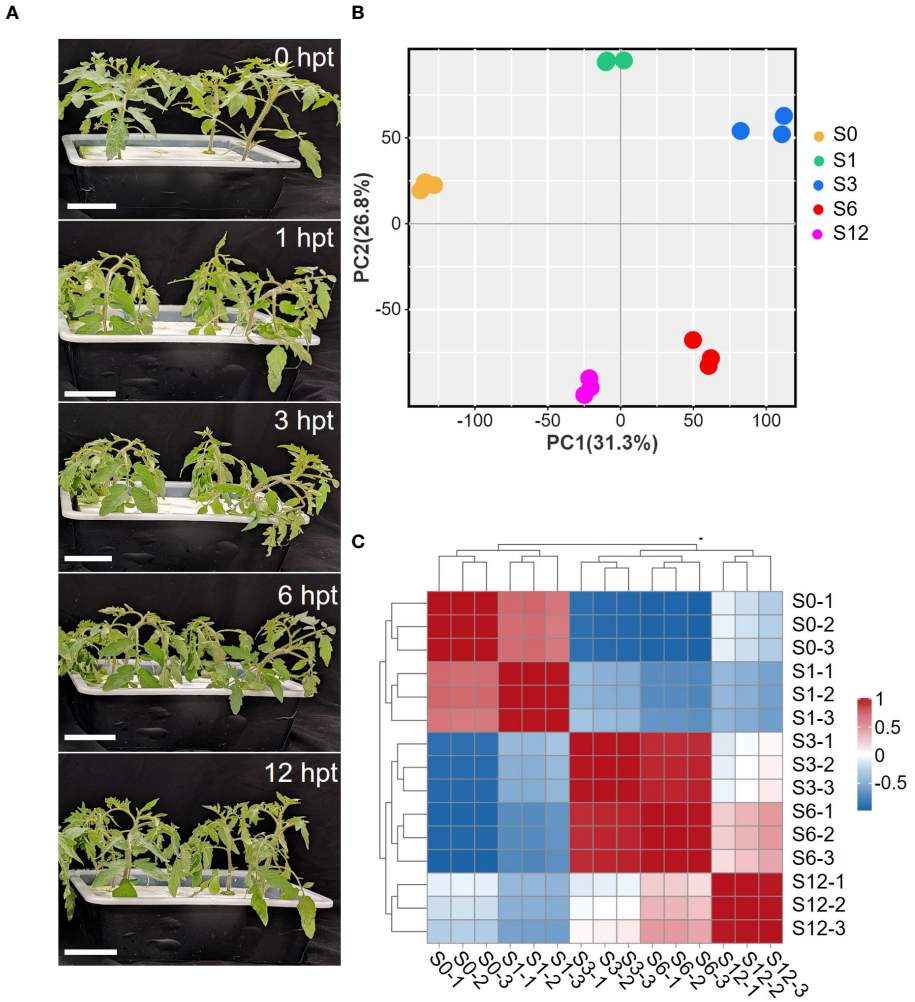

FIGURE 1
Phenotypic and transcriptome changes of tomato in response to salt stress. **(A)** Images of tomato plants at different treatment times (0, 1, 3, 6,12 hours) post treatment (hpt) in the presence of 150mM NaCl. **(B)** Principal component analysis (PCA) of RNA-seq data. Gene expression changes were investigated at 0h (S0), 1h (S1), 3h (S3), 6h (S6) and 12 hpt (S12) of salt stress treatment. The PCA was performed using normalized RNA-Seq data of all mapped genes. **(C)** Pearson's correlation analysis of RNA-seq data between each sample.

repeatability and reproducibility of the results. PCA showed an obvious separation of control group (S0) from salt treated groups, especially from the S3 and S6 samples (Figure 1B; Supplementary Table S3), suggesting that salt treatment significantly disturbed the transcriptome of tomato root.

Transcriptional changes induced by salt stress in tomato root

Differential expression genes (DEGs) were firstly analyzed based on the value of FPKM (Fragments Per Kilobase of transcript per Million mapped reads). A gene was considered to be expressed if all three repeats showed FPKM > 0. DEGs were selected by a threshold of log2 fold change ≥ 1 and adjusted p value < 0.05 when compared to S0 group. Based on these criteria, total 10,588 DEGs out of 22,047 expressed genes were identified from the salt treated samples (Supplementary Table S5), indicating that nearly half of the expressed genes were impacted by salt stress. A heatmap analysis on the expression of all the DEGs revealed various expression patterns among the salt-impacted genes (Figure 2A). Based on their expression patterns, DEGs were classified into 10 clusters by hierarchical clustering analysis based on their expression pattern (Figure 2B; Supplementary Tables S6, S7). Among these clusters, the expression patterns in clusters 6 to 10 were significantly pronounced. The DEGs in cluster 6 were highly enriched in Gene Ontology (GO) terms of cellular anatomical entity, cytoplasm, cell periphery and mitotic cell cycles. These DEGs showed a decreased expression at the first 3 hours post salt treatment, suggesting that the process of cell differentiation was inhibited when tomato roots were exposed to salt stress. The DEGs in clusters 7 and 8 showed significantly increased expression in S1-S3 (Cluster 7) and S3-S6 (Cluster 8) samples, respectively. The DEGs in these clusters were highly enriched in membrane elements and the processes of stimulus response, reflecting a reconfiguration of the membrane under salt stress. Protein modification and ubiquitination were

10.3389/fpls.2024.1394223

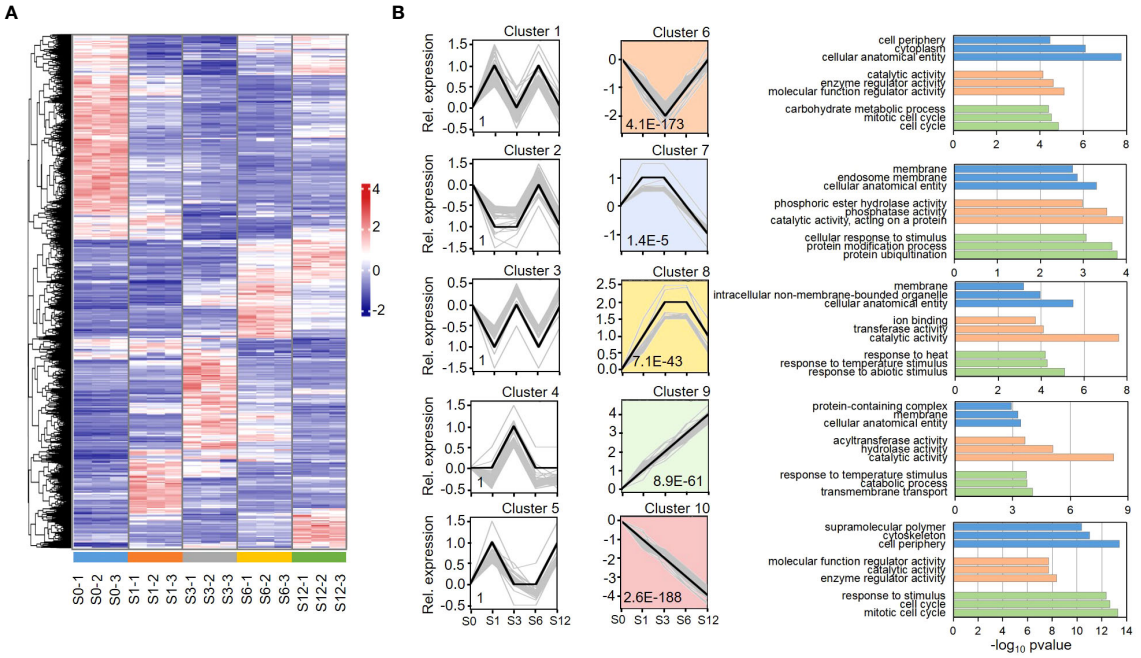

FIGURE 2
Hierarchical clustering and heatmap analyses of tomato DEGs. **(A)** Heatmap analysis shows dynamic expression pattern of DEGs during the early 12-hour response to salt stress in tomato root. **(B)** Hierarchical clustering analysis segregates DEGs into 10 clusters based on gene expression pattern. Y axis represents relative gene expression level based on normalized expression value. The *p* value of each cluster is shown inside the chart area, and the profound clusters are filled with colors. Top GO terms enriched in each profound cluster are shown on the right. GO terms of biological processes, molecular function and cellular component are shown in green, orange and blue bars. Detailed information of the clustered genes and list of all significant GO terms are provided in Supplementary Tables S6 and S7, respectively.

significantly enriched in cluster 7, revealing that protein turnover and metabolism was highly active during the first 3 hours of salt stress. The most pronounced expression patterns were observed in clusters 9 and 10 where DEGs showed linear enhancement (cluster 9) and depression (cluster 10) patterns along the treatment, respectively. The most highly enriched GO term in cluster 9 was catalytic activity, suggesting a continuous activation of enzymes during response to salt stress. Besides, GO terms of response to ROS and oxidative stress were also exclusively detected in cluster 9. Except in cluster 6, GO terms of mitotic cell cycle and cell periphery were also enriched in cluster 10. Multiple cell cycle related processes, such as cell cycle checkpoint signaling, DNA replication and phase transition, were enriched in cluster 6 and 10, further revealing a repression on cell differentiation during salt response.

Amino acid metabolic processes were significantly enriched in clusters 8 and 10. Cluster 8 contains genes involved in metabolism of aromatic amino acids, branched-chain amino acids, sulfur amino acids and alpha amino acids. While serine family amino acids catabolic process was pronounced in cluster 8, their biosynthetic process was only enriched in cluster 10. On the other hand, amino acid transmembrane transport was only significantly enriched in cluster 9. KEGG analysis (Supplementary Figure S1) further reveals that the metabolic pathways of many amino acids, including valine, leucine, isoleucine, serine, glycine, threonine, aspartate, glutamate, arginine, methionine, phenylalanine, tyrosine and tryptophan, were greatly influenced.

Biological processes of response to hormone were observed in highly enriched terms in clusters 6, 8 and 10, but not in cluster 9, suggesting that the process was highly dynamic but not continuously activated. Response to abscisic acid (ABA) and auxin were detected in both clusters 8 and 10. While response to cytokinin was enriched in cluster 10, responses to gibberellin and ethylene were enriched in cluster 8. KEGG analysis on plant hormone signaling pathways revealed that most of key steps in hormone signal transduction were significantly influenced in tomato root by salt stress (Supplementary Figure S2).

The genes involved in cytokinin, ABA and auxin signaling transduction showed various expression patterns as viewed by heatmap clustering (Figure 3; Supplementary Table S9), which reveals various expression pattern of these key factors. For example, while most of PYR/PYL genes was down-regulated by salt treatment, significant induction of PP2C was greatly observed at 3 hours after salt treatment (Figure 3B).

The numbers of DEGs (Supplementary Table S8) in the samples collected at each time point are shown in Figure 4A. The largest number of DEGs, 7,260 in total including 3,938 up-regulated and 3,322 down-regulated genes, was observed at 3 hours after salt treatment. Venn diagram data (Figures 4B–D) revealed 2,279 common DEGs (1,012 up-regulated and 1,099 down-regulated genes) among all pairwise comparisons (Supplementary Table S10). GO analyses were conducted to analyze the functions of all DEGs (Figure 5; Supplementary Table S11). Among the four comparison groups, several functional categories, including

10.3389/fpls.2024.1394223

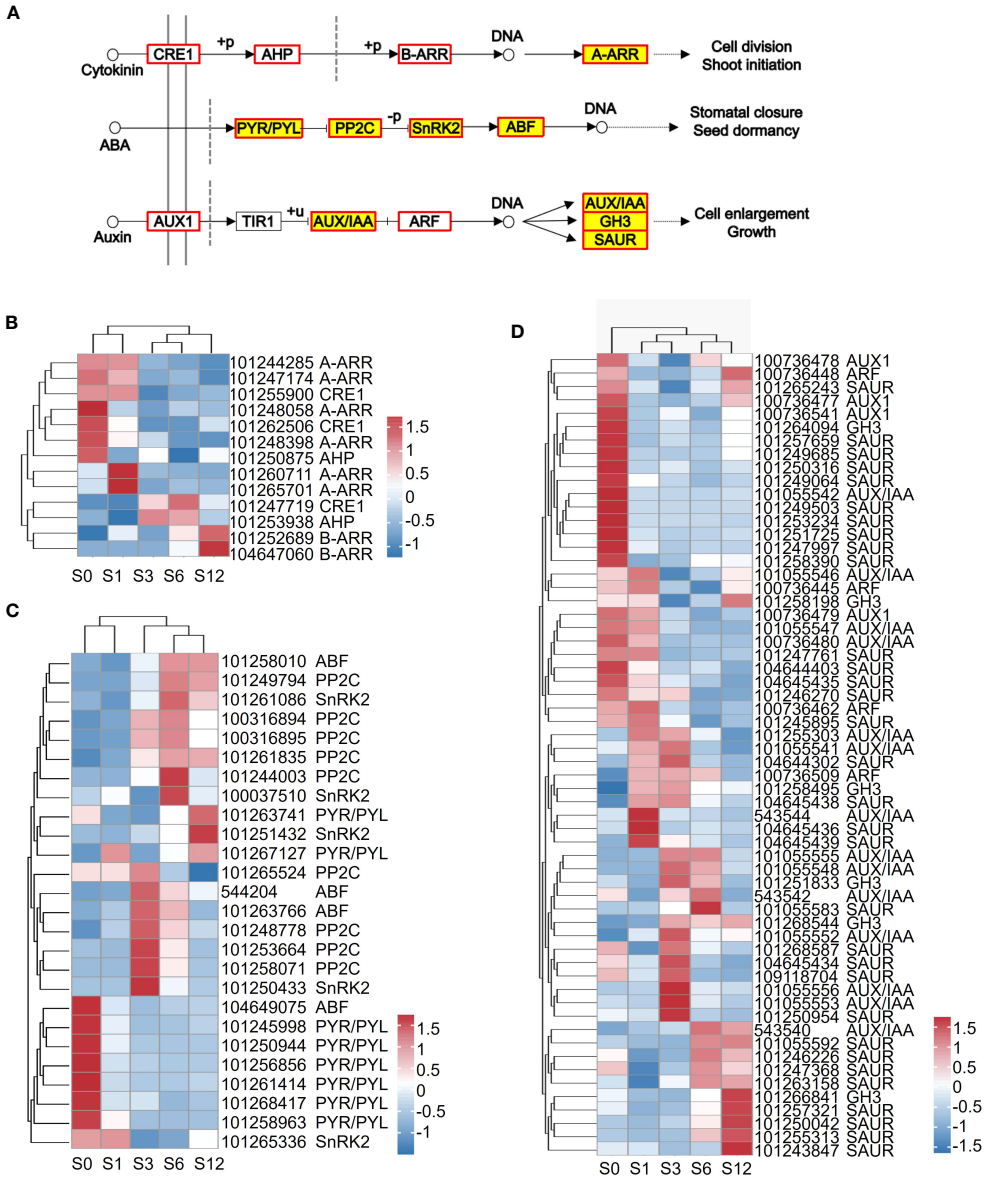

FIGURE 3
Expression of the annotated DEGs involved in plant hormone signal transduction KEGG pathway. **(A)** Overview of DEGs that code key factors functioning in cytokinin, ABA and auxin signal transduction. Red boxes represent genes that were regulated by salt stress, while red boxes filled in yellow represent the common genes found in the 1, 3, 6,12-hour samples treated under salt stress. **(B–D)** Heatmap analysis on the representative DEGs involved in cytokinin, ABA and auxin signaling transduction. The gene ID and potential family name are labeled on the right next to heatmap.

catalytic activity, cellular anatomical entity, cell periphery, membrane, response to hormone and response to stimulus, were strongly over-represented in all groups. It is worth noting that the DEGs from all salt treated samples were also highly enriched in the categories of RNA binding, RNA processing and RNA metabolic process (Supplementary Table S11), suggesting salt stress induces comprehensive changes in RNA metabolism. The common 2,279 DEGs contained genes are related to catalytic activity and responses to hormones and various stimuli (Supplementary Figure S3; Supplementary Table S12). Consistent with the previous clustering result, catalytic activity and cell cycle process were over-represented in the up-regulated and down-regulated common DEGs, respectively.

The expression of 738 transcription factors (TFs) belonging to 26 families were identified to be regulated by salt treatment (Supplementary Table S13). Among those TFs, 87 TFs were identified from the MYB family, 85 from the AP2/ethylene response factor (ERF) family, 80 from the zins finger (ZF) family, 75 from the bHLH family (Figure 6; Supplementary Table S13). Other TFs belonged to the superfamilies of homeobox (44), NAC (39), WRKY (31), MADS (28), bZIP (23), Dof (22) superfamilies were also noted. The distribution of these differentially expressed TFs along salt treatment is shown in Figure 6. A large proportion of TFs from MYB, heat stress transcription factor (HSF), AP2/ERF, MADS, Dof, homeobox, NAC, B3, WRKY and nuclear factor Y (NF-Y) families were up-regulated during the whole treatment. For example,

10.3389/fpls.2024.1394223

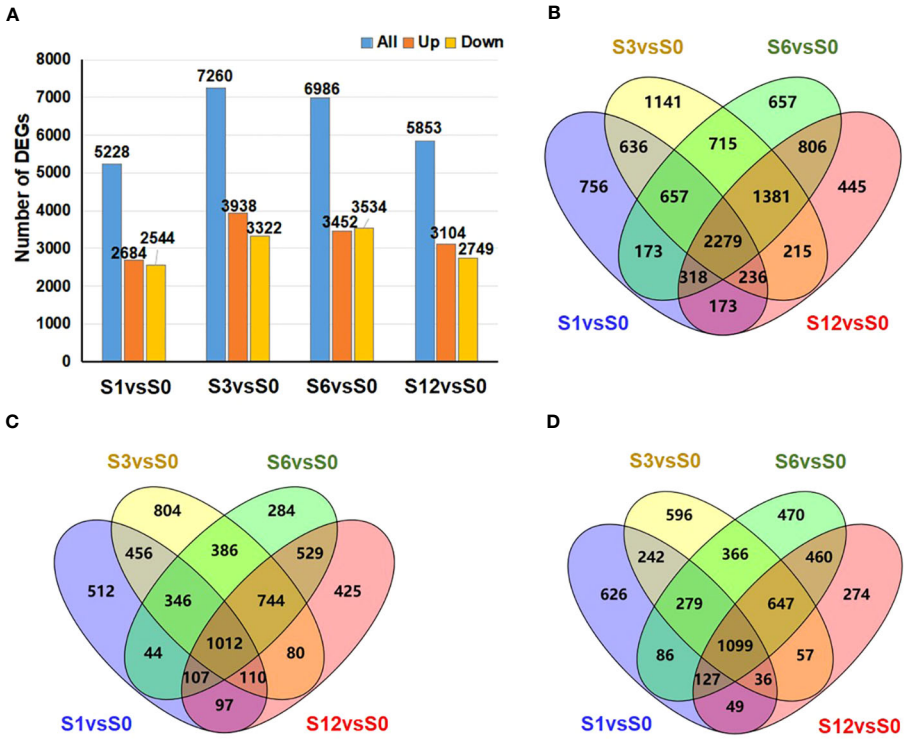

FIGURE 4
Number of DEGs during tomato root responses to salt stress. **(A)** Number of DEGs induced by salt treatment at different time point. Blue, orange and yellow bars represent the number of total DEGs, up-regulated DEGs, and down-regulated DEGs. **(B–D)** Venn diagram analysis to show the overlap or time-specific DEGs among different salt-treated groups. **(B)** all DEGs; **(C)** up-regulated DEGs; and **(D)** down-regulated DEGs.

25 out of 31 WRKY TFs showed increased expression under salt stress (Supplementary Table S13). On the other hand, most of TFs from AT-hook, TCP, and GATA showed down-regulation. Members of ZF and bHLH TFs exhibited diverse expression patterns during salt treatment (Figure 6; Supplementary Table S13). Some of them were activated by salt stress while others were significantly down-regulated. We also noticed that TFs from MADS, homeobox and NAC families were highly induced at 3 hours after treatment.

Analysis of alternative splicing events induced by salt stress

Alternative splicing events were analyzed using the rMATS software based on transcript data. Five major types of AS patterns (Figure 7A), including alternative 5' splice site (A5SS), alternative 3' splice site (A3SS), mutually exclusive exon (MXE), retained intron (RI) and skipped exon (SE) were determined. A total of 11,217 A5SS, 29,363 A3SS, 4,052 MXE, 7,902 RI and 85,812 SE events were identified from all tested samples (Supplementary Table S14). The total numbers of AS events based on three repeats for each salt treated group (9,365 events for S1, 9,488 events for S3, 10,447 events for S6 and 8,743 events for S12 groups) were higher than that observed in S0 group (8,072) (Figure 7B; Supplementary Table S14), suggesting that salt stress promoted significant AS changes in the tomato root. SE event was the most common AS events, counting for 57% in S0, 62.9% in S1, 64.6% in S3, 64.9% in S6 and 59.5% in S12 group (Supplementary Table S14). A3SS was the second most abundant AS pattern (20.6–24.5%), followed by A5SS (7.3–9.5%), RI (5.2–6.5%) and MXE (2.5–3.2%) (Supplementary Table S14). Although the ratio of each AS type to the total AS events varied in individual group, the ratio of SE event was higher in salt treated samples than that in S0 sample.

A gene was considered to incur a differentially alternative spliced (DAS) event when at least one of the AS transcripts was significantly expressed at a log2 fold change≥1 with adjusted p value < 0.05. When compared to the S0 group, a total of 2,169 DAS events in S1, 3,479 in S3, 3,092 in S6 and 2,669 in S12 were identified (Figure 8A; Supplementary Tables S15, S16). As some genes were alternatively spliced by more than one patterns, DAS events eventually generated a total of 3,709 DAS genes induced by salt stress, including 1164 DAS genes in S1, 1855 in S3, 1658 in S6 and 1429 in S12 groups (Supplementary Tables S15, S17). Although the highest counts of total raw AS events was observed in S6 group (Figure 7B), S3 group possessed the highest number of DAS events and genes, suggesting that more extensive changes occurred at 3 hours after salt treatment. While less than 10% DAS events were found to be differentially alternative spliced by RI pattern (Supplementary Table S15), SE was the most abundant DAS event that occurred under salt stress (Figure 8A; Supplementary Table S15).

GO enrichment analysis was performed on the DAS genes (Figure 8B; Supplementary Table S18). The top GO terms were mostly related to cellular anatomical entity, catalytic activity, membrane-bound organelle, nitrogen compound metabolic process and macromolecule metabolic process.

10.3389/fpls.2024.1394223

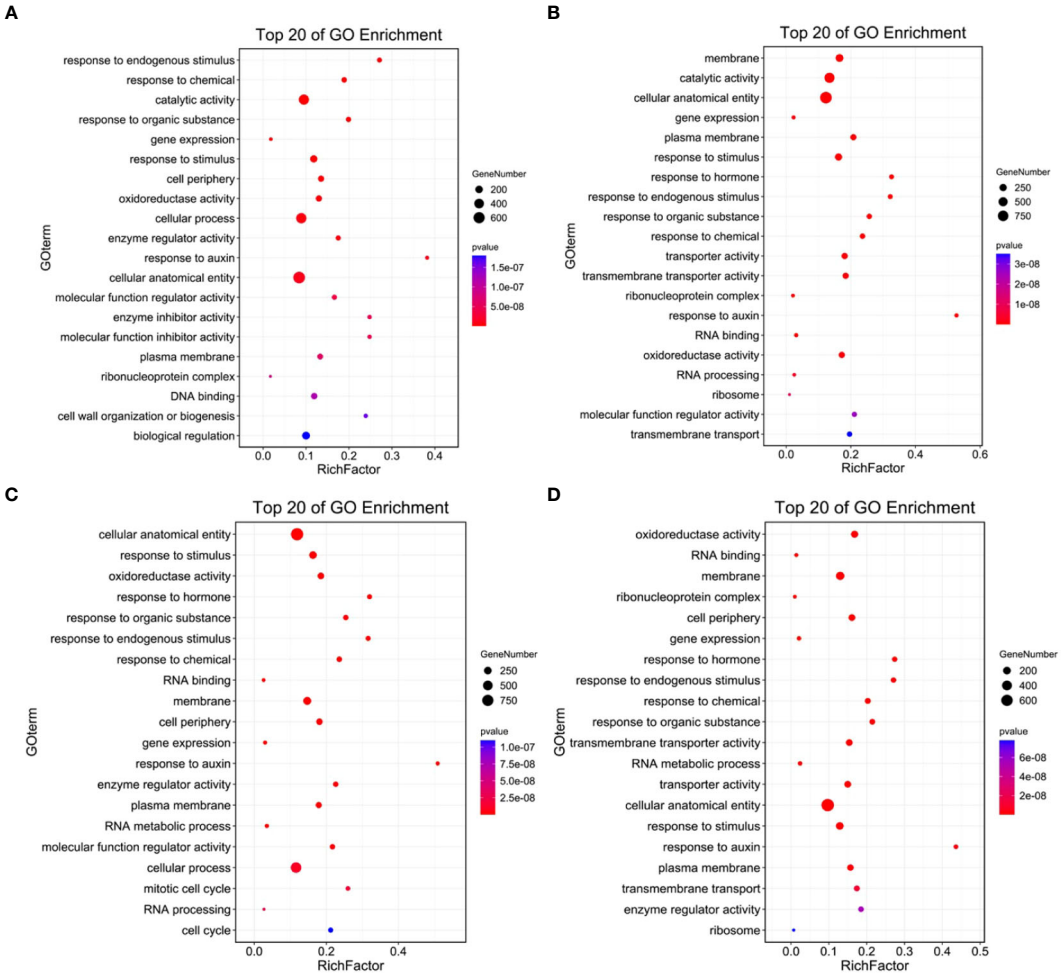

FIGURE 5
The enriched Gene Ontology (GO) terms of DEGs in salt treated samples. **(A–D)** Top 20 GO terms significantly enriched in the DEGs induced at 1 **(A)**, 3 **(B)**, 6 **(C)** and 12 **(D)** hours after salt treatment.

Venn diagram revealed that 368 DAS genes commonly alternatively spliced during the 12-hour salt treatment process (Supplementary Figure S4A; Supplementary Table S19). The top 20 GO terms enriched in the 368 common DAS genes were largely related to mitotic cycle, cytoskeleton and protein kinase (Supplementary Figure S4B; Supplementary Table S20).

The combined analysis on DEGs and DAS genes in response to salt stress

Comparison between DEG and DAS gene datasets revealed that 2,002 genes were differentially expressed due to the changes of AS events, while 1707 genes exhibited DAS-only events (Figure 8C; Supplementary Figure S5A; Supplementary Table S17). When expanded at each time point, the number of the overlapped genes between DEG and DAS events were 512 in S1 vs S0, 803 in S3 vs S0, 895 in S6 vs S0 and 689 in S12 vs S0 pairwise groups (Supplementary Figures S5B–E).

Compared to the GO analysis on the all 3,079 DAS genes (Figure 8B), the 1,707 DAS-only genes exhibited similar pathway enrichment on cellular anatomical entity, catalytic activity, membrane-bound organelle, nitrogen compound metabolic process and macromolecule metabolic process (Supplementary Figure S6A; Supplementary Table S18). When focusing on the 2,002 common genes between DEGs and DAS genes, however, mitotic cycle relevant pathways, such as spindle assembly, chromatid segregation and nuclear division, were found to be enriched (Supplementary Figure S6B; Supplementary Table S18).

Further investigation on the DAS genes revealed 117 genes coding serine/threonine-protein kinase (Figure 8D; Supplementary Table S17). Other profound gene families were pentatricopeptide repeat (PPR)-containing protein (96 genes) and E3 ubiquitin ligase (76 genes) (Figure 8D; Supplementary Table S17). Some TF families like ZF, MYB and bHLH were also detected. Among these gene families, most of the PPR-coding genes were detected in DAS only group.

Verification of AS patterns in DAS genes by RT-PCR

Six genes were selected to validate the alternative splicing pattern under salt stress by RT-PCR (Figure 9). In the study, semi-

10.3389/fpls.2024.1394223

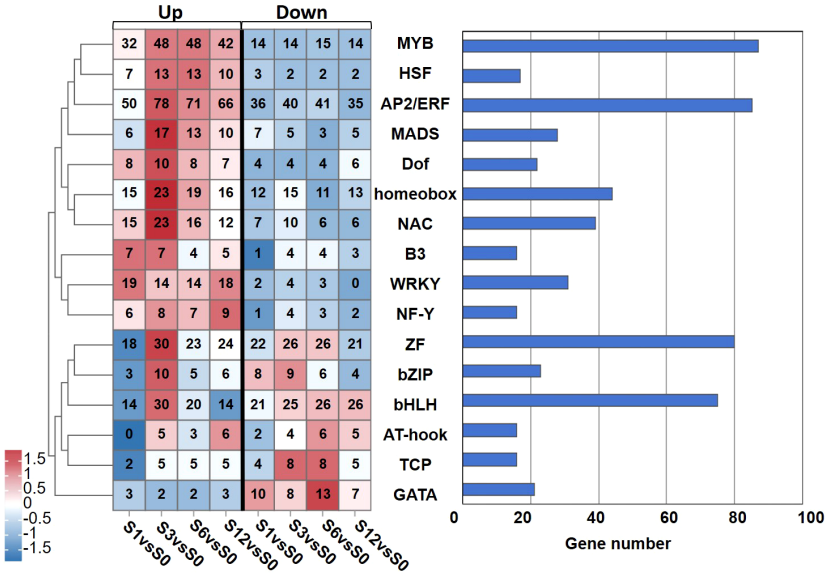

FIGURE 6
Numbers of the salt-responsive transcription factors (TFs) from the main TF families identified at different time points after salt treatment. Heatmap analysis on the distribution of up- and down-regulated TFs is shown in left panel, and total number of TFs from each family is presented in the chart on the right.

quantitative RT(sqRT)-PCR was performed to visualize the patterns of splice isoforms based on size disparity between differentially spliced transcripts (Harvey and Cheng, 2016), and quantitative RT(qRT)-PCR were carried out to quantify the expression level of each transcript. While the relative expression level of most of transcripts studied by qRT-PCR were consistent with the RNA-seq results (Figure 9; Supplementary Table S17), we observed more complex splicing events in some genes based on sqRT-PCR. Salt stress apparently increased skipping frequency of the second exon in the gene coding for a serine/argnine-rich splicing factor SR30 (101257012) (Figures 9A, B). The actual splicing pattern of F-box protein CPR1 gene (101260686) was more complicated than expected (Figures 9C, D). Except for the increase of splicing at alternative 3' splice site, extra bands were observed in the PCR products. A WRKY transcription factor (101265102) was highly induced at 12 hours after salt treatment, with an extra splicing variant detected at 6 and 12-hour treatment (Figures 9E, F). The increase of various splicing at alternative 5' splice site contributed to the expression increase of a heat stress transcription factor HsfA2 (101255223) (Figures 9G, H). Intron retention caused the increased expression of a gene coding multiple inositol polyphosphate phosphatase (101244492) (Figures 9I, J). While the expression level of a gene coding for SAGA-Tad1 like protein (101268618) (Figures 9K, L) was not significantly changed, the composition of splicing variants altered due to intron retention.

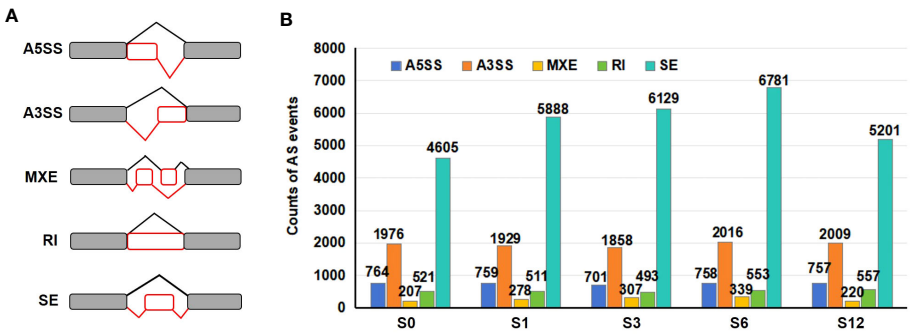

FIGURE 7
Distribution of alternative splicing events. **(A)** Diagram of five AS events detected in all 15 libraries. A5SS, alternative 5'splice site; A3SS, alternative 3' splice site; MXE, mutually exclusive exon; RI, retained intron; and SE, skipped exon. **(B)** The number of each AS event in control and salt-treated groups.

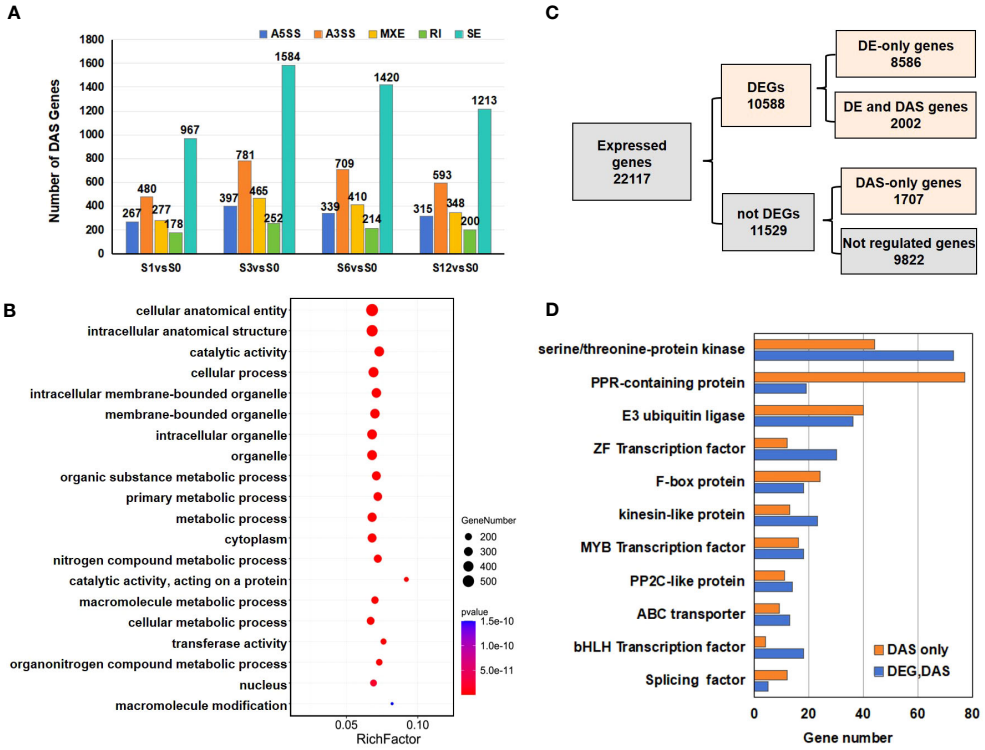

FIGURE 8
Numbers and functional analysis of DAS genes in salt treated samples. **(A)** The distribution of AS events and the number of DAS genes in salt treated samples. **(B)** The top 20 GO terms enriched in the DAS genes. **(C)** Flow chart to analyze the distribution of the 10588 DEGs and 3709 DAS genes. **(D)** List of significant DAS genes detected in the study.

The potential DEG genes responsible for AS events under salt stress

Given that the AS events were significantly altered in tomato root's response to salt stress, analysis of potential genes responsible for AS events in response to salt stress was performed (Figure 10; Supplementary Table S18). Based on the spliceosome pathway obtained from KEGG database (Figure 10A), more than 100 genes were found differentially expressed in one or more salt treated samples (Figure 10B; Supplementary Table S18). These genes encoded 42 types of splicing relevant factors, such as SR splicing factors, Prp family proteins, SnRNP proteins and other factors in U1, U2, U5, U4/6 complexes. Their expression showed dynamic changes throughout the salt stress treatment (Figure 10B; Supplementary Table S18).

Discussion

Salinity is one of the most significant environmental factors adversely affecting crop growth, development and yield. Tomato is moderately sensitive to salinity stress with seedlings especially susceptible due to its sensitive osmotic potential which is readily disrupted by salt stress during growth (Cuartero et al., 2006; Tanveer et al., 2019). Consequently, understanding of the underlying mechanisms of salinity tolerance will contribute to the breeding of salt tolerant tomato cultivars. To explore the gene regulatory network of tomato to salt stress, we investigated the early transcriptional responses to salt treatment over a 12-hour period in tomato roots.

The early morphological changes by tomato to salt stress (Figure 1) is consistent with the view that salt-specific signaling pathways are rapidly triggered in plant roots during the very early stages of salt stress (Galvan-Ampudia et al., 2013; Choi et al., 2014). The response of plant roots to salt stress involves complex regulation of gene expression at multiple levels, including at transcription, post-transcription, translation, post-translation, and metabolism, which eventually result in phenotypic changes (Barkla et al., 2013; van Zelm et al., 2020). Here we show that transcriptomic analysis of tomato roots under salt stress revealed a considerable and dynamic expression of transcripts in tomato roots during the early 12-hour treatment process of salt exposure. The gene expression patterns of continuously up or down-regulation, peak expression at 1 or 3 hours, and reduction at the first 3 hours were highly pronounced (Figure 2). The GO terms enriched in those clusters revealed the important changes of key biological processes, such as hormone signaling, cell cycle, amino acid metabolism and response to oxidative stress, during the 12-hour salt treatment.

This study revealed that amino acid metabolism was greatly enhanced at the early response of tomato root to salt treatment (Figure 2; Supplementary Table S7; Supplementary Figure S1). Amino acid metabolism is involved in various strategies during plant adaption to abiotic stress conditions (Huang and Jander, 2017; Hildebrandt, 2018; Batista-Silva et al., 2019; Reshi et al., 2023).

10.3389/fpls.2024.1394223

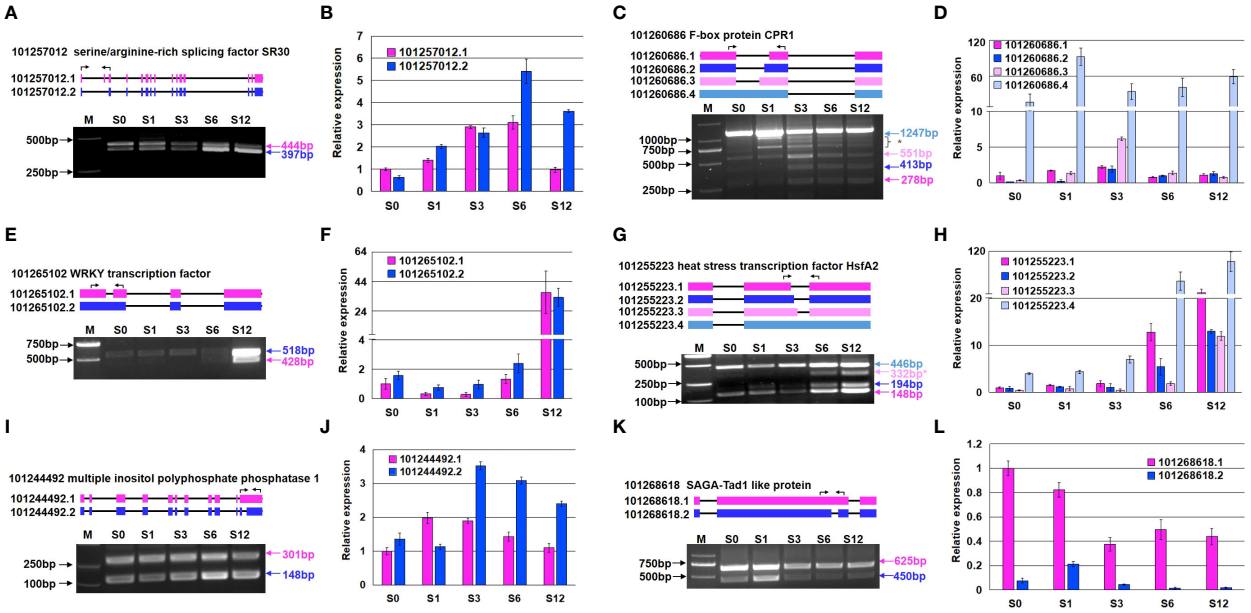

FIGURE 9
Validation of AS events in six representative genes by sqRT-PCR and qRT-PCR. **(A, B)** Expression of two transcripts of a serine/arginine-rich splicing factor SR30-like protein (101257012). **(C, D)** Expression of four transcripts of a F-box protein (101260686). **(E, F)** Expression of two transcripts of a WRKY transcription factor (101265102). **(G, H)** Expression of four transcripts of a heat stress transcription factor HsfA2 (101255223). **(I, J)** Expression of two transcripts of a multiple inositol polyphosphate phosphatase (101244492). **(K, L)** Expression of two transcripts of a SAGA-ted1-like protein (101268618). Panels **(A, C, E, G, I, K)** show the results of sqRT-PCR, and panels **(B, D, F, H, J, L)** depict the results of qRT-PCR. The asterisk (*) next to the band represents an unknown or abnormal alternative splice form. The black arrow on top of diagram indicates the location sites of the specific primers used for sqRT-PCR. Molecular markers are labeled on the left side, and the size of each transcript on the right side of gel picture. The transcript expression levels in panels **(B, D, F, H, J, L)** were relative to the transcript 1 of each gene and obtained from three independent replicates. The primers used for RT-PCR are listed in Supplementary Table S22.

Accumulation of free amino acids have been generally observed in diverse plants under various abiotic stress (Hildebrandt et al., 2015; Huang and Jander, 2017) and the enhancement of amino acid biosynthesis and amino acid transmembrane transport have been reported to improve plant tolerance to salt stress (Batista-Silva et al., 2019; Shohan et al., 2019). While some amino acids like proline are known to be potential ROS scavengers to protect plant cell from oxidative damage (Hayat et al., 2012), several amino acids, such as phenylalanine, tyrosine and tryptophan, arginine, methionine and lysine, act as precursors for the synthesis of nitrogenous secondary metabolites and signaling molecules (Tzin and Galili, 2010; Batista-Silva et al., 2019; Heinemann and Hildebrandt, 2021). Therefore, enhancement of amino acid metabolism is likely to be an important adaptive strategies to eliminate the adverse effects of salt stress in tomato root. On the other hand, it's known that the high levels of ROS concentration can affect amino acid metabolism, specially the site-specific chemical modification of amino acids such as arginine, lysine, proline, threonine and tryptophan, which cause increased vulnerability to proteolytic degradation (Moller et al., 2007). In this study, most of the DEGs involved in response to ROS and oxidative stress exhibited a continuously up-regulated expression pattern, suggesting the continuous accumulation of ROS throughout treatment of salt stress (Figure 2; Supplementary Table S7, cluster 9). Thus, the ROS accumulation induced by salt stress may contribute to the considerable changes of amino acid metabolic and catabolic processes under salt tress.

Plant hormones play vital roles in maintaining plant growth and enable plants to survive under conditions of salt stress (Ryu and Cho, 2015; Yu et al., 2020). It was reported that tomatoes could adapt to salt stress by dynamically regulating their hormone levels to establish new hormone balance (Wang et al., 2023a). The levels of ABA, SA, and JA and their respective signal transduction pathways were reported to be significantly increased, while decrease in the levels of GA and IAA were observed during the early response to salt stress (Wang et al., 2023a). In the current study, we also observed the dynamic regulation of plant hormone signaling transduction. Regulation of ABA and auxin-mediated signaling pathways were found to be significantly pronounced throughout the early response to salt stress (Figure 5; Supplementary Tables S7, S11). ABA is the primary hormone that promotes plant salt tolerance (Sah et al., 2016; Vishwakarma et al., 2017; Pye et al., 2018) where auxins promote plant growth (Zhang et al., 2022). The majority of genes involved in both hormone pathways appeared in expression clusters exhibiting continuous down-regulation or enhanced expression within the first 6 hours. This suggests that the regulation of salt tolerance and growth are closely intertwined. In contrast to a previous study (Wang et al., 2023a), significant regulation of the SA-mediated signaling pathway were not detected. On the other hand, response to JA was found to be prominent throughout the early response to salt stress (Supplementary Table S7). A previous study by Abouelsaad and Renault (2018) found that activation of JA signaling pathway enhanced tomato salt tolerance, aligning with our current result.

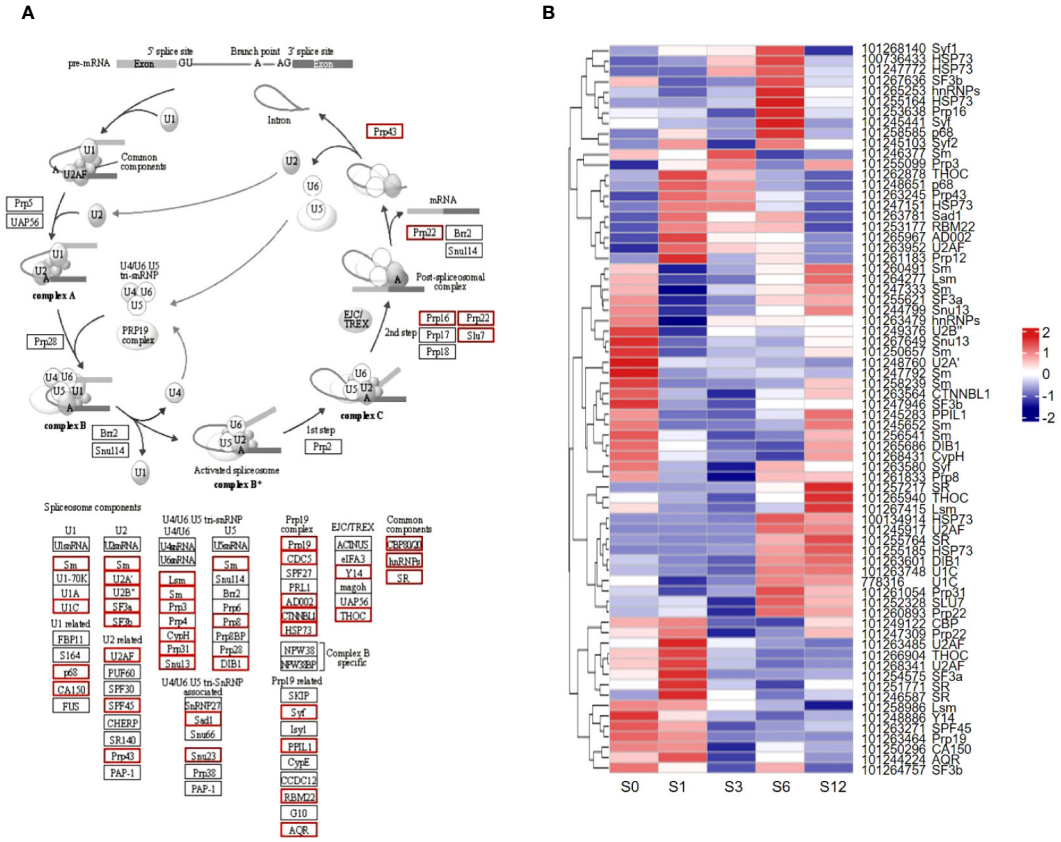

FIGURE 10
Differential expression of splicing related genes. **(A)** The spliceosome pathway based on KEGG analysis. Red boxes indicate differentially expressed genes. **(B)** Heatmap of differentially expressed spliceosome-related genes. NCBI gene IDs and potential gene names are listed on the right.

Cytokinin is another important hormone that modulates plant development and tolerance to various environmental stimuli (Mandal et al., 2022; Papon and Courdavault, 2022; Yin et al., 2023) by regulating cell cycle and differentiation, promoting antioxidant systems, impeding plant senescence, and cross-talking with stress-related phytohormones (Liu et al., 2020; Mandal et al., 2022). While defective cytokinin signaling mitigates high salinity in *Arabidopsis* via regulation of the lipid and flavonoid gene-to-metabolite networks, enhancement of cytokinin content was reported to improve tomato salt tolerance in tomato (Zizkova et al., 2015). We noticed that the pathway of response to cytokinin was only enriched in the cluster of down-regulated DEGs (Figure 2, cluster 10; Supplementary Table S7), suggesting that cytokinin-mediated signaling pathway was suppressed during the early response of tomato root to salt stress.

Transcription factors (TFs) play a central role to regulate the expression of the genes responsible for plant stress tolerance. Numerous TFs from the families like bZIP, NAC, WRKY, MADS, MYB, ZF, HSF and bHLH families are involved in conferring salt tolerance in various crop species (Duan et al., 2019; Zang et al., 2019; Li et al., 2020; Guo et al., 2021; Li et al., 2021; Wang et al., 2021a, Wang et al., 2021b; Liu et al., 2023; Rosca et al., 2023; Sukumaran et al., 2023; Ye et al., 2023; Wang et al., 2023b), including in tomato (Pan et al., 2010, Pan et al., 2012; Wang et al., 2013; Klay et al., 2014; Campos et al., 2016; Bai et al., 2018; Klay et al., 2018; Li et al., 2018; Waseem et al., 2019; Zhang et al., 2020; Guo et al., 2021; Qian et al., 2021; Chen et al., 2022) In this study, more than 700 TFs were found to be differentially expressed in tomato roots under salt stress (Supplementary Table S13) with members from MYB, ZF, bHLH and AP2/ERF gene families being the most abundant. Among these salt responsive TFs, several of them were previously reported to modulate tomato salt tolerance. For example, a R1-MYB type TF coding gene, *SlARS1* (Gene ID 101257705), that was reported to affect ABA-mediated stomatal conductance under salt stress (Campos et al., 2016), was found to be significantly induced under salt stress especially at 3-hour salt induction (Supplementary Table S13); SlWRKY13 previously proved to be negative regulator of tomato salt tolerance (Birhanu et al., 2020) was among the decreased WRKY TF group in this study. We also observed significant down-regulation of several AP2/ERF family TFs (Supplementary Table S13), such as *SlERF.B1* (Gene ID 543867) (Wang Y. et al., 2022) and *SlERF.B3* (Gene ID 108511945) (Klay et al., 2014) that negatively regulate tomato salt tolerance. Given the key roles of transcription factors in regulation of salt response in plants, the salt-sensitive TFs identified in this study deserve further investigation in the future.

Alternative splicing (AS) is an important post-transcriptional mechanism that regulates plant growth and development and is

prevalent during stress (Kelemen et al., 2013; Jabre et al., 2019; Punzo et al., 2020; Rosenkranz et al., 2022). In tomato, around 65% of the annotated protein-coding genes possess multiple transcript isoforms (Clark et al., 2019). Alternative splicing changes have been reported in tomato plants grown under phytotron vs greenhouse conditions (Wang et al., 2017), in inflorescences of cultivated and wild tomato species (Zhou et al., 2022), during fruit development regulation (Sun and Xiao, 2015; Wang et al., 2016), pollen responses to heat stress (Keller et al., 2017), tomato responses to drought stress (Lee et al., 2020), water deficit stress (Ruggiero et al., 2022), low nitrate stress (Ruggiero et al., 2022), phosphate starvation (Tian et al., 2021), and response to the fungal infection by *Trichoderma harzianum* (De Palma et al., 2019). Based on these studies, differential alternative splicing (DAS) was found to be tissue-specific, developmental stage-related or stress-responsive condition. As there is limited understanding regarding the involvement of alternative splicing in tomato's response to salt stress, we investigated the changes of AS events during early response of tomato root to salt stress in this stduy (Figure 3A, 4B). A total of 46,115 AS events, including A5SS, A3SS, RI, MXE and SE, were detected in the tomato root transcriptome (Figure 7; Supplementary Table S14), revealing a comprehensive and dynamic alteration in AS patterns in tomato roots during early responses to salt stress. An integrated genome-wide study (Clark et al., 2019) reported that RI was the prevalent AS event (18.9%) followed by alternative A5SS and A3SS, while SE was the least AS type, accounting for only 6%, among total 369,911 AS events in tomato. By contrast, SE was the most abundant AS event in tomato root under salt stress (Figure 7; Supplementary Table S14), suggesting that the alternative splicing pattern of SE might be susceptible to salt stress in tomato root. The dominance of SE in AS events was also previously reported in tomato root and shoot during phosphate starvation (Tian et al., 2021) and in date palm seedlings under salt stress (Xu et al., 2021), suggesting that AS patterns are not constant, but may change depending on the abiotic condition. On the other hand, RI event was reported to be the most frequent event induced by salt stress in *Arabidiopsis* (Ding et al., 2014b), wheat (Liu et al., 2018), cotton (Zhu et al., 2018) and Barley (Fu et al., 2019), while A3SS was the mostly affected AS events in rice by salt stress (Fu et al., 2019). Given that the differences in AS profiles are related to tissue type, stress condition and genotype (Gan et al., 2011; Vitulo et al., 2014; Martín et al., 2021; Zhou et al., 2022), the differences on the alternative splicing preference induced by salt may contribute to the evolutionary adaptation process in tomato.

Salt-induced AS of non-differentially expressed genes may contribute to the transcriptome reprogramming for salt tolerance of tomato root. Interestingly, except for unclassified genes, differentially alternative splicing induced by salt stress in tomato root were largely detected in the gene families of serine/threonine-protein kinase, PPR-containing protein, and E3 ubiquitin ligase (Figure 8D). Serine/threonine-protein kinases are key enzymes that reversibly phosphorylate the OH group of serine or threonine residues at the post-translational level. The network of serine/threonine kinases in plant cells is considered a central unit to accept and convert signaling information from sensing receptors of various stimulus and phytohormones and in turn guide responsive changes in gene expression, metabolism, plant growth and development (Hardie, 1999). One of the most representative serine/threonine-protein kinases belong to the SnRK2 family, which are involved in the ABA-dependent signaling pathway to regulate plant development and plant responses to diverse abiotic stresses (Kulik et al., 2011). Ubiquitin E3 ligases are major players that catalyze the covalent attachment of ubiquitin to target proteins (Mazzucotelli et al., 2006; Kelley, 2018). Ubiquitination of substrates is a dynamically regulated process and can generate diverse functional outcomes like potential degradation or activation of target proteins and changes in subcellular localization (Kelley, 2018). E3 ubiquitin ligases are thus well-known to be central regulators of many plants molecular processes, including plant hormone biosynthesis, signaling transduction and response to various stress conditions (Wang S. et al., 2022). AS susceptibility of serine/threonine kinases and E3 ubiquitin ligases in tomato root under salt stress poses as an additional complication in understanding the relationship between hormone signaling transduction and salt-responsive gene regulation. Pentatricopeptide (PPR) proteins are characterized by tandem arrays of a degenerate 35-amino-acid sequence motifs (Lurin et al., 2004). They are a large family of modular RNA-binding proteins with essential roles in organelle biogenesis, RNA editing, mRNA maturation and thus involved in many diverse biological processes during plant growth, development and stress acclimation (Barkan and Small, 2014). A previous genome-wide analysis revealed that the tomato genome has 471 PPR-coding genes (Ding et al., 2014a). In this study, extensive AS occurred in PPR-coding genes under salt stress as 96 out of the 471 PPR-coding genes were found to be differentially alternative spliced (Figure 8D; Supplementary Table S17). The dynamic AS changes of PPR-coding genes may also contribute to the gene regulation and transcriptome reprogramming under salt stress.

We also observed that some genes, such as the genes coding CPR1-like F-box protein and HsfA2 in Figure 9, were abnormally spliced under salt. These observations indicate that AS modulation in response to salt stress is more complicated than previously envisioned and that modulation of alternative splicing deserves more attention in future studies. The genes and their transcripts identified in the present study can be targeted for the improvement of tomato salt tolerance.

Analysis on the differential expression of spliceosome pathway-associated proteins (Figure 10) revealed the potential roles of specific groups of AS-associated proteins in regulating tomato root response to salt stress. Expression of many genes coding key component assembled in spliceosome machinery, such as small nuclear ribonucleoprotein complexes (snRNPs), U1, U2, U4, U5, and U6, was found to be affected in tomato root under salt stress. Except for core components of spliceosome machinery, the expression of trans-factors, including serine/arginine-rich (SR) proteins and heterogeneous nuclear ribonucleoprotein (hnRNP), were also significantly regulated under salt stress (Figure 10; Supplementary Table S21). In addition to differential expression,

alternative splicing in some of AS-related genes, such as SR-like splicing factors (Figure 8D; Supplementary Table S17), was also observed, which adds an additional complication of AS regulation during salt stress. It is reported that the salt-responsive regulation of SR gene isoforms may result in inaccurate identification of splicing sites and destabilization of the spliceosome complex (Albaqami et al., 2019; Xu et al., 2021; Laloum et al., 2023). Therefore, future studies on the AS events of splicing-related proteins will provide new insights on how genes are regulated in salt-stressed tomato.

Collectively, this study provides a comprehensive view of transcriptome changes and highlights the key role of AS in tomato root response to salt stress. A large number of DEGs and DAS genes involved in diverse metabolic pathways, such as hormone signaling transduction, DNA transcription, RNA binding and processing, were identified. The findings in this study expand our current understanding of transcriptional and post-transcriptional regulation in the response of tomato roots to salinity stress and provide an important gene resource for developing salt-tolerant tomato plants.

Materials and methods

Plant materials and salt stress treatment

Tomato seeds (*S. lycopersicum* cv. Ailsa Craig) were sown in a nutrient soil mixture with a ratio of 3:1 (w/w) and cultivated in an illumination incubator under standard conditions (16 hours of light at 26°C, followed by 8 hours of darkness at 20°C). After three weeks, the seedlings were transferred to pots filled with 1/2 Hoagland's nutrient solution following root rinsing under running water. After two additional weeks, seedlings of uniformed size were selected and treated with 150 mM NaCl. Three biological replicates of root samples were collected at 0, 1, 3, 6, and 12 hours post treatment. All samples were immediately frozen in liquid nitrogen and stored at -80°C for further use.

RNA extraction, library construction and sequencing

Total RNAs were extracted from root samples with TransZol UP Plus RNA kit (Tiangen Biotech, China). The mRNAs used for cDNA library construction were isolated from total RNAs using oligo-dT magnetic beads. A total of 15 cDNA sequencing libraries were constructed and sequenced using the DNBSEQ^{TM} technology (Beijing Genomics institution, China) following the manufacturer's recommendations to generate paired-end sequencing data.

RNA-seq analysis

The raw sequencing data was filtered by SOAPnuke v1.5.6 (https://github.com/BGI-flexlab/SOAPnuke) to remove low-quality reads, and the high-quality reads were mapped against the reference *S. lycopersicum* genome (Version SL3.1, https://www.ncbi.nlm.nih.gov/datasets/genome/GCF_000188115.5/) using the HISAT2 software (v2.1.0) (http://www.ccb.jhu.edu/software/hisat/index.shtml) with default parameters. Detection of differentially expressed genes was performed using Bowtie2 (v2.3.4.3) (http://bowtiebio.sourceforge.net/Bowtie2/index.shtml) and DESeq2 (v1.4.5) (http://www.bioconductor.org/packages/release/bioc/html/) with default parameters. The mapped reads were counted and normalized into fragments per kilobase of transcript per million (FPKM), and the expressed genes with a log2 fold change≥1 and adjusted p value < 0.05 were identified as differentially expressed genes (DEGs). Gene clustering was analyzed using the software of Dynamic Trend Analysis on https://www.omicshare.com/tools. Significantly enriched trends were determined according to a significance threshold p value<0.05 (Ernst and Bar-Joseph, 2006). Alternative splicing analysis were performed using rMATS (V3.2.5) (http://rnaseq-mats.sourceforge.net) with default parameters. Compared to control samples, alternative splicing events with adjusted p value < 0.05 were identified as differentially alternative spliced (DAS) events, and the genes that had at least one of the transcripts differentially expressed (log2 fold change≥1 and adjusted p value < 0.05) were considered to be DAS genes.

Pathway enrichment analysis

Gene Ontology (GO) analysis of the candidate gene groups was performed on https://geneontology.org/ that is powered by PATHER. Annotation version used in GO enrichment was GO Ontology database DOI:10.5281/zenodo.10536401 released on Jan 17, 2024. Kyoto Encyclopedia of Genes and Genomics (KEGG) enrichment was performed using KEGG Mapper on https://www.genome.jp/kegg/. The GO terms and KEGG pathways with p value<0.05 were defined as significantly enriched in the candidate gene groups.

Validation of alternative splicing

Semi-quantitative RT(sqRT)-PCR and quantitative RT(qRT)-PCR were performed to verify the AS pattern of six representive genes. Total RNA was subjected to first-strand cDNA synthesis using *EVo M-MLVRT* Mix Kit with gDNA Clean for qPCR Ver.2 (Vazyme, Nanjing, China) following the manufacturer's instructions. Specific primers of target genes (Supplementary Table S22) were designed using the NCBI primer design tool (https://www.ncbi.nlm.nih.gov/tools/primerblast). sqRT-PCR was conducted with HotStarTaq Plus DNA Polymerase Reagents (Qiagen) and the melting temperature (Tm) was optimized based on different sequences of the primers. PCR products were visualized via horizontal gel electrophoresis using a 2% agarose-TBE gel. Reactions of qRT-PCR were carried out on Applied Biosystems StepOnePlus instrument using SYBR Green Premix *Pro Taq* HS qPCR Kit (Vazyme, Nanjing, China). The gene encoding ribosomal protein L2 (RPL2) (Løvdal and Lillo, 2009) was used as internal

reference for qRT-PCR. Three independent replicates were tested for each transcript.

Data availability statement

The sequencing data are available at https://www.ncbi.nlm.nih.gov/sra/ at NCBI with accession number PRJNA1110838.

Author contributions

JG: Data curation, Investigation, Writing – original draft. YQ: Data curation, Formal analysis, Writing – original draft. YT: Investigation, Writing – original draft. LZ: Data curation, Writing – review & editing. TWO: Validation, Writing – review & editing. YY: Conceptualization, Methodology, Writing – original draft. LT: Conceptualization, Data curation, Supervision, Writing – original draft, Writing – review & editing.

Funding

The author(s) declare financial support was received for the research, authorship, and/or publication of this article. This work is supported by grants from the National Natural Science Foundation of China (NSFC, Grant No. 32272741) and Zhejiang A&F University Starting Funds of Scientific Research and Development (203402000101).

Conflict of interest

The authors declare that the research was conducted in the absence of any commercial or financial relationships that could be construed as a potential conflict of interest.

Publisher's note

Supplementary material

The Supplementary Material for this article can be found online at: https://www.frontiersin.org/articles/10.3389/fpls.2024.1394223/full#supplementary-material

References

Abouelsaad, I., and Renault, S. (2018). Enhanced oxidative stress in the jasmonic acid-deficient tomato mutant def-1 exposed to NaCl stress. *J. Plant Physiol.* 226, 136–144. doi: 10.1016/j.jplph.2018.04.009

Albaqami, M., Laluk, K., and Reddy, A. S. N. (2019). The Arabidopsis splicing regulator SR45 confers salt tolerance in a splice isoform-dependent manner. *Plant Mol. Biol.* 100, 379–390. doi: 10.1007/s11103–019-00864–4

Bai, Y., Kissoudis, C., Yan, Z., Visser, R. G. F., and van der Linden, G. (2018). Plant behaviour under combined stress: tomato responses to combined salinity and pathogen stress. *Plant J.* 93, 781–793. doi: 10.1111/tpj.13800

Balasubramaniam, T., Shen, G., Esmaeili, N., and Zhang, H. (2023). Plants' Response mechanisms to salinity stress. *Plants (Basel)* 12, 4810. doi: 10.3390/plants12122253

Barkan, A., and Small, I. (2014). Pentatricopeptide repeat proteins in plants. *Annu. Rev. Plant Biol.* 65, 415–442. doi: 10.1146/annurev-arplant-050213–040159

Barkla, B. J., Castellanos-Cervantes, T., de Leon, J. L., Matros, A., Mock, H. P., Perez-Alfocea, F., et al. (2013). Elucidation of salt stress defense and tolerance mechanisms of crop plants using proteomics–current achievements and perspectives. *Proteomics* 13, 1885–1900. doi: 10.1002/pmic.201200399

Batista-Silva, W., Heinemann, B., Rugen, N., Nunes-Nesi, A., Araujo, W. L., Braun, H. P., et al. (2019). The role of amino acid metabolism during abiotic stress release. *Plant Cell Environ.* 42, 1630–1644. doi: 10.1111/pce.13518

Birhanu, M. W., Kissoudis, C., and van der Linden, C. G. (2020). WRKY gene silencing enhances tolerance to salt stress in transgenic tomato. *J. Biol. Agric. Healthcare* 10, 14–25. doi: 10.7176/JBAH/10–17-03

Bonarota, M. S., Kosma, D. K., and Barrios-Masias, F. H. (2022). Salt tolerance mechanisms in the Lycopersicon clade and their trade-offs. *AoB Plants* 14, plab072. doi: 10.1093/aobpla/plab072

Campos, J. F., Cara, B., Perez-Martin, F., Pineda, B., Egea, I., Flores, F. B., et al. (2016). The tomato mutant ars1 (altered response to salt stress 1) identifies an R1-type MYB transcription factor involved in stomatal closure under salt acclimation. *Plant Biotechnol. J.* 14, 1345–1356. doi: 10.1111/pbi.12498

Chaves, M. M., Flexas, J., and Pinheiro, C. (2009). Photosynthesis under drought and salt stress: regulation mechanisms from whole plant to cell. *Ann. Bot.* 103, 551–560. doi: 10.1093/aob/mcn125

Chen, Y., Feng, P., Zhang, X., Xie, Q., Chen, G., Zhou, S., et al. (2022). Silencing of SlMYB50 affects tolerance to drought and salt stress in tomato. *Plant Physiol. Biochem.* 193, 139–152. doi: 10.1016/j.plaphy.2022.10.026

Choi, W. G., Toyota, M., Kim, S. H., Hilleary, R., and Gilroy, S. (2014). Salt stress-induced Ca2+ waves are associated with rapid, long-distance root-to-shoot signaling in plants. *Proc. Natl. Acad. Sci. U.S.A.* 111, 6497–6502. doi: 10.1073/pnas.1319955111

Clark, S., Yu, F., Gu, L., and Min, X. J. (2019). Expanding alternative splicing identification by integrating multiple sources of transcription data in tomato. *Front. Plant Sci.* 10. doi: 10.3389/fpls.2019.00689

Cuartero, J., Bolarín, M. C., Asíns, M. J., and Moreno, V. (2006). Increasing salt tolerance in the tomato. *J. Exp. Bot.* 5, 1045–1058. doi: 10.1093/jxb/erj102

De Palma, M., Salzano, M., Villano, C., Aversano, R., Lorito, M., Ruocco, M., et al. (2019). Transcriptome reprogramming, epigenetic modifications and alternative splicing orchestrate the tomato root response to the beneficial fungus Trichoderma harzianum. *Hortic. Res.* 6, 5. doi: 10.1038/s41438–018-0079–1

Ding, A., Li, L., Qu, X., Sun, T., Chen, Y., Zong, P., et al. (2014a). [Genome-wide identification and bioinformatic analysis of PPR gene family in tomato]. *Yi Chuan* 36, 77–84. doi: 10.3724/sp.j.1005.2014.00077

Ding, F., Cui, P., Wang, Z., Zhang, S., Ali, S., and Xiong, L. (2014b). Genome-wide analysis of alternative splicing of pre-mRNA under salt stress in Arabidopsis. *BMC Genomics* 15, 431. doi: 10.1186/1471–2164-15–431

Duan, S., Liu, B., Zhang, Y., Li, G., and Guo, X. (2019). Genome-wide identification and abiotic stress-responsive pattern of heat shock transcription factor family in Triticum aestivum L. *BMC Genomics* 20, 257. doi: 10.1186/s12864-019-5617-1

Ernst, J., and Bar-Joseph, Z. (2006). STEM: a tool for the analysis of short time series gene expression data. *BMC Bioinf.* 7, 191. doi: 10.1186/1471-2105-7-191

FAO (2021) *Global Map of Salt-affected Soils (GSASmap) V1.0.0.* Available at: https://www.fao.org/soils-portal/data-hub/soil-maps-and-databases/global-map-of-salt-affected-soils/en.

FAO (2022) *Agricultural production statistics 2000–2022.* Available at: https://openknowledge.fao.org/server/api/core/bitstreams/dc1b16d6–44af-4d50–9544-10fcb8a3779f/content.

Feng, J., Li, J., Gao, Z., Lu, Y., Yu, J., Zheng, Q., et al. (2015). SKIP confers osmotic tolerance during salt stress by controlling alternative gene splicing in Arabidopsis. *Mol. Plant* 8, 1038–1052. doi: 10.1016/j.molp.2015.01.011

Fu, L., Shen, Q., Kuang, L., Wu, D., and Zhang, G. (2019). Transcriptomic and alternative splicing analyses reveal mechanisms of the difference in salt tolerance between barley and rice. *Environ. Exp. Bot.* 166, 103810. doi: 10.1016/j.envexpbot.2019.103810

Galvan-Ampudia, C. S., Julkowska, M. M., Darwish, E., Gandullo, J., Korver, R. A., Brunoud, G., et al. (2013). Halotropism is a response of plant roots to avoid a saline environment. *Curr. Biol.* 23, 2044–2050. doi: 10.1016/j.cub.2013.08.042

Gan, X., Stegle, O., Behr, J., Steffen, J. G., Drewe, P., Hildebrand, K. L., et al. (2011). Multiple reference genomes and transcriptomes for Arabidopsis thaliana. *Nature* 477, 419–423. doi: 10.1038/nature10414

Gu, J., Xia, Z., Luo, Y., Jiang, X., Qian, B., Xie, H., et al. (2018). Spliceosomal protein U1A is involved in alternative splicing and salt stress tolerance in Arabidopsis thaliana. *Nucleic Acids Res.* 46, 1777–1792. doi: 10.1093/nar/gkx1229

Guo, J., Sun, B., He, H., Zhang, Y., Tian, H., and Wang, B. (2021). Current understanding of bHLH transcription factors in plant abiotic stress tolerance. *Int. J. Mol. Sci.* 22, 4921. doi: 10.3390/ijms22094921

Han, M., Niu, M., Gao, T., Shen, Y., Zhou, X., Zhang, Y., et al. (2024). Responsive alternative splicing events of opisthopappus species against salt stress. *Int. J. Mol. Sci.* 25, 1227. doi: 10.3390/ijms25021227

Hardie, D. G. (1999). PLANT PROTEIN SERINE/THREONINE KINASES: classification and functions. *Annu. Rev. Plant Physiol. Plant Mol. Biol.* 50, 97–131. doi: 10.1146/annurev.arplant.50.1.97

Harvey, S. E., and Cheng, C. (2016). Methods for characterization of alternative RNA splicing. *Methods Mol. Biol.* 1402, 229–241. doi: 10.1007/978-1-4939-3378-5_18

Hasanuzzaman, M., and Fujita, M. (2022). Plant responses and tolerance to salt stress: physiological and molecular interventions. *Int. J. Mol. Sci.* 23, 4810. doi: 10.3390/ijms23094810

Hasanuzzaman, M., and Fujita, M. (2023). Plant responses and tolerance to salt stress: physiological and molecular interventions 2.0. *Int. J. Mol. Sci.* 24, 15740. doi: 10.3390/ijms242115740

Hayat, S., Hayat, Q., AlYemeni, M. N., Wani, A. S., Pichtel, J., and Ahmad, A. (2012). Role of proline under changing environments: a review. *Plant Signal Behav.* 7, 1456–1466. doi: 10.4161/psb.21949

Heinemann, B., and Hildebrandt, T. M. (2021). The role of amino acid metabolism in signaling and metabolic adaptation to stress-induced energy deficiency in plants. *J. Exp. Bot.* 72, 4634–4645. doi: 10.1093/jxb/erab182

Hildebrandt, T. M. (2018). Synthesis versus degradation: directions of amino acid metabolism during Arabidopsis abiotic stress response. *Plant Mol. Biol.* 98, 121–135. doi: 10.1007/s11103-018-0767-0

Hildebrandt, T. M., Nunes Nesi, A., Araujo, W. L., and Braun, H. P. (2015). Amino acid catabolism in plants. *Mol. Plant* 8, 1563–1579. doi: 10.1016/j.molp.2015.09.005

Huang, T., and Jander, G. (2017). Abscisic acid-regulated protein degradation causes osmotic stress-induced accumulation of branched-chain amino acids in Arabidopsis thaliana. *Planta* 246, 737–747. doi: 10.1007/s00425-017-2727-3

Jabre, I., Reddy, A. S. N., Kalyna, M., Chaudhary, S., Khokhar, W., Byrne, L. J., et al. (2019). Does co-transcriptional regulation of alternative splicing mediate plant stress responses? *Nucleic Acids Res.* 47, 2716–2726. doi: 10.1093/nar/gkz121

Jamil, A., Riaz, S., Ashraf, M., and Foolad, M. R. (2011). Gene expression profiling of plants under salt stress. *Crit. Rev. Plant Sci.* 30, 435–458. doi: 10.1080/07352689.2011.605739

Jian, G., Mo, Y., Hu, Y., Huang, Y., Ren, L., Zhang, Y., et al. (2022). Variety-specific transcriptional and alternative splicing regulations modulate salt tolerance in rice from early stage of stress. *Rice (N Y)* 15, 56. doi: 10.1186/s12284-022-00599-9

Jin, Z., Lv, X., Sun, Y., Fan, Z., Xiang, G., and Yao, Y. (2021). Comprehensive discovery of salt-responsive alternative splicing events based on Iso-Seq and RNA-seq in grapevine roots. *Environ. Exp. Bot.* 192, 104645. doi: 10.1016/j.envexpbot.2021.104645

Kelemen, O., Convertini, P., Zhang, Z., Wen, Y., Shen, M., Falaleeva, M., et al. (2013). Function of alternative splicing. *Gene* 514, 1–30. doi: 10.1016/j.gene.2012.07.083

Keller, M., Hu, Y., Mesihovic, A., Fragkostefanakis, S., Schleiff, E., and Simm, S. (2017). Alternative splicing in tomato pollen in response to heat stress. *DNA Res.* 24, 205–217. doi: 10.1093/dnares/dsw051

Kelley, D. R. (2018). E3 ubiquitin ligases: key regulators of hormone signaling in plants. *Mol. Cell Proteomics* 17, 1047–1054. doi: 10.1074/mcp.MR117.000476

Keren, H., Lev-Maor, G., and Ast, G. (2010). Alternative splicing and evolution: diversification, exon definition and function. *Nat. Rev. Genet.* 11, 345–355. doi: 10.1038/nrg2776

Kesawat, M. S., Satheesh, N., Kherawat, B. S., Kumar, A., Kim, H. U., Chung, S. M., et al. (2023). Regulation of reactive oxygen species during salt stress in plants and their crosstalk with other signaling molecules-current perspectives and future directions. *Plants (Basel)* 12, 864. doi: 10.3390/plants12040864

Klay, I., Gouia, S., Liu, M., Mila, I., Khoudi, H., Bernadac, A., et al. (2018). Ethylene Response Factors (ERF) are differentially regulated by different abiotic stress types in tomato plants. *Plant Sci.* 274, 137–145. doi: 10.1016/j.plantsci.2018.05.023

Klay, I., Pirrello, J., Riahi, L., Bernadac, A., Cherif, A., Bouzayen, M., et al. (2014). Ethylene response factor Sl-ERF.B.3 is responsive to abiotic stresses and mediates salt and cold stress response regulation in tomato. *Sci. World J.* 2014, 167681. doi: 10.1155/2014/167681

Kulik, A., Wawer, I., Krzywinska, E., Bucholc, M., and Dobrowolska, G. (2011). SnRK2 protein kinases–key regulators of plant response to abiotic stresses. *OMICS* 15, 859–872. doi: 10.1089/omi.2011.0091

Laloum, T., Carvalho, S. D., Martin, G., Richardson, D. N., Cruz, T. M. D., Carvalho, R. F., et al. (2023). The SCL30a SR protein regulates ABA-dependent seed traits and germination under stress. *Plant Cell Environ.* 46, 2112–2127. doi: 10.1111/pce.14593

Lawlor, D. W., and Cornic, G. (2002). Photosynthetic carbon assimilation and associated metabolism in relation to water deficits in higher plants. *Plant Cell Environ.* 25, 275–294. doi: 10.1046/j.0016-8025.2001.00814.x

Lee, H. J., Eom, S. H., Lee, J. H., Wi, S. H., Kim, S. K., and Hyun, T. K. (2020). Genome-wide analysis of alternative splicing events during response to drought stress in tomato (*Solanum lycopersicum* L.). *J. Hortic. Sci. Biotechnol.* 95, 286–293. doi: 10.1080/14620316.2019.1656552

Li, P., Peng, Z., Xu, P., Tang, G., Ma, C., Zhu, J., et al. (2021). Genome-wide identification of NAC transcription factors and their functional prediction of abiotic stress response in peanut. *Front. Genet.* 12. doi: 10.3389/fgene.2021.630292

Li, W., Pang, S., Lu, Z., and Jin, B. (2020). Function and mechanism of WRKY transcription factors in abiotic stress responses of plants. *Plants (Basel)* 9, 1410. doi: 10.3390/plants9111515

Li, Z., Tian, Y., Xu, J., Fu, X., Gao, J., Wang, B., et al. (2018). A tomato ERF transcription factor, SlERF84, confers enhanced tolerance to drought and salt stress but negatively regulates immunity against Pseudomonas syringae pv. tomato DC3000. *Plant Physiol. Biochem.* 132, 683–695. doi: 10.1016/j.plaphy.2018.08.022

Liu, Z., Qin, J., Tian, X., Xu, S., Wang, Y., Li, H., et al. (2018). Global profiling of alternative splicing landscape responsive to drought, heat and their combination in wheat (Triticum aestivum L.). *Plant Biotechnol. J.* 16, 714–726. doi: 10.1111/pbi.12822

Liu, H., Tang, X., Zhang, N., Li, S., and Si, H. (2023). Role of bZIP transcription factors in plant salt stress. *Int. J. Mol. Sci.* 24, 7893. doi: 10.3390/ijms24097893

Liu, Y., Zhang, M., Meng, Z., Wang, B., and Chen, M. (2020). Research progress on the roles of cytokinin in plant response to stress. *Int. J. Mol. Sci.* 21, 6574. doi: 10.3390/ijms21186574

Løvdal, T., and Lillo, C. (2009). Reference gene selection for quantitative real-time PCR normalization in tomato subjected to nitrogen, cold, and light stress. *Anal. Biochem.* 387, 238–242. doi: 10.1016/j.ab.2009.01.024

Lurin, C., Andres, C., Aubourg, S., Bellaoui, M., Bitton, F., Bruyere, C., et al. (2004). Genome-wide analysis of Arabidopsis pentatricopeptide repeat proteins reveals their essential role in organelle biogenesis. *Plant Cell* 16, 2089–2103. doi: 10.1105/tpc.104.022236

Mandal, S., Ghorai, M., Anand, U., Samanta, D., Kant, N., Mishra, T., et al. (2022). Cytokinin and abiotic stress tolerance -What has been accomplished and the way forward? *Front. Genet.* 13. doi: 10.3389/fgene.2022.943025

Martín, E., Vivori, C., Rogalska, M., Herrero-Vicente, J., and Valcárcel, J. (2021). Alternative splicing regulation of cell-cycle genes by SPF45/SR140/CHERP complex controls cell proliferation. *RNA* 27, 1157–1576. doi: 10.1261/rna.078935.121

Mazzucotelli, E., Belloni, S., Marone, D., De Leonardis, A., Guerra, D., Di Fonzo, N., et al. (2006). The e3 ubiquitin ligase gene family in plants: regulation by degradation. *Curr. Genomics* 7, 509–522. doi: 10.2174/138920206779315728

Moller, I. M., Jensen, P. E., and Hansson, A. (2007). Oxidative modifications to cellular components in plants. *Annu. Rev. Plant Biol.* 58, 459–481. doi: 10.1146/annurev.arplant.58.032806.103946

Pan, I. C., Li, C. W., Su, R. C., Cheng, C. P., Lin, C. S., and Chan, M. T. (2010). Ectopic expression of an EAR motif deletion mutant of SlERF3 enhances tolerance to salt stress and Ralstonia solanacearum in tomato. *Planta* 232, 1075–1086. doi: 10.1007/s00425-010-1235-5

Pan, Y., Seymour, G. B., Lu, C., Hu, Z., Chen, X., and Chen, G. (2012). An ethylene response factor (ERF5) promoting adaptation to drought and salt tolerance in tomato. *Plant Cell Rep.* 31, 349–360. doi: 10.1007/s00299-011-1170-3

Papon, N., and Courdavault, V. (2022). ARResting cytokinin signaling for salt-stress tolerance. *Plant Sci.* 314, 111116. doi: 10.1016/j.plantsci.2021.111116

Punzo, P., Grillo, S., and Batelli, G. (2020). Alternative splicing in plant abiotic stress responses. *Biochem. Soc. Trans.* 48, 2117–2126. doi: 10.1042/BST20200281

Pye, M. F., Dye, S. M., Resende, R. S., MacDonald, J. D., and Bostock, R. M. (2018). Abscisic acid as a dominant signal in tomato during salt stress predisposition to phytophthora root and crown rot. *Front. Plant Sci.* 9. doi: 10.3389/fpls.2018.00525

Qian, Y., Zhang, T., Yu, Y., Gou, L., Yang, J., Xu, J., et al. (2021). Regulatory mechanisms of bHLH transcription factors in plant adaptive responses to various abiotic stresses. *Front. Plant Sci.* 12. doi: 10.3389/fpls.2021.677611

Reshi, Z. A., Ahmad, W., Lukatkin, A. S., and Javed, S. B. (2023). From nature to lab: A review of secondary metabolite biosynthetic pathways, environmental influences, and *in vitro* approaches. *Metabolites* 13, 895. doi: 10.3390/metabo13080895

Rosca, M., Mihalache, G., and Stoleru, V. (2023). Tomato responses to salinity stress: From morphological traits to genetic changes. *Front. Plant Sci.* 14. doi: 10.3389/fpls.2023.1118383

Rosenkranz, R. R. E., Ullrich, S., Lochli, K., Simm, S., and Fragkostefanakis, S. (2022). Relevance and regulation of alternative splicing in plant heat stress response: current understanding and future directions. *Front. Plant Sci.* 13. doi: 10.3389/fpls.2022.911277

Ruggiero, A., Punzo, P., Van Oosten, M. J., Cirillo, V., Esposito, S., Costa, A., et al. (2022). Transcriptomic and splicing changes underlying tomato responses to combined water and nutrient stress. *Front. Plant Sci.* 13. doi: 10.3389/fpls.2022.974048

Ryu, H., and Cho, Y. (2015). Plant hormones in salt stress tolerance. *J. Plant Biol.* 58, 147–155. doi: 10.1007/s12374-015-0103-z

Sah, S. K., Reddy, K. R., and Li, J. (2016). Abscisic acid and abiotic stress tolerance in crop plants. *Front. Plant Sci.* 7. doi: 10.3389/fpls.2016.00571

Sayyad-Amin, P., Jahansooz, M. R., Borzouei, A., and Ajili, F. (2016). Changes in photosynthetic pigments and chlorophyll-a fluorescence attributes of sweet-forage and grain sorghum cultivars under salt stress. *J. Biol. Phys.* 42, 601–620. doi: 10.1007/s10867-016-9428-1

Shohan, M. U. S., Sinha, S., Nabila, F. H., Dastidar, S. G., and Seraj, Z. I. (2019). HKT1;5 transporter gene expression and association of amino acid substitutions with salt tolerance across rice genotypes. *Front. Plant Sci.* 10. doi: 10.3389/fpls.2019.01420

Shrivastava, P., and Kumar, R. (2015). Soil salinity: A serious environmental issue and plant growth promoting bacteria as one of the tools for its alleviation. *Saudi J. Biol. Sci.* 22, 123–131. doi: 10.1016/j.sjbs.2014.12.001

Sukumaran, S., Lethin, J., Liu, X., Pelc, J., Zeng, P., Hassan, S., et al. (2023). Genome-wide analysis of MYB transcription factors in the wheat genome and their roles in salt stress response. *Cells* 12, 1431. doi: 10.3390/cells12101431

Sun, Y., and Xiao, H. (2015). Identification of alternative splicing events by RNA sequencing in early growth tomato fruits. *BMC Genomics* 16, 948. doi: 10.1186/s12864-015-2128-6

Tanveer, K., Gilani, S., Hussain, Z., Ishaq, R., Adeel, M., and Ilyas, N. (2019). Effect of salt stress on tomato plant and the role of calcium. *J. Plant Nutr.* 43, 28–35. doi: 10.1080/01904167.2019.1659324

Tester, M., and Davenport, R. (2003). Na+ tolerance and Na+ transport in higher plants. *Ann. Bot.* 91, 503–527. doi: 10.1093/aob/mcg058

Tian, P., Lin, Z., Lin, D., Dong, S., Huang, J., and Huang, T. (2021). The pattern of DNA methylation alteration, and its association with the changes of gene expression and alternative splicing during phosphate starvation in tomato. *Plant J.* 108, 841–858. doi: 10.1111/tpj.15486

Tzin, V., and Galili, G. (2010). New insights into the shikimate and aromatic amino acids biosynthesis pathways in plants. *Mol. Plant* 3, 956–972. doi: 10.1093/mp/ssq048

van Zelm, E., Zhang, Y., and Testerink, C. (2020). Salt tolerance mechanisms of plants. *Annu. Rev. Plant Biol.* 71, 403–433. doi: 10.1146/annurev-arplant-050718-100005

Vishwakarma, K., Upadhyay, N., Kumar, N., Yadav, G., Singh, J., Mishra, R. K., et al. (2017). Abscisic acid signaling and abiotic stress tolerance in plants: A review on current knowledge and future prospects. *Front. Plant Sci.* 8. doi: 10.3389/fpls.2017.00161

Vitulo, N., Forcato, C., Carpinelli, E. C., Telatin, A., Campagna, D., D'Angelo, M., et al. (2014). A deep survey of alternative splicing in grape reveals changes in the splicing machinery related to tissue, stress condition and genotype. *BMC Plant Biol.* 14, 99. doi: 10.1186/1471-2229-14-99

Wang, K., Jiao, Z., Xu, M., Wang, Y., Li, R., Cui, X., et al. (2016). Landscape and fruit developmental regulation of alternative splicing in tomato by genome-wide analysis. *Hortic. Plant J.* 2, 338–350. doi: 10.1016/j.hpj.2017.01.007

Wang, M., Liu, C., Li, S., Zhu, D., Zhao, Q., and Yu, J. (2013). Improved nutritive quality and salt resistance in transgenic maize by simultaneously overexpression of a natural lysine-rich protein gene, SBgLR, and an ERF transcription factor gene, TSRF1. *Int. J. Mol. Sci.* 14, 9459–9474. doi: 10.3390/ijms14059459

Wang, S., Lv, X., Zhang, J., Chen, D., Chen, S., Fan, G., et al. (2022). Roles of E3 ubiquitin ligases in plant responses to abiotic stresses. *Int. J. Mol. Sci.* 23, 2308. doi: 10.3390/ijms23042308

Wang, X., Niu, Y., and Zheng, Y. (2021a). Multiple functions of MYB transcription factors in abiotic stress responses. *Int. J. Mol. Sci.* 22, 6125. doi: 10.3390/ijms22116125

Wang, B., Wang, J., Yang, T., Wang, J., Dai, Q., Zhang, F., et al. (2023a). The transcriptional regulatory network of hormones and genes under salt stress in tomato plants (*Solanum lycopersicum* L.). *Front. Plant Sci.* 14. doi: 10.3389/fpls.2023.1115593

Wang, G., Weng, L., Li, M., and Xiao, H. (2017). Response of gene expression and alternative splicing to distinct growth environments in tomato. *Int. J. Mol. Sci.* 18, 475. doi: 10.3390/ijms18030475

Wang, Y., Xia, D., Li, W., Cao, X., Ma, F., Wang, Q., et al. (2022). Overexpression of a tomato AP2/ERF transcription factor SlERF.B1 increases sensitivity to salt and drought stresses, Sci. *Hortic* 304, 111332. doi: 10.1016/j.scienta.2022.111332

Wang, Y., Zhang, Y., Fan, C., Wei, Y., Meng, J., Li, Z., et al. (2021b). Genome-wide analysis of MYB transcription factors and their responses to salt stress in Casuarina equisetifolia. *BMC Plant Biol.* 21, 328. doi: 10.1186/s12870-021-03083-6

Wang, C., Zhang, L. J., and Huang, R. D. (2011). Cytoskeleton and plant salt stress tolerance. *Plant Signal Behav.* 6, 29–31. doi: 10.4161/psb.6.1.14202

Wang, F., Zhou, Z., Zhu, L., Gu, Y., Guo, B., Lv, C., et al. (2023b). Genome-wide analysis of the MADS-box gene family involved in salt and waterlogging tolerance in barley (Hordeum vulgare L.). *Front. Plant Sci.* 14. doi: 10.3389/fpls.2023.1178065

Waseem, M., Rong, X., and Li, Z. (2019). Dissecting the role of a basic helix-loop-helix transcription factor, slbHLH22, under salt and drought stresses in transgenic *solanum lycopersicum* L. *Front. Plant Sci.* 10. doi: 10.3389/fpls.2019.00734

Xu, Z., Zhang, N., Fu, H., Wang, F., Wen, M., Chang, H., et al. (2021). Salt stress modulates the landscape of transcriptome and alternative splicing in date palm (Phoenix dactylifera L.). *Front. Plant Sci.* 12. doi: 10.3389/fpls.2021.807739

Ye, X., Bi, Y., Ran, Q., Zhang, X., and Wang, B. (2023). The role of plant WRKY transcription factors against salt stress: a review. *Sheng Wu Gong Cheng Xue Bao* 39, 2600–2611. doi: 10.13345/j.cjb.220652

Yin, P., Liang, X., Zhao, H., Xu, Z., Chen, L., Yang, X., et al. (2023). Cytokinin signaling promotes salt tolerance by modulating shoot chloride exclusion in maize. *Mol. Plant* 16, 1031–1047. doi: 10.1016/j.molp.2023.04.011

Yu, H., Du, Q., Campbell, M., Yu, B., Walia, H., and Zhang, C. (2021). Genome-wide discovery of natural variation in pre-mRNA splicing and prioritising causal alternative splicing to salt stress response in rice. *New Phytol.* 230, 1273–1287. doi: 10.1111/nph.17189

Yu, Z., Duan, X., Luo, L., Dai, S., Ding, Z., and Xia, G. (2020). How plant hormones mediate salt stress responses. *Trends Plant Sci.* 25, 1117–1130. doi: 10.1016/j.tplants.2020.06.008

Yuan, F., Leng, B., and Wang, B. (2016). Progress in studying salt secretion from the salt glands in recretohalophytes: how do plants secrete salt? *Front. Plant Sci.* 7. doi: 10.3389/fpls.2016.00977

Zang, D., Wang, J., Zhang, X., Liu, Z., and Wang, Y. (2019). Arabidopsis heat shock transcription factor HSFA7b positively mediates salt stress tolerance by binding to an E-box-like motif to regulate gene expression. *J. Exp. Bot.* 70, 5355–5374. doi: 10.1093/jxb/erz261

Zhang, X., Chen, L., Shi, Q., and Ren, Z. (2020). SlMYB102, an R2R3-type MYB gene, confers salt tolerance in transgenic tomato. *Plant Sci.* 291, 110356. doi: 10.1016/j.plantsci.2019.110356

Zhang, Q., Gong, M., Xu, X., Li, H., and Deng, W. (2022). Roles of auxin in the growth, development, and stress tolerance of horticultural plants. *Cells* 11, 2761. doi: 10.3390/cells11172761

Zhang, J. G., Xu, C., Zhang, L., Zhu, W., Shen, H., and Deng, H. W. (2019). Identify gene expression pattern change at transcriptional and post-transcriptional levels. *Transcription* 10, 137–146. doi: 10.1080/21541264.2019.1575159

Zhao, B. S., Roundtree, I. A., and He, C. (2017). Post-transcriptional gene regulation by mRNA modifications. *Nat. Rev. Mol. Cell Biol.* 18, 31–42. doi: 10.1038/nrm.2016.132

Zhou, E., Wang, G., Weng, L., Li, M., and Xiao, H. (2022). Comparative analysis of environment-responsive alternative splicing in the inflorescences of cultivated and wild tomato species. *Int. J. Mol. Sci.* 23, 11585. doi: 10.3390/ijms231911585

Zhu, G., Li, W., Zhang, F., and Guo, W. (2018). RNA-seq analysis reveals alternative splicing under salt stress in cotton, Gossypium davidsonii. *BMC Genomics* 19, 73. doi: 10.1186/s12864-018-4449-8

Zizkova, E., Dobrev, P. I., Muhovski, Y., Hosek, P., Hoyerova, K., Haisel, D., et al. (2015). Tomato (*Solanum lycopersicum* L.) SlIPT3 and SlIPT4 isopentenyltransferases mediate salt stress response in tomato. *BMC Plant Biol.* 15, 85. doi: 10.1186/s12870-015-0415-7

frontiers | Frontiers in Plant Science

TYPE Original Research
PUBLISHED 14 August 2024
DOI 10.3389/fpls.2024.1385477

OPEN ACCESS

EDITED BY
Mehanathan Muthamilarasan,
University of Hyderabad, India

REVIEWED BY
Martin Cerny,
Mendel University in Brno, Czechia
Roshan Kumar Singh,
National Institute of Plant Genome Research (NIPGR), India

*CORRESPONDENCE
Els J. M. Van Damme
elsjm.vandamme@ugent.be

†PRESENT ADDRESSES
Simin Chen,
Guangzhou Municipal and Guangdong Provincial Key of Molecular Target & Clinical Pharmacology, the NMPA and State Key Laboratory of Respiratory Disease, School of Pharmaceutical Sciences and the Fifth Affiliated Hospital, Guangzhou Medical University, Guangzhou, China
Anikó Meijer,
BioLizard, Ghent, Flemish Region, Belgium
Subramanyam Kondeti,
National Institute of Agricultural Botany (NIAB), Cambridge, England, United Kingdom
Pieter Wytynck,
VIB-UGENT Center for Plant System Biology, Ghent, Belgium

RECEIVED 12 February 2024
ACCEPTED 24 July 2024
PUBLISHED 14 August 2024

CITATION
Chen S, De Zutter N, Meijer A, Gistelinck K, Wytynck P, Verbeke I, Osterne VJS, Kondeti S, De Meyer T, Audenaert K and Van Damme EJM (2024) Overexpression of the ribosome-inactivating protein *OsRIP1* modulates the jasmonate signaling pathway in rice.
Front. Plant Sci. 15:1385477.
doi: 10.3389/fpls.2024.1385477

Overexpression of the ribosome-inactivating protein *OsRIP1* modulates the jasmonate signaling pathway in rice

Simin Chen[1†], Noémie De Zutter[2], Anikó Meijer[1†], Koen Gistelinck[1], Pieter Wytynck[1†], Isabel Verbeke[1], Vinicius J. S. Osterne[1], Subramanyam Kondeti[1†], Tim De Meyer[3], Kris Audenaert[2] and Els J. M. Van Damme[1*]

[1]Department of Biotechnology, Faculty of Bioscience Engineering, Ghent University, Ghent, Belgium, [2]Laboratory of Applied Mycology and Phenomics, Department of Plants and Crops, Faculty of Bioscience Engineering, Ghent University, Ghent, Belgium, [3]Department of Data Analysis & Mathematical Modelling, Ghent University, Ghent, Belgium

Ribosome-inactivating proteins (RIPs) are plant enzymes that target the rRNA. The cytoplasmic RIP, called OsRIP1, plays a crucial role in regulating jasmonate, a key plant hormone. Understanding the role of OsRIP1 can provide insights into enhancing stress tolerance and optimizing growth of rice. Transcription profiling by mRNA sequencing was employed to measure the changes in gene expression in rice plants in response to MeJA treatment. Compared to wild type (WT) plants, *OsRIP1* overexpressing rice plants showed a lower increase in mRNA transcripts for genes related to jasmonate responses when exposed to MeJA treatment for 3 h. After 24 h of MeJA exposure, the mRNA transcripts associated with the gibberellin pathway occurred in lower levels in *OsRIP1* overexpressing plants compared to WT plants. We hypothesize that the mechanism underlying OsRIP1 antagonization of MeJA-induced shoot growth inhibition involves cytokinin-mediated leaf senescence and positive regulation of cell cycle processes, probably via OsRIP1 interaction with 40S ribosomal protein S5 and α-tubulin. Moreover, the photosystem II 10kDa polypeptide was identified to favorably bind to OsRIP1, and its involvement may be attributed to the reduction of photosynthesis in *OsRIP1*-overexpressing plants subjected to MeJA at the early timepoint (3 h).

KEYWORDS

ribosome-inactivating protein, *Oryza sativa*, *OsRIP1*, jasmonate signaling, photosynthesis

1 Introduction

Plants possess a sophisticated innate immune system to adapt to ever-changing environmental conditions. Jasmonates (JAs), salicylic acid and ethylene are the archetypal hormones and play critical roles in plant defense signaling (Pieterse et al., 2009; De Vleesschauwer et al., 2013). Other hormones such as gibberellins (GAs), abscisic acid, cytokinins and auxins have emerged as important regulators not only in plant growth and development, but also in plant immunity by interfering with the salicylic acid-jasmonate/ethylene backbone of plant basal immunity. The complicated network of communication among different plant hormone signaling pathways is often referred to as the hormone crosstalk in plant disease and defense (Robert-Seilaniantz et al., 2011; Klessig et al., 2018). JA, a lipid-derived plant hormone, functions as a core signal in plant developmental processes and in responses to abiotic stress and biotic stresses (Kazan and Manners, 2011; Yang et al., 2019). Different JA compounds are synthesized in the cytoplasm, such as methyl jasmonate (MeJA), JA–isoleucine and 12-hydroxyjasmonic acid (Wasternack and Strnad, 2016). These JAs are known to modulate plant defense upon insect herbivory and pathogen infection (Li et al., 2022).

The cell nucleus has attracted attention as a new source of yet unknown molecules involved in various signaling pathways of plant defense responses (Kalinina et al., 2018). Its primary function is ribosomal RNA (rRNA) synthesis and ribosome biogenesis. Ribosome-inactivating proteins (RIPs) with rRNA N-glycosylase activity target the 23S/25S/28S rRNAs, leading to irreversible inhibition of translation. A large number of studies indicate that plant RIPs play important roles in defense against pathogens and insects, which may partly be attributed to crosstalk mechanisms between these proteins and phytohormones or reactive oxygen species (ROS) (Zhu et al., 2018). The RIP family consists of 2 groups of proteins, type 1 RIPs which are single-chained proteins and type 2 RIPs composed of a type 1 RIP chain linked to a lectin chain. We previously reported that transgenic rice seedlings overexpressing *OsRIP1* (LOC_Os01g06740) exhibited reduced susceptibility to exogenous MeJA application (Wytynck et al., 2021). In addition, OsRIP1 has been reported as a JA-inducible protein (Kawahara et al., 2016), and emerging evidence reveals that transgenic rice plants targeting JA-related genes showed altered expression of the OsRIP1 gene, implying the intricate relationship between OsRIP1 and JA signaling. In the background of *Japonica* rice (*Oryza sativa* L.) variety Zhonghua 11, leaf expression of OsRIP1 was up-regulated significantly in OsBAG4-overexpressing rice plants (fold-change 4.41) (Supplementary Materials 1, Supplementary Figure S1) and in the ebr1 mutant (fold-change 2.01) (Supplementary Figure S2). EBR1 encodes an RING-type E3 ligase that interacts with OsBAG4, a Bcl-2-associated athanogene protein, leading to its ubiquitination and degradation (Kabbage and Dickman, 2008). *OsBAG4*-overexpressing rice plants and the mutant ebr1 were characterized by the activation of many defense-related genes involved in the JA and salicylic acid pathways, and enhanced resistance to bacterial blight caused by *Xanthomonas oryzae* pv. *oryzae* (*Xoo*) and fungal blast caused by *Magnaporthe oryzae* (You et al., 2016). OsJAZ1 (LOC_Os04g55920.1) has a negative effect on drought tolerance, and *OsJAZ1*-overexpressing plants under drought stress showed different expression levels for abscisic acid and the JA signaling as well as stress-responsive genes, including the up-regulation of *OsRIP1* (fold-change 3.15) (Supplementary Materials 1, Supplementary Figure S3) but the repression of both *OsbHLH006* and *OsbHLH148* (Fu et al., 2017). The latter two genes are both basic helix-loop-helix proteins and confer drought tolerance in rice through interacting with OsJAZ proteins in the JA signaling pathway (Seo et al., 2011; Miyamoto et al., 2013). Notably, *OsRIP1* and *OsJAZ12* transcripts were dramatically enhanced up to 26.22-fold (Supplementary Materials 1, Supplementary Figure S4) and 34.51-fold (Supplementary Figure S5) in the JA overproduction mutant, *cea62*, and in this mutant the JA pathway was activated by depletion of the hydroperoxide lyase OsHL3 (LOC_Os02g02000) from the CYP74B subfamily of the cytochrome P450 family, leading to resistance to the *Xoo* T1 strain (Liu et al., 2012). These observations all support the involvement of OsRIP1 in the JA signaling pathway in rice. In the present study, we focus on an in-depth investigation of OsRIP1 and JA-mediated pathways via transcriptome profiling analysis. Previously, transgenic rice plants from line H were demonstrated to exhibit 31-fold and 65-fold higher expression of OsRIP1 in shoots and roots, respectively, while in the case from line J this was 21-fold and 42-fold (Wytynck, 2020). In this study, we provide the first insight into how OsRIP1 antagonizes MeJA-induced leaf senescence using transgenic *OsRIP1*-overexpressing plants subjected to exogenous MeJA application. In addition, health parameters of plants and interaction partners for OsRIP1 were studied to uncover the physiological mechanisms underlying OsRIP1 functions in rice.

2 Materials and methods

2.1 Plant materials and seed sterilization

Seeds of wild type (WT) rice *Oryza sativa* cv. *Nipponbare* and *OsRIP1*-OE plants (T4 generation) from line J and line H (Wytynck et al., 2021) were dehusked, and soaked in 70% ethanol on a shaker (130 rpm) for 5 minutes, followed by 45 minutes washing in 5% NaOCl solution containing 0.01% Tween-20. After extensive washing with sterilized H_2O seeds were incubated overnight in H_2O on a shaker (130 rpm) at 28°C.

2.2 Phenotypic analysis of transgenic rice

Sterilized seeds were germinated in ½ solid MS medium (pH 5.8) supplemented with 30 g/l sucrose, 8 g/l Agarose SPI (Duchefa Biochemie, Netherlands) and 1.12 mg/l Gamborg B5 vitamins (Duchefa) in square Petri dishes, sealed with micropore tape. Seeds of transgenic plants from line J and line H were germinated on selective medium containing 4 mg/l phosphinothricin

(Duchefa). Petri dishes were wrapped with aluminum foil and incubated in the dark in a plant chamber at 28°C. After 4 days, the aluminum foil was removed, and germinated seeds were grown at 28°C with a 16-h light/8-h dark cycle for an additional 3 days. One-week-old rice seedlings were grown hydroponically in the ½ Hoagland solution under the same conditions in a plant cabinet. The ½ Hoagland solution was refreshed daily. 14-day-old plants were photographed and the phenotypic differences between WT and *OsRIP1*-OE transgenic plants were analyzed for biomass, shoot length and root length.

2.3 MeJA treatment

14-day-old plants were subjected to MeJA treatment. MeJA (Sigma-Aldrich, Darmstadt, Germany) was dissolved in absolute ethanol (Sigma-Aldrich) to obtain a 100 mM stock solution, and then added to the ½ Hoagland solution to reach the working concentration of 100 µM. Control seedlings were kept in the ½ Hoagland solution with 0.1% (v/v) ethanol. Shoots and roots were sampled at 3 h and 24 h, and stored at -80°C. All treatments were set up for biological triplicates.

2.4 mRNA sequencing

Four treatment groups were set up for each indicated timepoint (3 h and 48 h), namely mock-treated WT plants, MeJA-treated WT plants, mock-treated T4 *OsRIP1*-OE transgenic rice plants line J, and MeJA-treated T4 *OsRIP1*-OE transgenic rice plants line J. Three independent biological replicates were performed for each treatment, containing 10-12 individual plants per replicate. Total RNA was extracted from freshly ground material using the Spectrum Plant Total RNA kit (Sigma-Aldrich). Library preparation, sequencing and data analysis were performed as previously described (Ghaemi et al., 2020). For each time point, Gene Ontology (GO) enrichment analyses were performed for significantly differentially expressed genes (Adjusted P-values, FDR< 0.05, and $|\log_2\text{-FC}| > 1$) using PLAZA 4.5 (https://bioinformatics.psb.ugent.be/plaza/versions/plaza_v4_5_monocots/).

2.5 Transcript analysis by quantitative RT-PCR

The reverse-transcribed cDNA was synthesized using Maxima First-Strand Synthesis kit (Thermo Fisher Scientific, Waltham, Massachusetts, USA) after RNA extraction and DNAse treatment. Transcript levels for genes of interest were analyzed by reverse transcription quantitative polymerase chain reaction (RT-qPCR) using gene specific primers (Supplementary materials 1, Supplementary Table S1). EXP, EXPNar and EIF5C were selected as the reference genes. RT-qPCR was performed using the 96-well CFX Connect™ Real-Time PCR Detection System (BioRad, Hercules, California, U.S.) with iQ™ SYBR® Green Supermix (BioRad). The PCR amplification steps were 95°C for 10 min, followed by 41 cycles of 95°C for 15 sec, 60°C for 25 sec, 72°C for 20 sec. Three biological replicates with technical duplicates were performed for the RT-qPCR.

2.6 Evaluation of health parameters by multispectral imaging

After treatment with 100 µM MeJA, 14-day-old rice plants of WT, *OsRIP1*-OE line J and line H were cultured in a plant chamber at 28°C with 16 h light: 8 h dark. Plant health development was monitored longitudinally (0, 3, 6, 9, 24 and 48 h) through multispectral imaging analysis, including efficiency of photosystem II (Fv/Fm) (Baker, 2008), chlorophyll index (Chlldx) (Gitelson et al., 2003), modified anthocyanin reflectance index (mARI) (Gitelson et al., 2009) and biomass approximation based on the number of pixels occupied by the plant. At each timepoint, side-view images were captured to provide a more precise view of rice plants and leaves (n = 15 plants, 3 plants/image). At each timepoint 15 plants were used for the side-view images and discarded after the image acquisition. All the images were captured by a custom-build multispectral imaging- and microdispenser platform, equipped with WIWAM system and 6-Mp 16-bit 3CCD top-viewer camera (PhenoVation B.V., Wageningen, The Netherlands). Data processing was performed using the "Data Analysis Software" program (PhenoVation B.V.). Additionally, the phenotypic differences between WT and *OsRIP1*-OE transgenic plants were analyzed for biomass, shoot length and root length after 48 h of mock treatment or MeJA treatment, respectively.

2.7 Protein extraction from rice shoots

Frozen shoot samples from WT plants subjected to 100 µM MeJA treatment were crushed in the presence of liquid nitrogen. The powder was homogenized in ice-cold extraction buffer containing 25 mM Tris-HCl, 15 mM $MgCl_2$, 150 mM NaCl, 0.1% NP-40, 1 mM PMSF, 1 µM E64 and 0.1% benzonase (pH 7.6) in a ratio of 2:1 (2 ml of buffer per gram of plant material). Samples were vortexed for 30 seconds followed by 30 seconds cooling on ice for a total of 10 minutes, followed by incubation on a rotary shaker for 30 minutes. The supernatant was recovered by centrifugation at 14,000 rpm for 20 min at 4°C and used as the protein extracts for the pull-down assays. All steps were performed on ice. Protein content of the extracts was determined using the Bradford method (Bradford, 1976).

2.8 Recombinant production and purification of recombinant OsRIP1

Recombinant OsRIP1 was produced in *E. coli* strain Rosetta (DE3) grown at 14°C for 72 h, and purified as described previously (De Zaeytijd et al., 2019).

2.9 Pull-down assays

Pull-down assays were performed using purified recombinant OsRIP1 as bait and protein extracts from shoots of MeJA-treated WT plants as prey. Briefly, 100 µg total rice protein was supplemented with approximately 54 µg purified OsRIP1, and incubated for 30 min at 4°C. 25 µl of Ni-NTA agarose beads (Qiagen, Hilden, Germany) were equilibrated with binding buffer (mix of the phosphate buffer from OsRIP1 purification and plant protein extraction buffer in a ratio of 8.3:1). The beads were incubated with the mix of protein extracts and OsRIP1 for 30 min at 4°C. After centrifugation, the beads were washed once with the binding buffer containing 50 mM imidazole followed by three washes with trypsin digest buffer (20 mM Tris-HCl, 2 mM $CaCl_2$, pH 8.0). The beads were resuspended in 150 µl trypsin digest buffer and stored at -20°C prior to LC-MS/MS analysis. All incubations were performed on ice. Ni-NTA beads incubated with plant protein extracts only were used as a control. Four biological replicates were performed in total, one replicate was used for silver staining and Western blot analysis, and the other three replicates were used for LC-MS/MS analysis.

2.10 SDS-PAGE, silver staining, and Western blot analysis

Proteins were separated by SDS-PAGE using 15% acrylamide gels (Laemmli, 1970), followed by visualization with Pierce™ Silver Stain Kit (Thermo Scientific, Waltham, MA, United States). For Western blot analysis proteins were transferred from the acrylamide gel to polyvinylidene fluoride transfer membranes (FluoroTrans® PVDF, Pall Laboratory, USA). Membranes were blocked in Tris-buffered saline (TBS: 10 mM Tris, 150 mM NaCl, 0.1% (v/v) Triton X-100, pH 7.6) containing 5% (w/v) non-fat milk powder. Subsequently, membranes were incubated with the primary anti-His antibody (1:1000, Thermo Fisher Scientific) for 1 h. Membranes were washed three times with TBS prior to incubation with rabbit anti-mouse IgG secondary antibody labelled with horseradish peroxidase (1:10,000, Dako, Glostrup, Denmark) for another hour. Following two washes with TBS and one wash with 0.1 M Tris buffer (pH 7.6), blots were detected and visualized using 0.025% (w/v) 3,3'-diaminobenzidine tetrahydrochloride (Sigma-Aldrich) containing 0.003% (v/v) hydrogen peroxide.

2.11 LC-MS/MS analysis

All proteins were separated from Ni-NTA beads by trypsin digest. After acidification and purification, purified peptides were determined by LC-MS/MS analysis using an Ultimate 3000 RSLC nano LC (Thermo Fisher Scientific, Bremen, Germany) in-line connected to a Q Exactive mass spectrometer (Thermo Fisher Scientific) equipped with a pneuNimbus dual ion source (Phoenix S&T). LC-MS/MS runs were searched using the MaxQuant algorithm (version 1.6.3.4) with mainly default search settings, including a false discovery rate set at 1% on both the peptide and protein level. Spectra were searched against the OsRIP1-6x His sequence and *Oryza sativa* proteins in the Uniprot database (database release version of March 2021 containing 39,947 protein sequences) (www.uniprot.org). Only proteins with at least one unique or razor peptide were retained leading to the identification of 1,443 proteins. Proteins were quantified by the MaxLFQ algorithm integrated in the MaxQuant software. A minimum ratio count of two unique or razor peptides was required for quantification. Further data analysis was performed with the Perseus software (version 1.6.2.1) after loading the protein groups file from MaxQuant.

Reverse database hits were removed, and replicate samples were grouped. Proteins with less than three valid values in at least one group were removed and missing values were imputed from a normal distribution centered around the detection limit leading to a list of 950 quantified proteins that was used for further data analysis. To compare protein abundance between OsRIP1-treated and OsRIP1-nontreated (CTRL) samples, statistical testing for differences between these two groups was performed, using the package limma. Statistical significance for differential regulation was set at FDR = 0.05 and $|\log_2 FC| = 1$, and a volcano plot was also generated. The proteins shown to be differentially abundant between groups were visualized in a heatmap after non-supervised hierarchical clustering of z-scored protein LFQ intensities. The proteomics analyses were performed by the VIB Proteomics Core, Center for Medical Biotechnology, UGent Department of Biomolecular Medicine. Mass spectrometry was performed in triplicates.

2.12 Protein-protein docking

Protein-protein docking between OsRIP1 and the proteins identified in the pulldown assays has been performed using ClusPro 2.0 (Kozakov et al., 2017) with standard settings. Protein structure files in.pdb format have been obtained using AlphaFold2 (Jumper et al., 2021) using their respective Uniprot codes (Table 1) and selected based on model quality, with low-quality models being removed from further analysis. Simulations followed steps including rigid-body docking through the fast Fourier transform approach, root-mean square deviation clustering of structures, and refinement of the structures on the representative clusters. Poses were selected based on the most overrepresented clusters.

The representative pose for each complex between OsRIP1 and the target proteins underwent rescoring utilizing the Protein Interaction Z Score Assessment (PIZSA) online server (Roy et al., 2019), an empirical scoring function that assesses the stability of protein assemblies taking into consideration amino acid pair preferences. A distance threshold of 8 Å was applied, and PIZSA scores exceeding 0.8 were deemed indicative of possible binding, with values surpassing 1.0 indicating favorable binding.

2.13 Statistical analysis

Each treatment comprised at least three independent biological replicates. All results were presented as mean ± standard deviation (SD) except for the result of plant health parameters that were presented as

10.3389/fpls.2024.1385477

TABLE 1 Potential interaction partners of OsRIP1 as identified by LC-MS/MS after pull-down assays.

Log_2 (OsRIP1/ Ctrl)	Uniprot code	MSU (Locus ID)	Function/domain	Localization (Uniprot)	PIZSA Score	Output	GO terms
	Q9LGK6 (OsRIP1)	LOC_Os01g06740	rRNA N-glycosylase	Cytoplasm/ nucleocytoplasm	–	–	Translation (GO:0006412)
3.35	Q652S1	LOC_Os06g14740	NAD-binding domain, Sugar binding domain and a nucleotide binding domain	Cytoplasm	0.372	Unstable binding	Carbohydrate metabolic process (GO:0005975)
2.83	O65037	LOC_Os08g31228	50S ribosomal protein L27	Chloroplast	N/A	N/A	Translation (GO:0006412) Structural molecule activity (GO:0005198)
2.76	P12149	LOC_Os12g34062	30S ribosomal protein S12	Chloroplast	0.844	Possible binding	Translation (GO:0006412); structural molecule activity (GO:0005198)
2.71	A0A0P0VEB3	LOC_Os02g03890	Nuclear transport factor 2 domain and an RNA recognition motif	Cytoplasm	N/A	N/A	mRNA binding (GO:0003729); RNA binding (GO:0003723)
2.48	Q6ZBV1	LOC_Os08g10020	Photosystem II 10kDa polypeptide Psbr	Chloroplast membrane	1.864	Favorable binding	Photosynthesis (GO:0015979)
2.35	Q6K439	LOC_Os09g04790	Plastid-lipid associated protein/fibrillin domain, fibrillin-like protein 2	Chloroplast	-1.594	Unstable binding	
2.32	Q8W0D1	LOC_Os05g45660	RNA-binding protein	Cytoplasm	0.682	Unstable binding	mRNA binding (GO:0003729) RNA binding (GO:0003723)
1.78	Q2R4A1	LOC_Os11g29190	40S ribosomal protein S5 (Os11g0482000)	Cytoplasm	1.359	Favorable binding	Translation (GO:0006412); structural molecule activity (GO:0005198); RNA binding (GO:0003723)
1.69	Q2QVJ6	LOC_Os12g12580	NADP-dependent oxidoreductase	Cytoplasm	0.433	Unstable binding	
1.34	Q2QLR2	LOC_Os12g43600	Glycine-rich RNA-binding protein GRP1A	Cytoplasm	-1.005	Unstable binding	mRNA binding (GO:0003729); RNA binding (GO:0003723)
1.12	P28752	LOC_Os07g38730	Tubulin alpha-1 chain, α-tubulin	Cytoplasm	0.930	Possible binding	Structural molecule activity (GO:0005198)

N/A indicates that the predicted structures for these proteins are of poor quality and cannot be used to perform protein-protein docking.

mean ± standard error of mean. Data were analyzed by the t-test and one-way analysis of variance (ANOVA) using SPSS 17.0 (SPSS Inc., Chicago, IL). Multiple testing correction was performed with the Duncan correction, considering *$p < 0.05$, **$p < 0.01$, ***$p < 0.001$ as significance. For the analyses of the multispectral proxies, Mock and MeJA treated plants were pairwise compared as per independent sample t-test, implementing a Bonferroni multiple-significance test correction.

3 Results

3.1 Phenotypic analysis of OsRIP1-overexpressing transgenic rice plants

Phenotypic analysis on 14-day-old rice plants from two independent transgenic lines overexpressing OsRIP1 (*OsRIP1*-OE) revealed no visible morphological changes when compared to WT plants (Figure 1B). Under normal growth conditions no significant differences in total biomass and shoot length were observed for WT plants and plants from transgenic lines. Although plants from line J revealed a significantly shorter root length compared to plants from line H, no significant differences in root length were observed for line J compared to WT plants (Figure 1C).

MeJA exposure for 48h caused a significant inhibition of shoot growth in WT plants and plants from line H, unlike plants from line J. Moreover, plants from line H exhibited significantly longer roots compared to WT plants and line J during both normal growth conditions and MeJA exposure for 48 h (Figure 1C).

3.2 Effect of exogenously applied MeJA on health parameters of rice plants

To assess the effects of exogenously applied MeJA on WT plants and *OsRIP1*-OE plants of both line J and line H, the multispectral

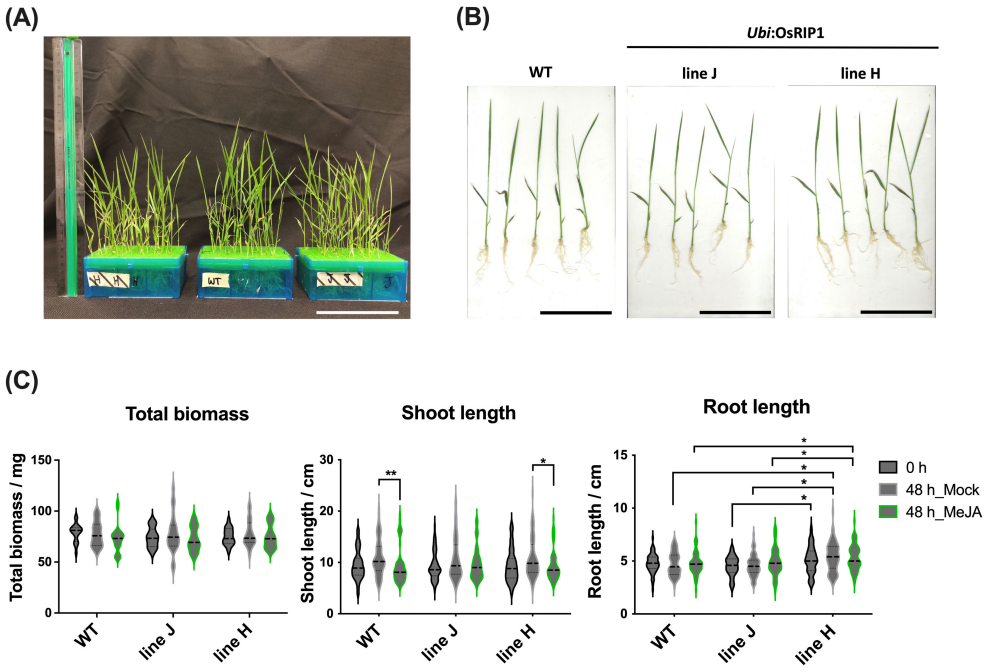

FIGURE 1
Phenotypic analysis of WT plants and T4 *OsRIP1*-OE transgenic rice plants (independent lines J and H) under normal growth conditions (0 h) and after 48 h of mock- or MeJA treatment. **(A)** Morphology of 14-day-old WT and T4 *OsRIP1*-OE rice plants hydroponically grown in the ½ Hoagland solution in 96-well tip boxes (at 0 h, before treatment). Ruler = 30 cm. **(B)** 5 individual plants of WT, lines J and H (at 0 h, before treatment). All scale bars = 10 cm. **(C)** The total biomass, shoot length and root length of plants of WT, lines J and H were measured under normal growth conditions. Each point represents means ± SD, from 60 individual plants (n = 60). The middle dotted line in the violin box refers to medians; the thin dotted lines refer to the median lower quartile and upper quartile; the width of the violin box represents the local distribution of feature values along the y axis. Statistically significant differences between points in the graphs are indicated by asterisks, *p < 0.05, **p < 0.01.

imaging platform was employed to visualize multispectral phenomics from the side view (n = 15 plants, 3 plants/image, Supplementary Materials 1, Supplementary Figure S7). All mock-treated plant groups consistently showed a non-significant increase in shoot biomass compared to the plants treated with MeJA for 48 h (Figure 2A; Supplementary Materials 1, Supplementary Figure S8A).

The effect of MeJA on the efficiency of photosystem II was evaluated as chlorophyll fluorescence (Fv/Fm; Figure 2B; Supplementary Materials 1, Supplementary Figure S8B). MeJA treatment for 3 h yielded slightly lower Fv/Fm-values in WT plants, while slightly higher Fv/Fm-values were apparent in plants of both line J and line H. MeJA treatment for 24 h resulted in significantly lower Fv/Fm-values in both line J and line H, while WT plants remained unaffected. This showed to be a transient effect since no significant differences were observed between plants of both line J and line H and WT plants after 48 h of MeJA exposure.

The effect of MeJA on the leaf chlorophyll content was evaluated as the chlorophyll index (ChlIdx; Figure 2C; Supplementary Materials 1, Supplementary Figure S8C). After 24 h, MeJA-treated plants from both transgenic lines showed impaired ChlIdx-values compared to the untreated (mock) plants, which was not the case for the WT plants.

Plants treated with MeJA were hallmarked by slightly lower (non-significant) mean mARI-values after 3 h for all three plant groups (Figure 2D; Supplementary Materials 1, Supplementary Figure S8D). This was a constant trend in WT plants as well as plants from line H up to 24 h. After 48h the opposite effect was observed, MeJA treatments resulted in slightly higher mARI values compared to mock treated plants. For plants from line J, the same trend was observed, except for timepoints 6 h and 9 h.

Transcriptome analysis and GO analysis revealed that the enrichment of "S-linalool synthase activity" (in shoots) and "terpene synthase activity" (in roots) in molecular function was characteristic for *OsRIP1*-OE plants from line J (Supplementary Materials 1, Supplementary Figure S9, Supplementary Tables S15, S16). Among these genes assigned was a monoterpene linalool encoded by *Os02g0121700* with a defensive function in plants (Supplementary Materials 1, Supplementary Figure S9; Supplementary Table S17).

3.3 OsRIP1 affects photosynthesis and cell cycle regulation in shoots under MeJA stress

mRNA sequencing was performed for shoot and root samples harvested from WT plants and T4 *OsRIP1*-OE transgenic plants from line J subjected to MeJA treatment or mock treatment. Plants from line J treated with MeJA for 3 h yielded 215 differentially

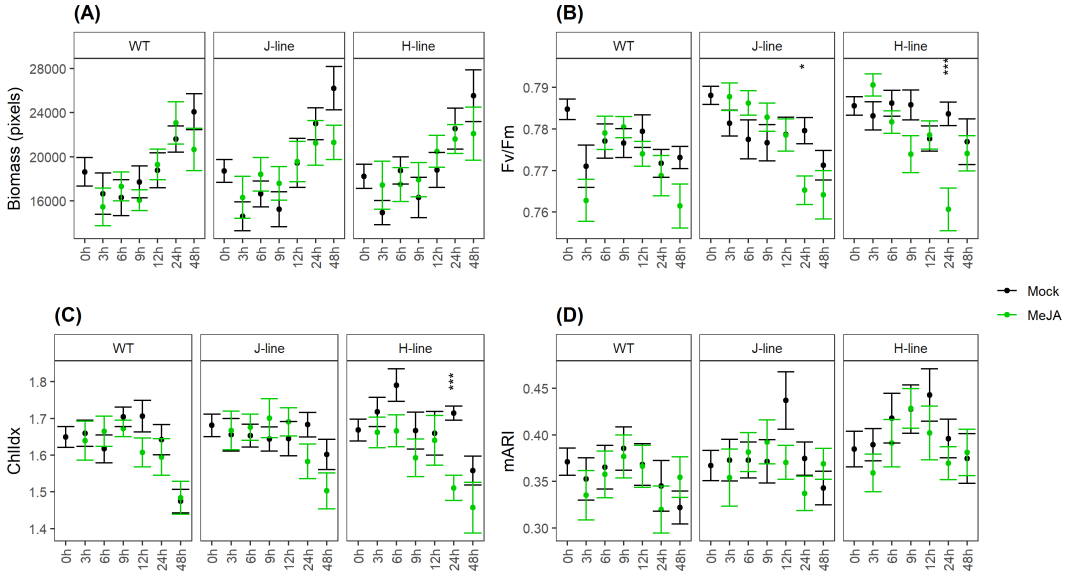

FIGURE 2
Multispectral parameters evaluated for WT plants and OsRIP1-OE plants under MeJA treatment and mock treatment based on side-view images throughout time (n = 15 plants) captured by the multispectral imaging platform. All the data represent the mean ± standard error. **(A)** estimated biomass (in pixels) of rice plants. Rice shoot biomass was evaluated as number of chlorophyll-containing pixels per plant. **(B)** chlorophyll fluorescence (Fv/Fm). **(C)** chlorophyll index (ChlIdx). **(D)** modified anthocyanin reflectance index (mARI). Significant differences (as per independent sample t-test with Bonferroni multiple-significance test-correction) between the mock and MeJA treatment are indicated by asterisks, *p < 0.05, ***p < 0.001.

expressed and down-regulated genes unique for shoots. Among these 199 annotated genes were significantly enriched in GO terms of "chlorophyll biosynthetic process", "regulation of cellular process" and "response to stimulus" (Figure 3B1; Supplementary Materials 1, Supplementary Table S2). We also identified 125 differentially expressed and up-regulated genes in these shoots (Figure 3A1) but no Gene Ontology (GO) enrichment results were found for the 114 annotated genes.

For 358 annotated genes down-regulated only in shoots of WT plants after MeJA exposure for 3 h (MeJA vs. mock, 3 h), GO enrichment analysis indicated two biological processes, in particular "DNA unwinding involved in DNA replication" and "DNA replication initiation" with the highest p-value (Figure 3B1; Supplementary Materials 1, Supplementary Table S3). When rice plants were subjected to MeJA stress for 24 h, GO terms of photosynthesis-related biological processes were over-represented in 330 down-regulated annotated genes only found in shoots of plants from line J (Figure 3A2). GO terms related to negative regulation of cell cycle were characteristic for the set of 437 down-regulated transcripts unique in WT plants exposed to MeJA for 24 h (Figure 3B2; Supplementary Table S6). GO ontology analyses were also performed for the root samples. An enrichment of the biological processes important for N metabolism such as the cellular nitrogen compound metabolic process (GO:0034641) was found in the set of down-regulated genes in roots of WT plants after MeJA treatment for 3 h, while this phenomenon was found in roots of *OsRIP1*-OE plants from line J at 24 h after MeJA exposure (Supplementary Materials 1, Supplementary Figure S6; Supplementary Tables S9–S14).

3.4 Transcript analysis for JA, GA, CK, cell cycle pathways and photosynthesis in shoots

Transcript numbers for genes related to JA signaling (Figures 4A–D), GA signaling (Figures 4E–H), cytokinin signaling (Figures 4I–L), salicylic acid signaling (Figures 4U–X), cell cycle (Figures 4M–P), and photosynthesis (Figures 4Q–T) were analyzed. MeJA treatment for 3 h activated many genes associated with the JA pathway. Among 82 common JA-related genes up-regulated after 3 h of MeJA treatment, 60 differentially expressed genes (DEGs) showed a higher up-regulation in WT plants compared to plants from line J (Table 2; Figure 4A). 24 up-regulated genes were unique for shoots of WT plants, while there were only 3 up-regulated unique DEGs for shoots of line J (Table 2; Figure 4A). After MeJA treatment for 24 h, a higher number of down-regulated genes were identified in shoots from line J than in WT plants (Table 2; Figure 4D), implying that OsRIP1 overexpression caused the delay of activation of the JA signaling in plants from line J compared to WT plants.

In the set of GA-related genes at 3 h after MeJA exposure, more down-regulated genes were identified in shoots from line J than in WT plants (Table 2; Figure 4F). Compared to plants from line J, 24 h exposure to MeJA led to a higher number of up-regulated genes and less down-regulated genes associated with the GA signaling in WT plants (Table 2; Figures 4G, H), suggesting that the mRNA transcripts associated with the GA pathway occurred in lower levels in *OsRIP1* overexpressing plants than in WT plants.

Compared to plants from line J, more cytokinin-related transcripts were found to be down-regulated in WT plants after 24

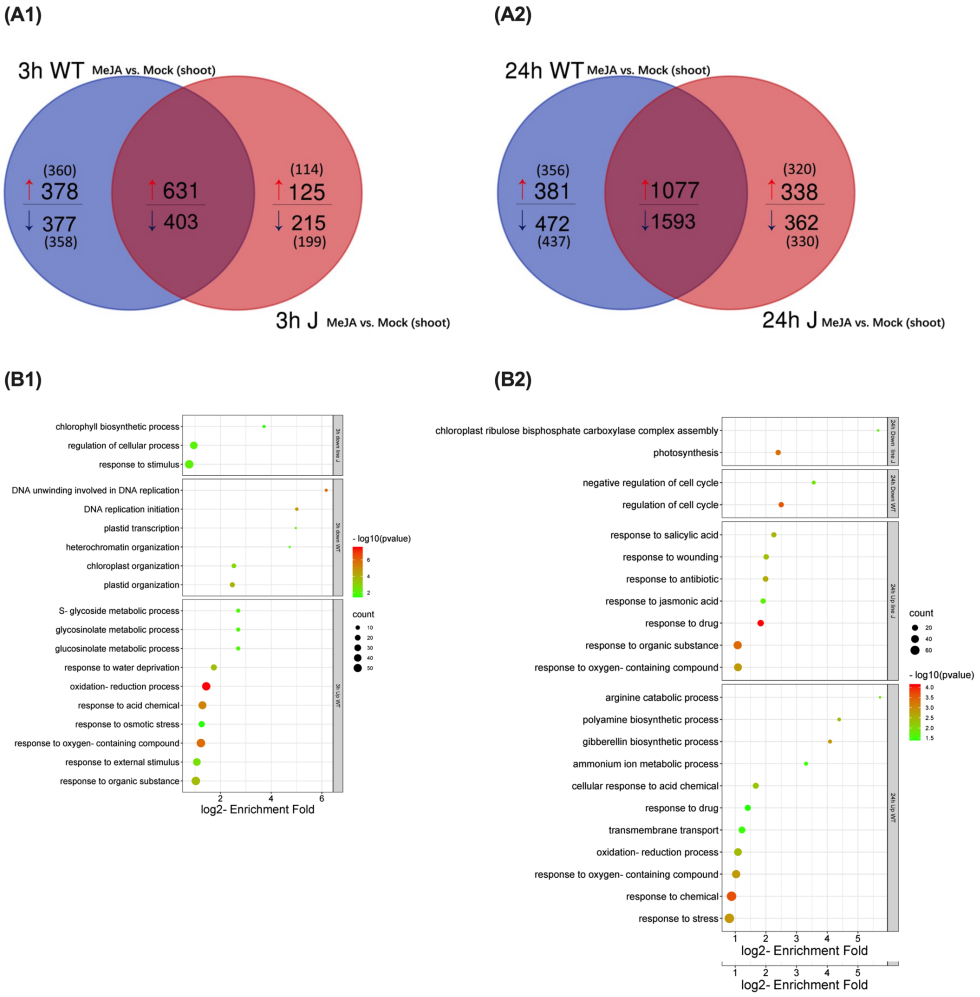

FIGURE 3
Gene ontology (GO) analysis for differentially expressed genes (DEGs) (log2 fold change [FC] > 1, log2 [FC] < -1, FDR < 0.05) unique for shoots of WT plants or *OsRIP1*-OE plants from line J after MeJA treatment (MeJA vs. mock) for 3 h and 24 h, respectively. **(A)** Venn diagram of DGEs (MeJA vs. mock) at 3 h **(A1)** or 24 h **(A2)** post MeJA treatment between WT plants and *OsRIP1*-OE plants from line J. **(B)** Enriched GO terms at 3 h **(B1)** or 24 h **(B2)** MeJA treatment in the category 'biological process'.

h of MeJA supplementation (Figure 4L). A similar phenomenon was observed for genes associated with cell cycle (Figure 4P). It is noted that 3 h of MeJA exposure caused down-regulation of cell cycle-related genes; the number of DEGs in WT plants was double compared to plants of line J (Figure 4N). Among photosynthesis-related DEGs suppressed by 24 h of MeJA treatment, two-thirds of the common down-regulated genes were found to be down-regulated at a higher level in WT plants than in plants of line J (Figure 4T). Despite the higher number of upregulated transcripts compared to those downregulated in either line within the salicylic acid (SA) mediated signaling pathway, the total number of transcripts with differential expression was limited (< 30) (Figures 4U–X), and most of the SA-mediated transcripts exhibited expression changes with a log2 fold change of less than 1 (data not shown). Additionally, slight differences were observed between the MeJA-induced expression changes in SA-related genes in WT plants and those from line J. Despite the well-established crosstalk between salicylic acid and jasmonate (Peng et al., 2021), in this case, MeJA exposure did not primarily affect the SA mediated signaling pathway in either WT plants or *OsRIP1*-overexpressing plants from line J.

3.5 RT-qPCR validation

To validate the mRNA-Seq data, 6 genes including 3 genes for photosynthesis (*OsRBCS2*, *OsRBCS4*, *OsRBCS5*), 2 genes involved in the JA signaling pathway (*OsHLH148*, *OsJAZ12*) and 1 gene encoding cytochrome P450 (*Cytochrome P450*) were selected for RT-qPCR analysis (Supplementary Materials 1, Supplementary Table S1; Figure 5). At 3 h after MeJA treatment, WT plants exhibited 3 more times of OsHLH148 transcript expression than plants from line J (Figure 5D). *OsbHLH148* transcript levels in shoots of plants from line J were more upregulated after 24 h of MeJA treatment compared to 3 h of MeJA treatment, but still significantly lower than that in WT plants (Figure 5D). Similarly, MeJA exposure resulted in less up-regulation of the expression of

10.3389/fpls.2024.1385477

TABLE 2 Differentially expressed genes (DEGs) associated with different pathways in shoots of WT plants and plants from line J at 3 h or 24 h after MeJA treatment (MeJA-WT vs mock-WT, MeJA-line J vs. mock-line J).

Pathway	Category	Common DEGs	DEGs with regulation folds: WT>J	DEGs with regulation folds: J>WT	Unique DEGs	Total DEGs
Jasmonate signaling	3h_WT_UP*	82	60	22	24	107
	3h_line J_UP	82	60	22	3	85
	3h_WT_DOWN	18	8	10	4	22
	3h_line J_DOWN*	18	8	10	3	22
	24h_WT_UP	109	53	56	11	120
	24h_line J_UP	109	53	56	11	120
	24h_WT_DOWN	25	9	16	7	32
	24h_line J_DOWN	25	9	16	5	30
Gibberellin signaling	3h_WT_UP	13	8	5	5	18
	3h_line J_UP	13	8	5	8	21
	3h_WT_DOWN	15	3	12	11	26
	3h_line J_DOWN	15	3	12	6	21
	24h_WT_UP	21	14	7	13	34
	24h_line J_UP	21	14	7	14	35
	24h_WT_DOWN	29	8	21	9	38
	24h_line J_DOWN	29	8	21	7	36
Cytokinin signaling	3h_WT_UP	36	25	11	22	58
	3h_line J_UP	36	25	11	6	42
	3h_WT_DOWN	46	28	18	17	63
	3h_line J_DOWN	46	28	18	9	55
	24h_WT_UP	55	29	26	10	65
	24h_line J_UP	55	29	26	5	60
	24h_WT_DOWN	81	40	41	30	111
	24h_line J_DOWN	81	40	41	5	86
Cell cycle	3h_WT_UP	12	7	5	6	18
	3h_line J_UP	12	7	5	4	16
	3h_WT_DOWN	10	7	3	18	28
	3h_line J_DOWN	10	7	3	4	14
	24h_WT_UP	9	4	5	4	13
	24h_line J_UP	9	4	5	0	9
	24h_WT_DOWN	69	32	37	22	91
	24h_line J_DOWN	69	32	37	7	76
Photosynthesis	3h_WT_UP	11	9	2	5	16
	3h_line J_UP	11	9	2	0	11
	3h_WT_DOWN	97	53	44	13	110
	3h_line J_DOWN	97	53	44	10	107
	24h_WT_UP	12	8	4	1	13

(Continued)

TABLE 2 Continued

Pathway	Category	Common DEGs	DEGs with regulation folds: WT>J	DEGs with regulation folds: J>WT	Unique DEGs	Total DEGs
	24h_line J_UP	12	8	4	2	14
	24h_WT_DOWN	120	40	80	9	129
	24h_line J_DOWN	120	40	80	7	127
Salicylic acid signaling	3h_WT_UP**	10	6	3	7	17
	3h_line J_UP**	10	6	3	0	10
	3h_WT_DOWN	3	3	0	1	4
	3h_line J_DOWN	3	3	0	1	4
	24h_WT_UP	16	9	7	6	22
	24h_line J_UP	16	9	7	1	17
	24h_WT_DOWN**	6	6	0	0	7
	24h_line J_DOWN**	6	6	0	0	7

*, one DEG up-regulated in WT but down-regulated in line J; **, one DEG with the same up-regulation or down-regulation folds in both WT plants and plants from line J.

OsJAZ12 in shoots of plants from line J compared to WT plants at 3 h (Figure 5E). 24 h of MeJA treatment stimulated more expression of *OsJAZ12* in plants from line J than 3 h of MeJA treatment (Figure 5E). MeJA application to WT plants for 3 h or 24 h had no discernible effect on *OsbHLH148* or *OsJAZ12* transcript levels (Figures 5D, E). These RT-qPCR expression profiles validate the mRNA-Seq data.

3.6 Identification of interaction partners of OsRIP1 using pull-down assays

Protein extracts from shoots of WT plants subjected to MeJA treatment were used as prey in pull-down assays to identify potential interaction partners of OsRIP1. Compared to the control group of proteins from Ni-NTA beads only treated with the plant protein extracts (Supplementary Figure S10A, lane 2), several proteins with a molecular weight between 17 kDa and 26 kDa appeared in the proteins from the bait samples (Supplementary Figure S10A, lane 1), and one additional one band of less 10 kDa was clearly present.

The three control samples and three bait samples were analyzed by LC-MS/MS runs. In all six samples 44,086 peptides were identified by LC-MS/MS system and attributed to a total of 1,443 proteins, in which 950 proteins could reliably be quantified. For the statistical analysis, protein intensities in bait samples were compared to those in control samples using a t-test approach with the settings at FDR = 0.05 and $|\log_2 FC| = 1$ (Supplementary Materials 2). The Log2 fold change and the statistical significance (-log(p-value)) can be seen on the volcano plot (Supplementary Figure S10C), and 12 proteins in total were found to be significantly enriched in the bait samples. Of these 12 proteins, OsRIP1 was abundantly present as expected due to the OsRIP1 addition to the bait samples. Other 11 enriched proteins were considered to represent potential interaction partners for OsRIP1, and their localization as well as defined functions were summarized in Table 1.

Among these 11 potential interactors, four interactors were known to carry nucleotide-binding/recognition domains, of which tubulin alpha-1 chain (α-tubulin), a GTP-binding protein was associated with cytoskeleton organization. Based on the information of subcellular localization in the Uniprot database, 4 out of 11 putative interactors are localized to the chloroplast, while 7 interactors are predicted to be located in the cytoplasm. Three potential interactors were ribosomal proteins, of which only one (40S ribosomal protein S5) is present in the cytoplasm and 2 others (50S ribosomal protein L27 and 30S ribosomal protein S12) reside in the chloroplast. In addition to two ribosomal proteins from the chloroplast, two more proteins containing a transit peptide were also identified plastid lipid associated protein 2 and photosystem II 10 kDa polypeptide, respectively. The transit peptide is required for their transport across the relevant membranes from their site of synthesis in the cytoplasm. Plastid lipid associated protein 2 belongs to the plastid-lipid associated protein/fibrillin family, while photosystem II 10 kDa polypeptide is known to participate in photosynthesis (Table 1).

According to the GO enrichment analysis, the biological processes over-represented in this subset of 12 proteins, including OsRIP1 and its 11 putative interaction candidates, are related to "translation" (GO:0006412) and "cellular amide metabolic process" (GO:0043603), whereas "mRNA binding" (GO:0003729), "RNA binding" (GO:0003723), "structural molecule activity" (GO:0005198) and "structural constituent of ribosome" (GO:0003735) are enriched in the category molecular function (Table 1).

Protein-protein docking was applied to understand the molecular interactions between OsRIP1 and the putative interaction candidates identified by the pull-down assays

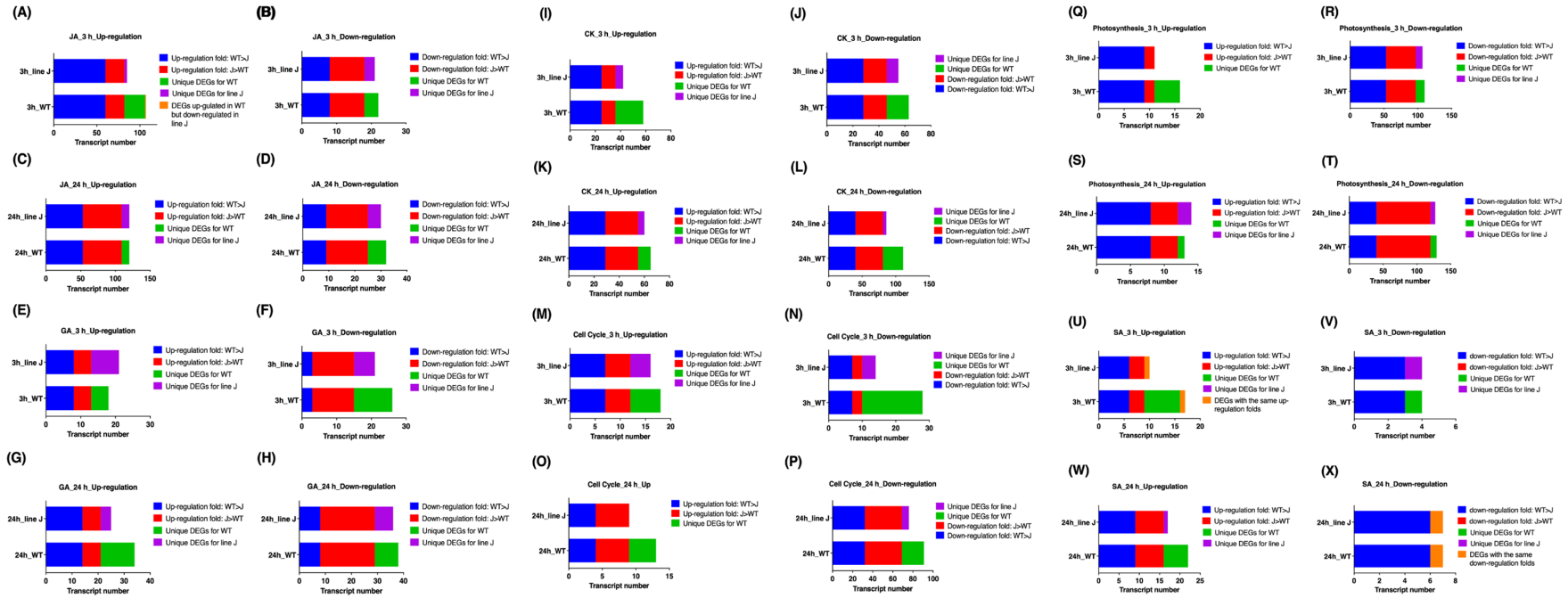

FIGURE 4
Abundance of transcripts for differentially expressed genes (DEGs) (FDR <0.05) involved in jasmonate (JA) pathway **(A–D)**, gibberellin (GA) pathway **(E–H)**, cytokinin (CK) pathway **(I–L)**, cell cycle **(M–P)**, photosynthesis **(Q–T)**, and salicylic acid (SA) pathway **(U-X)** in shoots after methyl jasmonate application for 3 or 24h. All up or down regulated DEGs were categorized into three groups, namely DEGs unique for the corresponding plants, DEGs with altered expression fold (WT > J), and DEGs with altered expression fold (J > WT). Blue and red bars represent number of transcripts identified in shoots of both WT plants and plants from line J. Bars in purple refer to number of transcripts only identified in shoots of plants from line J, while bars in green refer to number of transcripts only identified in shoots of WT plants.

10.3389/fpls.2024.1385477

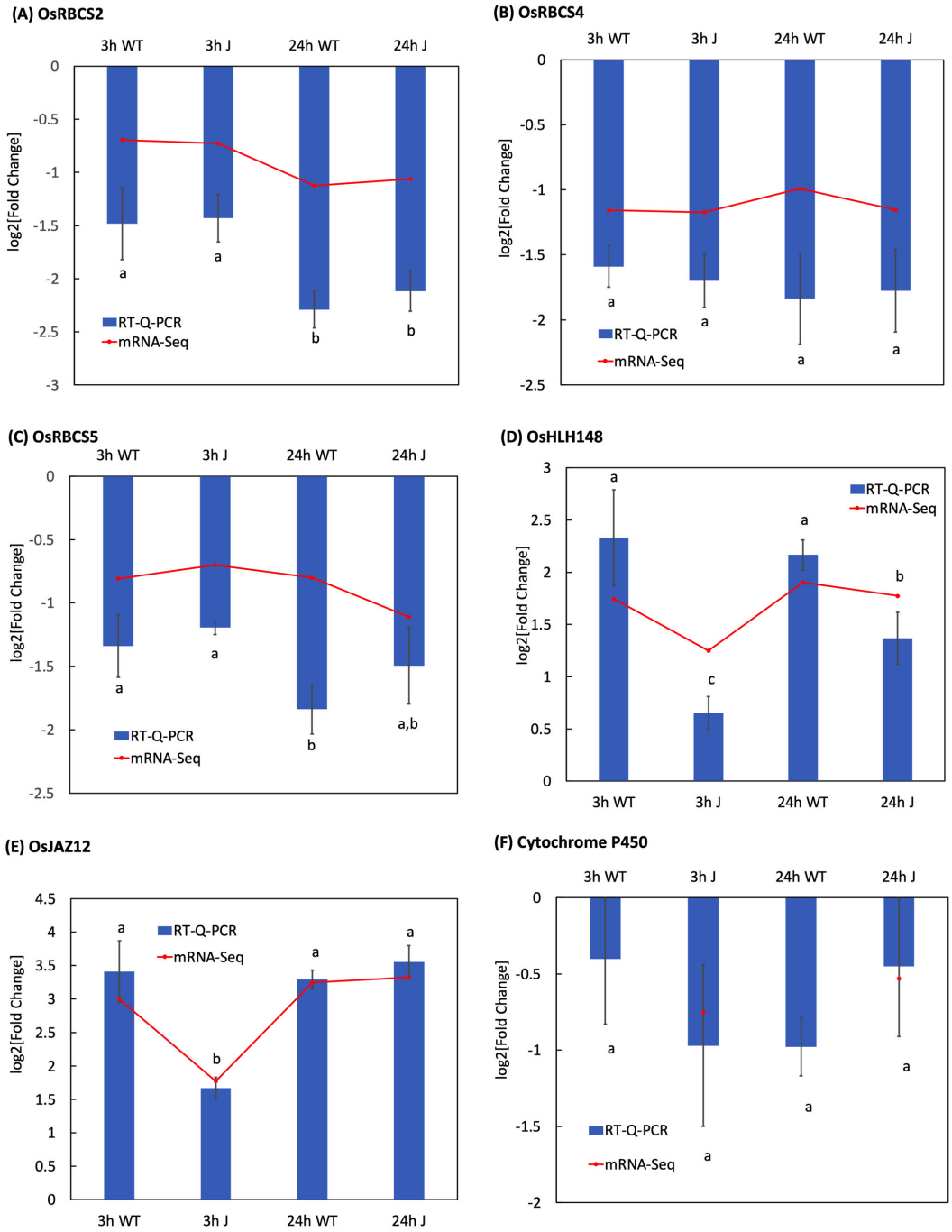

FIGURE 5
Transcript levels of genes of interest in MeJa-treated plants **(A–F)** measured using RT-qPCR relative to that in mock-treated groups (MeJa vs. mock). Each sample included three biological repeats. Three repeated biological experiments were carried out for each gene, and the error bar represents the SD of the means (n = 3). Statistically significant differences ($p < 0.05$) between points in the graphs are indicated with different letters; the same letters indicating no significant differences, with a>b>c.

(Table 1). Docking revealed a favorable binding of OsRIP1 with photosystem II 10 kDa polypeptide (Supplementary Materials 1; Supplementary Figure S11A), and 40S ribosomal protein S5 (Supplementary Figure S11B). Docking also suggested a binding with α-tubulin (Supplementary Materials 1; Supplementary Figure S11C), but unstable binding was predicted for the remaining proteins tested.

4 Discussion

Based on the previous findings showing that rice plants overexpressing *OsRIP1* show altered MeJA sensitivity the hypothesis was put forward that OsRIP1 participates in modulating the JA signaling pathway (Wytynck et al., 2021). In this study, we report that overexpression of *OsRIP1* exhibited no

visible adverse effects on the normal growth of 14-day-old rice plants compared to WT plants prior to MeJA exposure (Figure 1). However, the reduction in shoot length was more significant in WT plants when compared to plants from line H after exogenous application of 100 µM MeJA for 48 h, but this significant growth reduction was clearly absent in plants from line J (Figure 1C), in agreement with previous work showing that *OsRIP1* overexpression alleviated MeJA induction of shoot inhibition (Wytynck et al., 2021). All these findings suggested that constitutive expression of *OsRIP1* plays a role in enhanced tolerance to MeJA stress.

A monoterpene linalool encoded by *Os02g0121700* was identified as characteristic for *OsRIP1*-OE plants from line J (Supplementary Materials 1; Supplementary Figure S9, Supplementary Tables S15–S17). It exerts a defensive function in plants and could boost JA biosynthesis or signaling, and up-regulate the expression of defense-related genes in rice (Taniguchi et al., 2014), tomato (López-Gresa et al., 2017), as well as *Satsuma mandarin* (Shimada et al., 2017). Therefore, the presence of "S-linalool synthase activity" in the GO molecular function category for plants from line J (Supplementary Materials 1; Supplementary Figure S9; Supplementary Table S16) might highlight the increase in linalool concentrations as signaling molecules to enhance and coordinate the plant defense responses in *OsRIP1*-OE plants from line J.

Even though no significant MeJA-induced suppression of the shoot biomass was observed by the multispectral imaging platform during the time-course experiment (Figure 2A), the leaf growth inhibition in WT plants after the addition of exogenous MeJA (Figure 1) may be a consequence of down-regulation in DNA replication at the early timepoint 3 h post treatment (Figure 1B1) and subsequent negative regulation of the cell cycle after 24 h exposure to MeJA (Figure 1B2). These findings were supported by substantial reports highlighting that MeJA functions as a repressor in growth (Havko et al., 2016; Guo et al., 2018), cell division (Zhang and Turner, 2008) and cell expansion (Fattorini et al., 2009). The switch from the mitotic cell cycle to the endoreduplication cycle is delayed in plant cells after MeJA application. MeJA-induced disruption in leaf growth through arresting cells in G1 phase prior to the S-phase transition has been considered to inhibit the mitotic cycle, most probably by activating critical regulators of endoreduplication and affecting the expression of key determinants of DNA replication (Noir et al., 2013). Strikingly, we identified two putative interaction partners correlated to the regulation of cell cycle, 40S ribosomal protein S5 (RPS5) and α-tubulin. RPS5 is capable of favorable binding to OsRIP1 and is a structural component of the 40S small ribosomal subunit, it is believed to participate in translation through binding to the eIF-3 (Weijers et al., 2001; Browning and Bailey-Serres, 2015). Changes in ribosome biogenesis may affect global protein synthesis which would inevitably affect plant growth and development. In *Arabidopsis* plants with a mutation in the RPS5 gene (AtRPS5A) most cell-division processes were delayed or disrupted in the heterozygous mutant, and development was completely arrested at an early embryonic stage in the homozygous mutant (Weijers et al., 2001). Moreover, 6 out of top 50 positively co-expressed genes of RPS5A (Supplementary Materials 1; Supplementary Table S18) identified on the mRNA-Seq platform using the Genevestigator tool are clustered in the regulation of cytokinin (Supplementary Materials 1; Supplementary Table S2.19). RPS5A and its co-expressed genes (except one not differentially expressed) were suppressed in WT plants at 24 h following MeJA treatment but not in *OsRIP1*-OE plants from line J (Supplementary Materials 1; Supplementary Table S20). Cytokinins are tightly related to leaf senescence, and the decrease in cytokinin levels during leaf senescence is well-documented (Hönig et al., 2018; Liu et al., 2020). The marked difference in the cell cycle pathway showed more down-regulated genes in shoots of WT plants compared to plants from line J at both 3 h and 24 h after MeJA treatment (Table 2; Figures 4N, P). Accordingly, the number of down-regulated genes related to the cytokinin pathway found in WT plants were higher than that in plants of line J after MeJA treatment for 24 h (Figure 4L; Table 2).

Molecular docking also predicted a favorable binding between α-tubulin and OsRIP1. α-tubulin participates in the biological processes of microtubule cytoskeleton organization and the mitotic cell cycle (Gaudet et al., 2011; Sheoran et al., 2014). Furthermore, mutant studies demonstrated the involvement of α-tubulin in plant growth modification in rice and *Arabidopsis* (Thitamadee et al., 2002; Sunohara et al., 2009). We hypothesize that OsRIP1 functions as a regulatory protein to antagonize MeJA-mediated shoot growth inhibition, probably through interacting with 40S ribosomal protein S5 and/or α-tubulin to modulate cytokinin-mediated leaf senescence and positive regulation of cell cycle.

Externally applied MeJA inhibited N metabolism in roots of rice plants. The biological processes important for N metabolism were suppressed in roots of WT plants after MeJA treatment for 3 h, while this phenomenon was observed in roots of *OsRIP1*-OE plants from line J at 24 h after MeJA addition (Supplementary Materials 1; Supplementary Figure S6). These observations imply that OsRIP1 delayed N regulation in rice plants under MeJA stress. N deficiency remarkably reduced plant N marker traits such as chlorophyll content, total N content and protein content (Gutiérrez et al., 2007). Partially in line with previous results, impaired chlorophyll index (ChlIdx) was characteristic of *OsRIP1*-OE plants from both lines after 24 h of MeJA treatment, while this was absent in WT plants (Figure 2C). The N deficiency also has an important impact on the C metabolism (Guo et al., 2017). If plants maintain an adequate photosynthesis rate, it would certainly favor an efficient production of reduced C and the subsequent efficient use of N (Bi et al., 2014), since C and N metabolism are closely linked and tightly regulated (Schofield et al., 2009). Plants under low N stress exhibited a higher sensitivity to oxidative damage resulting from excessive light and were characterized by a significant suppression of the photosynthetic capacity (Mittler, 2002; Diaz et al., 2006). In the current study, one alternative explanation for the remarkable decline in the photosystem II efficiency (Fv/Fm) observed in shoots of *OsRIP1*-OE plants (Figure 2B) may be that MeJA limited N metabolism in root tissues and consequently decreased availability of C and energy in systemic leaves at 24 h after MeJA treatment. MeJA was reported to elicit rapid changes in C and N dynamics in tomato (Gómez et al., 2010). In addition, nitrogen metabolism is a critical process since nitrogen is an important constituent of hormones, DNA, RNA, and proteins. After 24 h of MeJA treatment, GO terms associated with the "Ribosome" pathway were assigned for the down-regulated

DEGs unique in roots of plants from line J (Supplementary Materials 1; Supplementary Figure S6B3). Oh et al. (2017) reported that protein degradation and protein translation pathways underwent extensive alterations in *Magnaporthe oryzae* under nitrogen starvation by comparative proteomic analysis. Yu et al. (2017) also established that N deficiency reduced the expression of many genes involved in translation, indicating translation is inhibited during nitrogen starvation.

The better performance of *OsRIP1*-OE plants from line J under MeJA stress might be attributed to negative regulation of photosynthesis pathways. MeJA elicitation suppressed the chlorophyll biosynthetic process at 3 h, and inhibited photosynthesis at 24 h after MeJA treatment in *OsRIP1-OE* plants from line J (Figures 3B1, B2). It has been firmly established that photosynthetic dysfunction is one of the typical senescence symptoms induced by MeJA application in barley (Kurowska et al., 2020), tomato (Ding et al., 2018), broccoli (Rahnamaie-Tajadod et al., 2017), and rice (Li et al., 2014). In our study, OsRIP1 confers rice tolerance to MeJA stress, which was accompanied by a large decrease in photosynthesis at the 24 h timepoint. Health parameters evaluated via the multispectral imaging platform showed that MeJA treatment at 24 h resulted in a clear rapid and transient decrease in Fv/Fm in *OsRIP1*-OE plants of both line J and line H, but not in WT plants (Figure 2A), which partly confirms the observations at transcriptome level (Figures 4S, T; Table 2). Notably, increasing evidence indicates that the difference in the degree of photosynthetic changes in the early stages of stresses could conversely be an indicator for the resistance level (Yang and Luo, 2021). Inoculation of powdery mildew induced a larger decline in photosynthesis in resistant barley than in susceptible barley plants (Swarbrick et al., 2006). Similar observations were also documented in tobacco upon infection with *Phytophthora nicotianae* (Scharte et al., 2005), and in *Arabidopsis* plants infected with *Pseudomonas syringae* (Bonfig et al., 2006).

A photosystem II 10 kDa polypeptide, Psbr, was identified by pull-down assays. Molecular docking predicted a preferable interaction between OsRIP1 and Psbr (Supplementary Materials 1; Supplementary Figure S11A), which function is associated with the oxygen-evolving complex of photosystem II. In contrast to Psbr that is located to the chloroplast thylakoid membrane while OsRIP1 was demonstrated to be present in the cytoplasm and the nucleus (De Zaeytijd et al., 2019). It is worth mentioning that most chloroplast proteins are synthesized in the cytoplasm and transported into the chloroplast through an orchestrated transport system (Schleiff and Becker, 2011). Psbr is a nuclear-encoded thylakoid lumenal protein (Liu et al., 2012), and we speculate that it can interact with OsRIP1 before entering the chloroplast. Further investigations are needed to proof the interactions.

OsRIP1 is suggested to predominately modulate redox-related responses (Supplementary Materials 1; Supplementary Figure S12; Supplementary Table S21) to MeJA treatment at 3 h by the analysis of gene regulatory network (Spurney et al., 2020) using DEGs with $\log_2$FC > 2. Furthermore, an upregulation of antioxidant enzymes was observed at 24 h in plants from line J (Supplementary Materials 1; Supplementary Table S22). Activation of antioxidant enzymes positively regulates plant defense systems, and a recent report showed that H_2O_2 application resulted in reduced oxidative stress by increasing the activity of antioxidant enzymes to protect rice plants form arsenic damage (Asgher et al., 2021).

Exogenous application of MeJA activated most JA-responsive genes (Table 2; Figure 4A–D), while approximately half of GA-responsive genes were up-regulated at both 3 h and 24 h (Table 2; Figures 4E–H). It is suggested that MeJA application activated the JA pathway to a larger extent than the GA pathway at 3 h and 24 h. Moreover, 3 h of MeJA treatment resulted in a higher activation of the JA signaling pathway in WT plants when compared to *OsRIP1*-OE plants from line J, while at 24 h of MeJA application a higher level of activation of the GA pathway was observed in WT plants compared to plants from line J. The interaction between different hormone signaling pathways in plants enables an optimal utilization of the available resources for either growth or defense. Numerous studies have revealed that JAs prioritize rice defense over GA-induced growth through negatively regulating GA signaling in herbivore-attacked plants (Yang et al., 2012; Li et al., 2015; MaChado et al., 2017). GA-JA antagonistic crosstalk has also been demonstrated in rice infected with *Xoo* (De Vleesschauwer et al., 2016) and *Meloidogyne graminicola* (Yimer et al., 2018). MaChado et al. (2017) proposed that JA indirectly represses shoot growth by antagonizing the GA pathway, perhaps through down regulation of photosynthesis based on the analysis of plants treated with exogenous JA and GA. The effect of MeJA treatment on WT plants in our study agrees with this hypothesis. In contrast to WT plants, OsRIP1 overexpression confers rice tolerance to MeJA stress through delaying the early activation of endogenous JA signaling cascades.

In summary, OsRIP1 is proposed to modulate redox-related responses at the 3 h timepoint, which may lead to further increasing the antioxidant enzyme activities and transient suppression of photosynthesis at 24 h post MeJA treatment. In addition, *OsRIP1* overexpression was suggested to modulate a lower level of the early activation of endogenous JA signaling pathway under exogenous MeJA treatment, resulting in a subsequent lower suppression of pathways involved in cytokinin signaling and cell cycle. Therefore, we speculated that OsRIP1 overexpression might be an important factor involved in the pathway determining rice tolerance to exogenous MeJA application.

Data availability statement

The mRNA-sequencing data used in this study have been submitted to the NCBI Sequence Read Archive (SRA) under BioProject ID PRJNA1104416. All other data mentioned in this article are available from the corresponding author upon reasonable request.

Author contributions

SC: Conceptualization, Data curation, Investigation, Methodology, Visualization, Writing – original draft, Writing –

review & editing. ND: Investigation, Methodology, Writing – review & editing. AM: Investigation, Writing – review & editing. KG: Investigation, Methodology, Writing – review & editing. PW: Investigation, Methodology, Writing – review & editing. IV: Investigation, Methodology, Writing – review & editing. VO: Investigation, Methodology, Writing – review & editing. SK: Investigation, Methodology, Writing – review & editing. TD: Writing – review & editing. KA: Conceptualization, Funding acquisition, Visualization, Writing – review & editing. EVD: Conceptualization, Funding acquisition, Project administration, Resources, Supervision, Writing – review & editing.

Funding

The author(s) declare that financial support was received for the research, authorship, and/or publication of this article. This work was supported in part by Guangzhou Elite Project and the Fund for Scientific Research – Flanders (Grant G006114N). The authors acknowledge the financial support from the Hercules foundation of the Flemish Government for the multispectral imaging platform (Project Number AUGE/15/17).

Conflict of interest

The authors declare that the research was conducted in the absence of any commercial or financial relationships that could be construed as a potential conflict of interest.

The author(s) declared that they were an editorial board member of Frontiers, at the time of submission. This had no impact on the peer review process and the final decision.

Publisher's note

Supplementary material

The Supplementary Material for this article can be found online at: https://www.frontiersin.org/articles/10.3389/fpls.2024.1385477/full#supplementary-material

References

Asgher, M., Ahmed, S., Sehar, Z., Gautam, H., Gandhi, S. G., and Khan, N. A. (2021). Hydrogen peroxide modulates activity and expression of antioxidant enzymes and protects photosynthetic activity from arsenic damage in rice (*Oryza sativa* L.). *J. Hazardous Materials* 401, 123365. doi: 10.1016/j.jhazmat.2020.123365

Baker, N. R. (2008). Chlorophyll fluorescence: A probe of photosynthesis *in vivo*. *Annu. Rev. Plant Biol.* 59, 89–113. doi: 10.1146/annurev.arplant.59.032607.092759

Bi, Y.-M., Meyer, A., Downs, G. S., Shi, X., El-Kereamy, A., Lukens, L., et al. (2014). High throughput RNA sequencing of a hybrid maize and its parents shows different mechanisms responsive to nitrogen limitation. *BMC Genomics* 15, 1–12. doi: 10.1186/1471-2164-15-77

Bonfig, K. B., Schreiber, U., Gabler, A., Roitsch, T., and BerGER, S. (2006). Infection with virulent and avirulent P. syringae strains differentially affects photosynthesis and sink metabolism in Arabidopsis leaves. *Planta* 225, 1–12. doi: 10.1007/s00425-006-0303-3

Bradford, M. M. (1976). A rapid and sensitive method for the quantitation of microgram quantities of protein utilizing the principle of protein-dye binding. *Analytical Biochem.* 72, 248–254. doi: 10.1016/0003-2697(76)90527-3

Browning, K. S., and Bailey-Serres, J. (2015). Mechanism of cytoplasmic mRNA translation. *Arabidopsis book/American Soc. Plant Biologists* 13, e0176. doi: 10.1199/tab.0176

De Vleesschauwer, D., Gheysen, G., and Höfte, M. (2013). Hormone defense networking in rice: tales from a different world. *Trends Plant Sci.* 18, 555–565. doi: 10.1016/j.tplants.2013.07.002

De Vleesschauwer, D., Seifi, H. S., Filipe, O., Haeck, A., Huu, S. N., Demeestere, K., et al. (2016). The DELLA protein SLR1 integrates and amplifies salicylic acid-and jasmonic acid-dependent innate immunity in rice. *Plant Physiol.* 170, 1831–1847. doi: 10.1104/pp.15.01515

De Zaeytijd, J., Rougé, P., Smagghe, G., and Van Damme, E. J. (2019). Structure and activity of a cytosolic ribosome-inactivating protein from rice. *Toxins* 11, 325. doi: 10.3390/toxins11060325

Diaz, C., Saliba-Colombani, V., Loudet, O., Belluomo, P., Moreau, L., Daniel-Vedele, F., et al. (2006). Leaf yellowing and anthocyanin accumulation are two genetically independent strategies in response to nitrogen limitation in Arabidopsis thaliana. *Plant Cell Physiol.* 47, 74–83. doi: 10.1093/pcp/pci225

Ding, F., Wang, M., and Zhang, S. (2018). Sedoheptulose-1, 7-bisphosphatase is involved in methyl jasmonate-and dark-induced leaf senescence in tomato plants. *Int. J. Mol. Sci.* 19, 3673. doi: 10.3390/ijms19113673

Fattorini, L., Falasca, G., Kevers, C., Mainero Rocca, L., Zadra, C., and Altamura, M. M. (2009). Adventitious rooting is enhanced by methyl jasmonate in tobacco thin cell layers. *Planta* 231, 155–168. doi: 10.1007/s00425-009-1035-y

Fu, J., Wu, H., Ma, S., Xiang, D., Liu, R., and Xiong, L. (2017). OsJAZ1 attenuates drought resistance by regulating JA and ABA signaling in rice. *Front. Plant Sci.* 8, 2108. doi: 10.3389/fpls.2017.02108

Gaudet, P., Livstone, M. S., Lewis, S. E., and Thomas, P. D. (2011). Phylogenetic-based propagation of functional annotations within the Gene Ontology consortium. *Briefings Bioinf.* 12, 449–462. doi: 10.1093/bib/bbr042

Ghaemi, R., Pourjam, E., Safaie, N., Verstraeten, B., Mahmoudi, S. B., Mehrabi, R., et al. (2020). Molecular insights into the compatible and incompatible interactions between sugar beet and the beet cyst nematode. *BMC Plant Biol.* 20, 1–16. doi: 10.1186/s12870-020-02706-8

Gitelson, A. A., Gritz, Y., and Merzlyak, M. N. (2003). Relationships between leaf chlorophyll content and spectral reflectance and algorithms for non-destructive chlorophyll assessment in higher plant leaves. *J. Plant Physiol.* 160, 271–282. doi: 10.1078/0176-1617-00887

Gitelson, A. A., Gurlin, D., Moses, W. J., and Barrow, T. (2009). A bio-optical algorithm for the remote estimation of the chlorophyll-a concentration in case 2 waters. *Environ. Res. Lett.* 4, 045003. doi: 10.1088/1748-9326/4/4/045003

Gómez, S., Ferrieri, R. A., Schueller, M., and Orians, C. M. (2010). Methyl jasmonate elicits rapid changes in carbon and nitrogen dynamics in tomato. *New Phytol.* 188, 835–844. doi: 10.1111/j.1469-8137.2010.03414.x

Guo, Q., Major, I. T., and Howe, G. A. (2018). Resolution of growth–defense conflict: mechanistic insights from jasmonate signaling. *Curr. Opin. Plant Biol.* 44, 72–81. doi: 10.1016/j.pbi.2018.02.009

Guo, X., Yu, C., Luo, L., Wan, H., Zhen, N., Xu, T., et al. (2017). Transcriptome of the floral transition in Rosa chinensis 'Old Blush'. *BMC Genomics* 18, 1–18. doi: 10.1186/s12864-017-3584-y

Gutiérrez, R. A., Lejay, L. V., Dean, A., Chiaromonte, F., Shasha, D. E., and Coruzzi, G. M. (2007). Qualitative network models and genome-wide expression data define carbon/nitrogen-responsive molecular machines in Arabidopsis. *Genome Biol.* 8, 1–13. doi: 10.1186/gb-2007-8-1-r7

Havko, N. E., Major, I. T., Jewell, J. B., Attaran, E., and Howe, G. A. (2016). Control of carbon assimilation and partitioning by jasmonate: an accounting of growth–defense tradeoffs. *Plants* 5, 7. doi: 10.3390/plants5010007

Hönig, M., Plíhalová, L., Husičková, A., Nisler, J., and Doležal, K. (2018). Role of cytokinins in senescence, antioxidant defense and photosynthesis. *Int. J. Mol. Sci.* 19, 4045. doi: 10.3390/ijms19124045

Jumper, J., Evans, R., Pritzel, A., Green, T., Figurnov, M., Ronneberger, O., et al. (2021). Highly accurate protein structure prediction with AlphaFold. *Nature* 596, 583–589. doi: 10.1038/s41586-021-03819-2

Kabbage, M., and Dickman, M. (2008). The BAG proteins: a ubiquitous family of chaperone regulators. *Cell. Mol. Life Sci.* 65, 1390–1402. doi: 10.1007/s00018-008-7535-2

Kalinina, N. O., Makarova, S., Makhotenko, A., Love, A. J., and Taliansky, M. (2018). The multiple functions of the nucleolus in plant development, disease and stress responses. *Front. Plant Sci.* 9, 132. doi: 10.3389/fpls.2018.00132

Kawahara, Y., Oono, Y., Wakimoto, H., Ogata, J., Kanamori, H., Sasaki, H., et al. (2016). TENOR: database for comprehensive mRNA-Seq experiments in rice. *Plant Cell Physiol.* 57, e7–e7. doi: 10.1093/pcp/pcv179

Kazan, K., and Manners, J. M. (2011). The interplay between light and jasmonate signaling during defense and development. *J. Exp. Bot.* 62, 4087–4100. doi: 10.1093/jxb/err142

Klessig, D. F., Choi, H. W., and Dempsey, D. M. A. (2018). Systemic acquired resistance and salicylic acid: past, present, and future. *Mol. Plant-Microbe Interact.* 31, 871–888. doi: 10.1094/MPMI-03-18-0067-CR

Kozakov, D., Hall, D. R., Xia, B., Porter, K. A., Padhorny, D., Yueh, C., et al. (2017). The ClusPro web server for protein-protein docking. *Nat. Protoc.* 12, 255–278. doi: 10.1038/nprot.2016.169

Kurowska, M. M., Daszkowska-Golec, A., Gajecka, M., Kościelniak, P., Bierza, W., and Szarejko, I. (2020). Methyl jasmonate affects photosynthesis efficiency, expression of HvTIP genes and nitrogen homeostasis in barley. *Int. J. Mol. Sci.* 21, 4335. doi: 10.3390/ijms21124335

Laemmli, U. K. (1970). Cleavage of structural proteins during the assembly of the head of bacteriophage T4. *Nature* 227, 680–685. doi: 10.1038/227680a0

Li, Y., Nie, Y., Zhang, Z., Ye, Z., Zou, X., Zhang, L., et al. (2014). Comparative proteomic analysis of methyl jasmonate-induced defense responses in different rice cultivars. *Proteomics* 14, 1088–1101. doi: 10.1002/pmic.201300104

Li, C., Xu, M., Cai, X., Han, Z., Si, J., and Chen, D. (2022). Jasmonate signaling pathway modulates plant defense, growth, and their trade-offs. *Int. J. Mol. Sci.* 23, 3945. doi: 10.3390/ijms23073945

Li, R., Zhang, J., Li, J., Zhou, G., Wang, Q., Bian, W., et al. (2015). Prioritizing plant defense over growth through WRKY regulation facilitates infestation by non-target herbivores. *Elife* 4, e04805. doi: 10.7554/eLife.04805

Liu, H., He, A., Jiang, G., Hussain, S., Wang, W., Sun, H., et al. (2020). Faster leaf senescence after flowering in wet direct-seeded rice was mainly regulated by decrease in cytokinin content as compared with transplanted-flooded rice. *Food Energy Secur.* 9, e232. doi: 10.1002/fes3.232

Liu, X., Li, F., Tang, J., Wang, W., Zhang, F., Wang, G., et al. (2012). Activation of the jasmonic acid pathway by depletion of the hydroperoxide lyase OsHPL3 reveals crosstalk between the HPL and AOS branches of the oxylipin pathway in rice. *PloS One* 7, e50089. doi: 10.1371/journal.pone.0050089

Liu, J., Yang, H., Lu, Q., Wen, X., Chen, F., Peng, L., et al. (2012). PsbP-domain protein1, a nuclear-encoded thylakoid lumenal protein, is essential for photosystem I assembly in Arabidopsis. *Plant Cell* 24, 4992–5006. doi: 10.1105/tpc.112.106542

López-Gresa, M. P., Lisón, P., Campos, L., Rodrigo, I., Rambla, J. L., Granell, A., et al. (2017). A non-targeted metabolomics approach unravels the VOCs associated with the tomato immune response against Pseudomonas syringae. *Front. Plant Sci.* 8, 1188. doi: 10.3389/fpls.2017.01188

MaChado, R. A., Baldwin, I. T., and Erb, M. (2017). Herbivory-induced jasmonates constrain plant sugar accumulation and growth by antagonizing gibberellin signaling and not by promoting secondary metabolite production. *New Phytol.* 215, 803–812. doi: 10.1111/nph.14597

Mittler, R. (2002). Oxidative stress, antioxidants and stress tolerance. *Trends Plant Sci.* 7, 405–410. doi: 10.1016/S1360-1385(02)02312-9

Miyamoto, K., Shimizu, T., Mochizuki, S., Nishizawa, Y., Minami, E., Nojiri, H., et al. (2013). Stress-induced expression of the transcription factor RERJ1 is tightly regulated in response to jasmonic acid accumulation in rice. *Protoplasma* 250, 241–249. doi: 10.1007/s00709-012-0400-z

Noir, S., Bömer, M., Takahashi, N., Ishida, T., Tsui, T.-L., Balbi, V., et al. (2013). Jasmonate controls leaf growth by repressing cell proliferation and the onset of endoreduplication while maintaining a potential stand-by mode. *Plant Physiol.* 161, 1930–1951. doi: 10.1104/pp.113.214908

Oh, Y., Robertson, S. L., Parker, J., Muddiman, D. C., and Dean, R. A. (2017). Comparative proteomic analysis between nitrogen supplemented and starved conditions in Magnaporthe oryzae. *Proteome Sci.* 15, 1–12. doi: 10.1186/s12953-017-0128-y

Peng, Y., Yang, J., Li, X., and Zhang, Y. (2021). Salicylic acid: biosynthesis and signaling. *Annu. Rev. Plant Biol.* 72, 761–791. doi: 10.1146/annurev-arplant-081320-092855

Pieterse, C. M., Leon-Reyes, A., van der Ent, S., and Van Wees, S. C. (2009). Networking by small-molecule hormones in plant immunity. *Nat. Chem. Biol.* 5, 308–316. doi: 10.1038/nchembio.164

Rahnamaie-Tajadod, R., Loke, K.-K., Goh, H.-H., and Mohd Noor, N. (2017). Differential gene expression analysis in Polygonum minus leaf upon 24 hours of methyl jasmonate elicitation. *Front. Plant Sci.* 8, 109. doi: 10.3389/fpls.2017.00109

Robert-Seilaniantz, A., Grant, M., and Jones, J. D. (2011). Hormone crosstalk in plant disease and defense: more than just jasmonate-salicylate antagonism. *Annu. Rev. Phytopathol.* 49, 317–343. doi: 10.1146/annurev-phyto-073009-114447

Roy, A. A., Dhawanjewar, A. S., Sharma, P., Singh, G., and Madhusudhan, M. S. (2019). Protein Interaction Z Score Assessment (PIZSA): an empirical scoring scheme for evaluation of protein-protein interactions. *Nucleic Acids Res.* 47, W331–W337. doi: 10.1093/nar/gkz368

Scharte, J., Schön, H., and Weis, E. (2005). Photosynthesis and carbohydrate metabolism in tobacco leaves during an incompatible interaction with Phytophthora nicotianae. *Plant Cell Environ.* 28, 1421–1435. doi: 10.1111/j.1365-3040.2005.01380.x

Schleiff, E., and Becker, T. (2011). Common ground for protein translocation: access control for mitochondria and chloroplasts. *Nat. Rev. Mol. Cell Biol.* 12, 48–59. doi: 10.1038/nrm3027

Schofield, R., Bi, Y. M., Kant, S., and Rothstein, S. (2009). Over-expression of STP13, a hexose transporter, improves plant growth and nitrogen use in Arabidopsis thaliana seedlings. *Plant Cell Environ.* 32, 271–285. doi: 10.1111/j.1365-3040.2008.01919.x

Seo, J. S., Joo, J., Kim, M. J., Kim, Y. K., Nahm, B. H., Song, S. I., et al. (2011). OsbHLH148, a basic helix-loop-helix protein, interacts with OsJAZ proteins in a jasmonate signaling pathway leading to drought tolerance in rice. *Plant J.* 65, 907–921. doi: 10.1111/j.1365-313X.2010.04477.x

Sheoran, I. S., Koonjul, P., Attieh, J., and Saini, H. S. (2014). Water-stress-induced inhibition of α-tubulin gene expression during growth, and its implications for reproductive success in rice. *Plant Physiol. Biochem.* 80, 291–299. doi: 10.1016/j.plaphy.2014.04.011

Shimada, T., Endo, T., Rodríguez, A., Fujii, H., Goto, S., Matsuura, T., et al. (2017). Ectopic accumulation of linalool confers resistance to Xanthomonas citri subsp. citri in transgenic sweet orange plants. *Tree Physiol.* 37, 654–664. doi: 10.1093/treephys/tpw134

Spurney, R. J., Van Den Broeck, L., Clark, N. M., Fisher, A. P., De Luis Balaguer, M. A., and Sozzani, R. (2020). tuxnet: a simple interface to process RNA sequencing data and infer gene regulatory networks. *Plant J.* 101, 716–730. doi: 10.1111/tpj.14558

Sunohara, H., Kawai, T., Shimizu-Sato, S., Sato, Y., Sato, K., and Kitano, H. (2009). A dominant mutation of TWISTED DWARF 1 encoding an α-tubulin protein causes severe dwarfism and right helical growth in rice. *Genes Genet. Syst.* 84, 209–218. doi: 10.1266/ggs.84.209

Swarbrick, P. J., Schulze-Lefert, P., and Scholes, J. D. (2006). Metabolic consequences of susceptibility and resistance (race-specific and broad-spectrum) in barley leaves challenged with powdery mildew. *Plant Cell Environ.* 29, 1061–1076. doi: 10.1111/j.1365-3040.2005.01472.x

Taniguchi, S., Hosokawa-Shinonaga, Y., Tamaoki, D., Yamada, S., Akimitsu, K., and Gomi, K. (2014). Jasmonate induction of the monoterpene linalool confers resistance to rice bacterial blight and its biosynthesis is regulated by JAZ protein in rice. *Plant Cell Environ.* 37, 451–461. doi: 10.1111/pce.12169

Thitamadee, S., Tuchihara, K., and Hashimoto, T. (2002). Microtubule basis for left-handed helical growth in Arabidopsis. *Nature* 417, 193–196. doi: 10.1038/417193a

Wasternack, C., and Strnad, M. (2016). Jasmonate signaling in plant stress responses and development–active and inactive compounds. *New Biotechnol.* 33, 604–613. doi: 10.1016/j.nbt.2015.11.001

Weijers, D., Franke-Van Dijk, M., Vencken, R.-J., Quint, A., Hooykaas, P., and Offringa, R. (2001). An Arabidopsis Minute-like phenotype caused by a semi-dominant mutation in a RIBOSOMAL PROTEIN S5 gene. *Development* 128 (21), 4289–4299. doi: 10.1242/dev.128.21.4289

Wytynck, P. (2020). *RIPs, a cereal killer?: the physiological role of rice ribosome-inactivating proteins (RIPs) in abiotic stress* (Ghent, Belgium: Ghent University).

Wytynck, P., Lambin, J., Chen, S., Demirel Asci, S., Verbeke, I., De Zaeytijd, J., et al. (2021). Effect of RIP overexpression on abiotic stress tolerance and development of rice. *Int. J. Mol. Sci.* 22, 1434. doi: 10.3390/ijms22031434

Yang, J., Duan, G., Li, C., Liu, L., Han, G., Zhang, Y., et al. (2019). The crosstalks between jasmonic acid and other plant hormone signaling highlight the involvement of jasmonic acid as a core component in plant response to biotic and abiotic stresses. *Front. Plant Sci.* 10, 1349. doi: 10.3389/fpls.2019.01349

Yang, H., and Luo, P. (2021). Changes in photosynthesis could provide important insight into the interaction between wheat and fungal pathogens. *Int. J. Mol. Sci.* 22, 8865. doi: 10.3390/ijms22168865

Yang, D.-L., Yao, J., Mei, C.-S., Tong, X.-H., Zeng, L.-J., Li, Q., et al. (2012). Plant hormone jasmonate prioritizes defense over growth by interfering with gibberellin signaling cascade. *Proc. Natl. Acad. Sci.* 109, E1192–E1200. doi: 10.1073/pnas.1201616109

Yimer, H. Z., Nahar, K., Kyndt, T., Haeck, A., Van Meulebroek, L., Vanhaecke, L., et al. (2018). Gibberellin antagonizes jasmonate-induced defense against Meloidogyne graminicola in rice. *New Phytol.* 218, 646–660. doi: 10.1111/nph.15046

You, Q., Zhai, K., Yang, D., Yang, W., Wu, J., Liu, J., et al. (2016). An E3 ubiquitin ligase-BAG protein module controls plant innate immunity and broad-spectrum disease resistance. *Cell Host Microbe* 20, 758–769. doi: 10.1016/j.chom.2016.10.023

Yu, C., Zhao, X., Qi, G., Bai, Z., Wang, Y., Wang, S., et al. (2017). Integrated analysis of transcriptome and metabolites reveals an essential role of metabolic flux in starch accumulation under nitrogen starvation in duckweed. *Biotechnol. Biofuels* 10, 1–14. doi: 10.1186/s13068-017-0851-8

Zhang, Y., and Turner, J. G. (2008). Wound-induced endogenous jasmonates stunt plant growth by inhibiting mitosis. *PloS One* 3, e3699. doi: 10.1371/journal.pone.0003699

Zhu, F., Zhou, Y.-K., Ji, Z.-L., and Chen, X.-R. (2018). The plant ribosome-inactivating proteins play important roles in defense against pathogens and insect pest attacks. *Front. Plant Sci.* 9, 146. doi: 10.3389/fpls.2018.00146

Frontiers in Plant Science

Cultivates the science of plant biology and its applications

The most cited plant science journal, which advances our understanding of plant biology for sustainable food security, functional ecosystems and human health.

Discover the latest Research Topics

See more →

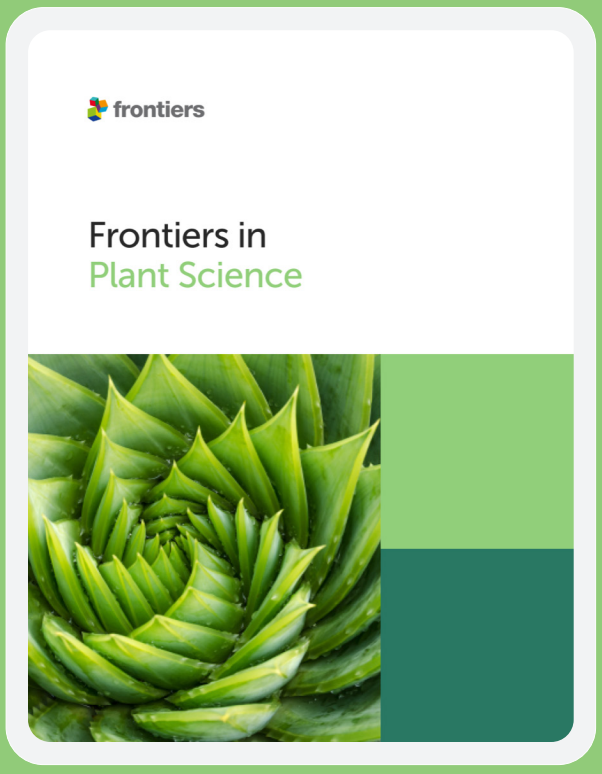

Frontiers

Avenue du Tribunal-Fédéral 34
1005 Lausanne, Switzerland
frontiersin.org

Contact us

+41 (0)21 510 17 00
frontiersin.org/about/contact